AFRL-RH-BR-TR-2010-0065

**Radio Frequency Radiation
Dosimetry Handbook
(Fifth Edition)**

Edited by

William P. Roach

**Directed Energy Bioeffects Division
Radio Frequency Radiation Branch**

July 2009

**Air Force Research Laboratory
711 Human Performance Wing
Human Effectiveness Directorate
Directed Energy Bioeffects Division
Radio Frequency Radiation Branch
Brooks City-Base, TX 78235-5147**

NOTICE AND SIGNATURE PAGE

This report was cleared for public release by the 88th ABW Public Affairs Office and is available to the general public, including foreign nationals. Copies may be obtained from the Defense Technical Information Center (DTIC) (http://www.dtic.mil).

AFRL-RH-BR-TR-2010-0065 has been reviewed and is approved for publication in accordance with assigned distribution statement.

_____//SIGNED//_____
TRAVIS BEMROSE, CAPT, USAF
Contract Monitor
Radio Frequency Radiation Branch

_____//SIGNED//_____
GARRETT D. POLHAMUS, DR-IV, DAF
Chief, Directed Energy Bioeffects Division
Air Force Research Laboratory
711 Human Performance Wing
Human Effectiveness Directorate

REPORT DOCUMENTATION PAGE		*Form Approved* *OMB No. 0704-0188*

Public reporting burden for this collection of information is estimated to average 1 hour per response, including the time for reviewing instructions, searching existing data sources, gathering and maintaining the data needed, and completing and reviewing this collection of information. Send comments regarding this burden estimate or any other aspect of this collection of information, including suggestions for reducing this burden to Department of Defense, Washington Headquarters Services, Directorate for Information Operations and Reports (0704-0188), 1215 Jefferson Davis Highway, Suite 1204, Arlington, VA 22202-4302. Respondents should be aware that notwithstanding any other provision of law, no person shall be subject to any penalty for failing to comply with a collection of information if it does not display a currently valid OMB control number. **PLEASE DO NOT RETURN YOUR FORM TO THE ABOVE ADDRESS.**

1. REPORT DATE *(DD-MM-YYYY)* 24/07/2009	2. REPORT TYPE Interim	3. DATES COVERED *(From – To)* November 2007 – February 2008

4. TITLE AND SUBTITLE

Radio Frequency Radiation Dosimetry Handbook (Fifth Edition)

5a. CONTRACT NUMBER
FA8650-07-D-6800

5b. GRANT NUMBER
N/A

5c. PROGRAM ELEMENT NUMBER
62202F

6. AUTHOR(S)

Edited by William P. Roach

5d. PROJECT NUMBER
7757

5e. TASK NUMBER
B3

5f. WORK UNIT NUMBER
55

7. PERFORMING ORGANIZATION NAME(S) AND ADDRESS(ES)

Air Force Research Laboratory, 711 Human Performance Wing,
Radio Frequency Radiation Branch
8262 Hawks Road
Brooks City-Base, TX 78235-5147

8. PERFORMING ORGANIZATION REPORT NUMBER

N/A

9. SPONSORING / MONITORING AGENCY NAME(S) AND ADDRESS(ES)
Air Force Materiel Command, Air Force Research Laboratory,
711 Human Performance Wing, Human Effectiveness Directorate,
Directed Energy Bioeffects Division
Radio Frequency Radiation Branch
8262 Hawks Road
Brooks City-Base, Texas 78235-5147

10. SPONSOR/MONITOR'S ACRONYM(S)
711 HPW/RHDR

11. SPONSOR/MONITOR'S REPORT NUMBER(S)
AFRL-RH-BR-TR-2010-0065

12. DISTRIBUTION / AVAILABILITY STATEMENT
Distribution A: Approved for public release; distribution unlimited. Public Affairs Case No. 11-069

13. SUPPLEMENTARY NOTES

14. ABSTRACT
This edition provides updated tables of published data and new information. Topics covered include: modeling low-to-high frequencies (0-3 GHz); experimental radio frequency dosimetry; high-resolution thermometry and microdosimetry in pulsed electromagnetic fields (EMF); biological effects of high peak power (HPP) pulses, electromagnetic pulse (EMP) and ultra-wideband (UWB) pulses; thermoregulation and thermal modeling; modeling thermal response of tissues irradiated with radio frequency energy; responses to radio frequency (RF) overexposure, personal exposure indicators for electromagnetic fields (3 kHz – 300 GHz); RF alerting signs, status of EMF standards and handbooks, radio frequency/microwave safety standards and terahertz-frequency bioeffects.

15. SUBJECT TERMS
Radio frequency radiation, high peak power, radio frequency dosimetry, thermometry, microdosimetry, electromagnetic fields, specific absorption rate, standards, electromagnetic pulse, ultra-wideband pulse, terahertz-frequency bioeffects

16. SECURITY CLASSIFICATION OF:			17. LIMITATION OF ABSTRACT	18. NUMBER OF PAGES	19a. NAME OF RESPONSIBLE PERSON Capt Travis Bemrose
a. REPORT Unclassified	b. ABSTRACT Unclassified	c. THIS PAGE Unclassified	SAR	398	19b. TELEPHONE NUMBER *(include area code)* N/A

Standard Form 298 (Rev. 8-98)
Prescribed by ANSI Std. Z39.18

THIS PAGE INTENTIONALLY LEFT BLANK

ii

DEDICATION

The Radio Frequency Radiation Dosimetry Handbook (Fifth Edition) is dedicated to the memory of Dr. John R. Leonowich and to the unflinching dedication of Dr. Eleanor R. Adair.

TABLE OF CONTENTS

FORWARD

The last Radio Frequency Radiation Dosimetry Handbook was published in October 1986. Its purpose was to provide a convenient compilation of information contained in the previous editions with updated tables of fresh data and new information. The idea of producing a radio frequency radiation dosimetry handbook grew out of conversations in the early 1970s with Professor Curtis C. Johnson, Chairman of Bioengineering at the University of Utah, Mr. John C. Mitchell, and Mr. Stewart J. Allen both of the United States Air Force School of Aerospace Medicine (USAFSAM) located then at Brooks Air Force Base, Texas. Thus, the first and subsequent editions were published under the watchful eyes of Professor Johnson, Mr. Mitchell, Mr. Allen, Lieutenant Luis Lozano, and Mr. William D. Hurt.

This latest installment of the Radio Frequency Radiation Dosimetry Handbook (Fifth Edition) owes its beginning, compilation, and existence to the diligent and steadfast efforts of Dr. Patrick A. Mason. Its purpose is to keep the current information from former additions with updates in research from the direct current (DC) range of the spectrum into the new region of Terahertz (THz) radiation. During the compilation of this work into the Fifth Edition, Dr. John A. Leonowich passed away and Dr. Eleanor R. Adair retired and to their tireless efforts on behalf of the safety of countless millions around the world, this Radio Frequency Radiation Dosimetry Handbook (Fifth Edition) is dedicated.

Chapter 1 by Professor Om P. Gandhi, ―Numerical Dosimetry – Modeling from Low-to-High Frequencies (0-3 GHz),‖ is written to address the importance of computational and experimental techniques developed for bioelectromagnetic problems for far-field and near-field exposures. Professor Gandhi illustrates the use of these techniques to calculate currents induced in the human body by electromagnetic fields and for specific absorption rate calculations from real world examples like handheld mobile telephones, wireless laptops and base stations, as well as low-frequency electronic article surveillance systems. In Chapter 2, ―Experimental Radio Frequency Dosimetry,‖ Mr. Stewart Allen describes the physical process required to achieve useful biological effects data and underscores the three conditions that are necessary to obtain accurate measurements of the biological response, accurate measurements of the radio frequency fields over the exposure volume in terms of incident field, and accurate measurement of the Specific Absorption Rate (SAR). Mr. Allen underscores the need for extrapolation from experimental data and equivalent human exposure, to complete the planning process before any dosimetry is initiated in order to maximize an outcome.

Dr. Andrei Pakhomov illuminates the proper techniques employed in the measurement of high-intensity short pulse radio frequency field exposures in Chapter 3, ―A Practical Guide to High-Resolution Thermometry and Microdosimetry in Pulsed Electromagnetic Fields.‖ Here Dr. Pakhomov describes the method of local SAR measurement which he states, ―…has proven to be fast, accurate, and reliable and it is likely to produce valid data whenever a temperature plateau after a pulsed exposure can be reliably detected.‖ In Chapter 4, ―Review of Literature on Biological Effects of High Peak Power (HPP) Pulses, Electromagnetic Pulse (EMP), and Ultra-Wideband (UWB) Pulses,‖ Dr. Ronald Seaman reviews the past and current literature. His material is divided into three main sections, HPP pulses, EMP, and UWB pulses. Each section is divided into subsections for in-vivo and in-vitro effects and the subsections in turn are divided

DISTRIBUTION A: APPROVED FOR PUBLIC RELEASE; DISTRIBUTION UNLIMITED.
PUBLIC AFFAIRS CASE NO. 11-069

into parts for acute, a few-pulses of exposures, and subchronic to chronic exposures involving many pulses.

From a more direct point of view, Dr. Eleanor Adair presents ―Thermoregulation and Thermal Modeling" in Chapter 5 and describes how radio frequency radiation may be regarded as part of the thermal environment to which humans and others may be exposed. Dr. Adair shows how heat is actively produced in the body through metabolic processes and may also be passively generated in body tissues by the absorption of radio frequency energy. She states that ―the balance between the production and loss of thermal energy is so efficiently regulated by behavioral and autonomic responses that minimal variation occurs in the core body temperature of an endotherm." In Chapter 6, ―Thermal Modeling," Professor David Nelson shows in great mathematical detail how a thermal model can be an invaluable tool for assessing thermal effects of RF radiation in humans and animals. He shows how there is some very significant limitations and drawbacks to the use of models in RFR dosimetry and that models are only as good as the data on which they are based. He states that, ―Ultimately, any model must be validated by comparison and calibration with accepted experimental results."

Chapter 7, ―Modeling Thermal Response of Tissues Irradiated with Radio Frequency Energy," written by Professor Kenneth Foster considers models for estimating the thermal response of tissue to exposure to RFR and reviews the thermal dose concept, SAR, for predicting tissue damage. The focus here is on applications to relevant dosimetry for safety analysis and his discussion excludes heat transfer of in vitro exposure systems, or heat transfer in tissues in which a boiling of tissue water or thawing frozen tissue may occur. In Chapter 8, ―Response to RF Overexposure," Professor Marvin Ziskin summarizes the biological consequences of exposure to radio frequency, electromagnetic energy for the health care provider. It provides guidance for the proper management of overexposures, where Professor Ziskin defines an overexposure as an exposure to radio frequency radiation in excess of national safety limit standards.

Dr. John Leonowich provides information necessary for field assessment in terms of exposure to fields operating between 3 kHz to 300 GHz. In Chapter 9, ―Personal Exposure Indicators for Electromagnetic Fields 3 kHz –300 GHz," the identification and control of man-made sources of all forms of non-ionizing radiation is highlighted as a high priority of radiation safety professionals. Here Dr. Leonowich considers radio frequency radiation (RFR) to cover the frequencies from 3 kHz to 300 MHz, and microwaves from 300 MHz to 300 GHz. In Chapter 10, ―RF Alerting Signs," Mr. Richard Tell describes hazard communication as the single most effective factor in maintaining safety in hazardous environments. He shows how such communications can take the form of written or verbal information or some form of safety awareness training. Mr. Tell describes how safety signage represents a common form of communication across a wide range of potential hazards and this applies equally to radio frequency environments.

Chapter 11, ―Current Status of EMF Standards and Handbooks - Information for the General Public," written by Professor Dina Simunic is where information on EMF standards of 48 countries are collected and presented. Further, information on published handbooks, reports, pamphlets, and fact sheets for the general public are presented. Chapter 12, ―Radio Frequency/Microwave Safety Standards," written by Mr. Ron Petersen describes radio frequency

radiation safety standards nationally and internationally from 1948 to the present day. Here he describes how contemporary science-based RF/microwave safety standards and guidelines are based on in-depth evaluations and interpretations of the extant scientific literature. He educates us that those RF safety standards updates are an on-going process and, as such, the recommendations in terms of safe limits of exposure evolve as the research becomes more focused and the quality of the research improves. Mr. Petersen notes that ―The simple single value frequency-independent limit proposed more than five decades ago has evolved into the sophisticated rather complex standards and guidelines now used throughout the world." Finally, Chapter 13, ―Terahertz-Frequency Bioeffects: Models and Standards," written by Dr. Robert Thomas and co-workers note that in the employment of new systems, safety is of interest to application developers as output limitations affect performance. Dr. Thomas notes that exposure limits for the 100-GHz to 10-THz frequency band fall within the overlapping ranges of laser safety limits and radio frequency limits and lacking any real scientific data presents the first theoretical consideration to safety by comparing data from theory to extrapolated safety standards for laser and RF. Dr. Thomas and his colleagues' work in Chapter 13 represent the first accounting for THz radiation safety concerns.

WILLIAM P. ROACH, Ph.D., CHP
Senior Science Advisor
Radio Frequency Radiation Branch
Brooks City-Base, Texas

Radio Frequency Radiation Dosimetry Handbook
(Fifth Edition)

Chapter 1. Numerical Dosimetry – Modeling from Low-to-High Frequencies (0-3 GHz)

Om P. Gandhi
Department of Electrical and Computer Engineering
University of Utah, Salt Lake City, Utah 84112-9606

gandhi@ece.utah.edu

1.1   Introduction

Electromagnetic fields are being increasingly used for many new and rapidly expanding applications. In addition to the traditional uses from domestic electrical power to broadcasting to microwave radar, some of the newer applications are for wireless telephones, wireless local-area networks (WLANs), electronic security systems, etc. Hardly a year goes by without a new application of electromagnetic (EM) fields for use by the public. This also creates public concern about the safety of these EM fields.

Fortunately, there are expert committees in many countries and some international committees that examine the human safety issues and suggest exposure levels that may not be exceeded. Most of the recently revised safety standards for exposure to electromagnetic fields are set in terms of limits of internal rates of electromagnetic energy deposition (Specific absorption rates or SARs) at radio frequency (RF) and microwave frequencies and of induced current densities for the various tissues at lower frequencies up to 10 MHz (IEEE, 1999; ICNIRP, 1998). Since 1996, the U.S. Federal Communications Commission (FCC) has required wireless systems such as portable handsets, wireless laptops and base stations to comply with radiofrequency radiation safety guidelines (U.S. FCC, 1996). Requirements for SAR certification for personal wireless devices and compliance with induced current density limits for low-frequency electronic article surveillance (EAS) systems (from a few Hz to a few MHz) have also been initiated in the European Union, Canada, Australia/New Zealand, Japan, and several other countries.

Over the last 30 years, increasingly sophisticated computational and experimental techniques have been developed for determination of SAR distributions or induced electric fields and current densities in anatomically-based models of the human body with present-day voxel resolutions on the order of 1-3 mm (Gandhi, 1995; Gandhi, Lazzi & Furse, 1996; Okoniewski & Stuchly, 1996). With the computational resources available today, even finer submillimeter resolutions are also possible provided the exposure is highly localized to smaller volumes of the body.

In this chapter, we discuss the important computational and experimental techniques developed for bioelectromagnetic problems both for far-field and near-field exposures. We illustrate the use of these techniques to calculate currents induced in the human body by electromagnetic fields (EMFs) and for calculation of SARs by using examples of some recent applications such as safety compliance testing of microwave devices e.g., handheld mobile telephones, wireless laptops and base stations; and of low-frequency EAS systems.

1.2   Safety Standards

The most commonly-used safety standards at the present time are the ANSI/IEEE C95.1 (IEEE, 1999) and ICNIRP (1998). The basic restrictions for both of these standards are in terms of induced current densities (or electric fields) at lower frequencies up to a few megahertz (MHz) and SARs at higher frequencies up to a few gigahertz (GHz). The basic restrictions for frequencies up to 10 GHz prescribed in the ICNIRP standard (ICNIRP, 1998) are given in Table 1-1.

Table 1-1. ICNIRP basic restrictions for time-varying electric and magnetic fields for frequencies up to 10 GHz (ICNIRP, 1998).*

Exposure	Frequency range	Current density J for head and trunk mA/m^2 (rms)	Whole-body average SAR W/kg	Localized SAR for head and trunk W/kg	Localized SAR (limbs) W/kg
Occupational exposure	Up to 1 Hz	40	---	---	---
	1-4 Hz	$40/f$	---	---	---
	4 Hz-1 kHz	10	---	---	---
	1-100 kHz	$f/100$	---	---	---
	100 kHz-10 MHz	$f/100$	0.4	10	20
	10 MHz-10 GHz	---	0.4	10	20
General public exposure	Up to 1 Hz	8	---	---	---
	1-4 Hz	$8/f$	---	---	---
	4 Hz-1 kHz	2	---	---	---
	1-100 kHz	$f/500$	---	---	---
	100 kHz-10 MHz	$f/500$	0.08	2	4
	10 MHz-10 GHz	---	0.08	2	4

* Note:
1. f is the frequency in Hertz.
2. Current densities J should be averaged over a cross section of 1 cm^2 perpendicular to the direction of induced current.
3. Localized SAR averaging mass is any 10 g of contiguous tissue.

The IEEE safety standard (IEEE, 1999), on the other hand, is given in terms of maximum permissible exposures (MPE) of incident external fields for controlled and uncontrolled environments corresponding to occupational and general public exposures, respectively. The IEEE MPEs are given in Table 1-2 for controlled and uncontrolled environments, respectively.

Table 1-2. The IEEE maximum permissible exposure limits for controlled (occupational) and uncontrolled (general public) environments (IEEE, 1999).*

Frequency range MHz	Controlled environments (Occupational)			Uncontrolled environments (General public)		
	E V/m	H A/m	Power density mW/cm^2	E V/m	H A/m	Power density mW/cm^2
0.003-0.1	614	163	---	614	163	---
0.1-3.0	614	16.3/f	---	614 (up to 1.34 MHz) 823.8/f (from 1.34-3.0 MHz)	16.3/f	---
3-30	1842/f	16.3/f	---	823.8/f	16.3/f	---
30-100	61.4	16.3/f	---	27.5	158.3/$f^{1.668}$	---
100-300	61.4	0.163	1.0	27.5	0.0729	0.2
300-3000	---	---	f/300	---	---	f/1500
3000-15,000	---	---	10	---	---	f/1500
15,000-300,000	---	---	10	---	---	10

* Note: f is the frequency in MHz.

As for the ICNIRP standard, the underpinning, here too, is in terms of whole-body average and localized SAR. For frequencies between 0.1 and 6000 MHz (6 GHz), the whole-body average SAR limits of 0.4 W/kg for controlled environments and 0.08 W/kg for uncontrolled environments are identical to those in the ICNIRP standard (see Table 1-1). In this same frequency range, the peak local SAR for any 1-g of tissue (defined as a tissue volume in the shape of a cube) should not exceed 8.0 and 1.6 W/kg for the head and trunk regions for controlled and uncontrolled environments, respectively. Both of these values are somewhat lower and only 80% of the peak local SARs of 10.0 and 2.0 W/kg suggested by ICNIRP for occupational and general public exposures, respectively. Another distinction between these two widely-used safety standards is that whereas the peak SARs are to be calculated (or measured) for any 1-g of tissue for the IEEE standard, a considerably larger averaging weight of 10-g of tissue is suggested by the ICNIRP standard for the tissues of the head and trunk. However, the peak local SARs for the limbs i.e., arms and legs are identical in both the IEEE and ICNIRP standards. The peak local 10-g averaged SARs in both of the standards are 20.0 and 4.0 W/kg for occupational and general public exposures, respectively.

As seen in Table 1-1 for the ICNIRP standard, for low-frequency exposures up to 10 MHz, the basic restrictions are in terms of maximum induced current densities averaged over a cross section of 1 cm^2 perpendicular to the current direction. The IEEE has recently created a standard for safety levels with respect to human exposure to electromagnetic fields 0-3 kHz (IEEE, 2002). In this standard, the basic restrictions are prescribed in terms of induced electric fields for the various regions of the body i.e., brain, heart, hands, wrists, feet and ankles, and all other tissues. The basic restrictions of induced electric fields should not be exceeded for any 5 mm length in any direction within the respective tissues.

The IEEE standard (1999) is used in the United States and a slightly modified version is used in Canada. The ICNIRP standard (1998) is used in the European Union and slightly-altered versions of this standard are used in Australia/New Zealand, Japan, Korea, and in many other countries. In any case, from the discussion of this section, it is clear that safety assessment of the various electromagnetic devices or environments involves determination of induced electric fields or current densities at low frequencies up to a few MHz and of whole-body average and peak 1- or 10-g tissue-averaged SARs at the higher frequencies.

1.3 Computational Techniques for High Frequencies

1.3.1 The FDTD Method with Uniform or Expanding Grid

The finite-difference time-domain (FDTD) method is extremely versatile for bioelectromagnetic problems. FDTD has been used for modeling whole-body or partial-body exposures due to spatially uniform or nonuniform near- or far-fields that are sinusoidally varying or transient in nature (Gandhi, 1995; Taflove & Brodwin, 1975; Spiegel, Fatmi, & Kunz, 1985; Sullivan, Gandhi, & Taflove, 1988; Chen & Gandhi, 1991). The latter includes the fields associated with an electromagnetic pulse (EMP).

In this method, the time-dependent Maxwell's equation is given by

$$\nabla \times \mathbf{E} = -\mu \frac{\partial \mathbf{H}}{\partial t} \tag{1}$$

$$\nabla \times \mathbf{H} = \sigma \mathbf{E} + \varepsilon \frac{\partial \mathbf{E}}{\partial t} \tag{2}$$

are implemented for a lattice of subvolumes or Yee space cells that may be cubical or parallelepiped with different dimensions Δx, Δy, and Δz in the x, y, and z directions, respectively. The components of $\mathbf{E}$ and $\mathbf{H}$ are positioned about each of the cells at half-cell intervals and calculated alternately (leapfrogged) with half-time steps ($\Delta t / 2$). The details of the method are given in several of the above-referenced publications and books (Kunz & Luebbers, 1993; Taflove & Hagness, 2000) and are, therefore, not repeated here.

In the FDTD method, it is necessary to represent not only the scatterer/absorber such as the human body or a part thereof, but also the electromagnetic sources, including their shapes, excitations, and so forth, if these sources are in the near-field region (Gandhi et al., 1996; Okoniewski & Stuchly, 1996). On the other hand, the far-field sources are described by means of incident plane-wave fields specified on a three-dimensional source "box" located typically 6 to 10 cells away from the exposed body. The source-body interaction volume is subdivided into cells of the type shown in Figure 1-1. The interaction space consisting of several hundred thousand to several million Yee cells is truncated by means of absorbing boundaries. The penetrating fields are tracked in time for all cells of the interaction space. The computation is

4

considered to be completed when either both the **E** and **H** fields have died off for an impulsive excitation or, for a sinusoidal excitation, when the sinusoidal steady-state is observed for all cells within the interaction space.
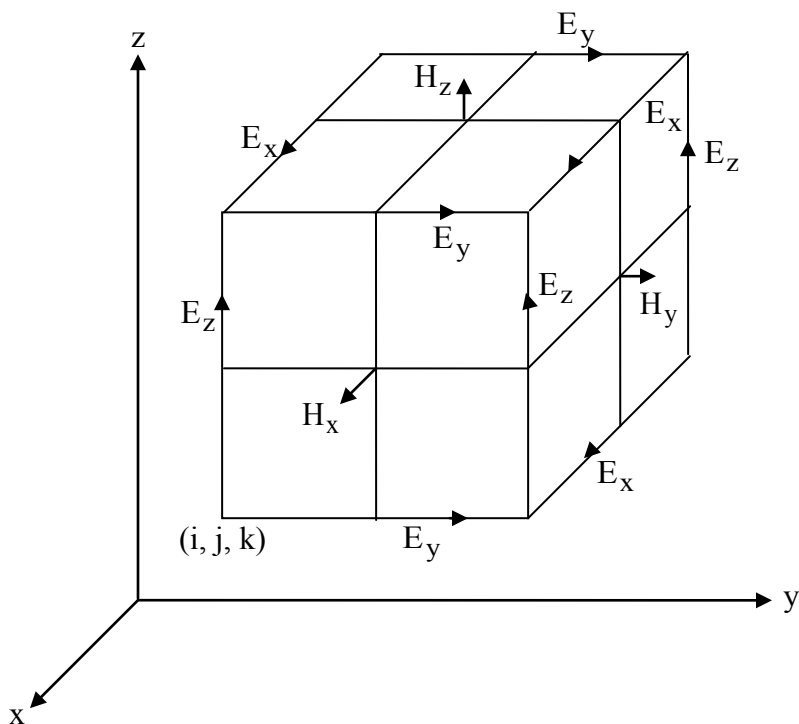
Figure 1-1. Unit cell of Yee lattice indicating positions for various field components.

Even though a uniform FDTD grid has mostly been used for the bioelectromagnetic problems, an expanding-grid formulation has also been proposed by Gao and Gandhi (1992). For near-field sources, this offers the advantage of modeling the tightly coupled regions such as the ear and the proximal side of the head with a fine resolution (small cell size) while allowing cell sizes to increase gradually as one moves further away from the regions of primary interest. The expanding-grid algorithm allows different cell-to-cell expansion factors (typically 1.05-1.10) along the three coordinate axes, and can reduce by a factor of 4 to 10 the total number of cells needed to model a given volume as compared to a uniform grid formulation where the cells with the finest resolution are used throughout the volume. Some of the applications of the expanding grid FDTD method to date are for calculations of induced current and SAR distributions for a worker model exposed to an RF dielectric heater (Gandhi, Wu, Chen, & Conover, 1997) and for SAR distributions due to cellular telephones (Wiart, Chaillou, & Drago, 1997; Tinniswood, Lazzi, & Gandhi, 1999). Another potential application is for dosimetry of the human body at higher frequencies where the interior of the exposed body is relatively shielded and may, therefore, be modeled with coarser cells or ignored altogether. For all of these applications, the coupled fields diminish rapidly into the exposed parts of the body. By using smaller cell sizes on

5

the order of 0.25-1.0 mm for the coupled region, one can determine the SARs with higher precision and better model the irradiating source as well (for example, the personal wireless device, its antenna, and the feed region).

Another approach to this problem of finer resolution for the higher SAR region is the use of subgridding (Okoniewski, Okoniewska, & Stuchly, 1997). Whereas a slowly expanding cell size with cell-to-cell expansion factors on the order of 1.05 to 1.1 are used in the expanding-grid formulation, a stepped expansion factor of two, and at times three, may be used in the subgridding method to represent the regions where the electromagnetic coupling is considerably lower.

1.3.1.1   The Parallelized FDTD Code

A parallelized FDTD code offers the advantages of scalability of memory size and speed to permit SAR calculations at increasingly higher frequencies where smaller grid-cell sizes are needed to resolve the wavelength within body tissues. Parallelized versions of the FDTD code have been developed for use on large parallel-processing machines such as IBM SP-2 (Tinniswood, Furse, & Gandhi, 1998a, 1998b). Although the parallel FDTD code can be run on all of the 64 nodes of the machine, 8 and 16 nodes are routinely used for simulations involving the magnetic resonance imaging (MRI)-based anatomical model having $5.974 \times 5.974 \times 6.0$-mm resolution. Thirty-two nodes are used for the larger, finer-grained anatomical models having $1.974 \times 1.974 \times 3.0$-mm resolution of the entire human body, or $0.9375 \times 0.9375 \times 3.0$-mm resolution of the head and neck for mobile telephone simulations (Tinniswood et al., 1998a). A general simulation strategy is to first apply the lower-resolution FDTD models to pinpoint resonant frequencies, for example, and then apply the higher-resolution models to accurately calculate the SAR distributions at these frequencies (Tinniswood et al., 1998b).

Availability of larger memory computers and improved FDTD codes have allowed SAR calculations for whole-body models with voxel resolutions of 1-2 mm (Tinniswood et al., 1998b; Dimbylow, 2002; Nagaoka et al., 2004).

1.3.2   The Frequency-Dependent FDTD Method

As previously mentioned, the frequency-dependent FDTD or $(FD)^2TD$ method is needed for short pulses where wide bandwidths are generally involved. Two general approaches have been used for the $(FD)^2TD$ method. One approach is to convert the complex permittivity from the frequency domain to the time domain and convolve this with the time-domain electric fields to obtain time-domain fields for dispersive material. This discrete time-domain method may be updated recursively for some rational forms of complex permittivity, which removes the need to store the time history of the fields and makes the method feasible. This method has been applied to materials described by a first-order Debye relaxation equation (Luebbers, Hunsberger, Kunz, Standler, & Schneider, 1990; Bui, Stuchly, & Costache, G., 1991; Sullivan, 1992), a second-order Lorentz equation with multiple poles (Luebbers & Hunsberger, 1992), and to a gaseous plasma (Luebbers, Hunsberger, & Kunz, 1991).

A second approach is to add a differential equation relating the electric flux density D to the electric field E and solve this new equation simultaneously with the standard FDTD equations. This method has been applied to lD and 2D examples with materials described by a first-order Debye equation or second-order single-pole Lorentz equation (Joseph, Hagness, & Taflove, 1991), and to 3D sphere and homogeneous two-thirds muscle-equivalent man model with properties described by a second-order Debye equation (Gandhi, Gao, & Chen, 1992, 1993). In the following, we describe this differential equation approach, which has been used for induced current and SAR calculations for a heterogeneous model of the human body (Furse, Chen, & Gandhi, 1994). The time-dependent Maxwell's curl equations used for the FDTD method are:

$$\nabla \times \mathbf{E} = -\frac{\partial \mathbf{B}}{\partial t} = -\mu \frac{\partial \mathbf{H}}{\partial t} \tag{3}$$

$$\nabla \times \mathbf{H} = \frac{\partial \mathbf{D}}{\partial t} \tag{4}$$

where the flux density vector **D** is related to the electric field through the complex permittivity $\varepsilon^*(\omega)$ of the local tissue by the following equation:

$$\mathbf{D} = \varepsilon^*(\omega)\mathbf{E} . \tag{5}$$

Since Equations 3 and 4 are solved iteratively in the time domain, Equation 5 must also be expressed in the time domain. This may be done by choosing a rational function for $\varepsilon^*(\omega)$ such as the Debye equation with two relaxation constants:

$$\varepsilon^*(\omega) = \varepsilon_0 \left[\varepsilon_\infty + \frac{\varepsilon_{s1} - \varepsilon_\infty}{1 + j\omega\tau_1} + \frac{\varepsilon_{s2} - \varepsilon_\infty}{1 + j\omega\tau_2} \right] . \tag{6}$$

Rearranging Equation 6 and substituting in Equation 5 gives

$$\mathbf{D}(\omega) = \varepsilon^*(\omega)\mathbf{E}(\omega) = \varepsilon_0 \frac{\varepsilon_s + j\omega\left(\varepsilon_{s1}\tau_2 + \varepsilon_{s2}\tau_1\right) - \omega^2\tau_1\tau_2\varepsilon_\infty}{1 + j\omega\left(\tau_1 + \tau_2\right) - \omega^2\tau_1\tau_2} \mathbf{E}(\omega) \tag{7}$$

where the dc (zero frequency) dielectric constant is given by

$$\varepsilon_s = \varepsilon_{s1} + \varepsilon_{s2} - \varepsilon_\infty . \tag{8}$$

Assuming $e^{j\omega t}$ time dependence, we can write Equation 7 as a differential equation in the time domain

$$\tau_1\tau_2\frac{\partial^2\mathbf{D}}{\partial t^2}+\left(\tau_1+\tau_2\right)\frac{\partial\mathbf{D}}{\partial t}+\mathbf{D}=\varepsilon_o\left[\varepsilon_s\mathbf{E}+\left(\varepsilon_{s1}\tau_2+\varepsilon_{s2}\tau_1\right)\right]\frac{\partial\mathbf{E}}{\partial t}+\varepsilon_\infty\tau_1\tau_2\frac{\partial^2\mathbf{E}}{\partial t^2}\quad. \tag{9}$$

For the (FD)^{2}TD method, we need to solve Equations 3 and 4 subject to Equation 9. As in Gandhi et al. (1992, 1993), we write these equations in the difference form, solve Equation 9 to find $\mathbf{E}$, Equation 3 to find $\mathbf{H}$, and Equation 4 to find $\mathbf{D}$ at each cell location. The $\mathbf{E}\rightarrow\mathbf{H}\rightarrow\mathbf{D}$ loop is then repeated until the pulse has died off.

1.3.2.1 Modeling of the Tissue Properties by Debye Equation with Two Relaxation Constants

For ultra-wideband calculations using the (FD)^{2}TD method, the measured properties for the various tissues have been fitted to the Debye Equation 6 with two relaxation constants (Gandhi et al., 1992, 1993; Furse et al., 1994). The measured properties of biological tissues (muscle, fat, bone, blood, intestine, cartilage, lung, kidney, pancreas, spleen, lung, heart, brain/nerve, skin, and eye) were obtained from (Durney et al., 1978). Optimum values for $\varepsilon_{s1},\varepsilon_{s2},\varepsilon_\infty,\tau_1,$ and τ_2 in Equation 6 were obtained by nonlinear least squares matching to the measured data for fat and muscle. All other tissues have properties falling roughly between these two. Optimum values shown in Table 1-3 for $\varepsilon_{s1},\varepsilon_{s2},$ and ε_∞ for all tissues were then obtained with τ_1 and τ_2 being the average of the optimized values for fat and muscle. This was done to facilitate volume averaging of the tissue properties in voxels of the heterogeneous man model. Having τ_1 and τ_2 constant for all tissues allowed linear (volume) averaging of the ε values for each tissue in a given voxel to calculate ε values for that voxel. The measured tissue properties and those computed from the Debye equation with τ_1 and τ_2 being the average of fat muscle are shown in Figure 1-2 for fat and muscle. Similar agreements were also obtained for the other tissue types.

8
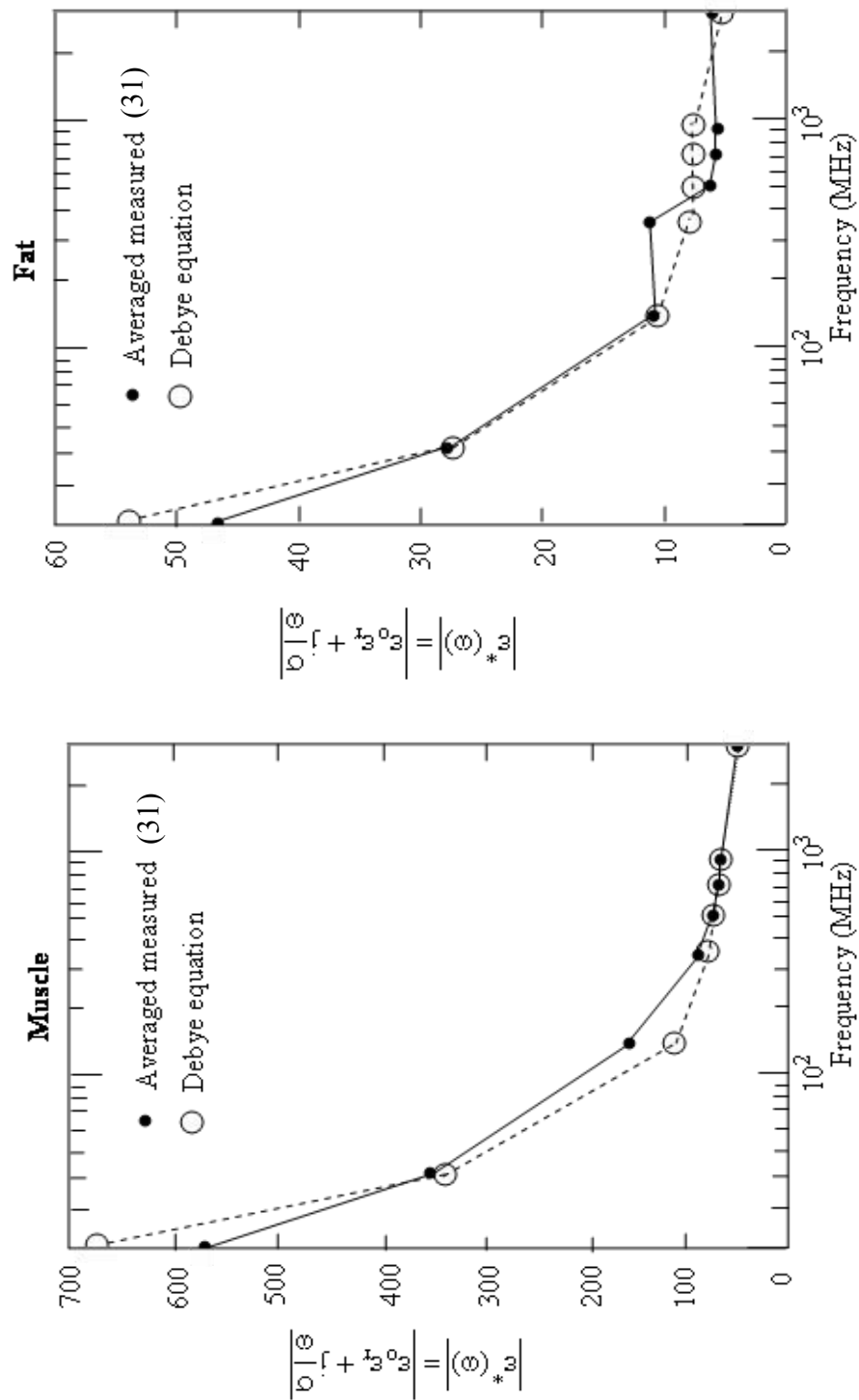
Figure 1-2. Fit of Debye equations with two relaxation constants (Equation 6) to measured tissue properties of (a) muscle and (b) fat (Furse et al., 1994).

9

Table 1-3. Debye constants for tissues (Furse et al., 1994).

$$\tau_1 = 46.2 \text{ ns}$$

$$\tau_2 = 0.091 \text{ ns}$$

(average of optimum for fat and muscle)

Tissue	ε_∞	ε_{s1}	ε_{s2}
Muscle	40.0	3984	59.1
Bone/Cartilage	3.4	313	7.1
Blood	35.0	3563	66.4
Intestine	39.0	4724	66.1
Liver	36.3	2864	57.1
Kidney	35.0	3332	67.1
Pancreas/Spleen	10.0	3793	73.9
Lung (1/3 tissue)	10.0	1224	13.1
Heart	38.5	4309	54.6
Brain/Nerve	32.5	2064	56.9
Skin	23.0	3399	55.6
Eye	40.0	2191	57.0

1.4 Methods For Low Frequencies

For exposures to EMFs from low-frequency sources such as power lines at 50/60 Hz, induction heaters and EAS devices in the kilohertz to megahertz range etc., several numerical techniques have been developed (Gandhi, 1995; Armitage, LeVeen, & Pethig, 1983; Gandhi, DeFord, & Kanai, 1984; DeFord & Gandhi, 1985; Gandhi & DeFord, 1988; Orcutt & Gandhi, 1990; Gandhi & Chen, 1992; Baraton & Hutzler, 1995; Furse & Gandhi, 1998; Dawson & Stuchly, 1998; Dimbylow, 1998; Dawson, Caputa, & Stuchly, 1999; Gustrau, Bahr, Rittweger, Goltz, & Eggert, 1999; Stuchly & Dawson, 2000; Gandhi, Kang, Wu, & Lazzi, 2001; Gandhi & Kang, 2001; Li & Gandhi, 2005). These methods are the admittance and impedance methods (Armitage et al., 1983; Gandhi et al., 1984; DeFord & Gandhi, 1985; Gandhi & DeFord, 1988; Orcutt & Gandhi, 1990), the finite-element method (Baraton & Hutzler, 1995), the scalar potential finite-difference (SPFD) method (Dawson & Stuchly, 1998; Dimbylow, 1998; Dawson et al., 1999), and the finite-difference time-domain method with frequency scaling (Gandhi & Chen, 1992; Furse & Gandhi, 1998; Gustrau et al., 1999). At low frequencies, it is possible to treat exposure to electric and magnetic fields separately and the induced electric fields or current densities added vectorially for each of the voxels (DeFord & Gandhi, 1985; Stuchly & Dawson, 2000). Using anatomically-based models with voxel resolutions of 1-6 mm, these methods have been used to calculate the induced electric fields and current densities for the various regions of the body. In the following, we describe the important aspects of some of the methods that have been used for bioelectromagnetic problems.

1.4.1 Impedance/Admittance Methods

Two relatively similar methods based on the formulation of the exposed volume as a three-dimensional impedance network or as an admittance network were proposed in 1983/84 and have been used for a number of low-frequency bioelectromagnetic problems over the years (Gandhi, 1995; Armitage et al., 1983; Gandhi et al., 1984; DeFord & Gandhi, 1985; Gandhi & DeFord, 1988; Orcutt & Gandhi, 1990; Gandhi et al., 2001; Gandhi, & Kang, 2001; Li & Gandhi, 2005). Because of duality of Kirchoff's laws of electrical engineering, either of the networks may be used to calculate the voltage or current distributions throughout the network.

In both of these methods, the biological body or an exposed part thereof is represented by a three-dimensional (3D) of admittances or impedances whose individual values are obtained from the complex conductivities $(\sigma + j\omega\varepsilon)$ for the various locations of the body. For example, the impedances for the various directions for the three-dimensional network can be written as

$$Z_m^{i,j,k} = \frac{\delta_m}{\delta_n \delta_p \left(\sigma_m^{i,j,k} + j\omega\varepsilon_m^{i,j,k} \right)} \tag{10}$$

where i, j, k indicate the voxel index; m is the direction, which can be x, y, or z, for which the impedance is calculated; $\sigma_m^{i,j,k}$ and $\varepsilon_m^{i,j,k}$ are the conductivities and the electrical permittivities for the voxel i, j, k; δ_m is the thickness of the voxel in the mth direction; and δ_n and δ_p are the widths of the voxel in directions at right angles to the mth direction.

In the impedance method formulation, it can be seen that the voxels need not be identical so that fairly thin features of the body can be modeled as well as the interfaces between the various tissues and organs. Also, the dielectric properties (σ, ε) for a given voxel can be directionally dependent. The admittance network formulation is convenient to find the voltage distribution for the exposed tissue volume for cases where the source/s may be prescribed in terms of applied voltages. An example of this is the induced voltage or electric field distribution for hyperthermia using capacitive electrodes (Orcutt & Gandhi, 1990). The admittance method has been used for calculation of cardiac-induced endogenous fields throughout the human body (Hart & Gandhi, 1998). Recognizing the equivalence of magnetostatic and electrostatic circuits e.g., at kilohertz frequencies as regards to the corresponding magnetic and electric fields thus created (Li & Gandhi, 2005), the admittance network formulation has been used to calculate the leakage magnetic fields of a tapered gap ferromagnetic deactivator typical of some of the electronic article surveillance (EAS) systems (Li & Gandhi, 2005).

The impedance method formulation has been found to be particularly useful for problems of exposure to spatially nonuniform magnetic fields for which the voltages or electromotive forces (EMFs) are induced for the various loops of the 3-D impedance network whose values are given by the following expression:

$$V_m^{i,j,k} = -\frac{d}{dt}\int B^{i,j,k} \cdot dS = -\left(\frac{d}{dt}B_m^{i,j,k}\right)\delta_n\delta_p \quad . \tag{11}$$

Using Kirchoff's current law, equations can be written for each of the nodes of the 3-D circuits such that the algebraic sum of the currents entering or leaving any node is zero. The simultaneous equations thus formulated are solved by using successive over-relaxation (SOR) technique. The x-, y-, and z-directed currents obtained for each of the voxel centers may be used to calculate the current densities J_x, J_y, J_z; the induced electric fields E_x, E_y, E_z; and the SARs, if needed.

Using tissue-classified anatomically-based models with resolutions of 1 to 6 mm, some of the applications of this method are: calculation of SAR distributions for operator exposure to nonuniform magnetic fields of induction heaters (Gandhi & DeFord, 1988), induced current densities and SARs due to capacitive-type electrodes used for hyperthermia (Orcutt & Gandhi, 1990), currents induced in the human body by electric and magnetic fields of electric blankets (Gandhi, 1995), current densities and electric fields induced by magnetic fields of EAS systems (Gandhi & Kang, 2001; Li & Gandhi, 2005), etc.

1.4.2 FDTD with Frequency Scaling

Because of the horrendous number of iterations, the FDTD method would be inapplicable for calculations at power-line as well as other low frequencies were it not for the quasi-static nature of the coupling as previously pointed out by Kaune and Gillis (1981) and Guy, Davidow, Yang and Chou (1982). Using a logic similar to these authors, the electric fields outside the body depend not on the internal tissue properties, but only on the shape of the body as long as the quasi-static approximation is valid, i.e., the size of the body is a factor of 10 or more smaller than the wavelength, and $|\sigma + j\omega\varepsilon| >> \omega\varepsilon_o$ where σ and ε are the conductivity and the permittivity of the tissues, respectively, $\omega = 2\pi f$ is the radian frequency, and ε_o is the permittivity of the free space outside the body. Under these conditions, the electric fields in air are normal to the body surface and the internal tissue electric fields are given from the boundary conditions in terms of the fields outside

$$j\omega\varepsilon_o\hat{n} \cdot \mathbf{E}_{air} = (\sigma + j\omega\varepsilon)\hat{n} \cdot \mathbf{E}_{tissue} \quad . \tag{12}$$

A higher quasi-static frequency f' may therefore be used for irradiation of the model and the internal fields E' thus calculated may be scaled back to frequency f of interest, e.g., 60 Hz. From Equation 12, we can write

$$\mathbf{E}_{tissue}(f) = \frac{\omega}{\omega'}\frac{(\sigma' + j\omega\varepsilon')}{(\sigma + j\omega\varepsilon)}\mathbf{E}'_{tissue}(f') \cong \frac{f\sigma'}{f'\sigma}\mathbf{E}'_{tissue}(f') \tag{13}$$

assuming that $\sigma + j\omega\varepsilon \cong \sigma$ at both f' and f.

12

This method has been shown to be very accurate for homogeneous or layered spheres (diameter = 33 cm) up to about 20 MHz (Gandhi & Chen, 1992). The fields $(\mathbf{E}')$, which are calculated at the higher frequency (f') using frequency scaling, are several orders of magnitude higher than $\mathbf{E}$, which would have been calculated at the low frequency (f), and therefore have less numerical round off error.

To demonstrate usefulness of this frequency scaling technique, Gandhi and Chen (1992) used a full-scale anatomically-based model of the human body and a frequency f' of 5-10 MHz to reduce the computation time by orders of magnitude. Since in the FDTD method, one needs to calculate in the time domain until convergence is obtained (typically 3-4 time periods), this frequency scaling to 5-10 MHz for f' reduces the needed number of iterations by almost five orders of magnitude. At the higher irradiation frequency f', $\sigma' = \sigma$ (i.e., conductivities of the various tissues at 60 Hz). Furthermore, they assumed the incident E-field $\mathbf{E}_i(f') = 60\,\mathbf{E}_i(f)/f'$ to obtain $\mathbf{E}_{tissue}(f)$ at say $\mathbf{E}_i(f) = 10$ kV/m. The incident magnetic field $\mathbf{H}_i(f')$ was similarly taken to be considerably lower $(= 60\,\mathbf{H}_i(f)/f')$ to account for the fact that the induced current densities and internal electric fields are proportional to the frequency of the incident fields and would therefore be higher at the assumed frequency f'.

Given in Figure 1-3 are the calculated vertical currents passing through the various cross sections of a $6 \times 6 \times 6$ mm MRI-based grounded model of the human body exposed to EMFs at 60 Hz for $\mathbf{E}_{inc} = 10$ kV/m vertically polarized, frontally incident, $\mathbf{B}_{inc} = 33.3\,\mu T$ from side to side of the model (Furse & Gandhi, 1998). Also given in Figure 1-3 is the measured current passing through the feet of an aluminum covered mannequin shown by a star with a value of 175 μA. An excellent agreement between calculated and measured values of the current through the feet is obtained.
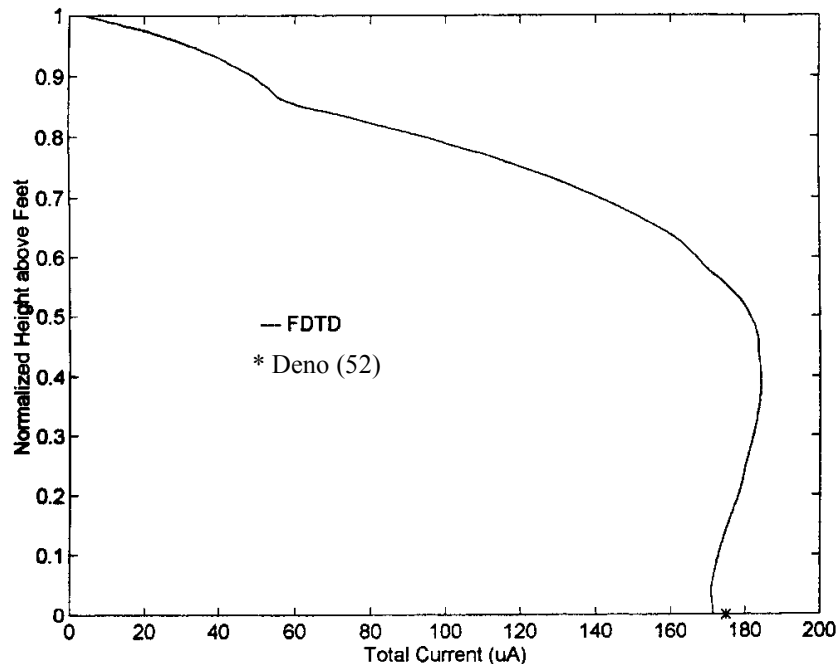
Figure 1-3. The calculated vertical currents passing through the various sections of a 6 x 6 x 6 mm MRI-based grounded model of the human body exposed to EMFs at 60 Hz. E_{inc} = 10 kV/m, vertically polarized, frontally incident; B_{inc} = 33.3 μ T from side to side of the model.

1.5   Some Applications for RF/Microwave Frequencies

1.5.1   Induced Currents/ SARs for Plane-Wave Exposure: Conditions for Whole-Body and Head Resonance

For plane-wave exposures at 10 to 915 MHz, the FDTD method has been used to calculate local, layer-averaged, and whole-body average SARs and induced currents for anatomically-based human models with resolutions from 2 to 26.2 mm (Chen & Gandhi, 1989; Gandhi, Gu, Chen, & Bassen, 1992; Tinniswood et al., 1998b). Figure 1-4 graphs the computed cross-section layer-average RF current distributions for one such human model at 40 and 60 MHz, assuming a vertically polarized incident electric field of 1 V/m (Gandhi et al., 1992). These frequencies are close to the whole-body resonances under the grounded and isolated conditions of the model, respectively.   Figure 1-5 graphs the corresponding layer-average SARs at these frequencies (Gandhi et al., 1992).   As expected, the highest SARs are calculated for the horizontal sections through the neck, knee, and ankle. The high neck SAR is due to its small cross section relative to the head and upper body on either side of the neck, which elevates the neck's layer-averaged current density. The high knee and ankle SARs are due to their high bone contents as well as their reduced cross-section areas relative to adjacent body parts.

The resonant frequency for whole-body exposure of a human to plane-wave illumination is about 40 MHz under grounded conditions and 65 to 75 MHz under isolated conditions or situations where the ground is several tens of centimeters removed from the feet (Chen &

14

Gandhi, 1989). For grounded and isolated conditions, respectively, whole-body absorption cross sections up to 6 and 4.5 times the physical cross section of the body have been calculated and measured for models of the human body (Chen & Gandhi, 1989; Gandhi et al., 1992; Tinniswood et al., 1998b; Gandhi, 1990).

Because of interest in possible neurological effects of RF radiation, the FDTD method has also been used to obtain SAR distributions and frequencies of maximum absorption for the head and neck for plane-wave exposure of grounded and isolated models of the human body (Gandhi et al., 1992; Tinniswood et al., 1998b). A high-resolution MRI-based model was constructed with a voxel size of $1.974 \times 1.974 \times 3.0$ mm. In addition, a coarse-resolution model with a voxel size of $5.922 \times 5.922 \times 6.0$ mm was constructed by combining $3 \times 3 \times 2$ cells of the high resolution model along the x, y, and z axes, respectively. The resonant frequencies for the head and neck are calculated to be 207 and 193 MHz for isolated and grounded conditions of the man model, respectively. The corresponding absorption cross sections are 3.27 and 2.62 times the physical (shadow) cross section for this region of the body (Gandhi, 1990).

15
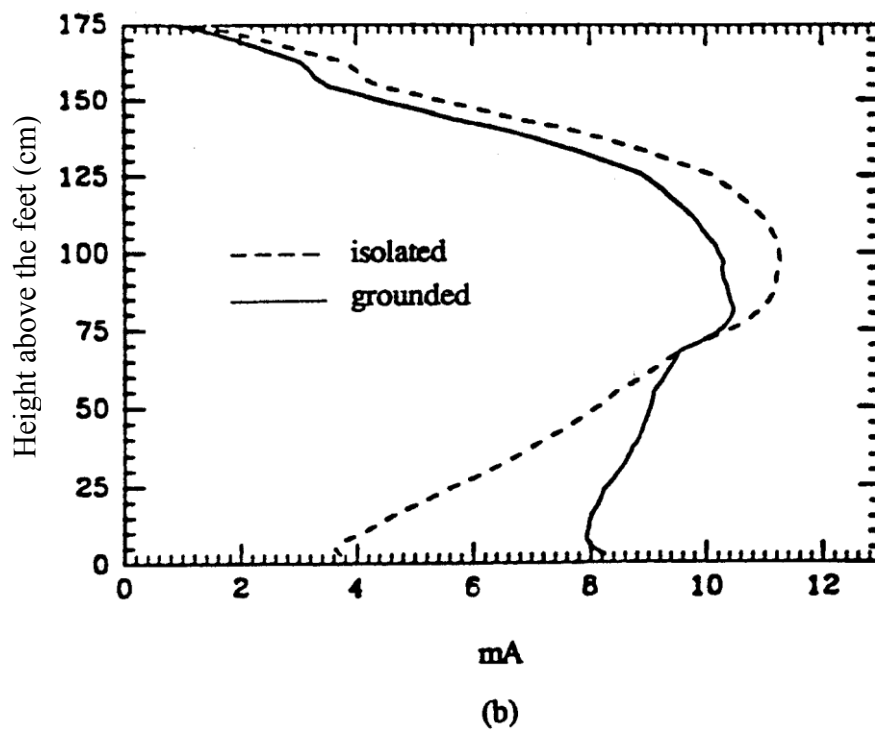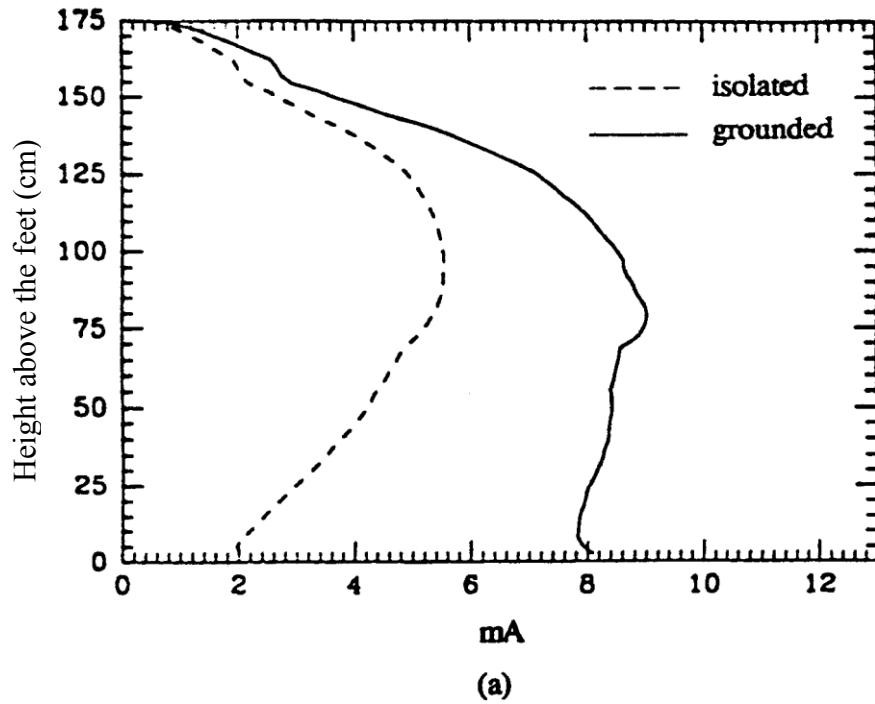
Figure 1-4. FDTD-computed cross-section layer-average RF current distributions for a human model exposed to a vertically polarized plane wave with a 1 V/m electric field at: (a) 40 MHz; (b) 60 MHz. Source: Chen & Gandhi, 1989.
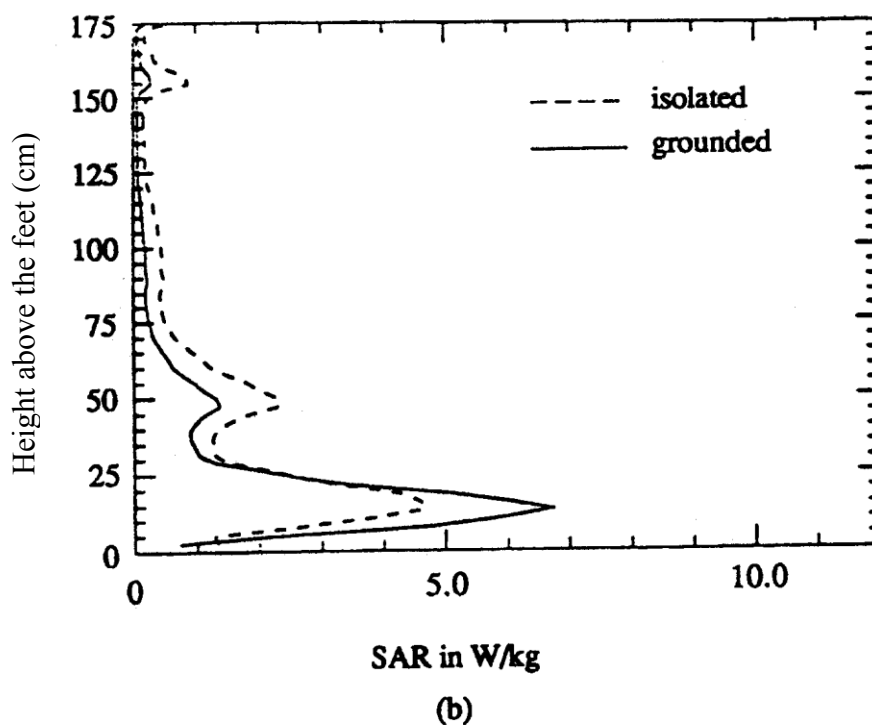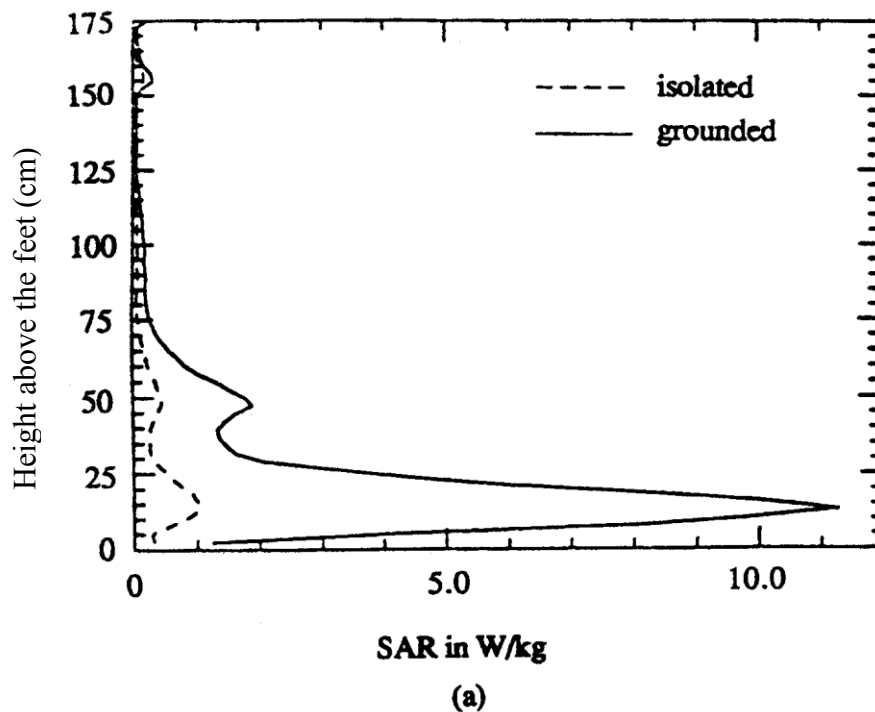
Figure 1-5. FDTD-computed cross-section layer-average SARs corresponding to the current distributions of Figure 1-4 for the human model exposed to a vertically polarized plane wave with a 1 V/m electric field at (a) 40 MHz; (b) 60 MHz. Source: Chen & Gandhi, 1989.

17

1.5.2   Coupling for a Human in the Vicinity of Base-Station Antennas

Of particular interest at the present time is the tremendous proliferation of wireless base stations, especially in metropolitan and urban settings. Some methods have been developed for assessing personnel safety which may be of concern for regions close to such base stations where electromagnetic fields can be fairly high (Bernardi et al., 2000; Gandhi & Lam, 2003). A relatively simple method that may be used for this and other near-field EM environments is the so-called "Spatial Components Method" (Gandhi & Lam, 2003).

1.5.2.1   The Spatial Components Method

In this method, the vertical and horizontal components of the electric field are calculated or measured for an imaginary vertical (xz) plane ($0 \leq x \leq A$; $0 \leq z \leq B$) but without the human. This so-called "plane of incidence" is taken to be grazing at the intended location of the model of the human. The measured distributions for vertical and horizontal electric field components E_z and E_x are then expressed in terms of space harmonics as follows:

$$E_z = \sum_{m,n=0}^{\infty} C_{mn} \cos\frac{m\pi x}{A} \cos\frac{n\pi z}{B} \tag{14}$$

$$E_x = \sum_{m,n=0}^{\infty} D_{mn} \cos\frac{m\pi x}{A} \cos\frac{n\pi z}{B} \tag{15}$$

where m and n are integers 0, 1, 2 ⋯ and the space harmonics are defined over the plane of incidence of dimensions A and B along horizontal (x) and vertical (z) directions, respectively. All of the components with magnitudes C_{mn} and D_{mn} that are 10% or larger than the maximum amplitude are included for truncated versions of Equations 14 and 15, respectively.

By defining the origin ($x = 0$, $z = 0$) at either the upper or lower corner rather than at the center of the measurement plane, one can express any general variation of the fields even though $\cos (m\pi x/A) \cos (n\pi z/B)$ type modal terms are considered. Since the EM fields beyond about two times the horizontal extent of the human body and 1.25 times the human height have been shown to have minimal coupling to the human, the dimensions A and B are taken to be 0.96 m and 2.28 m, respectively (Gandhi & Lam, 2003). The Spatial Harmonics Components Method relies on the pre-stored solutions for the internal E-fields (E_x, E_y, E_z) for the various voxels of the human body model to different space harmonics which may be added depending upon the magnitudes and phases of the various space harmonic components obtained on-site for the measured electric field distributions.

The applicability of this technique for on-site dosimetry has been validated by comparing the SAR distributions obtained for near-field regions of some commercial base station antennas at 835 and 1900 MHz with those obtained by using the conventional FDTD method (Gandhi & Lam, 2003). Like the ray-tracing method used in (Bernardi et al., 2000), the measured electric

18

field distributions for the commercial base station antennas were not readily available. Thus, the calculated field distributions in front of these transmitters were obtained using the FDTD method with a grid size of 3 cm at 835 MHz and 1.5 cm at 1900 MHz. Given in Figures 1-6 and 1-7 are two representative cases of human exposure in front of some typical base stations (Bernardi et al., 2000). In both of the figures, the calculated layer-average SARs using the spatial harmonic components method are compared with those obtained by the full FDTD method. Six components were found to be adequate at 835 MHz (in Figure 1-6) while 10 components were needed at 1900 MHz (Figure 1-7) to obtain a very good agreement of the SAR distributions with those obtained using the conventional FDTD method.

Comparison of the calculated whole-body average and peak 1-g SARs for the three base stations for different spacings to the human model are given in Tables 1-4 and 1-5, respectively. The whole-body average and peak 1-g SARs are less than 5-10 percent different than those obtained using the full FDTD simulation. This is remarkable since the harmonic components method takes less than one minute on a portable PC while the full FDTD simulation takes over an hour of computer time using the same PC.
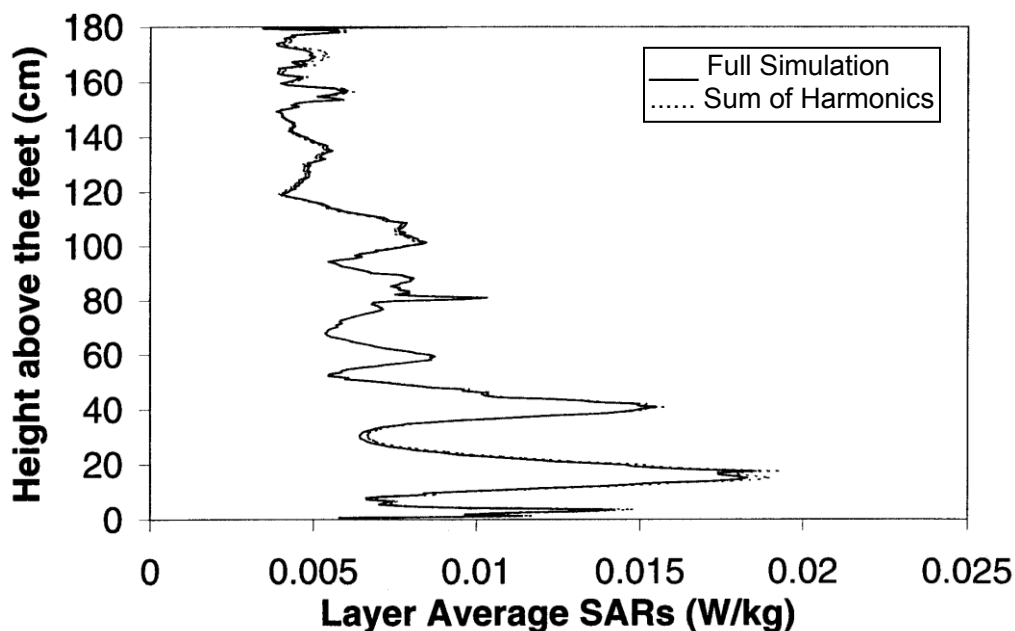
Figure 1-6. The calculated layer-averaged SAR distribution for the model of the human body due to a base station antenna made of an 18-cm-tall vertical dipole in front of a flat reflector of dimensions 24 x 24 cm. Frequency = 835 MHz, radiated power = 10 W, distance to the front plane of the model = 2 m.

19
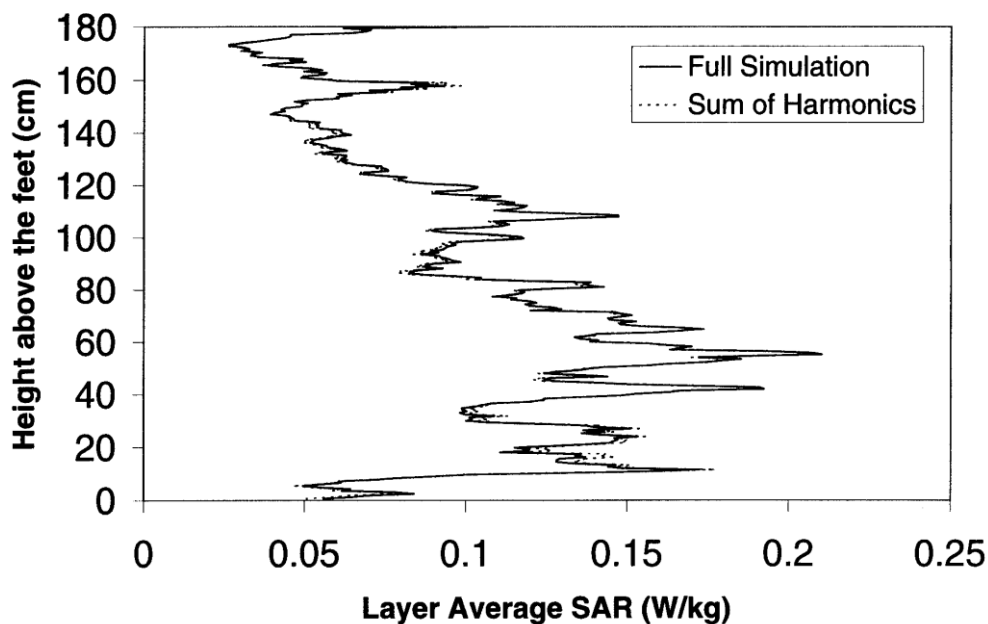
Figure 1-7. The calculated layer-averaged SAR distribution for the model of the human body due to an aperture type base station antenna of dimensions 38.1 x 20.3 cm along vertical and horizontal directions, respectively. Frequency = 1900 MHz, radiated power = 120 W, distance to the front plane of the model = 3 m.

Table 1-4. Comparison of whole-body average SARs and peak 1-g SARs obtained for various distances of the model from a base station at 824-849 MHz using the full FDTD simulation and the spatial harmonic components method (Gandhi & Lam, 2003).*

Distance (m)	Whole-body average SAR			Peak 1-g SAR		
	Full FDTD simulation (W/kg)	Harmonic components method (W/kg)	% difference	Full FDTD simulation (W/kg)	Harmonic components method (W/kg)	% difference
0.5	0.033	0.033	2.50	2.76	2.85	-3.38
0.765	0.023	0.023	0.00	1.69	1.73	-2.21
1	0.017	0.017	1.35	1.11	1.13	-1.65
2	0.006	0.006	0.09	0.38	0.36	4.41

* Assumed is a base station antenna using an 18-cm-tall vertical dipole in front of a flat reflector of dimensions 24 × 24 cm radiating 10 W of power. (See Figure 1-6 for layer-averaged SAR variation).

Table 1-5. Comparison of whole-body average SARs and peak 1-g SARs obtained for various distances of the model from a base station antenna at 1850-1910 MHz using the full FDTD simulation and the spatial harmonic components method (Gandhi & Lam, 2003).*

Distance (m)	Whole-body average SAR			Peak 1-g SAR		
	Full FDTD simulation (W/kg)	Harmonic components method (W/kg)	% difference	Full FDTD simulation (W/kg)	Harmonic components method (W/kg)	% difference
1	0.029	0.028	3.04	21.68	21.36	1.46
3	0.088	0.087	1.30	5.03	4.95	1.67
5	0.036	0.036	-1.65	2.48	2.42	2.33

* Assumed is an aperture-type base station antenna of dimensions 38.1 × 20.3 cm radiating 120 W of power. (See Figure 1-7 for layer-averaged SAR variation).

1.5.3   Coupling of an Ultra-wideband EMP to the Human Body

The $(FD)^2TD$ method has been used to calculate coupling of an ultrashort pulse to the heterogeneous model of the human body. From the calculated internal fields, vertical currents passing through the various cross sections of the body were calculated by using the following equations:

$$I_z(t) = \delta^2 \sum_{i,j} \frac{\partial D_z}{\partial t} \tag{16}$$

where δ is the cubic voxel size (= 1.31 cm for the model used here), and the summation is carried out for all voxels in a given layer. One can also calculate the layer-averaged absorbed energy density or specific absorption (SA) and the total energy W absorbed by the whole body using the following relationships:

$$SA\Big|_{\text{layer } k} = \frac{\delta t}{N_k} \sum_t \frac{\mathbf{E}(i,j,k,t)}{\rho(i,j,k)} \cdot \frac{\partial \mathbf{D}(i,j,k,t)}{\partial t} \; . \tag{17}$$

$$W = \delta t \cdot \delta^3 \sum_t \mathbf{E}(i,j,k,t) \cdot \frac{\partial \mathbf{D}(i,j,k,t)}{\partial t} \; . \tag{18}$$

In Equations 17 and 18, δt is the time step (= $\delta/2c$ = 0.02813 ns) used for the time-domain calculations, N_k is the number of voxels in layer k of the body, and $\rho(i,j,k)$ is the mass density

21

in kg/m^3 for each of the voxels in the corresponding layers. For the calculations of coupled energy, both the isolated models of the human body, as well as the model standing vertically on a conducting ground plane have been used.

A typical ultra-wideband pulse with prescribed peak amplitude of 1.1 V/m is shown in Figure 1-8 in the time domain. This ultra-wideband pulse has a rise time of about 0.2 ns and a total time domain of about 7-8 ns. The calculated Fourier spectrum of the prescribed pulse is shown in Figure 1-9. Most of the energy in the pulse is concentrated in the 200-900 MHz band with the peak of the energy being at about 500 MHz.

The incident fields were assumed to be vertically polarized, since this polarization is known to result in the strongest coupling for standing individuals. Using the $(FD)^2TD$ procedure described earlier, the temporal variations of total vertical currents for the various sections of the body were calculated both for the shoe-wearing grounded, and ungrounded exposure conditions of the model, respectively. The current variations for a couple of representative sections, such as those through the eyes and the bladder, are given in Figures 1-10a and 1-10b, respectively. The calculated peak currents for the various sections are on the order of 1.1 to 3.2 mA/(V/m).
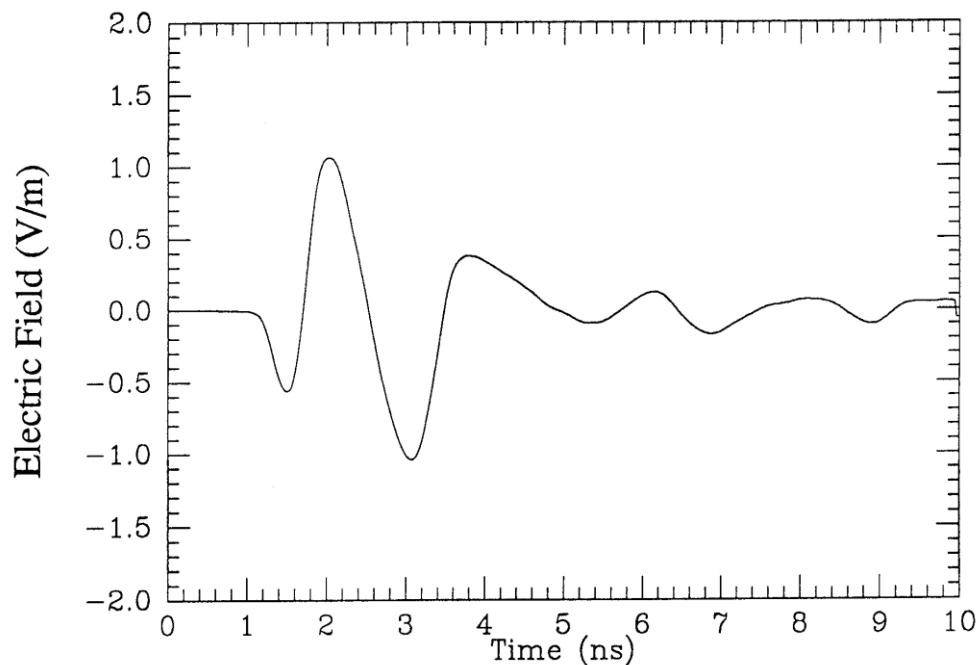
Figure 1-8. The prescribed electromagnetic pulse. Peak incident field = 1.1 V/m.
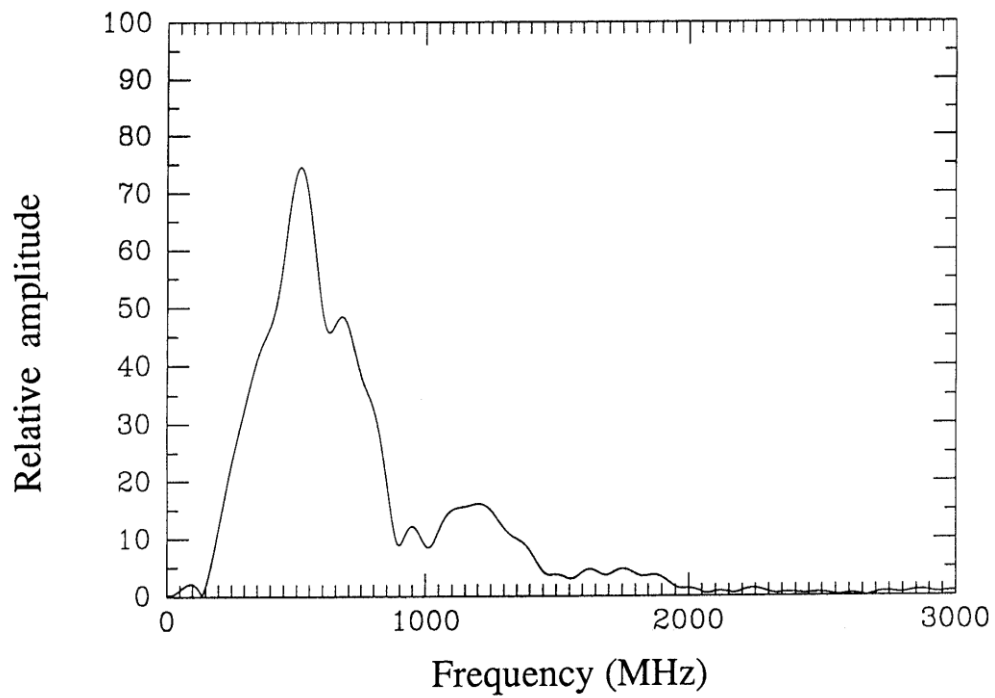
Figure 1-9. Fourier spectrum of the electromagnetic pulse of Figure 1-8.

23
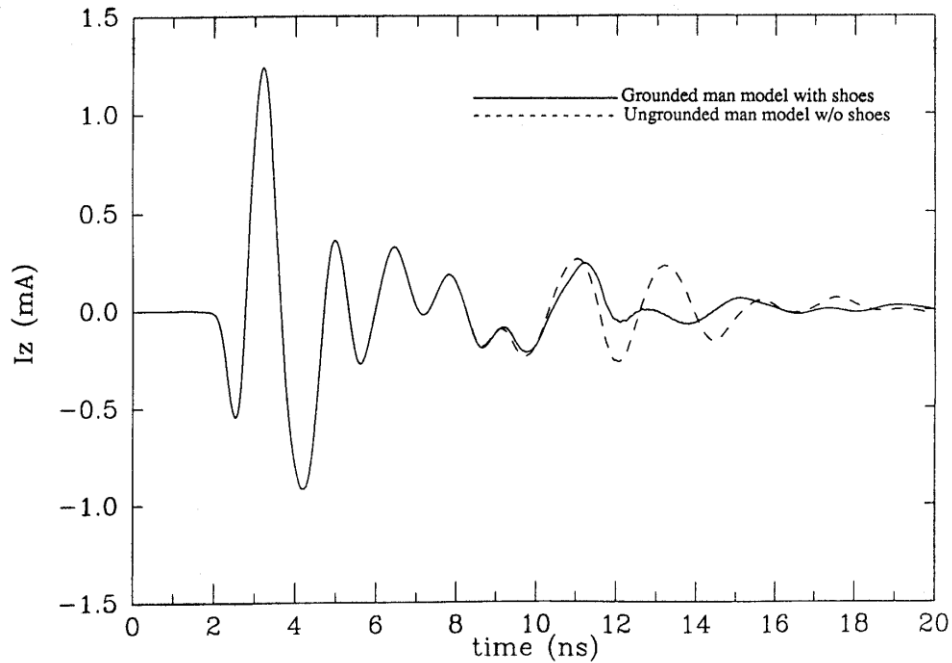
10a. Section through the eyes (height above the bottom of the feet = 168.3 cm).
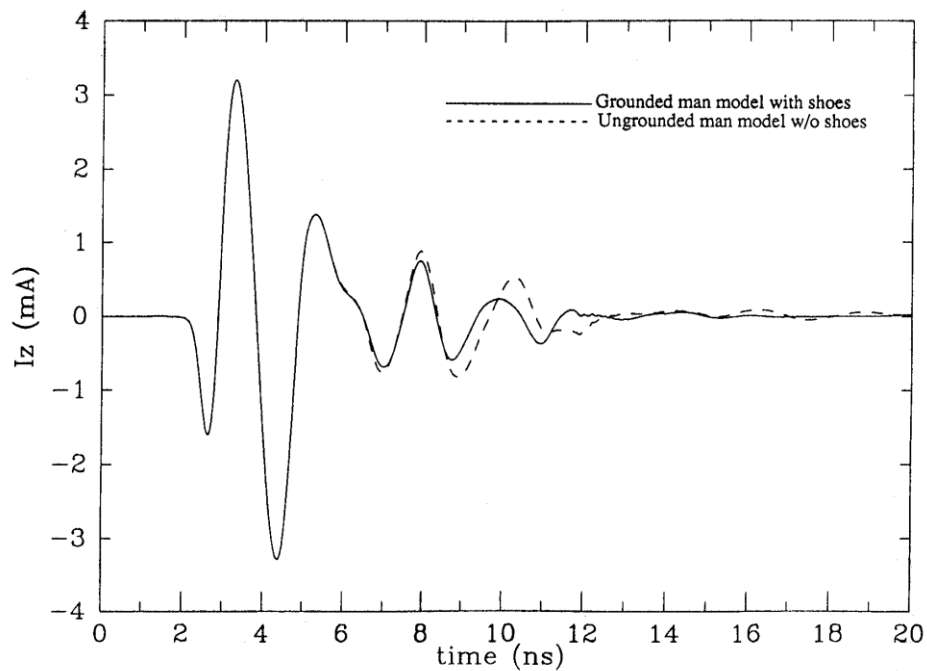
10b. Section through the bladder (height above the bottom of the feet = 91.0 cm.

Figure 1-10.   Currents induced for the various sections of the body for shoe-wearing grounded and ungrounded conditions of exposure. E_{peak} = 1.1 V/m.

24

It is interesting to note that there is very little difference in the induced currents whether the model is grounded or not. This is because most of the energy in the pulse is at frequencies in excess of 300 MHz, where the effect of the ground plane on the induced currents or the SARs is minimal (Gandhi et al., 1992).

The specific absorptions (SA) and the total absorbed energy for exposure to the ultra-wideband pulse of Figure 1-8 are calculated using Equations 17 and 18. The specific absorptions are plotted in Figure 1-11 as a function of height above the feet of the various sections of the body for isolated and shoe-wearing conditions. Note that because of the very limited time duration of the pulse (7-8 ns), the specific absorptions are on the order of 0.02 to 0.20 pJ/kg. Using Equation 18, the total energy absorbed by the body as a function of time has been calculated and is shown in Figure 1-12. The energy is virtually all absorbed in the first 6 to 8 ns. The total energy absorbed by the body exposed to a single pulse is calculated to be 2.0 and 1.91 pico Joules for isolated and shoe-wearing grounded conditions, respectively.
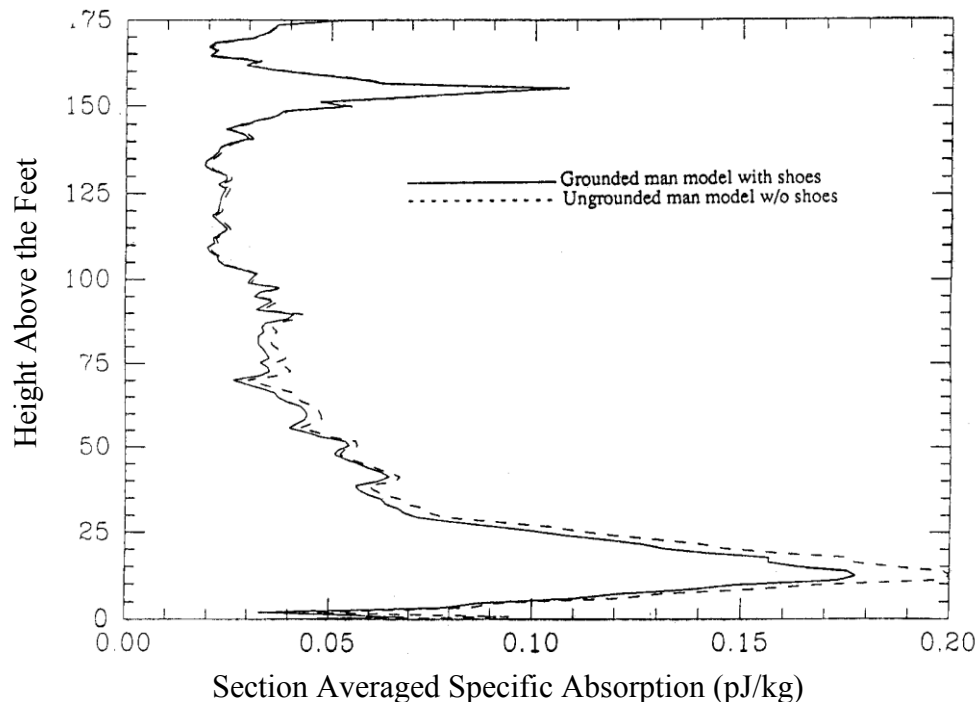
Figure 1-11. Variation of section or layer-averaged specific absorption for the ultra-wideband pulse of Figure 1-8. E_{peak} = 1.1 V/m.

25
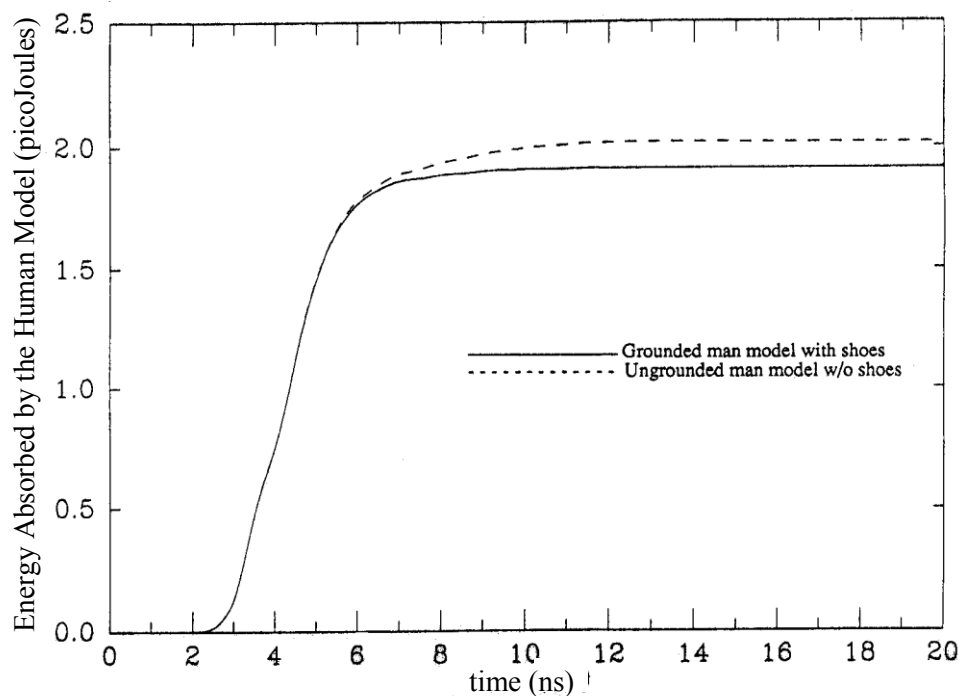
Figure 1-12. Energy absorbed by the human model for exposure to an ultra-wideband pulse of Figure 1-8.

1.5.3.1   A Convolution Procedure for Numerical Dosimetry for Pulsed EM Fields

To alleviate the problem of having to run computer-memory-intensive anatomically based models of the human body repeatedly, a simple and efficient technique based on convolution theory has been developed. In this procedure, the impulse response of the heterogeneous anatomically-based model is obtained and stored using an impulse in the time domain. This impulse response is convolved with the prescribed variation of the incident fields of an EMP. The convolution procedure is illustrated in the following with the example of the response of the human model for exposure to pulses or transients of prescribed shapes (Chen et a., 1994). For impulse response calculations, a narrow unit magnitude flat-top "impulse" of time duration $T' = 5$ to $10\,\delta t$ is assumed. The impulse-induced current response $H_i(t)$ for the various sections of the body (such as sections through the eyes, neck, heart, liver, etc.) is calculated and stored. Induced current $I_i(t)$ for these sections for a prescribed incident pulse $E(\tau)$ can then be calculated from the convolution integral

$$I_i(t) = \int_o^T E(\tau)\, H_i(t-\tau) d\tau \qquad (19)$$

26

where the integration time T is a period in excess of the time duration of the incident pulse. An alternate procedure that has also been found to be equally applicable is to work with Equation 19 in terms of the Fourier transforms $F\{H_i(t)\}, F\{E^{im}(t)\},$ and $F\{E(t)\}$ of the induced currents $H_i(t)$, the broadband initial impulse $E^{im}(t)$, and the prescribed pulse $E(t)$ for which the induced currents $I_i(t)$ are desired. In terms of the Fourier transforms, Equation 19 can be written as

$$I_i(t) = F^{-1} \left\{ \frac{F\{E(t)\} \, F\{H_i(t)\}}{F\{E^{im}(t)\}} \right\} \qquad (20)$$

where the discrete Fourier transforms needed for Equation 20 can be efficiently calculated using the Fast Fourier Transform (FFT) algorithm. Both of the above approaches are relatively simple and do not need a large computer memory, making it possible to use a small computer or PC for calculating the response of the human body to any desired incident pulse. We show in Figures 1-13a and 1-13b the comparison of the vertical currents induced for a couple of representative sections of the body for the ultra-wideband pulse of Figure 1-8. In both Figures 1-13a and 1-13b, the time-domain variations of the currents calculated with the simpler impulse response and the convolution method are in excellent agreement with the results obtained from the exact simulation with the conventional $(FD)^2TD$ method.

1.5.4 SAR Distributions Due to RF Magnetic Fields of MRI

MRI is an increasingly important tool for medical diagnostic applications. Emerging MRI technologies are leading to use of higher static magnetic fields and associated higher radio frequencies up to 400 MHz (Magin et al., 1991; Vaughan et al., 1994; Zhang et al., 1994). Sixteen-rung birdcage coils especially designed for imaging of the head, and the larger coils for imaging of the torso, are used not only for today's MRI machines (64 MHz, 1.5T biasing magnetic field) (Hayes et al., 1985), but are also planned for higher static-magnetic-field modalities (Magin et al., 1991; Vaughan et al., 1994; Zhang et al., 1994).

27
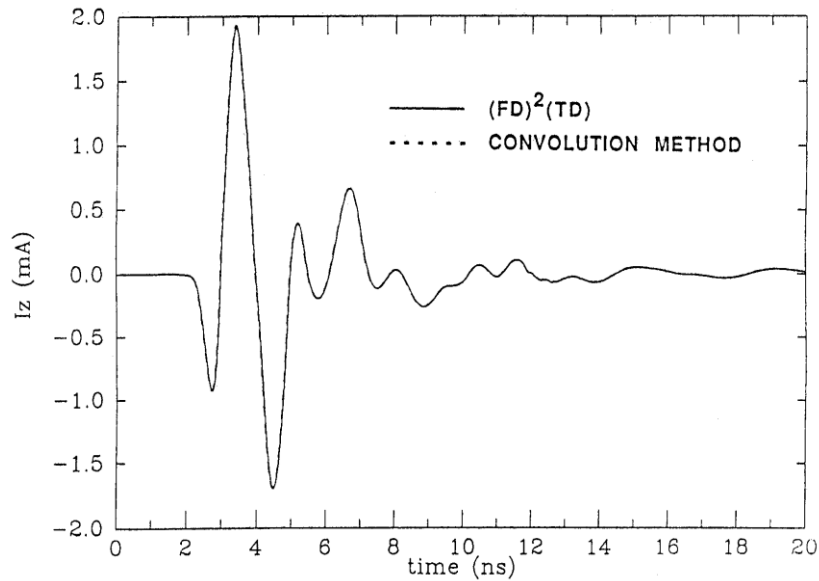
a. Section through the liver (height above the bottom of the feet = 123.8 cm).
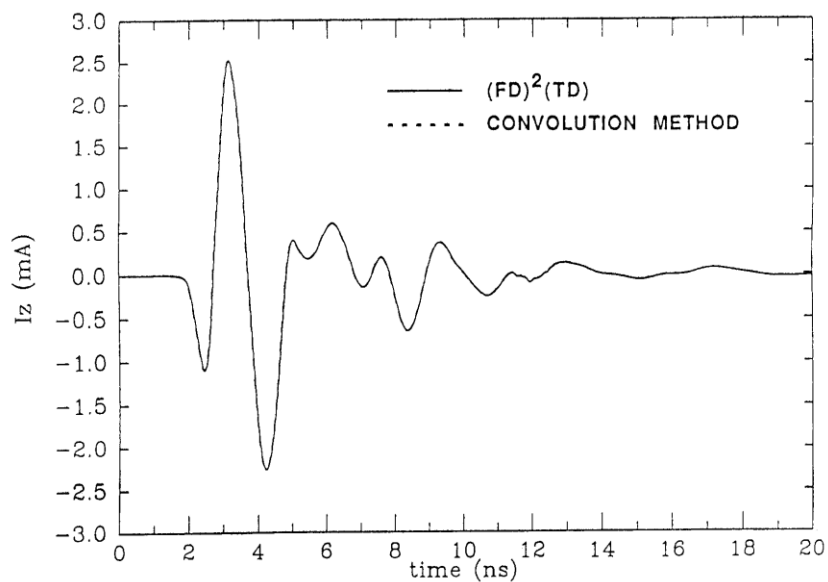
b. Section through the knees (height above the bottom of the feet = 50.4 cm).

Figure 1-13.   Comparison of the induced currents calculated using the convolution method with the conventional (FD)²TD method for two representative sections of the body. Shoe-wearing grounded model of the body was used for the calculations.

The safety standards proposed by the U.S. Food and Drug Administration (U.S. Food and Drug Administration, 1988) and the National Radiological Protection Board of the United

28

Kingdom (1990) limit SARs that can be induced within the human body. The FDTD method has been used for this purpose to calculate the coupled electromagnetic fields in heterogeneous, anatomically-based models of the human body for 16-rung birdcage coils having currents with progressive phase shifts of 22.5º between the adjacent rungs (Gandhi & Chen, 1999). These phase shifts are used to generate circularly polarized RF magnetic fields within the interior volume of the coil occupied by the parts of the body to be imaged. SAR distributions within the body have been obtained for head and body coils operating at 64 MHz and also at higher frequencies up to 400 MHz (Gandhi & Chen, 1999).

A related problem is to ensure the relative homogeneity of the RF magnetic fields within the body to meet the requirements of the imaging process. The FDTD method has been used for this purpose by calculating the distribution of internal RF magnetic fields (Jin et al., 1994; Chen & Jin, 1997).

1.5.5 SAR Distributions Due to Cellular Telephones

The finite-difference time-domain techniques has been used by many authors to calculate SAR distributions and radiation patterns of cellular telephones held close to the head (Gandhi, 1995; Gandhi et al., 1996; Okoniewski & Stuchly, 1996; Tinniswood et al., 1998a; Dimbylow & Mann, 1994; Jensen & Rahmat-Samii, 1995; Gandhi & Chen, 1995; Watanabe et al., 1996; Gandhi et al., 1999; Wang & Fujiwara, 2000). It is possible to use CAD-derived models of cellular telephones in order to represent the detailed construction of the telephone more accurately. An illustration of two CAD-derived telephones, one each at 835 and 1900 MHz, is given in Figure 1-14 (Tinniswood et al., 1998a; Gandhi et al., 1999). The anatomic model resolutions used by various authors are typically on the order of 1-3 mm. The calculated energy depositions are highly superficial with penetration depths on the order of 3-5 cm for the side of the head close to the radiating antenna. Shown in Figures 1-15a, b are two views of the calculated SAR distributions for a 1.974 × 1.974 × 3 mm resolution anatomic model of the human head for a cellular telephone radiating 600 mW of power at 835 MHz. This is the maximum power radiated by a cellular telephone in the analog AMPS mode. For calculations of SAR distributions, several numerical codes are presently available commercially so that they may be used to design a telephone that will meet the SAR compliance requirements and give desirable radiation patterns.

(a) 835 MHz model   (b) 1900 MHz model
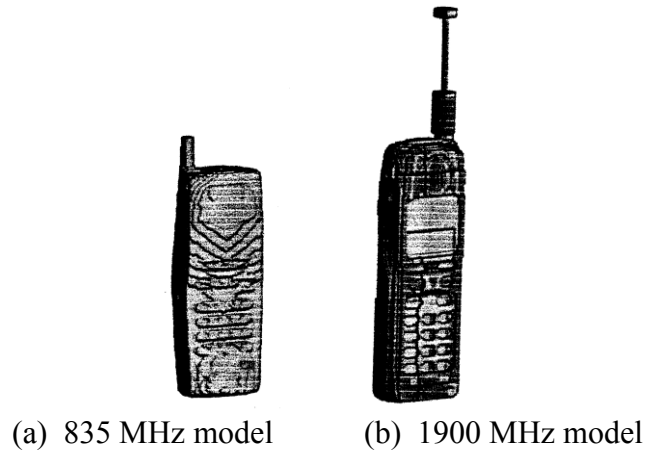
Figure 1-14. An illustration of two CAD-driven telephones used for SAR calculations.
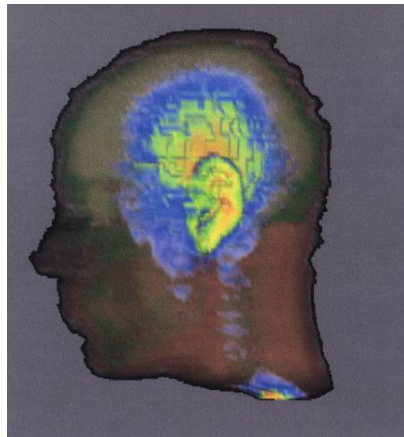
(a) The side of the head exposed to the cellular telephone.
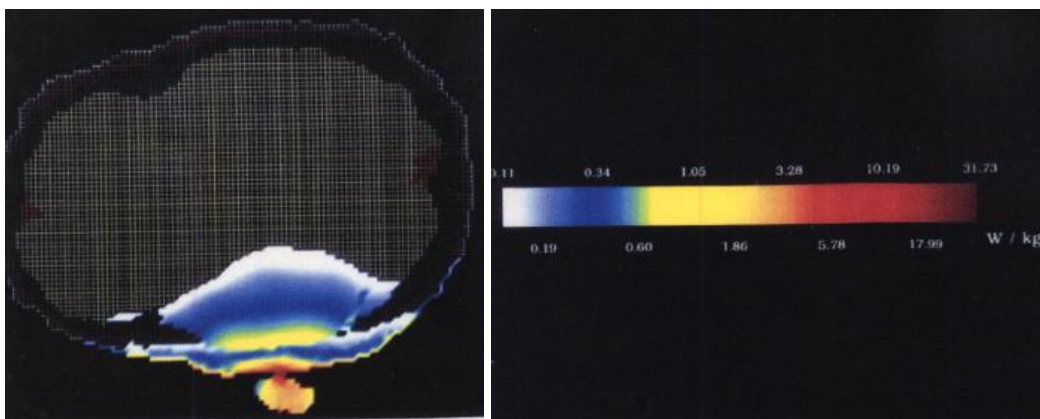
(b) A horizontal cross section of the head.

Figure 1-15. A typical SAR distribution for a cellular telephone radiating at 835 MHz. Shown here: (a) The side of the head exposed to the cellular telephone and (b) A horizontal cross section of the head.

30

Since different anatomic models of the human head have been used by various authors, the calculated SAR distributions are slightly different with peak 1-g SARs that may be up to 50% different even when identical antenna lengths and slant angles of the telephones vis à vis the head are used (Wang & Fujiwara, 2000). This variation in the calculated peak 1-g SAR may be reduced somewhat if care is taken in accurately positioning the telephone relative to the ear. In one such study, the effect of using different anatomical models of the head on SAR distributions is examined (Tinniswood et al., 1998a). For this study, two different anatomically-based models of the human head and neck derived from the MRI scans of two adult male volunteers are used. The first of these models, described in detail in (Gandhi, 1995; Gandhi et al., 1996) has a resolution of 1.974 × 1.974 × 3.0 mm. The second anatomic model described in (Tinniswood et al., 1998a) has a resolution of 0.9375 mm for each of the cubical voxels and is based on the head of a second individual. The head and neck parts of each of the models have been segmented into 15 tissue types, namely, muscle, fat, bone (skull), cartilage, skin, nerve, blood, parotid gland, eye humor, sclera and lens, cerebrospinal fluid (CSF), brain, and pineal and pituitary glands. Appropriate mass densities and dielectric properties depending on the irradiation frequency, listed in (Gandhi, 1995; Tinniswood et al., 1998a) were used to calculate SAR distribution using the FDTD method. The SAR results given in Table 1-6 use three different models: Model A with a resolution of 1.974 × 1.974 × 3 mm, its resampled version with a resolution of 0.987 × 0.987 × 1 mm (Model B), and a new 0.9375 mm resolution model (Model C). Given in Table 1-6 are the salient features of the calculated SARs and the powers absorbed for the various regions of the head for Models A, B, and C for a cellular telephone of handset dimensions 2.2 × 5.0 × 15.5 cm. Used for the SAR calculations is a handset with a quarter-wavelength (3.95 cm) long antenna radiating a time-averaged power of 125 mW (peak pulses of power output 1W with a duty cycle of 1/8) at 1900 MHz. As expected, the SAR distributions for Models A and B with different resolutions, but derived from the anatomic model of the same head, are very similar. The SARs calculated for Model C derived for a different individual are slightly different, but the peak 1-g SAR needed for compliance testing against the ANSI/IEEE and FCC guidelines (IEEE, 1999; U.S. FCC, 1996) is still within about 15% of that derived for Models A and B.

Table 1-6. SAR distributions for three anatomic models of the human head for a cellular telephone of handset dimensions 2.2 x 5.0 x 15.6 cm (Tinniswood et al., 1998a). Frequency = 1900 MHz, radiated power = 125 mW.

	Model A $1.974 \times 1.974 \times 3.0$ mm	Model B $0.987 \times 0.987 \times 1.0$ mm (resampled from Model A)	Model C 0.9375 mm^3
Peak 1-voxel SAR (W/kg)	5.88	10.97	6.77
Peak 1-g SAR (W/kg)	1.58	1.62	1.41
Peak 1-g SAR for brain (W/kg)	0.27	0.26	0.32
Power absorbed by head, neck and hand	58%	61.7%	61.5%
Brain average SAR (mW/kg)	9.33	9.33	12.31
CSF average SAR (mW/kg)	10.08	10.10	8.68
Lens average SAR (mW/kg)	1.17	1.17	1.61
Sclera average SAR (mW/kg)	1.41	1.44	2.50
Humour average SAR (mW/kg)	2.40	2.39	3.21

1.6 Some Applications for Low Frequencies

1.6.1 Coupling to the Human Body for EM Fields of High Voltage Power Transmission Lines

As given in Section 1.4.2, the FDTD method with frequency scaling may be used for calculating induced electric fields and current densities for various tissues for an anatomic model of the human standing under a high-voltage power transmission line (Gandhi & Chen, 1992; Furse & Gandhi, 1998). Shown in Figure 1-16 are the calculated results using the anatomically-based model where the conductivities used for the various tissues are as given in Table 1-7. Recognizing the anisotropy in the conductivity of the skeletal muscle, two different values of muscle conductivities are taken for curves (1) and (2). For these curves, a higher conductivity of 0.52 S/m is taken for the skeletal muscle and an average value of 0.11 S/m is taken for the muscle in the interior of the body. For curves (3) and (4), however, a lower conductivity of 0.11 S/m is taken for all of the muscle, interior or skeletal. The results shown in Figure 1-16 curves (1), (3), and (4) are for $E_{inc} = 10$ Kv/m (vertical) and $H_{inc} = 26.5$ A/m from side to side of the model. To point out the preponderance of the induced currents due to incident electric field, $H_{inc} = 0$ is assumed for the calculations shown in curve (2). It is interesting to note that the layer currents due to E-field exposure alone are almost 98-99 percent of the currents calculated for the combined electric and magnetic fields. It is also interesting to note that the calculated foot currents of 155-160 µA are in excellent agreement with 165 µA that would be projected from the measurements of Deno (1977) for the human.
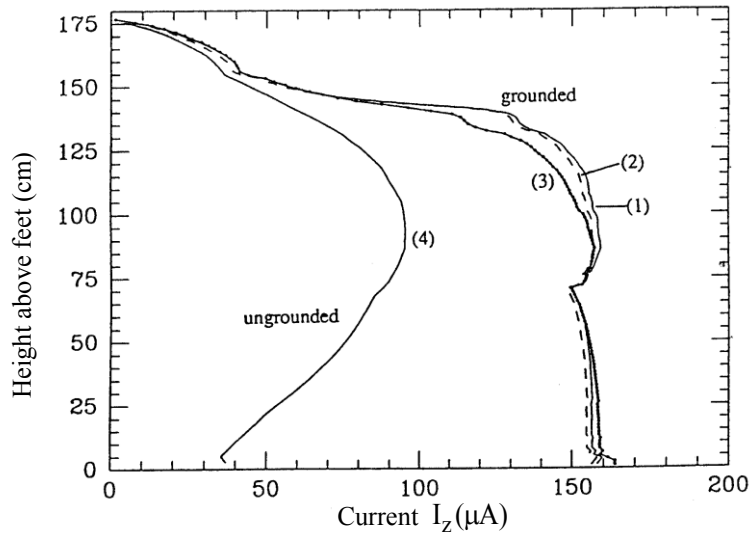
Figure 1-16. Calculated layer currents for anatomically-based grounded and ungrounded models exposed to EMFs at 60 Hz. For curves (1) and (2) σ = 0.11 S/m for the interior muscle. For curves (3) and (4) σ = 0.11 S/m for all of the muscle. E = 10 kVm (vertical), H = 26.5 A/m from side to side for all of the curves except for (2) for which only E-field exposure is assumed.

Table 1-7. Tissue conductivities used for calculations at the power-line frequency of 60 Hz.

Tissue Type	σ S/m
Air	0
Muscle	0.52 or 0.11
Fat, bone	0.04
Blood	0.6
Intestine	0.11
Cartilage	0.04
Liver	0.13
Kidney	0.16
Pancreas	0.11
Spleen	0.18
Lung*	0.04
Heart	0.11
Nerve, brain	0.12
Skin	0.11
Eye	0.11

* 33 percent lung tissue and 67 percent air for the dielectric properties
  of the lung were used.

33

1.6.2 Induced Electric Fields, Current Densities, and SARs for EAS and RFID Systems

Electronic Article Surveillance (EAS) and RF identification (RFID) systems based on the use of alternating magnetic fields at frequencies from 50/60 Hz up to 10-15 MHz are being rapidly introduced into society to prevent unauthorized removal of items from stores, libraries, and hospitals or for RF detection of identification cards to control access (Harris et al., 2000). The EAS and RFID systems may take the form of one or two-sided panels of current-carrying loops or pillars at or near the exit door, or loops hidden in the ceiling and/or the mat on the floor. Another manifestation is the magnetic tag deactivation systems that are mounted as checkout counter top devices. The net result is that an individual passing through or standing close to these devices is exposed to nonuniform vector magnetic fields emanating from these EAS and RFID systems.

As mentioned earlier, limits of induced current densities and SARs in the human body have been prescribed in the IEEE and ICNIRP standards (ICNIRP, 1998; IEEE, 2002) that may not be exceeded for exposure of the general public or for occupational situations. The basic restrictions specified in the ICNIRP guidelines (see Table 1-1) are to limit the induced current densities for the central nervous system (CNS) tissues e.g., the brain and the spinal cord for frequencies up to 100 kHz, current densities as well as SARs for frequencies between 100 kHz and 10 MHz and only SARs (both whole-body average and peak local 10-g SARs) for frequencies above 10 MHz. The European Standard EN50357 for compliance testing of EAS and RFID systems defines the procedures to be used for evaluation of human exposure to electromagnetic fields of these systems (CENELEC-European Committee for Electrotechnical Standardization, 2001). Since experimental compliance testing is tedious, computational methods using heterogeneous anatomically-based models of the human body may be used to show compliance of the new EAS devices.

For this application (Paul & Nasar, 1987), a full $1.974 \times 1.974 \times 2.93$ mm resolution model of the adult male described in (Gandhi, 1995), as well as scaled models of the 10- and 5-year-old children derived there from using the external dimensions typical of the children have been used (see Table 1-8).

Table 1-8. Some typical external dimensions and derived voxel sizes used for the anatomic models of the male adult and 10- and 5-year-old boys (Gandhi & Kang, 2001).

	Adult male	10-year-old boy	5-year-old boy
Head circumference[1] (cm)	53.8	52.3	51.0
Body weight (kg)	71.7	30.5	18.9
Height[1] (cm)	176	138	112
Body surface area[1] (cm^2)	17,400	9610	7510
Head surface area[1] (cm^2)	1305	1048	984
Voxel size for head (mm)	1.974×1.974×2.93	1.974×1.974×2.352	1.871×1.871×2.330
Voxel size for arms, torso, and legs (mm)	1.974×1.974×2.93	1.974×1.974×2.282	1.196×1.196×1.782

[1] See Reference (Lentner, 1984)

From Geigy Scientific Tables (Lentner, 1984), the head circumference does not change much from a 5-year-old child to an adult (about 5.5%) even though the surface area increases by about 33% and body height and weight increase significantly. Some typical external dimensions and derived voxel sizes for anatomic models of the male adult and 10- and 5-year-old boys are given in Table 1-8. The three models used for the calculations of different heights and weights but fairly similar circumferences of the head are visualized in Figure 1-17. Because of the fairly large size of the models with a grid size of 256 × 151 × 602 or approximately 23.3 million voxels, a Sun Microsystems UltraSparc II work station is used for the calculations of the induced electric fields from which the induced current densities are calculated using the tissue-dependent conductivities for each of the voxels. The problem requires a computer memory of 1.18 Gigabytes.

1.6.2.1   A Pass-Through EAS System

Even though the induced electric fields and current densities have been evaluated for several EAS device geometries mentioned in the previous section, we give details only for one such system to illustrate the procedure. A pass-by system assumed here is a 30-kHz one-sided EAS system consisting of two rectangular coils, each of width 50 cm and height 60 cm with an overlap of 10 cm, carrying in-phase currents of 100 A turns rms for each of the coils (46). This system is sketched in Figure 1-18.

a. Adult male.   b. Model of 10-year-old boy.   c. Model of 5-year-old boy.
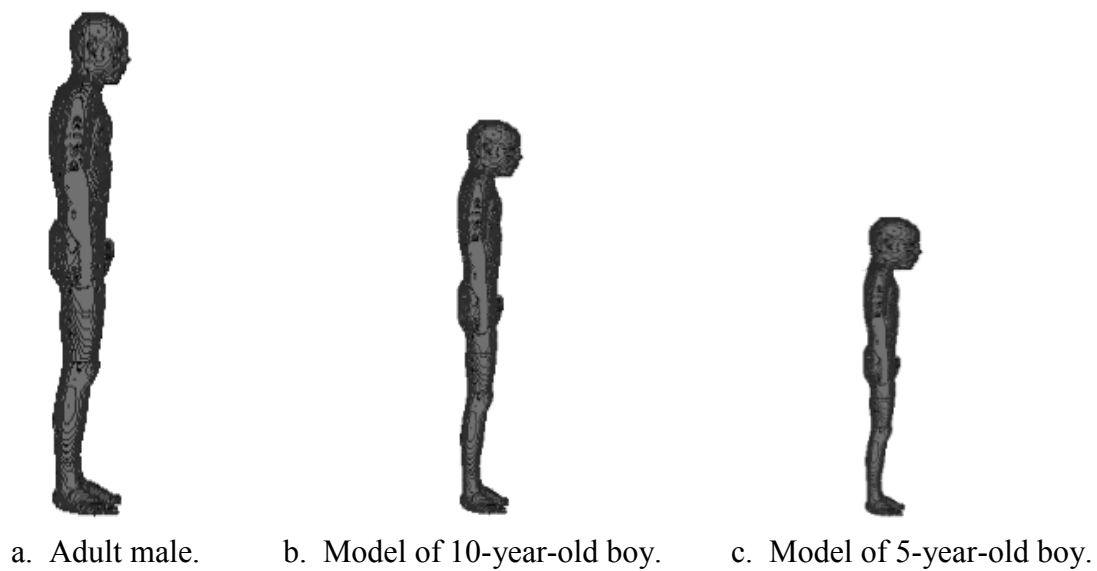
Figure 1-17. The three anatomic models used for calculations of induced electric fields and current densities.
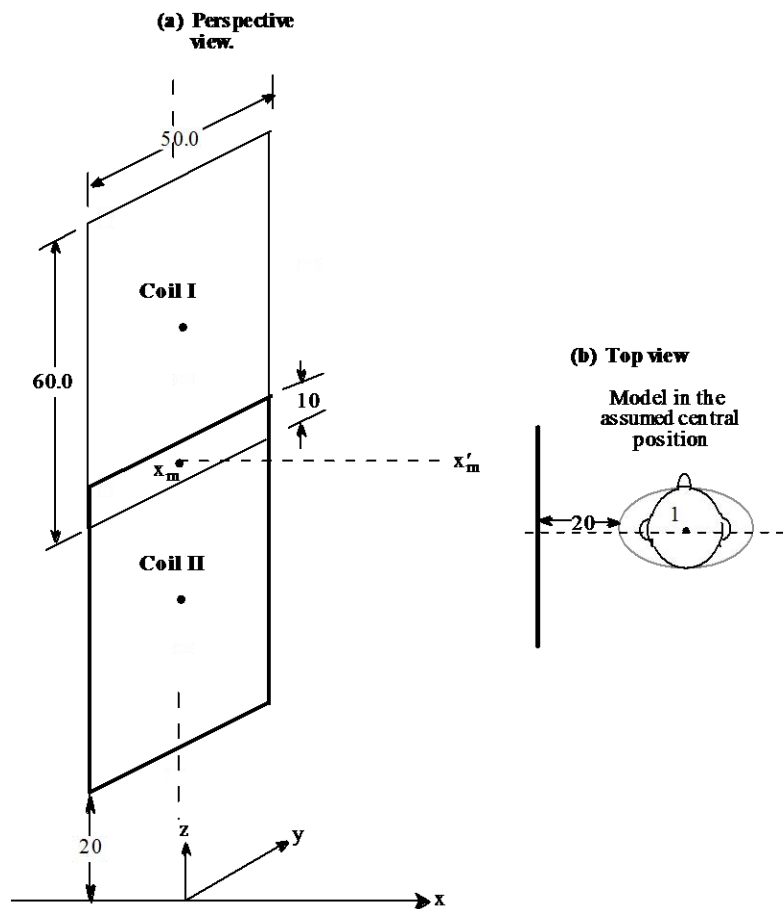
Figure 1-18. An assumed EAS system using a pair of rectangular coils with an overlap of 10 cm. The lower rung of the bottom coil is assumed to be 20 cm off the ground plane. The marked dimensions are in cm.

The dimensions and frequency used for this system are made up to illustrate the procedure and, to our knowledge, are not representative of any commercial products. This is done to protect the proprietary interests of the manufacturers. Using Biot-Savart's law of electromagnetics, a computer program is written to calculate the rms values of the magnetic fields B_x, B_y, B_z for the locations close to the assumed EAS system that are likely to be occupied by the various parts of the human. The calculated variations of the magnetic field components and the total magnetic field

$$B_{total} = \left(B_x^2 + B_y^2 + B_z^2 \right)^{1/2}$$

(21)

is sketched in Figure 1-19 for an imaginary vertical line that is centrally located (y = 0) at a distance x = 20 cm from the plane of the EAS panel. This is because of the placement of the human model such that this vertical line passes through the armpit tangential to the proximal side

37

of the torso recommended by European Standard EN50357 (CENELEC-European Committee for Electrotechnical Standardization, 2001) for compliance testing against ICNIRP guidelines.
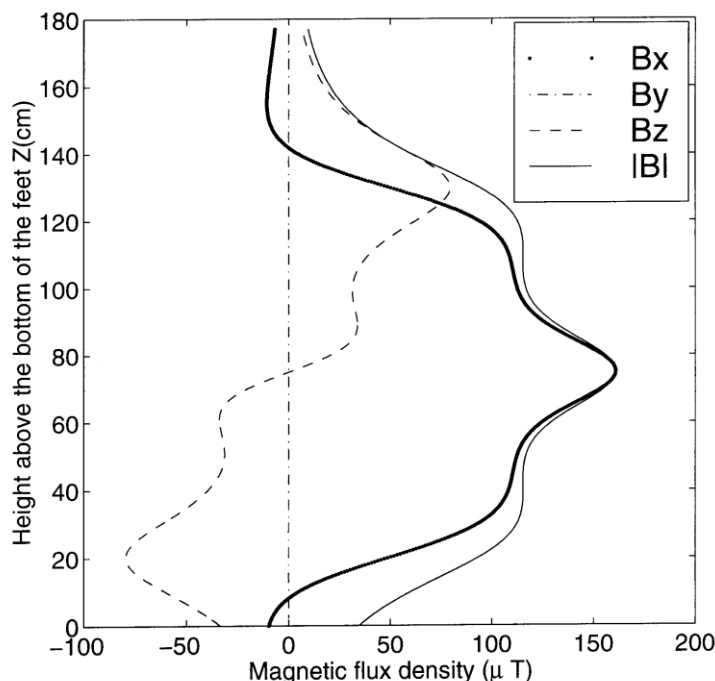
Figure 1-19. The calculated variation of the magnetic fields for a centrally-located vertical line (y=0) at a distance x = 20 cm from the plane of the EAS panel (see Figure 1-18).

From Figure 1-19, we can see that the magnetic fields are the highest for the region of the brain 100.2 < z < 111.2 cm for the model of the 5-year-old, intermediate for the model of the 10-year-old (125.8 < z < 137.2 cm) and lowest for the model of the adult (161.2 < z < 175.4 cm), respectively. As seen from Figure 1-19, the total magnetic field for the brain may be four to five times higher for the model of a 5-year-old child and two to three times higher for the model of a 10-year-old child as compared to that for an adult, respectively. For the spinal cord, the vertical coordinate z is between 60.6 to 100.2 cm for the 5-year-old, between 77.6 and 125.8 cm for the 10-year-old, and between 99.6 to 161.2 cm for the model of the adult. Here, too, the magnetic fields are higher for the regions of the spinal cord for both of the models of the children as compared to those for the model of the adult.

The impedance method described in Section 4.1 is used to calculate the induced electric fields and current densities for every voxel of the three models shown in Figure 1-17 with the proximal side of the torso at a distance of 20 cm from the yz plane passing through the EAS coils as suggested in EN50357 Compliance Standard (CENELEC-European Committee for Electrotechnical Standardization, 2001). From the component values of the x-, y-, or z-directed induced current densities J_x, J_y, and J_z, respectively, the total current densities (J) for each of the voxels are calculated using the following equation:

$$J = \left(J_x^2 + J_y^2 + J_z^2 \right)^{1/2}. \qquad\qquad (22)$$

The calculated organ-averaged and maximum 1 cm^2 area-averaged induced electric fields and current densities for the three human models for the pass-by EAS system of Figure 1-18 are given in Table 1-9. The maximum 1 cm^2 area-averaged current densities J_{max} for the brain and the spinal cord are considerably lower than the ICNIRP basic restriction at 30 kHz of 60 mA/m^2 for the general public for the model of the adult (see Table 1-1). Because of the shorter heights of the 10- and 5-year-old children, the brains of these models are in higher magnetic fields (see Figure 1-19) which results in the maximum current density for the 10-year-old model (64.6 mA/m^2) being close to the ICNIRP limit and that for the 5-year-old model (98.9 mA/m^2) being almost 65% higher than the ICNIRP limit of 60 mA/m^2 at 30 kHz. This is understandable since the average magnetic field for the region of the brain is about four times higher for the model of the 10-year-old and about five to six times higher for the model of the 5-year-old as compared to that for the adult, respectively.

Table 1-9. The calculated organ-averaged and maximum 1 cm^2 area-averaged electric fields (E) and current densities (J) for the models of the adult and 10- and 5-year-old children for the 30 kHz magnetic panel type EAS system (Gandhi & Kang, 2001).

Organ		Adult		10-year-Old		5-Year-Old	
		$J(mA/m^2)$	E(mV/m)	$J(mA/m^2)$	E(mV/m)	$J(mA/m^2)$	E(mV/m)
Brain	Organ-averaged	4.75	47.89	23.20	234.13	40.70	410.71
	Max. (1 cm^2)	17.63	177.83	64.64	652.23	98.93	998.27
Pineal gland	Organ-averaged	0.92	9.29	17.42	175.73	36.27	365.95
	Max. (1 cm^2)	-----	-----	-----	-----	-----	-----
Spinal cord	Organ-averaged	-----	-----	-----	-----	-----	-----
	Max. (1 cm^2)	32.64	538.61	40.19	663.20	43.71	721.29
Heart	Organ-averaged	92.69	185.39	120.08	240.16	130.33	260.66
	Max. (1 cm^2)	234.69	469.38	296.86	593.71	316.80	633.59
Liver	Organ-averaged	18.15	277.56	23.63	361.24	24.66	377.11
	Max. (1 cm^2)	86.68	1325.33	114.57	1751.76	121.11	1851.78
Kidneys	Organ-averaged	36.41	239.41	38.06	250.23	38.05	250.19
	Max. (1 cm^2)	88.08	579.09	81.26	534.26	78.07	513.26
Bladder	Organ-averaged	85.11	394.75	86.84	402.80	68.55	317.93
	Max. (1 cm^2)	234.21	1086.33	222.24	1030.81	170.34	790.09
Pancreas	Organ-averaged	28.61	188.08	38.64	254.02	46.72	307.19
	Max. (1 cm^2)	86.33	567.63	94.74	622.87	85.43	561.64

39

1.7 Conclusions and Future Directions

Dosimetry for electromagnetic fields from very low frequencies to microwave frequencies has advanced considerably over the last 15-20 years. Development of highly efficient numerical techniques makes it possible to get distributions of internal electric fields for SARs or for induced current densities for anatomically-realistic models of the human body with whole-body resolutions on the order of 1-2 mm and part-body resolutions of submillimeter voxel sizes. All of these techniques have been developed and tested for relatively uniform far-fields or highly nonuniform near-field sources. For personal wireless devices such as cellular telephones, source-body coupling is important and has been included by solving for E- and H-field distributions for the entire coupled region consisting of the shaped radiator (using CAD files) as well as the model of the human head.

Even though most of the focus in the past has been on safety compliance testing, these numerical techniques are now beginning to be used for important diagnostic and therapeutic applications. Some examples of therapeutic applications are designs of implantable and non-invasive devices such as pace makers and defibrillators and applicators for hyperthermia, hypothermia, transcranial magnetic stimulation, etc. Examples of diagnostic applications include detection of breast cancer and regions of abnormal electrical activity for the brain and the heart amongst many others.

1.8 References

Armitage, D. W., LeVeen, H. H., & Pethig, R. (1983). Radiofrequency-Induced Hyperthermia: Computer simulation of specific absorption rate distribution using realistic anatomical models. *Physics in Medicine and Biology, 28*, 31-42.

Baraton, P. & Hutzler, B. (1995). Magnetically-induced currents in the human body. *IEC Technology Trend Assessment.*

Bernardi, P., Cavagnaro, M., Pisa, S., & Piuzzi, E. (2000). Human exposure to radio base-station antennas in urban environment. *IEEE Transactions on Microwave Theory and Techniques, 48*, 1996-2002.

Bui, M. D., Stuchly, S. S., & Costache, G. I. (1991). Propagation of transients in dispersive dielectric media. *IEEE Transactions on Microwave Theory and Techniques, 39*, 1165-72.

CENELEC-European Committee for Electrotechnical Standardization. (2001). *Evaluation of human exposure to EM fields from devices used in electronic article surveillance (EAS), radiofrequency identification (RFID) and similar applications*. European Standard EN50357. CENELEC-European Committee for Electrotechnical Standardization, rue de Stassart 35, B-1050, Brussels, Belgium.

Chen, J. Y., Furse, C. M., & Gandhi, O. P. (1994). A simple convolution procedure for calculating currents induced in the human body for exposure to electromagnetic pulses. *IEEE Transactions on Microwave Theory and Techniques, 42*, 1172-75.

Chen, J. Y. & Gandhi, O. P. (1989). RF currents induced in an anatomically-based model of a human for plane-wave exposures (20-100 MHz). *Health Physics, 57*, 89-98.

Chen, J. Y. & Gandhi, O. P. (1991). Currents induced in an anatomically-based model of a human for exposure to vertically polarized electromagnetic pulses. *IEEE Transactions on Microwave Theory and Techniques, 39*, 31-39.

Chen, J., & Jin, J. M. (1997). Calculation of SAR and B_1-field within human head excited by MRI birdcage coils. *Proceedings of IEEE Antennas and Propagation Society International Symposium,* 2, 1210-13. Montreal, Canada.

Dawson, T. W., Caputa, K., & Stuchly, M. A. (1999). Numerical evaluation of 60 Hz magnetic induction in the human body in complex occupational environments. *Physics in Medicine and Biology*, *44*, 1025-40.

Dawson, T. W. & Stuchly, M. A. (1998). High resolution organ dosimetry for human exposure to low frequency magnetic fields. *IEEE Transactions on Magnetics, 34*, 708-18.

DeFord, J. F. & Gandhi, O. P. (1985). An impedance method to calculate currents in biological bodies exposed to quasi-static electromagnetic fields. *IEEE Transactions on Electromagnetic Compatibility, 27*, 168-73.

Deno, D. W. (1977). Currents induced in the human body by high voltage transmission line electric field: Measurement and calculation of distribution and dose. *IEEE Transactions on Power Apparatus and Systems, 96*, 1517-27.

Dimbylow, P. J. (1998). Induced current densities from low-frequency magnetic fields in a 2 mm resolution, anatomically realistic model of the body. *Physics in Medicine and Biology, 43*, 221-30.

Dimbylow, P. J. (2002). Fine resolution calculations of SAR in the human body for frequencies up to 3 GHz. *Physics in Medicine and Biology, 47*, 2835-46.

Dimbylow, P. J. & Mann, S. A. (1994). SAR calculations in an anatomically-based realistic model of the head for mobile communication transceivers at 900 and 1800 MHz. *Physics in Medicine and Biology, 39*, 1537-53.

Durney, C. H., Johnson, C. C., Barber, P. W., Massoudi, H., Iskander, M. F., Lords, J. J., Ryser, D. K., Allen, S. J., & Mitchell, J. C. (1978). *Radiofrequency Radiation Dosimetry Handbook*. (2nd ed.). SAM-TR-78-22. Brooks AFB, Texas.

Furse, C. M., Chen, J. Y., & Gandhi, O. P. (1994). A frequency-dependent finite-difference time-domain method for induced current and SAR calculations for a heterogeneous model of the human body. *IEEE Transactions on Electromagnetic Compatibility, 36*, 128-33.

Furse, C. M. & Gandhi, O. P. (1998). Calculations of electric fields and currents induced in a millimeter-resolution human model at 60 Hz using the FDTD method. *Bioelectromagnetics, 19*, 293-99.

Gandhi, O. P. (1990). Electromagnetic energy absorption in humans and animals. Chap. 8 in *Biological Effects and Medical Applications of Electromagnetic Energy*, Gandhi, OP ed., Englewood Cliffs, NJ: Prentice Hall Inc.

Gandhi, O. P. (1995). Some numerical methods for EM dosimetry: ELF to microwave frequencies. *Radio Science, 30*, 161-77.

Gandhi, O. P. & Chen, J. Y. (1992). Numerical dosimetry at power line frequencies using anatomically-based models. *Bioelectromagnetics,* Suppl. 1, 43-60.

Gandhi, O. P. & Chen, J. Y. (1995). Electromagnetic absorption in the human head from experimental 6-GHz handheld transceivers. *IEEE Transactions on Electromagnetic Compatibility, 37*, 547-58.

Gandhi, O. P. & Chen, X. B. (1999). Specific absorption rates and induced current densities for an anatomy-based model of the human for exposure to time-varying magnetic fields of MRI. *Magnetic Resonance in Medicine, 41*, 816-23.

Gandhi, O. P. & DeFord, J. F. (1988). Calculation of EM power deposition for operator exposure to RF induction heaters. *IEEE Transactions on Electromagnetic Compatibility, 30*, 63-68.

Gandhi, O. P., DeFord, J. F., & Kanai, H. (1984). Impedance method for calculation of power deposition patterns in magnetically induced hyperthermia. *IEEE Transactions on Biomedical Engineering, 31*, 644-51.

Gandhi, O. P., Gao, B. Q., & Chen, J. Y. (1992). A frequency-dependent finite-difference time-domain formulation for induced current calculations in human beings. *Bioelectromagnetics, 13*(6), 543-55.

Gandhi, O. P., Gao, B. Q., & Chen, J. Y. (1993). A frequency-dependent finite-difference time-domain formulation for general dispersive media. *IEEE Transactions on Microwave Theory and Techniques, 41*, 658-65.

Gandhi, O. P., Gu, Y. G., Chen, J. Y., & Bassen, H. I. (1992). Specific absorption rates and induced current distributions in an anatomically-based human model for plane-wave exposures (at frequencies 20-915 MHz). *Health Physics, 63*(3), 281-90.

42

Gandhi, O. P. & Kang, G. (2001). Calculation of induced current densities for humans by magnetic fields of electronic article surveillance devices. *Physics in Medicine and Biology, 46, 2759*-71.

Gandhi, O. P., Kang, G., Wu, D., & Lazzi, G. (2001). Currents induced in anatomic models of the human for uniform and nonuniform power frequency magnetic fields. *Bioelectromagnetics, 22*, 112-21.

Gandhi, O. P. & Lam, M. S. (2003). An on-site dosimetry system for safety assessment of wireless base stations using spatial harmonic components. *IEEE Transactions on Antennas and Propagation, 51*, 840-47.

Gandhi, O. P., Lazzi, G., & Furse, C. M. (1996). Electromagnetic absorption in the human head and neck for mobile telephones at 835 and 1900 MHz. *IEEE Transactions on Microwave Theory and Techniques, 44*, 1884-97.

Gandhi, O. P., Lazzi, G., Tinniswood, A., & Yu, Q-S. (1999). Comparison of numerical and experimental methods for determination of SAR and radiation patterns of handheld wireless telephones. *Bioelectromagnetics,* (Suppl. 4), 93-101.

Gandhi, O. P., Wu, D., Chen, J. Y., & Conover, D. L. (1997). Induced current and SAR distributions for a worker model exposed to an RF dielectric heater under simulated workplace conditions. *Health Physics, 72*, 236-42.

Gao, B. Q. & Gandhi, O. P. (1992). An expanding-grid algorithm for the finite-difference time-domain method. *IEEE Transactions on Electromagnetic Compatibility, 34*, 277-83.

Gustrau, F., Bahr, A., Rittweger, M., Goltz, S., & Eggert, S. (1999). Simulation of induced current densities in the human body at industrial induction heating frequencies. *IEEE Transactions on Electromagnetic Compatibility, 41*, 480-86.

Guy, A. W., Davidow, S., Yang, G. Y., & Chou, C. K. (1982). Determination of electric current distributions in animals and humans exposed to a uniform 60-Hz high intensity electric field. *Bioelectromagnetics, 3*, 47-71.

Harris, C., Boivin, W., Boyd, S., Coletta, J., Kerr, L., Kempa, K., & Aronow, S. (2000). Electromagnetic field strength levels surrounding electronic article surveillance (EAS) systems. *Health Physics, 78*, 21-7.

Hart, R. A. & Gandhi, O. P. (1998). Comparison of cardiac-induced endogenous fields and power frequency induced exogenous fields in an anatomical fields of the human body. *Physics in Medicine and Biology, 43*, 3083-99.

Hayes, C. E., Edelstein, W. A., Schenck, J. F., Mueller, O. M., & Eash, M. (1985). An efficient, highly homogeneous radio frequency coil for whole-body NMR imaging at 1.5 Tesla. *Journal of Magnetic Resonance, 63*, 622-28.

Institute of Electrical and Electronics Engineers, Inc. (IEEE). (1999). *IEEE standard for safety levels with respect to human exposure to radiofrequency electromagnetic fields, 3 kHz to 30 GHz* (IEEE Std C95.1). New York, NY: The Institute of Electrical and Electronics Engineers, Inc.

Institute of Electrical and Electronics Engineers, Inc. (IEEE). (2002). *IEEE standard for safety levels with respect to human exposure to electromagnetic fields, 0-3 kHz.* (IEEE Standard C95.6). New York, NY: The Institute of Electrical and Electronics Engineers, Inc.

International Commission on Non-Ionizing Radiation Protection (ICNIRP). (1998). Guidelines for limiting exposure to time-varying electric, magnetic and electromagnetic fields (Up to 300 GHz). *Health Physics, 74*(4), 494-522.

Jensen, M. A. & Rahmat-Samii, Y. (1995). EM interaction of handset antennas and a human in personal communication. *Proceedings of the IEEE, 83*, 7-17.

Jin, J. M., Shen, G., & Perkins, T. (1994). On the field inhomogeneity of birdcage coils. *Magnetic Resonance in Medicine, 32*, 418-22.

Joseph, R. M., Hagness, S. C., & Taflove, A. (1991). Direct time integration of Maxwell's equations in linear dispersive media with absorption for scattering and propagation of femtosecond electromagnetic pulses. *Optics Letters, 16*(18), 1412-14.

Kaune, W. T. & Gillis, M. F. (1981). General properties of the interaction between animals and ELF electric fields. *Bioelectromagnetics, 6*, 13-32.

Kunz, K. S. & Luebbers, R. J. (1993). *The finite-difference time-domain method.* Boca Raton, FL: CRC Press.

Lentner, C. (1984). *Geigy Scientific Tables,* 3. Basel, Switzerland: CIBA-GEIGY.

Li, Q-X & Gandhi, O. P. (2005). Calculation of magnetic field-induced current densities for humans from EAS countertop activation/deactivation devices that use ferromagnetic cores. *Physics in Medicine and Biology., 50*, 373-85.

Luebbers, R. & Hunsberger, F. (1992). FDTD for nth order dispersive media. *IEEE Transactions on Antennas and Propagation, 40*, 1297-1301.

Luebbers, R. J., Hunsberger, F., & Kunz, K. S. (1991). A frequency-dependent finite-difference time-domain formulation for transient propagation in plasma. *IEEE Transactions on Antennas and Propagation, 39*, 29-34.

Luebbers, R. J., Hunsberger, F. P., Kunz, K. S., Standler, R. B., & Schneider, M. (1990). A frequency-dependent finite-difference time-domain formulation for dispersive materials. *IEEE Transactions on Electromagnetic Compatibility, 32*, 222-27.

Magin, R. L., Liburdy, R. P., & Persson, B. (Eds.). (1991). Biological Effects and Safety Aspects of Nuclear Magnetic Resonance Imaging and Spectroscopy. *Annals of the New York Academy of Sciences*, *649*.

Nagaoka, T., Watanabe, S., Sakurai, K., Kunieda, E., Watanabe, S., Taki, M., & Yamanaka, Y. (2004). Development of realistic high-resolution whole-body voxel models of Japanese adult males and females of average height and weight, and application of models to radio-frequency electromagnetic-field dosimetry. *Physics in Medicine and Biology, 49*, 1-15.

National Radiological Protection Board. (1990). *Revised Advice on Acceptable Restrictions of Patient and Volunteer Exposure During Clinical Magnetic Resonance Diagnostic Procedures*, U.K.

Okoniewski, M., Okoniewska, E., & Stuchly, M. A. (1997). Three-dimensional subgridding algorithm for FDTD. *IEEE Transactions on Antennas and Propagation, 45*, 422-29.

Okoniewski, M. & Stuchly, M. A. (1996). A study of the handset antenna and human body interaction. *IEEE Transactions on Microwave Theory and Techniques, 44*, 1855-64.

Orcutt, N. & Gandhi, O. P. (1990). Use of the impedance method to calculate 3-D power deposition patterns for hyperthermia with capacitive plate electrodes. *IEEE Transactions on Biomedical Engineering, 37*, 36-43.

Paul, C. R. & Nasar, S. A. (1987). *Introduction to Electromagnetic Fields (2nd ed.)*. McGraw Hill.

Spiegel, R. J., Fatmi, M. B., & Kunz, K. S. (1985). Application of a finite-difference technique to the human radio-frequency dosimetry problem. *Journal of Microwave Power, 20*, 241-54.

Stuchly, M. A. & Dawson, T. W. (2000). Interaction of low-frequency electric and magnetic fields with the human body. *Proceedings of the IEEE, 88*, 643-64.

Sullivan, D. M. (1992). A frequency-dependent FDTD method for biological applications. *IEEE Transactions on Microwave Theory and Techniques, 40*, 532-39.

Sullivan, D. M., Gandhi, O. P., & Taflove, A. (1988). Use of the finite-difference time-domain method in calculating EM absorption in man models. *IEEE Transactions on Biomedical Engineering, 35*, 179-86.

Taflove, A. & Brodwin, M. E. (1975). Numerical solution of steady-state electromagnetic scattering problems using the time-dependent Maxwell's equations. *IEEE Transactions on Microwave Theory and Techniques, 23*(8), 623-30.

Taflove, A. & Hagness, S. C. (2000). *Computational Electrodynamics: the finite-difference time-domain method* (2nd ed.). Norwood, MA: Artech House.

Tinniswood, A. D., Furse, C. M., & Gandhi, O. P. (1998a). Computations of SAR distributions for two anatomically-based models of the human head using CAD files of commercial telephones and the parallelized FDTD code. *IEEE Transactions on Antennas and Propagation, 46*, 829-33.

Tinniswood, A. D., Furse, C. M., & Gandhi, O. P. (1998b). Power deposition in the head and neck of an anatomically-based model for plane-wave exposures. *Physics in Medicine and Biology, 43*, 2361-78.

Tinniswood, A. D., Lazzi, G., & Gandhi, O. P. (1999). The use of the expanding-grid FDTD method for simulation of CAD-derived personal wireless telephones. *Microwave and Optical Techology Letters, 22*, 24-29.

U.S. Federal Communications Commission (U.S. FCC). (1996). *Guidelines for evaluating the environmental effects of radiofrequency radiation* (*FCC* 96-326).

U.S. Food and Drug Administration. (1988). Magnetic Resonance Diagnostic Devices: Panel Recommendation and Report on Petitions for MR Reclassification. *Federal Register, 53*, 7575-7579.

Vaughan, J. T., Hetherington, H. P., Out, J. O., Pan J. W., & Pohost, G. M. (1994). High-frequency volume coils for clinical NMR imaging and spectroscopy. *Magnetic Resonance in Medicine, 32*, 206-18.

Wang, J. & Fujiwara, O. (2000). Dosimetry analysis and safety evaluation of realistic head models for portable telephones. *Transactions of the IEICE, J83-B*(5), 720-25.

Watanabe, S., Taki, M., Nojima, T., & Fujiwara, O. (1996). Characteristics of the SAR distributions in a head exposed to electromagnetic fields radiated by a handheld portable radio. *IEEE Transactions on Microwave Theory and Techniques, 44*, 1874-83.

Wiart, J., Chaillou, S., & Drago, S. (1997). Calculation of the power absorbed by the head using a nonuniform FDTD. *Proceedings of North American Radio Science Meeting,* Montreal, Canada, 666.

Zhang, N., Roos, M. S., Wang, S. T., & Vaughan, J. T. (1994). *An experimental study of a head coil for proton imaging and spectroscopy*. Paper presented at 2nd Meeting of Society of Magnetic Resonance, San Francisco, CA.

Radio Frequency Radiation Dosimetry Handbook
(Fifth Edition)

Chapter 2.   Experimental Radio Frequency Dosimetry

Stewart J. Allen
General Dynamics Information Technology
Air Force Research Laboratory, 711 Human Performance Wing,
Human Effectiveness Directorate, Directed Energy Bioeffects Division, Radio Frequency
Radiation Branch, Brooks City-Base, Texas 78235-5147

Stujallen@peoplepc.com

2.1   Introduction

To achieve useful biological effects data, three conditions must be met: 1) accurate measurements of the biological response, 2) accurate measurements of the radio frequency (RF) fields over the exposure volume in terms of incident field, and 3) accurate measurement of Specific Absorption Rate (SAR). Proper extrapolation from experimental subject to the equivalent human exposure must be completed in the planning process before any dosimetry is initiated. Theoretical calculations using Finite-Difference Time-Domain (FDTD) (Kunz & Luebbers, 1993; Mason et al., 2000; Gajsek et al., 2002) or other methods such as Mie theory (Guy, 1997) are desirable for comparison with the experimental results. Some of the basic principles involved in obtaining the biological and dosimetry data sets are the same, but this paper will concentrate on the details of the radio frequency field measurements.

2.2   Experimental Planning

Prior to initiation of an experimental protocol, one must first consider the problem to be addressed. If the question is ―What is the biological effect on mice exposed to 2450 MHz?‖ the mice would obviously be exposed to various levels of 2450 MHz fields and the effects of these fields measured. However, if the question is ―What is the effect of 2450 MHz on man?‖ and mice are used to measure the effect, the exposures to the mice must be done at a frequency greater than 2450 MHz.

2.2.1   Determination of appropriate exposure conditions

The extrapolation between animal and human exposures is presented in detail in Chapter 2 of the ―Radiofrequency Dosimetry Handbook 4th Edition‖ (Durney, et al., 1986). A brief discussion of the extrapolation process is presented here. Before an animal is exposed to RF fields, the desired human equivalent exposure condition should be calculated. The equivalent exposure frequency is calculated using the following equation:

$$a_1 f_1 = a_2 f_2 \qquad\qquad (1)$$

where a_1 = half length of the animal long axis; a_2 = half length of the human long axis; f_1 = frequency of animal exposure; and f_2 = frequency of human exposure.

For example, if a medium rat is to be used to investigate a 10 mW/ cm^2 exposure of the standard man to his resonance frequency. First, the resonance frequency of man exposed in E polarization (the long axis of the body aligned with the electric field vector) is determined to be 75 MHz (Figure 2-1) and a_2 = 0.875 m (Figure 6.3 Radiofrequency Dosimetry Handbook 4th Edition). The half-length of a medium rat is a_1 = 0.1 m (Figure 6.16 Radiofrequency Dosimetry Handbook 4th Edition).

Substituting into Equation 1:

$$f_1 = (0.875)\,(75)\,/\,0.1 = 660 \text{ MHz} . \qquad\qquad (2)$$

Reading the normalized SAR for the average man from Figure 2-1 at 75 MHz in E polarization (0.24 W/kg per mW/cm^2) and for the rat at 660 MHz in E polarization (0.8 W/kg per mW/cm^2) the equivalent exposure is calculated using Equations 3-5:

$$SAR_1\,PD_1 = SAR_2\,PD_2 . \qquad\qquad (3)$$

$$(0.8 \text{ W/kg per mW/cm}^2)\,PD_1 = (0.24 \text{ W/kg/mW/cm}^2)\,(10 \text{ mW/cm}^2) . \qquad (4)$$

$$PD_1 = \text{Rat Exposure} = 3.0 \text{ mW/cm}^2 . \qquad\qquad (5)$$

Thus, a rat exposed in E polarization to 3.0 mW/cm^2 at 660 MHz would be equivalent to exposing a human to 10 mW/cm^2 at his resonance frequency of 75 MHz. This type of calculation should be accomplished prior to conducting any animal experiment. One could perform the same calculation if the animal exposure is given and human equivalent exposure is desired.
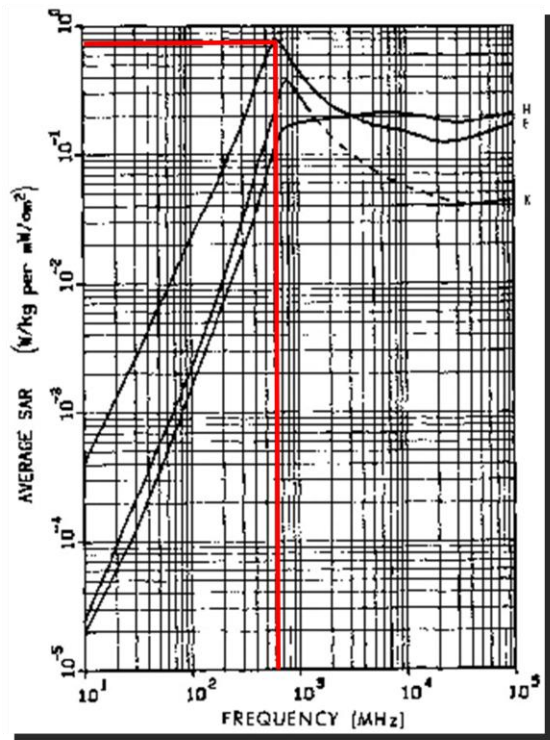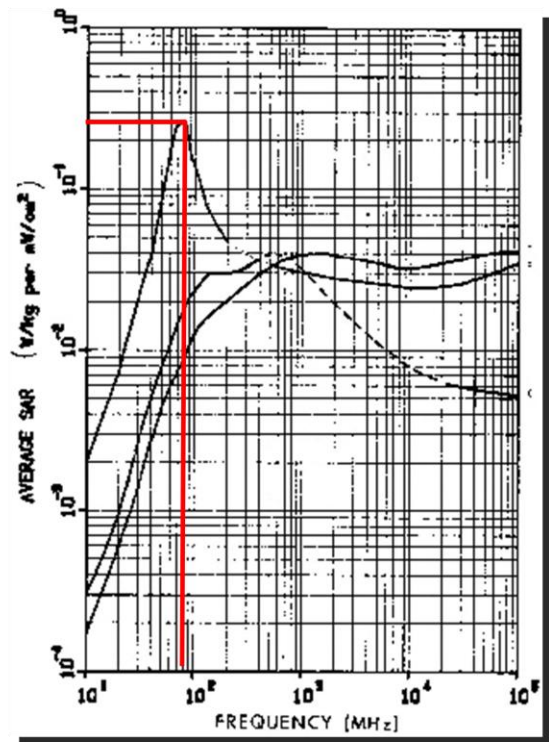
MEDIUM RAT   **STANDARD MAN**

Figure 2-1. SAR vs. Frequency (Source: Durney et al., 1986).

2.2.2   Instrumentation Check-out and Use

It is important to check all instruments to be used in the experiment to assure they are in good repair and calibrations are current. If calibration factors can be set in an instrument, it should be accomplished prior to the commencement of the experiment. If an isotropic probe is used, it should be oriented in K polarization with the handle pointing away from the antenna. If K polarization is not practical, align the probe in H polarization (handle aligned with the magnetic field). Do not take readings with the probe handle aligned with the E-field. Marks should be made on the probe at 45° intervals resulting in eight positions and the probe read for each position with the same transmitter output power. The eight readings are averaged and this value is divided by the maximum value. The probe is positioned for the maximum reading for all subsequent measurements and the value of the average divided by the maximum is multiplied by all subsequent readings to evaluate the fields. If the field measuring instrument stores calibration, this factor can be multiplied by the frequency correction factor and the result stored in the instrument. The output of the instrument reads the corrected field value.

49

2.2.3 Establishment of an Experimental Plan

To establish the RF field requirements, one should understand the interaction of biological systems with RF. Figure 2-2 shows a representation of the external field patterns for a human in E polarization, well above resonance (greater than 1 GHz) and at or below the resonance frequency (less than 100 MHz). As seen on the left side of the figure, the field is not distorted above or below the subject for frequencies above resonance for man in E polarization. There will be some scattering (not shown) of the field, but the absorbed power is a function of the exposed area. The higher the frequency, the more superficial the exposure (Durney et al., 1986, Table 11.4).

| Field pattern above resonance | Field pattern near and below resonance |
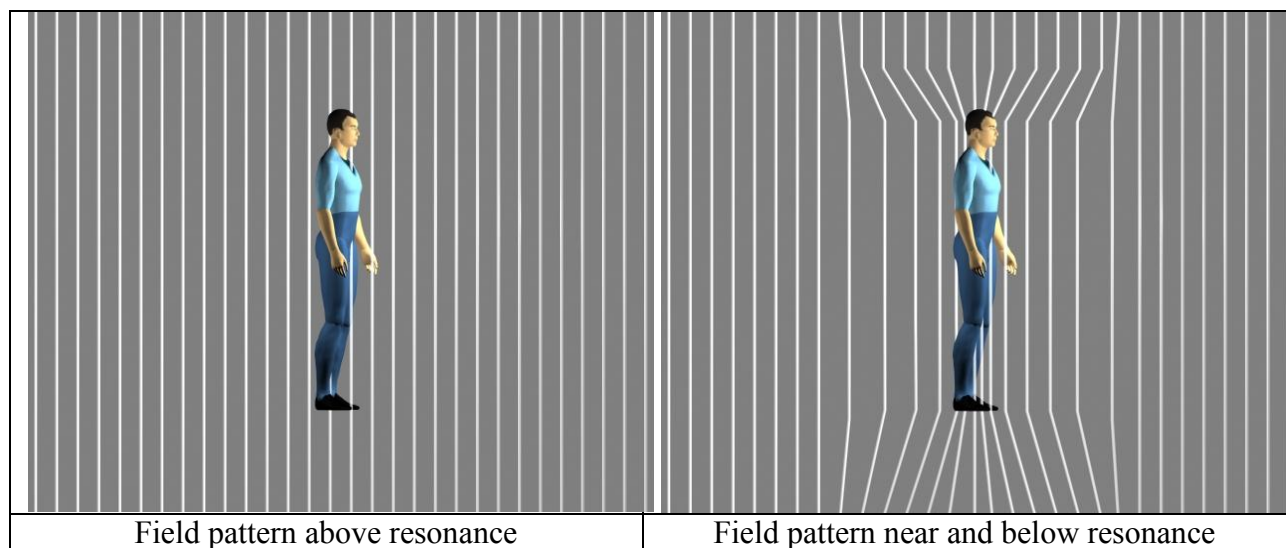
Figure 2-2. Representation of the external field patterns for a human in E polarization.

At resonance, the RF E-field is concentrated above and below the subject. The mode of interaction is one of induced current and the exposure is not a function of exposure area. As a matter of fact, if the standard man is exposed at his resonant frequency his SAR is greater than would be expected if his entire body surface area were exposed to 1 mW/cm^2 and total absorption occurred. These deep currents produce absorption in the body and the current density is a function of the conductivity of the various body tissues and the cross section through which the current flows. Incident electric field density and SAR are generally quite low on the surface of the body. As the frequency is lowered the total amount of absorption in the body decreases but the E-field is still concentrated at the head and feet and the deposition of energy is still deep within the body.

Using the Finite-Difference Time-Domain (FDTD) method to calculate the SAR distribution in a model of man produces the results shown in Figure 2-3. Note the transition from deep absorption to superficial absorption as the frequency is increased. Similar shifts in the absorption pattern are found in animals as a function of frequency. However, for a mouse the resonance frequency is approximately 2 GHz and superficial absorption occurs above 10 GHz.

50
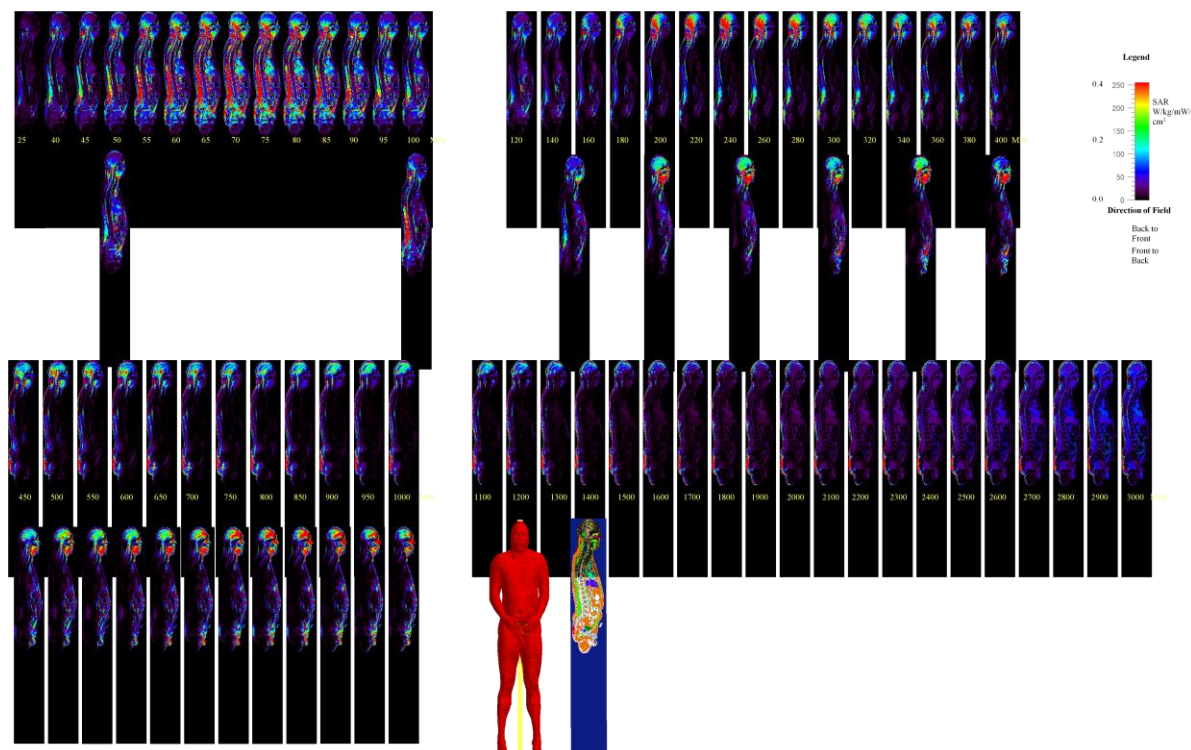
Figure 2-3. SAR as a function of frequency.

The change in uniformity of exposure as a function of distance from the antenna is illustrated in Figure 2-4. The man at the left would receive a non-uniform exposure while the man on the right would receive a uniform exposure. For the same power into the antenna, the man on the right would be exposed to a center beam power density of about 1/16th of that of the man on the right due to the distance increasing by approximately 4. In setting up experiments a compromise between field strength and uniformity is required, but the best condition is a plane wave exposure such as the man on the right. For a small animal such as a rat or mouse, plane wave exposure could be accomplished at the distance of the man on the left.

51
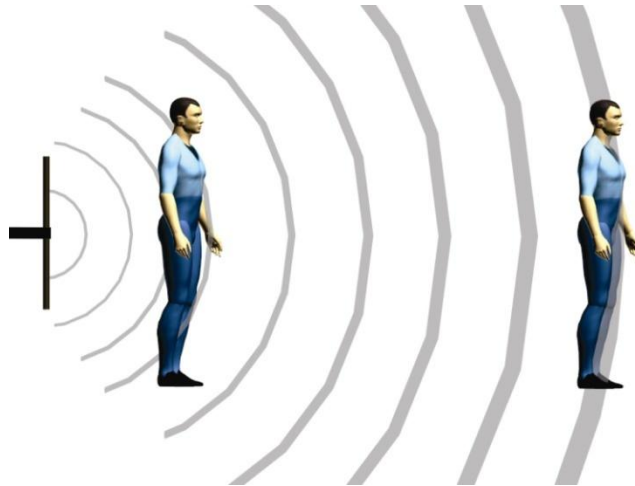
Figure 2-4. Change in uniformity of exposure as a function of distance from the antenna.

Most radio frequency bioeffects experiments are performed in an anechoic chamber with the field being propagated from a standard gain horn or open-ended waveguide. The use of a standard gain horn, though most common, may not be the preferred technique. The same field pattern can be accomplished with an open-end waveguide at a distance closer to the antenna than in the case of the standard gain horn. The open-ended waveguide has the advantage of exposures further into the far field for the same incident power density as the standard gain horn. The expected field can be calculated if the antenna gain is known and radiated power is measured. Radiated power equals Forward power – Reflected power. The expected power density can be calculated from Equation 6:

$$\text{PD} = \text{Numerical Antenna Gain} * \text{Radiated Power} / 4\,\pi\,D^2 \tag{6}$$

where D = Distance from antenna to measuring device (m) and PD = Power Density in W/m^2.

To convert to mW/cm^2 multiply by 0.1.

For pulsed fields:

$$\text{Average Radiated Power} = \text{Peak Radiated Power X Duty Factor} \tag{7}$$

$$\text{Duty Factor} = \text{Pulse Width X Pulse Repetition Frequency} \tag{8}$$

Note: The dB gain of a half-wave dipole is 2.2 and of an open-end waveguide is (2.2 + (4.5) (aperture area in wavelengths)).

If the long dimension of the waveguide is A and the short dimension is B, then:

$$\text{dB Gain} = (2.2 + (4.5)(A*B / \lambda^2)) \tag{9}$$

$$\text{Numerical Gain} = 10^{(\text{dB gain}/10)}. \tag{10}$$

52

2.3   Experimental Procedure

The order in which an experiment is performed is very important. The least complex measurements, the ones most predictable, are performed first. Then the next most complex measurement is performed until all required measurements are completed. For propagated fields in an anechoic chamber the order of measurement should be: 1) Measurement of centerline E-field or power density at the approximate distance exposures are likely to be made with a constant transmitter power over a 5- to 10-min period. If the drift is within acceptable limits move to step 2. 2) Measurement of the field as a function of distance, along the centerline, through the area in which exposures are to be made. If this measurement follows $1/D^2$ within experimental accuracy move to step 3. 3) Map the field over the exposure volume. If the field approximates a plane wave, average the exposure over the area to be occupied by the experimental subject. Note: All measurements should be made in free field with no subject present. 4) Utilize phantoms or cadavers to measure localized and whole-body SAR with the subject in the experimental exposure position.

2.4   Scientific Method

For all measurements, the scientific method (Figure 2-5) should be employed. The essential steps are: 1) establish an hypothesis 2) perform the measurements 3) compare the results of the measurements with the hypothesis 4) come to a conclusion as to whether the results support the hypothesis 5) report the results with sufficient details to allow others to replicate the measurements.

THE SCIENTIFIC METHOD

HYPOTHESIS

MEASUREMENT

RESULTS

CONCLUSIONS

REPORT
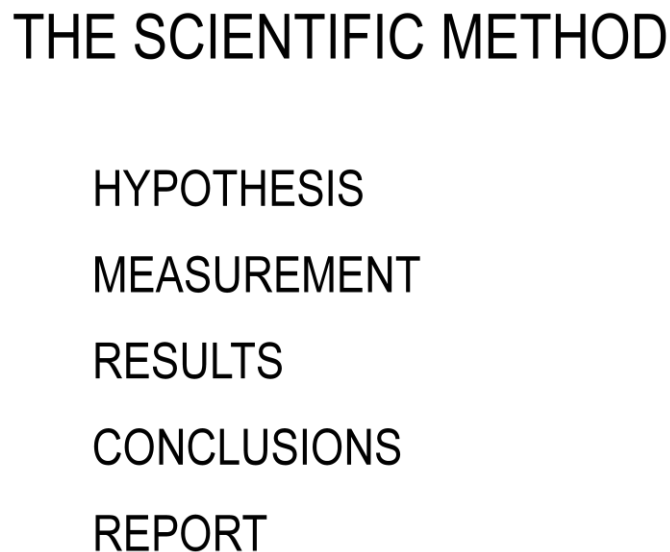
Figure 2-5. The Scientific Method.

53

For each of these steps the scientific method should be applied. Before the drift measurement is made a hypothesis should be arrived at as to how much drift is acceptable. Field measurement probes should read within ± 5% over a 10 min constant power run. Once the results are obtained, if the drift is below this level, the conclusion is that the next step can be performed, if not the reason for excessive drift must be determined. The cable from the readout to the probe should always be kept normal to the E-field especially for fields below 1000 MHz. If excessive drift is noted, a complete change of instruments should be made. This should resolve any drift problem, but if not, the instrument manufacturer should be contacted for their advice on proper resolution on the problem.

The far field should be calculated using the equation:

$$\text{Far Field} = 2*L^2 / \lambda \tag{11}$$

where L = longest dimension of the antenna; λ = Wavelength in meters = $3* 10^8 / F$ (meters) and F = frequency (Hz).

This equation gives an approximate distance to the far field. Obviously, near field conditions do not exist 1 cm inside this distance just as perfect far field conditions do not exist 1 cm beyond this point. Experiment should be set up as far outside the calculated distance to far field as transmitter power and chamber size allows.

Measurements of the field as a function of distance from the antenna should begin at the calculated far field distance and be measured at regular intervals well beyond the subject test position down the beam centerline. These data are entered into Excel or plotted using other techniques. Using a point at the approximate center of the scan the theoretical $1 / D^2$ curve is calculated using the equation:

$$PD = PD_o (D_o / D)^2 \tag{12}$$

where PD = Power Density at point D; PD_o = Power Density measured at point D_o; D_o = Distance to measured point; and D = Distance to calculated Power Density.

These data are plotted with the experimental data to compare experimental data with the theoretical $1 / D^2$. If the data compare within experimental accuracy, the field maps in the exposure plane should be taken. If not, the chamber should be checked for any metallic objects that might scatter the field. In small chambers, the problem might be due to reflections off the back or sidewalls.

Once the $1 / D^2$ data has been successfully completed the field is mapped over the subject exposure volume. The data read-out interval is dependent on the size of the subject. For a mouse, two readings, just in front of and just behind where the animal is to be exposed, would be sufficient. A rat might require 6 measurements, namely: nose, centerline, and tail, in front of and behind where the animal is to be exposed. If the animal is unrestrained the entire exposure volume should be mapped. A human or human phantom exposure requires a more detailed map

54

at 5 cm or smaller intervals in front of and behind, as well as along the centerline of the body to define the exposure condition. To avoid scatter off the subject, all incident power density measurements should be made without the subject.

2.4.1   Example of Use of Scientific Method

The 100-MHz Human exposure dosimetry experiment (Allen et al., 2003) is an example of how the scientific method was used in setting up an experiment. A half-wave dipole in a 90° corner reflector was excited with 100 MHz to provide the required exposure fields. The far field of this antenna was calculated to be 1.5 m. The hypothesis or expected field distribution at 2.25 m is a smooth rounded field with the maximum field occurring in the center of the scan. A scan was taken at 2.25 m and the results shown in Figure 2-6. These results obviously do not agree with the hypothesis with the highest field levels occurring on the perimeter of the scan instead of at the center, thus requiring further investigation.

Original 2.25 Meter Scan
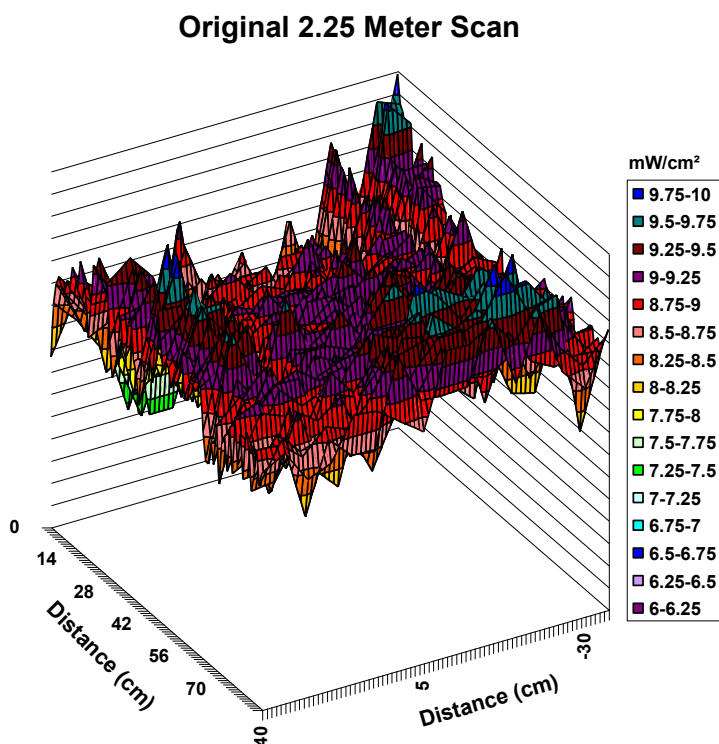
Figure 2-6. Scan results taken at 2.25 m.

The data in Figure 2-7 was obtained with the simplest measurement, i.e., drift at a fixed point. The hypothesis was that the instrument should not drift more than its guaranteed precision over a 7 − 10 min run in a fixed position. The data shows a 50% drift over seven minutes, thus: the conclusion that this is outside the normal range of accuracy. A new probe, cable, and read-

55

out were installed and the measurement repeated giving the results in Figure 2-8. The result of this measurement was ± 5% of the average, which was within the precision of the probe, thus: movement to the next step.

Stationary Drift Brooks 8762 Probe
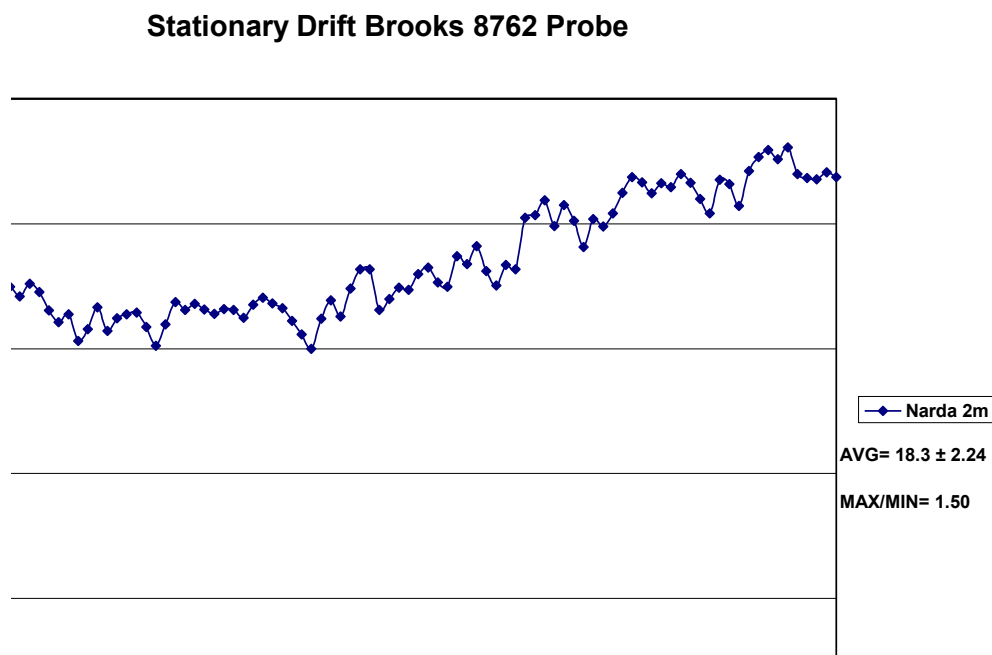
Figure 2-7. Stationary Drift Brooks 8762 Probe.

Stationary Drift NARDA 8762
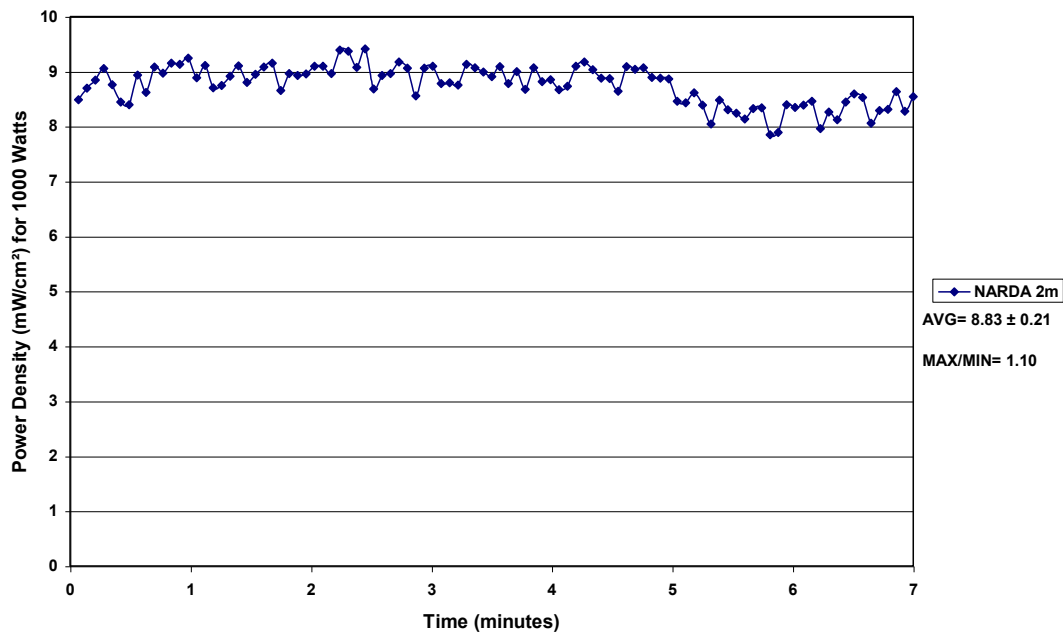
This probe was used to measure the power density as a function of distance from the dipole antenna. The result of the first set of measurements is shown in Figure 2-9. The power density should change as an inverse function of D^2, which was not the case for this measurement. The highest value of the field was measured at the farthest point from the antenna instead of the closest. It was hypothesized the cable behind the probe was approximately a half wavelength causing it to re-radiate the energy resulting in the observed pattern. The run was repeated with the cable normal to the E-field and the results are shown in Figure 2-10. These results are smooth and generally describe the expected field but do not follow the $1/D^2$. Another problem obviously exists.

57

Center Line Scan
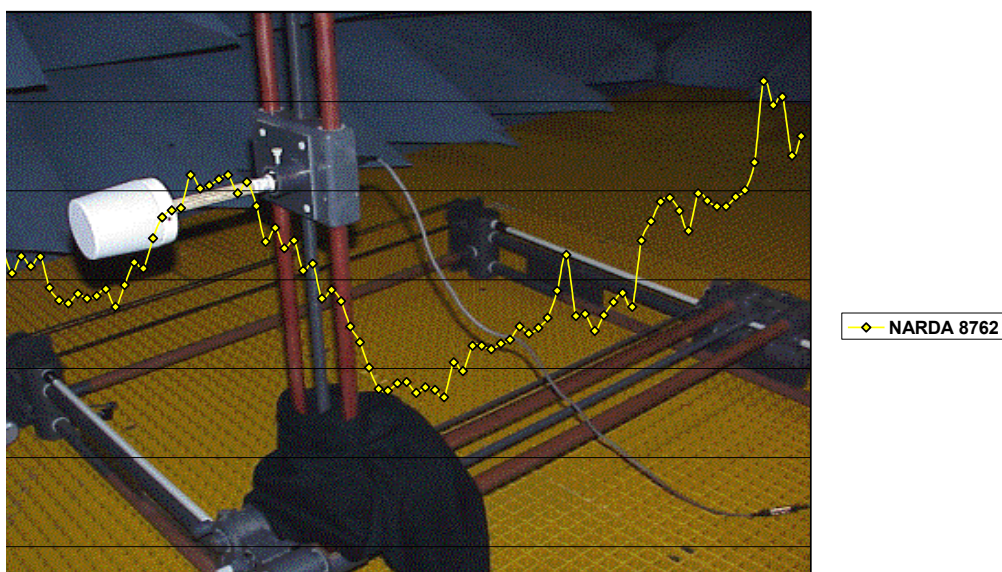
Figure 2-9. Result of first set of measurements.

Narda Cable Horizontal
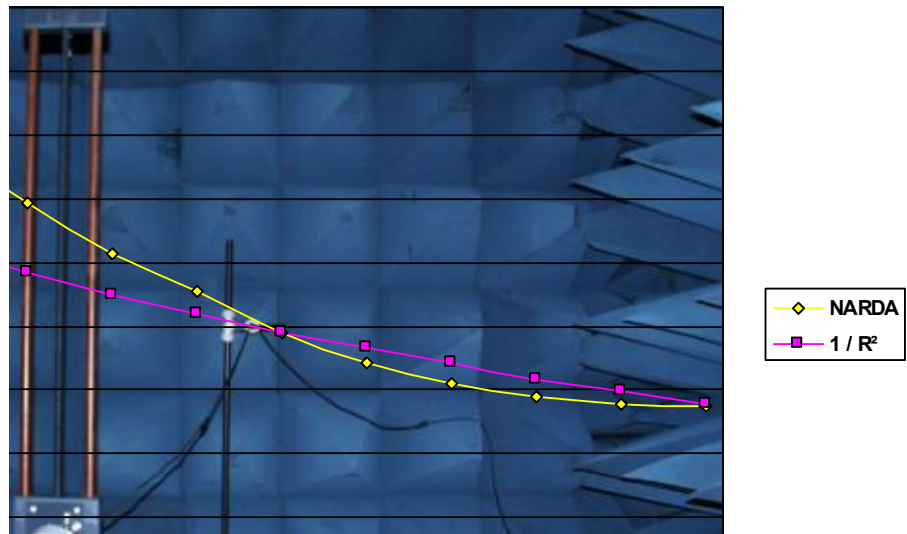
Figure 2-10. Results where run was repeated with the cable normal to the E-field.

Removing all cables from the field tested the hypothesis that the problem was due to conductors in the field. The air conditioner thermostat cable, which was located under the floor between the antenna and probe, was located and removed. After all cables were removed the measurement was repeated and the results are shown in Figure 2-11. These results are within the precision of the instrumentation, thus the conclusion that the $1/D^2$ condition has been met and the field map in the plane of exposure can now be accomplished.

...da Cable Horizontal- All Other Cables Removed
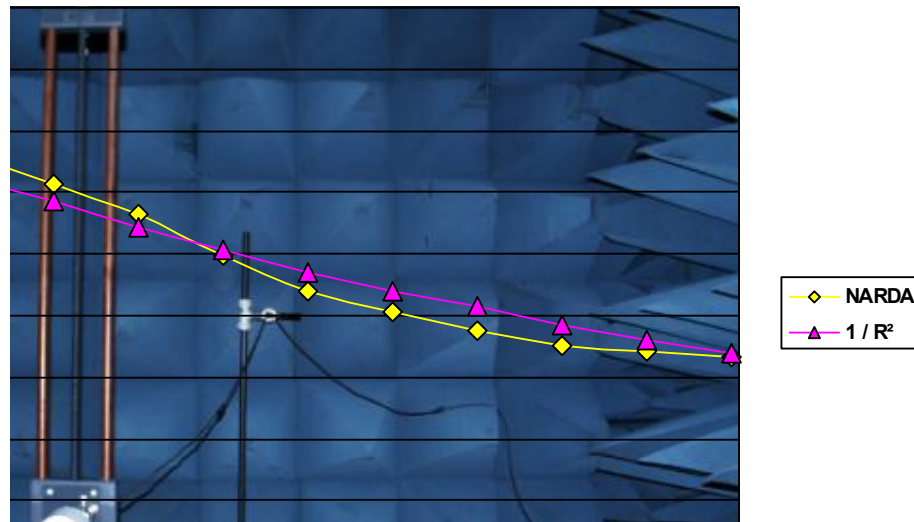
Figure 2-11. Results after all cables were removed and measurement repeated.

The field was scanned at 2.25 m from the dipole and the results presented in Figure 2-12. The shape of this curve and the values are within those expected. The exposure could be set on these values and the dosimetry report completed.

60
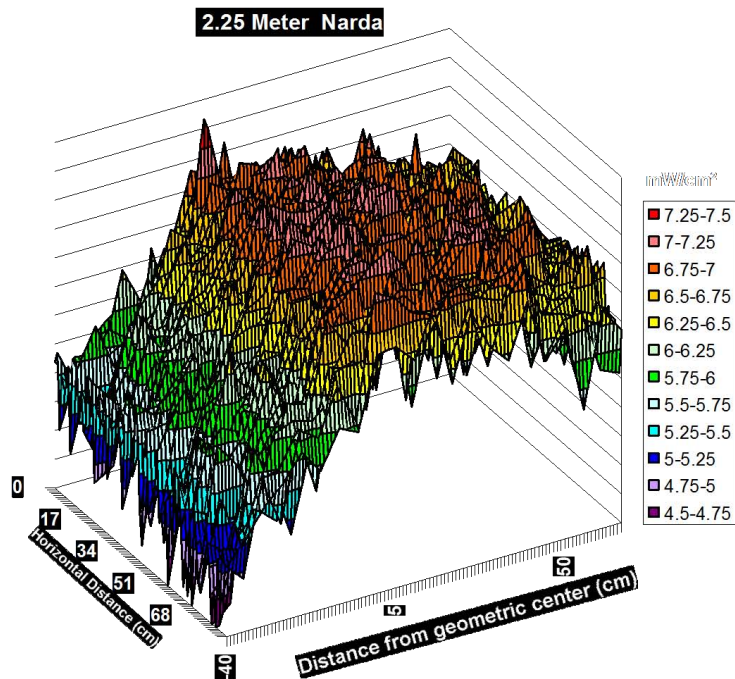
Figure 2-12. Results with field scanned at 2.25 m from the dipole.

2.5 Transverse Electromagnetic (TEM) Cells and Striplines

The TEM cell and stripline were devised to provide plane wave fields for long wavelength RF fields where extremely large anechoic chambers would be required to produce plane wave fields. These devices are useful at frequencies below 100 MHz where moderate sized chambers can produce uniform fields useable for small animals. For higher frequencies small anechoic chambers with dipole antennas or open-end waveguides are more suitable for uniform well-defined exposures. For both the TEM cell and stripline only the center third, both horizontal and vertical, of the device can be used to assure uniform exposures. If more than half of the space is filled, power can be capacitively coupled into the experimental subject resulting in extremely high peak SARs and SAR distributions not found in free field exposures. The field inside a TEM cell is shown in Figure 2-13. A group in Japan calculated these patterns using FDTD and posted the results on the Internet. These results can be found at: http://www2.crl.go.jp/ys/ys221/img/crl/D3-0e.html.

61

FDTD analysis of electromagnetic fields in a TEM-cell model shown below indicates the uniform area within -10% to + 10% of the nominal at the reference point is 1/3 of the separation between the outer conductor and septum.

Evaluation of a TEM-cell by using FDTD method
TEM-cell

Ex-field distribution

Electric field distribution in a TEM-cell

Ey-field distribution

Figure 2-13. Field inside a TEM cell.

A problem in using the stripline is that it radiates power into the area around it and if conductors or dielectric bodies are moved in the vicinity of the stripline the fields inside it can change. Because it is not a closed system, the SAR in a stripline cannot be determined by differential power measurement techniques. Since the stripline has no advantage and potentially more problems than a TEM cell or open-end waveguide, it should rarely, if ever, be used for biological experiments.

When higher-order modes and standing waves are not present, the E-field strength between the plates in the chamber can be found from:

$$E = V/d \tag{13}$$

where d = the distance from the septum to the outer wall, and

$$V = (PZ_o)^{1/2} \tag{14}$$

where V = the rms voltage between the center conductor and the outer conductor of the line; P = the input power in watts; and Z_o = the characteristic impedance of the chamber usually 50 Ohms.

The equivalent incident plane wave power density can be found from:

$$P_{inc} = E^2 / 3770 \text{ mW/cm}^2 \tag{15}$$

with the E-field in rms V/m.

Fields inside the TEM cell should be measured using appropriate E-field and H-field probes and the whole-body SAR determined by differential power techniques.

2.6   SAR Measurement

The SAR measurement is very useful in dosimetry. In cases where nonuniform exposures occur or where incident-power density cannot be measured, SAR is the only measurement that allows definition of the RF exposures. There are five basic techniques for measuring the SAR in biological systems and phantoms:

1. Differential power measured in a closed exposure system

2. Rate of temperature change in the biological test subject measured with noninterfering probes

3. Calorimetric techniques

4. Thermographic techniques

5. Implantable E-field probes

63

The latter four methods are also suitable for near-field SAR measurements.

2.6.1   Differential-Power Technique

For the differential-power technique, use directional couplers and power meters on all input and output ports of the exposure device. In the case of waveguide and TEM-mode exposure devices, monitor the input, output, and reflected powers and determine the absorbed power by:

$$P_E = P_I - P_O - P_R \tag{16}$$

where P_E = power (watts) absorbed by empty exposure device; P_I = input power (watts); P_O = output power (watts); and P_R = reflected power (watts).

Place the sample in the exposure device and determine P_S, the power absorbed by both the sample and exposure device, in a similar manner. Determine the total absorbed power for the sample by taking the difference between P_E and P_S. To determine the SAR, divide the total absorbed power by the mass of the sample.

The accuracy of these measurements can be improved by electronically measuring differential power i.e., using a differential amplifier or, for even more accuracy, digitizing the power meter readings to be stored in a computer. Controlling temperature of the couplers and power meter heads also will improve the stability of the measurements.

The fields in a circular waveguide system can be quantified by differential-power determination of the SAR in the animal being exposed. To do this, subtract from the input power, the power reflected out of the two transmitting and the two output ports. This requires five power meters.

2.6.2   Noninterfering Temperature-Probe Techniques

RF noninterfering probes can be used to determine SAR distributions in realistic phantoms, cadavers, and live animals. High-resolution systems using thermistor detectors on high-resistance lead wires can reliably measure 0.01 °C temperature changes in high-level RF fields. Lossy-line systems work best for frequencies above 100 MHz. For high fields below 100 MHz, line burnout may be a problem. Fiber-optic readouts are usable across the RF spectrum with minimal interference problems, but these instruments are not as stable as thermistor based units. Having the most sensitive technique possible is important if SAR distribution is to be measured. Less sensitive techniques require larger temperature rises, and more smearing of the SAR pattern will occur. Therefore, keep exposure time to a minimum to obtain minimum error from heat flow within the subject. Measure temperature rises in °C per minute; and for tissue and tissue-equivalent material, convert these data to SAR by

$$1 \text{ °C/min} = 58.6 \text{ W/kg} \tag{17}$$

which is based on a specific heat of tissue of 0.84. For liquids with a specific heat of 1, the conversion is 1 °C/min = 69.8 W/kg.

This measurement technique is the most accurate for assessing SAR distribution in phantoms and cadavers, allows temperature regulation to be measured in live animals, and is inexpensive. The major disadvantage is the time required to define the SAR in large or complex geometrical bodies.

2.6.3   Calorimetric Techniques

Calorimetric techniques prove extremely useful in measuring whole-body SAR for animal phantoms and cadavers. The two techniques in use are Twin-well and Dewar calorimetry.

Twin-well calorimetry yields accurate results and requires little effort from the experimenter after initial setup and calibration. Difficulties include long run times for making one measurement (approximately 1 day for a large rat), complexity of multiple thermocouple readouts that make it difficult to detect failure in one or two thermocouples, and relatively high cost.

The Dewar calorimeter technique is relatively inexpensive, is simple (calibration and operation anomalies are easily resolved), and requires a relatively short time for one reading (from 30 min for a mouse to 1 h for a rat). Accurate SAR determinations can be made with this technique, but they require experimenters to exercise extra precautions.

To check for heat loss during exposure, compare an SAR measurement immediately after exposure with a measurement that was delayed by a period equal to the exposure time. Water is usually used as the heat transfer medium. Use just enough water to allow total immersion of the cadaver. Adjust the water temperature to approximately 0.5 ℃ below the ambient air temperature; and after inserting the exposed animal, adjust the resultant temperature by varying exposure time to obtain a temperature rise of approximately 1 ℃. This achieves maximum stability in terms of calorimeter drift. When thermal equilibrium is reached (i.e., when the change in temperature is less than 0.01 ℃ during a 15-min period), measure the final temperature, T_F and use it to evaluate T_e for each cadaver:

$$T_e = [(Z_p + M_e\, C_e)(T_F - T_i\quad)]/(M_s\, C_s) + T_F \qquad (18)$$

where T_e = rationalized temperature of the cadaver upon insertion in the calorimeter; M_s = mass of the cadaver (kg); C_s = specific heat of the cadaver (J·kg^{-1}· K^{-1}); M_e = mass of water in calorimeter (kg); C_e = specific heat of water (J·kg^{-1}·K^{-1}); T_i = temperature of calorimeter just before insertion of cadaver (℃); T_F = final temperature of calorimeter (℃); and Z_p = heat capacity of calorimeter (J·K^{-1}).

The SAR in W/kg is determined by

$$SAR = C_s\, (T_e\, (exposed) - T_e\, (control))/\text{exposure time in seconds}$$

where $C_s = 3448$ for a rat or mouse and $C_e = 4185$.

65

The readout of the calorimeter can be automated by direct computer readout. This also facilitates computations.

2.6.4   Thermographic Techniques

A scanning thermographic camera can be used to provide detailed SAR distribution in phantoms and cadavers in a short time. Suitable material to separate sections of the phantom or cadaver must be used, and readout after termination of exposure must be rapid. If the output of the thermographic camera is put into a computer, average SAR can be easily computed. Personnel at the University of Washington have developed this technique, which is described in detail by Guy (1971). The technique has proven valuable in assessing SAR distribution for laboratory animals and models of man. The procedure originally involved using a thin sheet of plastic to facilitate separating the halves of the phantom, thus the procedure was limited to symmetrical models exposed to a linearly polarized field (E-field parallel to the interface) to avoid interrupting any induced currents that would normally flow perpendicular to the median plane of separation. For near-field measurements, however, the procedure was modified by replacing the plastic sheet with a silk screen, thus allowing easy separation without loss of electrical continuity Guy et al., (1975). The major disadvantage of this technique is the high cost of the required equipment.

2.6.5   Implantable Electric-Field Probes

Miniature electric-field probes with fiber-optics readout were developed by Bassen et al., (1977). Orthogonal probes are commercially available from SARTEST Ltd. located in Newdigate, UK. This system can be used to determine the E-field in a cadaver or phantom exposed to RF fields. SAR can be determined if the E-field is measured and the dielectric properties of the subject are known using the following equation:

$$SAR = \sigma E^2 / \rho_m \qquad (19)$$

where σ = effective conductivity (S/m); E = RMS electric field (V/m); and ρ_m = density of the subject (kg/m^3).

The advantages of this technique include instant readout (allowing SAR distribution to be determined by scanning techniques) and accurate measurements in low-level fields (this technique being at least 10 times as sensitive as any technique previously discussed). The primary problems include probe rigidity (requiring straight insertion into the subject) and frequency-range limitation. The use of orthogonal probes simplifies measurements, but single-axis probes can be used if they can be rotated to obtain three orthogonal readings.

2.7   Experimental Monitoring

During all dosimetry measurements as well as subject exposures, measurements of transmitter output and reflected power should be recorded at regular intervals. If possible, a field-monitoring instrument should be utilized to track field levels before and during dosimetry and subject exposures. All meters on the transmitter should be read at regular intervals. If all of

these measurements remain constant the experimental accuracy is assured. If deviation is detected in one or more of these measurements, an investigation into the cause should be undertaken before the experiment proceeds.

2.8   Report the Results

The last step of any dosimetry program is to report the findings. Enough detail should be included to allow others to repeat the measurements. Following the scientific method the test procedure should be well defined, the results clearly presented, and the conclusions concisely stated. This coupled with an equally precisely executed biological protocol results in data of great value to the scientific community.

2.9   References

Allen, S. J., Adair, E. R., Mylacraine, K. S., Hurt, W., & Ziriax, J. (2003). Empirical and theoretical dosimetry in support of whole body resonant RF exposure (100 MHz) in human volunteers. *Bioelectromagnetics, 24*(7).

Bassen, H., Herchenroeder, P., Cheung, A., & Neuder S. (1977). Evaluation of an implantable electric-field probe within finite simulated tissues. *Radio Science, 12*(06S), 15-25.

Durney, C. H., Massoudi, H., & Iskander, M. F. (1986). *Radiofrequency Radiation Dosimetry Handbook, Fourth Edition* (Report USAFSAM-TR-85-73). USAF School of Aerospace Medicine, Brooks AFB, TX.

Gajsek, P., Walters, T. J., Hurt, W. D., Ziriax, J. M., Nelson, D. A., & Mason, P. A. (2002). Empirical validation of SAR values predicted by FDTD modeling. *Bioelectromagnetics, 23*, 37-48, No. 1.

Guy, A. W. (1971). Analysis of electromagnetic fields induced in biological tissues by thermographic studies on equivalent phantom models. *IEEE Transactions on MIT, 19*, 205-214.

Guy, A. W., Webb, M. D., McDougall, J. A. (1975). A new technique for measuring power deposition patterns in phantoms exposed to EM fields of arbitrary polarization -- example, the microwave oven. *Proceedings for Microwave Power Symposium,* pp. 36-40. University of Waterloo, Waterloo, Ontario, Canada.

Guy, A. W. (1997). *Dosimetry of radiofrequency electromagnetic fields: Examples of results using numerical methods.* Health Physics Society Summer School Course on Non-Ionizing Radiation. San Antonio, TX.

Kunz, K. S. & Luebbers, R. J. (1993). *The finite-difference time-domain method for electromagnetic.* Boca Raton, FL: CRC Press.

Mason, P. A., Hurt, W. D., Walters, T. J., D'Andrea, J. A., Gajsek, P., Ryan, K. L., Nelson, D. A., Smith, K. I., & Ziriax, J. M. (2000). Effects of frequency, permittivity, and voxel size

on predicted specific absorption rate values in biological tissue during electromagnetic-field exposure. *IEEE Transactions on Microwave Theory and Techniques*, *48*(11).

68

Radio Frequency Radiation Dosimetry Handbook
(Fifth Edition)

Chapter 3.   **A Practical Guide to High-Resolution Thermometry and Microdosimetry in Pulsed Electromagnetic Fields**

Andrei G. Pakhomov
Frank Reidy Research Center for Bioelectrics,
Old Dominion University, Norfolk, VA

Andrei@pakhomov.net

3.1   Basic Terms and Definitions

Exposure of biological objects to electromagnetic fields (EMFs) gives rise to diverse bioeffects. Depending on the physical parameters of the applied field and studied biological endpoints, these bioeffects are conventionally divided into ―thermal‖ and ―non-thermal‖ categories. Thermal bioeffects, by definition, are a result of temperature rise caused by EMF absorption in tissues. Thermal effects in general are similar to the effects of conventional heating and can be attenuated by proper cooling of the object (although cooling by itself has no appreciable effect on EMF absorption). In practice, however, EMF exposure can produce spatial and temporal heating transients which are difficult or impossible to reproduce by conventional heating, leading to so-called ―specific‖ EMF bioeffects, such as microwave hearing (Lin, 1978).

In contrast, authentic non-thermal bioeffects, such as electroporation, are produced directly by the effect of electromagnetic field forces. These effects may be quantitatively and qualitatively different from known effects of temperature rise, and simple removal of the excessive heat produced by the field interaction with the biological system does not prevent or attenuate non-thermal effects.

In practice, it may be difficult to distinguish between thermal, specific thermal, and nonthermal effects. The existence of many alleged non-thermal effects and their physical nature remain the hottest topic in bioelectromagnetics, despite several decades of research.

In any biological experiment involving EMFs, and regardless of the particular mechanisms of how bioeffects are produced, the ―extent‖ of EMF interaction with the living object has to be characterized by certain metrics. The specific absorption rate (SAR, W/kg) is a convenient and universal metric for many types of EMF exposure, and it is defined as:

$$SAR = \sigma E^2 / \rho_m \tag{1}$$

where E is the induced electric field in tissue (V/m), σ is the electrical conductivity of the tissue (S/m), and ρ is the mass density of the tissue (kg/m^3).

Being a measure of the rate of energy transfer from the field into the tissue, SAR can also be conveniently estimated indirectly, from the rate of temperature rise in tissue under exposure. With the assumption that all the absorbed field energy is transformed into heat, and disregarding any heat dissipation, SAR (W/kg) at any location in the tissue is measured as:

$$SAR = c\Delta T/\Delta t \qquad\qquad (2)$$

where ΔT is the temperature increment (^{o}C), c is the specific heat capacity of the tissue (J/(kg x ^{o}C)), and Δt is the duration (sec) over which ΔT is measured. In practice, ΔT has to be measured over as short as possible time interval immediately after the onset of exposure, when the heat dissipation is minimal and can be disregarded.

Over time, SAR has been widely accepted as the principal exposure metric for many types of EMFs, particularly for radio frequency (RF) and microwave radiations. Nonetheless, several misconceptions exist. First, close connection between SAR and heating may be misinterpreted as a synonymy of these two parameters. Proponents of this position tend to disregard the fact of heat dissipation and obvious facts that the temperature can be intentionally kept the same or even lowered even at very high SAR values. The ―opposite‖ misconception is interpretation of any temperature rise as resulting directly from EMF energy absorption, whereas it could also be a result of conventional heat transfer from adjacent areas where the EMF absorption actually occurred.

Precise measurement of local temperature rise in objects exposed to intense pulsed EMFs is a complex technical problem. However, when performed correctly, these measurements provide information which is critical for correct interpretation of biological data. Moreover, such temperature measurements can provide the basis for a fast and elegant measurement of local SAR, with high precision and spatial resolution that exceeds the limits of other known methods.

3.2   Instruments and Techniques for Local Temperature Measurements in Intense Pulsed EMFs

3.2.1   General Considerations

One critical feature of thermometers intended for measurements during EMF exposure is their EMF compatibility, which has two different components. First, thermometers that have an electrical circuitry may be vulnerable to EMF pick-up: the electronic measurement circuitry, wire leads, and temperature probes may function as antennas, and erroneously report the detected electrical signal as a change in temperature. These artifacts can be minimized or eliminated by using thermometers equipped with remote sensors, and moving the electronic measurement circuitry to outside of the field; by aligning the wire leads perpendicular to the E-vector of the field and by shortening them; by using high-resistance wires; by reducing the physical dimensions of temperature probes; or by using non-metal temperature probes and connectors, as in fiber optic thermometers.

70

Another problem of EMF compatibility results from the fact that temperature sensors have dielectric properties which are very different from those of biological tissues and samples. Therefore, just the insertion of the probe into the sample may change EMF absorption and heating compared to the situation when no probe was present. It has been a common knowledge that metal probes may alter the local field and therefore should be avoided. However, it is much less known or appreciated that dielectric non-uniformities (e.g., plastic probes or air bubbles in biological samples) can also cause profound local field distortion (Alekseev & Ziskin, 2001), leading to erroneous measurements (an example of such behavior will shown in Figure 3-6 and discussed later). Perhaps the best practical way to reduce artifacts from introduction of temperature probes into EMF-exposed samples is reducing the size of probes.

Hence, minimization of temperature probes improves their EMF compatibility by decreasing both the EMF pick-up (by metal probes) and by decreasing the field distortion (by both metal and non-metal probes). In addition, using small probes has a number of other advantages. Smaller probes can be positioned in biological samples with less damage to surrounding tissues. Smaller probes have lower heat capacity, which means more accurate and faster reading of temperature changes (and the fast response is perhaps the most critical feature for using them in pulsed EMF dosimetry, see section 3.2.2). Finally, smaller probes have greater spatial resolution for temperature and SAR —mapping" within the exposed sample.

Using miniature temperature probes connected to a remote electronic circuitry for temperature reading and recording of measurements is a must for high-resolution local thermo- and dosimetry; however, other salient features of such thermometers need to be taken into account. These features include fast response and low noise of the electronic circuitry, good sensitivity, stability and accuracy of readings over time. Also, miniature temperature probes may be fragile and costly to replace.

3.2.2   Selection and Availability of Temperature Probes

A selection of miniature temperature probes that are (or have been) available on the market is shown in Figure 3-1.

VITEK model 101 Electrothermia Monitor is a thermistor probe that was manufactured by BSD Medical Devices, Salt Lake City, UT. Based on the original design by Bowman (1976), it became the first commercially available —non-field-perturbing" temperature probe. With the sensor size of about 1 mm, it has the sensitivity of about 5 mK and characteristic response time of about 240 ms (Burkhardt et al., 1996). This inexpensive probe has been employed widely in biological studies (Adair et al., 1984; Adey et al., 2000; Burr & Krupp, 1980; Chou et al., 1985; Galvin & McRee, 1986; McRee & Davis, 1984; Nawrot et al., 1985; Spiers et al., 1989) and remains in use in some laboratories, although its commercial production has been discontinued.

71
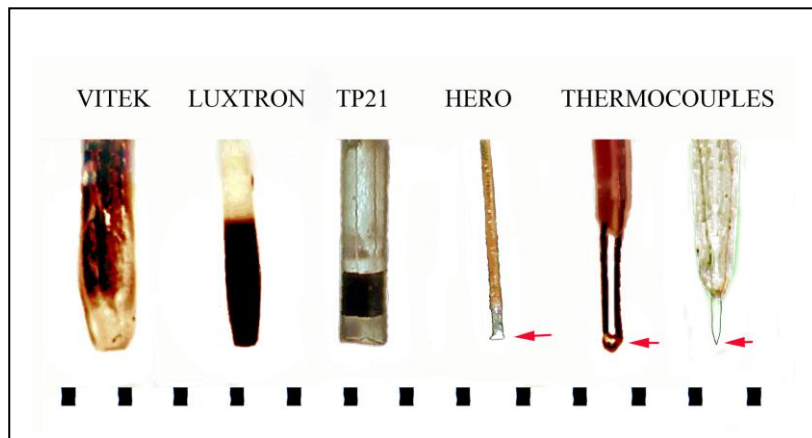
Figure 3-1. The appearance and comparative dimensions of some commercially-available temperature probes. The ruler divisions are 1 mm. For the smaller probes, the temperature-sensing element is identified by an arrow. See text for more information.

Different models of fluoroptic thermometers have been manufactured since 1978 by Luxtron Corporation (Santa Clara, CA). Fluoroptic temperature sensing is based on the fluorescence decay time of a special thermo-sensitive phosphorescent (phosphor) sensor, located at the end of a fiber optic cable. Despite their much higher cost compared to VITEC, Luxtron fluoroptic thermometers have also been popular among experimenters (Adair et al., 1992; Braithwaite et al., 1991; Kojima et al., 2004; Moriyama et al., 1991; Saalman et al., 1991; Shellock et al., 1989; Tattersall et al., 2001). Depicted temperature probe is from a Luxtron 850 model thermometer. With this device, the maximum measurement rate was about 30 samples/sec; however, at this rate, sequential measurements of a constant temperature could vary by as much as 0.5-1 °C (Pakhomov, Mathur & Murphy, 2003). Averaging of sequential measurements reduced the "noise," but also reduced the temporal resolution. Other authors reported a noise level of 100–250 mK and a response time of 250 ms for a 700-series Luxtron thermometer (Schuderer, 2004). Newer Luxtron fluoroptic thermometers with improved technical characteristics are now available (www.luxtron.com), with the smallest sensor being 0.5 mm in diameter.

TP-21-MO2 is a different type of a fiber optic sensor that is utilized in a REFLEX thermometer that was made by Nortech Fibronic Inc. (Quebec, QC, Canada). The manufacturer's specified temperature resolution is 0.1 °C and the probe's response time is 0.3 sec. The exact principle of operation of this probe has not been disclosed. Same as Luxtron and HERO temperature probes, TP-21 is completely immune to EMF pick-up. The highest acquisition rate by the REFLEX thermometer is limited to only 4 samples/sec; however, in our experience, the stability of readings over time and reproducibility of measurements were notably better than in the other tested fiber optic thermometers (Luxtron 850 and Veloce). REFLEX thermometers are no longer available on the market.

72
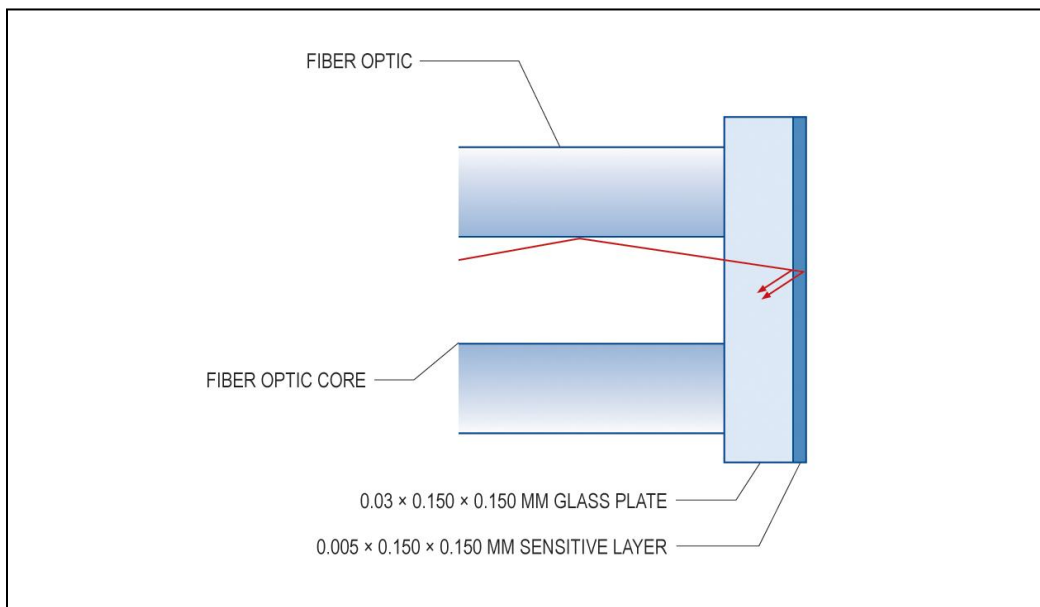
Figure 3-2. Detailed design and dimensions of the HERO fiber optic temperature sensor. Light reflections occur at the inner and outer layers of the sensitive layer. The diagram was kindly supplied by FISO Technologies, Inc. (Quebec, QC, Canada) and published with their permission.

FOT-HERO fiber optic probe manufactured by FISO Technologies (Quebec, QC, Canada) is by far the smallest and the fastest on the market. It utilizes a new technology of Fabry-Perot white-light interferometry (Choqueta et al., 2000). The heat-sensitive element is just a 5-μm thick film of SiH at the tip of the fiber optic cable (Figure 3-2), and the absolute change in the thickness of this film due to thermal expansion is measured with a help of a Veloce signal conditioner (up to 200 kHz sampling rate). HERO probe has an outstanding response time of less than 1 ms and the resolution of 0.03 °C at 1-ms averaging time (see www.fiso.com). The probe is indispensable for unique high-speed temperature measurements; its advantages, however, are somewhat offset by the high cost, fragileness, and appreciable sensitivity of temperature readings to the positioning and bending of the fiber optic cable.

Pre-manufactured thermocouples of various sizes are available, for example, from Omega Engineering Inc. (www.omega.com). Shown thermocouples are made of 125-μm (left) and 25-μm (right) copper and constantan wires (T-type thermocouples); the smaller one will be regarded below as a microthermocouple (MTC). Thermocouples, as well as leads connecting them to amplifiers or other devices, are not ―non-field perturbing." They may affect local field distribution just by the virtue of their presence in the field, and the field-induced currents may heat the thermocouple junction or affect the amplifier directly, producing erroneous readings. The response time in the smallest thermocouples is comparable to that of the HERO probe (e.g., it is 2 ms in MTC), which makes them a valuable tool for dosimetry applications described below.

When proper measures are taken to minimize possible EMF pick-up artifacts, thermocouples may be a convenient and inexpensive alternative to fiber optic thermometry, and they have often been employed in EMF bioeffects studies (Dunscombe et al., 1988; Dunscombe

73

et al., 1986; Gammampila et al., 1981; Gerig et al., 1992; Haveman et al., 2003; Moriyama et al., 1988; Pakhomov & Doyle, 2000; Pakhomov et al., 2002a; Pakhomov et al., 2000a; Pakhomov et al., 2000b; Pakhomov, Mathur & Murphy, 2003).

3.2.3 Comparative Evaluation of Temperature Probes' Performance Under a High Intensity Pulsed Microwave Exposure

3.2.3.1 Microwave Exposure Setup

We utilized the same setup that was employed previously (Pakhomov et al., 2003; Pakhomov et al., 2002a) for in vitro exposure of small biological objects to extremely high peak power microwave pulses (EHPP). EHPP were generated by either an MH300 system with an MF-IM65-01 RF plug-in (Epsco Inc., Itasca, IL), or by a model 337X magnetron transmitter (Applied Systems Engineering, Inc.). The following EHPP exposure parameters were used in this study: carrier frequency between 9 and 10 GHz (typically 9.6 GHz), peak output power 75-115 kW (MH300) or 230-260 kW (337X), pulse width from 0.5 to 2 μs, isolated pulses or brief pulse trains with up to 1 kHz repetition rate.

A separate transmitter (HP 8690A sweep oscillator with Hughes 8020H amplifier) was used to generate microwave pulses of the matching carrier frequency, but longer pulse duration (1-100 ms) and lower peak power (<20 W). Microwave pulses were transmitted via a waveguide (WR90, 22.86 x 10.16 mm) to a custom-made exposure chamber, which was mounted atop a waveguide flange and filled with a saline. The waveguide opening was sealed with a sapphire matching plate, flush with the flange (Figure 3-3). Incident and reflected powers in the waveguide were measured via directional couplers by an HP 438A power meter using HP 8481A power sensors. Reflection from the exposure chamber into the waveguide was less than 3%. EHPP shape was nearly rectangular, as monitored via an HP 432 detector on a TEK 2430A digital oscilloscope.
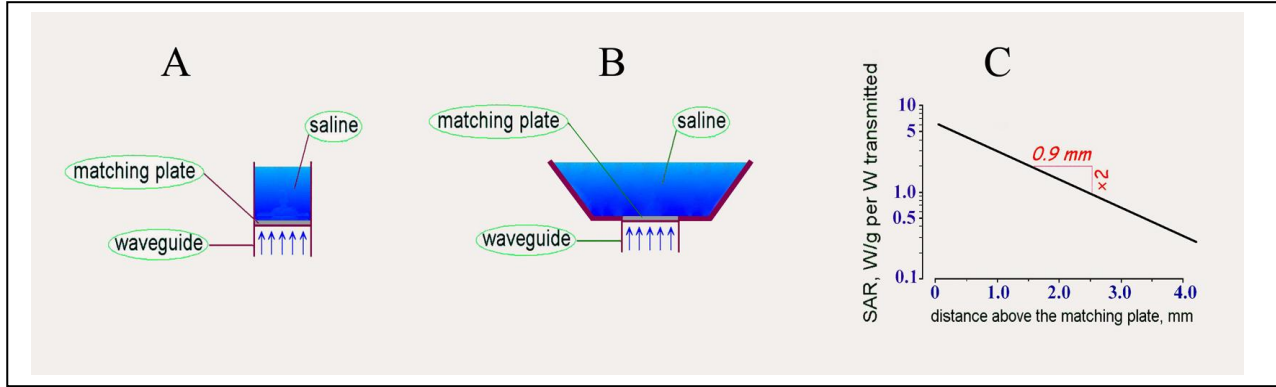
Figure 3-3. **Basic design of the exposure chamber that was employed in microdosimetry and the thermometry experiments. A, the original design after Chou and Guy (1978), and B, the modified design with improved access to the area immediately above the matching plate. C, calculated absorption in the saline along the axis of the waveguide as a function of distance above the matching plate. Calculations were performed using Equation 3 for 9.5 GHz at 25 °C. Note that local SAR decreased exponentially with the distance above the plate, at a rate of about twofold per 1 mm. With the saline depth of 10-20 mm, the microwave radiation intensity at the surface was attenuated by a factor of 2^{10}-2^{20}, so any microwave leakage to the outside of the exposure chamber and backward reflection from the saline air interface could be discarded.**

3.2.3.2 Exposure Chamber Design and Analytical Evaluation of Local SAR

Initially, the design of the exposure cell was similar to the one proposed by Chou and Guy (1978), Figure 3-3A. A vertical section at the end of the waveguide was separated by a quarter-wave matching plate and filled with saline. The waveguide walls in the cell were covered with a lacquer to prevent its electrical contact with the solution and possible corrosion. Complex dielectric constant of this solution at 9.3-9.7 GHz and at various temperatures was calculated by equations given by Stogryn (1971). With the solution normality of 0.12-0.14, its relative permittivity (ε_r) and conductivity (σ) at 25 °C were calculated as 63.4 and 15.9 S/m, respectively. To verify the calculations, the dielectric properties of the solution were also obtained experimentally using an HP 8510 measurement system (see Bao et al., 1996) for detailed procedures). Measured values (ε_r = 63, σ = 16 S/m) were virtually the same as the calculated ones. The respective linear loss coefficient of the solution was 3.71 Np/cm.

SAR in the solution along the axis of the waveguide decreased exponentially with increasing the distance above the matching plate, and could be calculated according to Chou and Guy (1978) as:

$$\text{SAR} = (1/\rho) \, \frac{2(P_i - P_r)}{S} \, 2\alpha e^{-2\alpha z} \quad \text{(W/g)} \tag{3}$$

where ρ is the saline density (g/cm^3). P_i and P_r are the incident and reflected power values (W; their difference will be regarded below as a "transmitted power"), S is the cross-section of the waveguide (2.32 cm^2), α is the linear loss coefficient in the saline (Np/cm), and z is the distance above the matching plate (cm). Based on this equation, a power of 100 kW transmitted to the

75

exposure cell would produce SAR values of 610, 304, 145, and 69 kW/g at the distances of at 0, 1, 2, and 3 mm above the plate, respectively (calculated for 9.5 GHz and 25 $^{\circ}$C). In other words, SAR in the saline decreased approximately twofold per millimeter.

In the later experiments, the waveguide walls beyond the matching plate were removed to form a larger reservoir (Figure 3-3B) with better access from the sides to the area where the SAR was the highest (immediately above the matching plate, along the axis of the waveguide). The entire reservoir was filled with the saline; because of shallow microwave penetration into the saline at the employed microwave frequencies, the removal of waveguide walls had no measurable effect on SAR in the chamber along the waveguide axis or in its immediate vicinity.

For testing of temperature probes, they were positioned 0.5-2 mm above the center of the matching plate. Peak SAR at this location reached 0.3-0.8 MW/g for EHPP and 5 to 50 W/g for millisecond-range pulses. Accurate measurement of local temperature and SAR in such a high-intensity pulsed microwave field and within a steep field gradient is perhaps among the most challenging tasks in practical microdosimetry. This is exactly the reason why we chose such ―unfavorable" conditions to compare the performance of different temperature probes and to evaluate their applicability for EMF microdosimetry.

3.2.3.3 Temperature Measurements

Three probes were selected for comparative evaluation of their performance under the extreme conditions of microwave exposure described above. The probes were (1) TP-21 with a REFLEX thermometer, (2) HERO with a VELOCE signal conditioner, and (3) a copper-constantan MTC (25-um wires), connected to a DAM50 DC amplifier (WPI) via a cold junction compensator (Omega). Zero DC level of the amplifier output was regularly checked with a model 181 nanovoltmeter (Keithley Instruments, Inc. Cleveland, OH) and was adjusted whenever a measurable drift was detected. Within a narrow range of temperature changes employed in this study (<10 °C), the inherent non-linearity of the thermocouple readings was negligible and could be disregarded.

For convenient handling, MTC was fixed in a custom-made glass holder. Bare wires ending with the thermocouple junction extended from the holder by 1-2 mm; they were covered with a lacquer for electrical insulation from the saline. The lacquer coating was made as thin as technically achievable, under a visual control using a microscope.

The three probes were positioned in the exposure chamber so that they were touching each other at the same level, 1-1.5 mm above the center of the matching plate. The precise and well-reproducible positioning was accomplished by means of three separate micromanipulators, and was controlled via a dissection microscope. To allow for the visual control of the probes' positions, they had to be inserted at about 45° angle to the field propagation vector (although strictly vertical insertion could have reduced EMF pick-up by MTC leads and decrease field distortion by other probes).

The outputs of the REFLEX thermometer, VELOCE signal conditioner, and DAM50 amplifier were connected to analog inputs of a BIOPAC MP100 Data acquisition system (WPI).

76

The calibration factor in each channel was fine tuned to obtain exactly identical temperature readings from the three probes (Figure 3-4). All temperature readings were monitored and stored on a PC.
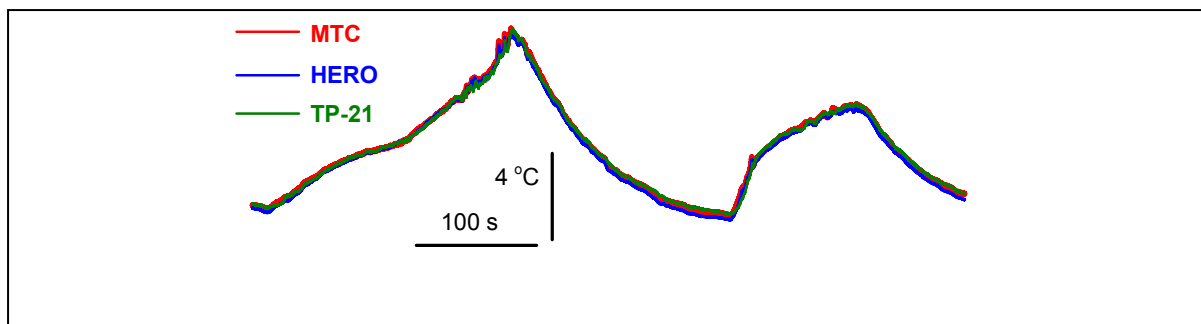
Figure 3-4. Concurrent recording of temperature changes by the MTC, HERO, and TP-21 temperature probes. The probes are brought together in the exposure chamber by means of three micromanipulators. The temperatures changes were caused by arbitrary additions of hot and cold saline into the exposure chamber (no EMF exposure), and were recorded using a BIOPAC data acquisition system. The goal of this experiment was to verify the identical calibration of the temperature probes and thermometers employed. See text for more detail.

3.2.3.4 Probes' Performance Under "Regular" Microwave Exposure

These experiments were performed using relatively long pulses (10-100 ms) at the transmitter output power less than 20 W. Calculated peak SAR values at the location of temperature sensors were within 10-40 W/g; the time average SAR values varied widely depending on the pulse repetition rate and duty cycle.

The ability of the probes to produce correct temperature readings during microwave irradiation was evaluated in two ways: (1) the probe's reading should match the concurrent readings of the other probes, and (2) the presence of the probe in the exposure chamber in the vicinity of the other probes should not affect readings of these probes.

When MTC and HERO were positioned in the exposure chamber together (in the absence of the TP-21 probe), their response to microwave heating was almost identical (Figure 3-5). Removal of the MTC from the exposure area had no effect on the HERO readings, indicating that possible field distortion and additional microwave heating in the vicinity of the MTC were negligible.

77
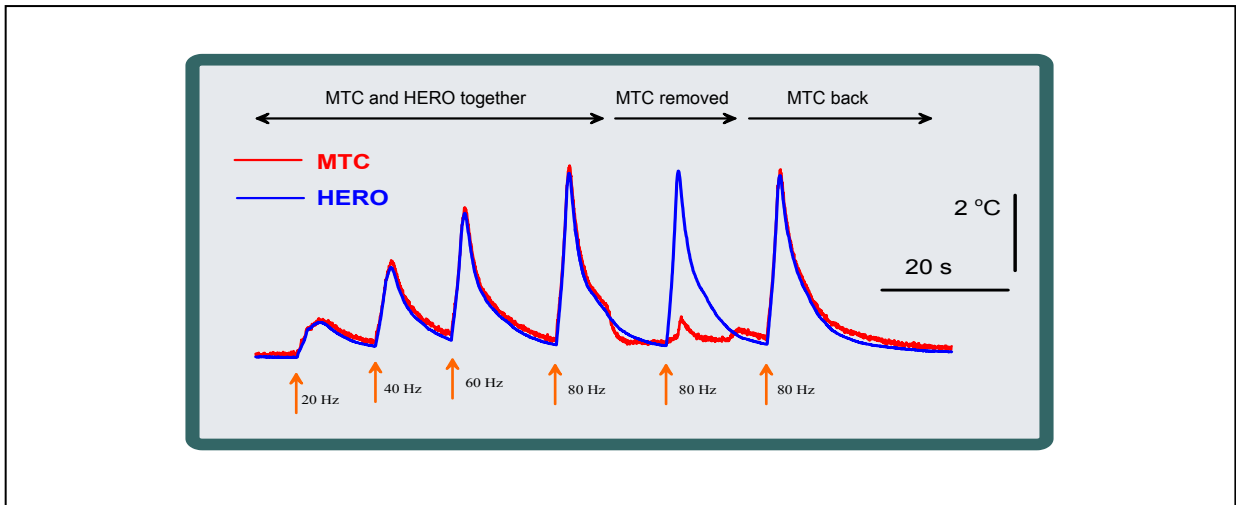
Figure 3-5. Readings of the temperature rise by a HERO probe and by an MTC positioned together in the exposure chamber. Exposures (shown by arrows): 2-sec trains of 10-ms pulses at different repetition rates, 15.5 W peak power output (peak SAR ~ 35 W/g). Note that withdrawal of the MTC had no effect on HERO readings in response to a microwave exposure. (When withdrawn, the MTC was at an arbitrary remote location within the exposure chamber; its readings during the "removed" time interval can be disregarded.)

Peak heating reading by the MTC could be slightly higher (Figure 3-5) or slightly lower (e.g., exposures ## 5 and 7 in Figure 3-6) than respective concurrent readings of the HERO readings probe. The reason for these small differences has not been fully understood; they could be caused by such factors as slightly uneven positioning of the probes relative to the irradiator; different size, shape, and material of the probes, leading to unequal field distortion and absorption changes in their immediate vicinity; different heat dissipation via the leads; or a combination of thereof.

The situation changed dramatically when the TP-21 probe was positioned in the immediate vicinity of the two smaller probes (Figure 3-6). Not only the TP-21 probe detected much higher temperature rise than two other probes, but it also affected the other probes' readings: The temperature rise reported by HERO and MTC in the presence of TP-21 was notably higher compared to the same exposure in the absence of TP-21. The difference of TP-21 readings from those of HERO and MTC could be as high as 5 °C and the effects of the withdrawal and re-introduction of the TP-21 probe on the readings of two other probes were well-reproducible.

In other experiments, TP-21 probe was deliberately positioned 0.5-1 mm above the other two probes, i.e., father away from the matching plate. Despite considerable additional attenuation of the field at these locations, readings of TP-21 were higher or just equal to those of the other probes.

78
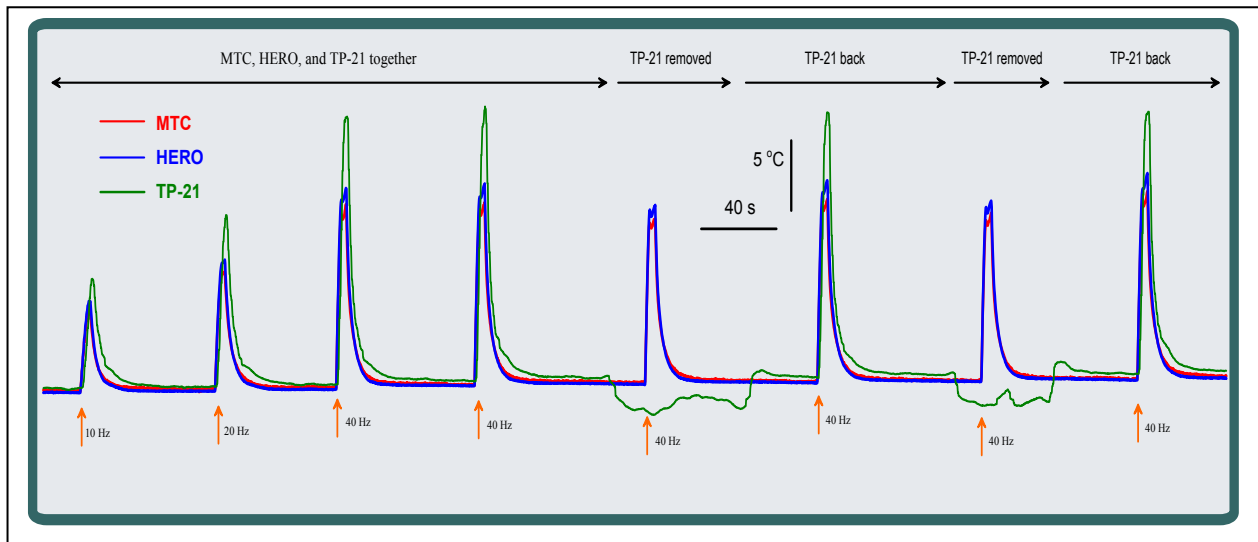
Figure 3-6. Concurrent recordings of microwave heating by MTC, HERO, and TP-21 probes. Exposures (shown by arrows): 5-sec trains of 20-ms pulses at different repetition rates, 10 W peak output (peak SAR ~ 25 W/g). Note that TP-21 readings of the microwave heating are substantially higher than that of the other two probes. Note also that readings of the HERO and MTC probes reversibly decreased when the TP-21 probe was withdrawn. See text and Figure 3-5 for more explanation.

The TP-21 probe is immune to microwave radiation and has no metal elements. It is probably safe to assume that this probe is capable of reporting correct temperature even when it is exposed to microwaves. This conjecture is well confirmed by the fact that we observed no pulse microwave pick-up or temperature changes when a TP-21 probe was exposed in air. Hence, the only explanation to higher temperature readings by this probe in saline is the local field distortion (as described in 3.2.1), resulting in higher local field intensity than it would be at the same location in the absence of the probe. In turn, higher local field intensity resulted in a profoundly greater heating in the immediate vicinity of TP-21. As a consequence, the smaller HERO and MTC probes also displayed higher temperature readings when they were situated in the area of field distortion near TP-21.

Based on the above findings, only the smallest probes (HERO and MTC) were used in subsequent experiments. An added (and, as it will be shown, a very important) benefit of using smaller probes is their negligible heat capacity and fast response to abrupt temperature changes.

3.2.3.5   Probes' Performance Under EHPP Microwave Exposure

These experiments employed 1- and 2-µs pulses at the transmitter peak output power of up to 250 kW; peak SAR at the location of the temperature probes reached 600-800 kW/g.

An example of simultaneous temperature readings with HERO and MTC probes exposed to EHPP is provided in Figure 3-7A. Exposure to a train of 3 EHPP (2 µs pulse width, 500 ms inter-pulse interval, 250 kW peak output, 700 kW/g peak SAR) caused a distinct stepwise temperature rise. In contrast to ―regular‖ microwave pulses (Section 3.2.3.4), EHPP irradiation

79

could induce transient artifacts in MTC measurements. These artifacts are probably caused by EMF pick-up and instant overheating of MTC, MTC's wires, and their immediate microenvironment. Thanks to the tiny volume and negligible heat capacity of the MTC, the excessive heat is fully dissipated in just 20-40 ms after exposure, without any measurable impact on the temperature of the medium. Indeed, temperatures measured by HERO probe were practically unaffected by the presence or absence of MTC, and vice versa. When the probes were situated in the exposure area together, their readings became identical shortly after the exposure.
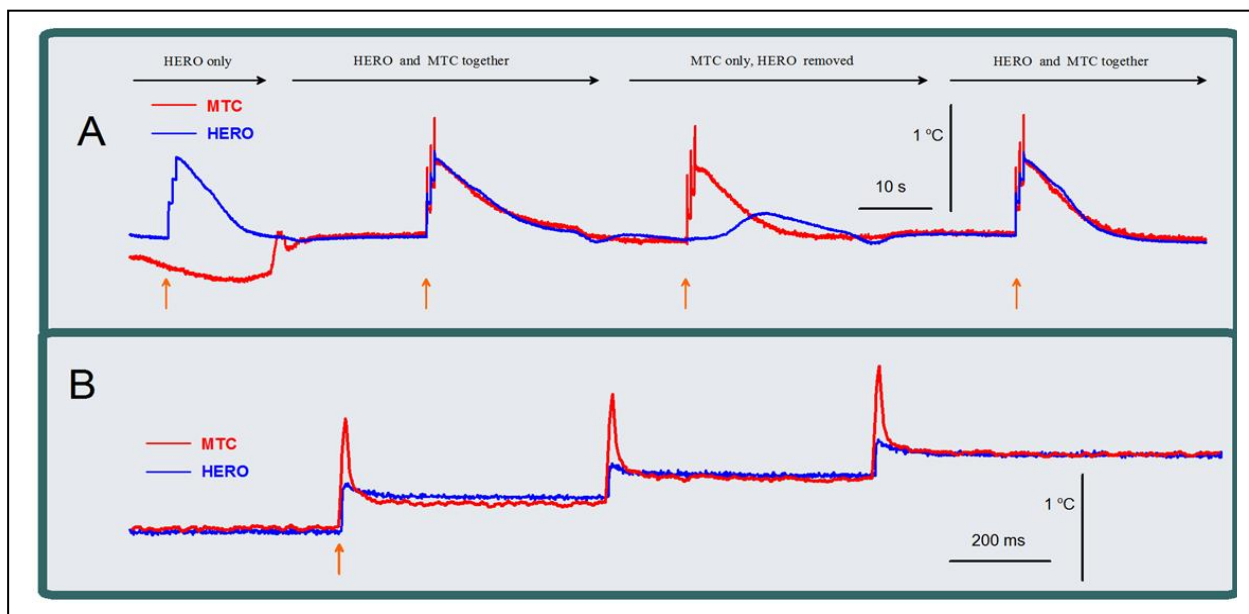
Figure 3-7. Concurrent temperature readings by HERO and MTC probes during exposures to trains of extremely-high power microwave pulses. All exposures were identical trains of 3 EHPPs: 2 μs pulse width, 500 ms inter-pulse interval, 250 kW peak output, 700 kW/g peak SAR. The onset of each exposure is identified by an arrow. A, alternate readings by both probes situated in the exposure area together and when one of the probes was withdrawn. Note that the presence of either probe in the exposure area had no apparent effect on readings of the other probe. B, the 2nd exposure from A, shown at an expanded time scale. Note transient EHPP pick-up artifacts, which affected MTC readings during the first 20-30 ms after each EHPP.

In other words, the MTC was capable of measuring correct temperature before the EHPP(s) and shortly (but not instantly) after it. The fact that the presence of the MTC did not actually affect heating of the surrounding medium was additionally confirmed in a different type of experiments (Pakhomov et al., 2000a), where the MTC-recorded heating curves served as "self-control" (Figure 3-8). The micromanipulator employed for MTC positioning allowed us to raise the MTC for the duration of exposure and then to slide it down to the exact original position. The upper heating curve in Figure 3-8 was recorded when the MTC was permanently kept at the bottom of the exposure chamber (*Position 1*). The lower curve (the same exposure parameters) started when the MTC was elevated into *Position 2*. After the exposure was over, the MTC was slid promptly into the *Position 1*.
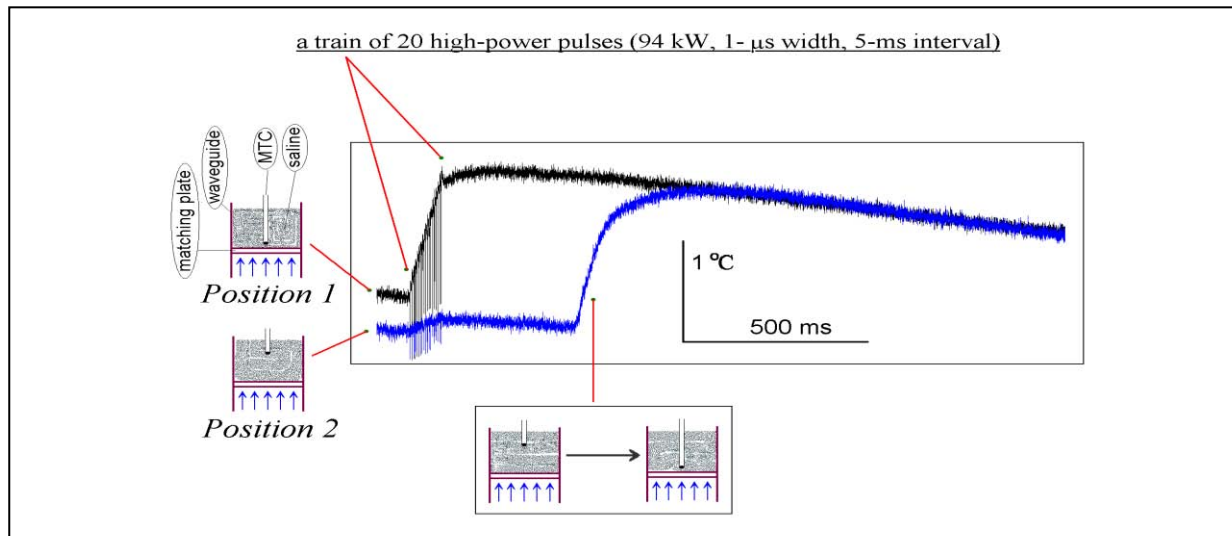
Figure 3-8. EHHP pick-up by MTC does not affect local heating in the surrounding medium. Upper trace (black): MTC was at the bottom of the exposure chamber (*Position 1*) during and after exposure (20 EHPP). Lower trace (blue): MTC was at the top of the chamber (*Position 2*) during the exposure, and was slid into the *Position 1* after the exposure was over. See text for further explanation. Adopted with changes from (Pakhomov et al., 2000a), with kind permission of Springer Science and Business Media.

Prior to recording the data shown in Figure 3-8, the saline in the chamber has already been repeatedly exposed to EHPP trains, in a series of experiments similar to the one illustrated. As a result, the starting temperature at the upper *Position 2* (farther away from the irradiator) was lower than in the *Position 1*. EHPP produced large artifacts and pronounced heating in the *Position 1*, but much smaller artifacts and only subtle heating in the *Position 2*. Due to large field attenuation, the presence of the MTC in the *Position 2* could have no effect on microwave heating in the *Position 1*.

Therefore, the temperature recorded after sliding the MTC down (blue curve) reflected microwave heating at the *Position 1*, not affected by the presence of the MTC there during exposure. However, this temperature was exactly the same as the one recorded with the MTC being in the *Position 1* throughout the exposure (black curve). This experiment was repeated numerous times, with various MTC positions and exposure parameters, and with the same result as illustrated. These experiments confirmed once again that the presence of MTC in the medium during exposure produced no considerable field distortion and did not measurably affect local heating.

3.2.3.6 Summary: Applicability of Different Probes for Microwave Thermometry and Dosimetry

The records presented in the Figure 3-6 provide an excellent example how a fiber optic probe (made only of dielectric materials) may produce erroneous readings when exposed in saline to microwave pulses (25 W/g peak SAR and 5 to 20 W/g time-average SAR). Although this probe is commonly regarded as ―non-field-perturbing‖ or an ―artifact-free,‖ these definitions

81

are not entirely correct. When exposed in a conductive medium, TP-21 can profoundly distort the local field in its vicinity, resulting in erroneous temperature readings. On the contrary, smaller probes made solely of dielectric materials (HERO) or of solely conductive materials (MTC) displayed almost identical readings. These results indicate once again that the size of the temperature probe, especially in intense microwave fields, may be a more important parameter than the materials it is made of.

At the same time, it is worth mentioning that the error in temperature readings by the TP-21 probe was logarithmically proportional to the time-average SAR. For the case illustrated in Figure 3-6, the readings of TP-21 exceeded those of two other probes by 4.5, 10.5, and 16.5% at the time-average SAR of 5, 10, and 20 W/g, respectively (Figure 3-9). One may anticipate that at low enough SAR the error becomes negligible, and TP-21 probe can be safely employed for temperature measurements. For the case illustrated in Figures 3-6 and 3-8, the apparent ―safety limit" will be at 2 W/g; however, this value may vary greatly depending on specific exposure conditions (frequency, surrounding medium, exact probe position, etc).
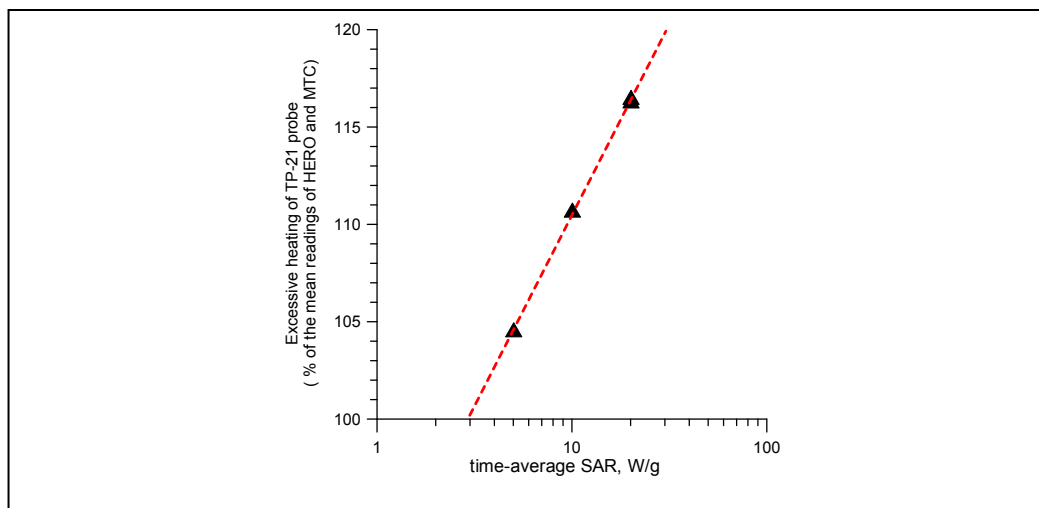
Figure 3-9. The error in temperature readings by TP-21 probe as a function of time-average SAR during exposure. Temperature readings of TP-21 are shown as a percentage of concurrent readings of HERO and MTC probes, measured in °C. The graph is based on the data illustrated in Figure 3-6.

Overall, the experimental data suggest that relatively large ―non-field-perturbing" temperature probes (e.g., TP-21, Luxtron, Vitek), which are undoubtedly useful for measurements in weak EMFs, may produce large errors in high-intensity, high-gradient and should be used with caution.

Since these probes appeared on the market, they have been a popular choice to measure local SAR from the rate of local microwave heating. Such measurements render accurate results when all of the following conditions apply: (1) The presence of the probe during exposure does introduce large measurement errors, like shown in Figure 3-6; (2) The field and heating gradients are relatively low, meaning that the change in these parameters within a distance comparable

with the size of the probe can be neglected; (3) Microwave heating should be slow enough to allow for adequate data sampling by a particular thermometer (sampling rates of different thermometers are largely in the range from 1 to 30 Hz); (4) Microwave heating should be fast enough to reliably detect and record the initial linear portion of the heating curve, prior to any considerable heat dissipation. Alternatively, the rate of heat dissipation can sometimes be accurately measured and included in the equation for calculating SAR (e.g., (Chemeris et al., 2006)).

The above procedure of local SAR measurements has been widely used and addressed in published literature, including this Handbook and its previous editions. Hence, this method will not be further discussed in this chapter, with the exception of one underappreciated problem. This problem arises from the fact that local heating in tissues during exposure can be produced directly by the EMF absorption at the given locality, and indirectly, by heat flow from neighboring areas which might have absorbed more radiation and thereby reached a higher temperature. In an artificial "extreme" situation shown in Figure 3-10A (two absorptive layers separated by an aluminum foil), a temperature sensor placed in the EMF-shielded absorptive layer will still record a heating curve that can be erroneously used for SAR calculation. (Note that SAR definition is based on the local E-field, not on the heating rate (Section 1); hence, in the absorptive layer shielded by the foil, SAR is equal to zero by definition, irrespective of the local heating rate during exposure.) The indirect heating component can be recognized by a delayed start of the heating curve after the onset of EMF exposure, typically leading to S-shaped heating curves. However, this delay can be easily omitted if the sampling rate of the temperature probe is slow (Figure 3-10B); or it can be misinterpreted by the experimenter as a meter "noise" and disregarded.

In real life situations, SAR measurement errors introduced by the indirect heating can be very significant and perhaps sometimes approach the 100% level, like in the hypothetical setting shown in Figure 3-10. Large errors may be expected, for example, when skin is exposed to mm-waves, and local SAR under the skin is measured with a subcutaneous temperature probe (mm-waves are mostly absorbed within skin, so subcutaneous heating will have a large indirect component). This type of error in local SAR determination is very difficult to account or correct for, and it is inherent for methods that require collection of thermometry data over extended time intervals. In contrast, the method of "instant" SAR determination with fast temperature probes described below (Section 3.2.4) is completely immune to this error.

Overall, the size, the slow response, and potential errors in readings of the larger temperature probes limit their utility for high-resolution thermometry and dosimetry, especially in high-gradient and high-intensity fields. When possible, preference should be given to the smaller probes, of which only two types can be found on the market, namely MTC and HERO.

These smaller probes performed equally well with "regular" microwave pulses, but not with EHPP. EMF pick-up artifacts were clearly present in MTC readings, but they lasted no more than 20-40 ms after each microwave pulse. In practice, the repetition rate of EHPP in biological experiments is usually kept low, e.g., 0.5-2 Hz or less (otherwise, heating will exceed limits of biological function). In these cases, the time-average temperature readings by MTC will not be affected by the short-live pick-up artifacts. Indeed, in experiments described in

(Pakhomov et al., 2000a), slow concurrent recording of EHPP heating by MTC and by a Luxtron probe looked virtually identical. The EMF pick-up transients can also be removed by low-pass filtering of the MTC signal, although it must be clearly understood that this procedure is purely cosmetic.
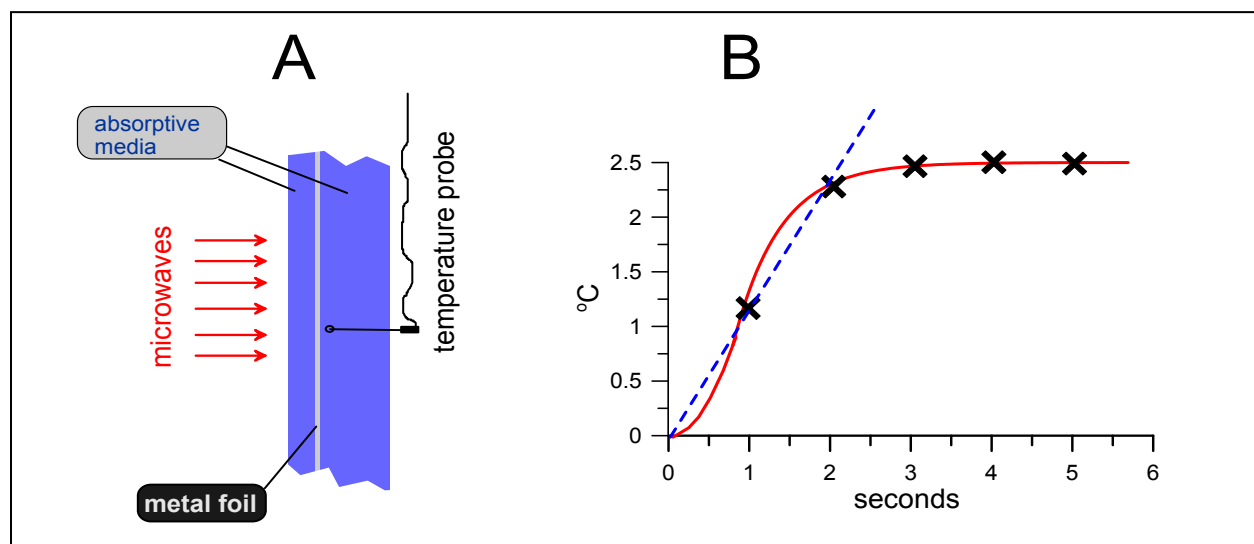
Figure 3-10. Illustration of local SAR measurement error resulting from indirect heating. A, a hypothetical exposure setting where two layers of an absorptive material are separated by a metal foil. Microwaves will only be absorbed in front of the foil. However, temperature may also rise in the area shielded by the foil, because of heat flow from the exposed area. A temperature probe is located in the shielded area behind the metal foil. A sample heating curve for a location in the shielded area is measured with a thermometer having a discrete sampling rate of 1 Hz (black symbols), the S-shaped onset of the curve will not be detected. An experimenter who is not aware that the area was shielded will mistakenly calculate local SAR from the slope of the apparently linear portion of the curve (dashed line). If the absorptive media is water (C = 4.2 J/°C x g)), the calculated local SAR will be about 5 W/g. Actually, SAR in the shielded area is zero by definition.

EMF pick-up artifacts are an inherent property of ―artifact-prone‖ probes such as thermocouples. Proper positioning of the probe leads and their shielding are the most efficient ways to minimize these artifacts, although the results are sometimes unpredictable. In our setup, the layer of saline ensured very efficient shielding of the leads, but, depending on specific exposure conditions and settings, the magnitude of possible artifacts may be many times greater than reported here. In general, thermocouples, as well as other ―artifact-prone‖ probes should not be used for temperature measurements unless they are proven to perform properly under specific exposure settings. Interestingly, this rule does not apply to the precision local microdosimetry technique using MTC (described below), as the temperature readings are taken before and after the exposure (not during it) and therefore are not distorted by the artifacts.

The uniqueness of HERO probe used with VELOCE signal conditioner is in combining the ―artifact-free‖ performance features of a fiber optic sensor with the minimum thermal mass and virtually instant response typical of the MTC. HERO probe outperforms other temperature sensors and potentially can be considered a ―golden standard.‖ However, based on our experience with a HERO/VELOCE thermometer (manufactured in 2002), the device was tricky

to calibrate and calibration values could be rather unstable. For example, moderate bending or simple repositioning of the fiber optic cable, as well as subtle movement of the cable plug-in (such as touching it with a finger) could shift the output zero and calibration values, requiring re-calibration. VELOCE conditioner itself has no indicators and any temperature (or output voltage) readout can only be obtained using external devices. Although VELOCE was supplied with specific guidelines and software to communicate with a computer, we found it greatly advantageous to employ an MP100 data acquisition system with Acknowledge™ software instead. Overall, HERO/VELOCE thermometer was an indispensable tool for unique, high-speed, high-resolution, artifact-free, one-time measurements; however, it may be troublesome to use it for routine everyday measurements. (Note: we have not assessed the latest modification of this thermometer, which might be already improved by the manufacturer.)

3.2.4   Modern Temperature Probes that are Not Commercially Available

Recently, Schuderer and co-authors (2004) reported that a novel thermistor probe for temperature evaluations in radio frequency-heated environments has been developed and tested. The probe's sensitive area is based on a highly resistive 50 μm × 100 μm layer of amorphous germanium processed on a glass tip. The authors stated that the temperature resolution of the probe is 4 mK and its response time is of the order of 10 ms. The influence of RF electric fields on the signal is minimized due to the high resistance of the sensor and the leads. The probe was successfully used by the authors to determine the highly nonuniform absorption distribution gradients.

Thanks to its small size, short response time, and immunity RF fields, the probe appears well suited for dosimetry measurements. Indeed, this thermistor probe has offered clear advantages over such probes as Luxtron or Vitek. However, no comparison was made between this new probe and MTC or HERO detectors.

3.3   Pulsed EMF Microdosimetry Using MTC and Hero Temperature Probes

3.3.1   General Considerations

As shown in Section 3.2, MTC and HERO are the most suitable probes for high-resolution, fast temperature measurements with minimum local field distortion. In this chapter, we will show these probes can be utilized for precision microdosimetry in high-intensity pulsed EMF. Although a HERO/VELOCE thermometer would be a top choice for this task, the cost of this device may be prohibitively high for most experimenters (in 2002, the cost was about $8,000 for VELOCE and $750 for each HERO probe). Therefore, we will largely focus on the use and performance of MTC, to demonstrate that it can be reliably used in many microdosimetry applications, despite possible EMF pick-up artifacts.

A conventional way to calculate SAR from temperature rise is based on the measurement of the initial slope of the heating curve during EMF exposure (see Section 3.1 and also Figure 3-15). When MTC is used for this purpose, EMF pick-up transients may obscure the initial slope, making accurate measurements impossible (e.g., see the top record in Figure 3-11). Therefore,

MTC could not be employed in the conventional manner for measuring local SAR from EHPP exposure, so an alternative procedure had to be developed.
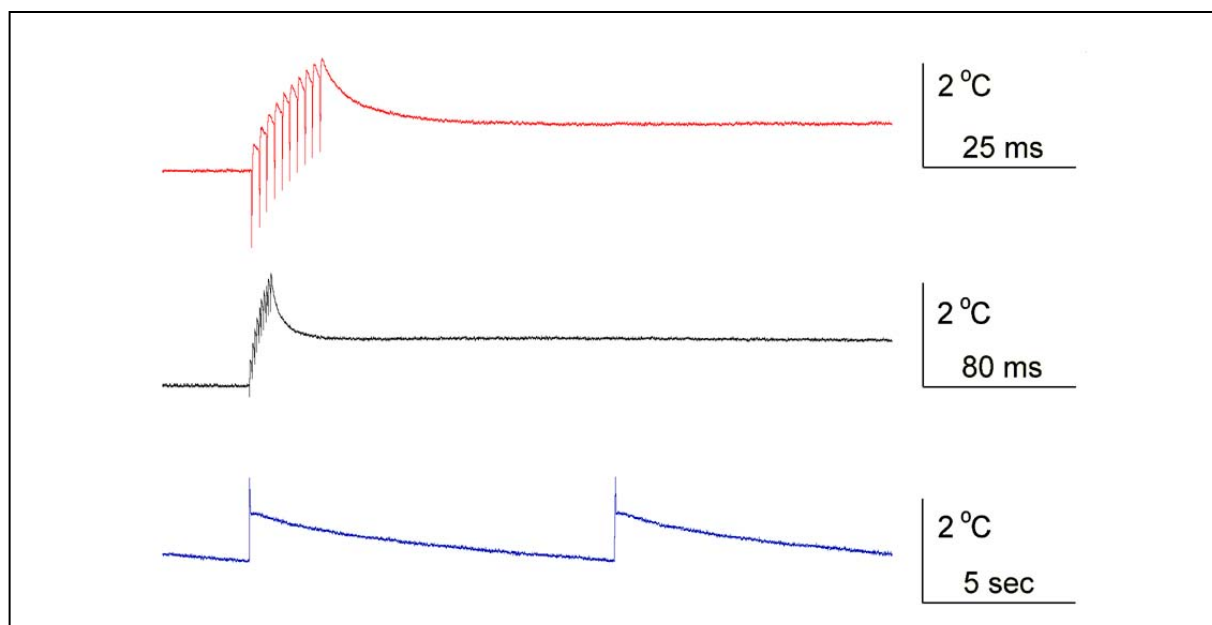
Figure 3-11. The shape of heating/cooling curves recorded by MTC at different time scales. Heating was produced by identical trains of 10 EHPP (110 kW peak transmitted power, 1 μs width, 1 ms interpulse interval, 1 train/12 s). Note EHPP pick-up artifacts (they also mark the time when the EHPP train was applied), brief temperature decline after the exposure is over, and a long-lasting temperature plateau afterwards. Exposures were performed in the chamber shown in Figure 3-3, A; MTC was positioned in saline about 1 mm above the center of the matching plate. Adopted with changes from (Pakhomov et al., 2000a), with kind permission of Springer Science and Business Media.

3.3.2 A Key to Microdosimetry in Intense Pulsed Fields: The Temperature Plateau Phenomenon

An unexpected observation from the temperature curves measured with MTC and HERO probes (but not with any other probes) was the presence of an extended temperature plateau after a short microwave pulse or a brief train of pulses (Figures 3-7B, 3-11, 3-12). It should be emphasized that this was an actual plateau, and not a part of the declining slope that was artificially expanded to make it appear flat. The presence of this plateau was a distinguishing feature of fast MTC and HERO recordings and typically could not be detected when using larger and slower probes. Perhaps this fact explains why, despite numerous studies in the area of EMF thermometry and dosimetry, the plateau phenomenon has not been described until recently (Pakhomov et al., 2000a).
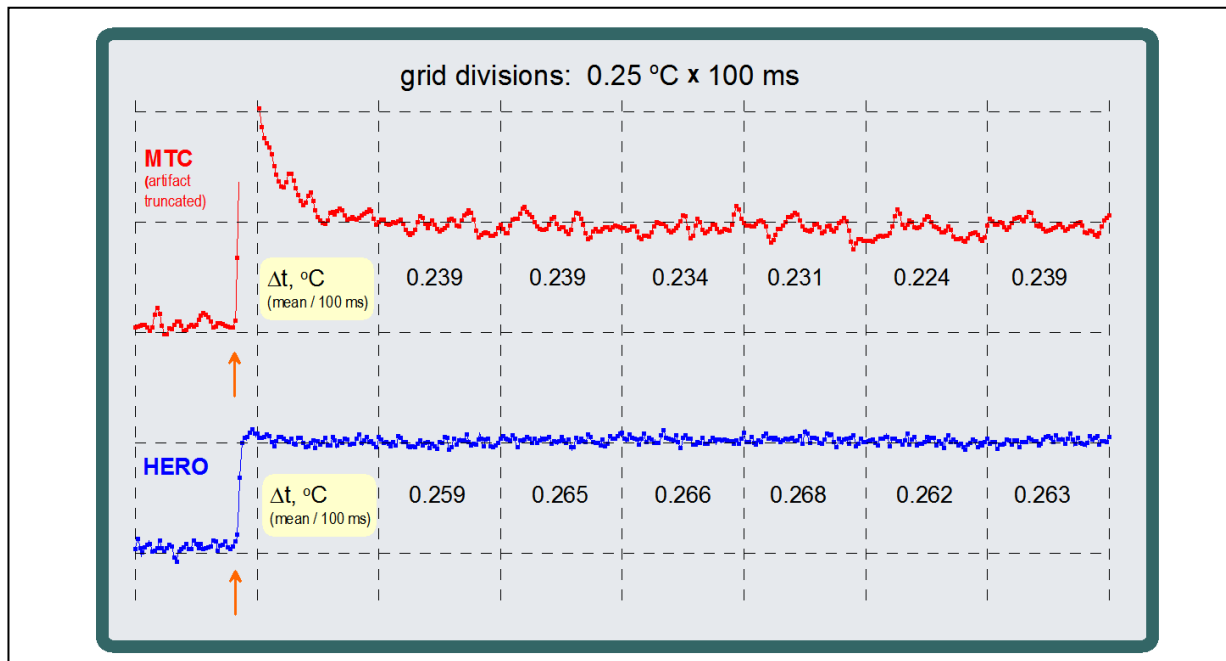
Figure 3-12. Examples of the temperature plateau following exposure to a single extremely-high peak power microwave pulse (pulse duration 2 μs, peak transmitted power about 240 kW). Exposure setting is the same as in Figure 3-11, except for using the chamber shown in Figure 3-3B. The same temperature recording was made using MTC (top) or HERO probe (bottom). The time when the EHPP was delivered is shown by arrows. Numbers in each square show the temperature difference from the pre-exposure level (ΔT, °C), as averaged over a respective 100-ms interval identified by grid divisions. Note that the temperature stayed practically constant (within 3 digits of precision!) for at least 700 ms after the microwave pulse, meaning the detection of a true post-exposure temperature plateau. Note also that the initial EMF pick-up artifact is not present when using HERO probe, which is artifact-free. Slightly higher readings of the HERO probe compared to the MTC, similar to those seen in Figure 3-6, could be a result of minor field distortion in the immediate vicinity of this probe.

At a first glance, the existence of temperature plateau after an exposure is somewhat counterintuitive. If an object's temperature has been increased above the background during the EMF heating, one may expect it to go down immediately once the external influx of energy is discontinued. However, measurements taken with the smallest and fastest probes show unambiguously that the temperature decrease after cessation of exposure may occur after a short delay, forming a post-exposure temperature plateau. Potential reasons for plateau formation, at a conceptual level, are explained below and illustrated in Figure 3-13.

Figure 3-13A depicts a hypothetical situation when a temperature probe is placed inside a sphere made of an absorptive material. It is also assumed that the presence of the temperature probe causes no field distortion, does not affect heating in the sphere, and that some sort of an EMF exposure caused uniform heating of the sphere above its environment. In this case, cessation of EMF exposure will have no immediate effect on the temperature readings by the probe. First, the surface layers of the sphere will begin to cool down to the environment temperature; next, the intermediate-depth layers will start to cool down; ultimately, the process will reach the center of the sphere in the vicinity of the probe, which will then display a temperature decline. However, this process takes some finite time, and there will be a distinct

87

delay between turning off the EMF field and the onset of the temperature decline, displayed as a post-exposure plateau on the temperature curve. The time duration of this plateau will depend on many parameters (e.g., the size of the sphere, the rate of heat conduction), but the principal conclusion from this hypothetical example is that the presence of a post-exposure temperature plateau is indeed expected and makes no surprise in such exposure setting.
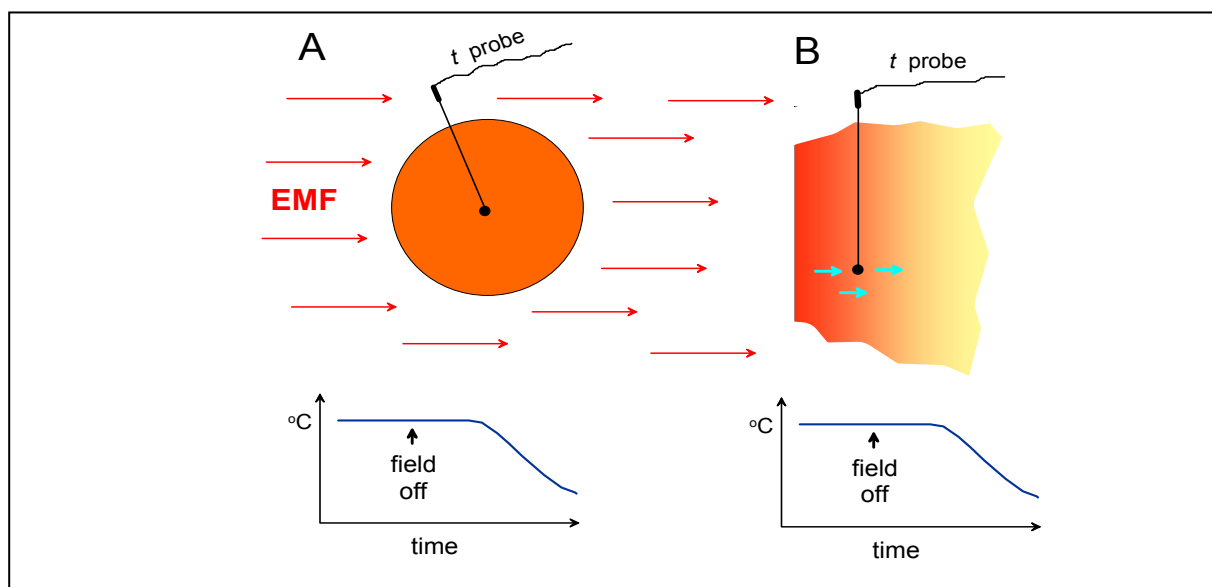
Figure 3-13. Hypothetical exposure settings that illustrate situations when local temperature inside of an EMF-heated object may remain unchanged for a finite time interval after cessation of exposure. In A, the temperature probe is located within a sphere that has been heated to a uniform temperature by some modality of EMF exposure. In B, the probe is placed into a medium that has attained a uniform temperature gradient during the EMF exposure; the exposed surface is assumed to be warmer (red) than deeper layers (yellow). Blue arrows show the direction of heat flow once the exposure is terminated. In both A and B settings, the temperature probe may record a short-lived temperature plateau after the exposure is turned off. See text for more explanation.

Figure 3-13B depicts a more realistic situation, when an absorptive object has been non-uniformly heated by an EMF exposure. The object is assumed to have semi-infinite structure, meaning that it has one flat surface and the other surfaces are far away, so they need not to be accounted for. We assume again that the presence of the temperature probe had no effect, and expect that the irradiated surface of the cylinder experiences maximum heating, whereas deeper areas will be heated less and less, due to gradual power loss when the field propagates through the object. Hence, irradiation will produce a temperature gradient in this object; for simplicity, we will consider the situation when the attained temperature is the same at any given depth from the surface and that the temperature change with the distance from the surface is linear (although in real-life exposure conditions it will usually be closer to exponential).

In this setting, once the EMF radiation is turned off, the temperature sensor will be instantly subject to two opposite processes: it will be cooled down by heat conduction to the deeper (cooler) layers, but concurrently it will also be warmed up by heat conduction from the upper (warmer) layers. In the idealized situation, two processes completely balance each other,

88

resulting in a temperature plateau that will last for a certain time after the irradiation is discontinued.

One may argue that real-life EMF exposures will seldom, if ever, produce field and temperature distribution patterns such as described above. However, if we consider only a very small volume within a large exposed object, these patterns may be indistinguishable from the idealized situation. Hence, with a microscopic temperature probe that measures instant temperature in its immediate vicinity, the idealized assumptions may indeed be true for real-life situations.

This idea can be illustrated by the following example: When a rat is exposed to 2.45-GHz microwaves at a high incident power density (e.g., 100 mW/cm^2), the heating of the animal's body will be highly non-uniform, and temperature gradients will vary greatly depending on the exact location, type of tissue, and body orientation with respect to the EMF source. However, when we consider a smaller volume of a relatively uniform tissue (e.g., only the liver), heating of this volume and temperature gradients within it will probably be much more uniform. Furthermore, if we consider just a small volume of, say, 1 or 0.5 mm^3 inside the liver, the field and temperature distribution within this small volume will be close to the idealized situation. Then, for the reasons discussed above (Figure 3-13), a tiny temperature probe placed within this volume should record a short-lived temperature plateau after the radiation is turned off. Note that the volume of the MTC is less than 0.0001 mm^3 (not counting the leads), and it is not surprising that the tissue volume in its immediate vicinity will ―behave" similarly to what is expected under idealized exposure conditions.

The time duration of the post-exposure plateau will vary depending on how big is the volume near the probe that has uniform temperature or temperature gradient structure and uniform heat conduction properties. For example, the plateau may last 100 ms if the uniform volume is 1 mm^3, and 20 ms if it is 0.5 mm^3 (the numbers are arbitrary); and no plateau will be detected if the probe is positioned at an interface of two distinctly different materials (e.g., touching the bottom of the exposure chamber in Figure 3-3).

In this chapter, we only attempted to explain the principle mechanism of how a post-exposure temperature plateau may form, and do not attempt to make any quantitative predictions, such as what are the borderline conditions for plateau detection in a particular microenvironment, using a specific probe, and under specific exposure conditions. Such calculations would be rather complex and their utility limited, due the countless variety of exposure conditions. As far as practical applications are concerned, the plateau can be readily and routinely detected if (1) the temperature probe is small enough, such as MTC or HERO, (2) the temperature data are acquired at a rate of no less than 100 Hz (1000 Hz preferred), so that a plateau that lasts only a few tens of milliseconds will not be missed, (3) the high-frequency cut-off filter of a signal amplifier, if one is used, should be no less than 50-100 Hz; any low-frequency filters must be disabled to allow DC recording, (4) the overall duration of EMF exposure (a pulse or a train of pulses) should not exceed 10-100 ms, (5) the EMF intensity is high enough to produce measurable heating during this brief exposure, and (6) the probe is positioned so that it is surrounded by a uniform absorptive medium, not at the interface of media with different absorptive and heat conduction properties. Failure to meet the above conditions does not necessarily prevent one from the

89

detection of the post-exposure temperature plateau, but the probability of this event will be decreased.

With EHPP exposure and temperature recording using MTC, the plateau is not instant after the exposure is turned off. Typically, the plateau occurs after a brief (~10-20 ms) decline of the reported temperature (Figures 3-11, 3-12, and 3-14). The reasons for this artifact may be one or both of the following: (1) relaxation of the EMF pick-up signal in the electronic circuitry of the amplifier, and (2) additional heating of the MTC by EMF-induced currents in the MTC itself and in its leads. In the latter case, the brief decline of temperature truly reflects dissipation of this ―additional" heat from the MTC into the surrounding medium. Fortunately, the size and the heat capacity of the MTC are so small that the additional heating of the medium by the presence of MTC typically does not affect the level of the following plateau. For example, in Figure 3-13A, the plateau levels were identical after EHPP trains that ended with different sizes of the temperature artifact (the largest artifact occurred with the shortest (1-ms) interval between EHPP). This brief initial artifact was not present when the temperature changes were recorded with HERO probe (which is artifact-free), but the plateau level was practically the same as with the MTC probe that picked up a large artifact (Figure 3-12).

3.3.3 Post-Exposure Temperature Plateau, Specific Absorbed Dose (SAD), and Specific Absorption Rate (SAR)

Based on the discussion above, the presence of the post-exposure plateau means that, at the given location, the dissipation of heat generated by EMF absorption was negligible, or that the opposite heat flows were balanced and cancelled each other. In either case, heat dissipation can be disregarded, so the plateau level (i.e., the difference between the temperature before the exposure and the plateau) is linearly proportional to the absorbed energy (which, in turn, is proportional to the delivered energy). Indeed, when the delivered energy is kept constant, the level of the plateau does not change, regardless of the particular pulse repetition rate or overall train duration (Figure 3-14A). Likewise, equal increments in the amount of delivered energy (by adding extra four pulses to the train, Figure 3-14B) produced proportional and identical increments in the measured plateau level.

Hence, the local SAD (J/g) can be accurately measured from the post-exposure temperature plateau level as:

$$SAD = C\,\Delta T \qquad\qquad (4)$$

where C is the specific heat capacity of the medium (J/(kg x ^{o}C)), and where ΔT is the plateau level (^{o}C).
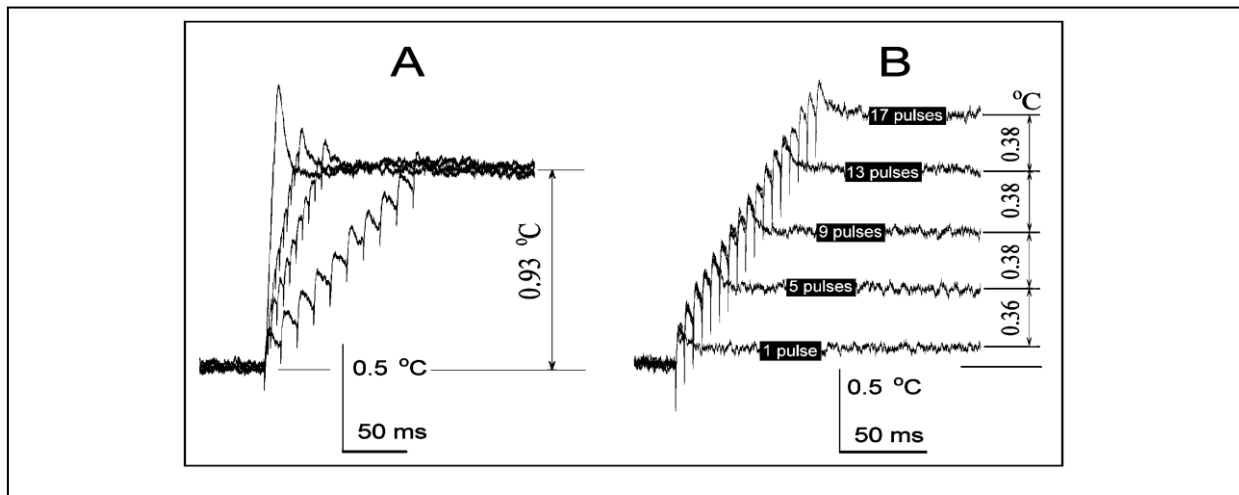
Figure 3-14. **The post-exposure plateau level does not depend on the pulse repetition rate (A) and is proportional to the delivered (and absorbed) energy (B). Heating was produced by EHPP trains (1-μs pulse width, ~100 kW peak transmitted power); pick-up artifacts show the exact time when microwave pulses were applied. Temperature was measured as a mean value for a 40-ms period. A: Trains of 10 pulses (therefore, delivering the same dose) were applied with interpulse intervals of 1, 3, 5, and 13 ms. The post-exposure plateau level (0.93 °C) did not depend on of the interpulse interval or the amplitude of the pick-up artifacts. B: Changing the absorbed dose by varying the number of pulses in the EHPP changes the level of post-exposure temperature plateau in the linear manner. Heating by a single pulse was about 0.09 °C. Reproduced from (Pakhomov et al., 2000a) with kind permission of Springer Science and Business Media.**

Once the SAD is known, we no longer need to measure the initial slope of the heating curve to calculate SAR. Instead, SAR (W/g) can be easily calculated as a ratio of SAD and known duration of the EMF pulse (Δt, sec):

$$SAR = SAD / \Delta t = C \, \Delta T / \Delta t . \qquad (5)$$

In case if heating is produced by a train of pulses, Δt is the product of the pulse number and individual pulse duration (sec). This ―alternative‖ method of fast and accurate measurement of local SAR is illustrated in Figure 3-15.

91
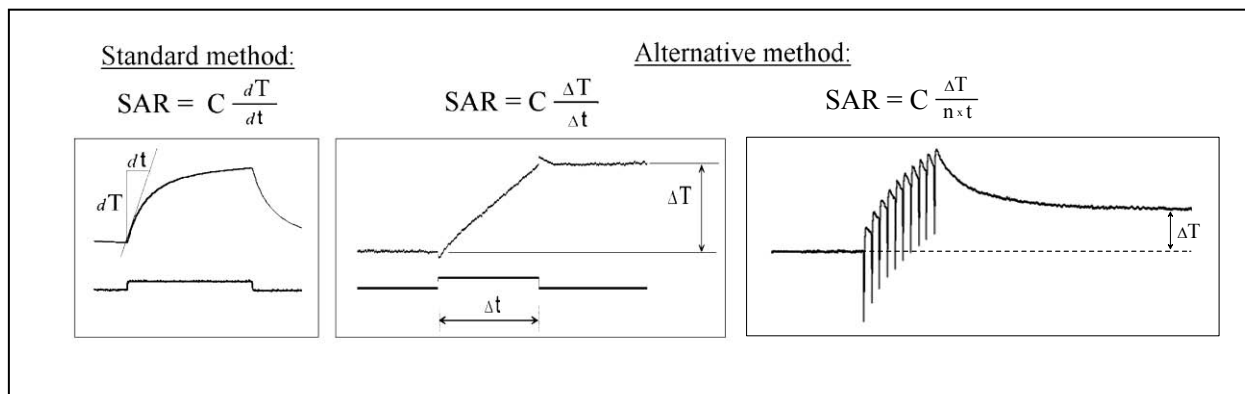
Figure 3-15. Standard and alternative methods of specific absorption rate (SAR) measurement from heating dynamics. Shown are the microwave pulse duration (lower traces) and sample heating curves (upper traces). The standard method uses the initial slope of the heating curve (C is the specific heat capacity of medium). The alternative method calculates SAR from the level of the after-pulse plateau and the duration of the pulse, or of all pulses in a train (in the right fragment, *n* is the number of pulses and *t* is the known duration of each pulse). Both methods can be used with the same result when the plateau is present and no artifacts are recorded. However, the alternative method is the only choice when the initial slope cannot be measured accurately. Some fragments have been reproduced from (Pakhomov et al., 2000a) with kind permission of Springer Science and Business Media.

The final step to justify the alternative method was to compare measured SAR values with those predicted theoretically by the equation 3. SAR measurements were performed with MTC in well-defined exposure conditions (Figure 3-3A), and the comparison results are shown in Figures 3-16 and 3-17.

In Figure 3-16A, heating of 0.1 $^{\circ}$C was produced by a single high-power pulse. Calculated and measured SARs were 585 and 420 kW/g, respectively. As stated by Bassen and Babij, "an absolute accuracy of ± 3 dB … is the best-case measurement uncertainty that can be achieved when attempting to determine the maximum and minimum … SARs within an irradiated biological body" (1990, p. 169). In our exposure system and with the use of MTC, the difference between calculated and measured SARs was only 1.4 dB.

The match was even better for exposure to low-power, longer microwave pulses (Figure 3-16B). Measured values were only 0.4-0.5 dB apart from the calculated ones. This small error could result from the combined inaccuracy of power meters, field probes and other devices, or even to some imperfection of the analytical equation itself (the equation is for TE_{10} wave propagation mode, but other modes can also arise in the waveguide after the matching plate). Figure 3-15 also demonstrates that the presence of the temperature plateau after a microwave pulse is not a specific attribute of exposure to extremely high-power pulses. The plateau can be as well pronounced with reasonably low amplitude pulses of ms-range duration, and SAR measurements with MTC are accurate as long as the plateau is present.

92
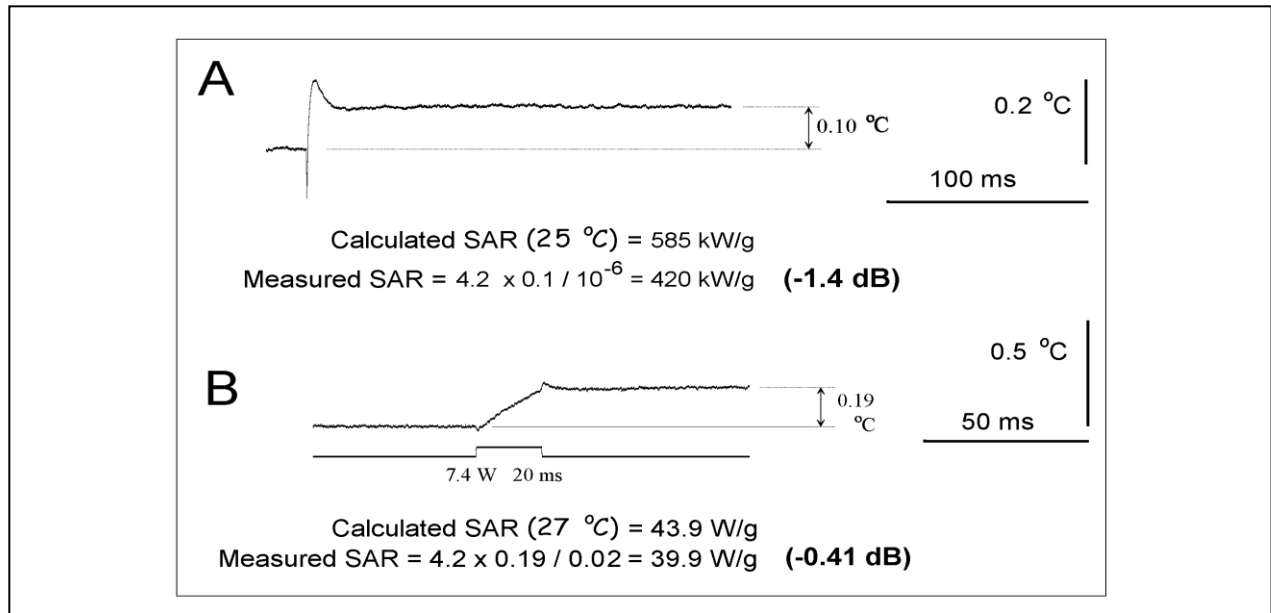
Figure 3-16. Comparison of calculated and MTC measured local SAR values. A, exposure to a single extremely-high-power pulse (96 kW transmitted power, 1 μs width); the moment of exposure coincides with the artifact on the heating curve. B, a moderate power pulse (7.4 W, 20 ms width, indicated on the lower trace). The temperature before the pulse and during the plateau was measured as a mean of a 25-ms period. Calculated SAR values were obtained using Equation (3), see text. The difference of the measured and calculated SAR was -1.4 dB (A) and -0.41 dB (B). Reproduced from (Pakhomov et al., 2000a) with kind permission of Springer Science and Business Media.

Figure 3-17 gives an example of the ―local field mapping‖ with MTC and illustrates the spatial resolution of the method. Heating curves recorded in spots as close as 0.5 mm to each other were substantially different, and measured SAR values were always close to the calculated ones.

93
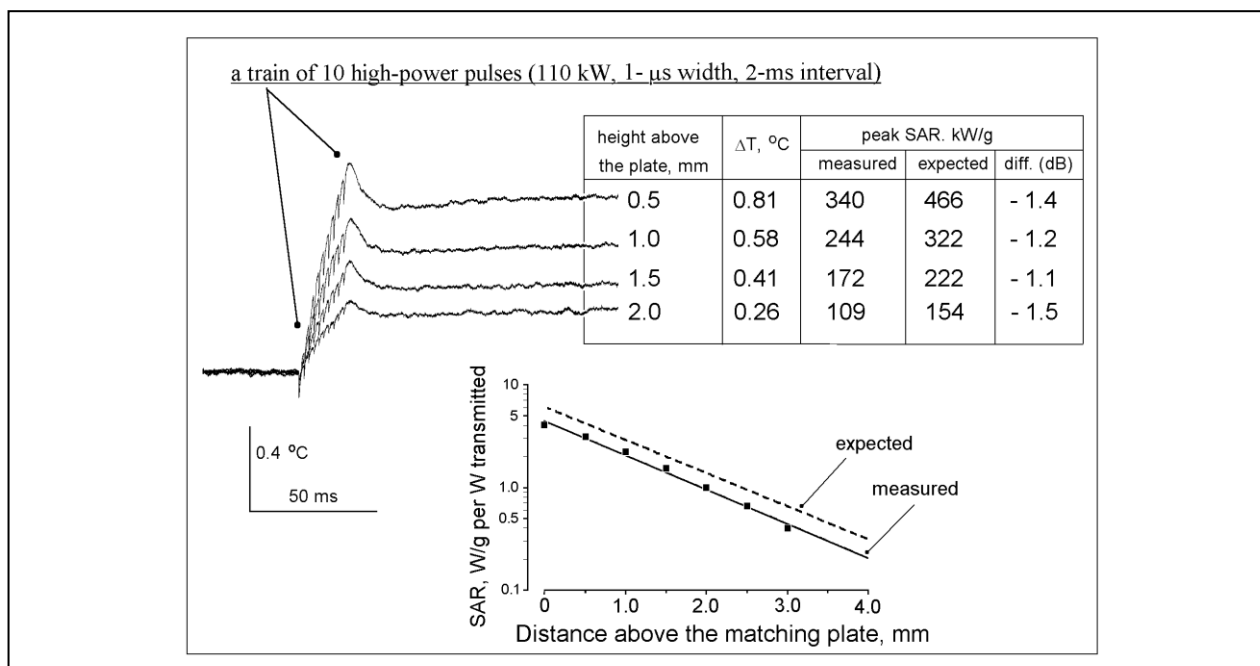
Figure 3-17. Local SAR in the exposure chamber as a function of the distance above the matching plate, along the axis of the waveguide. Heating curves (left) produced by a train of 10 high-power pulses (110 kW output, 1-μs width) were recorded at the heights from 0 to 3 mm above the matching plate (for clarity, only four curves are shown). The respective heights, plateau levels, and local SAR values are provided in the table. The "expected" local SAR values at the same distances above the matching plate were calculated using Equation (3). In the graph below, the expected and measured local SAR have been normalized to the transmitted power and plotted against the distance above the matching plate. Reproduced from (Pakhomov et al., 2000a) with kind permission of Springer Science and Business Media.

Similarly, MTC was used for horizontal field mapping in a plane parallel to the matching plate. Horizontal field distribution was calculated according to standard waveguide equations for TE_{10} mode (Paris & Hurd, 1969). Again, measured and calculated values were within ±1.5 dB apart.

3.3.4   Verification of the Local SAR Measurement Technique in a Different Exposure Setting

Explanations for the formation of the post-exposure temperature plateau, as discussed above in Section 3.3.2, did not rely on a particular type of the radiation or a specific exposure set-up. The same is also true for Equations 4 and 5, which are employed to calculate SAR from the temperature plateau level. In principle, this method of local SAR measurement should be valid for various radiation modalities (not limited to microwaves or even to EMFs) and various exposure settings. The only requirements that enable the use of this method are (1) irradiation should be performed as a single pulse or a brief train of pulses, (2) the energy deposited by this pulse (or the train) is sufficient to produce a measurable temperature rise, and (3) the pulse (or the train) duration are short enough not to obscure the temperature plateau.

94

Hence, this method was additionally tested in exposure conditions very different from those described above. A volume of 0.45 ml of a mammalian cell culture medium (RPMI 1640 supplemented with 10% fetal bovine serum, obtained from American Type Tissue collection, Manassas, VA) was placed in an electroporation cuvette with 2-mm gap between two conductive walls (Bio-Rad Laboratories, Hercules, CA); the cuvette is shown in the inset of Figure 3-18. The conductive walls were connected to a Blumlein line pulse generator (custom built at the Old Dominion University, Norfolk, VA, see (Kolb, Kono, & Schoenbach, 2006) for design details) to produce a high voltage, 10-ns duration electrical pulse into the sample. The Blumlein line was charged from a high-voltage DC power supply (HR-100, American High Voltage, Elko, NV) until a breakdown voltage was reached across a spark gap in a pressurized switch chamber. The breakdown voltage (and, consequentially, the voltage of the 10-ns pulse delivered to the sample) was varied from 10 to 25-30 kV by increasing the pressure of SF6 gas in the switch chamber. The shape and voltage of the pulse delivered to the sample were monitored on a 500-MHz digital oscilloscope (TDS3052B, Tektronix, Wilsonville, OR) via a custom-made high-voltage probe. The pulse shape was close to rectangular, with some additional oscillations caused by impedance mismatch and the capacitance of the load.

Assuming that the pulse shape is perfectly rectangular, the power dissipation in the sample during the pulse can be calculated straightforward as U2/R, where U is the applied voltage (V) and R is the ohmic resistance of the sample (in our case, it was about 8 Ohm). With the parallel-plate design of the cuvette, the E-field in the sample is close to uniform, so SAR (W/g) can be calculated as:

$$SAR = U^2/(R\ M) \tag{6}$$

where M is the mass of the sample (0.45 g). In our experiments, these ―expected" SAR values were compared with those measured using a HERO probe and Veloce signal conditioner. The probe was placed in the medium in the gap between the conductive walls, approximately in the geometrical center of the electroporation cuvette. Temperature data were filtered at 1 kHz and sampled at 10 kHz. To improve the signal-to-noise ratio, up to 12-15 independent runs were averaged off line.

An example of such temperature recording, with a clear post-exposure temperature plateau, is shown in Figure 3-18. The voltage applied across the sample was 10.4 kV, yielding the SAR value of 30 MW/g using Equation 6. At the same time, the plateau level detected by the HERO probe was about 0.06 °C, which corresponds to SAR of 24 MW/g, using Equation 5. Thus, the ―expected" and HERO-measured SAR values were remarkably close; in other similar experiments using various voltages, the difference of the expected and measured SAR did not exceed 1.5 dB. Although this difference can probably be explained by a combined inaccuracy of measurement or less than perfect shape of the electric pulse, it may also be indicative of the fact that the pulse energy was not entirely transferred into heat. For example, some of this energy could be spent in an electrochemical reactions, e.g., between the aluminum walls of the cuvette and water or other constituents of the medium.
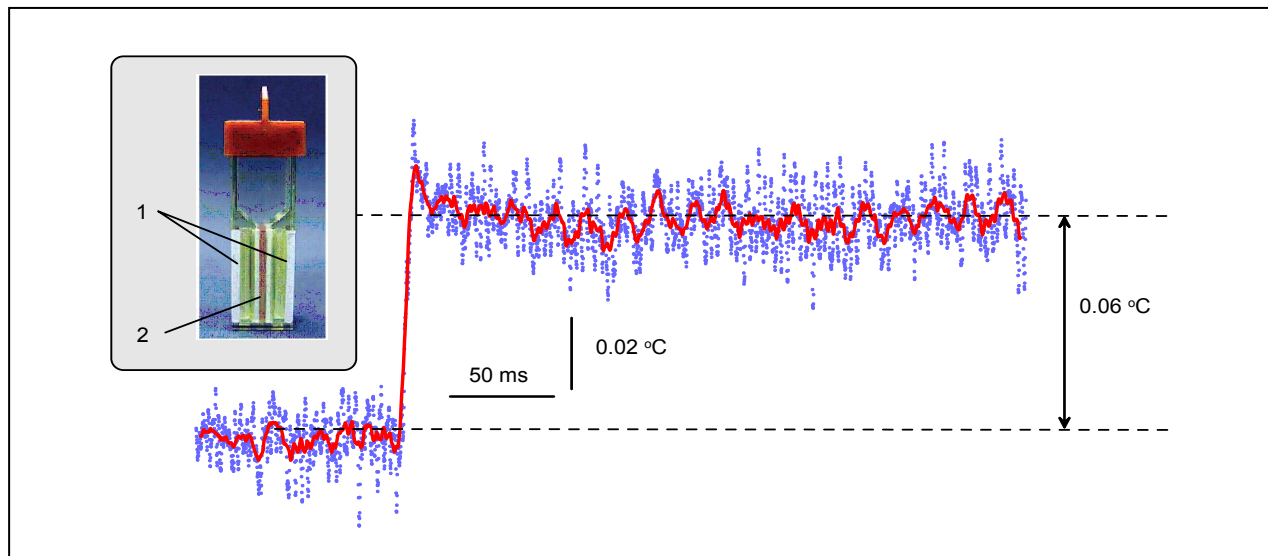
Figure 3-18. Heating of the medium in an electroporation cuvette by a 10-ns electrical pulse. Individual data points (blue) show the temperature readings sampled at 10 kHz using HERO/VELOCE thermometer system. Solid red line is the "running average" of 49 data points. Heating produced by this single pulse of 10.4 kV (52 kV/cm) was approximately 0.06 °C, which corresponded to the SAR value of 24 MW/g. The expected SAR value, calculated from the pulse voltage and electrical resistance of the sample (8 Ohm), was 30 MW/g. See text for more detail. The inset shows the electroporation cuvette with a 2-mm gap between the conductive walls (1) filled with the sample medium (1).

Regardless of these details, the experiments clearly established that the post-exposure temperature plateau is not unique for the exposure system shown in Figure 3-3; the plateau can be found in totally different exposure setting and using a different type of pulsed energy. Furthermore, the procedure of local SAR calculation from the plateau level remains valid and accurate in these different exposure conditions.

Note also that with pulse duration as small as 10 ns, the slope of the heating curve obviously cannot be measured by any conventional means, even if the EMF pick-up artifacts are entirely absent. In such cases, measuring SAR from the post-exposure temperature plateau is probably the only possible approach, aside from theoretical calculations.

3.4 Summary

In this chapter, we have reviewed practical methods and techniques for high-resolution thermometry and microdosimetry in high-intensity pulsed RF fields. The methods were first reported in (Pakhomov et al., 2000a; Pakhomov, Mathur & Murphy, 2003), and, over the years, were repeatedly employed in varied biological studies (Pakhomov et al., 2003; Pakhomov et al., 2002a.; Pakhomov et al., 2002b; Pakhomov et al., 2000b; Walker et al., 2006). The described method of local SAR measurement has proven to be fast, accurate, and reliable; it is likely to produce valid data whenever a temperature plateau after a pulsed exposure can be reliably detected (regardless of the radiation wavelength, incident power, absorptive media properties or

96

exposure set-up). When biological experiments are performed at radiation intensities too low to produce a measurable temperature plateau after a pulse, the intensity can be cranked up just for dosimetry purposes. In this case, SAR values measured at the increased field intensity can be linearly scaled down (proportionally to the output power) to determine actual local SAR in the biological experiments.

3.5   References

Adair, E. R., Adams, B. W., & Akel, G. M. (1984). Minimal changes in hypothalamic temperature accompany microwave-induced alteration of thermoregulatory behavior, *Bioelectromagnetics*, *5*, 13-30.

Adair, E. R., Adams, B. W., & Hartman, S. K. (1992). Physiological interaction processes and radio-frequency energy absorption, *Bioelectromagnetics, 13*, 497-512.

Adey, W. R., Byus, C. V., Cain, C. D., Higgins, R. J., Jones, R. A., Kean, C. J., Kuster, N., MacMurray, A., Stagg, R. B., & Zimmerman, G. (2000). Spontaneous and nitrosourea-induced primary tumors of the central nervous system in Fischer 344 rats exposed to frequency-modulated microwave fields, *Cancer Research*, *60*, 1857-1863.

Alekseev, S. I., & Ziskin, M. C. (2001). Distortion of millimeter-wave absorption in biological media due to presence of thermocouples and other objects. *IEEE Transactions on Biomedical Engineering, 48*, 1013-1019.

Bao, J. Z., Swicord, M., & Davis, C. (1996). Microwave dielectric characterization of binary mixtures of water, methanol, and ethanol. *Journal of Chem. Physics, 104*, 4441-4450.

Bassen, H. I. & Babij T. M. (1990). Experimental techniques and instrumentation. In: O.P. Gandhi (Ed.), *Biological Effects and Medical Applications of Electromagnetic Energy* (pp. 141-173). Englewood Cliffs, New Jersey: Prentice Hall.

Bowman, R. R. (1976). A probe for measuring temperature in radio-frequency heated material. *IEEE Transactions on Microwwave Theory and Techniques*, *24*, 43-45.

Braithwaite, L., Morrison, W., Otten, L. & Pei, D. (1991). Exposure of fertile chicken eggs to microwave radiation (2.45 GHz, CW) during incubation: technique and evaluation, *Journal of Microwave Power and Electromagnetic Energy, 26*, 206-214.

Burkhardt, M., Pokovi´c, K., Gnos, M., Schmid, T., & Kuster, N. (1996). Numerical and experimental dosimetry of Petri dish exposure setups. *Bioelectromagnetics*, *17,* 483-493.

Burr, J. G. & Krupp, J. H. (1980). Real-time measurement of RFR energy distribution in the Macaca mulatta head. *Bioelectromagnetics*, *1,* 21-34.

Chemeris, N. K., Gapeyev, A. B., Sirota, N. P., Gudkova, O. Y., Tankanag, A. V., Konovalov, I. V., Buzoverya, M. E., Suvorov, V. G., & Logunov, V. A. (2006). Lack of direct DNA

damage in human blood leukocytes and lymphocytes after in vitro exposure to high power microwave pulses. *Bioelectromagnetics*, *27*, 197-203.

Choqueta, P., Juneaua, F., & Bessetteb, J. (2000). New generation of Fabry-Perot fiber optic sensors for monitoring of structures. *SPIE's 7th Annual International Symposium on Smart Structures and Materials* (pp. 1-9), Vol. MC-00077R1, Newport Beach, CA.

Chou, C. K. & Guy, A. W. (1978). Effects of electromagnetic fields on isolated nerve and muscle preparations. *IEEE Transactions on Microwave Theory and Techniques*, *26*, 141-147.

Chou, C. K., Guy, A. W., McDougall, J. A., & Lai, H. (1985). Specific absorption rate in rats exposed to 2,450-MHz microwaves under seven exposure conditions. *Bioelectromagnetics, 6,* 73-88.

Dunscombe, P. B., Constable, R. T., & McLellan, J. (1988). Minimizing the self-heating artefacts due to the microwave irradiation of thermocouples. *International Journal of Hyperthermia*, *4*, 437-445.

Dunscombe, P. B., McLellan, J., & Malaker, K. (1986). Heat production in microwave-irradiated thermocouples. *Medical Physics*, *13*, 457-461.

Galvin, M. J. & McRee, D. I. (1986). Cardiovascular, hematologic, and biochemical effects of acute ventral exposure of conscious rats to 2450-MHz (CW) microwave radiation. *Bioelectromagnetics, 7*, 223-233.

Gammampila, K., Dunscombe, P. B., Southcott, B. M., & Stacey, A. J. (1981). Thermocouple thermometry in microwave fields. *Clinical Physics and Physiological Measurement*, *2*, 285-292.

Gerig, L. H., Szanto, J., & Raaphorst, G. P. (1992). The clinical use of thermocouple thermometry. *Frontiers of Medical and Biological Engineering, 4*, 105-117.

Haveman, J., Smals, O. A., & Rodermond, H. M. (2003). Effects of hyperthermia on the rat bladder: a pre-clinical study on thermometry and functional damage after treatment. *International Journal of Hyperthermia, 19,* 45-57.

Kojima, M., Hata, I., Wake, K., Watanabe, S., Yamanaka, Y., Kamimura, Y., Taki, M., & Sasaki, K. (2004). Influence of anesthesia on ocular effects and temperature in rabbit eyes exposed to microwaves. *Bioelectromagnetics*, 25, 228-233.

Kolb, J. F., Kono, S., & Schoenbach, K. H. (2006). Nanosecond pulsed electric field generators for the study of subcellular effects. *Bioelectromagnetics*, 27, 172-187.

Lin, J. C. (1978). *Microwave auditory effects and applications*. Charles C. Thomas, Springfield.

McRee, D. I. & Davis, H. G. (1984). Whole-body and local dosimetry in rats exposed to 2.45-GHz microwave radiation. *Health Physics*, *46*, 315-320.

Moriyama, E. Matsumi, N., Shiraishi, T., Tamiya, T., Satoh, T., Matsumoto, K., Furuta, T., & Nishimoto, A. (1988). Hyperthermia for brain tumors: improved delivery with a new cooling system. *Neurosurgery*, *23*, 189-195.

Moriyama, E., Salcman, M., & Broadwell, R. D. (1991). Blood-brain barrier alteration after microwave-induced hyperthermia is purely a thermal effect: I. Temperature and power measurements. *Surgical Neurology*, *35*, 177-182.

Nawrot, P. S., McRee, D. I., & Galvin, M. J. (1985). Teratogenic, biochemical, and histological studies with mice prenatally exposed to 2.45-GHz microwave radiation. *Radiation Research, 102*, 35-45.

Pakhomov, A. G. & Doyle, J. (2000). Effect of pulsed microwaves on the population spike in rat hippocampal slices. In: P. Kostarakis and P. Stavroulakis (Eds.), *Biological effects of EMFs. Proc. millennium international workshop on biological effects of electromagnetic fields* (pp. 480-485). Heraklio, Crete, Greece.

Pakhomov, A. G., Doyle, J., Stuck, B. E., & Murphy, M. R. (2003). Effects of high power microwave pulses on synaptic transmission and long term potentiation in hippocampus. *Bioelectromagnetics*, *24*, 174-181.

Pakhomov, A. G., Du, X., Doyle, J., Ashmore, J., & M. R., Murphy. (2002a). Patch-clamp analysis of the effect of high-peak power and CW microwaves on calcium channels. In: P. Kostarakis (Ed.), *Biological effects of EMFs* (Vol. 1, pp. 281-288).

Pakhomov, A. G., Gajsek, P., Allen, L., Stuck, B. E., & Murphy, M. R. (2002b). Comparison of dose dependences for bioeffects of continuous-wave and high-peak power microwave emissions using gel-suspended cell cultures. *Bioelectromagnetics*, *23*, 158-167.

Pakhomov, A. G., Mathur, S. P., Akyel, Y., Kiel, J. L., & Murphy, M. R. (2000a). High-resolution microwave dosimetry in lossy media. In: B. Klauenberg and D. Miklavcic (Eds.), *Radio frequency radiation dosimetry*, Kluwer Academic Publishers, Netherlands (pp. 187-197).

Pakhomov, A. G., Mathur, S. P., Doyle, J., Stuck, B. E., Kiel, J. L., & Murphy, M. R. (2000b). Comparative effects of extremely high power microwave pulses and a brief CW irradiation on pacemaker function in isolated frog heart slices. *Bioelectromagnetics*, *21*, 245-254.

Pakhomov, A. G., Mathur, S. P., & Murphy, M. R. (2003). High-resolution temperature and SAR measurement using different sensors., *25th Annual Meeting of the Bioelectromagnetics Society* (pp. 224-225). Wailea, Maui, HI

99

Paris, D. T. & Hurd, F. K. (1969). *Basic Electromagnetic Theory*. New York: McGraw-Hill Companies.

Saalman, E., Norden, B., Arvidsson, L., Hamnerius, Y., Hojevik, P., Connell, K. E., & Kurucsev, T. (1991). Effect of 2.45 GHz microwave radiation on permeability of unilamellar liposomes to 5(6)-carboxyfluorescein. Evidence of non-thermal leakage. *Biochimica et Biophysica Acta*, *1064*, 124-130.

Schuderer, J., Schmid, T., Urban, G., Samaras, T., & Kuster, N. (2004). Novel high-resolution temperature probe for radiofrequency dosimetry. *Physics in Medicine and Biology*, *49*, N83-N92.

Shellock, F. G., Schaefer, D. J., & Crues, J. V. (1989). Alterations in body and skin temperatures caused by magnetic resonance imaging: is the recommended exposure for radiofrequency radiation too conservative? *British Journal of Radiology, 62*, 904-909.

Spiers, D. E., Adair, E. R., & Baummer, S. C. (1989). Acute thermoregulatory responses of the immature rat to warming by low-level 2,450-MHz microwave radiation. *Biology of Neonate*, *56*, 48-56.

Stogryn, A. (1971). Equations for calculating the dielectric constant of saline water. *IEEE Transactions on Microwave Theory and Techniques*, *19*, 733-736.

Tattersall, J. E., Scott, I. R., Wood, S. J., Nettell, J. J., Bevir, M. K., Wang, Z., Somasiri, N. P., & Chen, X. (2001). Effects of low intensity radiofrequency electromagnetic fields on electrical activity in rat hippocampal slices. *Brain Research, 904*, 43-53.

Walker, K., 3rd, Pakhomova, O. N., Kolb, J., Schoenbach, K. S., Stuck, B. E., Murphy, M. R., & Pakhomov, A. G. (2006). Oxygen enhances lethal effect of high-intensity, ultrashort electrical pulses. *Bioelectromagnetics, 27*, 221-225.

Radio Frequency Radiation Dosimetry Handbook
(Fifth Edition)

Chapter 4.   Review of Literature on Biological Effects of High Peak Power (HPP) Pulses, Electromagnetic Pulse (EMP), and Ultra-Wideband (UWB) Pulses

Ronald L. Seaman, Ph.D.
General Dynamics Information Technology
P.O. Box 35505
Brooks City-Base, TX 78235 USA

ronald.seaman.ctr@brooks.af.mil

4.1   Introduction

Systems emitting pulsed energy at microwave frequencies (300 MHz to 300 GHz) are used for military and civilian applications that include communication and detection. The emitted pulses can be divided into two types.

One type of pulsed energy consists of short bursts of power at a microwave frequency. The microwaves are said to be pulse-modulated and the resulting signal can be represented in the frequency domain by a narrow band of frequencies centered at the microwave frequency. For many applications, the pulses are referred to as being high peak power (HPP) pulses because of the large ratio of the power during the pulse to the time averaged power. The pulse is generally thought of as having a rectangular power profile with a duration, or width, of a few nanoseconds to a few microseconds, and a maximum, or peak, power density in W/cm² or W/m².

The second type of pulsed energy is in the form of short electric-field pulses. Over the years, these have been termed electromagnetic pulse (EMP), ultra-wideband (UWB) pulses, or, more recently in some applications, ultra-broadband (UBB) pulses. Pulse durations range from 0.5 ns to 10 µs or longer and the pulses can be represented in the frequency domain by broad spectra extending into the microwave region. They have relatively little energy at any one frequency. Over time, UWB pulses have become shorter and shorter, and the term ―UWB‖ now usually refers to pulses with durations of less than 10 ns or so. Pulses are commonly described in terms of their time domain parameters of pulse duration, rise time, and peak electric field, the last in V/m. In vitro studies of UWB-like pulses have been conducted using "nanopulses" that have the same range of durations as UWB pulses.

Biological effects of pulsed microwaves and other electromagnetic fields published in the open scientific literature and other reports in the last few years are reviewed here. The coverage consists almost entirely of peer-reviewed published material. In some cases, older material is included because of its uniqueness or for historical continuity. A large proportion of the research consists of studies using animals, isolated tissues, and cells in culture. Cited reviews and research articles can be consulted for other sources of information on a particular topic. Other

reviews include general summaries of earlier work and other sources such as conference proceedings (Lu & de Lorge, 2000; Pakhomov & Murphy, 2000). In cases in which a cited reference is a government report the DTIC accession number, where available, is given to facilitate retrieval. DTIC is the Defense Technical Information Center, which can be accessed at http://www.dtic.mil/ or http://stinet.dtic.mil/str/.

Some areas of research have not been included in order to focus attention on biological effects. Although the operation of cell, or mobile, phones involves pulse modulated microwave radiation, the literature on biological effects of phone emissions are not included. Papers specifically dealing with exposure apparatus for delivering the energy as well as details of exposure systems used in the reviewed papers are not covered. Theoretical analyses and modeling topics related to biological effects are also not covered.

Material is divided into three main sections: HPP pulses, EMP, and UWB pulses. The EMP literature is included because of the similarity between EMP and UWB pulses and the importance of responses to a single pulse of energy. The HPP section includes material on TEMPO pulses for the sake of completeness. Each section is divided into subsections for in vivo and in vitro effects and the subsections in turn are divided into parts for acute, few-pulse exposures and subchronic to chronic exposures involving many pulses.

In reporting results from experiments, commonly accepted terminology is used to describe the magnitude of the amount of electromagnetic energy. For microwave studies, the specific absorption rate (SAR) in W/kg is a measure of the rate of energy deposition in tissue per unit of mass. The specific absorption (SA) in J/kg, a measure of energy deposited, is the time integral of SAR. If energy is absorbed at a constant rate, then SA is simply the product of SAR and the duration of exposure. Specific absorption is used as a preferred measure of effective microwave energy for pulsed microwaves, where SA is given for a single pulse. Voltage pulses applied directly to tissue or a biological preparation are described in terms of the induced electric field in V/m or V/cm. The electric field is found by dividing the applied voltage by the separation distance of the contact electrodes.

4.2 High Peak Power (HPP) Pulse

4.2.1 Animal Studies with HPP Pulses

4.2.1.1 Single-Pulse HPP Effects

4.2.1.1.1 Microwave Hearing and Startle Modification with HPP Pulses

Microwave hearing is the auditory sensation resulting from microwave energy impinging on the head (Chou et al., 1982; Elder & Chou, 2003). Investigation of microwave hearing began in the 1960's (e.g., Frey, 1961, 1962, 1967) but only one original research report on auditory system response has appeared since 1990 (Röschmann, 1991). Microwave hearing is an undisputed effect of pulse modulated microwaves (Guy et al., 1975). Sensation occurs readily with exposure of the head to pulsed microwaves with very small time-averaged power and energy densities. With temperature increase caused by each pulse estimated to be only

102

10^{-6}-10^{-5}°C at sensation threshold (Guy et al., 1975; Chou et al., 1982; Lin, 1978, 1990; Elder & Chou, 2003), the effect is clearly not due to gross heating of tissue.

Auditory sensations in humans and responses in animals in microwave hearing are directly related to characteristics of individual pulses, and to pulse repetition frequency when this is at auditory frequencies. Threshold energy densities for human perception are reported as 2.3-40 µJ/cm² , the product of incident power density and pulse duration (also called energy fluence) (Elder & Chou, 2003). Thresholds for detection by the auditory systems in a variety of animal preparations are 1.5-1240 µJ/cm² fluence and 0.6-180 mJ/kg specific absorption (SA) in the head (Seaman & Lebovitz, 1989; Elder & Chou, 2003). Amplitude of the pressure transient at microwave sensation threshold has been estimated in a finite-difference time-domain (FDTD) model of the human head to be 0.18 Pa (Watanabe et al., 2000).

Single microwave pulses impinging on the heads of rats being startled by an intense burst of acoustic noise or by an air puff were capable of altering the respective startle response (Seaman et al., 1994). Effective microwave pulses had peak head-neck SAR and SA of 15-86 kW/kg and 16-86 mJ/kg, respectively, for 0.96 µs pulses used in the acoustic startle experiment and 55-113 kW/kg and 525-1056 mJ/kg, respectively, for 7.82 µs pulses used in the air-puff experiment. Although SA in both experiments was above thresholds for auditory sensations, the role of microwave hearing was not studied.

4.2.1.2 Microwave Convulsions and Stunning with HPP-Like Pulses

A small number of papers in the open literature report the induction of convulsions, stunning, and/or hypoactivity due to a single pulse of microwave energy to the head. Although the single pulses were longer than those used for communication and detection purposes, these studies are included for the purpose of completeness. Values of SA are estimated here from reported temperature changes by using the relationship SA = dTxc, where SA is the specific absorption (in J/kg), dT is the temperature change (in °C), and c is a representative specific heat capacity of tissue (3700 J/kg-°C).

Mice became —hypokinetic" following exposure to less than lethal pulse energies at 2450 MHz in a microwave fixation apparatus and began to recover within 5 min after exposure (Modak et al., 1981). The elevation of brain temperature was 2 and 4 °C for pulses 15 and 25 ms long, respectively. And the estimated head SAs are 7.4 and 14.8 kJ/kg. The 25-ms pulse caused a significant reduction in brain acetylcholine content.

Rats exposed to a 220-ms pulse of microwave energy at 2450 MHz appeared —stunned and hypoactive" for 5-10 s after exposure (Miller et al., 1987). The estimated SA in this case is 11.5 kJ/kg.

Rats with heads exposed to a 50-360 ms pulse of microwave energy at 915 MHz were —stunned" when brain SA was 28 kJ/kg or greater (Guy & Chou, 1982). The reaction consisted of seizures for about a minute after exposure followed by an —unconscious state" lasting 4-5 min.

103

4.2.1.3 Microwave Fixation with HPP-Like Pulses

Microwave fixation is the process in which microwave energy is delivered to the head of an experimental animal to ―fix" tissues, specifically brain tissue for neurochemical studies. Heating of the tissue by the single application of microwave energy denatures enzymes and essentially stops chemical reactions as well as being lethal to the animal. The more rapid the heating, the more representative is the chemistry of the brain to that of the animal just before fixation. Several papers reported enough information for the SA to be estimated as done above for stunning.

The range of effective pulse energies reported for rats and mice was 1-12.5 kJ and the range of effective SA is 72-198 kJ/kg (Butcher & Butcher, 1976; Delaney & Geiger, 1996; Maruyama et al., 1978; Medina & Stavinoha, 1977; Moroji et al., 1977; Schneider et al., 1982; Merritt et al., 1975; Stavinoha et al., 1977). The range of pulse durations in these studies was 0.15-1.5 s.

4.2.1.4 TEMPO Studies

A number of studies have been performed with TEMPO (Transformer Energized Megavolt Pulsed Output) devices developed to radiate high voltage pulses with durations of 20-80 ns. Because of their irregular power profile with time, TEMPO pulses can be represented in the frequency domain by a band of frequencies more broad than pulse-modulated microwaves but less broad than EMP and UWB pulses. TEMPO pulses are often described by the center frequency (CF) of this band.

Several studies examined behavior of rats during and after exposure to TEMPO pulses. In one of the earliest TEMPO studies, rats were exposed to a single 85 ns pulse with 1.3-GHz CF and estimated incident power density of 0.75-0.99 kW/cm² (Klauenberg et al., 1988). Exposure to a single pulse caused a startle-like response in some animals, but this might have been due to the sound produced by the TEMPO source. In the same study, exposure to ten pulses at 1 Hz led to alteration in baseline activity and disruption of ongoing performance on a rotarod device.

In another TEMPO study of rats, exposure to pulses with 85-ns duration and 2.11-GHz CF caused no change in subsequent performance in an operant task or in tests of avoidance behavior (Hjeresen et al., 1989). Up to 50 pulses with peak power density averaging 10.8 kW/cm² were delivered over 5 min. In a third reported study of rats, exposure to pulses with 200 80-ns duration and 3.0-GHz CF over about 25 min altered performance in a subsequent time discrimination task (Raslear et al., 1993). The authors referred to an acoustic stimulus that was coincident with each TEMPO pulse.

Two studies have been reported exposing monkeys to TEMPO pulses. Exposure of the head to 27-51 pulses with 93-ns duration and 2.37-GHz CF during 20 min of a vigilance task involving discrimination of acoustic tone frequency did not change performance (D'Andrea et al., 1989). The pulses, delivered during acoustic signals used in the task, had peak power of 7-11 kW/cm². In another study, a similar behavioral test with exposure to pulses with 20-60-ns duration and 3.0-GHz CF also showed no change in performance (D'Andrea et al., 1993). Pulses

104

were delivered every 7.5 s and had a peak power density of 45.6 kW/cm². Steps were taken in these two studies to reduce the acoustic signal accompanying each TEMPO pulse.

One TEMPO study examined the effect of the pulses on rat cardiovascular parameters (Jauchem & Frei, 1995). Aortic cannulas inserted prior to exposure were used to determine heart rate and blood pressure during exposure to 10 TEMPO pulses. Two types of pulses were used in separate experiments: pulses with 40-85-ns duration, 1.7-1.8-GHz CF, and 4.5 kW/cm² mean estimated peak power density and pulses with 40-70-ns duration, 1.2-1.4- GHz CF, and 32.6 kW/cm² mean estimated peak power density. No significant change in heart rate was seen in the experiment using pulses with 1.7-1.8-GHz CF. A significant transient increase in blood pressure seen with the first one or two pulses was not present after attenuation of the sound produced by the TEMPO source.

4.2.1.5 Repetitive-Pulse HPP Effects

The study of animals exposed for minutes to hours to microwave radiation has a history of several decades that includes exposure to microwave pulses. A comprehensive review of this extensive literature is not made here. Rather, the reader is referred to reviews for more complete coverage (Lai, 1994; Black & Heynick, 2003; D'Andrea et al., 2003a, 2003b; Elder, 2003a, 2003b; Heynick et al., 2003). The material presented here is a summary of the most recent work on pulsed microwaves and related history for some studies.

The potential interaction of pulsed microwave exposure with neurodegenerative processes was investigated in different experiments. In one set of experiments, a low dose (10 mg/kg) of 3-nitropropionic acid (3-NP), a neurotoxin known to cause degeneration in the rat caudate-putamen, was used to induce mild chemical hypoxia in the brain (Seaman et al., 2002a, 2004b). After each of two daily 3-NP doses, animals were exposed for 30 min to 1250-MHz microwaves as 5.9-μs pulses delivered at 10 Hz with whole-body average SAR of 0, 0.6, or 6 W/kg. Locomotor activity and response to a startling acoustic stimulus were measured immediately after the second exposure and up to 4 weeks afterward. Although changes in activity and startle-response measures were seen in some cases, no significant change was seen for 3-NP, microwave exposure, or their interaction at the end of the experiment. This was not the case for a study of ultrastructure in the caudate-putamen in tissue taken immediately after the second 3-NP and microwave exposures (Seaman & Phelix, 2005). Changes in the endoplasmic reticulum of medium-sized "spiny" neurons were seen after 3-NP administration in sham-exposed animals and in animals exposed at 6 W/kg with or without 3-NP. Exposure at 0.6 W/kg resulted in no change for sham-exposed animals. However, exposure at 0.6 W/kg after 3-NP administration eliminated the effect of 3-NP on the endoplasmic reticulum. The results of this study are consistent with the idea that exposure at the smaller SAR was able to prevent the change in ultrastructure caused by 3-NP.

In another set of experiments, rotenone, a neurotoxin known to cause degeneration in the rat substantia nigra and caudate-putamen, was subcutaneously infused at 2 mg/kg/day with an implanted osmotic minipump (Seaman et al., 2003, 2004a). Animals were exposed for 6 min on the fourth and fifth days after minipump implantation to 1250-MHz microwaves as 6-μs pulses delivered at 10 Hz with whole-body average SAR of 0, 0.4, or 4 W/kg. In testing on the sixth

day after implantation, rotenone-treated animals exhibited a longer time to initiate movement and a reduced number of exploratory vertical movements. In an experiment with exposures delivered by an open-ended waveguide, these rotenone effects were diminished after exposures at 0.4 W/kg (Seaman et al., 2003) while in another experiment with exposures at the same SAR in circular waveguide the effects were not affected by exposure (Seaman et al., 2004a). The difference in effect indicates that some aspect of the exposures differed enough to cause different effectiveness of exposure to interact with effects of rotenone.

Reports in the literature suggested that pulsed microwaves could have specific effects on the eye (Kues et al., 1985, 1992; Lim et al., 1993). A Tri-Service study was also performed to provide more information on potential effects of HPP exposure on the retina (Lu et al., 2000). Rhesus monkeys were exposed to 1250 MHz microwaves as 5.59-µs pulses with 1.04 MW peak power in nine 4-h sessions over 3 weeks. Pulses were delivered at 0, 0.59, 1.18, and 2.79 Hz to provide different average power densities at the eyes that resulted in retinal SAR of 0, 4.3, 8.4, and 20.2 W/kg, respectively. Fundus pictures and angiograms were within normal limits across the study. Minor changes in the electroretinogram were seen and seemed to be SAR-dependent. Minor changes in retinal histopathology were also seen, but no evidence of degeneration was found. A summary table of selected previous studies of microwave effects on lens, cornea, retina, and electroretinogram was included in the paper (Lu et al., 2000).

A considerable amount of controversy surrounds two areas of research with pulsed microwaves. One of these areas is the effect on learning and memory in rats. Performance deficits were seen in a radial arm maze after 45-min exposure in circular waveguide to 2-µs pulses of 2450-MHz radiation with whole-body average SAR of 0.6 W/kg (Lai et al., 1994). Deficits were seen in a water maze after 1-h circular waveguide exposure to similar pulses but at whole-body average SAR of 1.2 W/kg (Wang & Lai, 2000; Lai, 2004). The results of the radial arm maze were not obtained in a similar study also using circular waveguide exposures (Cobb et al., 2004). The various results generated discussion in the literature (Jauchem, 2005; Lai, 2005; Cassel, 2005). Several other studies have since been carried out with variations on microwave exposure parameters and animal model without showing deficits (Sienkiewicz et al., 2000; Dubreuil et al., 2002, 2003; Yamaguchi et al., 2003; Cassel et al., 2004; Cosquer et al., 2005a, 2005b).

The other controversial area involves the effect of exposure to pulsed microwaves on DNA damage and repair. Single-strand DNA breaks were seen in the brains of rats at 4 h after exposure for 2 h in circular waveguide to 2-µs pulses of 2450-MHz radiation with whole-body average SAR of 0.6 or 1.2 W/kg (Lai & Singh, 1995). The number of breaks was SAR dependent. Similar results were obtained in follow-up experiments at 1.2 W/kg (Lai & Singh, 1996, 1997). Damage after exposure to continuous-wave microwave was also seen (Lai & Singh, 1995; Sarker et al., 1994). This work along with a number of other studies have been summarized and critiqued in reviews (Meltz, 2003; Vijayalaxmi & Obe, 2004). More recent work has produced some evidence for the occurrence of breaks but most evidence is for the absence of breaks after exposure to microwaves (e.g., Lagroye et al., 2004; Belyaev et al., 2006; Paulraj & Behari, 2006).

4.2.2 In Vitro Studies with HPP Pulses

Studies that expose isolated tissue samples and cellular preparations have the potential to reveal effects at the tissue and cell level in the absence of confounding interactions with other tissues or cell types. Coupling of microwave pulses to small preparations has been successfully accomplished by taking advantage of the smaller wavelength at 9.2-9.3 GHz, frequencies higher than used in most studies, and utilizing customized techniques (Pakhomov et al., 2000, 2002, 2003).

Application of pulses delivered at regular repetition frequencies resulted in changes that were quite similar to those seen by equivalent heating. This was the case for decrease in interbeat interval of isolated beating frog heart slices when exposed to 1 μs microwave pulses at 50 Hz repetition frequency that gave peak SAR of 250-350 MW/kg and peak SA of 250-350 J/kg (Pakhomov et al., 2000). The decrease in intervals was duplicated by lower power microwave pulses delivered with the same time average power and consequently producing the same heating. In an experiment looking at the density of yeast cells after exposure to 0.5 μs microwave pulses at 10 Hz repetition frequency that gave peak SAR up to 650 MW/kg and peak SA up to 320 J/kg, the effects were not significantly different from those obtained using exposure to continuous-wave microwaves producing the same heating (Pakhomov et al., 2002). In another type of experiment, a slice of rat hippocampus was exposed to microwave pulses with 0.5-2 μs duration and 0.5-10 Hz repetition frequency that gave peak SAR up to 500 MW/kg and peak SA up to 250-1000 J/kg (Pakhomov et al., 2003). The evoked population spike used as an index of synaptic response was changed by microwave exposure in the same way as long as microwave pulse duration and repetition frequency were set to give the same average power, which gave the same heating. Long term potentiation of the evoked population spike, a standard test in this preparation, was also studied and it, too, showed changes consistent with thermal mediation.

The hippocampal slice was also studied using this exposure system to deliver microwave pulses synchronized with the evoked population spike potential (Doyle et al., 2006). Peak SAR and pulse SA were similar to those in the previous hippocampal work: 740 MW/kg and 1480 J/kg, respectively. Single microwave pulses were delivered at four different times relative to the electrical stimulus that evoked the population spike. Sham exposures and exposures with unsynchronized microwaves were also performed. The population spike was depressed when the microwave pulse was delivered 1 ms after the electrical stimulus but not for other times used. Because the temperature change resulting from a pulse was 0.3-0.4 °C regardless of pulse timing, the depression specific to the single time interval seemed to be unrelated to the gross temperature of the preparation.

4.3   Electromagnetic Pulse (EMP)

4.3.1   Animal Studies with EMP

4.3.1.1   Single-Pulse EMP Effects

The earliest studies on the biological effects of EMP were done using large outdoor transmission lines to expose animals. This work along with other aspects of EMP is included in a summary technical report (Patrick & Vault, 1990).

Performance of rats in a maze was affected for up to 10 min by exposure to three pulses of 600 kV/m but appeared to recover after about 30 min (Hirsch et al., 1968; Hirsch & Bruner, 1972). The pulses had a rise time of 3 ns and an exponential fall time with time constant of 550 ns. No change in a performance task was found for monkeys exposed to eight of these pulses with amplitudes 300-600 kV/m (Hirsch & Bruner, 1972) and no change was seen in blood chemistry of dogs exposed to 10 pulses of 330 kV/m (Hirsch & Bruner, 1972). The exposed rats and monkeys in these studies exhibited a startle-like response to many of the pulses, which were reported not to produce sound detectable to the investigators (Hirsch et al., 1968; Hirsch & Bruner, 1972).

4.3.2   Repetitive-Pulse EMP Effects

Effects of longer EMP exposures were also studied at the outdoor facility with pulses having exponential decay with the same 550-ns time constant delivered at 5 Hz. Three studies used pulses with 5-ns rise time and 477-kV/m peak electric field. With continuous exposure 5 days a week for 38 weeks, no effect on blood chemistry or cell counts, bone marrow, or offspring was seen in rats and no change in onset or incidence of leukemia was seen in leukemia-prone mice (Skidmore & Baum, 1974). With continuous exposure for 94 weeks, no effect on blood chemistry or cell counts, bone marrow, reproductive capability, or tumor incidence was seen in rats (Baum et al., 1976). With daily exposures of 8 h per day for 45 days, no effect on blood cell counts, bone marrow, or reproductive capability was seen in dogs (Baum, 1979). In a study using pulses with 11-ns rise time and 266-kV/m peak electric field applied for 1 h, no significant effect was seen on electroencephalogram (EEG) or Sidman avoidance behavior in a rhesus monkey (Mattsson & Oliva, 1976). At another facility, no change in pentobarbital sleeping time or blood chemistry was seen in rabbits exposed for up to 2 h to 100-200-kV/m EMP-like pulses with rise time less than 100 ns and exponentially decreasing sinusoid lasting 400 ns delivered at 10-38 Hz (Cleary et al., 1980).

In contrast to reports that describe no EMP effect, various effects have been reported for pulses with 20-ns rise time, 25-30-μs duration, and 20-120-kV/m peak electric field. Changes were seen in apoptotic rate in lymphocytes taken from dogs up to 120 days after exposure to single 20-, 60-, or 120-kV/m pulses or ten 120-kV/m pulses (Cui et al., 2001). The following three studies are summarized from English-language abstracts. After exposure to five 60-kV/m pulses, changes were seen in the amino acid content of rat hippocampus and related to slower learning of the animals (Li et al., 2003). Also after exposure to five 60-kV/m pulses, effects

<div align="center">108</div>

were seen in gestation and offspring development in mice (Wang et al., 2003a) as well as in testosterone and Leydig cells of the testes in male mice (Wang et al., 2003b).

4.3.3 In Vitro Studies with EMP

Preparations of isolated cells and organelles have also been used in studies of EMP biological effects. The studies are summarized from English-language abstracts. In one study, cells of the human lung carcinoma cell line GLC-82 showed increased apoptosis rate with changes in pro-apoptotic and anti-apoptotic pathways after exposure to five 60-kV/m pulses (Cao et al., 2002). Isolated rat liver mitochondria showed changes in membrane mobility and lipid peroxidation after exposure to an unspecified number of 60-kV/m pulses (Wang et al., 2002). Isolated cardiac myocytes showed changes in spontaneous beating rate, ion content, and conformation after unspecified exposure to EMP or high power microwave pulses (Deng et al., 2005). The lack of available exposure details makes these studies in isolated preparations difficult to assess.

4.4 Ultra-wideband (UWB) Pulse and Nanopulse

4.4.1 Animal Studies with UWB Pulses

Two UWB studies used free-field exposures with 8-ns, 250-kV/m pulses at 60 Hz. In the first study, performance on a primate equilibrium platform was measured in Macaque monkeys previously trained on the device (Sherry et al., 1995). No difference in performance was seen immediately after or 1, 2, 3, 4, or 5 d after each of two 2-min exposures. In the second study, a number of endpoints were examined in rats exposed for 2 min by comparing results with corresponding sham-exposed animals (Walters et al., 1995). No difference was seen in swimming performance or functional observation battery 3 h after exposure or in serum enzymes in blood taken 2 or 48 h after exposure. No difference was seen in immunocytochemical staining for brain c-fos protein in tissue taken 2 h after exposure.

In a more recent report using free-field exposure, rats and rabbits were exposed to 1-2-ns, 10-13-kV/m UWB pulses at 6 Hz for 1 h (Petrova et al., 2005). Immediately after exposure, the EEG of exposed rats exhibited differences in spectral content, particularly at frequencies near the pulse repetition frequency of 6 Hz. Information sufficient to judge the significance of the differences was not reported. The EEG along with electromyogram (EMG) of exposed rabbits was followed for more than 21 h after exposure. Beginning at about 18 h after exposure, the animals showed differences in sleep EEG patterns relative to controls. The differences included increased duration of slow sleep and paradoxical sleep. The investigators appeared to have used implanted metal electrodes for the EEG recordings and the effect of this methodology on the EEG and EMG is not known.

In a cardiovascular study, anesthetized rats were exposed to 6-ns, 19-20-kV/m UWB pulses at 1000 or 2000 Hz using parallel-plate transmission line (Jauchem et al., 1999). The electrocardiogram (ECG) and arterial blood pressure were recorded before, during, and after 0.5-5-s exposures. The three types of exposure used did not result in any change in heart rate or blood pressure averaged over 10 or 30-s intervals.

109

Another study using parallel-plate transmission line looked at convulsions induced by pentylenetetrazol in rats (Miller et al., 1999). Animals were injected with the convulsant and exposed 20 s later to 1.9 ns, 40-kV/m UWB pulses at 1000 Hz for 2 min. No difference was seen between UWB-exposed and sham-exposed groups in latency to initial seizure, latency to full convulsion, duration of seizure, and time to death.

A teratology study exposing pregnant rats (dams) and, in one experiment, both dams and their male pups to 1.8 ns, 55-kV/m UWB pulses at 1000 Hz was also conducted using parallel-plate transmission line (Cobb et al., 2000). In the experiment with dams exposed for 2 min on gestation days 3-18, female and male pups were tested for developmental indices and stress vocalizations and male pups were tested on a water maze and later for reproductive capability. In the experiment with dams exposed on gestation days 3-18 and pups exposed for 2 min on postnatal days 1-10, male pups were assessed for hippocampal morphology 12 d later and operant conditioning 25 d later. The few spurious differences seen over all endpoints between UWB-exposed and sham-exposed groups were attributed to the large number of statistical tests performed.

Another study using parallel-plate transmission line involved repeated UWB exposures of tumor-prone mice to 1.9-ns, 40-kV/m pulses at 1000 Hz (Jauchem et al., 2001). Animals were exposed for 2 min once a week for 12 weeks and followed for 64 weeks after the exposures. No difference due to UWB exposure was seen in animal weight, tumor incidence, tumor size, or time to death.

Studies of possible effects of UWB exposure on the nervous system were investigated using a giga transverse electromagnetic cell (GTEM) to expose animals to 0.9-1.03-ns, 99-105-kV/m pulses. Measured endpoints were nociception, or pain sensation, and spontaneous locomotor activity in exposed mice. In the first study, some mice were pretreated with an injection of morphine in order to test possible UWB modification of the effect of morphine on nociception (Seaman et al., 1998). Groups of mice were studied in different experiments with exposures of 15, 30, or 45 min with pulses at 60 or 600 Hz. No effect of UWB exposure was seen on nociception or activity of the mice. In addition, no modification of the effect of morphine was seen. In the second study (Seaman et al., 1999), mice were exposed for 15 min at 600 Hz with some animals injected before exposure with N^G-nitro-L-arginine methyl ester (L-NAME), an inhibitor of nitric oxide synthase. The effects of L-NAME were to increase latency of response to a thermal stimulus and to increase spontaneous activity. Exposure to UWB pulses had no effect on latency, activity, or latency changes due to L-NAME. However, exposure to UWB pulses did eliminate the L-NAME-induced increase in activity, indicating a possible interaction with the mechanisms of nitric oxide production.

Mice were also exposed to UWB pulses in a GTEM in another study investigating damage in immature red blood cells (Vijayalaxmi et al., 1999). Peripheral blood and bone marrow were collected from mice at 18 or 24 h after a 15-min exposure to 0.92-0.97-ns, 91-103-kV/m pulses and the incidence of micronuclei was determined in polychromatic erythrocytes. No effect of UWB exposure was seen at either time point in this standard genotoxic test.

In another study using a GTEM, arterial blood pressure was recorded from anesthetized rats for 2 min before, during, and 2 min after 2-min exposures to 0.97-0.99-ns, 87-104-kV/m UWB pulses (Jauchem et al., 1998). No change was seen in 30-s averages of heart rate and blood pressure over the 6 min of recording.

Another cardiovascular study using anesthetized rats exposed in a GTEM to 0.78-0.79-ns, 106-kV/m UWB pulses looked at immediate changes in the cardiac cycle as reflected in the ECG (Seaman & Jauchem, 2004). Arterial blood pressure was recorded as before (Jauchem et al., 1999) as well as the ECG. Each animal received multiple 25-ms bursts of pulses during the R wave or T wave of the ECG or no pulses. No significant effect on various ECG timing intervals or heart rate was seen and no obvious effect on blood pressure was noted.

Two studies on long-term cardiovascular effects of UWB exposure in rats were conducted using a GTEM. In both studies the single UWB exposure was 6 min long to correspond to the averaging time in an exposure standard (IEEE, 1999). In the first study, blood pressure waveforms, measured using a tail cuff method, were used to derive blood pressure parameters and heart rate at 45 min, 24 h, 72 h, 1 week, 2 weeks, 3 weeks, and 4 weeks after exposure to pulses delivered at 500 or 1000 Hz (Lu et al., 1999). No difference in heart rate was seen at any time point. However, significant reductions in systolic, diastolic, and/or mean blood pressure were seen at all time points. In a replication study, UWB pulses were again delivered at 500 or 1000 Hz for 6 min and blood pressure and heart rate were determined in the same ways as before at 18 min, 24 h, and 2 weeks (Lu & Mathur, 2002). Significant decreases in systolic blood pressure were seen at 18 min and 2 wk after exposure in this second study.

4.4.2 In Vitro Studies with UWB Pulses

4.4.2.1 Single-Pulse UWB Effects

As part of evaluating the effect of UWB pulses on excitable tissues such as nerve and muscle, one prefers to have a strength-duration curve that plots the threshold for applied electric field or current density to stimulate an action potential for pulses with nanosecond durations. Traditional strength duration curves available in the research literature for excitable tissues did not extend to pulses shorter than about 10 μs. A study providing a strength duration relationship for shorter pulse durations was recently reported (Rogers et al., 2004). For 1.2-ns UWB pulses, threshold was 2.4 MV/m. The strength-duration curve was found to have the shape of traditional curves and to extrapolate to shorter durations based on constant stimulus electrical charge.

The term "nanopulse" is used to describe nanosecond voltage pulses applied to biological preparations by direct contact in order to obtain intense electric fields. The pulses are similar to UWB pulses in pulse duration, ranging from a few nanoseconds to 300 ns. Unlike UWB pulses, however, the propagation of nanopulses is not a major concern because contact electrodes are used to apply them. The seemingly unique ability of nanopulses is to affect organelles inside a cell with little or no effect on the cell membrane (Schoenbach et al., 2001, 2002; Deng et al., 2003; Beebe & Schoenbach, 2005). Electric fields used in the various preparations to study nanopulse effects are in the range of 2.5-15 MV/m.

111

A number of nanopulse experiments have shown effects on cells without immediate cell lethality that might be expected with severe disruption of the cell plasma membrane. Integrity of the membrane soon after nanopulse application has been confirmed experimentally for at least some conditions (Hall et al., 2005; Frey et al., 2006). Release of stored calcium into the cytoplasm might be the most studied effect of nanopulses (Beebe et al., 2003a, 2004; Vernier et al., 2003, 2004c; Buescher et al., 2004; White et al., 2004; Sun et al., 2006). The possibility of cell death as a result of sufficient perturbation of intracellular processes has also been examined. Apoptosis, a natural cell death process executed by the cell, and inhibition of growth have been observed, (Beebe et al., 2002, 2003a, 2003b; Stacey et al., 2003; Vernier et al., 2003, 2004a, 2004b; Hall et al., 2005). Activation of caspases (cysteinyl-aspartate-cleaving proteases), molecules that mediate apoptosis, was also detected in some of these studies. Cell death and other cellular responses to nanopulses have been studied in a variety of cell types (Hair et al., 2003; Chen et al., 2004; Pakhomov et al., 2004; Vernier et al., 2004c; Nuccitelli et al., 2006; Vernier et al., 2006; Walker et al., 2006).

4.4.2.2 Repetitive-Pulse UWB Effects

An early study using a 0.3-0.4-ns voltage pulse looked at histology of isolated spinal cord and brainstem from bullfrogs (Sandler et al., 1975). The tissue sample was inserted into a coaxial transmission line with 0.51 cm separation between inner and outer conductors. Six voltage pulses applied at 250 Hz resulted in a calculated peak electric field of 130 kV/m in the sample. In light microscopy no cell damage was found in the large motor neurons of exposed tissue and nuclear groups had normal appearance.

The GTEM used for exposing rodents to UWB pulses has also been used to expose other biological preparations. Exposure of yeast cells (*Saccharomyces cerevisiae*) to 1.01-1.02-ns, 101-104-kV/m pulses with 164-166-ps rise time at 16 or 600 Hz for 30 min resulted in no significant effect on colony-forming ability, occurrence of mutations, or chromosome recombinations (Pakhomova et al., 1997). Exposure with the same UWB parameters of yeast cells previously exposed to ultraviolet radiation resulted in no change in UV-induced reciprocal and non-reciprocal recombination, mutagenesis, or cell survival (Pakhomova et al., 1998). Exposure of RAW 264.7 macrophages to 0.98-ns, 103-kV/m pulses with 162-ps rise time (means) at 600 Hz for 30 min resulted in increased production of nitric oxide by the cells, but only when they had been incubated in medium containing nitrate (Seaman et al., 2002b). Exposure to 0.79-ns, 100-kV/m pulses at 250 Hz for 90 min led to increased activation of NF-KB (nuclear factor kappa B) in human monocytes (Natarajan et al., 2006) similar to what had also been seen with HPP exposure (Natarajan et al., 2002). But because this was only seen at certain times after exposure, the authors concluded that such an increase would have minimal functional effect.

Another GTEM used to study the biological effects of UWB effects delivered pulses of 10-ns duration. In one study using a 2-h exposure to these pulses (unreported rise time and apparently unstable 5- to 20-kV/m peak amplitude), increased proliferation of AML-12 mouse hepatocytes was seen 8-24 h after their exposure (Dorsey et al., 2005). In another study using 0.25- to 4-h exposures to these pulses with ~100 ps rise time and 0.18-, 1.8-, and 18-kV/m peak

112

amplitudes, a significant increase in cell proliferation was seen for exposures that were at least 4 h long and only for 18-kV/m pulses (Sylvester et al., 2005). The effect was larger for pulses at 1 and 10 kHz relative to sham-exposed control and, in the 4-h exposures, also pulses at 100 and 1000 kHz. In another study, evidence was found for differences in the fertility of the nematode worm *C. elegans* after exposures to 18-kV/m pulses in the GTEM or 62-kV/m pulses in another system at 1, 10, or 100 kHz in both systems (Bojjawar et al., 2006).

In one brief report, a "BTEM" cell, described as having a frequency range of DC to 17 GHz, was used to expose umbilical blood, sheep red cells, and HeLa cells to UWB pulses with 1.2-ns rise time and 2.4-ns duration for 0-3 h (Wang et al., 1997). Electric field amplitude and pulse repetition rate, however, were not specified. Changes in "T-lymph" cell size and shape as well as incidence of abnormal nuclei were reported to increase with exposure duration.

4.5   Conclusions

The review of literature on biological effects of pulsed microwave and electric fields reveals a diverse collection of experiments. This is the case even for the limitations imposed on coverage of this review. The literature seems clear on certain points but shows unresolved topics in some areas. Evolving applications of pulsed electromagnetic fields such as mobile phones and new types of pulses for communication and detection will make this field of study even more challenging in the future.

4.6   References

Baum, S. J. (1979). Tests of biological integrity in dogs exposed to an electromagnetic pulse environment. *Health Physics*, *36*, 159-165.

Baum, S. J., Ekstrom, M. E., Skidmore, W. D., Wyant, D. E., & Atkinson, J. L. (1976). Biological measurements in rodents exposed continuously throughout their adult life to pulsed electromagnetic radiation. *Health Physics*, *30*, 161-166.

Beebe, S. J., & Schoenbach, K. H. (2005). Nanosecond pulsed electric fields: A new stimulus to activate intracellular signaling. *Journal of Biomedicine and Biotechnology*, *2005*, 297-300.

Beebe, S. J., Blackmore, P. F., White, J., Joshi, R. P., & Schoenbach, K. H. (2004). Nanosecond pulsed electric fields modulate cell function through intracellular signal transduction mechanisms. *Physiological Measurement*, *254*, 1077-1093.

Beebe, S. J., Fox, P. M., Rec, L. J., Somers, K., Stark, R. H., & Schoenbach, K. H. (2002). Nanosecond pulsed electric field (nsPEF) effects on cells and tissues: Apoptosis induction and tumor growth inhibition. *IEEE Transactions on Plasma Sciences, 30,* 286-292.

Beebe, S. J., Fox, P. M., Rec, L. J., Willis, E. L., & Schoenbach, K. H. (2003a). Nanosecond, high-intensity pulsed electric fields induce apoptosis in human cells. *Journal of the Federation of American Societies for Experimental Biology, 17*, 1493-1495.

Beebe, S. J., White, J., Blackmore, P. F., Deng, Y., Somers, K., & Schoenbach, K. H. (2003b). Diverse effects of nanosecond pulsed electric fields on cells and tissues. *DNA and Cell Biology*, *22*, 785-796.

Belyaev, I. Y., Koch, C. B., Terenius, O., Roxstrom-Lindquist, K., Malmgren, L. O., Sommer, W. H., Salford, L. G., & Persson, B. R. (2006). Exposure of rat brain to 915 MHz GSM microwaves induces changes in gene expression but not double stranded DNA breaks or effects on chromatin conformation. *Bioelectromagnetics*, *27*, 295-306.

Black, D. R., & Heynick, L. N. (2003). Radiofrequency (RF) effects on blood cells, cardiac, endocrine, and immunological functions. *Bioelectromagnetics*, Suppl 6, S187-S195.

Bojjawar, T., Jalari, M., Aamodt, E., Ware, M. F., & Haynie, D. T. (2006). Effect of electromagnetic nanopulses on C. elegans fertility. *Bioelectromagnetics, 27*, 515-520.

Buescher, E. S., Smith, R. R., & Schoenbach, K. H. (2004). Submicrosecond intense pulsed electric field effects on intracellular free calcium: Mechanisms and effects. *IEEE Transactions on Plasma Sciences*, *32*, 1563-1572.

Butcher, L. L., & Butcher, S. H. (1976). Brain temperature and enzyme histochemistry after high intensity microwave irradiation. *Life Sciences, 19*, 1079-1087.

Cao, X. Z., Zhao, M. L., Wang, D. W., & Dong, B. (2002). [Apoptosis of human lung carcinoma cell line GLC-82 induced by high power electromagnetic pulse]. *Ai Zheng*, *21*, 929-933. Chinese.

Cassel, J. C. (2005). Radial arm maze performance of rats following repeated low-level microwave radiation exposure by Cobb et al. [BEMS, 2004, 25:49-57] and letter to the editor by Lai [BEMS, 2005, 26:81]. [Letter to the editor]. *Bioelectromagnetics*, *26*, 526-7.

Cassel, J. C., Cosquer, B., Galani, R., & Kuster, N. (2004). Whole-body exposure to 2.45 GHz electromagnetic fields does not alter radial-maze performance in rats. *Behavioural Brain Research*, *155*, 37-43.

Chen, N., Schoenbach, K. H., Kolb, J. F., James, Swanson R., Garner, A. L., Yang, J., Joshi, R. P., & Beebe, S. J. (2004). Leukemic cell intracellular responses to nanosecond electric fields. *Biochemical and Biophysical Research Communications*, *317*, 421-427.

Chou, C. K., Guy, A. W., & Galambos, R. (1982). Auditory perception of radio-frequency electromagnetic fields. *Journal of Acoustical Society of America*, *71*(6), 1321-1334.

Cleary, S. F., Nickless, F., Liu, L. M., & Hoffman, R. (1980). Studies of exposure of rabbits to electromagnetic pulsed fields. *Bioelectromagnetics*, *1*, 345-352.

Cobb, B. L., Jauchem, J. R., & Adair, E. R. (2004). Radial arm maze performance of rats following repeated low level microwave radiation exposure. *Bioelectromagnetics*, *25*, 49-57.

Cobb, B. L., Jauchem, J. R., Mason, P. A., Dooley, M. P., Miller, S. A., Ziriax, J. M., & Murphy, M. R. (2000). Neural and behavioral teratological evaluation of rats exposed to ultra-wideband electromagnetic fields. *Bioelectromagnetics*, *21*, 524-537.

Cosquer, B., Galani, R., Kuster, N., & Cassel, J. C. (2005a). Whole-body exposure to 2.45 GHz electromagnetic fields does not alter anxiety responses in rats: A plus-maze study including test validation. *Behavioural Brain Research*, *156*, 65-74.

Cosquer, B., Kuster, N., & Cassel, J. C. (2005b). Whole-body exposure to 2.45 GHz electromagnetic fields does not alter 12-arm radial-maze with reduced access to spatial cues in rats. *Behavioural Brain Research*, *161*, 331-334.

Cui, Y., Yang, H., Gao, Y., Cui, X., Xiong, C., Gao, L, & Wang, D. (2001). Effect and mechanism of electronic magnetic pulse on peripheral lymphocytes in dogs. *Chinese Medical Journal (Engl)*, *114*, 1019-1021.

D'Andrea, J. A., Cobb, B. L., Knepton, J., & Bates, F. (1993). *Behavioral performance in monkeys exposed to Tempo high-peak-power microwave pulses at 3 GHz* (NAMRL-1389). Naval Aerospace Medical Research Laboratory. DTIC Accession Number ADA280551.

D'Andrea, J. A., Knepton, J., Cobb, B. L., Klauenberg, B. J., Merritt, J. H., & Erwin, D. N. (1989). *High peak power microwave pulses at 2.37 GHz: No effect on vigilance performance in monkeys*. Joint Naval Aerospace Medical Research Laboratory Research Report, NAMRL-1348, and USAF School of Aerospace Medicine, USAFSAM-TR-89-21. DTIC Accession Number ADA219570.

D'Andrea, J. A., Adair, E. R., & de Lorge, J. O. (2003a). Behavioral and cognitive effects of microwave exposure. *Bioelectromagnetics*, Suppl 6, S39-S62.

D'Andrea, J. A., Chou, C. K., Johnston, S. A., & Adair, E. R. (2003b). Microwave effects on the nervous system. *Bioelectromagnetics*, Suppl 6, S107-S147.

Delaney, S. M., & Geiger, J. D. (1996). Brain regional levels of adenosine and adenosine nucleotides in rats killed by high-energy focused microwave irradiation. *Journal of Neuroscience Methods, 64*, 151-156.

Deng, H., Wang, D., Peng, R., Wang, S., Chen, J., Zhang, S., Dong, B., & Wang, X. (2005). [The electroporation effects of high power pulse microwave and electromagnetic pulse irradiation on the membranes of cardiomyocyte cells and the mechanism therein involved]. *Sheng Wu Yi Xue Gong Cheng Xue Za Zhi*, *22*, 672-676, 694. Chinese.

Deng, J., Schoenbach, K. H., Buescher, E. S., Hair, P. S., Fox, P. M., & Beebe, S. J. (2003). The effects of intense submicrosecond electrical pulses on cells. *Biophysical Journal*, *84*, 2709-2714.

Dorsey, W. C. Ford, B. D., Roane, L., Haynie, D. T., & Tchounwou, P. B. (2005). Induced mitogenic activity in AML-12 mouse hepatocytes exposed to low-dose ultra-wideband electromagnetic radiation. *International Journal of Environmental Research and Public Health*, *2*, 24-30.

Doyle, J., Stuck, B., Murphy, M. R., & Pakhomov, A. G. (2006). Suppression of synaptic transmission in hippocampus by extremely-high power microwave pulses synchronized with neuronal excitation. In S. N. Ayrapetyan, & M. S. Markov (Eds.), *Bioelectromagnetics* (pp. 123-133). Netherlands: Springer.

Dubreuil, D., Jay, T., & Edeline, J. M. (2002). Does head-only exposure to GSM-900 electromagnetic fields affect the performance of rats in spatial learning tasks? *Behavioural Brain Research*, 129, 203-210.

Dubreuil, D., Jay, T., & Edeline, J. M. (2003). Head-only exposure to GSM 900-MHz electromagnetic fields does not alter rat's memory in spatial and non-spatial tasks. *Behavioural Brain Research*, 145, 51-61.

Elder, J. A. (2003a). Ocular effects of radiofrequency energy. *Bioelectromagnetics*, Suppl 6, S148-S161.

Elder, J. A. (2003b). Survival and cancer in laboratory mammals exposed to radiofrequency energy. *Bioelectromagnetics*, Suppl 6, S101-S106.

Elder, J. A., & Chou, C. K. (2003). Auditory response to pulsed radiofrequency energy. *Bioelectromagnetics*, Suppl 6, S162-S173.

Frey, A. H. (1961). Auditory system response to radio frequency energy. *Aerospace Medicine*, 32, 1140-1142.

Frey, A. H. (1962). Human auditory system response to modulated electromagnetic energy. *Journal of Applied Physiology*, *17*, 689-692.

Frey, A. H. (1967). Brain stem evoked responses associated with low-intensity pulsed UHF energy. *Journal of Applied Physiology,* 23, 984-988.

Frey, W., White, J. A., Price, R. O., Blackmore, P. F., Joshi, R. P., Nuccitelli, R., Beebe, S. J., Schoenbach, K. H., & Kolb, J. F. (2006). Plasma membrane voltage changes during nanosecond pulsed electric field exposure. *Biophysical Journal*, *90*, 3608-3615.

Guy, A. W., & Chou, C. K. (1982). Effects of high-intensity microwave pulse exposure of rat brain. *Radio Science, 17*(5S), 169S-178S.

116

Guy, A. W., Chou, C. K., Lin, J. C., & Christensen, D. (1975). Microwave-induced acoustic effects in mammalian auditory systems and physical materials. *Annals of the New York Academy of Sciences*, *247*, 194-218.

Hair, P. S., Schoenbach, K. H., & Buescher, E. S. (2003). Sub-microsecond, intense pulsed electric field applications to cells show specificity of effects. *Bioelectrochemistry, 61*, 65-72.

Hall, E. H., Schoenbach, K. H., & Beebe, S. J. (2005). Nanosecond pulsed electric fields (nsPEF) induce direct electric field effects and biological effects on human colon carcinoma cells. *DNA and Cell Biology, 24*, 283-291.

Heynick, L. N., Johnston, S. A., & Mason, P. A. (2003). Radio frequency electromagnetic fields: cancer, mutagenesis, and genotoxicity. *Bioelectromagnetics*, Suppl 6, S74-S100.

Hirsch, F. G., & Bruner, A. (1972). Absence of electromagnetic pulse effects on monkeys and dogs. *Journal of Occupational Medicine, 14*, 380-386.

Hirsch, F. G., McGiboney, D. R., & Harnish, T. D. (1968). The psychologic consequences of exposure to high density pulsed electromagnetic energy. *International Journal of Biometerorology*, *12*, 263-270.

Hjeresen, D. L., Umbarger, K. O., Klauenberg, B. J., & Erwin, D. N. (1989). *Lack of behavioral effects of high-peak-power microwave pulses from an axially extracted virtual cathode oscillator* (Technical Report USAFSAM-TR-89-24). Brooks Air Force Base: USAF School of Aerospace Medicine. DTIC Accession Number ADA220779.

Institute of Electronics and Electrical Engineers (IEEE). (1999). *IEEE standard for safety levels with respect to human exposure to radio frequency electromagnetic fields, 3 kHz to 300 GHz* (IEEE Std C95.1-1991).

Jauchem, J. R. (2005). Lai's letter on Radial arm maze performance of rats following repeated low level microwave radiation exposure. *Bioelectromagnetics, 25*, 49-57 (2005). [Letter to the editor]. *Bioelectromagnetics*, 26, 525.

Jauchem, J. R., & Frei, M. R. (1995). High-peak-power microwave pulses: Effects on heart rate and blood pressure in unanesthetized rats. *Aviation, Space, and Environmental Medicine, 66*, 992-997.

Jauchem, J. R., Frei, M. R., Ryan, K. L., Merritt, J. H., & Murphy, M. R. (1999). Lack of effects on heart rate and blood pressure in ketamine-anesthetized rats briefly exposed to ultra-wideband electromagnetic pulses. *IEEE Transactions on Biomedical Engineering*, *46*, 117-120.

Jauchem, J. R., Ryan, K. L., Frei, M. R., Dusch, S. J., Lehnert, H. M., & Kovatch, R. M. (2001). Repeated exposure of C3H/HeJ mice to ultra-wideband electromagnetic pulses: Lack of effects on mammary tumors. *Radiation Research*, *155*, 369-377.

Jauchem, J. R., Seaman, R. L., Lehnert, H. M., Mathur, S. P., Ryan, K. L., Frei, M. R., & Hurt, W. D. (1998). Ultra-wideband electromagnetic pulses: Lack of effects on heart rate and blood pressure during two-minute exposures of rats. *Bioelectromagnetics*, *19*, 330-333.

Klauenberg, B. J., Merritt, J. H., & Erwin, D. N. (1988). *Behavioral effects of exposure to the Tempo high-power microwave system* (Technical Report USAFSAM-TR-87-35). Brooks Air Force Base: USAF School of Aerospace Medicine. DTIC Accession Number ADA193305.

Kues, H. A., Hirst, L. W., Lutty, G. A., D'Anna, S. A., & Dunkelberger, G. R. (1985). Effects of 2.45-GHz microwaves on primate corneal endothelium. *Bioelectromagnetics*, *6*, 177-188.

Kues, H. A., Monahan, J. C., D'Anna, S. A., McLeod, D. S., Lutty, G. A., & Koslov, S. (1992). Increased sensitivity of the non-human primate eye to microwave radiation following ophthalmic drug pretreatment. *Bioelectromagnetics*, *13*, 379-393.

Lagroye, I., Anane, R., Wettring, B. A., Moros, E. G., Straube, W. L., Laregina, M., Niehoff, M., Pickard, W. F., Baty, J., & Roti Roti, J. L. (2004). Measurement of DNA damage after acute exposure to pulsed-wave 2450 MHz microwaves in rat brain cells by two alkaline comet assay methods. *International Journal of Radiation Biology*, *80*, 11-20.

Lai, H. (1994). Neurological effects of radiofrequency electromagnetic radiation. In J. C. Lin (Ed.), *Advances in electromagnetic fields in living systems, Vol. 1* (pp. 27-80). New York: Plenum.

Lai, H. (2004). Interaction of microwaves and a temporally incoherent magnetic field on spatial learning in the rat. *Physiology & Behavior*, *82*, 785-789.

Lai, H. (2005). Comment on "Radial arm maze performance of rats following repeated low level microwave radiation exposure". *Bioelectromagnetics*, *26*, 81.

Lai, H., & Singh, N. P. (1995). Acute low-intensity microwave exposure increases DNA single-strand breaks in rat brain cells. *Bioelectromagnetics*, *16*, 207-210.

Lai, H., & Singh, N. P. (1996). Single- and double-strand DNA breaks in rat brain cells after acute exposure to radiofrequency electromagnetic radiation. *International Journal of Radiation Biology*, *69*, 513-521.

Lai, H., & Singh, N. P. (1997). Melatonin and a spin-trap compound block radiofrequency electromagnetic radiation-induced DNA strand breaks in rat brain cells. *Bioelectromagnetics*, *18*, 446-454.

Lai, H., Horita, A., & Guy, A.W. (1994). Microwave irradiation affects radial-arm maze performance in the rat. *Bioelectromagnetics*, *15*, 95-104.

Li, Y. H., Wang, D. W., Peng, R. Y., Li, Z. J., Dong, B., Dong, F. T., Liang, Y. Q., & Hu, W. H. (2003). [Effects of electromagnetic pulse on contents of amino acids in hippocampus of rats]. *Zhonghua Lao Dong Wei Sheng Zhi Ye Bing Za Zhi*, *21*, 323-325. Chinese.

Lim, J. I., Fine, S. L., Kues, H. A., & Johnson, M. A. (1993). Visual abnormalities associated with high-energy microwave exposure. *Retina*, *13*, 230-233.

Lin, J. C. (1978). *Microwave auditory effects and applications*. Springfield, IL: Charles C. Thomas.

Lin, J. C. (1990). Auditory perception of pulsed microwave radiation. In O. P. Gandhi (Ed.), *Biological effects and medical applications of electromagnetic energy*. (Chapter 12, pp. 277-318). Englewood Cliffs, NJ: Prentice Hall.

Lu, S.-T., & de Lorge, J. O. (2000). Biological effects of high peak power radiofrequency pulses. In J. C. Lin (Ed.), *Advances in electromagnetic fields in living systems Vol. 3* (pp. 207-264). New York: Plenum Press.

Lu, S.-T., & Mathur, S. P. (2002). Hypotension induced by ultra-wide-band pulses: Dose response, replication, orthostatic response and heart rate variability. In *Proceedings of Second International Workshop on Biological Effects of Electromagnetic Fields* (pp. 409-418).

Lu, S.-T., & Mathur, S. P., Akyel, Y., & Lee, J. C. (1999). Ultrawide-band electromagnetic pulses induced hypotension in rats. *Physiology & Behavior*, *67*, 753-761.

Lu, S.-T., Mathur, S. P., Stuck, B., Zwick, H., D'Andrea, J. A., Ziriax, J. M., Merritt, J. H., Lutty, G., McLeod, D. S., & Johnson, M. (2000). Effects of high peak power microwaves on the retina of the rhesus monkey. *Bioelectromagnetics*, *21*, 439-454.

Maruyama, Y., Iida, N., Horikawa, A., & Hosoya, E. (1978). A new microwave device for rapid thermal fixation of the murine brain. *Journal of Microwave Power*, *13*, 53-57.

Mattsson, J. L., & Oliva, S. A. (1976). Effect of electromagnetic pulse on avoidance behavior and electroencephalogram of a rhesus monkey. *Aviation, Space, and Environmental Medicine*, *47*, 644-648.

Medina, M. A., & Stavinoha, W. B. (1977). Labile intermediary metabolites in rat brain determined after tissue inactivation with microwave irradiation. *Brain Research, 132,* 149-152.

Meltz, M. L. (2003). Radiofrequency exposure and mammalian cell toxicity, genotoxicity, and transformation. *Bioelectromagnetics*, Suppl 6, S196-S213.

119

Merritt, J. H., Medina, M. A., & Frazer, J. W. (1975). Neurotransmitter content of mouse brain after inactivation by microwave heating. *Research Communications in Chemical Pathology and Pharmacology, 10*, 751-754.

Miller, D. B., Blackman, C. F., & O'Callaghan, J. P. (1987). An increase in glial fibrillary acidic protein follows brain hyperthermia in rats. *Brain Research, 415*, 371-374.

Miller, S. A., Bronson, M. E., & Murphy, M. R. (1999). Ultrawideband radiation and pentylenetetrazol-induced convulsions in rats. *Bioelectromagnetics, 20*, 327-329.

Modak, A. T., Stavinoha, W. B., & Deam, A. P. (1981). Effect of short electromagnetic pulses on brain acetylcholine content and spontaneous motor activity of mice. *Bioelectromagnetics*, *2*(1), 89-92.

Moroji, T., Takahashi, K., Ogura, K, Toishi, T., & Arai, S. (1977). Rapid microwave fixation of rat brain. *Journal of Microwave Power*, *12*, 273-286.

Natarajan, M., Nayak, B. K., Galindo, C., Mathur, S. P., Roldan, F. N., & Meltz, M. L. (2006). Nuclear translocation and DNA-binding activity of NFKB (NF-kappaB) after exposure of human monocytes to pulsed ultra-wideband electromagnetic fields (1 kV/cm) fails to transactivate kappaB-dependent gene expression. *Radiation Research*, *165*, 645-654.

Natarajan, M., Vijayalaxmi, Szzliagyl, M., Roldan, F. N., & Meltz, M. L. (2002). NF-kappaB DNA-binding activity after high peak power pulsed microwave (8.2 GHz) exposure of normal human monocytes. *Bioelectromagnetics*, *23*, 271-277.

Nuccitelli, R., Pliquett, U., Chen, X., Ford, W., James Swanson, R., Beebe, S. J., Kolb, J. F., & Schoenbach, K. H. (2006). Nanosecond pulsed electric fields cause melanomas to self-destruct. *Biochemical and Biophysical Research Communications*, *343*, 351-360.

Pakhomov, A. G., & Murphy, M. R. (2000). A comprehensive review of the research on biological effects of pulsed radiofrequency radiation in Russia and the former Soviet Union. In J.C. Lin (Ed.), *Advances in electromagnetic fields in living systems, Vol. 3* (pp. 265-290). New York: Plenum Press.

Pakhomov, A. G., Doyle, J., Stuck, B. E., & Murphy, M. R. (2003). Effects of high power microwave pulses on synaptic transmission and long term potentiation in hippocampus. *Bioelectromagnetics*, *24*, 174-181.

Pakhomov, A. G., Gajsek, P., Allen, L., Stuck, B. E., & Murphy, M. R. (2002). Comparison of dose dependences for bioeffects of continuous-wave and high-peak power microwave emissions using gel-suspended cell cultures. *Bioelectromagnetics, 23*, 158-167.

Pakhomov, A. G., Mathur, S. P., Doyle, J., Stuck, B. E., Kiel, J. L., & Murphy, M. R. (2000). Comparative effects of extremely high power microwave pulses and a brief CW irradiation on pacemaker function in isolated frog heart slices. *Bioelectromagnetics*, *21*, 245-254.

Pakhomov, A. G., Phinney, A., Ashmore, J., Walker, K. III, Kolb, J. F., Kono, S., Schoenbach, K. H., & Murphy, M. R. (2004). Characterization of the cytotoxic effect of high-intensity, 10-ns duration electrical pulses. *IEEE Transactions on Plasma Science, 32*, 1579-1586.

Pakhomova, O. N., Belt, M. L., Mathur, S. P., Lee, J. C., & Akyel, Y. (1997): Lack of genetic effects of ultrawide-band electromagnetic radiation in yeast. *Electro– and Magnetobiology*, *16*, 195-201.

Pakhomova, O. N., Belt, M. L., Mathur, S. P., Lee, J. C., & Akyel, Y. (1998). Ultra-wide band electromagnetic radiation does not affect UV-induced recombination and mutagenesis in yeast. *Bioelectromagnetics, 19*, 128-130.

Patrick, E. L., & Vault, W. L. (1990, March). *Bioelectromagnetic effects of the electromagnetic pulse (EMP)* (Technical Report HDL-TL-90-2). Adelphi, MD: Harry Diamond Laboratories. DTIC Accession Number ADA221552.

Paulraj, R., & Behari, J. (2006). Single strand DNA breaks in rat brain cells exposed to microwave radiation. *Mutation Research*, *596*, 76-80.

Petrova, E. V., Gulyaeva, N. V., Titarov, S. I., Rozhnov, Y. V., & Koval'zon V. M. (2005). Actions of pulsed ultra-broadband electromagnetic irradiation on the EEG and sleep in laboratory animals. *Neuroscience Behavioral Physiology*, 35, 165-70. [translation of *Ross Fiziol Zh Im I M Sechenova*, *89*, 786-794, (2003)].

Raslear, T. G., Akyel, Y., Bates, F., Belt, M., & Lu, S.-T. (1993). Temporal bisection in rats: the effects of high-peak-power pulsed microwave irradiation. *Bioelectromagnetics*, *14*, 459-478.

Rogers, W. R., Merritt, J. H., Comeaux, J. A., Jr., Kuhnel, C. T., Moreland, D. F., Teltschik, D. G., Lucas, J. H., & Murphy, M. R. (2004). Strength-duration curve for an electrically excitable tissue extended down to near 1 nanosecond. *IEEE Transactions on Plasma Sciences, 32*, 1587-1599.

Röschmann, P. (1991). Human auditory system response to pulsed radiofrequency energy in RF coils for magnetic resonance at 2.4 to 170 MHz. *Magnetic Resonance in Medicine, 21*, 197-215.

Sandler, S. S., Smith, G. S., & Albert, E. N. (1975). Electromagnetic field effects in nerve tissue. *Aviation, Space, and Environmental Medicine*, *46*, 1414-1417.

Sarkar, S., Ali, S., & Behari, J. (1994). Effect of low power microwave on the mouse genome: A direct DNA analysis. *Mutation Research*, *320*, 141-147.

121

Schneider, D. R., Felt, B. T., & Goldman, H. (1982). On the use of microwave radiation energy for brain tissue fixation. *Journal of Neurochemistry*, *38*, 749-752.

Schoenbach, K. H., Beebe, S. J., & Buescher, E. S. (2001). Intracellular effect of ultrashort electrical pulses. *Bioelectromagnetics*, *22*, 440-448.

Schoenbach, K. H., Katsuki, S., Stark, R. H., Buescher, E. S., & Beebe, S. J. (2002). Bioelectrics – New applications for pulsed power technology. *IEEE Transactions on Plasma Sciences, 30*, 293-300.

Seaman, R. L., & Jauchem, J. R. (2004). Rat electrocardiogram during acute exposure to synchronized bursts of ultra wideband pulses. *IEEE Transactions on Plasma Sciences*, *32*, 1644-1652.

Seaman, R. L., & Lebovitz, R. M. (1989). Thresholds of cat cochlear nucleus neurons to microwave pulses. *Bioelectromagnetics, 10*, 147-160.

Seaman, R. L., & Phelix, C. F. (2005). Acute effects of pulsed microwaves and 3-nitropropionic acid on neuronal ultrastructure in the rat caudate-putamen. *Bioelectromagnetics*, *26*, 82-101.

Seaman, R. L., Beblo, D. A., & Raslear, T. G. (1994). Modification of acoustic and tactile startle by single microwave pulses. *Physiology & Behavior*, *55*, 587-595.

Seaman, R. L., Belt, M. L., Doyle, J. M., & Mathur, S. P. (1998). Ultra-wideband electromagnetic pulses and morphine-induced changes in nociception and activity in mice. *Physiology & Behavior*, *65*, 263-270.

Seaman, R. L., Belt, M. L., Doyle, J. M., & Mathur, S. P. (1999). Hyperactivity caused by a nitric oxide synthase inhibitor is countered by ultra-wideband pulses. *Bioelectromagnetics*, *20*, 431-439.

Seaman, R. L., Mathur, S. P., Phinney, A. M., Garcia, A. S., & Ashmore, J. L. (2002a). Changes in rat motor activity by pulsed microwave radiation depend on type of activity, time after exposure, and state of animal. In *Proceedings of Second International Workshop on Biological Effects of Electromagnetic Fields* (pp. 388-393).

Seaman, R. L., Parker, J. E., Kiel, J. L., Mathur, S. P., Grubbs, T. R., & Prol, H. K. (2002b). Ultra-wideband pulses increase nitric oxide production by RAW 264.7 macrophages incubated in nitrate. *Bioelectromagnetics*, *23*, 83-87.

Seaman, R. L., Fleming, S. M., Prosolovitch, K., Chesselet, M. F., Lu, S. T., Mathur, S. P., DiCarlo, C. D., Garcia, A. S., Grado, A. R., & Garza, T. H. (2003). Effects of exposure to pulsed microwaves on movement initiation in rats exposed to the mitochondrial toxin

122

rotenone. *Abstracts of 6th Congress of the European Bioelectromagnetics Association* (p. 127).

Seaman, R. L., Chesselet, M. F., Mathur, S. P., DiCarlo, C. D., Fleming, S. M., Ashmore, J. L., Garza, T. H., & Grado, A. R. (2004a). Sensorimotor function in rotenone treated rats after acute exposure to 1.25 GHz microwave pulses in circular waveguide. In *Proceedings of Third International Workshop on Biological Effects of Electromagnetic Fields* (pp. 633-640).

Seaman, R. L., Mathur, S. P., & Dick, E. J., Jr. (2004b). *Short-term motor activity and acoustic startle after microwave exposure and toxin-induced hypoxia*. WRAIR/USAMRD Technical Report submitted June 2003 in Final Report for U.S. Army Medical Research and Materiel Command contract DAMD17-94-C-4069, May 2004.

Sherry, C. J., Blick, D. W., Walters, T. J., Brown, G. C., & Murphy, M. R. (1995). Lack of behavioral effects in non-human primates after exposure to ultrawideband electromagnetic radiation in the microwave frequency range. *Radiation Research, 143*, 93-97.

Sienkiewicz, Z. J., Blackwell, R. P., Haylock, R. G., Saunders, R. D., & Cobb, B. L. (2000). Low-level exposure to pulsed 900 MHz microwave radiation does not cause deficits in the performance of a spatial learning task in mice. *Bioelectromagnetics, 21*, 151-158.

Skidmore, W. D., & Baum, S. J. (1974). Biological effects in rodents exposed to 10^8 pulses of electromagnetic radiation. *Health Physics, 26*, 391-398.

Stacey, M., Stickley, J., Fox, P., Statler, V., Schoenbach, K., Beebe, S. J., & Buescher, S. (2003). Differential effects in cells exposed to ultra-short, high intensity electric fields: cell survival, DNA damage, and cell cycle analysis. *Mutation Research, 542*, 65-75.

Stavinoha, W. B., Frazer, J., & Modak, A. T. (1977). Microwave fixation fro the study of acetylcholine metabolism. In D. J. Jenden (Ed.), *Cholinergic mechanisms and psychopharmacology* (pp. 169-179). New York: Plenum Press.

Sun, Y., Vernier, P. T., Behrend, M., Wang, J., Thu, M. M., Gundersen, M., & Marcu, L. (2006). Fluorescence microscopy imaging of electroperturbation in mammalian cells. *Journal of Biomedical Optics*, 11, #024010.

Sylvester, P. W., Shah, S. J., Haynie, D. T., & Briski, K. P. (2005). Effects of ultra-wideband electromagnetic pulses on pre-neoplastic mammary epithelial cell proliferation. *Cell Proliferation, 38*, 153-63.

Vernier, P. T., Sun, Y., Marcu, L., Craft, C. M., & Gundersen, M. A. (2004a). Nanoelectropulse-induced phosphatidylserine translocation. *Biophysical Journal, 86*, 4040-4048.

Vernier, P. T., Sun, Y., Marcu, L., Craft, C. M., & Gundersen, M. A. (2004b). Nanosecond pulsed electric fields perturb membrane phospholipids in T lymphoblasts. *Federation of Europoean Biochemical Societies Letters, 572*, 103-108.

Vernier, P. T., Thu, M. M. S., Marcu, L., Craft, C. M., & Gundersen, M. A. (2004c). Nanosecond electroperturbation – Mammalian cell sensitivity and bacterial spore resistance. *IEEE Transactions on Plasma Science*, *32*, 1620-1625.

Vernier, P. T., Sun, Y., Marcu, L., Salemi, S., Craft, C. M., & Gundersen, M. A. (2003). Calcium bursts induced by nanosecond electric pulses. *Biochemical and Biophysical Research Communications, 310*, 286-295.

Vernier, P. T., Ziegler, M. J., Sun, Y., Chang, W. V., Gundersen, M. A., & Tieleman, D. P. (2006). Nanopore formation and phosphatidylserine externalization in a phospholipid bilayer at high transmembrane potential. *Journal of the American Chemical Society*, *128*, 6288-6289.

Vijayalaxmi & Obe, G. (2004). Controversial cytogenetic observations in mammalian somatic cells exposed to radiofrequency radiation. *Radiation Research*, *162*, 481-496.

Vijayalaxmi, Seaman, R. L., Belt, M. L., Doyle, J. M., Mathur, S. P., & Prihoda, T. J. (1999). Frequency of micronuclei in the blood and bone marrow cells of mice exposed to ultra-wideband electromagnetic radiation. *International Journal of Radiation Biology*, *75*, 115-120.

Walker, K., 3rd, Pakhomova, O. N., Kolb, J., Schoenbach, K. S., Stuck, B. E., Murphy, M. R., & Pakhomov, A. G. (2006). Oxygen enhances lethal effect of high-intensity, ultrashort electrical pulses. *Bioelectromagnetics, 27*, 221-225.

Walters, T. J., Mason, P. A., Sherry, C. J., Steffen, C., & Merritt, J. H. (1995). No detectable bioeffects following acute exposure to high peak power ultra-wide band electromagnetic radiation in rats. *Aviation, Space, and Environmental Medicine, 66*, 562-567.

Wang, B., & Lai, H. (2000). Acute exposure to pulsed 2450-MHz microwaves affects water-maze performance of rats. *Bioelectromagnetics*, *21*, 52-56.

Wang, B., Yang, J., Guo, Q., Xu, R., Liu, C., Zhang, H., Zou, F., & Wang, Z. (1997). Experimental study and mechanism analysis on bioeffects by nanosecond electromagnetic pulses. *Science in China Series C: Life Sciences*, *40*, 301-304.

Wang, C., Cong, J., Xian, H., Cao, X., Sun, C., & Wu, K. (2002). [The effects of electromagnetic pulse on fluidity and lipid peroxidation of mitochondrial membrane]. *Zhonghua Lao Dong Wei Sheng Zhi Ye Bing Za Zhi*, *20*, 266-268. Chinese.

Wang, S. M., Wang, D. W., Peng, R. Y., Chen, H. Y., Gao, Y. B., Cao, X. Z., Cui, X. M., & Zhao, M. L. (2003a). [Effect of electromagnetic pulse irradiation on mice reproduction]. *Zhonghua Lao Dong Wei Sheng Zhi Ye Bing Za Zhi, 21*, 329-331. Chinese.

Wang, S. M., Wang, D. W., Peng, R. Y., Gao, Y. B., Yang, Y., Hu, W. H., Chen, H. Y., Zhang, Y. R., & Gao, Y. (2003b). [Effect of electromagnetic pulse irradiation on structure and function of Leydig cells in mice]. *Zhonghua Nan Ke Xue*, *9*, 327-330. Chinese.

Watanabe, Y., Tanaka, T., Taki, M., & Watanabe, S. (2000). FDTD analysis of microwave hearing effect. *IEEE Transactions on Microwave Theory and Techniques*, *49*, 2126-2132.

White, J. A., Blackmore, P. F., Schoenbach, K. H., & Beebe, S. J. (2004). Stimulation of capacitative calcium entry in HL-60 cells by nanosecond pulsed electric fields. *Journal of Biological Chemistry, 279*, 22964-22972.

Yamaguchi, H., Tsurita, G., Ueno, S., Watanabe, S., Wake, K., Taki, M., & Nagawa, H. (2003). 1439 MHz pulsed TDMA fields affect performance of rats in a T-maze task only when body temperature is elevated. *Bioelectromagnetics*, *24*, 223-230.

Radio Frequency Radiation Dosimetry Handbook
(Fifth Edition)

Chapter 5.   Thermoregulation and Thermal Modeling

Eleanor R. Adair, Ph.D.
Senior Scientist Emeritus
Air Force Research Laboratory, 711 Human Performance Wing,
Human Effectiveness Directorate, Directed Energy Bioeffects Division, Radio Frequency
Radiation Branch, Brooks City-Base, Texas 78235-5147

5.1   Introduction

The study of thermoregulation – the responses that maintain a constant internal body temperature – has flourished since Claude Bernard (1885) first demonstrated that the temperature of the blood varies in different parts of the body. Bernard established that food taken into the body is metabolized in the tissues and that the bloodstream distributes the released energy throughout the body. The relative stability of the internal body temperature was part of his concept of the constancy of the ‗milieu intérieur,‘ a necessity for optimal functioning and health of the organism. He pointed out that the vasomotor nerves control the transfer of heat from deep in the body to the skin and that this is a mechanism of the utmost importance to thermoregulation in endotherms. Bernard‘s discoveries underlie the modern science of thermophysiology and help us to understand how man and animals can remain relatively independent of the thermal environment, even when the environment contains potent or unusual thermal stressors.

Thermal loads on the body can result from changes in metabolic heat production and from changes in the characteristics of the environment (temperature, ambient vapor pressure, air movement, insulation, and other environmental variables that may alter the skin‘s temperature). Thermalizing energy deposited in body tissues by exposure to radio frequency electromagnetic energy can be a unique exception to the normal energy flows in the body, although metabolic activity in skeletal muscle can deposit large amounts of thermal energy directly into deep tissues.

All living organisms respond vigorously to changes in body temperature. Cold-blooded animals, called ectotherms because they derive thermal energy mainly from outside the body, regulate their body temperatures largely through behavioral selection of a preferred microclimate. Warm-blooded animals, called endotherms because they can generate heat in their bodies and dissipate it to the environment through physiological processes, often rely on behavioral thermoregulation. Behavior is important to thermoregulation because it is mobilized rapidly and aids the conservation of the body‘s energy and fluid stores. When behavioral responses, which include the thermostatic control of the immediate microclimate, are difficult or impossible, the body temperature of endothermic species is regulated by autonomic mechanisms.

126

These mechanisms control metabolic heat production, the distribution of heat within the body tissues, and the avenues and rate of heat loss from the body to the environment. The material that follows focuses primarily on these autonomic thermoregulatory mechanisms, which are automatic, well understood, and amenable to modeling.

5.2   Basic Thermal Physiology

5.2.1   Heat Exchange Between Organism and Environment

Radio frequency radiation may be regarded conveniently as part of the thermal environment to which humans and other endotherms may be exposed. Figure 5-1 is a schematic representation of the sources of heat in the body and the different routes by which thermal energy may be transferred between the body and the environment. Heat is actively produced in the body through metabolic processes (M) and may also be passively generated in body tissues by the absorption of radio frequency energy (A_{RFR}). If the body temperature is to remain stable, this thermal energy must be continually transferred to the environment. As outlined above, the balance between the production and loss of thermal energy is so efficiently regulated by behavioral and autonomic responses that minimal variation occurs in the core body temperature of an endotherm.

Thermal energy may be lost (Figure 5-1) by evaporation of water from the respiratory tract (E_{res}) or from the skin by sweating (E_{sw}), by dry-heat transfer from the skin surface via radiation (Q_r) or convection (Q_c), and by doing work (W) on the environment. Heat transfer by conduction (Q_k) is usually insignificant in most species unless they are recumbent. When the environment is thermally neutral, dry-heat loss predominates in the form of convective transfer to the air and radiant transfer to the surrounding surfaces. A small amount of heat is continually lost by the diffusion of water through the skin (not shown in the figure).
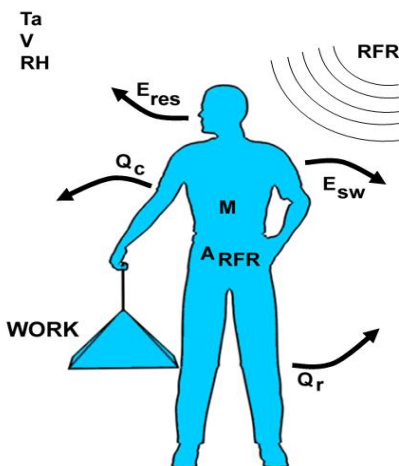
Figure 5-1. A schematic diagram of the sources of body heat (including radio frequency radiation) and the important energy flows between man and the environment. The body is in thermal equilibrium if the rate of heat loss equals the rate of heat gain. Figure modified from Berglund (1983).

127

When the temperature of the environment rises above thermoneutrality, or during vigorous exercise or defervescence, the evaporation of sweat (E_{sw}) dissipates large amounts of body heat. Evaporative water loss through sweating occurs in humans, the great apes, certain other non-human primates, and a few other species such as horses and camels. Many animals – such as dogs, cats, and rabbits – use panting (increased respiratory frequency coupled with copious saliva production) to lose heat by evaporation. Other species, such as rodents, have no such physiological mechanisms and must rely on behavioral responses, which include seeking shade, burrows, or aqueous environments and/or grooming their bodies with water, urine, or saliva to aid evaporative cooling. Table 5-1 includes several thermoregulatory characteristics of certain animals.

The rate of heat loss from an endotherm is governed by the thermal characteristics of the environment, as indicated in Figure 5-1; these include the air temperature (T_a) but also the air movement (v) and humidity (RH). Two other environmental variables that affect heat transfer (not shown in the figure) are the mean radiant temperature of surrounding surfaces, especially those close to the body, and the amount of insulation (fur, fat, feathers, clothing).

When the thermal energy produced in the body (including that derived from absorbed radio frequency radiation (RFR)) is equal to that exchanged with the environment, the body is said to be in thermal balance. Under these conditions the body temperature remains stable. When heat production exceeds heat loss, thermal energy is stored in the body and the body temperature rises (hyperthermia). Conversely, when more heat is lost to the environment than can be produced or absorbed, the body temperature falls (hypothermia).

Table 5-1. Thermoregulatory characteristics of animals.

Species	Body Temperature ºC Normal	Min.	Max.	Thermoregulatory Mechanisms Sweating	Shivering	Panting	Thermopreferendum ºC
Man*[ab] Homo sapiens	37	27	42	Yes	Yes	No	23- 26 (50% RH)
Rhesus monkey[c] Macacaca mulatta	39-39	25	43	Yes	Yes	No	-------
Patas monkey[d] Erythrocebus patas	38-40	---	42-43	Yes	Yes	No	-------
Squirrel monkey[e] Saimiri sciureus	38-39	25	42-43	Yes	Yes	No	35-36
Dog**[f] Canis familiaris	38-39	24	42	No	Yes	Yes	12-16
Cat[g] Felix domesticus	38-39	19	42	No	Yes	Yes	-------
Domestic pig[h] Sus scrofa	38-39	---	42	No	Yes	Yes	30-32+
Sheep (fleeced)[h] Ovis aries	38-39	---	42	Yes	Yes	Yes	-------
Rabbit[i] Oryctolaris cuniculus	39	20	42	No	Yes	Yes	-------
Guinea pig[j] Cavis porcellus	39	17	43	No	Yes	Yes	29
Rat[jk] Rattus norvegicus	37-38	20	42	No	Yes	No	29-30
Mouse[j] Mus musculus	37	20	42-44	No	Yes	No	32

* Assumes man is lightly clothed, sedentary in still air.
** Value for Alaskan husky is well below that for most other subspecies.
[a]Cabanac (1983), [b]Elizondo (1977), [c]Johnson and Elizondo (1979),
[d]Mahoney (1980), [e]Stitt and Hardy (1971), [f]Adams (1971), [g]Adams et al. (1970), [h]Whittow (1971), [i]Gonzalez, et al. (1971), [j]Hart (1971), [k]Berry et al. (1984)

5.2.2   The Thermoregulatory Profile

The particular thermoregulatory effector response mobilized at any given time, and its vigor, will depend on the prevailing thermal environment. The ambient temperature is frequently the only environmental variable specified in research reports, but the specification of air movement and relative humidity is equally important. Figure 5-2 shows a schematic thermoregulatory profile of a typical endotherm. It illustrates how the principal autonomic responses of heat production and heat loss depend on the ambient temperature. The responses are considered to be steady state rather than transient, and the ambient air is considered to have minimal movement and water content. Three distinct zones can be defined in terms of the prevailing autonomic adjustment. Below the lower critical temperature (LCT), thermoregulation is accomplished by changes in metabolic heat production, other responses remaining at minimal

129

strength. As the ambient temperature falls further and further below the LCT, heat production increases proportionately. In a cool environment RF energy absorbed by an endotherm will spare the metabolic system in proportion to the field strength and will have no effect on other autonomic responses.

At ambient temperatures above the LCT, metabolic heat production is at the low resting level characteristic of the species, evaporative heat loss is minimal, and changes in thermal conductance accomplish thermoregulation. Conductance is a measure of heat flow from the body core to the skin and reflects the vasomotor tone of the peripheral vasculature. As the constricted peripheral vessels begin to dilate, warm blood from the body core is brought to the surface so that the heat may be lost to the environment by radiation and convection. These vasomotor adjustments take place within a range of ambient temperatures, called the thermoneutral zone (TNZ) that is peculiar to each species. Insofar as they are known, the TNZs for animals commonly used in the laboratory are indicated in Table 5-1. If an endotherm at thermoneutrality is exposed to RFR, augmented vasodilation may occur so that the heat generated in deep tissues can be quickly brought to the skin surface for dissipation to the environment.
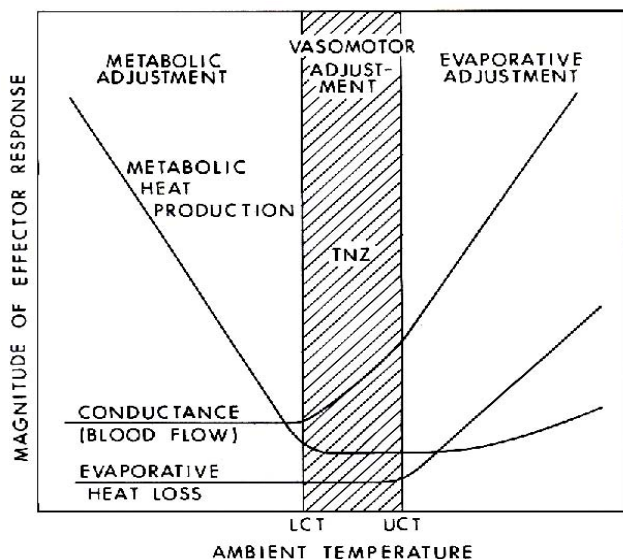
Figure 5-2. Thermoregulatory profile of a typical endothermic organism to illustrate the dependence of principal types of autonomic responses on environmental temperature. LCT = lower critical temperature; UCT = upper critical temperature; TNZ = thermoneutral zone.

The upper limit of the TNZ is known as the upper critical temperature (UCT). At this ambient temperature the endotherm is fully vasodilated and dry heat loss (by convection and radiation) is maximal. Further increases in ambient temperature provoke the mobilization of heat loss by evaporation, either from the skin (sweating) or the respiratory tract (panting). Humans and certain other mammals have the ability to sweat copiously to achieve thermoregulation in hot environments. It is reasonable to assume that if these species were exposed to RFR at ambient temperatures above the UCT, their sweating rate would increase in proportion to the field strength. Other mammals, notably the rodents, neither sweat nor pant and when heat stressed must depend on behavioral maneuvers to achieve some degree of thermoregulation; if the

130

opportunity for behavioral thermoregulation is curtailed, these animals can rapidly become hyperthermic when heat stressed. The basic thermoregulatory profile of the selected laboratory animal must therefore be considered in detail as part of the experimental design of any research into the biological consequences of exposure to RFR; changes in any measured thermoregulatory response will depend on the functional relationship between that response and the prevailing ambient temperature. Other types of responses (e.g., food and water consumption) also may be indirectly affected by the thermoregulatory profile if they interfere with efficient thermoregulation.

Humans exhibit profound adaptability in the face of environmental stress, particularly in warm environments. Figure 5-3 illustrates some of the archival data collected by Hardy and DuBois (1940) for nude men and women exposed in a calorimeter to a wide range of ambient temperatures. Because of the vigorous responses of heat production and heat loss, the rectal temperature varies less than 1 ºC across a 20 ºC range of calorimeter temperatures. The TNZ is extremely narrow, occurring at about 28 ºC in the calorimeter and closer to 30 ºC in the natural environment. Above the TNZ, evaporative heat loss (whole-body sweating) is initiated that can attain rates of 2-3 L/h and up to 10-15 L/d (Wenger, 1983). Assuming normal hydration, it is difficult to increase metabolic heat production (by exercise) to levels that cannot be dissipated by sweating, unless the ambient temperature or vapor pressure is very high. Since human evaporative heat loss is controlled by both peripheral and internal signals (Nadel et al., 1971a, 1971b), only an extraordinarily hostile thermal environment, which includes a source of RFR, can be expected to seriously threaten the thermoregulatory system of humans.

131
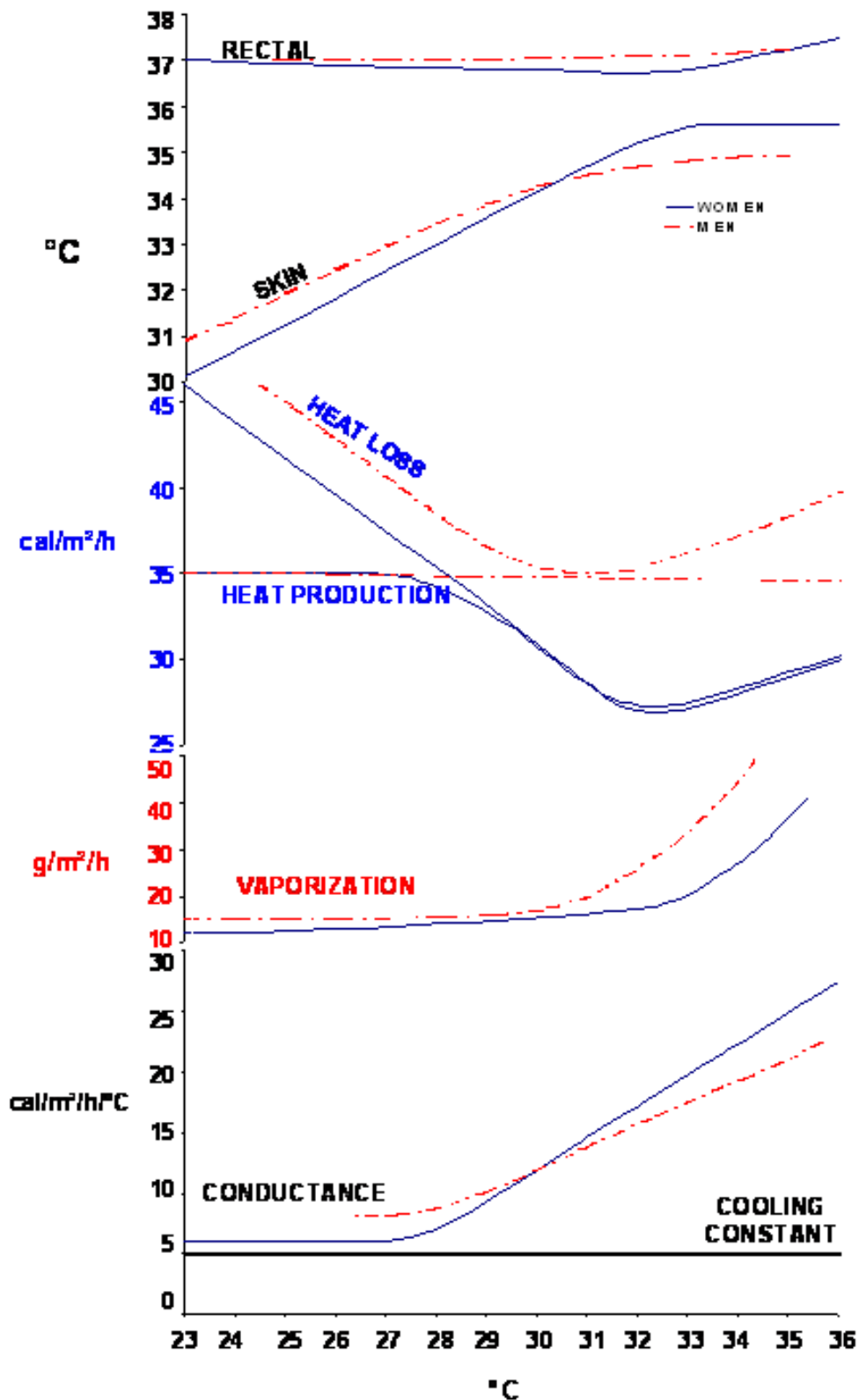
Figure 5-3. Thermoregulatory profile of nude adult humans equilibrated in a calorimeter to different ambient temperatures. Data adapted from Hardy and DuBois (1940).

132

Way et al. (1981) and Stolwijk (1983) have predicted minimal increases in brain and body temperatures during local absorption of significant amounts of RF energy, because of the rapid mobilization of evaporative heat loss and a significant increase in tissue blood flow. Under the assumption that RF exposure provides a thermal stress comparable to exercise (Nielsen & Neilsen, 1965) or an ambient temperature well above the TNZ, such response changes would be predicted from knowledge of the human thermoregulatory profile in Figure 5-3. On the other hand, significant localized temperature elevations in certain body sites (e.g., legs, arms, neck) have been predicted by a two-dimensional heat-transfer model of man exposed to a unilateral planewave at resonant and near-resonant frequencies (Spiegel et al., 1980). Some of these predictions have been supported by FD-TD modeling of a 70-kg seated human exposed at the resonant frequency of 100 MHz (Adair et al., 2003a). For additional discussion of predictive modeling, see section 5.8 below.

5.2.3 Body Heat Balance

The most important principle involved in the study of autonomic thermoregulation of endotherms is the first law of thermodynamics – the law of conservation of energy (Bligh & Johnson, 1973). In the steady state, the heat produced in the body is balanced by the heat lost to the environment, so that heat storage is minimal. This relationship can be expressed by a heat-balance equation:

$$M \pm W = R + C + E \pm S \qquad (1)$$

where M is the rate at which thermal energy is produced through metabolic processes; W is the power, or rate at which work is produced by or on the body; R is the rate of heat exchange with the environment via radiation; C is the rate of heat exchange with the environment via convection; E is the rate of heat loss due to the evaporation of body water; and S is the rate of heat storage in the body.

All terms in Equation 1 must be in the same units, e.g., watts (the unit used throughout this handbook). Physiologists often express these quantities in kilocalories per hour, which can be converted to watts by multiplying by the conversion factor 1.163. As Equation 1 is written, negative values of $R, C,$ and E may all cause a rise in the body temperature; positive values may cause a fall. Work (W) is positive when accomplished by the body (e.g., riding a bicycle), and this potential energy must be subtracted from metabolic energy (M) to find the net heat (H) developed within the body. When W is negative (e.g., walking downstairs), this heat is added to M. While W may be a significant factor for humans or beasts of burden, it may be considered negligible for other endotherms, particularly in a laboratory setting. Usually, evaporative heat loss (E) is positive; when E is negative, condensation occurs and thermal injury is possible.

Because heat exchange by radiation, convection, or evaporation is always related in some way to the surface area of the body, each term in Equation 1 is usually expressed in terms of energy per unit surface area, e.g., watts per square meter. The most commonly used measure of the body surface area is that proposed by DuBois and DuBois (1916),

$$A_D = 0.202w^{0.425}h^{0.725} \tag{2}$$

where A_D is DuBois surface in square meters; w is the body mass in kilograms; and h is the height in meters.

As noted by Kleiber (1961), h for similar body shapes is proportional to a mean linear dimension equal to $w^{1/3}$. Therefore, to compare humans of different sizes, Equation 2 may be generalized as

$$A_D = k_1w^{0.425}k_2w^{1/3 \times 0.725} = k_1k_2w^{(0.425 + 0.242)} = k_1k_2w^{2/3} \ . \tag{3}$$

The ratio of surface area to body mass varies between species, so it is difficult to establish a general rule for the determination of surface area. Many methods have been devised for the direct measurement of surface area of experimental animals, most of which are inaccurate to some degree. In nearly all cases, the surface area is some function of $w^{2/3}$.

Although Equation 1 has no term for rate of heat transfer through conduction (which is usually insignificant under normal conditions), conduction combined with mass transfer forms the significant mode of heat transfer called convection. Convective heat transfer in air (C) is a linear function of body surface area (A), and the convective heat transfer coefficient (h_c) is a function of ambient air motion to the 0.6 power ($v^{0.6}$). The amount of heat the body loses through convection depends on the difference between the surface temperature of the skin (T_{sk}) and the air temperature, usually taken as the dry-bulb temperature (T_{db}). The value of the heat transfer coefficient depends on certain properties of the surrounding medium, such as density and viscosity, as well as a shape/dimension factor for the body. Clothing complicates the analysis and is often evaluated in terms of insulation (clo) units.

Heat transfer by radiation is independent of ambient temperature. The wavelengths of the radiation exchanged between two objects are related to their respective surface temperatures; the net heat transfer by radiation is proportional to the difference between their absolute temperatures to the fourth power and to the relative absorptive and reflective properties of the two surfaces. In general, the net radiant heat exchange (where h_r = radiant-heat-transfer coefficient) between a nude man and the environment involve an estimation of the mean radiant temperature (MRT). MRT (alternate symbol T_r) can be derived from the temperature (T_g) of a blackened hollow sphere of thin copper (usually 0.15-m diameter) having heat transfer characteristics similar to those for the human body (Woodcock et al., 1960):

$$MRT = (1 + 0.222V^{0.5})(T_g - T_{db}) + T_{db} \quad [°C] \ . \tag{4}$$

Clothing complicates this analysis, as it does heat transfer by convection (h_c) and other modes. A combined heat transfer coefficient (h) is equal to the sum of h_c and h_r. Evaluation of these heat transfer coefficients is necessary to the application of the heat balance Equation (1) to practical problems of the thermal environment. Additional evaluations include both the metabolic requirements (see below) for any particular ongoing activity and the general nature of the clothing insulation used. The thermal insulation of a clothing ensemble can be evaluated by summarizing the insulation values of each garment worn by the subject. Table 5-2 lists

individual values (clo) for insulation of various garments. Details of the applications of clo values may be found in the ASHRAE Handbook (1986).

Table 5-2. Clo units for individual items of clothing and formula for estimating total intrinsic insulation Clo = 0.82 (Σ Individual Items).

MEN			WOMEN		
Clothing		**clo**	**Clothing**		**clo**
Underwear					
Sleeveless		0.06	Bra and panties	0.05	
T Shirt		0.09	Half slip		0.13
Briefs	0.05		Full slip		0.19
Long underwear upper		0.35	Long underwear upper	0.35	
Long underwear lower		0.35	Long underwear lower	0.35	
Torso					
Shirt			Blouse		
Light, short sleeve	0.14		Light	0.20	
long sleeve	0.22		Heavy		0.29
Heavy, short sleeve	0.25				
long sleeve		0.29	Dress		
(Plus 5% for tie or turtleneck)			Light	0.22	
			Heavy		0.70
Vest			Skirt		
Light		0.15	Light	0.10	
Heavy		0.29	Heavy		0.22
Trousers			Slacks		
Light		0.26	Light	0.26	
Heavy		0.37	Heavy		0.44
Sweater			Sweater		
Light		0.20	Light	0.17	
Heavy		0.37	Heavy		0.37
Jacket			Jacket		
Light		0.22	Light	0.17	
Heavy		0.49	Heavy		0.37
Footwear					
Socks			Stockings		
Ankle length	0.04		Any length	0.01	
Knee high	0.10		Panty hose		0.01
Shoes			Shoes		
Sandals		0.02	Sandals		0.02
Oxfords		0.04	Pumps		0.04
Boots		0.08	Boots	0.08	

Heating by RFR may further complicate the analysis of radiant- and convective-heat exchange between a person and his environment, although Berglund (1983) has demonstrated that this complex situation can be analyzed by conventional methods.

The final avenue of heat loss available to humans is that due to the evaporation of water. The latent heat of vaporization of water at normal body temperature is 0.58 kcal/g; the body loses this amount of heat when water is evaporated from its surfaces. Water from the respiratory surfaces is continually being lost in the expired air. Water also continually diffuses through the

135

skin; this is called insensible water loss or insensible perspiration. These two avenues contribute equally to a heat loss that totals about 25% of the resting metabolic heat production of a man in a thermoneutral environment.   However, the major avenue of evaporative heat loss in humans is sweating, which depends on the vapor pressures of the air and the evaporating surface and is thus a direct function of both dry bulb (T_{db}) and wet bulb (T_{wb}) temperatures. When $T_{db} = T_{wb}$, the air is at 100% relative humidity and thus no water can be evaporated from the skin surface; at less than 100% relative humidity, evaporation can occur. The interrelationships between these variables can be determined from a standard psychrometric chart (ASHRAE Handbook, 1986), an example of which is shown in Figure 5-7 and described in Section 5.4.2.2. In Equation 1, E represents the evaporative cooling allowed by the environment (E_{max}) and is in no way related to the level of evaporative cooling required (E_{req}) by the person.

5.3   Thermoregulation in Humans and Animals

5.3.1   Metabolic Rates of Humans and Animals

Because the metabolic heat production per unit body mass, or ―specific metabolic rate,‖ varies greatly with body size and proportion (somatotype), several measures of this variable are in wide use. Figure 5-4 is a log-log plot of metabolic heat production versus body mass for several animals and humans. The solid line has a slope of 0.75 and reveals a strong correlation between body mass raised to the 0.75 power and metabolic heat production. This empirical observation has prompted researchers to adopt power per unit body mass, in watts per kilogram, as the standard metric for animal metabolic rate.
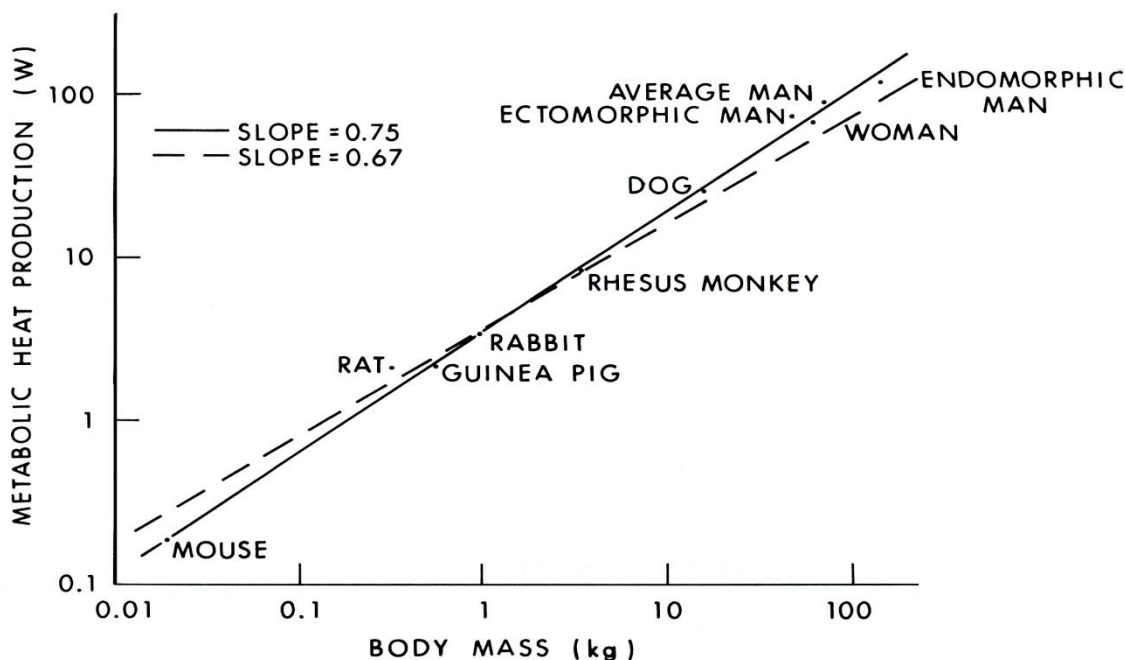
Figure 5-4. Logarithm of total metabolic heat production plotted against logarithm of body mass (Data taken from Tables 5-2 and 5-4).

The metabolic heat production (*M*) of placental animals (most mammals) can be estimated by the following formula:

$$M = 3.39w^{0.75} \quad [\text{W}] \tag{5}$$

where w is the mass of the animal in kilograms. Another useful equation relates the metabolic heat produced by the body to the rate of oxygen consumption (ASHRAE Handbook, 1986):

$$M = [0.23(RQ) + 0.77](5.87)(V_{O2})(60/A_D) \quad [\text{W/m}^2] \tag{6}$$

where RQ is the respiratory quotient, or ratio of V_{CO2} produced to V_{O2} inhaled; RQ in man may vary from 0.83 (resting) to over 1.0 (heavy exercise); V_{O2} is the oxygen consumption in liters /minute at standard conditions (0 ºC, 760 mm Hg); 5.87 is the energy equivalent of 1 L of oxygen at standard conditions in watt-hours/L when RQ = 1.

Formulas for the metabolic heat production of other classes of mammals can be found in Gordon (1977).

Another widely accepted form for expressing metabolic heat production is power per unit surface area. The dashed line in Figure 5-5, with a slope of 0.67, represents how surface area increases with mass for geometrically similar shapes. This corresponds to the approximate formula for the body surface area (SA) of these animals:

$$SA = 0.09w^{0.67} \quad [\text{m}^2] \tag{7}$$

Although surface area does not describe the animal data as well as $w^{0.75}$, it is as suitable a measure as any for human metabolic heat production. For accurate calculations of human metabolic heat production, the DuBois area (Equation 2) should be used.

5.3.1.1 Human Data

Metabolic heat production (*M*) is often called ―metabolic rate‖ (MR). Table 5-2 lists resting metabolic rates for normal healthy humans of varying age and somatotype. The specific metabolic rate (SMR) is clearly seen to be a function of body size and shape. The basal metabolic rate (BMR) is defined as the heat production of a human in a thermoneutral environment (33 ºC), at rest mentally and physically, and at a time exceeding 12 h from the last meal. The standard BMR for man is about 250 ml O_2/min, or 84 W, or 0.8 MET (where 1 MET = 58.2 W/m^2). The BMR also corresponds to about 1.2 W/kg for a 70-kg ―standard‖ man. The BMR is altered by changes in body mass, diet, and endocrine levels, but probably not by living in the heat (Goldman, 1983). In resting man most of the heat is generated in the core of the body – the trunk, viscera, and brain – despite the fact that these regions represent only about one-third of the total body mass. The heat is conducted to the other body tissues, and its elimination from the body is controlled by the peripheral vasomotor system.

Table 5-3 shows the wide variation of metabolic rates during various activities. All of these data are given for a healthy, normal 20- to 24-year-old male except as noted. The range of

137

metabolic rates for humans – considering work performed and assorted physiological variables such as age, sex, and size – is roughly 40 to 800 W/m^2 (1 to 21 W/kg for ―standard" man), depending on physical fitness and level of activity. The influence of age and sex on the metabolic rate of humans is shown in Figures 5-6 and 5-7. Other factors that may influence the metabolic rate are endocrine state, diet, race, pregnancy, time of day, and emotional state. If deep body temperature is altered, from either heat storage in warm environments or febrile disease, a comparable change occurs in the metabolic rate (Stitt et al., 1974). Similar changes occur when deep body temperature rises during exposure to RFR (Adair & Adams, 1982; Adair et al., 1997, 1998, 2001a, 2003b).

Table 5-3. Resting metabolic rates for normal healthy humans of specific age and somatotype (adapted from Ruch & Patton, 1973).

Gender/Age	Average Weight (kg)	Average Height (m)	Body Surface Area (m^2)	Metabolic Rate		
				W	(W/m^2)	W/kg
Man (20-40 yr old)						
Average	70	1.75	1.85	88.2	47.7	1.26
Ectomorphic	47.18	1.76	1.57	74.9	47.7	1.59
Endomorphic	141	1.76	2.5	119.3	47.7	0.85
Woman (20-40 yr old)						
Average	61.14	1.61	1.64	70.4	42.9	1.15
Ectomorphic	43.09	1.45	1.31	56.2	42.9	1.30
Endomorphic	88.45	1.73	1.73	86.7	42.9	0.98
Average male child						
10-yr old	32.3	1.38	1.12	64.5	57.6	2.00
5-yr old	19.5	1.12	0.78	48.0	61.6	2.46
1-yr old	10	0.74	0.43	27.5	64.0	2.75

Table 5-4. Variation of metabolic rate with activity for a normal 20-24 year-old male* (Adapted from Ruch & Patton, 1973).

Activity	Metabolic Rate			
	(W)	**(W/m^2)**	**(W/kg)**	**METS****
Sleeping	75	41	1.1	0.7
Resting quietly (~basal)	88.2	48	1.3	0.8
Sitting upright	110	58	1.5	1
Standing, clerical work***	130	70	1.8	1.2
Walking 3 mph	300	160	4.3	2.7
Bicycling	540	290	7.7	5
Swimming	750	410	11	7
Maximum sustained exercise	750	410	11	7
Running (sprinting)	1300	700	18	12
Maximum peak exercise****				
Average male	850-1600	460-860	12-23	
Average female	700-1100	410-700	11-18	
Trained male athlete	2000	1080	29	

* Female included under "maximum peak exercise", ** 1 MET = 58.2 W/m^2 (Ruch & Patton, 1973),
*** (Newburgh, 1949), **** (Astrand & Rodahl, 1970)
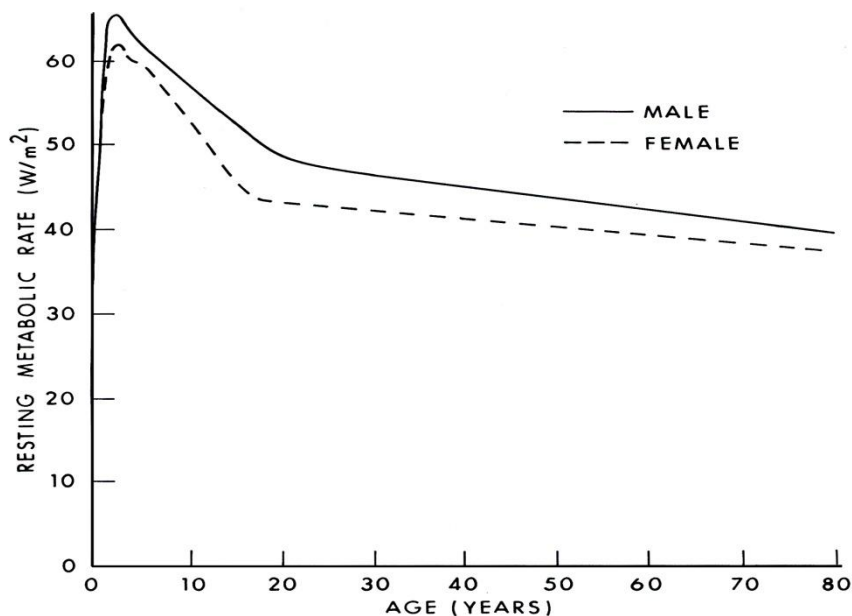
Figure 5-5. Variation of human resting metabolic rate (RMR) with age and sex, expressed as power per unit surface area (Ruch & Patton, 1973).

139
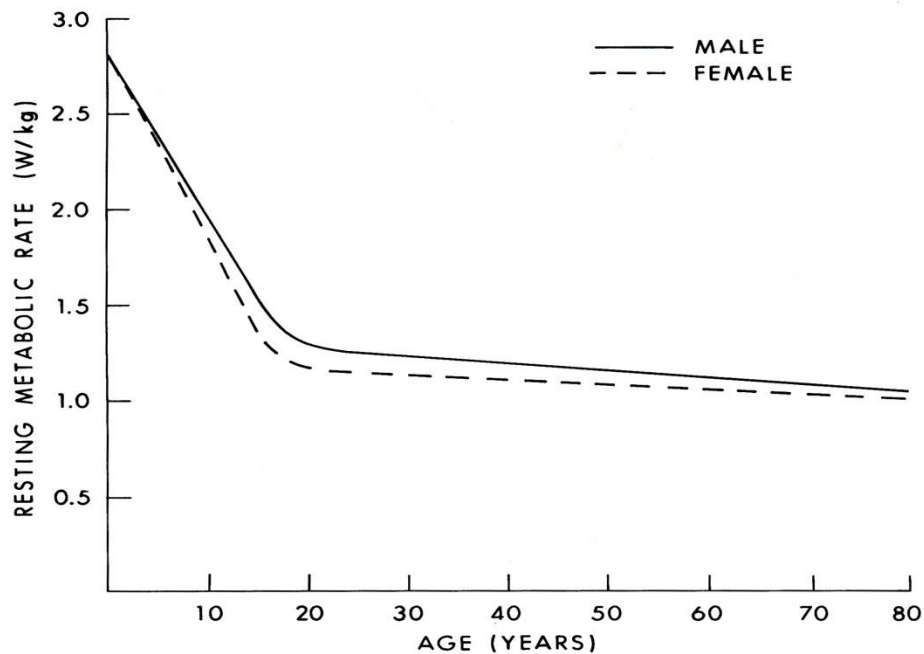
Figure 5-6. Variations of human resting metabolic rate (RMR) with age and sex, expressed as power per unit body mass. Data from Figure 5-6 is converted by means of average height and weight given in Dreyfuss (1967).

5.3.1.2   Animal Data

Resting metabolic rates (MR) for some adult laboratory animals are shown in Table 5-5 in three different forms: total MR for the weight given, specific MR, and standardized MR. A rough idea of metabolic heat production can be gained from an animal's oxygen consumption (V_{O2}) by using the formula:

$$M = 335 \, V_{O2} \quad [W] \tag{8}$$

where V_{O2} = liters of oxygen consumed per minute. The energy equivalent of oxygen is approximately 4.8 kcal/L O_2 for a typical animal diet, and the respiratory quotient (RQ) is approximately 0.85.

140

Table 5-5. Resting metabolic rate for adult laboratory animals.

Animal (Reference)	Average Weight	Metabolic Rate		
	(kg)	W	W/kg	W/kg$^{0.75}$
Rhesus monkey**[a]	3.5	8.26	2.36	4.34
Squirrel monkey[b]	1.1	4.93	4.47	4.59
Baboon**[a]	13	40.7	2.26	4.66
Dog:				
German Shepherd[c]	32	44.2	1.38	3.29
Brittany Spaniel[c]	15.9	26.2	1.65	3.29
Beagle[c]	13.5	23.2	1.72	3.29
Rabbit[d]	1	3.57	3.57	3.57
Guinea pig**[e]	0.58	2.26	3.83	3.4
Rat:**[e]				
Small	0.11	0.94	8.51	4.9
Medium	0.32	2.08	6.51	4.9
Large	0.52	3	5.77	4.95
Mouse:[f]				
Small	0.015	0.15	10	3.5
Medium	0.02	0.19	9.31	3.5
Large	0.025	0.22	8.88	3.5

* W = MR for given weight; W/kg = specific MR; W/kg$^{0.75}$ = standardized MR
** MR data given as totals for 24-hr period.
[a]Bourne (1975), [b]Rosenblum & Cooper (1968), [c]Benedict (1938), [d]Heilbrun (1952), [e]Altman & Dittmer (1968), [f]Pennycuik (1967)

5.3.2   Avenues of Heat Loss

Changes in vasomotor tonus and evaporation of body water through active sweating (or panting in certain endotherms) are both mechanisms of body heat loss. As detailed in Section 5.3 (Figures 5-2 and 5-3), vasomotor control normally operates to regulate the body temperature

when an endotherm is in a thermoneutral environment, i.e., within the TNZ. Sweating (or panting) is activated in warmer environments and during exercise and defervescence.

5.3.2.1 Vasomotor Control

Convective heat transfer via the circulatory system is controlled by the sympathetic nervous system. Below the LCT, vasoconstriction of the peripheral vasculature in arm, leg, and trunk skin minimizes heat loss from the skin, leaving a residual conductive heat flow of 5-9 W/m per °C difference between body core and skin. For a body in the TNZ, when the peripheral vessels are vasodilated, each liter of blood at 37 °C that flows to the skin and returns 1 °C cooler allows the body to lose about 1 kcal, or 1.16 W•h, of heat (Hardy, 1978). During vigorous exercise in the heat, peripheral blood flow can increase almost tenfold; this increase is essential to eliminate the increased metabolic heat produced in the working muscles.

Thermal conductance represents the combined effect of two channels of heat transfer in the body – conductive heat transfer through layers of muscle and fat, and convective heat transfer by the blood. Tissue thermal conductance K (W/m^2•°C) is the rate of heat transfer per unit area across a layer of tissue. Although K cannot be measured directly in the human organism, it can be estimated for resting humans under the assumption that all the heat is produced in the core of the body and is transferred to the skin and thence to the environment. Thus:

$$H_L = K(T_{re} - T_{sk}) \quad [W/m^2] \tag{9}$$

in which H_L represents the heat loss (neglecting that lost through respiration), T_{re} is rectal or core temperature, and T_{sk} is the average skin temperature. In the cold (22 – 28 °C), conductance is minimal for both men and women, ranging between 6 and 9 W/m^2•°C. In warm environments, conductance increases rapidly, and women show a faster increase than men (Cunningham, 1970; see also Figure 5-3).

5.3.2.2 Sweating

Evaporation of sweat from the skin surface efficiently removes heat even in environments warmer than the skin. In this case, evaporative heat loss must take care of both metabolic heat and that absorbed from the environment by radiation and convection. We have no reason to believe that thermalizing energy from absorbed RFR will be dealt with any differently than heat produced by normal metabolic processes or absorbed by exposure to warm environments. Normal secretory functioning of the approximately 2.5 million sweat glands on the skin of a human being is essential to the prevention of dangerous hyperthermia. Secretion is controlled by the sympathetic nervous system and occurs when the ambient temperature rises above 30 °C or the core body temperature rises above 37 °C. Local sweating rate also depends on the local skin temperature (Nadel et al., 1971a). Physically fit individuals and those acclimated to warm environments sweat more efficiently and at a lower body temperature than normal (Nadel, 1974). Dehydration or increased salt intake will alter plasma volume and decrease sweating efficiency (Greenleaf, 1973).

The maximum sweat rate for humans and the length of time it can be maintained are limited. The maximum rate of sweat production by an average man is about 30 g/min. If the ambient air movement and humidity are low enough for all this sweat to be evaporated, the maximum cooling will be about 675 W/m^2; however, conditions are not usually this ideal – some sweat may roll off the skin or be absorbed by layers of clothing. A more practical limit of cooling is 350 W/m^2, or 6 METS, which represents about 17 g/min for the average man (ASHRAE Handbook, 1986).

5.4 Human Thermoregulatory Control During RF Exposure

5.4.1 Thermoregulatory Control

The thermoregulatory system functions as a negative-feedback control system with a reference or ―set‖ temperature. Thermally-sensitive neural elements (thermosensors) are distributed around the body to provide information about the local temperature of body tissues. The thermosensors located in the skin are the most important; other sites include the medial preoptic/anterior hypothalamic area of the brainstem (locus of the ―central thermostat‖), midbrain, medulla, spinal cord, cortex, and deep abdominal structures. Neural signals from the sensors are integrated by a central controller, the integrated signal is compared with the internal reference, and an output command is generated to energize appropriate responses whenever a load error occurs. A negative load error (body temperature lower than set point) will increase heat production; a positive load error will increase heat loss. As detailed below, the particular effector response that is mobilized, as well as its strength, will depend on the prevailing environmental conditions.

5.4.2 Human Heat Tolerance and Environmental Factors

5.4.2.1 RF Energy Deposition

The basic problem posed by excessive body heating from any source, including absorbed RF energy, is whether the heat-loss capability of the thermoregulatory system is sufficient to prevent heat storage in the body. Thus, for a human being exposed to a RF field, Equation 1 may be rewritten as:

$$(M \pm W) + A_{\text{rf}} = R + C + E \pm S \tag{10}$$

where A_{rf} represents the rate of energy absorption from the RF field. If we neglect the work factor (W), the sum of the heat production, of the heat exchange by convection (H_c) and radiation (H_r), and of the absorbed RF energy will yield a useful estimate of the evaporative cooling required (E_{req}) as:

$$E_{\text{req}} = M \pm H_c \pm H_r + A_{\text{rf}} \ . \tag{11}$$

If the maximum available evaporative cooling (E_{max}) is less than E_{req}, S will be positive and the body temperature will rise.

143

5.4.2.2   Human Heat Tolerance

In general, the degree of body heat stress can be predicted by the simple ratio of E_{req}/E_{max}, which yields a measure of the percentage of the skin surface that is wet with sweat. Values of $E_{req}/E_{max} < 20\%$ yield a state of thermal comfort, while higher percentages indicate tolerance limits (Gagge, 1937). This same ratio has also been called the Heat Stress Index (HSI) (Belding & Hatch, 1955). HSI values greater than 30% are judged to be uncomfortable but tolerable and may interfere with concentration and fine motor performance; values from 30 - 60% have finite tolerance times, while values from 60 – 100% represent severe, intolerable conditions. Tolerance limits can also be determined from a standard psychrometric chart (Figure 5-7), which diagrams the ambient vapor pressure in terms of both wet-bulb and dry-bulb temperatures. A Comfort-Health-Index (C-H-I) has also been derived from such a chart and is expressed in terms of the dry-bulb temperature (T_{db}) at 50% RH. Human responses change as the C-H-I ranges from 50 °C (rapid body heating, circulatory collapse, unbearable conditions) through 35 °C (―danger line" for heat stroke, slightly uncomfortable) to 20 °C (vasoconstriction of extremities, muscular pains, cold and uncomfortable sensation).
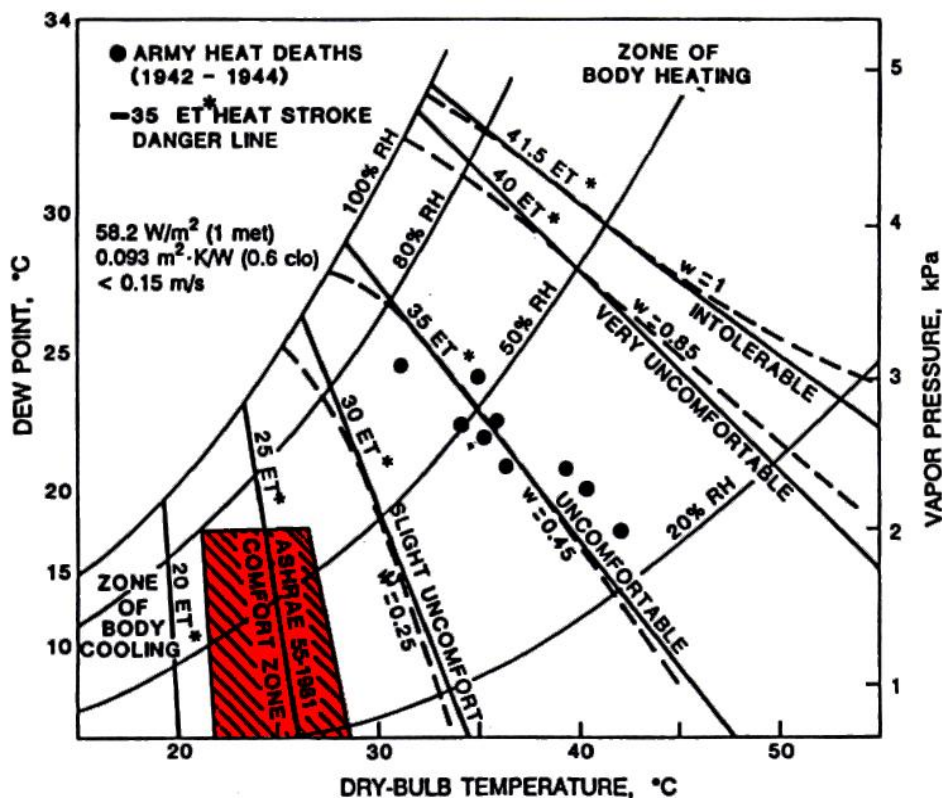
Figure 5-7. A standard psychrometric chart that delineates the zone of thermal comfort (red area), zone of body heating, and zone of body cooling in terms of dew point, ambient vapor pressure, and dry bulb temperature. ET* defines the limits of thermal comfort (ASHRAE Handbook, 1986).

Clothing is also considered a part of the thermal environment since it presents a resistance to the flow of heat from the skin to the environment; this resistance is a direct function

144

of the thickness of the air layer trapped by the clothing. The standard insulation unit, called the clo, was empirically derived and equals 0.155 °C m² W⁻¹ (Gagge et al., 1941). It has been suggested (ASHRAE, 1986) that for each 0.1 clo deviation from the usual 0.6 clo insulation baseline for sedentary office workers (1MET), the air temperature for comfort can be offset by 0.55 °C; this temperature offset can be doubled if the workload is increased to 4 – 5 METs.

5.4.2.3 Exercise

During exercise, the internal body temperature rises because heat generated in the working muscles is distributed throughout the body by increased blood flow. This increased blood flow, combined with peripheral vasodilation, also brings excess body heat to the surface for dissipation. In the steady state, the heat produced by moderate exercise is efficiently lost to the environment so that the internal body temperature stabilizes at an elevated level that depends primarily on the workload, whatever the ambient temperature.

During passive exposure to RF fields, thermalizing energy may be selectively deposited in specific tissue beds; the particular pattern of energy deposition varies with many physical factors of both the radiation and the target. Similarly, during exercise the source of heat lies in specific groups of muscle fibers; the particular pattern of heating varies with the activity. However, some have argued that these two scenarios may generate different thermoregulatory responses because the absorption of RF energy is ―unique‖ (Elder & Cahill, 1984). This view limits the application of voluminous data on exercise physiology to the prediction of human thermophysiological responses to RF fields.

An early study by Nielsen and Nielsen (1965) demonstrated the equivalence of thermophysiological responses during exercise and during passive heating by diathermy. In their experiments, short-wave diathermy was used to deposit heat directly into the deep tissues of the trunk of human subjects. In other test sessions, the same subjects exercised on a stationary bicycle at a work rate adjusted so that the heat load during cycling and diathermic heating was the same (approximately 5 times the resting *M* or 5 METs). Four ambient temperatures (T_a), ranging from cool to warm, were studied. In the steady-state at all T_a, the rectal temperature increased by the same amount during the two procedures. Thermal conductance, assessed by changes in peripheral blood flow, and sweating rates were also comparable. Thus, passive heating by diathermy and the heat generated by active exercise produced the same kind of thermal disturbance in the body as a whole, although the distribution of heat in individual tissue compartments of the body may have been very different in the two cases. These findings indicated that the thermoregulatory consequences of whole-body RF energy deposition may be predicted by the consequences of equivalent heat loads produced by exercise.

5.4.2.4 Febrile States

The elevated body temperatures produced by exercise and those occurring during febrile disease must be differentiated. Strenuous exercise may elevate the deep body temperature to a level above the normal, regulated (or ―set‖) level; the magnitude of the heat loss response is directly related to this deviation as the body attempts to defend the normal level. However,

145

during fever there is an elevation in the "set" level that is defended just as is the normal "set" level during normothermia. These differences are clearly described by Shimada and Stitt (1983).

The elevated body temperature during fever is generated differently in different T_a. In warm T_a, heat loss will be curtailed and vasoconstriction will occur; if these responses are inadequate to increase heat storage, heat production will be increased.   In cold T_a, greatly increased heat production, including vigorous shivering (chill), is the only way to raise the body temperature. Stitt (1979) has shown that when a pyrogenic substance is introduced into the body and the set point elevated, the thermoregulatory controller will mobilize any response appropriate to increase the storage of body heat.

Adair et al. (1997) hypothesized that a febrile animal might utilize energy from an environmental RF field to generate a fever in response to an injection of pyrogen into the hypothalamus, thus sparing metabolic energy stores. Four squirrel monkeys were implanted with Delrin injection cannulae and re-entrant tubes in the medial preoptic/anterior hypothalamic area so that a 1 μL volume of 250 ng PGE_1 in saline could be injected on demand to produce a 0.6 °C fever that lasted 60-90 min. In each test, following a 90-min equilibration to T_a = 26 °C, the PGE_1 was injected and a 30-min RF exposure to either 450 or 2450 MHz CW microwaves was introduced either immediately, or 30, or 60 minutes post-injection. This procedure allowed evaluation of the potential synergism between RF energy and fever during the three different phases of the fever cycle (chill, plateau, and defervescence).   Two whole-body specific absorption rates (SARs) (1.5 and 3.0 W/kg) were studied at each frequency. Control conditions included 1) PGE_1 injection without subsequent RF exposure, 2) RF exposure following a saline injection, and 3) tests in the absence of injections and RF exposure. The major finding was that during the chill and plateau phases of the fever cycle, RF energy did indeed substitute for metabolic energy in the generation and maintenance of the fever.   However, during defervescence, RF exposure tended to exacerbate the fever and prevent the efficient loss of heat stored in the body. These responses were dose dependent and also related in complex ways to RF frequency.

5.4.3   Whole-Body RF Exposure

5.4.3.1   Human Physiology and Heat

Human core temperature can be as low as 36 °C in the early morning and as high as 40 °C during exercise or environmental stress. The core temperature of humans is generally stable in most thermal environments; however, skin surface temperature is directly related to the environmental temperature (including radiant heat).   Sensations of heat or cold, as well as feelings of comfort and discomfort, are primarily related to the skin surface temperature and the property of skin wettedness.   Humans have exquisitely sensitive behavioral and autonomic mechanisms to maintain both core and surface temperatures. Failure of temperature regulation is described by heat related disorders (heat cramps, heat exhaustion and heat stroke) and may occur at core temperatures as low as 38 ºC.

146

5.4.3.2   RF Heating / Clinical and Laboratory Studies

Studies of human beings deliberately exposed to RF energy are rare and most of those reported involve partial-body RF exposure. In volunteers undergoing magnetic resonance imaging (MRI), when SAR = 2.7 to ~6.0 W/kg for 30 min, core body temperature (tympanic) could rise as much as 0.4 ºC during MRI and was a direct function of SAR. Increases in local skin temperature, local skin blood flow, sweating, and heart rate were also SAR-related, but negligible (Shellock, et al., 1989a, 1989b, 1994). As the frequency of partial-body RF exposure increases, wavelength decreases and the RF energy is absorbed closer to the surface of the skin. In laboratory studies of volunteers undergoing 45-min RF exposure at normalized peak SAR = 6.0 to 15.4 W/kg in controlled thermal environments, core body temperature (esophageal) remained stable within ± 0.1 °C of the equilibrated level and metabolic heat production changed little in resting subjects (Adair et al., 1998, 1999a, 1999b, 2001a, 2001b, 2003a). Individual physiological responses (skin temperatures, sweating rate, skin blood flow) were a function of ambient temperature (T_a=24, 28, 31 °C), frequency (100, 450, 2450 MHz), and field strength (4, 6, and 8 mW/cm^2 at 100 MHz; 18 and 24 mW/cm² at 450 MHz; 27, 35, 50, and 70 mW/cm² at 2450 MHz). Corresponding normalized peak SARs at 2450 MHz were 6.0, 7.7, 11.2, and 15.4 W/kg, the highest being well outside the IEEE C95.1 (1999) guidelines.

For whole-body exposure, the maximal absorption of RF energy occurs when the long axis of the body is parallel to the electric field vector (E-polarization) and the longest dimension of the body is about 0.4 of the free space wavelength (resonant frequency) (Durney et al., 1986). RF exposure of non-human primates at resonance yields somewhat less efficient thermoregulation than does exposure to sub-resonant or supra-resonant frequencies (Adair et al., 1992; Krupp, 1983; Lotz, 1985; Lotz & Saxton, 1988). Although the threshold for a reduction in metabolic heat production (*M*) may be lower at resonance, the magnitude of the response change may be less for a given SAR than at non-resonance and the body temperature may rise. However, the hyperthermia is modest and well regulated. The situation is similar to that of humans during exercise (Adair, 1996). Some have expressed concern that human exposure at resonance may pose a greater hazard than exposure at other frequencies. Experiments recently completed, where seated adults undergo 45-min RF whole-body exposures at resonance (100 MHz), demonstrate that autonomic heat loss mechanisms (blood flow and sweating) are rapidly mobilized to dissipate heat generated deep in the body. No increase in core temperature occurs, even at a power density that is 8 times the IEEE C95.1-1991 standard at 100 MHz (Adair et al., 2003a).

5.4.3.3   Heat Stroke and Other Heat-Related Effects

5.4.3.3.1   Cardiovascular Effects

Many deaths that occur during periods of very hot weather are not only due to hyperthermia but also to hemoconcentration, which can lead to increased incidence of coronary and cerebral artery thrombosis in elderly people (Donaldson et al., 2003). This risk appears minimal in healthy adults. Sweating can cause serious loss of body water even in young adults, if water intake is restricted. Dehydration can cause heat cramps, heat exhaustion, and ultimately

DISTRIBUTION A: APPROVED FOR PUBLIC RELEASE; DISTRIBUTION UNLIMITED.
PUBLIC AFFAIRS CASE NO. 11-069

to a failure of sweating and of circulation to the skin, with a rapid rise of core temperature. Heat stroke will ensue if supportive treatment is not administered. People taking certain drugs, or vulnerable for other reasons, may also be prone to heat stroke.

5.4.3.3.2 Gastrointestinal (GI) and Other Effects

Excessive whole-body heating is also associated with damage to a variety of critical organs, including the heart, kidney, lungs, liver and gastro-intestinal (GI) tract. In addition to the direct effect of increased tissue temperature as a result of heating, a redistribution of blood flow away from organs such as the GI tract, can potentiate this damage and contribute to other pathologies. For instance, dysfunction of the protective GI mucosa can produce an increase in intestinal permeability, which involves diffusion of bacterial products such as endotoxin from the GI lumen to the blood.

5.4.3.3.3 Central Nervous System (CNS) Effects in Humans

The adverse effects of heat and heat related disorders in the normal population are more frequent than initially thought. The main leading causes of death are cardiovascular diseases followed by traumatic injuries to the CNS. However, until now very little attention has been paid to the heat/related illnesses as one of the important factors in CNS injuries. Early reports of heat-related human deaths seldom included post mortem study of the CNS. One study showed that in most victims, heat induced brain damage was apparent following 4 to 14 days of the initial heat insult. The main causes of death were micro haemorrhages in the leptomeninges and a pronounced increase in volume swelling of the brain (brain edema) that compresses the vital centers. The most vulnerable areas of the brain were the cerebellum and the cerebral cortex, while the brain stem and hypothalamus showed minimal damage. No attempt was made to study changes in the hippocampus. Following heat-related illness, the body temperature at death ranged between 39 to 41.6 °C.   However, this and subsequent investigations of CNS pathology of heat victims, did not examine endothelial cell damage or cellular alterations in the hippocampus and spinal cord. Also, the methods used to study cell changes were primitive and no specific staining of nerve cells, glial cells, or myelin were used. Thus, details of neuropathology of the human CNS are still not well known and require careful further investigation using modern techniques.

5.4.3.3.4 Central Nervous System (CNS) Effects in Animals

Animal studies using CNS as the target organ following whole-body heating are rare. Thus, knowledge of the exposure temperature that leads to changes in brain function is still lacking. However, exposure of rats at 38 °C for 4 h results in cellular damage in different parts of the brain. The hippocampus is the most vulnerable organ of the brain and specific cell damage can be seen in the CA3 and 4 regions. Since the hippocampus is related to memory function, damage to this organ following heat injury can lead to memory impairment. This new field of research requires further investigation. Also, in animals the endothelial cells of the brain and spinal cord are more vulnerable to heat injury, and leakage of serum proteins leading to edema formation can be seen in several brain regions following heat exposure at 38 °C for 4 h, suggesting that the crucial factor could be alteration in blood/brain barrier function. Impairment

148

of the fluid microenvironment of the brain results in brain dysfunction leading to cell death, apoptosis, and necrosis. However, the detailed mapping of cell injury and expression of several pathological markers in the heat-injured brain is still incomplete.

5.4.4 Partial-Body RF Exposure

If a non-human primate undergoes partial-body exposure to RF energy, the magnitude of the change in *M* reflects the total absorbed energy, as though it were integrated over the whole body (Adair, 1988). If an animal is exposed to RF energy at SARs greater than those that reduce *M* to the resting level, thermoregulation will be accomplished by mobilization of the next response in the thermoregulatory hierarchy, changes in vasomotor state or conductance, i.e., blood flow, as shown in Figure 5-2 (Adair, 1985; Candas et al., 1985; Lotz & Saxton, 1987).

A series of laboratory studies has been conducted in which human volunteers were exposed for 45 min to continuous wave (CW) RF energy (at 2 to 4 peak power densities) in three controlled thermal environments (T_a = 24, 28, and 31 °C) (Adair et al., 1998, 1999a, 2001a, 2001b). The frequencies explored (450 and 2450 MHz) deposited RF energy relatively close to the skin surface, a condition that resulted in SAR- and frequency-dependent increases in skin temperatures but no significant change in core body temperature, measured in the esophagus at the level of the heart. This stability of core temperature resulted from the efficient mobilization of autonomic heat loss responses, principally skin blood flow and sweating, which were presumably initiated by signals from thermal receptors in the skin. These studies involved partial-body exposure of the subject volunteers. Given small anechoic chambers and transmitting systems of modest peak output power (e.g., 1 kW or less), it is impossible to achieve both whole-body exposure and a peak power density (PD) that is appropriate for scientific investigation. The best compromise for these studies was to expose the dorsal aspect of the head, upper arms, and trunk of the seated subject, which represented about 34% of the total skin surface area.

5.4.5 Sensitive Tissues and Organs

The rate at which biological cells are killed by heat is an exponential function that depends on both the temperature applied and the duration of exposure. In clinical hyperthermia treatments, it is useful to normalize the time-at-temperature data to a common unit that may be applied to various heating regimes. Sapareto and Dewey (1984) proposed a simple method, termed "thermal isoeffective dose," by which one time-temperature combination can be converted to another. In this method, time-temperature data are converted to an equivalent number of minutes at 43 °C. This temperature is close to the point of discontinuity (break point) of functions in many Arrhenius plots of time-temperature data (Dewey, 1994). The equation for converting one time-temperature combination to another is:

$$\text{CEM } 43 \text{ °C} = tR^{(43-T)} \tag{12}$$

where CEM 43 °C = cumulative equivalent minutes at 43 °C, t = time (minutes), T = average temperature during the time interval t, and R = number of minutes required to compensate for a 1.0 °C temperature change above or below the break point. Sapareto and Dewey's (1984) method assumes that R = 0.25 below the break point, which is consistent with much rodent data. This value indicates that the time to achieve an isoeffect at a defined temperature is increased by a factor of 4 for each degree drop below the break point. On the other hand, above the break point R = 0.43 for rodent cells, indicating that the time to achieve an isoeffect is increased only by a factor of 2.2 for each degree rise above the break point (Dewhirst et al., 2003). Note that the break point on Arrhenius plots is slightly higher for human (43.5 °C) than for rodent cells (43.0 °C), based on in vitro data. However, there is very little human data available apart from a few measurements of thermally induced skin necrosis (Moritz & Henriques, 1947; Buettner, 1951; Song et al., 1990). Most of the available data have been collected on mice, rats, and rabbits, with some data on dogs and pigs. Since the characteristics of porcine skin are quite similar to those of humans, future work on the thermal sensitivity of tissues and organs might be conducted on pigs as the best approximation to humans.

Hyperthermia, in terms of CEM 43 °C at various durations from < 1 min to > 80 min, reveals the thermal sensitivity of many animal tissues. Based on histopathological analysis, testicular and brain tissues appear to be the most sensitive to thermal insult for exposures of short duration. Changes in BBB function can also be significant. Bone marrow, kidney, and spleen show minor changes of an acute nature. Minor changes in testicular function may persist for some time. Hyperthermia of longer duration (up to 40 min) exacerbates effects on the brain and BBB, produces minor morphological effects on cornea, retina, and eyelid, and may damage the prostate and rectum. Still longer exposures (up to 80 min) impair the function of peripheral nerves, damage other parts of the eye (sclera, choroid, lens, anterior chamber, ciliary body) and impact liver, muscle, skin, and fat. Exposures longer than 80 min produce significant damage to most of the tissues in the body of rabbits, dogs, and pigs. Evidently, rodents do not survive CEM 43 °C exposures much longer than 40 min. On the other hand, based on an exhaustive survey of the hyperthermia literature, Dewhirst et al. (2003) state that there are virtually no data that relate to the sensitivity of tissues in the human body. It is of interest that thermal damage to human skin, in terms of CEM 43 °C would require a continuous exposure of 10-12 hours at that temperature.

5.5 Human Perception of RF Fields

5.5.1 Introduction

Since RF exposure generates heat in body tissues, such energy can be part of the thermal environment to which humans and animals may potentially be exposed. Although physiological responses (e.g., sweating) may be initiated automatically by thermal stimuli, the sensation of tissue warming is necessary to initiate appropriate behavioral action. The stimulation of temperature-sensitive nerve endings located within the outermost 0.6 mm of mammalian skin probably underlies the sensations of changes in skin temperature (Hardy & Oppel, 1937). Whether or not RF exposure produces a warmth sensation depends on many parameters of the signal, e.g., frequency, modulation, intensity, duration, as well as the body locus and the exposed

150

surface area. Many of these parameters influence the magnitude of thermal sensations derived from exposure to infrared (IR) radiation (Stevens, 1983). IR energy is absorbed in the most superficial layers of skin in close proximity to the temperature-sensitive nerve endings; a similar absorption profile should be obtained for the higher microwave frequencies (10 GHz and above). However, lower RF frequencies will be absorbed in complex patterns at other depths, making prediction of thermal sensation difficult.

5.5.2 Perception Thresholds

5.5.2.1 Archival Data

Absolute thresholds for the detection of RF irradiation by human observers were determined in several archival studies (Schwan et al., 1966; Eijkman & Vendrijk, 1961; Vendrijk & Vos, 1958; Hendler, 1968; Hendler & Hardy, 1960; Hendler et al., 1963). All of these studies involved brief exposures (10 sec or less) and restricted areas of forehead or forearm skin. In general, the shorter the wavelength of the irradiation, the less energy was required to provoke a just-detectable sensation of warmth (Michaelson, 1972). When a 37 cm² area of forehead was irradiated for 4 sec, the mean absolute threshold of warmth was 33.5 mW/cm² at 3 GHz, 12.6 mW/cm² at 10 GHz, and 4.2 mW/cm² at frequencies > 1000 GHz (far-IR). Irradiation of small areas of skin by 3- or 10-GHz pulsed (0.4 µsec pulse with, 2500 pps) microwaves had to last at least 5 sec in order for the minimal intensity to evoke a thermal sensation and the exact intensity depended on the area stimulated. At shorter stimulus durations, the intensity had to be greatly increased to evoke comparable warmth sensations. This phenomenon is called temporal summation and the shortest duration at which only intensity matters is called the "critical duration" (Stevens, 1983).

Justesen et al. (1982) incorporated indirect assessment of absorbed RF energy during 10-sec exposures of the human forearm (average area = 107 cm²) to 2.45-GHz CW fields. Warmth sensations were reported when the energy density of the RF field was ~29 mJ/cm², compared to ~1.8 mJ/cm² when the same skin area was exposed to far-IR radiation. These thresholds corresponded to power densities of 27 and 1.7 mW/cm² and, thus, were similar to results reported in the earlier studies cited above.

5.5.2.2 Recent Extensions of Classical Data

Blick et al. (1997) measured the threshold for thermal sensation across a range of five RF frequencies from 2.45 to 94 GHz plus far-IR (~3000 GHz). Judgments of threshold warmth sensation, across a skin area of 327 cm² centered on the subject's back, were determined at each frequency using a double-staircase psychophysical procedure. The stimulus duration was 10 sec and the interstimulus interval was 1 minute. Thresholds were determined at each frequency for a group of 16 adult male volunteers. Thresholds of warmth were a linear function of frequency when the data were plotted in log log coordinates. The threshold at 2.45 GHz (63.1 ± 6.7 mW/cm²) was more than an order of magnitude larger than that measured at 94 GHz (4.5 ± 0.6 mW/cm²); in turn, the latter was not significantly different from the IR threshold (5.34 ± 6.7 mW/cm²). In general, measured warmth thresholds reflected the skin depth at each frequency and a theoretical analysis (Riu et al., 1997) suggested that a constant temperature increase of

151

~0.07 °C at or near the surface of the skin was the adequate stimulus for perception. This analysis also indicated that the depth at which the thermal receptors are located is not a relevant parameter, as long as it is within 0.3 mm of the surface.

5.5.2.3 Suprathreshold Functions Including Pain

No new data on pain sensations derived from RF exposure have appeared in the literature since the classical studies of Cook (1952a, 1952b), although these early data should be confirmed and extended. Cook investigated the potential of 9.4- and 10-cm microwaves to induce pain sensation in two exposure areas (53.2 and 9.5 cm²) of human skin (forearm, thigh, and calf). The subject was instructed to report when a burning pain sensation occurred and the latency to report was noted. The temperature of the skin at pain threshold was measured with a copper/constantan thermocouple held at the center of the irradiated surface. The final skin surface temperature at pain threshold was 46.1 ± 1.0 °C. Cook concluded that the pain threshold, aroused by microwave irradiation, was directly related to the skin temperature. However, the power density of the radiation at threshold could depend on area exposed, exposure time, initial skin temperature, anatomical site, and thermal conductivity. Cook provided a theoretical analysis based on thermal flow theory that explained the results measured with short exposures. Longer exposures had to involve vasomotor responses in the capillaries, a conclusion also reached by Riu et al. (1997) for the adequate RF stimuli for the sensation of warmth.

5.6 Human Overexposure Data

Chiang and Shao (1989) reported that ―hundreds of male volunteers‖ in China have received RF irradiation as a contraceptive procedure. A group of 53 volunteers was treated with 2450-MHz energy localized to the testes once a month for 30 minutes (Fang et al., 1982). If the testes were heated to 40 – 42 °C, sperm counts were reduced to $<5x10^9$/L by 7 weeks after the first irradiation and persisted at this level. Neither a change in sexual function nor deleterious side effects were reported. However, no data were presented on the effectiveness of the treatment as a contraceptive and there was a suggestion that the near field exposures used provided inhomogeneous exposure to the testes. A more recent study, reporting a similar attempt to use RF energy to induce temporary sterility in adult males, also gave data related to the thermal effects of long-term, partial-body exposure at high intensities (Liu et al., 1991). Thirteen male volunteers underwent localized RF exposures of the testes at 915 or 2450 MHz in weekly sessions that lasted 30 min each. Irradiation was carefully restricted to the testes. Power levels were 20 to 30 watts, sufficient to raise the scrotal skin temperature 10 °C above its normal level. Seven subjects received over 100 such sessions, the remainder somewhat fewer. Six months after termination of the exposures, biopsies of testicular tissue were taken for microscopic examination. While considerable cellular damage was evident, no significant gross morphological abnormalities were found. Further, despite evidence of greatly reduced spermatogenesis during the treatment, sterilization was not reliably achieved by this method, as two of the men fathered children during the course of the study. A major conclusion was that human testicular tissue appeared much more resistant to thermal injury than equivalent tissue in experimental animals, such as similarly-exposed rats or rabbits.

Other data on RF overexposure of human beings in the military and/or industrial environments have been collected over the years. A report by Mitchell (1985) indicated that over the preceding 10 years, 300 reported overexposure incidents were investigated. Of these, 58 were confirmed overexposures, the remainder being within the permissible exposure limit (PEL) of 10 mW/cm² in any 6-min period. Of the 58 overexposures, most of which were in the frequency range between 1.5 and 10 GHz, 45% of the individuals felt a clear warming sensation and terminated the exposure within less than 6 min. The power densities ranged from 15 to 160,000 mW/cm² (with most between 40 and 1000 mW/cm²) and nearly all were partial-body exposures. The clinical findings of the overexposure victims were inconsistent, even for intense localized exposure. Erythema and/or edema were rarely found. Abnormalities of the ocular lens that were noted were not associated with visual impairment. Follow-up tests of serum enzyme levels, blood counts, blood pressures, sedimentation rates, and EKGs were all clinically unremarkable. Unfortunately, a nearly complete lack of pre-exposure baseline data hampered the evaluation of any abnormal findings.

A study involving extensive workups of 34 patients overexposed to RFR was recently published (Reeves, 2000). The purported overexposures occurred between 1973 and 1985 and each patient received a comprehensive clinical diagnostic workup at the USAF School of Aerospace Medicine at Brooks AFB. An intensive review of the evaluations was conducted with the objective of advising attending physicians on symptoms and physical signs to focus on, required extent of the workup, need for laboratory studies, additional testing and referrals. Exposure characteristics recorded included RF frequency, average incident power density, estimated exposure durations, and calculated dose. Patient symptoms recorded included sensation of warmth, headache, muscle pain, lacrimation and/or photophobia. Clinical laboratory data included a hemogram, tissue destructive screen, a hepatic screen, and thyroid studies. Statistical analysis showed that there was a slight positive association of certain effects (muscle pain, lacrimation and/or photophobia) with the product of power density and exposure time. Other laboratory studies included urinalysis, serum testosterone levels, sperm counts, electrolytes, serum lipids, fasting blood sugar, EKG, pulmonary function tests, chest and abdominal X-rays. These latter showed no correlation with field strength or the product of field strength and exposure duration. Extensive neurology consultation, psychometric testing, and psychiatric consultation yielded no correlation with field strength or the product of field strength and exposure duration. Principle findings included a positive association of a sensation of warmth with power density, but a negative association between an abnormal tissue destruction screen and power density. A few patients reported burning pain that resolved over several weeks. The major conclusion drawn from this study was that patients with suspected RFR overexposures need to be seen promptly at a medical facility. However, rather than perform extensive evaluations of such patients, a careful history and physical examination with laboratory studies should be performed. It is also very important to address fully the patient's concern about RFR effects.

5.7   Clinical Data of Humans Exposed To MRI

The exposure of patients to the magnetic resonance imaging (MRI) environment at 64 MHz may produce tissue heating that is related to the changing fields of the RF coils. A considerable amount of literature describes thermoregulatory responses of humans to those fields

153

during a variety of MRI procedures in the clinic. An early study (Kido et al., 1987) measured blood pressure (BP), heart rate (HR), respiration rate (RR), and axillary temperature in 27 volunteers during MRI scans of both trunk and head at 1.5T and two RF power levels. Recently, more attention has been paid to equilibration of the patients prior to MRI scans, control of T_a, specification of SAR, and assessment of several physiological variables. Shellock and Crues (1988a, 1988b) measured skin, sublingual, and corneal temperatures of 35 patients during MRI with a head coil (1.5T at 64 MHz). The estimated peak SARs ranged from 2.54 to 3.05 W/kg. An average corneal temperature rise of 0.5 °C (range = 0.0 to 1.8 °C) was statistically significant (P< 0.001) as were slight elevations in the T_{sk} of head regions (P < 0.01) compared to pre-scan levels. Sublingual temperature did not change. In another study (Shellock et al., 1989a), sublingual and T_{sk} were measured in 6 subjects before (20 min), during (30 min), and after (20 min) MRI in a 1.5T body coil at SARs from 2.7 to 4.0 W/kg. SkBF was also measured. Although the 30-min scans did not establish a thermal steady state, the measured temperature changes were not significantly different from zero. Scrotal MRI of 8 men at 1.5 T (range of whole-body SAR from 0.56 to 0.84 W/kg) and an average duration of 23 min produced a maximal rise of 3.0 °C in scrotal surface temperature (Shellock et al., 1990). The authors claimed that this temperature elevation was well below the threshold for a reduction in spermatogenesis, confirmed by Berman (1984).

That measured tissue temperature changes during MRI are attributable to RF exposure during the procedure was demonstrated by experiments in which 6 male subjects were exposed to 1.5T static magnetic fields only (Shellock, 1992; Shellock et al., 1989b). Sublingual and several T_{sk} were measured during 20-min scans that followed a 20-min equilibration to a $T_a = 21$ °C. No change from the equilibrated level occurred in any measured body temperature. The general conclusion drawn from MRI data at 1.5T, is that tissue temperature changes are small and far below hazardous levels (Shellock, 1992).

5.7.1   MRI Exposure Data (Laboratory Studies of Humans)

Schaefer (1988) reported results of 20-min whole-body MRI scans (SAR = 4.0 W/kg) of 11 adult volunteers. The scan was preceded and followed by 20-min baseline periods. Measured variables included T_{esoph}, several T_{sk}, M, HR, RR, and BP. Although the initial baseline did not produce a steady state, no change in the group mean T_{esoph} occurred until the end of the 20-min MRI scan when the increase was 0.3 °C (P<0.005). During the scan, T_{sk} near the isocenter of the scanner rose up to 3.0 ± 0.5 °C, but these increases were judged to be non-hazardous. BP did not change, but slight elevations were recorded in HR and RR. In general, this study and that by Shellock et al. (1989b) indicate that MRI scans at whole-body SARs up to 4.0 W/kg do not produce significant changes in T_{co} and that T_{sk} elevations are within the normal variation produced by changes in T_a or during normal activity. However, the MRI exposure environment is atypical. The penetrating RF field is primarily magnetic, with a small contribution from the electric field (Bottomley et al., 1985); thus, the ohmic heating that occurs is greatest at the surface and least at the center of the body.

A more recent report (Shellock et al., 1994) describes 16-min MRI exposures of 6 human volunteers in a body coil at 1.5 T, 64 MHz. Subjects were equilibrated to $T_a = 21.3 - 23.3 \pm 0.4$ °C for about 15 min prior to the exposure. Tympanic membrane temperature (T_{tymp}) was

154

recorded immediately before and after the MRI exposure, and HR, oxygen saturation, SkBF, and 6 T_{sk} were recorded at 2-min intervals during the procedure. The RF exposure was at a calculated whole-body SAR of 6.0 W/kg, achieved by use of a "prototype pulse sequence". The authors reported statistically-significant (P < .05) increases in T_{tymp} and 5 T_{sk}, HR, and SkBF. These changes were not considered deleterious and such a high SAR appears to be well tolerated by persons with normal thermoregulatory function. However, the report suffers from a lack of technical detail with respect to the purported whole-body SAR achieved.

5.7.2 Modeling Human Responses to MRI

As a test of a modeling effort (see below), Adair and Berglund (1992) reported the results of tests on two normal male subjects who underwent a series of three 20-min MRI scans (1.5T) of the trunk at a whole-body SAR of 1.2 W/kg. Each session began with a 30-min equilibration to $T_a = 22 \pm 1$ °C and successive 20-min scans were separated by a 35-min re-equilibration period. T_{esoph} and several T_{sk} were monitored continuously, as was sweat rate from chest and thigh. Judgments of thermal sensation and discomfort were obtained periodically throughout each test. For both subjects, T_{sk} of chest and thigh increased 1.1 °C during each scan but T_{esoph} was very stable throughout the 170 minutes of the test session. This stability occurred despite an overall rise of about 2.5 °C in T_{sk} and periodic sweating. As the test session progressed, both subjects reported increased sensations of warmth that were directly related to the increased T_{sk}.

5.8 Predictive Models of Human Physiological Response to RF Environments

5.8.1 Introduction to Thermoregulatory Modeling

The operating characteristics of the thermoregulatory system appear to be similar to those of an automatic control system involving negative feedback. The body temperature of endotherms appears to be regulated at a set, or reference, level. Temperature sensors located in the skin and various other parts of the body detect temperature perturbations and transmit this information to a central integrator or controller that integrates the sensory information, compares the integrated signal with the set point, and generates an output command to the effector systems for heat production or heat loss. The responses thus mobilized tend to return the body temperature back to the set level.

These hypothetical constructs aid our understanding of thermoregulatory processes and let us formulate simulation models that can be used to predict human response to a wide variety of thermal stressors. Models have been of many types from verbal descriptions to highly sophisticated electrical analogs and mathematical models. Many simulation models have been used to predict human responses to RF energy (Fan et al., 1971). Of particular relevance are the theoretical models of Mumford (1969) and Guy et al. (1973) that use a heat stress index to describe the human response to particular environmental and RF heat loads. A model by Emery et al. (1976) used several sweat rates to calculate the thermal response of the body to absorbed RF energy. On the other hand, a two-dimensional, combined RF-heat-transfer model (Spiegel et al., 1980) predicted rapid localized temperature increments in the thigh of a nude male resting in a thermoneutral environment and exposed to 80 MHz at 50 mW/cm^2. Similar temperature increments were calculated for the steady state at power densities as low as 10 mW/cm^2. If the

155

altered tissue blood flow for temperatures in excess of 40 ºC (Cunningham, 1970) could be added to this model, these predictions might be modified.

The modeling of physiological responses becomes important when its purpose is to simulate experiments that cannot be performed or to extrapolate variables that are not attainable through experiment. The basis of thermophysiological modeling is the energy (heat) balance Equation 1. These models incorporate the physical characteristics of the body, the heat production and heat loss responses, and all relevant environmental parameters. In such models, absorbed RF energy is added to metabolic energy and must be balanced by appropriate heat loss responses in order to prevent body heat storage.

A model by Stolwijk and Hardy, first published in 1966, updated by Stolwijk and Hardy (1977), is still used as a basis for predicting the possible thermoregulatory outcomes of RF energy deposition in selected parts of the human body. The model was used, for example, to simulate the deposition of 100 watts of RF energy into the core compartment of the head for 30 min in a thermoneutral T_a of 30 °C (Stolwijk, 1980, 1983). This simulated exposure caused only a small increase in brain temperature because of the high rate of brain blood flow and the mobilization of vigorous heat loss through sweating. Because heat loss far exceeded heat production plus the RF energy input, all body temperatures were predicted to fall. Attempts by others, e.g., Kritikos and Schwan (1975), to improve on this model have had varying degrees of success that have been described elsewhere (Adair, 1995).

5.8.2   Predictions of a Two-Node Model

A simpler model was adapted to predict the consequences of human exposure to RF fields in the MRI environment (Adair & Berglund, 1986). The model has only 2 nodes (core and skin) but in most other respects is similar to the Stolwijk and Hardy formulation. It predicts physiological heat loss responses in real time in terms of T_a, air movement (v), and whole-body SAR. Assuming a criterion elevation in deep body temperature (ΔT_{co}) of 0.6 °C, $T_a = 20$ °C, and v = 0.8 m/sec, the model predicts that a 70-kg patient could undergo a MRI scan of indefinite duration at SAR $\leq$ 5 W/kg. Lowering T_a or increasing v permits a rise in lower permissible SAR for a given ΔT_{co}. Stricter ΔT_{co} criteria result in lower permissible SARs and shorter exposure durations. The limiting response is usually the rate of SkBF, although sweating can play a role in limiting ΔT_{co}.

Restrictions on the rate of SkBF, ranging from 0 to 89% of normal, have also been studied with this model (Adair & Berglund, 1989). Model predictions showed that restrictions of up to 67% of SkBF would yield a tolerable ΔT_{co} ($\leq$ 1 °C) during MRI scans (SAR $\leq$ 4 W/kg) of 40 min or less under normal clinical conditions. Increased T_a and RF exacerbate the thermal stress imposed by absorbed RF energy, while severely impaired SkBF encourages short MRI exposures (20 min or less) at SAR $\leq$ 3 W/kg.

156

After generating predictions based on many values of each parameter, a nomogram was developed based on the fact that, at any given T_a, a person can absorb some level (SAR) of RF energy indefinitely; i.e., achieve thermal equilibrium with the prevailing conditions. When SAR is low, T_{co} will rise initially and then stabilize at an elevated level. If SkBF is impaired, the maximal SAR at which thermal equilibrium is attained will be lower. Figure 5-8 shows the maximal SAR for equilibrium in two T_a (20 and 27 °C) as a function of the impairment in SkBF. The solid line defines the limit of the zone of stable T_{co} at T_a = 20 °C; the dashed line defines the same limit for T_a = 27 °C. Thus, raising the T_a by 7 °C decreases the maximal SAR for equilibrium by ~1 W/kg. If the SAR under consideration exceeds the maximal value for thermoequilibrium, a continuous rise in T_{co} can be expected during RF exposure. The model predicts that the rate of ΔT_{co} depends on the impairment in SkBF, T_a, RH, and the clothing insulation (clo) (McCullough et al., 1989). Adair and Berglund (1989) provided explicit corrections to the predictions of their model as a function of departure of SkBF, T_a, RH, and clo from those specified in Figure 5-8.
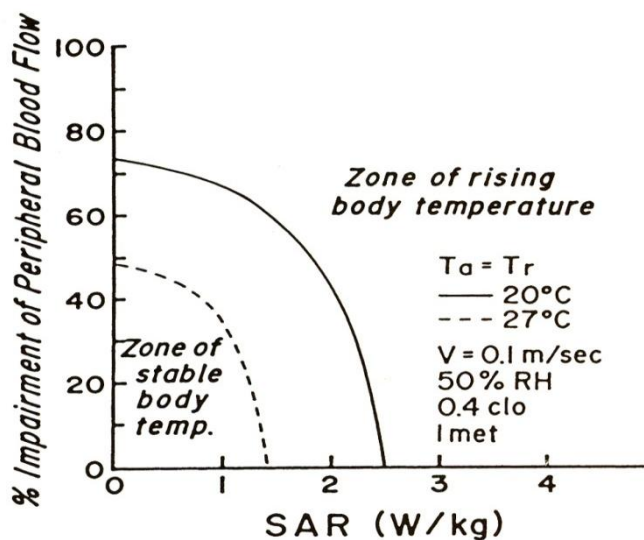
Figure 5-8. Predictions of a two-node model showing zones of stable and rising body temperatures in two environments during 40-min MRI scans at different SARs when peripheral blood flow is impaired (Adair & Berglund, 1989).

Schaefer (1992) used these predictions to calculate the effect of T_a during a 60-min MRI scan on the average ΔT_{co} under conditions of 40% impairment of SkBF and clo = 0.2. He calculated that a scan at SAR = 4 W/kg would result in a ΔT_{co} of only 1 °C when T_a = 19 °C. Further, a 1-hr RF exposure at SAR = 1 W/kg, even at T_a = 27 °C, should result in no rise in T_{co}. These predictions do not conflict with clinical data or with ongoing laboratory studies of human volunteers.

5.8.3 Amplification of the Modeling Process: Incorporation of FD-TD Images

A variety of human and animal studies confirm that, even when no changes can be measured in deep or peripheral body temperatures, thermoregulatory mechanisms are mobilized

157

to dissipate heat generated in body tissues during RF exposure at resonance. A review was undertaken to identify the loci of temperature-sensitive neurons (thermosensors) in the mammalian body, their operating characteristics, and how they may be selectively stimulated by absorbed RF energy.

Research results (Adair et al., 2003a) indicated that when seated human volunteers underwent 45-min whole-body RF exposures at resonance (100 MHz), no change was measured in core (esophageal) temperature despite maximal energy penetration at this frequency. Minimal temperature changes were recorded in the skin, locus of peripheral thermosensors, yet vigorous sweating and increased blood flow were rapidly mobilized. The subjects had no sensation of skin warming, even at power densities greatly in excess of current RF safety standards. A comparable study at 220 MHz, recently completed, has yielded similar results. We needed to identify regions of high local SAR within the central nervous system (CNS) that would coincide with the loci of thermosensors specific to thermoregulatory heat loss responses. Finite Difference-Time Domain (FD-TD) modeling of a 70-kg seated human adult (Gasjek et al., 2002) was then utilized to determine the optimal RF frequency to stimulate warm sensors located in the CNS that could initiate these specific heat loss mechanisms.

Vertical FD-TD images, encompassing head and trunk, were generated at both frequencies and compared with anatomical maps of brainstem nuclei and other CNS regions known to harbor thermosensitive cells. Mid-sagittal sections of the models showed high rates of RF energy absorption [normalized local SAR ≥ 1 (W/kg)/(mW/cm^2)] in the ventricles of the brain, particularly the third ventricle, where the choroid plexus produces cerebrospinal fluid. The cerebrospinal fluid bathes the medial preoptic-anterior hypothalamic (PO/AH) nuclei as well as the length of the spinal cord, both of which contain concentrations of thermosensors that are known to exert control over the body temperature. Large aggregates of these warm sensitive cells in multiple layers, firing at rates of ~0.25 pps/°C, provide for convergence and enhancement of output signals so that minute temperature changes in the fluid ($\Delta T = 0.02$ °C) can ultimately initiate heat loss responses (Adair, 1999). Exploration of regions of high local SAR, at many frequencies and for models of different characteristics, is now underway in earnest and will greatly aid the understanding of thermophysiological responses measured in humans during RF exposures.

5.9 Data for Heat Response Calculations

5.9.1 Introduction

Much is known about the upper limits of human tolerance to hot, humid environments that contain no source of RF energy (Givoni & Goldman, 1972; Provins et al., 1962). Knowing what the human tolerance time would be for a given SAR would be useful. This section describes calculations of the approximate SAR that will produce a critical internal body temperature in a standard human exposed for 60 min in a specified hot and humid environment.

The two physiological mechanisms that deal with heat stress in the human body, vasomotor and sudomotor, are each a complex function of many variables. The problem can be simplified, however, if we assume that the body is calling upon its maximum thermoregulatory

158

capacity. Under most conditions of severe thermal stress, evaporative cooling is limited by the evaporation rate, not the sweating rate since the maximum sweating rate is over 2 L/h. If the psychrometric conditions (air temperature, relative humidity, and air velocity), skin temperature, and clothing characteristics are known, the heat storage in the body can be calculated by the fundamental heat-balance Equation 1.

Agreement is not complete on the physiological criteria that best describe the limits of human thermal tolerance. Several researchers (Craig et al., 1954; Goldman et al., 1965; Wyndham et al., 1965) have used a rectal temperature (T_{re}) of 39.2 ℃ as a useful criterion for setting the upper level of heat-stress tolerance in clinical trials. Others have advocated the use of more subjective criteria such as faintness and loss of mental and physical ability (Bell & Walters, 1969; Bell et al., 1965; Machle & Hatch, 1947). Since quantitative calculations based on such subjective criteria are not practical, for the purposes of the following calculations we have defined a T_{re} = 39.2 ℃ as the danger level for man. With this definition, the critical rate of heating for a 1-h period is that which will cause a rise in T_{re} of 2.2 ℃/h, assuming a normal beginning rectal temperature of 37 ℃ and neglecting any temporal lag in the T_{re} response.

We utilized data for the change in mean skin temperature (T_{sk}) as a function of time collected in an experiment recorded by Ellis (1972), in which a healthy 28-yr-old male exposed to a hot, humid environment was judged by observers to have reached his tolerance limit in 61 min. His final rectal temperature was 39.4 ℃. His skin temperature rose bimodally from 36.9 ℃ to 38.4 ℃ during the first 20 min of exposure, then increased more slowly to 39.3 ℃ in the next 41 min because of the onset of sweating.

If these data for T_{re} and T_{sk} are assumed to be generally true for a man heat stressed to his tolerance point in 1 h, we should be able to calculate lesser amounts of heat storage imposed on the body by less severe environmental conditions that permit greater rates of evaporative cooling. Also, substituting an equivalent amount of heat energy absorbed during exposure to RF for metabolic energy seems reasonable. Such an equivalence was demonstrated by Nielsen and Nielsen (1965) when they measured identical thermoregulatory responses to exercise and to diathermic heating. This assumption would be expected to be valid for RF energy at frequencies up to the post-resonance range (perhaps up to about 1 GHz for the average man), but might not be valid at higher frequencies where the RF exposure causes primarily surface heating. Consequently, the results calculated in the next section are restricted to conditions where the RF heating does not occur primarily on the surface. The substituted equivalent RF heat load, expressed in watts per kilogram of body mass, is designated the SAR_{60} – the specific absorption rate that would produce a rectal temperature of 39.2 ℃ in the irradiated subject in 60 min. The SAR_{60} is intended to represent the maximum SAR that a healthy average man can tolerate, with regard to thermal conditions alone, for 60 min in a given environment, assuming both that the capacity to thermoregulate is normal and that the other criteria for metabolic heat production, posture, clothing, and behavior specified below are valid.

5.9.2   Calculations

For the following calculations, the required parameters for man and the environment are listed in Table 5-6. Standard values obtained from physiology texts (Kerslake, 1972;

159

Mountcastle, 1974; Newburgh, 1949; Ruch & Patton, 1973; Guyton & Hall, 2000) are given for the sample calculations. The symbols, units, and conversion factors used in this section conform, for the most part, to the uniform standards proposed by Gagge et al. (1969).

The calculations are based on a modification of the fundamental heat balance Equation 1, which neglects the work factor (W), groups together the terms for dry-heat losses ($R + C$), and incorporates the electromagnetic power absorbed (P):

$$M + P = (R + C) + E + S \tag{12}$$

or

$$S = M - (R + C) - E + P \tag{13}$$

in which all symbols are as previously defined. The total heat load is given by:

$$H = \Delta T_{re} \, c_p \, w \quad [\text{kcal}] \tag{14}$$

where ΔT_{re} is the change in rectal temperature caused by the heat load H. The evaporation rate is given by:

$$E = h_e \, A_w \, (P_{sk} - P_a) + 0.0023 \, M \, (44 - P_a) \quad [\text{W}] . \tag{15}$$

The dry heat losses due to radiation and convection can be represented by:

$$(R + C) = (h_r \, A_r + h_c \, A_c)(T_{sk} - T_a) \quad [\text{W}] . \tag{16}$$

160

Table 5-6. Specification of parameters used in calculating SAR60.

Parameters for a Standard Physiological Man	Symbol and Numerical Value
Mass	w = 70 kg
Height	h = 1.75 m
Surface area	A_D = 1.85 m^2
Convection, radiation area	$A_r = A_c$ = 1.3 m^2
Wetted area	A_w = 1.7 m^2
Rate of metabolic heat production	M
Sitting at rest	M = 110 W or 1.57 W/kg
With thermal stress, T_{re} = 37C	M = 120 W or 1.71 W/kg
At T_{re} = 39.2 ºC	M = 153 W or 2.18 W/kg
Average M over 1-h period	M = 137 W or 1.96 W/kg
Critical rectal temperature	T_{re} = 39.2 ºC
Normal rectal temperature	T_{re} = 37.0 ºC
Specific heat of body	C_p = 0.83 (kcal/ ºC · kg)

Psychrometric Conditions	Symbol and Numerical Value
Wind velocity	v = 1.35 m/s
Evaporation coefficient	h_e = 21 W (m^2 · torr)
Convective coefficient	h_c = 9.5 W/ (m^2 · ºC)
Radiation coefficient	h_r = 8 W/ (m^2 · ºC)
Ambient temperature range	T_a = 30 to 68 ºC
Relative humidity	a = 0.8, 0.5, 0.2
Saturated ambient water-vapor pressure	P_{wa} is given in referenced tables in units of torr as a function of T_a
Ambient water-vapor pressure	$P_a = a · P_{wa}$
Saturated skin-vapor pressure	P_{sk} is given in referenced tables in units of torr as a function of T_{sk}

Combining Equations 13, 15, and 16 and using values from Table 5-6 results in:

$$S = M - [0.0023\,M(44 - P_a) + 36(P_{sk} - P_a)] - 23(T_{sk} - T_a) + P \quad [W] . \tag{17}$$

This equation is first solved for the particular psychrometric conditions of interest with no RF power absorbed (P = 0). Over a 1-h period, the heat load due to the environment alone is given by:

$$H = \int_{0}^{60\,\text{min}} S \cdot dt . \tag{18}$$

The solution is –60 kcal when $T_a = 40\ °C$ and $\upsilon_a = 0.8$. By Equation 14, the heat load that causes a 2.2 °C rise in T_{re} was 128 kcal for this particular man.

The power, P, that will cause a 2.2 °C rise in T_{re} in 1 h is the difference between H and 128 kcal:

$$P = 1.16\ \frac{W}{Kcal\ /\ h}\ (128 - H) = 218\ W.$$

The SAR_{60} is simply:

$$SAR_{60} = \frac{P}{70\ kg} = 3.11\ \frac{W}{kg} .$$

By using the SAR curves for an average man, we can plot the incident power density that will produce the SAR_{60} for any given frequency and polarization, as shown in Figure 5-9. The calculated SAR_{60} values plotted on this graph represent the worst possible case for man, which is, according to the data for the prolate spheroidal model, E polarization at resonance (70 MHz).

In Figure 5-9, the intercept of each curve with the horizontal axis indicates the ambient conditions (temperature and relative humidity) that will produce a rectal temperature of 39.2 °C with no RF irradiation. For example, with a relative humidity of 80% and an ambient temperature of 42 °C, the SAR_{60} is zero. This means that under these conditions a rectal temperature of 39.2 °C will occur in 1 h with no irradiation. Similarly, the curve shows that if the ambient temperature was 41 °C and the relative humidity 80%, the SAR_{60} would be 1.25 W/kg; under these conditions a rectal temperature of 39.2 °C would be reached in 60 min. The other curves in the figure indicate that the same SAR (1.25 W/kg) would occur at 49 °C and 50% relative humidity and at 63 °C and 20% relative humidity. From the ordinate on the right, we read that at this SAR_{60}, the incident power density for E polarization at resonance would be 5 mW/cm^2.

The incident power densities at other frequencies and/or polarizations can be determined by using the dosimetric curves to find what power density produces an SAR of 1.25 W/kg for the given frequency and polarization in question.

162

RELATIVE HUMIDITY
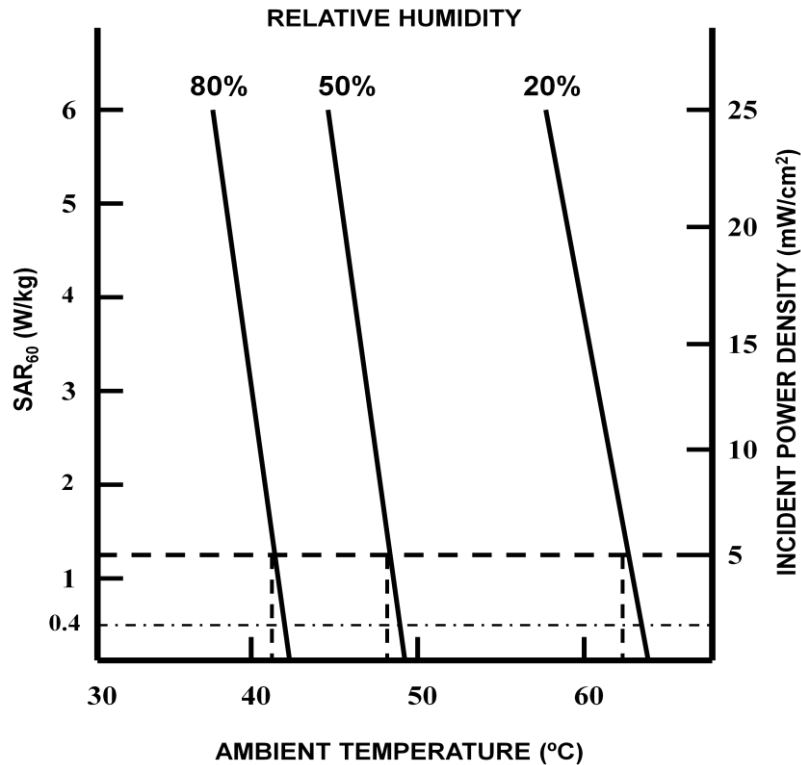
Figure 5-9. Calculated SAR$_{60}$ values in an average man, unclothed and quiet, irradiated by an electromagnetic planewave with E polarization at resonance (about 70 MHz). Dashed horizontal lines indicate the psychrometric conditions (in still air) that yield a SAR$_{60}$ of 1.25 W/kg and 0.4 W/kg at this frequency.

If the ambient temperature were 41 °C and the relative humidity only 20%, a very high SAR would be required to produce a rectal temperature of 39.2 °C in 60 min, a value too high to be read from Figure 5-9. This shows that, as expected, in warm environments the relative humidity has a great effect on the body's ability to dissipate an added thermal burden by evaporation. We cannot emphasize strongly enough that the SAR$_{60}$ is only an estimate of the upper limit of thermal tolerance for a healthy nude man. Many other factors must be considered, not the least of which is the great disparity in thermoregulatory response from individual to individual. Figure 5-9 shows the relative independence of the SAR$_{60}$ on the prevailing ambient temperature at any given ambient humidity level. Thus, at such moderate SARs, hyperthermic levels of body temperature can be expected only if the body is already operating at near-critical environmental conditions. Under such hostile conditions, even small increases in metabolic heat production, such as very light work, will also initiate an elevation in the body temperature. The basis for RF exposure guidelines currently in force (0.4 W/kg) is also indicated on the curves in Figure 5-9, under the assumption of a 60-min averaging time. (The 6-min averaging time specified in the current guidelines is far too short to achieve a thermal steady-state, such as that represented in Figure 5-9.) The reduction in ambient temperature required, at any relative humidity, to accommodate an SAR$_{60}$ of 0.4 W/kg is less than can be precisely achieved or measured, given present technology; therefore, no temperature or humidity factors should be used to adjust 0.4 W/kg RF exposures.

163

A healthy person exposed to the environments represented in the SAR curves would be expected to experience considerable thermal discomfort along with the rise in core temperature, rise in heart rate, and profuse sweating. All of these responses would increase over time until, at about 60 min, the person would be on the verge of collapse and exhibiting the unpleasant but reversible symptoms reported in experiments on human heat tolerance.

Because of the approximations used in the calculations described here and the great differences in thermoregulatory response found from person to person, we emphasize that the calculated data given in this chapter of the Handbook are intended to serve only as guidelines and to give a qualitative indication of anticipated responses.

5.10 References

Adair, E. R. (1985). Thermal physiology of RFR interactions in animals and humans. In J. C. Mitchell (Ed.), *Proceedings of a Workshop on Radiofrequency Radiation Bioeffects.* (USAF Report SAM-TR-85-14) (pp. 37-54). Brooks AFB, TX: USAF School of Aerospace medicine.

Adair, E. R., (1988). Microwave challenges to the thermoregulatory system. In M. E. O'Connor & R. F. Lovely (Eds.), *Electromagnetic Waves and neurobehavioral Function (*pp. 179-201*)*. New York, Alan R. Liss.

Adair, E. R., (1995). Thermal physiology of radiofrequency radiation (RFR) interactions in animals and humans. In B. J. Klauenberg, M. Grandolfo & D. N. Erwin (Eds.), *Radiofrequency Radiation Standards: Biological Effects, Dosimetry, Epidemiology, and Public Health Policy* (pp. 245-269). New York: Plenum Press.

Adair, E. R. (1996). Thermoregulation in the presence of microwave fields. In C. K. Polk & Postow, E. (Eds.), *CRC Handbook of Biological Effects of Electromagnetic Fields (Second Edition)* (pp. 403-434). Boca Raton: CRC Press.

Adair, R. K. (1999). A model of the detection of warmth and cold by cutaneous sensors through effects on voltage-gated membrane channels. *Proceedings of the National Academy of Sciences, 96*, 11825-11829.

Adair, E. R. & Adams, B. W. (1982). Adjustments in metabolic heat production by squirrel monkeys exposed to microwaves. *Journal of Applied Physiology: Respiration, Environment, and Exercise Physiology, 52*, 1049-1058.

Adair, E. R., Adams, B. W. & Hartman, S. K. (1992). Physiological interaction processes and radiofrequency energy absorption. *Bioelectromagnetics*, *13*, 497-512.

Adair, E. R., Adams, B. W., Kelleher, S. A. & Street, J. W. (1997). Thermoregulatory responses of febrile monkeys during microwave exposure. *Annals of the New York Academy of Sciences, 813*, 497-507.

Adair, E. R. & Berglund, L. G. (1986). On the thermoregulatory consequences of NMR imaging. *Magnetic Resonance Imaging, 4*, 321-333.

Adair, E. R. & Berglund, L. G. (1989). Thermoregulatory consequences of cardiovascular impairment during NMR imaging in warm/humid environments. *Magnetic Resonance Imaging, 7*, 25-37.

Adair, E. R. & Berglund, L. G. (1992). Predicted thermophysiological responses of humans to MRI fields. In R. L. Magin, R. P. Liburdy, & B. Persson (Eds.), *Biological Effects and Safety Aspects of Nuclear Magnetic Resonance Imaging and Spectroscopy*, *Annals of the New York Academy of Sciences*, *649*, 188-200.

Adair, E. R., Cobb, B. L., Mylacraine, K. S. & Kelleher, S. A. (1999b). Human exposure at two radio frequencies (450 and 2450 MHz): Similarities and differences in physiological response. *Bioelectromagnetics*, *20*, (Suppl. 4), 12-20.

Adair, E. R., Kelleher, S. A., Berglund, L. G. & Mack, G. W. (1999a). Physiological and perceptual responses of human volunteers during whole-body RF exposure at 450 MHz. In Bersani, F. (ed.), *Electricity and Magnetism in Biology and Medicine* (pp. 613-616). New York: Kluwer Academic/Plenum.

Adair, E. R., Kelleher, S. A., Mack, G. W. & Morocco, T. S. (1998). Thermophysiological responses of human volunteers during controlled whole-body radio frequency exposure at 450 MHz. *Biioelectromagnetics, 19,* 232-245.

Adair, E. R., Mylacraine, K. S. & Allen, S. J. (2003a). Thermophysiological consequences of whole-body resonant RF exposure (100 MHz) in human volunteers. *Bioelectromagnetics, 24*, 489-501.

Adair, E. R., Mylacraine, K. S. & Cobb, B. L. (2001a). Partial-body exposure of human volunteers to 2450 MHz pulsed or CW fields provokes similar thermoregulatory responses. *Bioelectromagnetics, 22*, 246-259.

Adair, E. R., Mylacraine, K. S. & Cobb, B. L. (2001b). Human exposure to RF energy at levels outside the C95.1 standard does not increase core temperature. *Bioelectromagnetics, 22*, 429-439.

Adair, E. R., Ziriax, J. M., Mylacraine, K. S. & Allen, S. J. (2003b). Characteristics of mammalian temperature sensitive neurons and their role in RF exposure. *Bioelectromagnetics Society Abstract Book*, Maui HI.

Adams, T. (1971). Carnivores. In G. C. Whittow (Ed.). *Comparative Physiology of Thermoregulation* (Vol. II, pp. 151-189). New York: Academic Press.

Adams, T., Morgan, M. L., Hunter, W. S., & Holmes, K. R. (1970). Temperature regulation of the unanesthetized cat during mild cold and severe heat stress. *Journal of Applied Physiology, 29*, 852-858.

Altman, P. L. & Dittmer, D. D. (1968). *Metabolism.* Bethesda, MD: Federation of American Societies for Experimental Biology.

American Society of Heating, Refrigerating and Air Conditioning Engineers (ASHRAE). (1986). Physiological principles and thermal comfort. In *ASHRAE Handbook, 1986 Fundamentals* (pp. 8.1-8.29). Atlanta, GA: ASHRAE.

Astrand, P.O. & Rodahl, K. (1970). *Textbook of work physiology*. New York: McGraw-Hill.

Belding, H. S. & Hatch, T. F. (1955). Index for evaluating heat stress in terms of resulting physiological strain. *Heating, Piping and Air Conditioning, 27*, 129-136.

Bell, C. R., Hellon, R. F., Hiorns, R. W., Nicol, P. B., & Provins, K. A. (1965). Safe exposure of men to severe heat. *Journal of Applied Physiology*, *20*(2), 288-292.

Bell, C. R. & Walters, J. D. (1969). Reactions of men working in hot and humid conditions. *Journal of Applied Physiology, 27*, 684-686.

Benedict, F. G. (1938). *Vital Energetics; A Study in Comparative Basal Metabolism.* Publication No. 503. Washington, DC: Carnegie Institution of Washington.

Berglund, L. G. (1983). Characterizing the thermal environment. In E. R. Adair (Ed.), *Microwaves and Thermoregulation* (pp. 15-31). New York: Academic Press.

Berman, E. (1984): Reproductive effects. In Elder, J.A. & D. Cahill (Eds.) *Biological Effects of Radiofrequency Radiation*. Report # EPA-600/8-83-026A, pp. 5.29-5.42.

Berry, J. J., Montgomery, L. D. & Williams, B. A. (1984). Thermoregulatory responses of rats to varying environmental temperatures. *Aviation, Space, and Environmental Medicine, 55*, 546-549.

Blick, D. W., Adair, E. R., Hurt, W. D., Sherry, C. J., Walters, T. J. & Merritt, J. H. (1997). Thresholds of microwave-evoked warmth sensation in human skin. *Bioelectromagnetics, 18*, 403-409.

Bligh, J. & Johnson, K. G. (1973). Glossary of terms for thermal physiology. *Journal of Applied Physiology, 35*, 941-961.

Bottomley, P. A., Redington, R. W., Edelstein, W. A. & Schenck, J. F. (1985). Estimating radiofrequency power dissipation in body NMR imaging. *Magnetic Resonance in Medicine, 2*, 336-349.

166

Bourne, G H. (1975). *The Rhesus Monkey.* New York: Academic Press.

Buettner, K. (1951). Effects of extreme heat and cold on human skin. II. Surface temperature, pain and heat conductivity in experiments with radiant heat. *Journal of Applied Physiology, 3*, 703-713.

Cabanac, M. (1983). Thermoregulatory behavioral responses. In E. R. Adair (Ed.), *Microwaves and Thermoregulation* (pp. 307-357). New York: Academic Press.

Candas, V., Adair, E. R. & Adams, B. W. (1985). Thermoregulatory adjustments in squirrel monkeys exposed to microwaves at high power densities. *Bioelectromagnetics, 6*, 221-234.

Chiang, H. & Shao, B. (1989). Biological responses to microwave radiation:Reproduction, development and immunology. In J. C. Lin (Ed.), *Electromagnetic Interaction with Biological Systems* (pp. 141-163). New York: Plenum Press.

Cook, H. F. (1952a). A physical investigation of heat production in human tissues when exposed to microwaves. *British Journal of Applied Physics, 3*, 1-6.

Cook, H. F. (1952b). The pain threshold for microwave and infra-red radiations. *Journal of Physiology, 118*, 1-11.

Craig, F. N., Garren, H. W., Frankel, H., & Blevins, W. V. (1954). Heat load and voluntary tolerance time. *Journal of Applied Physiology, 6*, 634-644.

Cunningham, D. J. (1970). An evaluation of heat transfer through the skin in extremity. In J. D. Hardy, A. P. Gagge, & J. A. J. Stolwijk (Eds.), *Physiological and behavioral Temperature Regulation* (pp. 302-315). Springfield, IL: Charles C. Thomas.

Dewey, W. C. (1994). Arrhenius relationships from the molecule and cell to the clinic. *International Journal of Hyperthermia, 10*, 457-483.

Dewhirst, M. W., Viglianti, B. L., Lora-Michiels, M., Hanson, M. & Hoopes, P. J. (2003). Basic principles of thermal dosimetry and thermal thresholds for tissue damage from hyperthermia. *International Journal of Hyperthermia, 19*(3), 267-294.

Donaldson, G. C., Keatinge, W. R., Saunders, R. D. (2003). Cardiovascular responses to heat stress and their adverse consequences in healthy and vulnerable human populations. *International Journal of Hyperthermia, 19*(3), 225-235.

Dreyfuss, H. (1967). *The Measure of Man: Human Factors in Design.* New York: Whitney Library of Design.

DuBois, D. & DuBois, E. F. (1916). A formula to approximate surface area, if height and weight are known. *Archives of Internal Medicine, 17*, 863-871.

Durney, C. H., Massoudi, H. & Iskander, M. F. (1986). *Radiofrequency Radiation Dosimetry Handbook, Fourth Edition* (Report No. USAFSAM-TR-85-73). Brooks AFB, TX: USAF School of Aerospace Medicine.

Eijkman, E. & Vendrik, A. J. H. (1961). Dynamic behavior of the warmth sense organ. *Journal of Experimental Psychology, 62*, 403-408.

Elder, J. A. & Cahill, D. F. (Eds.). (1984). *Biological Effects of Radiofrequency Radiation.* Research Triangle Park, NC: U.S. Environmental Protection Agency.

Elizondo, R. (1977). Temperature regulation in primates. *International Review of Physiology, 15*, 71-118.

Ellis, F. P. (1972). Mortality from heat illness and heat-aggravated illness in the United States. *Environmental Research,* 5, 1-58.

Emery, A. F., Short, R. E., Guy, A. W., Kraning, K. K. & Lin, J. C. (1976). The numerical thermal stimulation of the human body when undergoing exercise or nonionizing electromagnetic irradiation. *Journal of Heat Transfer, 98*, 284-291.

Fan, L. T., Hsu, F. T, & Hwang, C. L. (1971). A review on mathematical models of the human thermal system. *IEEE Transactions on Biomedical Engineering, 18*(3), 218-234.

Fang, B.R., Lu, Q., Zou, R.B. and Liu, Y.H. (1982): Application of microwave in male contraception. *Chinese Journal of Urology, 3*, 75. (in Chinese). Cited in Liu et al. (1991).

Gagge, A. P. (1937). A new physiological variable associated with sensible and insensible perspiration. *American Journal of Physiology, 120*, 277-287.

Gagge, A. P., Burton, A. C. & Bazett, H. C. (1941). A practical system of units for the description of the heat exchange of man with his environment. *Science, 94*, 428-430.

Gagge, A. P., Stolwijk, J. A. J. & Nishi, Y. (1969). The prediction of thermal comfort when thermal equilibrium is maintained by sweating. ASHRAE *Transactions,* 75 (II), 108-125.

Gasjek, P., Walters, T. J., Hurt, W. D., Ziriax, J. M., Nelson, D. A. & Mason, P. A. (2002). Empirical validation of SAR values predicted by FDTD modeling. *Bioelectromagnetics, 23*, 37-48.

Givoni, B. & Goldman, R. F. (1972). Predicting rectal temperature response to work, environment, and clothing. *Journal of Applied Physiology, 32*(6), 812-822.

168

Goldman, R. F. (1983). Acclimation to heat and suggestions, by inference, for microwave radiation. In E. R. Adair (Ed.), *Microwaves and Thermoregulation* (pp. 275-282). New York: Academic Press.

Goldman, R. F., Green, E. B., & Iampietro, P. F. (1965). Tolerance of hot, wet environments by resting man. *Journal of Applied Physiology, 20*(2), 271-277.

Gonzalez, R. R., Kluger, M. J., & Hardy, J. D. (1971). Partitional calorimetry of the New Zealand white rabbit at temperatures 5-35 degrees C. *Journal of Applied Physiology, 31*, 728-734.

Gordon, M. S. (1977). *Animal Physiology: Principles and Adaptations.* New York: Macmillan Company.

Greenleaf, J. E. (1973). Blood electrolytes and exercise in relation to temperature regulation in man. In E. Schoenbaum & P. Lomax (Eds.), *The Pharmacology of Thermoregulation* (pp. 72-84). Basel: Karger.

Guy, A. W., Johnson, C. C., Lin, J. C., Emery, A. F., & Kraning, K. K. (1973). *Electromagnetic power deposition in man exposed to high frequency fields and the associated thermal and physiologic consequences* (USAFSAM-TR-73-75). Brooks AFB, TX: USAF School of Aerospace Medicine.

Guyton, A. C., & Hall, J. E. (2000). *Textbook of Medical Physiology* (10th ed.). Philadelphia: WB Saunders.

Hardy, J. D. (1978). Regulation of body temperature in man – an overview. In J. A. J. Stolwijk (Ed.), *Energy Conservation Strategies in Buildings* (pp. 14-37). New Haven, CT: Yale University Printing Service.

Hardy, J. D. & DuBois, E. F. (1940). Differences between men and women in their response to heat and cold. *Proceedings of the National Academy of Sciences, 26*, 389-398.

Hardy, J. D. & Oppel, T. W. (1937). Studies in temperature sensation III. The sensitivity of the body to heat and the spatial summation of the warmth sense organ responses. *Journal of Clinical Investigation, 16*, 533-540.

Hart, J. S. (1971). Rodents. In G. C. Whittow (Ed.). *Comparative Physiology of Thermoregulation* (Vol. II, pp. 1-149). New York: Academic Press.

Heilbrunn, L. V. (1952). *An Outline of General Physiology.* Third edition. Philadelphia: Saunders, pp. 818.

Hendler, E. (1968). Cutaneous receptor response to microwave irradiation. In J. D. Hardy (Ed.), *Thermal Problems in Aerospace Medicine* (pp. 149-161). Surrey, Unwin, Ltd.

Hendler, E. & Hardy, J. D. (1960). Infrared and microwave effects on skin heating and temperature sensation. *IRE Transactions on Medical Electronics* ME, *7*, 143-152.

Hendler, E., Hardy, J. D. & Murgatroyd, D. (1963). Skin heating and temperature sensation produced by infrared and microwave radiation. In C. M. Hertzfield (Ed.), *Temperature: Its Measurement and Control in Science and Industry* (pp. 211-230). New York: Reinhold.

Johnson, G. S. & Elizondo, R. S. (1979). Thermoregulation in Macaca mulatto: A thermal balance study. *Journal of Applied Physiology: Respiratory, Environmental and Exercise Physiology, 46*, 268-277.

Justesen, D. R., Adair, E. R., Stevens, J. C. & Bruce-Wolfe, V. (1982). A comparative study of human sensory thresholds: 2450 MHz vs. far-infrared radiation. *Bioelectromagnetics, 3*, 117-125.

Kerslake, D. M. (1972). *The Stress of Hot Environments*. Oxford, England: Cambridge University Press.

Kido, D. K., Morriss, T. W., Erickson, J. L., Plewes, D. B. & Simon, J. H. (1987). Physiologic changes during high field strength MR imaging. *American Journal of Roentgenology*, *148*, 1215-1218.

Kleiber, M. (1961). *The Fire of Life*. New York: John Wiley and Sons.

Kritikos, H. N. & Schwan, H. P. (1975). The distribution of heating potential inside lossy spheres. *IEEE Transactions on Biomedical Engineering, 22*, 457-463.

Krupp, J. H. (1983). In vivo temperature measurements during the whole-body exposure of *Macaca mulatto* to resonant and non-resonant frequencies. In E. R. Adair (Ed.), *Microwaves and Thermoregulation* (pp. 95-107). New York: Academic Press.

Liu, Y-H., LI, X-M., Zou, R-P., & Li, F-B. (1991). Biopsies of human testes receiving multiple microwave irradiation: An histological and ultramicroscopical study. *Journal of Bioelectricity, 10*, 213-230.

Lotz, W. G. (1985). Hyperthermia in radiofrequency exposed rhesus monkeys: A comparison of frequency and orientation effects. *Radiation Research, 102*, 59-70.

Lotz, W. G. & Saxton, J. L. (1987). Metabolic and vasomotor responses of rhesus monkeys exposed to 225-MHz radiofrequency energy. *Bioelectromagnetics, 8,* 73-89.

Lotz, W. G. & Saxton, J. L. (1988). Thermoregulatory responses of the rhesus monkey during exposure at a frequency (225 MHz) near whole-body resonance. In M. E. O'Connor & R.

H. Lovely (Eds.), *Electromagnetic Fields and Neurobehavioral Function* (pp. 203-218). New York: Alan R. Liss.

Machle, W. & Hatch, T. F. (1947). Heat: Man's exchanges and physiological responses. *Physiological Reviews, 27*, 200-227.

Mahoney, S. A. (1980). Cost of locomotion and heat balance during rest and running from 0 to 55 degrees C in a patas monkey. *Journal of Applied Physiology, 49*, 789-800.

McCullough, E. A., Jones, B. W., & Tamura, T. (1989). A data base for determining the evaporative resistance of clothing. *ASHRAE Transactions*, *95*, 316-328.

Michaelson, S. M. (1972). Cutaneous perception of microwaves. *Journal of Microwave Power, 7*, 67-73.

Mitchell, J. C. (1985). Human exposures to radiofrequency radiation (RFR): A review of RFR accidents. In J. D. Mitchell (Ed.), *Proceedings of a Workshop on radiofrequency Radiation Bioeffects* (USAF Report No. USAFSAM-TR-85-3) (pp. 135-141). Brooks AFB, TX: USAF School of Aerospace Medicine.

Moritz A. & Henriques, F. (1947). Studies of thermal injury II. The relative importance of time and surface temperature in the causation of thermal burns. *American Journal of Pathology, 23*, 695-720.

Mountcastle, V. B. (1974). *Medical Physiology, Vol. II.* St. Louis: C.V. Mosby Co.

Mumford, W. W. (1969). Heat stress due to RF radiation. *Proceedings of the IEEE, 57*(2), 171-178.

Nadel, E. R. (1974). Mechanisms of thermal acclimation to exercise and heat. *Journal of Applied Physiology, 37*(4), 515-520.

Nadel, E. R., Bullard, R. W. & Stolwijk, J. A. J. (1971a). Importance of skin temperature in the regulation of sweating. *Journal of Applied Physiology*, *31*, 80-87.

Nadel, E. R., Mitchell, J. W., Saltin, B. & Stolwijk, J. A. J. (1971b). Peripheral modifications to the central drive for sweating. *Journal of Applied Physiology, 31*, 828-833.

Neilsen, B. & Nielsen, M. (1965). Influence of passive and active heating on the temperature regulation of man. *Acta Physiologica Scandinavica, 64*, 323-331.

Newburgh, L. H. (Ed.). (1949). *Physiology of Heat Regulation and the Science of Clothing*. London: W.B. Saunders, Ltd.

Pennycuik, P. R. (1967). A comparison of the effects of a variety of factors on the metabolic rate of the mouse. *Australian Journal of Experimental Biology and Medical Science, 45*, 331-346.

Provins, K. A., Hellon, R. F., Bell, C. R., & Horns, R. W. (1962). Tolerance of heat of subjects engaged in sedentary work. *Ergonomics, 5*, 93-97.

Reeves, G. I. (2000). Review of extensive workups of 34 patients overexposed to radiofrequency radiation. *Aviation, Space and Environmental Medicine, 71*(3), 206-215.

Riu, P. J., Foster, K. R., Blick, D. W. & Adair, E. R. (1997). A thermal model for human thresholds of microwave-evoked warmth sensations. *Bioelectromagnetics, 18*, 578-583.

Rosenblum, L. A. & Cooper R. W. (1968). *The Squirrel Monkey.* New York: Academic Press,

Ruch, T. C. & Patton, H. D. (1973). *Physiology and Biophysics, Vol. III.* Philadelphia: Saunders.

Sapareto, S. A. & Dewey, W. C. (1984). Thermal dose determination in cancer therapy. *International Journal of radiation Oncology and Biological Physics, 10*, 787-800.

Schaefer, D. J. (1988). Safety aspects of magnetic resonance imaging. In F. W. Wherli, D. Shaw, & J. B. Kneeland (Eds.), *Biomedical Magnetic Resonance Imaging: Principles, Methodology and Applications* (pp. 553-578). New York: VCH Publishers.

Schaefer, D. J. (1992). Dosimetry and effects of MR exposure to RF and switched magnetic fields. In R. L. Magin, R. P. Liburdy, & B. Persson (Eds.), *Biological Effects and Safety Aspects of Nuclear Magnetic resonance Imaging and Spectroscopy. Annals of the New York Academy of Sciences*, 649, 225-229.

Schwan, H. P., Anne, A. & Sher, I. (1966). *Heating of Living Tissue.* U.S. Naval Engineering Center, Philadelphia. Report NAEC-ACEL-534, Feb. 18.

Shellock, F. G. (1992). Thermal responses in human subjects exposed to magnetic resonance imaging. In R. L. Magin, R. P. Liburdy, & B. Persson (Eds.), *Biological Effects and Safety Aspects of Nuclear Magnetic Resonance Imaging and Spectroscopy. Annals of the New York Academy of Sciences*, 649, 260-272.

Shellock, F. G. & Crues, J. V. (1988a). Corneal temperature changes induced by high field-strength MR imaging with a head coil. *Radiology, 167*, 809-811.

Shellock, F. G. & Crues, J. V. (1988b). Temperature changes caused by MR imaging of the brain with a head coil. *American Journal of Nuclear Radiology, 9*, 287-291.

Shellock, F. G., Rothman, B. & Sarti, D. (1990). Heating of the scrotum by high-field strength MR imaging. *American Journal of Roentgenology, 154*, 1229-1232.

Shellock, F. G., Schaefer, D. J. & Crues, J. V. (1989a). Alterations in body and skin temperatures caused by magnetic resonance heating: Is the recommended exposure for radiofrequency radiation too conservative? *British Journal of Radiology, 62*, 904-909.

Shellock, F. G., Schaefer, D. J. & Crues, J. V. (1989b). Exposure to a 1.5 T static magnetic field does not alter body and skin temperatures in man. *Magnetic Resonance in Medicine, 11*, 371-375.

Shellock, F. G., Schaefer, D. J. & Kanal, E. (1994). Physiologic responses to an MR imaging procedure performed at a specific absorption rate of 6.0 W/kg. *Radiology, 192*, 865-868.

Shimada, S. G. & Stitt, J. T. (1983). Body temperature regulation during euthermia and hyperthermia. In E. R. Adair (Ed.), *Microwaves and Thermoregulation* (pp. 139-160). New York: Academic Press.

Song, C. W., Chelstrom, L. M. & Haumschild, D. J. (1990). Changes in human skin blood flow by hyperthermia. *International Journal of Radiation Oncology and Biological Physics, 18*, 903-907.

Spiegel, R. J., Deffenbaugh, D. M., & Mann, J. E. (1980). A thermal model of the human body exposed to an electromagnetic field. *Bioelectromagnetics, 1*(3), 253-270.

Stevens, J. C. (1983). Thermal sensation: Infrared and microwaves. In E. R. Adair (Ed.), *Microwaves and Thermoregulation* (pp. 191-201). New York: Academic Press.

Stitt, J. T. (1979). Fever versus hyperthermia. *Federation Proceedings, 38*, 39-43.

Stitt, J. T. & Hardy, J. D. (1971). Thermoregulation in the squirrel monkey (*Saimiri sciureus*). *Journal of Applied Physiology, 31*, 48-54.

Stitt, J. T., Hardy, J. D., & Stolwijk, J. A. (1974). PGE1 fever: Its effect on thermoregulation at different low ambient temperatures. *American Journal of Physiology, 227*, 622-629.

Stolwijk, J. A. J. (1980). Mathematical models of thermoregulation. *Annals of the New York Academy of Sciences, 335*, 998-106.

Stolwijk, J. A. J. (1983). Thermoregulatory response to microwave power deposition. In E. R. Adair (Ed.), *Microwaves and Thermoregulation* (pp. 279-305). New York: Academic Press.

Stolwijk, J. A. J. & Hardy, J. D. (1966). Temperature regulation in man – a theoretical study. *Pflugers Archive, 291*, 129-162.

Stolwijk, J. A. J. & Hardy, J. D. (1977). Control of body temperature. In D. H. K. Lee (Ed.), *Handbook of Physiology. Section 9. Reactions to Environmental Agents* (pp. 45-68). Bethesda, MD: American Physiological Society.

Vendrik, A. J. H. & Vos, J. J. (1958). Comparison of the stimulation of the warmth sense organ by microwave and infrared. *Journal of Applied Physiology, 13*, 435-444.

Way, W. L., Kritikos, H. & Schwan, H. P. (1981). Thermoregulatory physiologic responses in the human body exposed to microwave radiation. *Bioelectromagnetics*, 2, 341-356.

Wenger, C. B. (1983). Circulatory and sweating responses during exercise and heat stress. In E. R. Adair (Ed.), *Microwaves and Thermoregulation* (pp. 251-276). New York: Academic Press.

Whittow, G. C. (1971). Ungulates. In G. C. Whittow (Ed.). *Comparative Physiology of Thermoregulation* (Vol. II, pp. 191-281). New York: Academic Press.

Woodcock, A. H., Pratt, R. L., & Breckenridge, J. R. (1960). *Theory of the globe thermometer*. Research Study Report BP-7, Quartermaster R&E Command, U.S. Army Natick Laboratories, Natick, MA.

Wyndham, C. H., Strydom, N. B., Morrison, J. F., Williams, C. G., Bredell, G. A. G., Maritz, J. S., & Munro, A. (1965). Criteria for physiological limits for work in heat. *Journal of Applied Physiology, 20*(1), 37-45.

Radio Frequency Radiation Dosimetry Handbook
(Fifth Edition)

Chapter 6.   Thermal Modeling

David A. Nelson
Professor and Chairman
Department of Mechanical Engineering
University of South Alabama, Mobile, AL 36688

danelson@usouthal.edu

6.1   Introduction

The term ―thermal modeling" as used here refers to mathematical and numerical methods which can be employed to describe the relationship between tissue temperature and power density or specific absorption rate (SAR). There are two major applications of thermal modeling in radio frequency radiation (RFR) dosimetry:

- **Indirect Measurement of SAR.** A thermal model may be used to infer SAR from temperature measurements in an animal carcass or a phantom. Such models can be relatively simple, as it is not necessary to reflect thermal effects of blood flow, metabolism, thermoregulation, or other physiological factors.

- **Thermal Dosimetry.** Thermal modeling can be useful in the assessment or prediction of thermal effects in live animals or humans subjected to a known SAR. Such applications may demand more sophisticated models than are needed for indirect SAR measurement. This is especially true in cases where the energy absorption is highly localized, or when evaluating thermal effects of low-power exposures. Those situations may demand models which can provide temperature results with a high degree of spatial resolution, or reflect subtle changes in thermophysiological state.

This chapter discusses some principles of thermodynamics and heat transfer which are relevant to modeling RF heating in tissues and animals. A numerical approach is described which can be applied to predicting tissue temperatures in animals and human subjects.

6.2   Energy Balance

The First Law of Thermodynamics states the rate at which the energy E of a system changes is the sum of the rates of work ($\dot{W}$) and heat transfer ($\dot{Q}$),

$$\frac{dE}{dt} = \sum \dot{Q}_i + \sum \dot{W}_j. \qquad (1)$$

Note the summations, as there may be multiple, simultaneous heat transfer and work terms for a given system.

For solids and liquids which do not experience a significant change in volume, the change in energy of a stationary system is proportional to the change in the average temperature, $\bar{T}$:

$$dE = mC \cdot d\bar{T} \qquad (2)$$

where m is the mass of the system, C is the specific heat of the material (units of energy per temperature, per mass; e.g., $kJ \cdot °C^{-1} \cdot kg^{-1}$). Equation (1) then can be written as follows:

$$mC\frac{d\bar{T}}{dt} = \sum \dot{Q}_i + \sum \dot{W}_j. \qquad (3)$$

The heat transfer and work rates represent the various energy transfers in and out of the system. These include surface heat loss/gain, in addition to energy sources/sinks within the system. As illustrated in Figure 6-1, those terms may include any or all of the following:

- metabolism
- muscle contraction/extension
- absorption of electromagnetic energy
- heat conduction through tissue
- heat convection (also known as "advection") associated with fluid flow through tissues (blood, lymph)
- convection heat transfer (surface)
- radiation heat transfer (surface)
- evaporation (surface)

The first three terms (metabolism, muscle contraction/extension, absorption of electromagnetic (EM) energy) are often referred to as energy "sources" in the tissue. Thermodynamically, these are considered *work* terms in the energy balance equation (Equation 3). That distinction is of little practical importance however. The sum of all the work (or source) and heat transfer terms is simply the net energy gained (or lost) by the system.

176
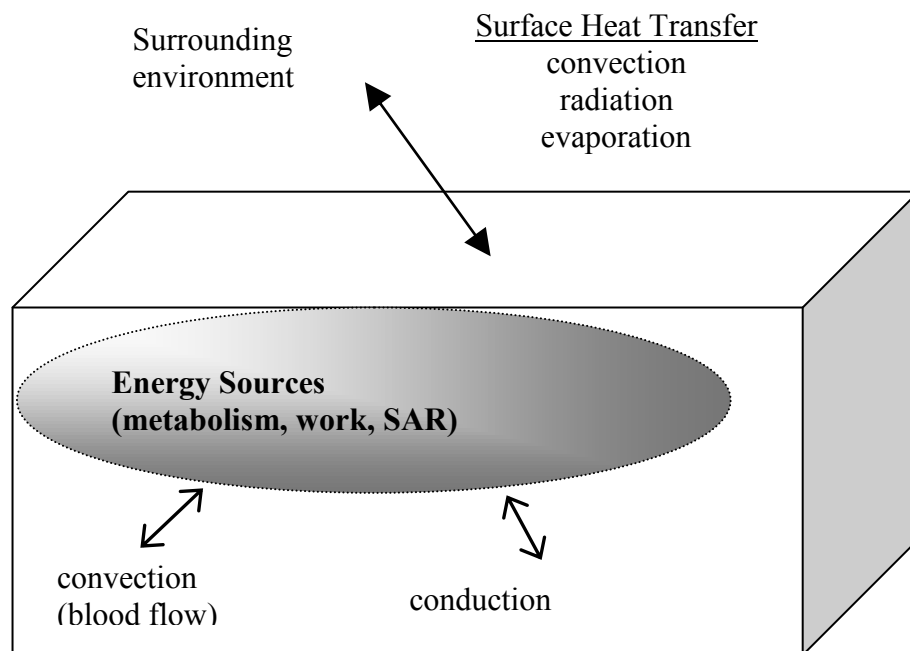
Figure 6-1. **An arbitrary volume of tissue may have energy sources which include mechanical work, metabolism, and electromagnetic work (SAR). Heat transfer within the tissue space primarily is through blood flow (convection) and conduction. Heat transfer between tissue and the surroundings occurs via convection (air movement), evaporation and radiation.**

6.2.1 Lumped Thermal Models

The termed ―lumped model" (also called ―lumped capacitance analysis") refers to an analytical approach in which local, spatial variations in temperature are neglected. This greatly simplifies the analysis, as it eliminates the need to calculate or measure temperatures throughout the tissue volume. A time-varying spatially-averaged temperature $\bar{T}(t)$ describes the temperature throughout the sample.

In RF dosimetry, lumped models commonly are employed to estimate the SAR from temperature measurements over time in dead animals, phantoms and tissue-equivalent materials. The use of a lumped model is justified when the volume of tissue (or tissue-equivalent material) is small, and when the SAR is high relative to the rate of heat loss from the surface.

In situations in which the SAR is quite high, the heat transfer and work terms (excluding the SAR) may be negligible. In those cases the rate of energy storage is approximately equal to the SAR. For a homogeneous sample, the rate of average temperature increase therefore is a linear function of the average SAR:

$$\frac{d\bar{T}}{dt} = \frac{SAR}{C}. \tag{4}$$

This provides a convenient method for estimating the average SAR by measuring the rate of temperature increase. Consider a tissue in which $C = 3.5 \times 10^3$ J·kg^{-1}·°C^{-1} (skeletal muscle, e.g. see Table 6-1). A temperature increase of 1.0 °C per min. (1.67×10^{-2} °C·s^{-1}) implies an SAR of $\left(3.5 \times 10^3 \text{ J·kg}^{-1}\cdot\text{°C}^{-1}\right) \times \left(1.67 \times 10^{-2} \text{ °C·s}^{-1}\right) = 58$ W·kg^{-1}.

Note the rate of temperature increase – for a given SAR – is inversely proportional to the specific heat of the tissue or material. The temperature of fat, for instance ($C = 2.3 \times 10^3$ J·kg^{-1}·°C) increases at a rate which is 1.5 times that of muscle for a given SAR value. Thus a temperature increase of 1.0 °C per min. in fat indicates an SAR of 38 W·kg^{-1}.

The relationship described by Equation 4 is valid only for relatively high, short-duration exposures in which there is little heat exchange with surrounding tissues or the environment, and in which metabolism and blood flow are not thermally significant. The average temperature of the sample will increase continuously – although at a decreasing rate – until a steady-state temperature is reached.

In exposures of dead animals, a steady-state temperature will be reached when the rate of heat transfer to the surroundings equals mass $m \times SAR$. This may not be until the temperature has reached several degrees above the ambient temperature. The SAR often can be determined – with reasonable accuracy – through measurement of the rate of temperature increase during exposure of a dead animal.

While dead animals commonly are used for RF dosimetry, investigation of potential thermal effects of RF may require determining temperatures in live animal or human subjects. In those cases the rate of temperature increase in a tissue or organ reflects the thermal effects of blood flow and metabolism, as well as heat transfer to the surrounding tissue or environment. In homeotherms, thermoregulation (either autonomic or behavioral) also may alter the temperature response to RF heating very significantly.

For in vivo experiments, the steady-state temperature is a function of blood flow to the tissue and the rate of heat transfer to surrounding tissues or the environment. Metabolism is rarely a major factor in the tissue temperature response to RF exposure, even for tissues and organs which have high metabolic rates (e.g., liver, brain). Liver, for instance has a metabolic rate of approximately 20 W·kg^{-1} (Table 6-1). Note however that organs with high metabolic rates generally have high rates of blood flow (oxygen demand is proportional to metabolic rate), which serves to maintain a normothermic temperature in the tissue. Thus, the rate of temperature increase still may be approximately linear with SAR, at least for short-term exposures, even in tissues and organs with high metabolic rates.

178

Blood flow can affect significantly the tissue temperature response to RF exposure, however. Unlike metabolism, the thermal effect of blood flow is a strong function of tissue temperature. (The metabolic rate is a weak function of temperature.) The rate of tissue – blood heat exchange is proportional to the temperature difference between the arterial blood and the tissue. As the tissue temperature increases therefore, so does the rate of heat removal by the blood. In tissues with high rates of blood perfusion (liver, brain), the *initial* rate of temperature increase still may be approximately proportional to the SAR. The temperature increase is effectively ―clamped;‖ however, it will approach a steady-state, or equilibrium tissue temperature at which the SAR equals the rate of heat transfer to the blood. Neglecting metabolism and heat transfer to the surroundings, the equilibrium temperature T_{eq} can be estimated according to Equation 5:

$$(T_{eq} - T_a) = \frac{\rho_t \cdot SAR}{\dot{m}_b C_b}$$
(5)

where T_a is the (deep arterial) blood temperature, ρ_t is the mass density of the tissue, $\dot{m}_b$ is the mass flow-rate of blood per unit tissue volume, and C_b is the specific heat of blood $(3.6 \times 10^3 \ \mathrm{J \cdot kg^{-1} \cdot {}^\circ C^{-1}})$. Typical values for the blood flow rate and mass density are provided in Table 6-1 for a variety of tissues.

Again using liver as an example, the initial rate of temperature increase for $\mathrm{SAR} = 10 \ \mathrm{W \cdot kg^{-1}}$, as predicted by Equation 4 is $2.8 \times 10^{-3} \ {}^\circ\mathrm{C \cdot s^{-1}}$ $\left[\left(10 \ \mathrm{W \cdot kg^{-1}}\right) / \left(3600 \ \mathrm{J \cdot kg^{-1} \cdot {}^\circ C^{-1}}\right) \right]$, or $0.17 \ {}^\circ\mathrm{C \cdot min^{-1}}$. The temperature will increase at that rate initially, but will asymptotically approach a steady-state temperature approximately 1.4 °C above the arterial temperature ($T_{eq} - T_a = 1.4 \ {}^\circ\mathrm{C}$), according to Equation 5.

This tissue heating analysis is appropriate for high-power, short duration exposures of homogeneous tissue. As it neglects heat transfer to surrounding tissues and to the environment, a temperature increase calculated according to Equation 5 can be considered an upper limit for most exposure scenarios.

Table 6-1. Estimated thermal properties of various human tissues and fluids.

Tissue	Mass density kg·m⁻³	Spec. Heat J·kg⁻¹·°C⁻¹	Thermal Cond. W·m⁻¹·°C⁻¹	Blood flow L·s⁻¹·m⁻³	Metabolism W·kg⁻¹
Bile(approx props)	1.01E+03	3.99E+03	5.76E-01	N/A	0.00E+00
Bladder	1.04E+03	3.31E+03	4.26E-01	1.46E+00	6.70E-01
Blood (whole)	1.06E+03	3.60E+03	4.88E-01	N/A	0.00E+00
Blood vessel(a)	1.00E+03	4.00E+03	5.00E-01	6.67E-01	0.00E+00
Body fluid(a)	1.00E+03	4.00E+03	5.00E-01	0.00E+00	0.00E+00
Bone(cancellous)	1.99E+03	1.59E+03	3.00E-01	0.00E+00	0.00E+00
Bone(cortical)	1.99E+03	1.59E+03	3.00E-01	0.00E+00	3.07E-01
Bone(marrow)	1.00E+03	1.59E+03	3.00E-01	0.00E+00	7.00E-01
Cartilage	1.10E+03	2.30E+03	2.20E-01	0.00E+00	1.41E+00
Cerebellum	1.04E+03	3.50E+03	4.90E-01	9.76E+00	1.08E+01
Cerebral spinal fluid	1.01E+03	4.20E+03	6.20E-01	0.00E+00	0.00E+00
Eye (aqueous humor)	1.00E+03	4.00E+03	5.78E-01	0.00E+00	0.00E+00
Eye (retina)	1.04E+03	3.68E+03	5.65E-01	9.14E+00	6.60E+00
Eye (sclera)	1.01E+03	3.90E+03	5.00E-01	0.00E+00	0.00E+00
Eye(cornea)	1.08E+03	4.18E+03	5.80E-01	0.00E+00	0.00E+00
Eye(lens)	1.08E+03	3.90E+03	5.00E-01	0.00E+00	0.00E+00
Fat	9.16E+02	2.30E+03	2.04E-01	3.60E-03	3.28E-01
Gall bladder	1.03E+03	3.50E+03	4.70E-01	2.37E+00	1.55E+00
Glands	1.05E+03	3.60E+03	5.30E-01	9.45E+00	0.00E+00
Gray matter	1.04E+03	3.68E+03	4.90E-01	9.75E+00	1.08E+01
Heart	1.06E+03	3.72E+03	5.87E-01	7.84E+00	9.10E+00
Hypothalamus	1.04E+03	3.68E+03	4.90E-01	9.75E+00	1.08E+01
Intestine (large)	1.04E+03	3.64E+03	5.43E-01	4.48E+00	4.50E-01
Intestine (small)	1.04E+03	3.70E+03	5.60E-01	4.50E+00	4.50E-01
Kidney	1.05E+03	3.89E+03	5.39E-01	1.95E+01	4.10E+00
Ligaments	1.22E+03	3.04E+03	5.34E-01	0.00E+00	0.00E+00
Liver	1.05E+03	3.60E+03	4.97E-01	1.95E+01	2.02E+01
Lung (inner)	5.50E+02	3.72E+03	5.18E-01	3.01E+01	1.60E+00
Lymph	1.03E+03	3.97E+03	5.92E-01	0.00E+00	0.00E+00
Mucous membrane	1.04E+03	3.97E+03	5.16E-01	0.00E+00	0.00E+00
Muscle	1.04E+03	3.50E+03	4.20E-01	5.16E-01	6.30E-01
Nails	1.30E+03	1.89E+03	9.90E-02	0.00E+00	0.00E+00
Nerve (spine)	1.04E+03	3.50E+03	6.00E-01	3.43E+00	1.08E+01
Pancreas	1.05E+03	3.50E+03	3.45E-01	1.05E+01	4.10E+00
Rectum	1.04E+03	3.64E+03	5.43E-01	4.48E+00	4.50E-01
Skin/abdomen	1.00E+03	3.72E+03	4.70E-01	1.44E+00	3.39E-01
Skin/arms	1.00E+03	3.72E+03	4.70E-01	1.40E+00	3.39E-01
Skin/face	1.00E+03	3.72E+03	4.70E-01	1.17E+01	3.39E-01

180

Tissue	Mass density kg·m^{-3}	Spec. Heat J·kg^{-1}·°C^{-1}	Thermal Cond. W·m^{-1}·°C^{-1}	Blood flow L·s^{-1}·m^{-3}	Metabolism W·kg^{-1}
Skin/feet	1.00E+03	3.72E+03	4.70E-01	2.05E+00	3.39E-01
Skin/hands	1.00E+03	3.72E+03	4.70E-01	3.35E+00	3.39E-01
Skin/head	1.00E+03	3.72E+03	4.70E-01	7.15E+00	3.39E-01
Skin/legs	1.00E+03	3.72E+03	4.70E-01	1.19E+00	3.39E-01
Skin/neck	1.00E+03	3.72E+03	4.70E-01	2.91E+00	3.39E-01
Skin/shoulders	1.00E+03	3.72E+03	4.70E-01	1.01E+00	3.39E-01
Skin/thorax	1.00E+03	3.72E+03	4.70E-01	1.08E+00	3.39E-01
Spleen	1.05E+03	3.72E+03	5.45E-01	1.58E+01	4.10E+00
Stomach	1.05E+03	3.60E+03	5.30E-01	4.53E+00	4.10E+00
Testicles	1.04E+03	3.80E+03	5.30E-01	1.46E+00	2.30E-01
Tooth	2.17E+03	1.17E+03	4.50E-01	0.00E+00	7.00E-01
White matter	1.04E+03	3.60E+03	4.90E-01	9.79E+00	1.08E+01

6.3   Multi-Dimensional Analysis

Often, analysis of the thermal effect of RF exposure requires determination of the spatial distribution of the temperature, as well as the temperature change over time. For example, if the SAR is spatially non-uniform, it may be important to determine the temperature increase in regions of high SAR. Alternatively, there may be tissues or organs that are particularly susceptible to thermal effects or damage. In such cases, a lumped analysis approach will not provide the appropriate information. While a lumped model can be used to estimate SAR in a tissue sample or a small animal carcass, its applicability is limited. It is not very useful in modeling thermal effects in living animals, or in cases where the SAR is highly non-uniform.

If the objective is the prediction or evaluation of thermal effects from low to moderate SAR (local or whole-body) in a live animal or human, the analysis can be complicated by heat transfer effects (both internal and surface), metabolism, muscle work, blood flow, and tissue heterogeneity. In homeotherms, it may also demand consideration of thermoregulatory feedback and mechanisms. This requires a more detailed thermal model which combines some fundamental principles of heat transfer and physiology.

6.3.1   Bio-Heat Transfer Fundamentals

Within a tissue volume, energy is transported by (i) heat conduction through tissue, and (ii) movement of blood and other fluids (convection[1]).

---

[1] The term "advection" is sometimes used to refer to transport by bulk fluid motion, as with blood flow.

6.3.1.1 Conduction

Heat conduction is described by Fourier's Law of Conduction, which states the rate of conduction heat transfer per unit area is proportional to, and in the opposite direction of, the temperature gradient:

$$\vec{q}''_{cond} = -k\vec{\nabla}T \tag{6}$$

where k represents the thermal conductivity of the tissue and $\vec{\nabla}T$ is the temperature gradient vector. (See Appendix for the definition of the temperature gradient and the del operator $\vec{\nabla}$). The double-prime (e.g. $-\vec{q}''$ ") denotes a rate of heat transfer per unit area ($W \cdot m^{-2}$, for instance). Thermal conductivity has units of energy per unit time, and per unit length and temperature ($W \cdot m^{-1} \cdot °C^{-1}$). Thermal conductivity values for most biological tissues are in the range of 0.1 to 1.0 $W \cdot m^{-1} \cdot °C^{-1}$. Nominal values of thermal conductivity for various human tissues are provided in Table 6-1.

Note the temperature dimension in the thermal conductivity represents a temperature difference (or gradient); hence the thermal conductivity can be expressed in terms of absolute temperature (kelvins (K)) or °C without conversion. In other words, 1 $W \cdot m^{-1} \cdot °C^{-1}$ = 1 $W \cdot m^{-1} \cdot K^{-1}$.

Equation 6 assumes the material is isotropic; i.e., it conducts heat as easily in one direction as in another. Some tissues are anisotropic; skeletal muscle, for instance, has a distinct fiber orientation and might be expected to exhibit some degree of thermal anisotropy. Measurements in meat samples (Hill et al., 1967) indicate thermal conductivities of bovine and porcine skeletal muscle vary slightly, depending on whether the measurement is made parallel to, or normal to the direction of fiber orientation. The difference is less than 10% however, and probably is not significant, given other inherent uncertainties in applying ex vivo measurements to in vivo problems. In most other tissues the degree of anisotropy is so small that it can be extremely difficult to measure (Bowman et al., 1975) and will not affect calculations significantly.

If a tissue can be treated as an isotropic medium with no metabolism and no blood flow, the temperature distribution over space and time can be described as follows:

$$\vec{\nabla}\cdot\left(k\vec{\nabla}T\right) = \rho C \frac{\partial T}{\partial t}. \tag{7}$$

If the tissue is homogeneous, and the thermal conductivity does not vary with temperature, then Equation 7 can be written

$$\nabla^2 T(\vec{x},t) = \frac{1}{\alpha} \frac{\partial T(\vec{x},t)}{\partial t} \tag{8}$$

where thermal diffusivity, $\alpha = \dfrac{k}{\rho C}$ has units of $L \cdot t^{-2}$ (e.g., $\text{m} \cdot \text{s}^{2}$) and describes the dynamic temperature response to a change in thermal environment. Note the temperature $T(\vec{x}, t)$ is written explicitly as a function of spatial location and time.

In general, the thermal conductivity and other properties are temperature-dependent. Fortunately, most bioheat transfer problems involve relatively small temperature differences ($<10\,°\text{C}$) such that the temperature dependencies of thermal properties do not affect calculations significantly.

6.3.1.2 Blood Flow (Convection)

One difficulty in developing thermal models of tissue is that of describing the role of blood flow in determining tissue temperature. This is because a physiologically accurate description would require knowing the temperature of the blood at every point in the vascular system, as well as complete, detailed knowledge of the vascular anatomy. Since arterial blood is exchanging heat with the surrounding tissues (including venous blood) throughout the system, the arterial blood temperature varies throughout the circulatory system. This implies it would be necessary to know the path taken by each differential volume of blood in the circulatory system, and determine its temperature history in order to fully describe how the blood heats or cools a volume of tissue. For most situations and applications, that approach is not practical.

An alternative approach is to treat the blood as local heat source (or sink), in which the heat transfer to (from) the tissue is proportional to the rate of blood flow to the tissue and the temperature difference between the blood and the tissue. This is the basis for the Bio-Heat Transfer Equation (BHTE), first proposed by Pennes (1948):

$$\nabla^2 T(\vec{x},t) + \rho \cdot \frac{q_m}{k} + \frac{\rho_{bl} C_{bl}}{k} \cdot \omega \cdot \left[T_a - T(\vec{x},t) \right] = \frac{1}{\alpha} \frac{\partial T(\vec{x},t)}{\partial t} \tag{9}$$

where ω is the blood flow per unit tissue volume and $T_a - T(\vec{x},t)$ represents the temperature difference between arterial blood and the tissue. In Equation 9, q_m is the local metabolic rate per unit mass, k is the thermal conductivity, ρ and ρ_{bl} are the mass densities of the local tissue and blood respectively, C_{bl} is the specific heat of blood, and ω is the rate of blood flow per unit volume of tissue.

The arterial blood temperature T_a in the BHTE is "deep arterial" temperature, or the mixed blood pool temperature. As the deep arterial temperature cannot be measured directly, the esophogeal temperature is considered a good estimate in humans. The colonic temperature may be used as a surrogate of deep arterial temperature in laboratory animals.

A premise of the BHTE is that heat transfer between the blood and the tissues is confined to the capillary bed. That justifies treating the blood as a local, volumetric source/sink which is at the deep arterial temperature and is proportional to the local blood perfusion rate.

In reality, most of the heat transfer between a volume of blood and the body occurs before the blood reaches the capillary bed. While the blood temperature changes only slightly in the larger vessels (diameter approximately 0.6 mm and larger), it approaches thermal equilibrium with surrounding tissues by the time the blood reaches the arterioles (diameter approximately 0.02 mm) (Chen, 1985). This suggests there is very little heat exchange between capillary blood and the surrounding tissues, and contradicts a premise of the Pennes BHTE. The Pennes model is still useful as a model for blood-tissue heat exchange, however. It simply means the user must be mindful of the inherent limitations of the Pennes BHTE, especially when attempting to apply it in situations involving very small spatial scales, or where there may be significant counter-current heat exchange between arterio-venous paired vessels (Wissler, 1998).

Note that Equation 9 does not include any electromagnetic work term. If the SAR work term is added to the BHTE, the tissue energy balance becomes

$$\nabla^2 T(\vec{x},t) + \rho \cdot \frac{q_m}{k} + \frac{\rho_{bl} C_{bl}}{k} \cdot \omega \cdot \left[T_a - T(\vec{x},t) \right] + \rho \cdot \frac{SAR}{k} = \frac{1}{\alpha} \frac{\partial T(\vec{x},t)}{\partial t}. \quad (10)$$

Equation 10 is the governing equation used to describe tissue temperature during RFR exposures. When applying Equation 10 in skeletal muscle or myocardium, however, it may be necessary to add a term to represent the energy input due to the work of contraction/extension.

6.3.2 Surface Heat Transfer

The BHTE (Equation 10) describes the energy balance within the tissue space. Determining the tissue temperature, however, also requires knowledge of the heat loss/gain occurring at the surface. The principal mechanisms of surface heat transfer are convection, thermal radiation, and evaporation.

6.3.2.1 Convection

The rate of convective heat transfer from the skin (or clothing) surface to the air is described by a simple linear equation (Newton's Law of Cooling):

$$q''_{conv} = h_c (T_s - T_{air}) \quad (11)$$

where q''_{conv} is the heat transfer rate per unit surface area and h_c is an empirically-determined convection coefficient, sometimes called the *film coefficient*.

The fundamental task in modeling convection heat transfer is estimating the value of the film coefficient h_c. The film coefficient may reflect contributions both from forced convection

184

and free convection (the latter is also known as —natural convection"). Free or natural convection refers to fluid movement which is driven by temperature differences. Very simply, warm air rises, since it less dense than cold air. Forced convection is simply convection that is not free.

The local convection coefficient h_c, reflecting mixed convection conditions (combination of forced and natural convection), can be calculated for the human body from the following equation:

$$h_c = \left[a_{nat} \left(T_s - T_{air} \right)^{0.5} + a_{frc} v + a_{mix} \right]^{0.5}$$
(12)

where T_s and T_{air} are the surface and air temperatures and v is the ambient air velocity. The values of the coefficients a_{nat}, a_{frc} and a_{mix} are empirically-determined and will vary by body region. Appropriate values for the coefficients may be found in Fiala et al. (1999).

6.3.2.2 Thermal Radiation

Radiation heat transfer is the transfer of energy between surfaces via the emission and absorption of electromagnetic energy. Although this definition would seem to include RFR heating, thermal radiation refers to emission and absorption at wavelengths approximately in the range $0.1\,\mu\text{m}$ - $100\,\mu\text{m}$, which includes the ultraviolet, visible, and infrared portions of the spectrum (Mills, 1992). The rate of thermal radiation heat transfer to or from a surface is simply the net of the rates of energy absorption and emission. The rate of energy emission by a surface is a function of the surface temperature. At the short wavelengths relevant to thermal radiation, there is effectively no energy penetration and absorption is modeled purely as a surface phenomenon.

Modeling radiation heat transfer between surfaces can be an extremely challenging task, especially in situations where there are several surfaces at different temperatures and/or complicated geometries. The analysis can be simplified in some situations in which there is no significant radiation exchange between body parts (such as might occur, e.g., between medial surfaces of the legs) and if the surroundings are at a single temperature. In such cases the radiation heat transfer rate q_{rad} from the skin surface to the surroundings, per unit skin surface area, can be described by the following equation, which is derived from the Stefan-Boltzmann Law:

$$q''_{rad} = \varepsilon \cdot \sigma (T_s^4 - T_{surr}^4)$$
(13)

where σ is the Stefan-Boltzmann constant ($\sigma = 5.6697 \times 10^{-8}\ \text{W} \cdot \text{m}^{-2} \cdot \text{K}^{-4}$) and ε is the surface emissivity – a dimensionless property which has values in the range $0 - 1$. Note the surface and surroundings temperatures T_s and T_{surr} are expressed in *kelvins* (units of absolute temperature).

The surface emissivity of human skin is approximately 0.95 for both men and women (Togawa, 1989) and is independent of pigmentation (Mitchell et al., 1967). Assuming a value of 1.0 is generally appropriate (Yang, 1989).

Note in Equation 13 that the rate of radiation heat transfer is a function of the fourth power of surface temperature and the temperature surroundings. Such nonlinearities can cause very significant problems when attempting to calculate skin temperatures in a bio-heat transfer model. It is helpful to linearize the model where possible, such that the heat transfer rate is a function of the first power of temperature (or temperature difference). In situations where the temperatures T_s and T_{surr} are "close" (which is true for most situations of interest here), an approximate linear equation can be derived from Equation 13 by factoring the fourth-order temperature difference. This allows radiation heat transfer to be described – at least approximately – by a simple linear equation:

$$q''_{rad} \approx h_r (T_s - T_{surr}) \tag{14}$$

where the radiation heat transfer coefficient $h_r = \varepsilon \sigma \left(T_{sk} + T_{surr} \right) \left(T_{sk}^2 + T_{surr}^2 \right)$. Again, note temperatures are expressed in *kelvins* (K). For a skin surface temperature of 33 °C (306 K) and surroundings at 20 °C for example, and assuming an emissivity value of unity, this yields a radiation heat transfer coefficient $h_r = 6.1 \ \text{W} \cdot \text{m}^{-2} \cdot {}^{\circ}\text{C}^{-1}$ and a radiation heat loss rate of $79 \ \text{W} \cdot \text{m}^{-2}$. This likely is a slightly higher rate of heat loss than would obtain under these conditions; typical radiation heat transfer coefficients are in the range $3.8 - 5.1 \ \text{W} \cdot \text{m}^{-2} \cdot {}^{\circ}\text{C}^{-1}$ for environmental temperatures $0 \ {}^{\circ}\text{C} < T_{surr} < 50 \ {}^{\circ}\text{C}$ (Datta, 2002). Shitzer and Eberhart (1985) suggest a radiation coefficient calculated according to

$$h_r = 3.5 \cdot \left[1 + 0.0055 \left(\bar{T}_s + T_{surr} \right) \right]. \tag{15}$$

The net radiation heat transfer for the body generally will be less than that calculated from integrating the rate per unit area (obtained from Equation 14) over the body surface, as some regions are "shaded" and will not radiate to the surroundings. For instance, the medial surfaces of the arms and legs do not view the surroundings fully; hence they will have very limited radiation heat transfer rates. The effective whole-body radiation area can be estimated using a correction factor f_r, such that the total, net radiation heat transfer rate q_{rad} between the subject and the surroundings can be estimated according to Equation 16:

$$q_r \approx h_r A_s f_r (\bar{T}_{sk} - T_{surr}) \tag{16}$$

where A_s is the total surface area. For humans (male or female), the estimated correction factor is $f_r = 0.696$ for a seated subject and $f_r = 0.725$ for standing (Fanger, 1970). The body surface area A_s is the DuBois area,

$$A_s = 0.202 \cdot M^{0.425} H^{0.725} \tag{17}$$

where M is the subject's body mass (kg), and H is the standing height (m). Equation 17 thus provides an estimate of body surface area of an adult human, in m^2.

6.3.2.3 Evaporation

Evaporative heat transfer is often referred to as *latent* heat loss, to distinguish it from the *sensible* heat transfer associated with a change in temperature. In humans and – to a lesser extent – some non-human primates, evaporation of sweat can produce very high rates of surface heat loss.

The rate of heat loss is proportional to the rate of moisture evaporation from a surface, $q_{evap} = \dot{m}_{evap} \lambda_{fg}$ where $\dot{m}_{evap}$ is the mass rate of evaporation and λ_{fg} is the heat of vaporization ($\lambda_{fg} = 2.430 \times 10^3$ J$\cdot$g^{-1} at 30 °C). The mass rate of evaporation is a function of the amount of moisture on the skin surface and on the ambient humidity (vapor pressure). The rate can be affected by sweat secretion, transpiration through skin, the permeability or wicking of clothing, and environmental conditions.

Surface evaporative heat loss from the skin E_s is proportional to the difference between the saturation pressure $P_{sat,sk}$ at the skin surface temperature, and the ambient vapor pressure $P_{v,amb}$:

$$E_s = w \cdot U_{e,cl}^* \left(P_{sat,sk} - P_{v,amb} \right) \tag{18}$$

where w is a dimensionless skin wettedness factor, ranging from $w = 0.06$ (no sweating; transpiration only) to $w = 1.0$ (skin is fully wetted). The quantity $U_{e,cl}^*$ is a conductance term which represents the moisture permeability of clothing. The skin wettedness reflects the rate of sweat secretion per unit surface area $\dot{m}_{sw}$, relative to the rate of evaporation from the skin surface:

$$w = 0.06 + 0.94 \cdot \left(\dot{m}_{sw} \lambda_{fg} \right) \cdot \left[U_{e,cl}^* \left(P_{sat.sk} - P_{v,amb} \right) \right]^{-1}. \tag{19}$$

In the absence of active sweat secretion ($\dot{m}_{sw} = 0$), moisture is still lost from the skin surface via transpiration. Additional latent heat transfer occurs from the respiratory tract, as described in Section 6.3.2.5.

6.3.2.4 Clothing Insulation

The insulating value of a garment or clothing ensemble is described in terms of a whole-body thermal resistance per unit surface area R_{cl} (units K$\cdot$m$^2\cdot$W^{-1}). Sometimes the insulation (*I*)

187

value is expressed in *clo* units ($1 \text{ clo} = 0.155 \text{ K} \cdot \text{m}^2 \cdot \text{W}^{-1}$), where 1 clo is the nominal insulation value of a typical business suit. A pair of shorts has an insulation value of 0.1 clo, while a polar weather suit may have a value as high as 4 clo (Fanger, 1970).

For a subject with surface area A_s, the rate of sensible heat transfer q_T is proportional to the difference between area-weighted mean skin temperature $\bar{T}_s$ and the ambient operative temperature T_0:

$$q_T = \frac{\left(\bar{T}_s - T_0\right) A_s}{R_{cl} + \dfrac{R_a}{f_{cl}}}. \tag{20}$$

The quantities R_{cl} and R_a represent the whole-body thermal resistance of the garment and of the air layer surrounding the manikin, respectively. The area factor $f_{cl,j}$ describes the relative increase in surface of the garment, compared with the exposed skin. The operative temperature T_0 is the average of the radiative surface temperature of the surroundings and the ambient air temperature, weighted by their respective heat transfer coefficients (ASHRAE, 2001).

The whole-body resistance or insulation (clo value) may not provide sufficient detail for predicting local surface temperatures or heat loss. Since it represents the whole-body effect, there is no difference between wearing a hat, or a pair of socks with the same clo value. A more useful value is the local resistance, which states the thermal resistance value in terms of power per unit body surface area which is covered by the article of clothing. This localized resistance represents the actual resistance of the garment as it affects the portion of the body that it covers – not as it affects the entire body.

The localized garment resistance describes the incremental effect on heat loss associated with wearing a given article of clothing, denoted here by the subscript *j*, applied over the portion of the body covered by garment *j*. The heat loss from the clothed portion of body $q_{cl,j}$ can be expressed in terms of the localized garment resistance $R_{cl,j}^*$, the localized resistance of the air layer $R_{a,j}^*$, and the surface areas of the garment-covered skin ($A_{s,j}$) and the garment ($A_{cl,j}$). [Note the asterisk (*) superscript denotes a localized value.] That relationship is stated by Equation 21:

$$q_{cl,j} = \frac{\left(\bar{T}_{s,j} - T_0\right) A_{cl,j}}{R_{cl,j}^* \left(\dfrac{A_{cl,j}}{A_{s,j}}\right) + R_{a,j}^*} \tag{21}$$

where $\bar{T}_{s,j}$ is the area-weighted, mean surface temperature of the skin that is covered by garment *j*.

188

Localized and whole-body insulation (clo) values for 106 different garments are given a Table 6-2. The localized values were calculated from the whole-body values, as determined by McCullough et al. (1985). The clo values can be converted easily to resistance (R or $R*$) values using the factor $1 \text{ clo} = 0.155 \text{ K} \cdot \text{m}^2 \cdot \text{W}^{-1}$.

6.3.2.5 Respiration

Heat transfer in the respiratory tract consists of latent (E_{rsp}) and sensible (C_{rsp}) terms, both of which are proportional to the minute respiratory volume; hence they scale with total metabolic energy production rate q_m.

The respiratory evaporative heat transfer rate E_{rsp} is a function of the difference in moisture content between expired and inspired air, as described by Fanger (1970):

$$E_{rsp} = 3.47 \cdot q_m \left(0.029 - 4.95 \cdot 10^{-3} P_{v,amb} \right) \tag{22}$$

where $P_{v,amb}$ is the ambient water vapor pressure (kPa).

The sensible respiratory heat transfer rate C_{rsp} is associated with the temperature change between the inspired and expired air and associated water vapor

$$C_{rsp} = .0014 \cdot q_m \left[\left(32.6 + 0.066 \cdot T_{surr} + 0.203 \cdot P_v \right) - T_{surr} \right] \tag{23}$$

where T_{surrr} is the ambient temperature (°C).

Of the two respiratory heat transfer terms, the evaporative rate E_{rsp} typically is much larger than the sensible rate C_{rsp}. Under extremely dry conditions, E_{rsp} may approach 10% of the whole-body metabolic rate. This compares with approximately 1% of metabolic rate for C_{rsp} at an ambient temperature of 28 °C (less at higher ambient temperatures). Note that under ambient temperatures which exceed core temperature, sensible heat transfer may represent a small heat *load* on the body ($C_{rsp} < 0$). The latent heat term is almost always a heat loss from the body however, except in rare cases where a subject is inhaling very hot, saturated air.

189

Table 6-2. Whole-body and local insulation and area factor values for various garments.

Garment Number, j	Garment Description and Fabric Type	$I_{cl,j}$, *clo*	$I^*_{cl,j}$, *clo*	$f^*_{cl,j}$
	Shirts			
1	Long-sleeve, bow at neck (broadcloth)	0.33	0.79	1.25
2	Long-sleeve, shirt collar (broadcloth)	0.33	0.80	1.24
3	Long-sleeve, shirt collar (flannel)	0.42	1.22	1.24
4	Short-sleeve, shirt collar (broadcloth)	0.25	0.75	1.23
5	Short-sleeve, sport shirt (double knit)	0.18	0.64	1.05
6	3/4 length sleeve, boat neck* (broadcloth)	0.34	1.07	1.24
7	Cap sleeve, boat neck* (broadcloth)	0.27	1.22	1.25
8	Sleeveless, scoop neck (broadcloth)	0.18	0.83	1.27
9	Tube top (double knit)	0.07	1.20	1.08
10	Long-sleeve, sweat shirt (fleece-backed knit)	0.38	1.62	1.13
	Sweaters			
11	Long-sleeve, V-neck (thin knit)	0.28	0.97	1.09
12	Long-sleeve, V-neck cardigan (thin knit)	0.26	1.12	1.10
13	Short-sleeve, V-neck (thin knit)	0.23	1.12	1.11
14	Short-sleeve, V-neck cardigan (thin knit)	0.20	1.20	1.13
15	Sleeveless, V-neck (thin knit)	0.15	0.85	1.11
16	Long-sleeve, round neck (thick knit)	0.40	1.83	1.13
17	Long-sleeve, round neck cardigan (thick knit)	0.35	2.13	1.15
18	Sleeveless, round neck (thick knit)	0.25	2.55	1.14
19	Long-sleeve, turtleneck (thin knit)	0.29	0.91	1.11
20	Long-sleeve, turtleneck (thick knit)	0.41	1.69	1.13
	Suit Jackets and Vests (lined)			
21	Single-breasted suit jacket (denim)	0.44	1.40	1.24
22	Single-breasted suit jacket (tweed)	0.52	2.04	1.24
23	Double-breasted suit jacket (denim)	0.50	1.86	1.26
24	Double-breasted suit jacket (tweed)	0.56	2.49	1.26
25	Work jacket (duck)	0.51	1.32	1.38
26	Vest (denim)	0.13	1.04	1.24
27	Vest (tweed)	0.20	5.15	1.24
	Trousers and Coveralls			
28	Straight, long, fitted (denim)	0.21	0.53	1.20
29	Straight, long, fitted (tweed)	0.30	0.93	1.20
30	Straight, long, loose (denim)	0.32	0.83	1.44
31	Straight, long, loose (tweed)	0.40	1.27	1.44
32	Walking shorts (denim)	0.12	0.58	1.24
33	Walking shorts (tweed)	0.21	2.11	1.24
34	Short shorts (denim)	0.09	0.65	1.28
35	Sweat pants (fleece-backed knit)	0.34	1.25	1.23

Trousers and Coveralls (cont)

190

Garment Number, j	Garment Description and Fabric Type	$I_{cl,j}$, clo	$I_{cl,j}^*$, clo	$f_{cl,j}^*$
36	Work pants (duck)	0.36	1.00	1.46
37	Overalls (denim)	0.41	0.92	1.33
38	Coveralls (gabardine)	0.61	0.80	1.26
39	Insulated coveralls (multi-component)	1.09	1.63	1.28
	Skirts			
40	A-line, ankle length (denim)	0.41	1.06	1.76
41	A-line, ankle length (tweed)	0.46	1.36	1.76
42	A-line, 6" below knee (denim)	0.32	0.93	1.63
43	A-line, 6" below knee (tweed)	0.39	1.43	1.63
44	A-line, 6" above knee (denim)	0.18	0.72	1.43
45	A-line, 6" above knee (tweed)	0.27	2.01	1.43
46	A-line, knee length (denim)	0.25	0.81	1.51
47	A-line, knee length (tweed)	0.34	1.65	1.51
48	Straight, knee length, with slit (denim)	0.23	0.82	1.44
49	Straight, knee length, with slit (tweed)	0.31	1.60	1.44
50	Bias flair, knee length (denim)	0.26	0.79	1.63
51	Bias flair, knee length (tweed)	0.35	1.55	1.63
52	Full gathered, knee length (denim)	0.25	0.82	1.54
53	Full gathered, knee length (tweed)	0.33	1.53	1.54
54	Knife pleated, knee length (denim)	0.27	0.96	1.54
55	Knife pleated, knee length (tweed)	0.37	2.15	1.54
	Dresses			
56	Long-sleeve, shirt collar, A-line (broadcloth)	0.44	0.70	1.30
57	Long-sleeve, shirt collar, A-line (tweed)	0.59	1.03	130
58	Long-sleeve, shirt collar, A-line, belt (broadcloth)	0.46	0.74	1.26
59	Long-sleeve, shirt collar, A-line, belt (tweed)	0.59	1.03	1.26
60	Short-sleeve, shirt collar, A-line, belt (broadcloth)	0.38	0.72	1.25
61	Sleeveless, scoop neck, A-line (broadcloth)	0.34	0.87	1.40
62	Sleeveless, scoop neck, A-line (tweed)	0.38	1.05	1.40
	Sleepwear			
63	Long-sleeve, long gown (tricot)	0.52	0.63	1.60
64	Long-sleeve, long gown (flannel)	0.69	0.87	1.60
65	Long-sleeve, short gown (tricot)	0.38	0.60	1.38
66	Long-sleeve, short gown (flannel)	0.53	0.93	1.38
67	Short-sleeve, long gown (tricot)	0.47	0.62	1.59
68	Short-sleeve, short gown (tricot)	0.33	0.59	1.34
69	Sleeveless, long gown (tricot)	0.41	0.61	1.65
70	Sleeveless, short gown (tricot)	0.29	0.63	1.36
71	Thin strap, long gown (tricot)	0.36	0.61	1.57
72	Thin strap, short gown (tricot)	0.23	0.62	1.29
73	Hospital gown (print cloth)	0.44	0.92	1.40

Garment Number, j	Garment Description and Fabric Type	$I_{cl,j}$, **clo**	$I_{cl,j}^{*}$, **clo**	$f_{cl,j}^{*}$
	Sleepwear (cont)			
74	Long-sleeve, long pajamas (broadcloth)	0.64	0.85	1.38
75	Long-sleeve, long pajamas (flannel)	0.73	0.99	1.38
76	Short-sleeve, long pajamas (broadcloth)	0.57	0.89	1.37
77	Long pajama trousers (broadcloth)	0.29	0.71	1.44
78	Body sleeper with feet (knit fleece)	0.92	1.18	1.44
	Robes			
79	Long-sleeve, wrap, long (velour)	0.73	0.96	1.50
80	Long-sleeve, wrap, long (terrycloth)	0.89	1.22	1.53
81	Long-sleeve, wrap, long (pile knit)	1.25	1.89	1.58
82	Long-sleeve, wrap, short (broadcloth)	0.55	0.93	1.35
83	Long-sleeve, wrap, short (velour)	0.60	1.06	1.37
84	3/4 length sleeve, wrap, short (velour)	0.55	1.11	1.32
85	Long-sleeve, button front, long (broadcloth)	0.66	0.81	1.57
86	Long-sleeve, button front, long (velour)	0.72	0.90	1.59
87	Long-sleeve, button front, short (broadcloth)	0.57	0.92	1.46
88	Short-sleeve, button front, short (broadcloth)	0.63	1.04	1.48
89	Long-sleeve, button front, short (velour)	0.50	0.94	1.46
	Underwear/Footwear			
90	Briefs (knit)	0.05	0.57	1.08
91	Panties (tricot)	0.04	0.39	1.08
92	Bra (knit/foam)	0.02	0.37	1.20
93	Half slip (tricot)	0.21	0.86	1.34
94	Full slip (tricot)	0.24	0.71	1.30
95	T-shirt (knit)	0.10	0.37	1.09
96	Thermal long underwear top (knit)	0.24	0.60	1.12
97	Thermal long underwear bottoms (knit)	0.19	0.51	1.14
98	Pantyhose (knit)	0.02	0.04	1.00
99	Ankle length athletic socks (knit)	0.03	1.30	1.14
100	Calf length athletic socks (knit)	0.04	0.42	1.07
101	Calf length dress socks (knit)	0.04	0.49	1.08
102	Knee socks (thick knit)	0.07	0.57	1.05
103	Thongs/sandals (vinyl)	0.03	4.81	1.20
104	Hard-soled street shoes (vinyl)	0.04	1.43	1.43
105	Slippers (quilted fleece)	0.06	1.42	1.44
106	Soft-soled athletic shoes (canvas)	0.04	1.43	1.43

6.4 Numerical Models of Tissue Heating

In situations where the lumped analysis approach is not valid, a multi-dimensional numerical model can be employed to predict the temperature – as a function of time and space – in tissue samples, whole animals and humans. A finite difference thermal model often can be used to calculate tissue temperatures with a high degree of spatial and temporal resolution. The finite difference method for thermal modeling is conceptually similar to the –Finite-Difference –

192

Time-Domain" (FDTD) method for electromagnetic field modeling, which is commonly used to calculate SAR values in heterogeneous tissues, animals and humans.

The finite difference method entails representing the tissue space as a rectangular grid. When applied to a three-dimensional space or object, this results in a series of cuboid volume elements, or *voxels* which form the basis for analysis. The same voxelized model often can be used for both FDTD analysis (to get the SAR distribution) and subsequently, the thermal analysis.
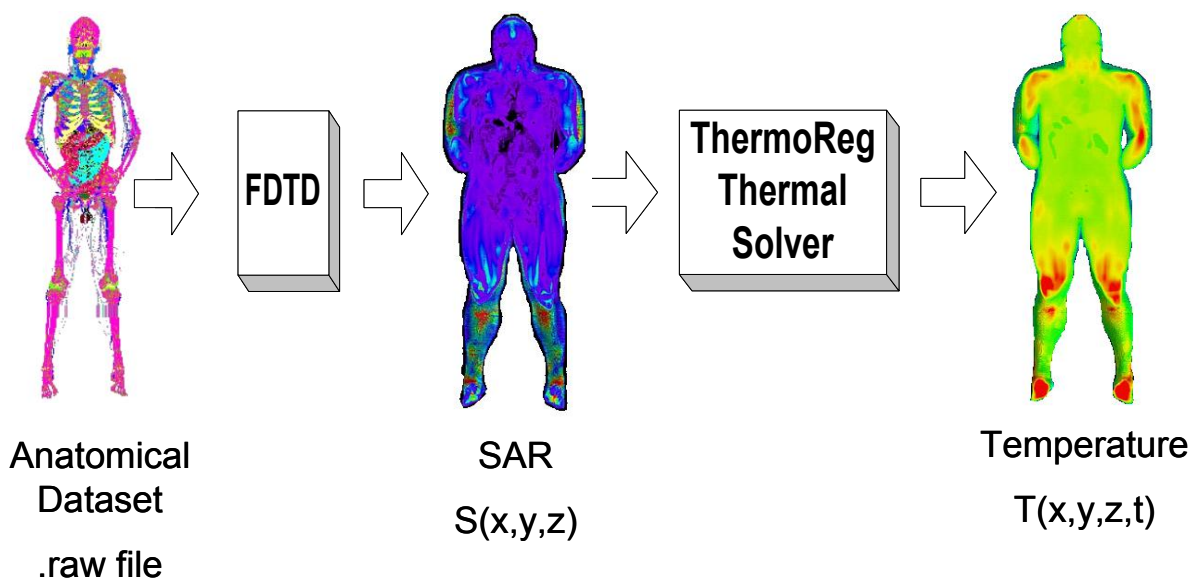

| Anatomical Dataset .raw file | SAR S(x,y,z) | Temperature T(x,y,z,t) |

Figure 6-2. An heterogeneous tissue data set (".raw file") is used as the geometry in the FDTD calculations to determine local SAR values. The same raw file, along with the calculated SAR data, is used to determine local tissue temperatures over time using the ThermoReg finite difference thermal solver.

The BHTE is discretized – in space and time – resulting in one algebraic equation written for each voxel, all of which must be solved at each time step. ThermoAnalytics, Inc. (Calumet, MI) has developed a voxel-based bio-heat transfer computer code, ***ThermoReg***, which incorporates active thermoregulation for simulating whole-body radio frequency (RF) heating, when used in conjunction with a finite-difference, time-domain (FDTD) code or similar solver to calculate SAR values. Thermoreg incorporates the effects of physiological heat sources and thermoregulatory mechanisms, clothing and environmental loads.

Human thermoregulatory feedback is described by a modified version of the model of Fiala et al. (2001). ThermoReg can also be used to simulate heating in animals by disabling the human thermoregulation function, provided the appropriate tissue-coded model ("raw file") is available.

A brief, general description of the ThermoReg model is provided below. Additional information and test case results can be found at www.ThermoReg.info.

6.4.1 Model Summary

The geometry for the human voxel model is a variant of the "Brooks man" model (Gajsek et al., 2001), which is a tissue-segmented version of the National Library of Medicine Visible Man (Ackerman et al., 1995). The simulated subject has a body mass of 104 kg and a DuBois surface area of 2.2 m^2. Each pixel of each slice of the Visible Man was assigned a numeric code, corresponding to a specific tissue type (Table 6-1).

As the model is based on the modified Pennes BHTE (i.e., Equation 10), blood flow is treated as a tissue heat source, proportional to the rate of flow and to the temperature difference between the mixed, deep arterial temperature T_a and the local tissue temperature. The change in the deep arterial temperature T_a is calculated at each time step by summing all heat flow terms to or from the blood pool over the preceding time interval, for all N voxels of the model. If counter-current heat exchange in the vasculature is negligible, then the blood arterial temperature T_a entering a given voxel is equal to the blood pool temperature. A finite-difference expression for the change in the arterial blood temperature is then written as follows:

$$\rho_{bl} V_{bl} c_{bl} \frac{\left(T_a^{k+1} - T_a^k\right)}{\Delta t} = \sum_{n=1}^{N} V_n \beta_n \left(T_n^k - T_a^k\right) \tag{24}$$

where n takes on values from 1 to N (the number of voxels in the model), and the superscripted indices k and $k+1$ refer to the current and next time steps.

6.4.1.1 Active Thermoregulation

The thermoregulatory algorithm of the model is based on control equations for a whole-body, compartment model of human thermoregulation (Fiala et al., 2001). Skin and core (hypothalamus) temperature errors (deviations from respective set-points) provide afferent signals for vasomotor drive and sweating.

The afferent core temperature error signal is determined from the mean hypothalamic temperature (ensemble voxel average), minus the hypothalamic set point temperature (37 °C). The afferent skin temperature signal is determined from a weighted skin temperature (WST), minus the skin set point temperature (34.4 °C). The weighting factors for the WST are applied on a regional basis to the voxel-averaged, mean skin surface temperature for each surface region. The magnitude of each weighting factor reflects (i) the surface of the region, relative to the total body surface area, and (ii) the importance of afferent temperature signals from the region in determining thermoregulatory feedback.

6.4.2 Tissue Temperature Results

Tissue temperatures calculated by ThermoReg for the seated Brooks Man are shown as Figures 6-3 to 6-5. In each case, the results are depicted at the conclusion of 45 minutes in an indoor environment which is at 24 °C and 40% RH. The average ambient air velocity is

194

$v = 0.1 \, \text{m} \cdot \text{s}^{-1}$. The man is simulated wearing only a pair of cotton shorts. His metabolic rate (1 met) corresponds to a sedentary activity level.

Figure 6-3 depicts the results of a sham exposure (no RF). Note the skin temperatures are in the range 30 – 34 °C (nom.), while internal tissue temperatures are normothermic. Figure 6-4 illustrates the subject model following 45 minutes of exposure to 100 MHz RFR (- EHK orientation) at power density of $4 \, \text{mW} \cdot \text{cm}^{-2}$, under the same environmental conditions as for Figure 6-3. While the skin temperatures are little changed – with the exception of the head region – there is a noticeable increase in the internal tissue temperature levels. This suggests thermoregulatory feedback is able to control surface temperature under these conditions, primarily through sweating and vasodilation.

At higher power density ($8 \, \text{mW} \cdot \text{cm}^{-2}$; Figure 6-5) both skin and internal temperatures are markedly elevated at the end of 45 minutes exposure. Maximum temperatures do not exceed 40 °C, however, suggesting there is little likelihood of tissue damage under these conditions.
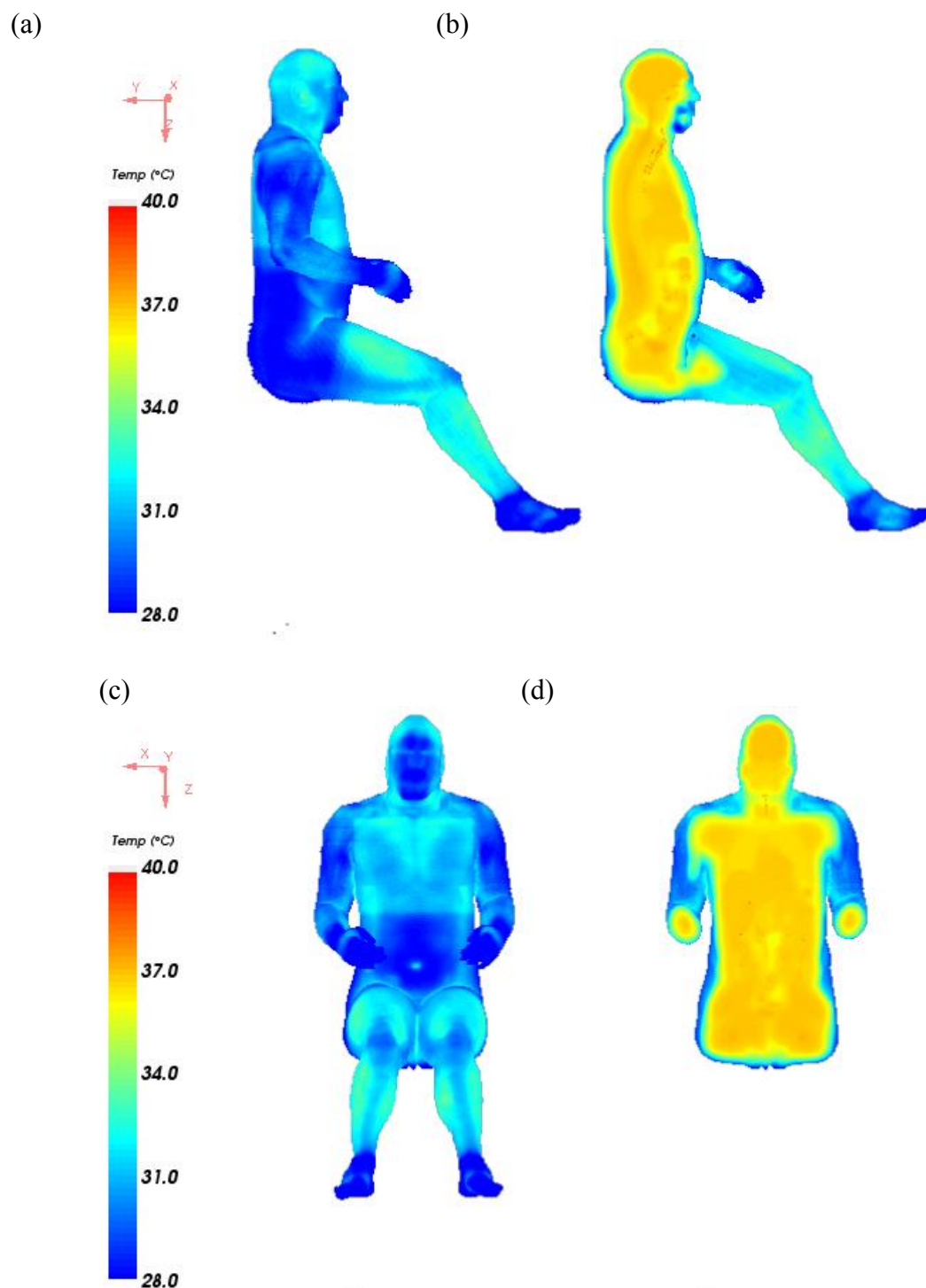
Figure 6-3. Tissue temperature, as calculated in ThermoReg for a seated, adult male exposed to a 24 °C, 40% RH environment for 45 min (no RF): (a) side view of skin surface (b) sagittal mid-plane section (c) front skin surface (d) coronal mid-plane section. The subject is simulated wearing only a pair of cotton shorts.
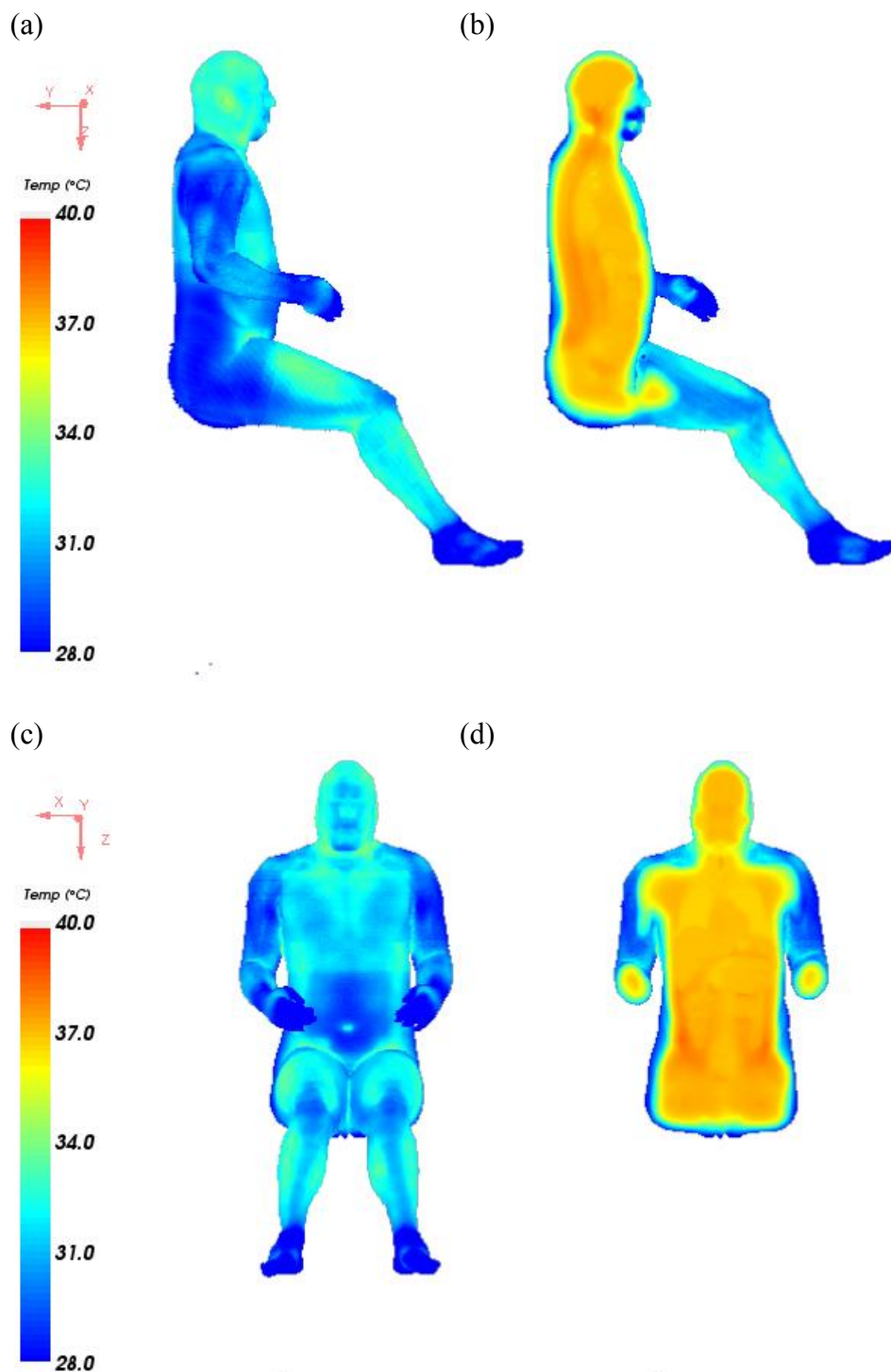
196

Figure 6-4. Tissue temperatures, as calculated in ThermoReg for a seated, adult male in a 24 °C, 40% RH environment exposed to 100 MHz (-EHK) whole-body RFR at a power density of $4\,\mathrm{mW\cdot cm^{-2}}$ for 30 minutes: (a) side view of skin surface (b) sagittal mid-plane section (c) front skin surface (d) coronal mid-plane section.

DISTRIBUTION A: APPROVED FOR PUBLIC RELEASE; DISTRIBUTION UNLIMITED.
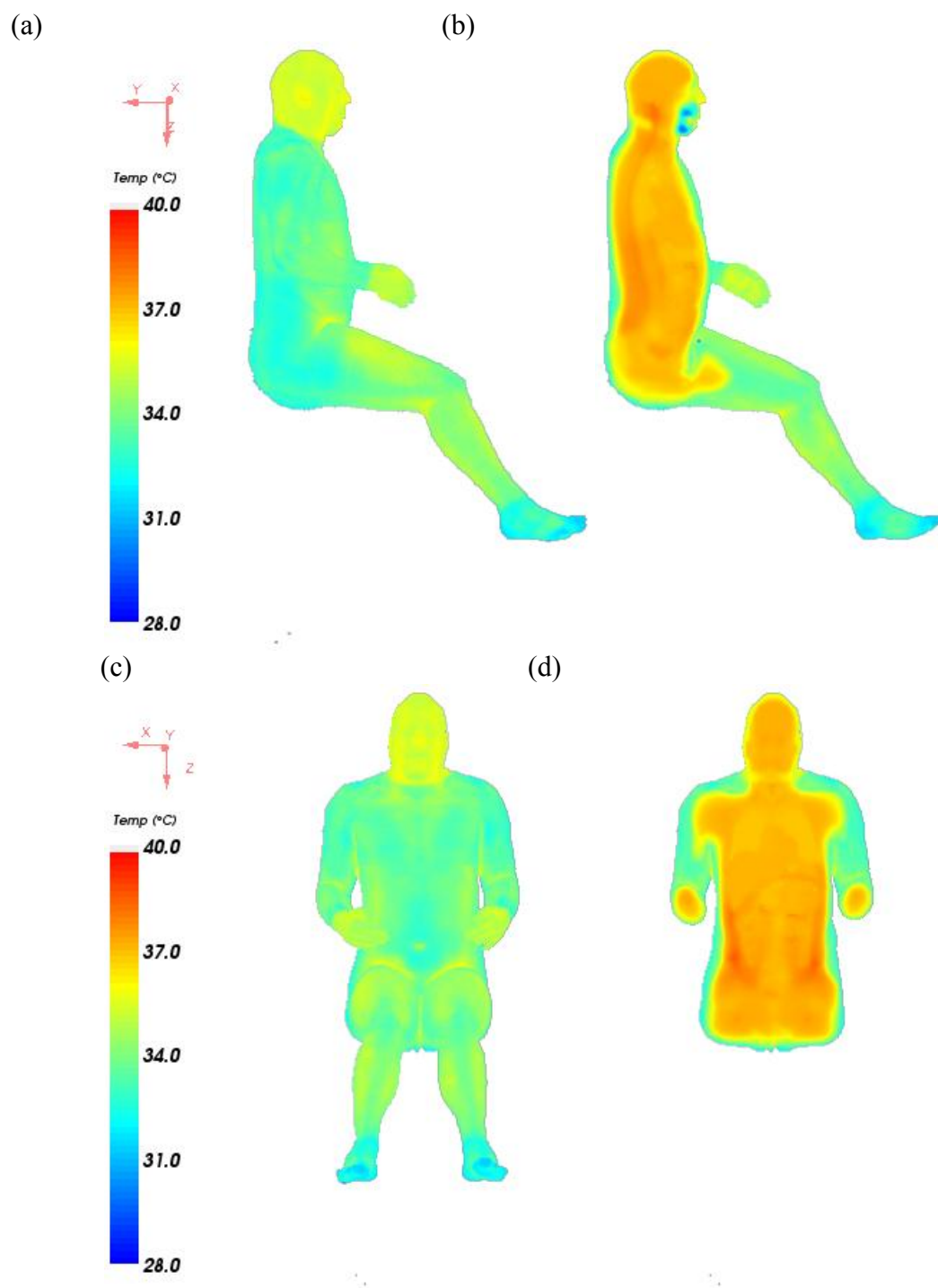PUBLIC AFFAIRS CASE NO. 11-069

Figure 6-5. Tissue temperatures, as calculated in ThermoReg for a seated, adult male in a 31 °C, 40% RH environment exposed to 100 MHz (-EHK) whole-body RFR at a power density of $8\ \mathrm{mW}\cdot\mathrm{cm}^{-2}$ for 30 minutes: (a) side view of skin surface (b) sagittal mid-plane section (c) front skin surface (d) coronal mid-plane section.

6.5 Summary

A thermal model can be an invaluable tool for assessing thermal effects of RF radiation in humans and animals. A model can be used to examine potentially synergistic effects of exposure to extreme thermal environments and RF exposure, or to simulate environments outside the accepted safe exposure levels. Model simulations are much cheaper and faster than human or animal exposures, allowing a wider range of conditions to be examined.

There are some very significant limitations and drawbacks to the use of models in RFR dosimetry. Models are only as good as the data on which they are based. Ultimately, any model must be validated by comparison and calibration with accepted experimental results. Additionally, most models are based on a limited number of subjects and may not accurately reflect variations in thermal response associated with a subject's gender, body size or type, and level of acclimatization. Thus, the results of thermal models should be interpreted cautiously and – where possible – confirmed by experimentation.

199

6.6   Appendix

In a Cartesian (xyz) coordinate system the "del" operator is

$$\vec{\nabla} = \hat{i}\,\frac{\partial}{\partial x} + \hat{j}\,\frac{\partial}{\partial y} + \hat{k}\,\frac{\partial}{\partial z} \qquad\qquad (A.1)$$

where $\hat{i}, \hat{j}, \hat{k}$ represent the unit vectors in the x, y, and z directions, respectively.

When the del operator is applied to a scalar (temperature, e.g.), the result is a vector which represents the "directional derivative" or gradient of the scalar. Thus, the temperature gradient is simply:

$$\vec{\nabla} T = \hat{i}\,\frac{\partial T}{\partial x} + \hat{j}\,\frac{\partial T}{\partial y} + \hat{k}\,\frac{\partial T}{\partial z}\;. \qquad\qquad (A.2)$$

The dot product of the del operator and the gradient is a scalar quantity, known as the Laplacian. In Cartesian coordinates the Laplacian of temperature is:

$$\nabla^2 T = \frac{\partial^2 T}{\partial x^2} + \frac{\partial^2 T}{\partial y^2} + \frac{\partial^2 T}{\partial z^2}\;. \qquad\qquad (A.3)$$

6.7   References

Ackerman, M. J., Spitzer, V. M., Scherzinger, A. L., & Whitlock, D. G. (1995). The Visible Human data set: an image resource for anatomical visualization. *Medical Information for patients, 8*(2), 1195-1198.

ASHRAE. (2001). *Handbook: Fundamentals*. Atlanta, GA: American Society of Heating, Refrigerating and Air-Conditioning Engineers, Inc.

Bowman, H. F., Cravalho, E. G., & Woods, M. (1975). Theory, Measurement, and application of thermal properties of biomaterials. *Annual Review Biophysics & Bioengineering, 4*, 43-80.

Chen, M. M. (1985). The Tissue Energy Balance Equation. In Shitzer A., & Eberhart R. C. (Ed.), *Heat Transfer in Medicine and Biology* (pp. 153-164). New York: Plenum Press.

Datta, A. K. (2002). *Biological and Bioenvironmental Heat and Mass Transfer*. New York: Marcel Dekker.

Fanger, P. O. (1970). *Thermal Comfort Analysis and Applications in Environmental Engineering*. New York: McGraw-Hill.

Fiala, D., Lomas, K. J., & Stohrer, M. (1999). A computer model of human thermoregulation for a wide range of environmental conditions: the passive system. *Journal of Applied Physiology, 87,* 1957-1972.

Fiala, D., Lomas, K. J., & Stohrer, M. (2001). Computer prediction of human thermoregulatory and temperature responses to a wide range of environmental conditions. *International Journal of Biometeorology, 45,* 143-159.

Gajsek, P., Hurt, W. D., Ziriax, J. M., & Mason, P. A. (2001). Parametric dependence of SAR on permittivity values in a man model. *IEEE Transactions on Biomedical Engineering, 48,* 1169-1177.

Hill, J. E., Leitman, J. D., & Sunderland, J. E. (1967). Thermal Conductivity of Various Meats. *Food Technology, 21,* 1143-1148.

McCullough, E. A., Jones, B. W., & Huck, J. (1985). A comprehensive data base for estimating clothing insulation. *ASHRAE Transactions, 91,* 29-47.

Mills, A. F. (1992). *Heat Transfer*. Homewood, IL: Richard D. Irwin, Inc.

Mitchell, D., Wyndham, C. H., & Hodgson, T. (1967). Emissivity and transmittance of excised human skin in its thermal emission wave band. *Journal of Applied Physiology, 23,* 390-394.

Pennes, H. H. (1948). Analysis of tissue and arterial blood temperatures in the resting human forearm. *Journal of Applied Physiology, 1,* 93-122.

Shitzer, A., & Eberhart, R. C. (1985). Heat generation, storage and transport processes. In A. Shitzer & R.C. Eberhart (Eds.), *Heat Transfer in Medicine and Biology: Analysis and Applications* (pp. 137-152). New York: Plenum Press.

Togawa, T. (1989). Non-contact skin emissivity: measurement from reflectance using step change in ambient radiation temperature. *Clinical Physics and Physiological Measurement, 10,* 39-48.

Wissler, E. H. (1998). Pennes' 1948 paper revisited. *Journal of Applied Physiology, 85,* 35-41.

Yang, W. (1989). *Biothermal Fluid Sciences: Principles and Applications*. New York: Hemisphere Publishing Corp.

Radio Frequency Radiation Dosimetry Handbook
(Fifth Edition)

Chapter 7.   Modeling Thermal Response of Tissues Irradiated with Radio Frequency Energy

Kenneth R. Foster
Professor, Department of Bioengineering
University of Pennsylvania, Mail Code 6321, 240 Skirkanich Hall
210 S. 33rd Street, Philadelphia PA 19104

kfoster@seas.upenn.edu

7.1   Introduction

The Specific Absorption Rate (SAR) is the universally accepted measure of exposure to radio frequency radiation (RFR). However, for thermal effects the biological responses are more directly the result of heating of tissue. These thermal effects can be due to local increases in temperature of tissue, or from thermoregulatory responses as the body manages the additional heat load imposed by the absorbed energy (even though the increase in tissue temperature within the body might be very small).

This chapter considers models for estimating the thermal response of tissue to exposure to RFR, and reviews the thermal dose concept for predicting tissue damage. The focus is on applications relevant to dosimetry for safety analysis. The discussion excludes heat transfer of in vitro exposure systems, or heat transfer in tissues in which a phase transition (e.g., boiling of tissue water or thawing frozen tissue) occurs.

An enormous amount of literature exists on heat transfer in tissue, focusing both on fundamental mechanisms of heat transfer and on practical applications for hyperthermia and other medical purposes. While the principles of heat transfer in tissue are well understood, the anatomical complexity of tissue requires the use of simplified models for any practical application, which raises the issues of model accuracy and validity.

This chapter focuses on a simple quantitative description of heat transfer in tissue and its applications. This is the so-called bioheat equation, which was first proposed by Pennes (1948) in a paper that has been cited more than 700 times since its original publication. The implications of this equation for the heating behavior of tissue from RFR are discussed, with respect to thermal time constants and definition of averaging volumes. This chapter includes a table of recommended parameters for different tissues, as well as a much longer table that gives a picture of the dispersion in parameters that are found in the literature. Finally, this chapter discusses the likely ranges of validity and limits of this modeling approach.

7.2 The Bioheat Equation

7.2.1 Formulation of the Equation

Pennes' bioheat equation can be written

$$k_t \nabla^2 T - \rho_b \rho_t m_b C_b (T - T_b) + \dot{q}_m + \dot{q}_{env} + \rho_t SAR = \rho_t C_t \frac{\partial T}{\partial t} \qquad (1)$$

where T = the temperature of the tissue ($^{\circ}$C) above mean arterial temperature T_b, k_t = the thermal conductivity of tissue (W/m $^{\circ}$C), SAR = the electromagnetic power deposition rate (W kg^{-1}), C_t (C_b) = the heat capacity of blood or soft tissue (assumed in the following discussion to be the same) (W sec kg^{-1} $^{\circ}$C^{-1}), ρ_t, ρ_b = the density of tissue and blood (kg m^{-3}), $\dot{q}_m$ and $\dot{q}_{env}$ = energy inputs from metabolic processes and the environment, (watt m^{-3}), and m_b = the blood perfusion rate (m^3 kg^{-1} sec^{-1}).

In the physiology literature, blood perfusion is commonly cited as a volumetric flow (e.g., liters of blood per kg of tissue per minute) which can be converted to a mass flow using the density of blood (assumed to be 1000 kg m^{-3} in preparing the tables in this chapter). The terms ($\dot{q}_m, \dot{q}_{env}$) represent rates of heat input from metabolic processes and the environment.

For practical modeling applications, Equation 1 can be simplified considerably. The material properties (density, heat capacity) of all soft high water content tissues are similar (being determined chiefly by water content) and can be expressed as C and ρ using approximate values of heat capacity and density of soft tissue. Also, when calculating the increase in temperature above baseline due to RFR exposure, the heat input from metabolic or environmental sources can often be ignored; a full thermoregulatory model would have to include such effects.

With these simplifications, Equation 1 becomes

$$k \nabla^2 T - \rho^2 C m_b (T - T_b) + \rho SAR = C \rho \frac{\partial T}{\partial t}. \qquad (2)$$

This is the usual expression for heat conduction (Fourier's Law) modified with an additional term that quantifies the removal of heat by blood perfusion due to convection. In this simple continuum model, blood itself does not appear explicitly, but acts as an invisible sink for energy. In some applications (typically for hyperthermia treatment planning), investigators have developed hybrid models in which the bioheat equation is used to determine heat transfer in tissues away from major blood vessels, with the vessels themselves considered as separate geometric entities.

7.2.2 Boundary Conditions

Heat transfer mechanisms at the skin include convection (heat loss to the surrounding air), evaporation of water, and radiation of energy from the tissue into space. The literature on human thermoregulation contains extended discussion of the effects of environmental conditions, clothing, etc. on these mechanisms. When modeling the increases in tissue temperature due to RFR absorption, it is often satisfactory to lump all of these effects together, and apply a boundary condition at the tissue-air interface using a heat transfer coefficient h (W m^{-2} °C^{-1})

$$k\nabla T \bullet n = -h(T - T_a) \tag{3}$$

where T_a = the ambient air temperature, and n = the unit vector normal to the surface.

For a nude man in a thermally neutral environment with low air flow rates, Stolwijk and Hardy (1977) cite a heat transfer coefficient h (combining both radiative and convective cooling effects) of 6.9 W m^{-2} C^{-1}.

For many modeling applications a number of simplifications are possible. For localized RFR exposure, thermal gradients produced by the RFR in tissue near the surface of the body are often sufficiently large that heat transfer is primarily by conduction into deeper layers of tissue, and only a small fraction of the absorbed RF energy is lost to the surrounding air. In such cases, it may be adequate to assume insulated boundary conditions (h=0) at the tissue surfaces that are in contact with air.

7.2.3   Parameter Values

This chapter includes two tables of parameter values for use with the bioheat equation. Table 7-1 summarizes single values of the parameters, which, in the judgment of the scientist who compiled the data, represent ―best values" from a variety of literature sources (Samaras & Kuster, personal communication). Two Appendices (supplied by Holmes) provide detailed tables of values taken from the primary literature, which gives a good picture of the dispersion in available data (Holmes, 1997).

It should be noted in connection with Table 7-1 that there is wide variation in values for parameters reported in the literature, particularly for blood perfusion. For purposes of modeling effects of RFR exposure, it may be more important for different groups to agree on consistent sets of values to use, rather than to try to identify a single set of ―correct" values.

Table 7-1. Thermal properties of tissue and derived quantitites* - summary data. Note that reported values of these properties vary considerably in the literature, even for similar tissues from the same species.

Name	Density [kg/m3]	Thermal Conductivity [W/m/K]	Specific Heat Capacity [J/(kg K)]	Heat Generation Rate [W/kg]	Blood perfusion m_b [m^3/(kg sec)]	τ_1 [sec]	τ_2/L^2 [sec/cm^2]	1/v [cm]	$\sqrt{4\alpha}$ [cm sec$^{-1/2}$]
Aorta	1060	0.51	3824	0	1.7E-04	5.66	794.79	0.08	0.071
Bladder	1040	0.56	3900	1.54	1.3E-06	739.50	724.29	1.01	0.074
Blood	1060	0.51	3824	0	1.7E-04	5.66	794.79	0.08	0.071
Bone	1990	0.4	1289	0.307	3.7E-07	1370.21	641.28	1.46	0.079
Bone Marrow (Infiltrated)	1027	0.6	4191	5.55	0.0E+00	n/a	717.36	n/a	0.075
Bone Marrow (NotInfiltrated)	980	0.6	4191	5.82	0.0E+00	n/a	684.53	n/a	0.076
Brain (Grey Matter)	1039	1.13	3675	6.833	1.1E-05	86.05	337.90	0.50	0.109
Brain (White Matter)	1043	0.5	3621	6.807	4.0E-06	242.68	755.34	0.57	0.073
Breast fat	916	0.5	2524	0.323	4.5E-07	2425.52	462.40	2.29	0.093
Cartilage	1100	0.47	3664	1.455	8.3E-07	1090.69	857.53	1.13	0.068
Cerebellum	1040	0.53	3640	6.827	9.3E-06	103.00	714.26	0.38	0.075
Cerebrospinal Fluid	1007	0.6	4191	0	0.0E+00	n/a	703.39	n/a	0.075
Cervix	1013	0.56	3700	1.524	1.2E-05	84.60	669.30	0.36	0.077
Colon	1044	0.56	3653	9.1	1.3E-05	76.41	681.02	0.33	0.077
Cornea	1032	0.52	3793	0	6.3E-07	1529.68	752.76	1.43	0.073
Dura	1013	0.35	2947	0	6.3E-07	1572.44	852.95	1.36	0.068
Eye Tissues(Sclera)	1032	0.4	3000	0	6.3E-07	1529.68	774.00	1.41	0.072
Fat	916	0.25	2524	0.328	4.5E-07	2425.52	924.79	1.62	0.066
Gall Bladder	1040	0.47	3496	1.56	1.3E-06	739.50	773.58	0.98	0.072
Gall Bladder Bile	1026	0.47	3496	1.56	1.3E-06	749.59	763.17	0.99	0.072
Heart	1060	0.54	3720	9.057	1.5E-05	62.88	730.22	0.29	0.074
Kidney	1046	0.52	3745	45.89	4.4E-05	21.95	753.32	0.17	0.073
Lens Cortex	1090	0.4	3664	0	6.3E-07	1448.29	998.44	1.20	0.063
Lens Nucleus	1090	0.4	3664	0	6.3E-07	1448.29	998.44	1.20	0.063
Liver	1050	0.51	3600	11.43	1.7E-05	56.73	741.18	0.28	0.073
Lung	655	0.44	3625	2.595	6.7E-06	228.96	539.63	0.65	0.086
Muscle	1041	0.53	3546	0.461	4.7E-07	2058.05	696.49	1.72	0.076
Nerve	1038	0.46	3664	6.84	9.2E-06	105.27	826.79	0.36	0.070
Ovary	1025	0.53	3600	62.44	5.1E-05	19.13	696.23	0.17	0.076
Skin	1100	0.35	3437	1.473	1.6E-06	562.21	1080.20	0.72	0.061
Small Intestine	1044	0.56	3653	12.452	1.7E-05	57.46	681.02	0.29	0.077
Spleen	1054	0.54	3603	14.321	1.9E-05	49.84	703.25	0.27	0.075
Stomach	1050	0.53	3553	4.952	6.2E-06	152.76	703.90	0.47	0.075
Tendon	1110	0.5	3500	1.441	8.3E-07	1080.86	777.00	1.18	0.072
Testis	1044	0.53	3746	61.3	1.6E-06	617.85	737.89	0.92	0.074
Thyroid	1050	0.53	3553	60.95	1.7E-04	5.75	703.90	0.09	0.075
Tongue	1041	0.53	3546	0.461	4.7E-07	2058.05	696.49	1.72	0.076
Trachea	1100	0.47	3664	1.455	8.3E-07	1090.69	857.53	1.13	0.068
Uterus	1041	0.5	3580	0.451	6.3E-07	1530.15	745.36	1.43	0.073
Vitreous Humor	1009	0.59	3932	0	0.0E+00	n/a	672.44	n/a	0.077

* We thank T. Samaras and N. Kuster for these data.

205

Thermal conductivity and heat capacity properties are chiefly determined by the water content of the tissue, which varies over narrow limits for tissues of a given type. There is some dispersion in the values for these properties in the literature, which may in part reflect experimental errors and in part variations in the condition of the tissue used in different studies.

Giering et al. (1996) provided an extensive table of heat capacities of tissues. To illustrate the dispersion in values, these authors quoted a range from 3550 to 3800 m^2 sec^{-2} K^{-1} for the heat capacity of human muscle, and 2200 to 2430 m^2 sec^{-2} K^{-1} for human fat (all values at 37 ^oC). The specific heat C was summarized by a correlation relation with the mass fraction of water W in the tissue:

$$C \ (m^2 \sec^{-2} \ ^oC^{-1}) = 4190(0.37 + 0.63W) \ . \tag{4}$$

Chato (1985) summarized the thermal conductivity of various tissues. To give an example of the dispersion in the data, he cites a range of values of 0.34-0.68 W m^{-1} C^{-1} for muscle in vitro. Chato quoted a correlation equation for the thermal conductivity k of tissue:

$$k \ (W\,m^{-1}\,^oC^{-1}) = 0.054 + 0.573W \ \ for \ W > 0.2 \ . \tag{5}$$

Blood perfusion in tissue is highly dependent on physiological circumstances. It varies among individuals and, in any individual, with environmental and physiological conditions. Blood flow in the same tissue type also varies with species.

Blood perfusion data from muscle in humans and other species illustrate this variability (Appendix B). In this table (derived from Holmes, 1997), the blood flow measured in human skeletal muscle (non-exercising subjects) varied from 3-4.5 (10^{-7}) m^3 kg^{-1} sec^{-1}. It increases by up to an order of magnitude with exercise (Ch. 2). Blood flow in heart muscle in various species is more than two orders of magnitude larger than that measured in non-exercising skeletal muscle.

Moreover, blood perfusion in muscle is highly temperature-dependent, increasing by an order of magnitude for an 8 ^oC increase in tissue temperature. Lang et al. (1999) proposed the following temperature dependence for the blood perfusion in muscle for use with the bioheat equation for planning hyperthermia treatments:

$$m_b \rho_t^2 \bullet 10^6 = \begin{cases} 0.45 + 3.55 \exp(\dfrac{-(T - T_b - 8.0)^2}{12}), T - T_b \leq 8.0 \\ 4.00, \qquad\qquad\qquad\qquad\quad T - T_b > 8.0 \end{cases} (units \ m^3 \ kg^{-1}sec^{-1}). \tag{6}$$

By contrast, blood perfusion in other organs, notably the human brain, is much more constant.

As discussed below, the bioheat equation is based on a highly oversimplified model of heat transfer in tissue, and consequently the blood perfusion m_b that appears in it has a very unclear relationship to blood perfusion as measured in a tissue using standard physiological methods. Consequently, m_b is best regarded as a model-dependent parameter, and not to be

206

identified with blood perfusion as measured (for example) with tracer techniques. The effect of this on thermal modeling will be discussed below.

7.2.4 Scaling Properties of the Bioheat Equation

It is useful to consider the scaling properties of the equation, which yields insights into the heating of tissue by RFR that supplement the results of more detailed numerical or analytical solutions to the equation for particular cases.

7.2.4.1 Spatial Scaling and Thermal Averaging Volumes

The characteristics of the bioheat equation can be studied conveniently using the Green's function, which is the solution of the equation assuming a point or line source of heat. With no boundary conditions and zero initial conditions, the Green's functions for the bioheat equation are (Yeung & Atalar, 2001):

$$
\begin{aligned}
&\text{Steady-state cylindrical} \quad G(r) = \frac{\rho_t}{2\pi k_t} K_0(vr) \\[2mm]
&\text{Steady-state spherical} \quad\;\; G(R) = \frac{\rho_t}{4\pi k_t R} e^{-vR} \\[2mm]
&\text{Time-dependent cylindrical} \quad G(r,t) = \frac{\rho_t}{4\pi k_t t} e^{-(r^2/4\alpha t)} e^{-av^2 t} \\[2mm]
&\text{Time-dependent spherical} \quad G(R,t) = \frac{\alpha \rho_t}{k_t (4\pi \alpha t)^{3/2}} e^{-(R^2/4\alpha t)} e^{-av^2 t} \; .
\end{aligned}
\tag{7}
$$

In the above expressions, K_o is a Bessel function, v is defined by

$$
v = \rho \sqrt{m_b c / k_t}
$$

α_t is the thermal diffusivity of tissue

$$
\alpha_t = \frac{k}{\rho C}
$$

and R and r are the distance from the point or line source of heat, respectively.

The time-dependent increases in temperature produced by an actual source of heat are found by convolving the appropriate Green's function with the SAR. Because the convolution operation is a form of averaging, the Green's functions provide a physically motivated way to define an averaging volume, which has considerable importance in setting exposure guidelines. Equations 7 yield two different length scales in terms of which an averaging volume can be defined. These are

$$R_1 = \sqrt{4\alpha t} \approx 0.05\sqrt{t} \ \text{cm} \ \text{sec}^{-1/2}$$

$$R_2 = 1/v = \frac{\sqrt{k_t}}{\rho\sqrt{m_b c}} \approx 1-2 \ \text{cm} \tag{8}$$

(using parameter values that are in the range of those typically reported for soft tissue). The first of these, R_1, is the well-known Einstein diffusion length, a measure of the distance that heat diffuses in time. The second, R_2, is a measure of the distance at which the temperature pattern from a point source falls off due to convective cooling of tissue by blood flow.

For very short times after the source has been turned on, the Green's function is spread out over a distance comparable to R_1, limited in spatial extent by the diffusion of heat. Consequently, the temperature increase at any point reflects an average of the absorbed power over this distance scale. At longer times, as the steady-state is approached, the appropriate averaging distance would increase to R_2. For standards setting, the steady-state (maximum) temperature increase would undoubtedly be of greatest interest, and the appropriate averaging volume would be a sphere of radius of the order of R_2 which corresponds to distances of several cm^3 from the source or averaging volumes of several cm^3 assuming typical values of blood flow.

7.2.4.2 Temporal Scaling and Thermal Averaging Times

Some general insights into the time-dependent properties of heating of tissue by RFR can be gained by considering the temporal scaling characteristics of the bioheat equation (Foster et al., 1998). Two different time scales can be defined from the bioheat equation

$$\tau_1 = \frac{1}{m_b \rho}$$

$$\tau_2 = \frac{\rho C L^2}{k} \tag{9}$$

which characterize heat transfer by blood flow and heat conduction, respectively. Recasting Equation 2 in non-dimensional form yields:

$$\nabla^2 T^* - \frac{\tau_2}{\tau_1}T^* + SAR^*(r^*,t^*) = \frac{\partial T^*}{\partial t^*} \tag{10}$$

where

$$T^* = \frac{k(T-T_b)}{\rho SAR_0 L^2}$$

$$x^* = \frac{x}{L}$$

$$t^* = \frac{t}{\tau_2} \tag{11}$$

$$SAR^* = \frac{SAR}{SAR_0}.$$

208

In the above expressions, L is a measure of the distance scale of the heating pattern, and SAR_o is a measure of the maximum SAR in the region of interest. The temperature is with reference to baseline, i.e., the temperature above that of the tissue in the absence of RF heating.

In the above expressions, the smaller of τ_1 and τ_2 determines the dominant mechanism of heat transport. If $\tau_1 \gg \tau_2$, which occurs for very localized heating, thermal conduction dominates and Equation 2 reduces to the standard Fourier expression for heat conduction. In the opposite case ($\tau_1 \ll \tau_2$), which occurs when the SAR pattern is broad and uniform, heat removal by blood perfusion dominates. For materials whose thermal properties are similar to those of soft tissues and with physiologically appropriate values of blood flow, the transition from conduction to convection-dominated heat transfer typically corresponds when the spatial extent of the SAR pattern is on the order of millimeters. This is the situation with millimeter wave radiation, for which the energy penetration depth in tissue is very shallow.

In the early transient regime (at short times after the exposure has begun when effects of heat transfer are negligible) the rate of rise in local temperature T in non-dimensional units is simply

$$\left. \frac{dT^*}{dt^*} \right)_0 = SAR^* \approx 1$$

or, in dimensioned form (12)

$$\left. \frac{dT}{dt} \right)_0 = \frac{SAR}{C} .$$

For an SAR of 10 W/kg (roughly equal to the IEEE and ICNIRP basic restrictions for partial body exposure) this corresponds to a maximum rate of temperature increase of about 0.15 ^oC/min. In the steady-state, ignoring both loss of heat to the surrounding air and heat conduction, the steady-state temperature will approach

$$T_{ss}^* \approx \frac{\tau_1}{\tau_2} SAR^*$$ (13)

or, in dimensioned form

$$T_{ss} \approx \frac{SAR}{\rho m_b C} .$$ (14)

Using a value of the blood perfusion parameter m_b that is in the range mentioned in the physiological literature (3 cm^3/100 g tissue minute or, in MKS units $5 \cdot 10^{-7}$ m^3 kg^{-1} sec^{-1}), this corresponds to a steady-state temperature increase of about 1 ^oC. Heat conduction and other effects would further reduce this temperature increase.

Considering the effects of both blood perfusion and heat conduction (but not loss of heat to the environment through the boundary conditions on the heated region), the steady-state temperature increase can be expressed as the product of the SAR with an effective thermal response time τ_{eff}

209

$$T_{ss} \approx \frac{dT}{dt}\bigg)_0 \tau_{eff}$$
$$= \frac{SAR}{C}\tau_{eff} .$$

(15)

This is equivalent to the initial rate of increase in temperature in the absence of heat conduction, times an effective thermal time constant τ_{eff}. The effective response time τ_{eff} is intermediate between τ_1 and τ_2, and approaches the smaller of the two in limiting cases when the heat transfer is limited by conduction or convection.

One important implication of the scaling considerations discussed above concerns the possibility of ―selective" heating of small regions of tissue by RFR, which has sometimes been mentioned in the literature. But thermal conduction works strongly to oppose the establishment of localized temperature increases. For example, if a small spherical object of radius R is exposed to RFR at a uniform SAR, and is surrounded by unheated material, the maximum temperature increase ΔT in the sphere is

$$\Delta T \approx \frac{SAR}{C}\tau_{eff}$$

where

(16)

$$\tau_{eff} = \frac{\rho C R^2}{k} .$$

For a sphere whose thermal properties are similar to those of soft tissue, the effective time constant τ_{eff} ranges from a few minutes for centimeter-sized regions, down to microseconds for micron-sized objects. To produce significant temperature fluctuations over small (millimeter or smaller) distance scales would require very high SARs. This may occur with pulsed RFR of very high peak power but very low duty cycle or pulsed laser energy, but is not likely to be a significant factor with RFR at ordinary exposure parameters.

7.2.4.3   Analytical Solutions to the Bioheat Equation

Equation 2 can be solved analytically for a number of special cases, including RFR-heated spheres and cylinders of tissue (cf. Foster et al., 1978; Foster & Erdreich, 1999).

A useful special case is a planar tissue surface exposed to RFR with insulated boundary conditions. This would be a useful approximation for millimeter wave exposure to tissue, in which thermal gradients near the surface of the tissue are sufficiently large that convective cooling by blood can be ignored. In that case, the bioheat equation reduces to the usual heat conduction equation

$$k\nabla^2 T + \frac{I_o \mathrm{T}}{L} e^{-x/L} = C_p \rho \frac{\partial T}{\partial t}$$

(17)

210

where T is the energy transmission coefficient (fraction of incident energy that is transmitted into the tissue), L is the energy penetration depth into the tissue, and I_o is the intensity of the incident beam. Equation 17 can be solved to yield the surface temperature T_{sur}

$$T_{sur}(t) = C_1\sqrt{t} - C_2(1 - e^{t/\tau}erfc\sqrt{t/\tau})$$
where

$$C_1 = \frac{2I_o T}{\sqrt{\pi k \rho C}}$$
$$C_2 = \frac{I_o TL}{k}$$
$$\tau = \frac{\rho CL^2}{k}.$$

(18)

The first term in the right side of Equation 18 is the temperature increase that would result from purely surface heating, while the second term is a correction that takes into account the finite penetration distance of the energy into the tissue.

This simple one-dimensional model, which ignores blood flow, is reasonable for RFR at sufficiently high frequency (typically above 10 GHz) is incident on the body. Insulated boundary conditions are appropriate in such cases because nearly all of the heat transfer is by conduction into the tissue (a consequence of the large thermal gradients near the tissue surface) and not by radiation or convection into the surrounding air. This simple model accurately predicted the temperature increase in tissue due to short (3 second) exposures to millimeter wave energy even though there were no adjustable parameters in the model (Walters et al., 2000). It works because transfer of the electromagnetically induced heat away from the exposed area is dominated by conduction (a physiologically trivial process) and not convection by blood flow.

7.2.4.4   Numerical Solutions to Bioheat Equation

There exists immense literature on the numerical solution of the bioheat equation in tissues subject to heating from various energy sources including RFR. Applications include therapy (hyperthermia dose planning) and radiation hazard studies.

Many of these studies are extensions of conventional RFR dosimetry studies that are based on the finite-difference time-domain (or other numerical) solution of the electromagnetic field equations using a detailed numerical model of the body such as Visible Man. In such studies, it is straightforward to extend the electromagnetic calculations to solve the bioheat equation, based on tables of thermal parameters such as given in Table 7-1 below. An example of such a study conducted for purpose of hazard assessment (for mobile phones) is by Van Leeuwen et al. (1999).

At least three commercial FDTD electromagnetic simulation programs are presently being extended to include solution of the bioheat equation in this way. In the near future, it will

211

be a routine matter to include thermal simulations, based on the bioheat equation, as an add-on to detailed calculation of SAR pattern using numerical models of the human body.

7.2.4.5 Limits of Validity of the Bioheat Equation

Pennes' bioheat equation is widely accepted and is almost universally employed in thermal modeling studies involving exposure of the human body to RFR. However, several important issues arise that bear on the validity of this approach.

Conceptual issues. Pennes' bioheat equation has been subject to a number of devastating critiques over the years. On face value, the equation violates the First Law of Thermodynamics - energy disappears into the heat sink term – and thus it cannot be a complete description of transfer of heat in a tissue.

That objection aside, narrative accompanying the bioheat equation typically states that the heat sink is provided by blood in the capillary bed, and the strength of the sink is proportional to the difference between local tissue temperature and mean arterial or core body temperature. Both of these assumptions are clearly wrong. In tissues, capillaries are thermally equilibrated with their surrounding tissue and cannot be a source of heat exchange. Rather, significant heat transfer between tissue and blood occurs at the level of ―thermally significant‖ vessels that are ca. 100 microns or more in diameter (e.g., Weinbaum et al., 1997). The ability of these vessels to remove heat from a region of tissue depends on their size, flowrate, and their thermal interaction. An example of the latter is countercurrent heat exchange, which reduces the ability of blood in the countercurrent vessels to carry heat away from a region of tissue. When a region of tissue is subject to heating from external sources, such as RFR, blood entering the region of interest will not be at core body temperature, but will have been heated before arriving at the point of interest.

These problems with the bioheat equation above have been extensively discussed, and indeed much research literature exists on the subject. Numerous attempts have been made to develop conceptually valid alternatives to the bioheat equation. One approach has been to use a modified heat conduction model, using an effective thermal conductivity to represent the effects of blood flow. Another approach has been to retain the bioheat equation, but adjusting the blood perfusion parameter m_b by an "efficacy function" in the range of 0.5-1.0 to take into account countercurrent heat exchange (Brinck & Werner, 1995).

Despite these objections, there is a broad consensus among investigators in bioheat transfer that Pennes' bioheat equation remains a useful approximation to bioheat transfer in tissue. For example, Kolios et al. (1998) reported that the bioheat equation provided a much better fit to the transient increase in temperature near a heat source in tissue than an alternate model (which used an effective thermal conductivity to describe the effects of blood flow). That study, however, involved heating under circumstances in which the temperature increase would not be expected to depend strongly on the value of blood perfusion parameter (e.g., transient heating from a small source).

Clearly, because of the variability in the blood flow in tissue, temperature calculations using the bioheat equation should be treated with caution when the results depend critically on

the blood perfusion parameter. Calculations based on the bioheat equation are likely to be <u>most accurate</u> when:

- The SAR pattern is localized (so that heat conduction effects dominate over blood perfusion effects)
- The exposure is short-term (so that the steady-state temperature profile, which is strongly influenced by blood perfusion, has not been reached)
- Experimental conditions are such that literature values of tissue blood flow are likely to be reasonable approximations for the situation at hand
- The local temperature increase is insufficient to produce large thermoregulatory changes in local blood flow.

7.3   Examples of Modeling the Thermal Response of the Human Body to RFR

A great many studies have been done, in which the thermal response of tissue to RFR has been calculated using a variety of thermal models. The approaches range from numerical solution of the bioheat equation using simplified homogeneous models of tissue, to solutions involving detailed anatomical models of the body including consideration of major blood vessels. For each application, a suitable choice has to be made to achieve a reasonable tradeoff between model accuracy and computational time and cost.

Various approaches include:

7.3.1   Numerical Solution of Bioheat Equation for Idealized Tissue Models

A good example of this approach is the study by Nelson et al. (2000), who modeled the head as a series of four concentric shells, representing scalp, skull, cerebrospinal fluid, and brain, and calculated its thermal response to millimeter wave irradiation at 100 GHz. The study included an analysis of the effects of varying several parameters of physiological interest (surface convection coefficient, evaporation rate of sweat, and blood flow to the scalp).

7.3.2   High Resolution Calculation of SAR Using Imaging Techniques and Use of Bioheat Equation to Predict Temperature

This approach has reached a high level of sophistication in hyperthermia treatment planning (including RF hyperthermia), where the need is to maintain the temperature of a treated region of tissue within narrowly fixed limits using external sources of power at SARs up to the range of hundreds of W/kg (e.g., Roemer, 1999).

As an example of this approach, Van de Kamer et al. (2002) obtained a high-resolution (mm) SAR distribution in the body and used Pennes' bioheat equation to predict temperature increase. This work was undertaken to explore the requirements for spatial resolution in SAR data for purposes of hyperthermia treatment planning. The authors concluded that small-scale variations in SAR due to dielectric inhomogeneities could lead to undesirable temperature elevations ("hot spots") in localized tissue regions, which cannot be predicted by SAR patterns computed with lower spatial resolution. For both the low and high resolution SAR patterns, the

213

investigators used the same thermal model (solving the bioheat equation without considering the effects of discrete blood vessels).

7.3.3 Hybrid Models Using the Bioheat Equation and Vessel-By-Vessel Analysis

Perhaps the most significant development in recent years has been the development of hybrid models, which combine a continuum approximation to heat transfer using the bioheat equation with a separate analysis of major blood vessels. For purposes of hyperthermia treatment planning, this work is motivated by the fact that tissue is cooled by blood flow in nearby major vessels, which reduces the effectiveness of hyperthermia treatment in those regions. This approach has been facilitated by new imaging techniques that allow investigators to quickly develop anatomical models of individual patients, including the anatomy of major blood vessels. Important work along these lines has been reported by groups led by Langendijk (e.g., Craciunescu et al., 2001).

As an example of this approach, Van Den Berg et al. (2006) obtained three dimensional blood perfusion maps in the prostates of patients, imaging blood vessels larger than about 1 mm. The investigators calculated the temperature increase in the prostate from RF hyperthermia using three different models with increasing amounts of information about blood perfusion, to study the effects of ―pre-heating" of blood entering the treatment area and factors leading to inadequate heating of a tumor in the prostate.

7.3.4 Thermal Models for the Body Incorporating Thermoregulation

A variety of models have been developed for predicting the thermal and physiological response of the body to RFR that incorporate thermoregulatory mechanisms. These are most appropriate for whole-body exposures to RFR in which thermoregulation is anticipated to play a significant role in the thermal response of the body, or where physiological endpoints (e.g., changes in sweat rate or skin blood flow) are of interest.

Over the years, a variety of lumped parameter models for the human thermoregulatory system have been developed, which can be adapted to modeling of the effects of exposure of the body to RFR. One approach along these lines was described by Foster and Adair (2004), who used an existing model for the human thermoregulatory system which was used to predict physiological changes in humans subject to whole-body RFR exposure described by Stolwijk & Hardy (1977). In this model, each segment of the body (limbs, head, and torso) is represented by four concentric compartments representing skin, fat, muscle, and body core. Heat exchange among the compartments and with the environment is governed by a set of rules intended to model the human thermoregulatory response. The compartments are homogeneous, i.e., the model uses a lumped parameter approach that considers only heat flow between compartments, not within individual compartments. This thermal model had been developed over a period of several years in a research program started by Stolwijk and Hardy (1977), who independently evaluated the several hundred parameters in the model by means of thermophysiological measurements on male college students. Foster and Adair (2004) found that this model, with no change in parameter values, did an excellent job of predicting thermophysiological responses of

214

a cohort of human volunteers who extended (45 minute) exposures to RFR at several frequencies, at levels considerably above present exposure guidelines.

Other investigators have incorporated detailed information about SAR distributions in the body with thermoregulatory mechanisms including exchange of heat with the environment. For example, Bernardi et al. (2003) described a hybrid model, using detailed calculations of SAR and calculation of local temperature increase (using the bioheat equation) together with a whole-body model for the human incorporating thermoregulatory mechanisms. Such models promise to provide information about both local increases in tissue temperature, and global physiological effects of the added heat to the body.

7.4   Thermal Wave Effects

The Fourier law of heat conduction (and by extension the bioheat equation) is unphysical, in that they imply that heat conduction occurs instantly after the temperature gradient is set up. In reality, there is a slight time delay after a temperature change is imposed before heat diffusion begins, which is characterized in terms of a wave equation. This time delay is described in terms of a thermal relaxation time of tissue (Shih et al., 2005). The value of the relaxation time is uncertain and somewhat controversial among different investigators; Shih et al. (2005) suggested that it is of the order of 1 s. Certainly, due to the structural complexity of tissue, the diffusion of heat is very complex over short time scales, and small scale temperature fluctuations will be present. While the effect is normally insignificant, it may affect thermal dose calculations for exposures with very abrupt heating at high SARs.

7.5   Thermal Injury of Tissue and Thermal Dose

The kinetics of thermal injury to tissue is characterized by an exponential relation between the time required to produce injury and the temperature at which the tissue is maintained, which can be interpreted in terms of the activation energy for protein denaturation. An Arrhenius plot for tissue damage shows a breakpoint at about 43.5 $^{\circ}$C for human tissues which has been interpreted as reflecting the buildup of thermal tolerance during long heating times below this temperature (Dewhirst et al., 2003). This approach leads to the definition of the thermal isoeffective dose, which allows investigators to relate the effects of different exposures to RFR resulting in different temperature-time patterns.

In a widely cited paper, Sapareto and Dewey (1984) proposed a measure of thermal dose to tissue, in terms of a cumulative number of minutes at which the tissue is held at 43 $^{\circ}$C. The cumulative equivalent minutes, CEM 43 $^{\circ}$C, is defined as

$$\text{CEM 43 } ^{\circ}\text{C} = \frac{t}{60} R^{43-T}$$
$$= \frac{1}{60} \int R^{43-T(t)} dt \tag{19}$$

where t is the time in seconds. The second expression above would be used if the temperature varies with time. In this approach, CEM 43 ^oC represents the entire thermal history of the exposure. A typical value of R for human tissue is 0.23 below and 0.43 above the breakpoint temperature of 43 ^oC. This expression gives the equivalent number of minutes in which tissue must be held at 43 ^oC to produce the same thermal damage as produced by exposure for time t at temperature T. The thermal dose, as opposed to SAR or temperature increase, is a biologically meaningful measure of exposure, at least for producing thermal damage to tissue.

Dewhirst et al. (2003) present an extensive table of values of CEM43 associated with thermal damage to tissue. While the threshold for thermal damage varies with animal model, values of CEM43 exceeding 10 (minutes) have been reported for producing thermal injury in a number of different animal tissues. Tissues characteristically show very sharp thresholds in CEM43 ^oC for producing thermal damage. For example, if 60 minutes at 43.5 ^oC is needed to produce complete necrosis in ear skin, a 30% reduction in heating time will completely avoid the injury (Dewhirst et al., 2003). While sparse data are available for thresholds for thermal damage to human tissues, it seems clear that RFR exposure leading to small (<1 minute) values of CEM43 ^oC present negligible risk of thermal injury.

7.6   Discussion

This chapter considers models for predicting the thermal response of the body to exposure to RFR, focusing on applications based on the bioheat equation. While thermal models clearly succeed, at some level, in predicting the thermal response of the body to RFR, the approach is not rigorous and significant issues can arise about the validity of such models.

7.6.1   Choice of Model

The basic principles of heat transfer in tissue are well known. However, convective heat transfer due to blood perfusion takes place at the level of thermally significant (> 100 μm diameter) blood vessels, which are numerous and complex in geometry. A rigorous analysis that explicitly considers all such vessels in the body would be impossible in any practical sense. Consequently, something less than a full scale model is needed. The issue then becomes one of choosing an appropriate tradeoff of cost (computational effort and amount of data required) for accuracy and validity of the model. The following comments are based on suggestions by Suyama offered in a different context[2].

Choosing an appropriate model will depend on a variety of considerations that depends on the particular needs at hand. The model should provide an appropriate level of detail, both in terms of spatial and temporal resolution, to address the research questions at hand. For example, in a study involving thermoregulatory responses of humans to whole-body exposure to RFR at levels comparable to international exposure guidelines, it may not be necessary to know the detailed temperature distribution within the body, but only the total amount of heat generated in major regions of the body. It is seldom necessary to know the detailed temperature variations

---

[2] http://www.cs.memphis.edu/cec03bmc/M3/pose1.htm

over a cellular or subcellular distance scale in tissue (although that may be needed for situations involving RFR pulses of extreme peak power and low duty cycle).

Given the potentially immense investments required to develop detailed thermal models of the body, investigators would be well advised to begin with simple models and refine them only if preliminary results indicate the need for more detail or for more accurate simulations.

7.6.2 Validity of Model

Given the approximate nature of the bioheat equation, the question arises of the validity of heat transfer models based on this equation. The major issue is external validity, i.e., the ability of a thermal model to predict temperature increases that will be produced by RFR exposure in a variety of circumstances. This has two main components:

7.6.2.1 Correctness of Parameter Values

Thermal or thermoregulatory models of the body can depend on a large number (perhaps hundreds) of parameters, of which one group (blood perfusion parameters m_b) is both variable and uncertain. Investigators would be well advised to conduct a sensitivity analysis of their model, to ensure that the conclusions remain accurate given the anticipated level of uncertainty in the parameter values. Values of m_b taken from tables such as Table 7-1 or Appendix B below should be examined with particular care.

7.6.2.2 Experimental Testability

The external validity of a model depends on its ability to make accurate predictions under a variety of circumstances that may be different than those under which the model was developed in the first place. In this connection, it is worth noting that the vast majority of modeling efforts discussed above were in the forward direction only, i.e. the investigators calculated temperature increases using a variety of models on the basis of thermal parameters taken from the literature. Where it has been tested, the bioheat equation has been successful in predicting the increase in tissue temperature due to RFR exposure, but there will always be uncertainties as to the best values of the blood flow parameter m_b to use in any particular application.

The take-home lesson from this chapter is that thermal modeling, particularly when the need arises to include physiologically vital processes such as blood flow, is more complicated than dosimetric calculations of SAR. Engineers should avoid the temptation to consider the bioheat equation as a kind of fifth Maxwell's equation, and be aware that the parameter values used in the equation, particularly m_b, are subject to considerable uncertainty and variability. That said, thermal modeling has been highly successful for therapeutic applications of RFR and it can provide important insights into possible biological effects of exposure to this form of radiant energy.

7.7   References

Bernardi, P., Cavagnaro, M., Pisa, S. & Piuzzi, E. (2003). Specific absorption rate and temperature elevation in a subject exposed in the far-field of radio-frequency sources operating in the 10-900-MHz range. *IEEE Transactions Biomedical Engineering, 50*, 295-304.

Brinck, H. & Werner, J. (1995). Use of vascular and non-vascular models for the assessment of temperature distribution during induced hyperthermia. *International Journal of Hyperthermia*, *11*, 615-626.

Chato, J. C. (1985). Selected thermophysical properties of biological materials. In A. Shitzer & R. C. Eberhart (Eds.), *Heat Transfer in Medicine and Biology* (Vol. 2, App. 2, pp. 413-418). New York: Plenum.

Craciunescu, O. I., Raaymakers, B. W., Kotte, A. N., Das, S. K., Samulski, T. V., & Lagendijk, J. J. (2001). Discretizing large traceable vessels and using DE-MRI perfusion maps yields numerical temperature contours that match the MR noninvasive measurements. *Medical Physics, 28*, 2289-2296.

Dewhirst, M. W., Viglianti, B. L., Lora-Michiels, M., Hanson, M. & Hoopes, P. J. (2003). Basic principles of thermal dosimetry and thermal thresholds for tissue damage from hyperthermia. *International Journal of Hyperthermia, 19*, 267-294.

Foster, K. R., Kritikos, H. N., & Schwan H. P. (1978). Effect of blood flow and surface cooling on the microwave heating of tissue. *IEEE Transactions on Biomedical Engineering*, BME-*25*, 313- 316.

Foster, K. R., Lozano-Nieto, A., Riu, P. J., & Ely, T. S. (1998). Heating of tissue by microwaves: a model analysis. *Bioelectromagnetics*, *19*, 420-428.

Foster K. R. & Erdreich, L. S. (1999). Thermal models for microwave hazards, *Bioelectromagnetics*, *20*, Suppl. 4, 52-63.

Foster, K. R. & Adair, E. R. (2004). Modeling thermal responses in human subjects following extended exposure to radiofrequency energy. *Biomedical Engineering OnLine, 3*, 4. Retrieved April 27, 2009 from http://www.biomedical-engineering-online.com/content/3/1/4

Giering, K., Lamprecht, I., & Minet, O. (1996). Specific heat capacities of human and animal tissues. *Proceedings of SPIE, 2624*, 188-196.

Holmes, K. R. (1997). *Biological structures and heat transfer*. Allerton International Conference on Bioheat Transfer, Allerton, IL.

Kolios, M. C., Worthington, A. E., Sherar, M. D., & Hunt, J. W. (1998). Experimental evaluation of two simple thermal models using transient temperature analysis. *Physics in Medicine and Biology, 43*, 3325-40.

Lang, J., Erdmann, B., & Seebass, M. (1999). Impact of nonlinear heat transfer on temperature control in regional hyperthermia. *IEEE Transactions on Biomedical Engineering, 46*, 1129-38.

Nelson, D. A., Nelson, M. T., Walters, T. J., & Mason, P. A. (2000). Skin heating effects of millimeter-wave radiation – thermal modeling results. *IEEE Transactions on Microwave Theory and Techniques, 48*, 2111-2120.

Pennes, H. H. (1948). Analysis of tissue and arterial blood temperature in the resting forearm. *Journal of Applied Physiology, 1*, 93-122.

Roemer, R. B. (1999). Engineering aspects of hyperthermia. *Annual Review of Biomedical Engineering, 1*, 347–376.

Sapareto, S. A, & Dewey, W. C. (1984). Thermal dose determination in cancer therapy. *International Journal of Radiation Oncology • Biology • Physics, 10*, 787-800.

Shih, T. C., Kou, H. S., Liauh, C. T., & Lin, W. L. (2005). The impact of thermal wave characteristics on thermal dose distribution during thermal therapy: a numerical study. *Medical Physics, 32*, 3029-3036.

Stolwijk, J. A. J., & Hardy, J. D. (1977). Control of body temperature. In H. K. Douglas (Ed.), *Handbook of Physiology,* Section 9, 45-69. Bethesda, MD: American Physiological Society.

Van den Berg, C. A., Van de Kamer, J. B., De Leeuw, A. A., Jeukens, C. R., Raaymakers, B. W., van Vulpen, M, & Lagendijk, J. J. (2006). Towards patient specific thermal modeling of the prostate. *Physics in Medicine and Biology, 51*, 809-825.

Van de Kamer, J. B., van Vulpen, M., de Leeuw, A. A., Kroeze, H., & Lagendijk, J. J. (2002). CT-resolution regional hyperthermia treatment planning. *International Journal of Hyperthermia, 18*, 104-16.

Van Leeuwen, G. M., Lagendijk, J. J., Van Leersum, B. J., Zwamborn, A. P., Hornsleth, S. N., & Kotte, A. N. (1999). Calculation of change in brain temperatures due to exposure to a mobile phone. *Physics in Medicine and Biology, 44*, 2367-2379.

Walters, T. J., Blick, D. W., Johnson, L. R. , Adair, E. R. & Foster, K. R. (2000). Heating and pain sensations produced in human skin by millimeter waves: validation of a simple thermal model. *Health Physics, 78*, 259-267.

Weinbaum, S., Xu, L. X., Zhu, L., & Ekpene, A. (1997). A new fundamental bioheat equation for muscle tissue: Part I–Blood perfusion term. *Journal of Biomechanical Engineering, 119*, 278-288.

Yeung, C. J. & Atalar, E. (2001). A Green's function approach to local RF heating in interventional MRI. *Medical Physics, 28*, 826-832.

7.8   Appendices

From Holmes, K. R. (1997). Biological structures and heat transfer. Allerton International Conference on Bioheat Transfer, Allerton, IL. (Used by permission of K. R. Holmes)

7.8.1   Appendix A: Thermal Properties of Tissues

The following physiological properties were compiled by Professor Kenneth R. Holmes (krholmes@ux1.cso.uiuc.edu) and were published in part previously. The tabulation includes values for both the native thermal conductivity of biomaterials (Appendix A) and the blood perfusion rates for specific tissues and organs (Appendix B). Original sources are documented in the dedicated list of references at the end of each appendix. Knowledge of the perfusion behavior of tissues is important in that the flow of blood can have a direct quantitative effect on the temperature distribution within living tissue.

APPENDIX A

THERMAL CONDUCTIVITY DATA FOR SPECIFIC TISSUES AND ORGANS

FOR HUMANS AND OTHER MAMMALIAN SPECIES

Professor Kenneth R. Holmes

TISSUE		k (W/mK)	%H$_2$O	Reference
Kidney	whole (rabbit)	.502	81	6
	whole (rabbit)	.495		16
	whole (human)	.543	84	4
	cortex (rabbit)	.465 - .490 (n=7)	76.6 - 79.8	1
	cortex (dog)	.491		16
	cortex (human)	.499		16
	medulla (rabbit)	.502 - .544 (n=7)	82.0 - 86.0	1
	medulla (dog)	.507		16
	medulla (human)	.499		16
Aorta	human	.476 ± .041 (SD) (n=12)		2
Arterial plaque				
	fatty	.484 ± .044 (SD) (n=13)		2
	fibrous	.485 ± .022 (SD) (n=12)		2
	whole (human)	.492 ± .009 (SD) (n=10)		5
	plasma	.582		10
	plasma (human)	.570 ± .010 (SD) (n=10)		5
Spleen	(human)	.543	80	4
Liver	(rabbit)	.493	72	6
	(rat)	.498 - .528 (n=4)		3
	(sheep)	.495 ± .017 (SD) (n=9)		5
	(dog)	.550 ± .010 (SD) (n=7)		5
	(dog)	.574		11
	(pig)	.498		16
	(human)	.469		16
	(human)	.564	77	4
Heart	(rat)	.521 - .531 (n=2)		3
	(dog)	.527		11
	(dog)	.487		16

221

Muscle	(rat)	.505 - .530 (n=7)		3
	(cow)	.410 - .426		7
	(pig)	.518 - .618		7
	(pig)	.460		17
	(sheep)	$.478 \pm .019$ (SD) (n=10)		5
Fat (cow)		.185 - .233		7
	(cow)	.222		17
	(pig)	.317 - .402		7
	(pig)	.159		17
	blubber (Minke whale)	.200 - .280	3 - 30	8
	blubber (Harp seal)	$.190 \pm .010$		9
	(human)	.201 - .217		17
Brain	whole	.527	78	4
	cerebral cortex	.564	83	4
	cerebral cortex	.504		16
	white matter	.502	71	4
Tumor	periphery	.511		11
	core	.561		11
	colon cancer (human)	.545		16
Bone		.410 - .630		15
Skin		.210 - .410		15
	crocodile, middle of back	.432		12
	crocodile, tail, ventral	.334		12
	epidermis			
	foot pad (cat)	.116 - .290		13
	(hydrated)	.295 - .580		13
	elephant (freeze/thaw)	.475	62.5	14
	rhinoceros "	.452	60.1	14
	Giraffe (formalin fixed)	.442	60.0	14
	epidermis (human)	.209		17
	epidermis (pig)	.209		17
	dermis (human)	.293 - .322		17
Pure water		.627		17

$$c = [\%H_2O + 0.4 * (100 - \%H_2O)] * 41.9 \ \text{J/kg K} \qquad 4$$
$$\rho = 1.05(10^3) \ \text{kg/m}^3 \qquad 4$$

222

7.8.1.1 References to Appendix A

Balasubramaniam, T. A., & Bowman, H. F. (1977). Thermal conductivity and thermal diffusivity of biomaterials: A simultaneous measurement technique. *Journal of Biomechanical Engineering*, *99*, 148-154.

Chato, J. C. (1968). A method for the measurement of the thermal properties of biological materials. In J. C. Chato (Ed.), *Thermal Problems in Biotechnology*, ASME symposium series, American Society of Mechanical Engineers, New York.

Chato, J. C. (1990). Fundamentals of bioheat transfer. In M. Gautherie (Ed.), *Thermal Dosimetry and Treatment Planning* (p. 51). New York: Springer-Verlag.

Cohen, M. L. (1977). Measurement of the thermal properties of human skin. A review. *Journal of Investigative Dermatology*, *69*, 333-338, and its references.

Cooper, T. E., & Trezek, G. J. (1971). Correlation of thermal properties of some human tissue with water content. *Aerospace Medicine*, *42*, 24-27.

Drane, C. R. (1981). The thermal conductivity of the skin of crocodilians. *Comparative Biochemistry and Physiology, 68A*, 107-110.

Dumas, A. & Barozzi, G. S. (1984). Laminar heat transfer to blood flowing in a circular duct. *International Journal of Heat and Mass Transfer*, *27*, 391-398.

Grayson, J., (1952). Internal calorimetry in the determination of thermal conductivity and blood flow. *Journal of Physiology*, *118*, 54-72.

Holmes, K. R. Unpublished data.

Holmes, K. R. & Adams, T., (1975). Epidermal thermal conductivity and stratum corneum hydration in cat footpad. *American Journal of Physiology*, *228*, 1903-1908.

Holmes, K. R. & Chen, M. M. (1979). Local thermal conductivity of Para-7 fibrosarcoma in hamster. *1979 Advances in Bioengineering*, ASME, New York, NY, 147-149.

Holmes, K. R., Ryan, W., & Chen, M. M. (1983). Thermal conductivity and H_2O content in rabbit kidney cortex and medulla. *Journal of Thermal Biology*, *8*, 311-313.

Kvadsheim, P. H., Folkow, L. P. & Blix, A. S. (1994). A new device for measurement of the thermal conductivity of fur and blubber. *Journal of Thermal Biology*, *19*, 431-435.

Kvadsheim, P. H., Folkow, L. P., & Blix, A. S. (1996). Thermal conductivity of Minke whale blubber. *Journal of Thermal Biology*, *21*, 123-128.

Valvano, J. W., Allen, J. T., & Bowman, H. F. (1981). The simultaneous measurement of thermal conductivity, thermal diffusivity, and perfusion in small volumes of tissue. *ASME 81-WA/HT-21*.

Valvano, J. W., & Chitsabesan, B. (1987). Thermal conductivity and diffusivity of arterial wall and atherosclerotic plaque. *Lasers in Life Sciences*, *1*, 219-229.

Valvano, J. W., Cochran, J. R., & Diller, K. R. (1985). Thermal conductivity and diffusivity of biomaterials measured with self-heated thermistors. *International Journal of Thermophysics*, *6*, 301-311.

7.8.2 Appendix B. Blood perfusion

(1 ml/min/gm corresponds to 1.7 (10^{-5}) $m^3kg^{-1}sec^{-1}$)

BLOOD PERFUSION DATA FOR SPECIFIC TISSUES AND ORGANS

FOR HUMANS AND OTHER MAMMALIAN SPECIES

Professor Kenneth R. Holmes

ORGAN	BLOOD FLOW (ml/min/gm)	SPECIES (¶ unanesthetized)	Ref.
Brain	0.36 ± 0.04 (SE)	dog (n=11)	36
Brain	0.78 ± 0.06 (SE)	rat (n=7)	30
Brain	1.52 ± 0.23 (SE)	fetal sheep¶ (n=12)	32
Brain	0.82 ± 0.06 (SE)	neonatal sheep¶ (n=13)	37
Brain	0.64 ± 0.03 (SE)	sheep¶ (n=7)	37
Brain	1.14 ± 0.14 (SD)	rat¶ (12 mo old)(n=5)	33
Brain	0.65 ± 0.07 (SD)	rat (n=10)	33
Brain	1.31 ± 0.22 (SD)	rat¶ (24 mo old)(n=5)	33
Brain	0.43 ± 0.14 (SD)	rat (n=7)	33
Mean Cerebral	0.373 ± 0.062	dog	2
Mean Cerebral	0.491 ± 0.078	baboon	2
Cerebrum	0.48 ± 0.03	cat	18
Cerebrum	0.53 ± 0.06	cat	18
Cerebrum	0.32 ± 0.06	monkey	18
Cerebrum	0.39 ± 0.03	monkey	18
Cerebrum	0.79 ± 0.12	pig¶	19
Cerebrum	1.17 ± 0.11 (SE)	rat¶ (n=8)	31
Cerebrum	0.61 ± 0.06 (SE)	rat (n=7)	31
Cerebrum	0.72 ± 0.05 (SE)	rat (n=7)	31
Cerebrum	0.50 ± 0.04 (SE)	rat (n=7)	31
Cerebrum	0.60 ± 0.06 (SE)	cat (n=8)	34
Cerebrum	1.29 ± 0.03 (SE)	cat (n=8) (hypercapnic)	34
cerebral cortex	0.446 ± 0.061	dog	2
cerebral cortex	0.447 ± 0.036	dog	3
cerebral cortex	0.64 ± 0.05	cat	18
cerebral cortex	0.75 ± 0.11	cat	18
cerebral cortex	0.40 ± 0.11	monkey	18
cerebral cortex	0.50 ± 0.11	monkey	18
frontal cortex	1.06 ± 0.05	rat	4
parietal cortex	1.07 ± 0.05	rat	4
occipital cortex	0.98 ± 0.08	rat	4

225

cerebral white	0.240 ± 0.037	dog	2
cerebral white	0.305 ± 0.022	dog	3
cerebral white	0.20 ± 0.05	monkey	18
cerebral white	0.21 ± 0.06	monkey	18
cerebral white	0.29 ± 0.03	cat	18
cerebral white	0.20 ± 0.03 (SE)	cat (n=8)	34
cerebral white	0.35 ± 0.09 (SE)	cat (n=8) (hypercapnic)	34
White matter	0.164 ± 0.022	baboon	2
corpus callosum	0.249 ± 0.035	dog	3
corpus callosum	0.62 ± 0.03	rat	4
Grey matter	0.552 ± 0.077	baboon	2
cortical grey	0.87 ± 0.11 (SE)	cat (n=8)	34
cortical grey	1.94 ± 0.37 (SE)	cat (n=8) (hypercapnic)	34
caudate nucleus	0.88 ± 0.03	rat	4
caudate nucleus	0.65 ± 0.06	cat	18
caudate nucleus	0.87 ± 0.11	cat	18
caudate nucleus	0.39 ± 0.05	monkey	18
caudate nucleus	0.47 ± 0.05	monkey	18
caudate nucleus	0.85 ± 0.10 (SE)	cat (n=8)	34
caudate nucleus	1.31 ± 0.19 (SE)	cat (n=8) (hypercapnic)	34
Choroid plexus	4.18 ± 0.60 (SE)	neonatal sheep[¶] (n=13)	37
Choroid plexus	7.53 ± 1.11 (SE)	sheep[¶] (n=7)	37
Hypothalamus	1.03 ± 0.06	rat	4
Pituitary	1.08 ± 0.24 (SE)	neonatal sheep[¶] (n=13)	37
Pituitary	1.13 ± 0.16 (SE)	sheep[¶] (n=7)	37
Thalamus	0.92 ± 0.07	rat	4
thalamus-midbrain	0.62 ± 0.07 (SE)	cat (n=8)	34
thalamus-midbrain	1.64 ± 0.32 (SE)	cat (n=8) (hypercapnic)	34
Hippocampus	0.68 ± 0.06	rat	4
Cerebellum	0.63 ± 0.04	cat	18
Cerebellum	0.70 ± 0.07	cat	18
Cerebellum	0.60 ± 0.08 (SE)	cat (n=8)	34
Cerebellum	1.63 ± 0.31 (SE)	cat (n=8) (hypercapnic)	34
Cerebellum	0.40 ± 0.08	monkey	18
Cerebellum	0.50 ± 0.02	monkey	18
Cerebellum	0.78 ± 0.06	pig[¶]	19
Cerebellum	1.31 ± 0.19 (SE)	rat[¶] (n=8)	31
Cerebellum	1.02 ± 0.12 (SE)	rat (n=7)	31
Cerebellum	1.04 ± 0.08 (SE)	rat (n=7)	31
Cerebellum	0.78 ± 0.07 (SE)	rat (n=7)	31

226

Cerebellum	1.31 ± 0.19 (SE)	rat (n=8)	31
Cerebellum	1.02 ± 0.12 (SE)	rat (n=7)	31
Cerebellum	1.04 ± 0.08 (SE)	rat (n=7)	31
Cerebellum	0.78 ± 0.07 (SE)	rat (n=7)	31
Pons	0.50 ± 0.03 (SE)	cat (n=8)	34
Pons	1.18 ± 0.25 (SE)	cat (n=8) (hypercapnic)	34
Medulla	0.37 ± 0.06 (SE)	cat (n=8)	34
Medulla	1.07 ± 0.20 (SE)	cat (n=8) (hypercapnic)	34
Medulla	0.84 ± 0.04	rat	4
Brain stem	0.52 ± 0.03	cat	18
Brain stem	0.58 ± 0.03	cat	18
Brain stem	0.33 ± 0.06	monkey	18
Brain stem	0.36 ± 0.03	monkey	18
Brain stem	0.46 ± 0.06	pig	19
Brain stem	0.55 ± 0.05 (SE)	cat (n=8)	34
Brain stem	1.44 ± 0.28 (SE)	cat (n=8) (hypercapnic)	34
Spinal cord	0.22 ± 0.02	cat	18
Spinal cord	0.31 ± 0.03	cat	18
Spinal cord	0.20 ± 0.03	monkey	18
Spinal cord	0.21 ± 0.03	monkey	18
Nerve, sciatic	0.27 ± 0.03 (SE)	rat (n-14)	29
inner cortex	2.57 ± 0.22 (SE)	sheep (n=6)	40
inner cortex	4.38 ± 1.19	dog	11
inner cortex	3.35 ± 0.42	dog	3
inner cortex	3.96	dog	7
inner cortex	3.24 ± 0.004	rabbit	5
inner cortex	4.7 ± 0.4	rat	13
outer 1/4 cortex	4.24 ± 0.40	dog	12
next 1/4	6.24 ± 0.61	dog	12
next 1/4	3.55 ± 0.45	dog	12
inner 1/4	1.73 ± 0.13	dog	12
medulla	0.35 ± 0.09 (SE)	sheep (n=6)	40
medulla	0.77 ± 0.064	dog	3
outer medulla	1.2	human	6
outer medulla	1.30	dog	7
outer medulla	2.10 ± 0.28	dog	11
inner medulla	0.25	human	6
Adrenal gland	7.62 ± 2.55 (SE)	fetal sheep (n=12)	32

Kidney	3.018 ± 0.412 (SE)	dog (n=11)	36
Kidney	3.99 ± 0.88 (SD)	rat[¶] (12 mo old)(n=5)	33
Kidney	3.64 ± 0.92 (SD)	rat (n=10)	33
Kidney	4.82 ± 1.39 (SD)	rat[¶] (24 mo old)(n=5)	33
Kidney	2.31 ± 0.82 (SD)	rat (n=7)	33
Kidney	1.54 ± 0.12 (SE)	fetal sheep[¶] (n=12)	32
Kidney	3.00 ± 0.14 (SE)	neonatal sheep[¶] (n=13)	37
Kidney	4.19 ± 0.32 (SE)	sheep[¶] (n=7)	37
Kidney	4.32 ± 0.30	dog	3
Kidney	3.2 ± 0.3	rabbit	17
Kidney	2.80 ± 0.05	pig[¶]	19
Kidney	4.7 ± 0.3	rat	13
Kidney	5.55 (4.87-8.76)	rat (n=14)	26
Kidney	6.23 ± 0.49	rat (n=9)	27
Kidney	4.38 ± 0.51 (SE)	rat (n=7)	30
Kidney	4.38 ± 0.44 (SE)	rat (n=7)	30
Kidney	7.63 ± 0.46 (SE)	rat[¶] (n=8)	31
Kidney	6.16 ± 0.39 (SE)	rat (n=7)	31
Kidney	5.96 ± 0.42 (SE)	rat (n=7)	31
Kidney	5.46 ± 0.53 (SE)	rat (n=7)	31
whole cortex	4.0-5.0	human[¶]	6
whole cortex	3.63 ± 0.54 (range = 3.0-4.4)	pig	8
whole cortex	3.71 ± 0.284	pig (n=4)	25
whole cortex	4.69 ± 0.347	pig (n=6)	25
whole cortex	5.06 ± 0.251	pig (n=6)	25
whole cortex	3.25 ± 0.20 (SE)	sheep[¶] (n=6)	40
outer cortex	3.81 ± 0.23 (SE)	sheep[¶] (n=6)	40
outer cortex	6.32 ± 0.33	dog	3
outer cortex	7.56 ± 0.70	dog	11
outer cortex	4.62	dog	7
outer cortex	8.84 ± 0.014	rabbit	5
outer cortex	8.7 ± 0.6	rat	13
middle cortex	9.53 ± 0.013	rabbit	5

228

Adrenal gland	1.83 ± 0.12 (SE)	neonatal sheep (n=13)	37
Adrenal gland	1.99 ± 0.13 (SE)	sheep[¶] (n=7)	37
Adrenal gland	1.341 ± 0.297 (SE)	dog (n=11)	36

Muscle

skeletal	0.027 (average)	human[¶]	16
skeletal	0.12 ± 0.02 (SE)	neonatal sheep[¶] (n=13)	37
skeletal	0.04 ± 0.01 (SE)	sheep[¶] (n=7)	37
skeletal	0.18 ± 0.07 (SD)	rat[¶] (12 mo old)(n=5)	33
skeletal	0.03 ± 0.01 (SD)	rat (n=10)	33
skeletal	0.22 ± 0.12 (SD)	rat[¶] (24 mo old)(n=5)	33
skeletal	0.05 ± 0.02 (SD)	rat (n=7)	33
skeletal	0.39 ± 0.20 (SD)	rat (n=12)	41

resting thigh

1.5 cm depth	0.018 ± 0.011	human[¶]	14
3.0 cm depth	0.026 ± 0.013	human[¶]	14
resting thigh	0.020-0.022	human[¶]	15

vastus medialis

& triceps	0.14 ± 0.03	pig[¶]	19

gracilis	0.049 ± 0.064	dog	2

masseter	0.09 ± 0.01 (SE)	rat (n=7)	30

cremaster	0.16 ± 0.03 (SE)	rat (n=7)	30
cremaster	0.07 ± 0.018 (SE)	rat[¶] (n=8)	31
cremaster	0.06 ± 0.008 (SE)	rat (n=7)	31
cremaster	0.05 ± 0.013 (SE)	rat (n=7)	31
cremaster	0.04 ± 0.012 (SE)	rat (n=7)	31

diaphragm	0.93 ± 0.19 (SE)	rat[¶] (n=8)	31
diaphragm	0.22 ± 0.02 (SE)	rat (n=7)	31

229

diaphragm	0.24 ± 0.04 (SE)	rat (n=7)	31
diaphragm	0.35 ± 0.04 (SE)	rat (n=7)	31
diaphragm	0.144 ± 0.017 (SE)	dog (n=11)	36
rectus abdominus	0.18 ± 0.029 (SE)	rat[¶] (n=8)	31
rectus abdominus	0.04 ± 0.008 (SE)	rat (n=7)	31
rectus abdominus	0.09 ± 0.025 (SE)	rat (n=7)	31
rectus abdominus	0.09 ± 0.027 (SE)	rat (n=7)	31
gastrocnemius	0.11 ± 0.022 (SE)	rat[¶] (n=8)	31
gastrocnemius	0.04 ± 0.003 (SE)	rat (n=7)	31
gastrocnemius	0.15 ± 0.084 (SE)	rat (n=7)	31
gastrocnemius	0.06 ± 0.019 (SE)	rat (n=7)	31
tibialis anterior	0.36 ± 0.068 (SE)	rat[¶] (n=8)	31
tibialis anterior	0.03 ± 0.004 (SE)	rat (n=7)	31

tibialis anterior	0.17 ± 0.11 (SE)	rat (n=7)	31
tibialis anterior	0.08 ± 0.03 (SE)	rat (n=7)	31
psoas	0.26 ± 0.034 (SE)	rat[¶] (n=8)	31
psoas	0.04 ± 0.004 (SE)	rat (n=7)	31
psoas	0.09 ± 0.037 (SE)	rat (n=7)	31
psoas	0.07 ± 0.022 (SE)	rat (n=7)	31
heart	3.72 ± 0.45 (SE)	fetal sheep[¶] (n=12)	32
heart	2.16 ± 0.23 (SE)	neonatal sheep[¶] (n=13)	37
heart	1.13 ± 0.09 (SE)	sheep[¶] (n=7)	37
heart	5.45 ± 0.59 (SE)	rat (n=7)	30
heart	5.31 ± 0.59 (SE)	rat[¶] (n=8)	31
heart	2.83 ± 0.60 (SE)	rat (n=7)	31
heart	2.23 ± 0.37 (SE)	rat (n=7)	31
heart	3.19 ± 0.55 (SE)	rat (n=7)	31
heart	6.61 ± 2.20 (SD)	rat[¶] (12 mo old)(n=5)	33
heart	5.45 ± 1.62 (SD)	rat (n=10)	33
heart	8.66 ± 2.74 (SD)	rat[¶] (24 mo old)(n=5)	33
heart	3.67 ± 1.03 (SD)	rat (n=7)	33
right ventricle	0.92 ± 0.12	pig[¶]	19
left ventricle	1.45 ± 0.09	pig[¶]	19
left ventricle	1.58 ± 0.13	dog	20
left ventricle	1.09 ± 0.35	dog	21
left ventricle	0.61 ± 0.41	dog	22
left ventricle	0.88 ± 0.14	dog	23
epicardium	0.89 ± 0.14	dog	24
epicardium	0.86 ± 0.14	dog	24
endocardium	1.14 ± 0.18	dog	24
endocardium	1.08 ± 0.18	dog	24
GI			
intestine	0.47 ± 0.05 (SE)	fetal sheep[¶] (n=12)	32
intestine	0.389 ± 0.04	dog	3

tract	2.05 ± 0.25	rat[1] (n=8)	31
tract	1.31 ± 0.11	rat (n=7)	31
tract	1.26 ± 0.09	rat (n=7)	31
tract	1.19 ± 0.14	rat (n=7)	31
stomach	1.27 ± 0.21 (SE)	rat[1] (n=8)	31
stomach	0.46 ± 0.04 (SE)	rat (n=7)	31
stomach	0.53 ± 0.05 (SE)	rat (n=7)	31
stomach	0.52 ± 0.07 (SE)	rat (n=7)	31
stomach	1.31 ± 0.30 (SD)	rat[1] (12 mo old)(n=5)	33
stomach	0.55 ± 0.21 (SD)	rat (n=10)	33
stomach	1.50 ± 0.45 (SD)	rat[1] (24 mo old)(n=5)	33
stomach	0.42 ± 0.21 (SD)	rat (n=7)	33
stomach	0.53 ± 0.26 (SD)	dog (n=12)	39

duodenum	1.11 ± 0.46 (SD)	dog (n=12)	39
duodenum	0.901 ± 0.132 (SE)	dog (n=11)	36
duodenum	3.63 ± 0.70 (SD)	rat[¶] (12 mo old)(n=5)	33
duodenum	2.33 ± 0.89 (SD)	rat (n=10)	33
duodenum	3.31 ± 0.64 (SD)	rat[¶] (24 mo old)(n=5)	33
duodenum	2.00 ± 0.76 (SD)	rat (n=7)	33
jejunum	0.642 ± 0.086 (SE)	dog (n=11)	36
jejunum	0.263 ± 0.034 (SE)	cat (n=12	35
ileum	0.498 ± 0.083 (SE)	dog (n=11)	36
small bowel	1.00 ± 0.45 (SD)	dog (n=12)	39
small bowel	2.09 ± 0.17 (SE)	neonatal sheep[¶] (n=13)	37
small bowel	0.81 ± 0.06 (SE)	sheep[¶] (n=7)	37
small bowel	2.81 ± 0.46 (SE)	rat[¶] (n=8)	31
small bowel	1.73 ± 0.18 (SE)	rat (n=7)	31
small bowel	1.67 ± 0.13 (SE)	rat (n=7)	31
small bowel	1.52 ± 0.20 (SE)	rat (n=7)	31
cecum	1.89 ± 0.19 (SE)	rat[¶] (n=8)	31
cecum	1.52 ± 0.08 (SE)	rat (n=7)	31
cecum	1.51 ± 0.15 (SE)	rat (n=7)	31
cecum	1.55 ± 0.22 (SE)	rat (n=7)	31
colon	1.24 ± 0.57 (SD)	dog (n=12)	39
colon	0.711 ± 0.065 (SE)	dog (n=11)	36
large bowel	0.92 ± 0.06 (SE)	neonatal sheep[¶] (n=13)	37
large bowel	0.55 ± 0.09 (SE)	sheep[¶] (n=7)	37
large bowel	1.33 ± 0.29 (SE)	rat[¶] (n=8)	31
large bowel	0.66 ± 0.09 (SE)	rat (n=7)	31
large bowel	0.59 ± 0.07 (SE)	rat (n=7)	31
large bowel	0.70 ± 0.13 (SE)	rat (n=7)	31

233

Pancreas	0.008-0.016	dog	1
Pancreas	0.545 ± 0.070 (SE)	dog (n=11)	36
Pancreas	0.652 ± 0.26 (SD)	dog (n=12)	39
Liver			
hep art. + portal	2.65 ± 0.530	pig (n=4)	25
hep art. + portal	2.53 ± 0.184	pig (n=6)	25
hep art. + portal	3.17 ± 0.228	pig (n=6)	25
hep art. + portal	1.40 ± 0.15 (SE)	rat[¶] (n=8)	31
hep art. + portal	1.19 ± 0.07 (SE)	rat (n=7)	31
hep art. + portal	1.22 ± 0.09 (SE)	rat (n=7)	31
hep art. + portal	1.25 ± 0.16 (SE)	rat (n=7)	31
via portal vein	1.25	rat	25
via portal vein	1.19 ± 0.12 (SE)	rat[¶] (n=8)	31
via portal vein	0.98 ± 0.05 (SE)	rat (n=7)	31
via portal vein	0.98 ± 0.10 (SE)	rat (n=7)	31
via portal vein	0.93 ± 0.12 (SE)	rat (n=7)	31
Prostate	0.18 ± 0.02	rat (n=9)	27
Prostate	0.31-0.79	dog (n=11)	38
Bone			
Femur	0.096 ± 0.039	rat	9
Tibia	0.083 ± 0.032	rat	9
Femur	0.14 ± 0.01	pig[¶]	19
Skin	0.20 ± 0.02 (SE)	neonatal sheep[¶] (n=13)	37
Skin	0.09 ± 0.01 (SE)	sheep[¶] (n=7)	37
Skin	0.18 ± 0.03 (SE)	rat[¶] (n=8)	31
Skin	0.12 ± 0.03 (SE)	rat (n=7)	31
Skin	0.15 ± 0.02 (SE)	rat (n=7)	31
Skin	0.17 ± 0.02 (SE)	rat (n=7)	31
Skin			
in the cold	approx. 0.02	human forearm[¶]	10

234

via hepatic art.	0.24 ± 0.04	pig	3
via hepatic art.	0.22 ± 0.04	pig[¶]	19
via hepatic art.	0.15 ± 0.03	rat (n=9)	27
via hepatic art.	0.22 ± 0.05 (SE)	rat[¶] (n=8)	31
via hepatic art.	0.21 ± 0.05 (SE)	rat (n=7)	31
via hepatic art.	0.23 ± 0.02 (SE)	rat (n=7)	31
via hepatic art.	0.31 ± 0.07 (SE)	rat (n=7)	31
via hepatic art.	0.10 ± 0.05 (SE)	fetal sheep[¶] (n=12)	32
via hepatic art.	0.10 ± 0.03 (SE)	neonatal sheep[¶] (n=13)	37
via hepatic art.	0.14 ± 0.05 (SE)	sheep[¶] (n=7)	37
via hepatic art.	0.02 ± 0.02 (SD)	rat[¶] (12 mo old)(n=5)	33
via hepatic art.	0.07 ± 0.04 (SD)	rat (n=10)	33
via hepatic art.	0.03 ± 0.01 (SD)	rat[¶] (24 mo old)(n=5)	33
via hepatic art.	0.11 ± 0.07 (SD)	rat (n=7)	33
via hepatic art.	0.178 ± 0.050 (SE)	dog (n=11)	36
via hepatic art.	0.31 ± 0.30 (SD)	rabbit (n=5)	42
Spleen	1.46 ± 0.14	dog	3
Spleen	1.381 ± 0.199 (SE)	dog (n=11)	36
Spleen	3.60 ± 0.16	pig[¶]	19
Spleen	1.64 ± 0.14 (SE)	rat[¶] (n=8)	31
Spleen	1.52 ± 0.22 (SE)	rat (n=7)	31
Spleen	2.35 ± 0.49 (SE)	rat (n=7)	31
Spleen	2.01 ± 0.22 (SE)	rat (n=7)	31
Spleen	5.43 ± 1.13 (SE)	fetal sheep[¶] (n=12)	32
Spleen	4.03 ± 0.73 (SE)	neonatal sheep[¶] (n=13)	37
Spleen	1.88 ± 0.27 (SE)	sheep[¶] (n=7)	37
Spleen	1.51 ± 0.54 (SD)	rat[¶] (12 mo old)(n=5)	33
Spleen	0.75 ± 0.37 (SD)	rat (n=10)	33
Spleen	1.13 ± 0.38 (SD)	rat[¶] (24 mo old)(n=5)	33
Spleen	0.40 ± 0.15 (SD)	rat (n=7)	33
Prostate	0.17 (.11-.21)	rat (n=14)	26

thermoneutral	0.04-0.05	human forearm[¶]	10
hyperthermic	near or >0.20	human forearm[¶]	10
thermoneutral	0.9 ± 0.09	pig[¶]	19
Subcutaneous tissue	0.48 ± 0.15	rat (n=29)	41
Tumor	0.25 ± 0.11	rat (n=12)	41
	1.79 ± 0.70	rabbit (n=5)	42
Fat	0.21 ± 0.06	pig[¶]	19
Testes	0.45 ± 0.06	rat (n=9)	27
Lungs	1.14 ± 0.14 (SE)	fetal sheep[¶] (n=12)	32

7.8.2.1   References to Appendix B

Andersson, L., Dahn, I., Nelson, K. E., & Norgren, A. (1967). Method for measuring prostate blood flow with Xenon[133] in the dog. *Investigative Urology, 5*, 140-148.

Baer, R. W., Payne, B. D., Verrier, E. D., Vlahakes, G. J., Molodowitch, D., Uhlig, P. N., & Hoffman, J. I. E. (1984). Increased number of myocardial blood flow measurements with radionuclide-labeled microspheres. *American Journal of Physiology*, *246*, H418-434.

Baumbach, G. I., & Heistad, D. D. (1985). Heterogeneity of brain blood flow and permeability during acute hypertension. *American Journal of Physiology*, *249*, H629-H637.

Bhattacharya, J., & Beilin, L. J. (1980). Left ventricular cannulation for microsphere estimation of rabbit renal blood flow. *American Journal of Physiology*, *238*, H736-H739.

Burton, M. A., Kelleher, D. K., Gray, B. N., & Morgan, C. K. (1990). Effect of temperature on liver tumour blood flow. *European Journal of Cancer, 26*, 999.

Capurro, N. L., Goldstein, R. E., Aamodt, R., Smith, H. J., & Epstein, S. E. (1979). Loss of microspheres from ischemic canine cardiac tissue. *Circulation Research*, *44*, 223-227.

Crandell, S. S., Fisher, D. J., & Morriss, F. H., Jr. (1985). Effects of ovine maternal hyperglycemia on fetal regional blood flows and metabolism. *American Journal of Physiology*, *249*, E454-E460.

Crystal, G. J., Boatwright, R. B., Downey, H. F., & Bashour, F. A. (1979). Shunting of microspheres across the canine coronary circulation. *American Journal of Physiology*, *236*, H7-H12.

Damber, J.-E., Bergh, A., Daehlin, L., Petrow, V., & Landstrom, M. (1992). Effects of 6-methylene progesterone on growth, morphology, and blood flow of the Dunning R3327 prostatic adenocarcinoma. *The Prostate*, *20*, 187-197.

Drake, A. J., & Noble, M. I. M. (1976). Myocardial blood flow measured by carbonized microspheres before and after cardiac denervation. *9th European Conference on Microcirculation, Antwerp, Bibliotheca Anatomica*, *15*, 53-56.

Fan, F-C., Schuessler, G. B., Chen, R. Y. Z., & Chien, S. (1979). Determinations of blood flow and shunting of 9- and 15- atmospheres in regional beds. *American Journal of Physiology*, *237*, H25-H33.

Goodhead, B. (1969). Accute pancreatitis and pancreatic blood flow. *Surgery, Gynecology & Obstetrics*, *129*, 331-340.

Gores, G. J., Kost, L. J., & LaRusso, N. F. (1986). The isolated perfused rat liver: conceptual and practical considerations. *Hepatology*, *6,* 511-517.

Gyrd-Hansen, N. (1968). Renal clearances in pigs. *Acta Veterinaria Scandinavica*, *9*, 183-198.

Haws, C. W., & Heistad, D. D. (1984). Effects of nimodipine on cerebral vasoconstrictor responses. *American Journal of Physiology*, *247*, H170-H176.

Hernandez, E. J., Hoffman, J. K., Fabian, M., Siegel, J. H., & Eberhart, R. C. (1979). Thermal quantification of regional myocardial perfusion and heat generation. *American Journal of Physiology*, *236*, H345-H355.

Johnson, J. M., Brengelmann, G. L., Hales, J. R. S., Vanhoutte, P. M., & Wenger, C. B. (1986). Regulation of the cutaneous circulation. *Federation Proceedings*, *45*, 2841-2850.

Jonsson, O., Widmark, A., Grankvist, K., Damber, J.-E, & Henriksson, R. (1992). Effects of clonidine-induced hypertension on blood flows in prostatic adenocarcinoma (Dunning R3327) and normal tissue. *The Prostate*, *20*, 225-232.

Kapin, M. A., & Ferguson, J. L., (1985). Hemodynamic and regional circulatory alterations in dog during anaphylactic challenge. *American Journal of Physiology*, *249*, H430-H437.

Keele, C. A., & Neil, E. (Eds.) (1971). *Samson Wright's Applied Physiology* (12th ed.) (p. 62). London: Oxford Press.

Koehler, R. C., Traystman, R. J., & Jones, Jr., M. D., (1985). Regional blood flow and O_2 transport during hypoxic and CO hypoxia in neonatal and adult sheep. *American Journal of Physiology*, *248*, H118-H124.

Kvietys, P. R., Shepherd, A. P., & Granger, D. N. (1985). Laser-Doppler, H_2 clearance, and microsphere estimates of mucosal blood flow. *American Journal of Physiology*, *249*, G221-G227.

Lassen, N. A., Lindbjerg, J., & Munck, O. (1964). Measurement of bloodflow through skeletal muscle by intramuscular injection of xenon-133. *Lancet*, *1*, 686-689.

Lovell, R. A. (1989). The toxicity of microcystin-LR in swine and mice. PhD Thesis. University of Illinois.

Marcus, M. L., Bischof, C. J., & Heistad, D. D. (1981). Comparison of microsphere and xenon-133 clearance method in measuring skeletal muscle and cerebral blood flow. *Circulation Research*, *48*, 748-761.

Mattsson, J., Alpsten, M., Appelgren, L., & Peterson, H-I, (1980). Influence of Noradrenalin on local tumor blood flow. *European Journal of Cancer, 16*, 99-102.

Mimran, A., & Casellas, D. (1979). Microsphere size and determination of intrarenal blood flow distribution in the rat. *Pflugers Archive*, *382*, 233-240.

Mraovitch, S., Iadecola, C., & Reis, D. J. (1983). Vasoconstriction unassociated with metabolism in cerebral cortex elicited by electrical stimulation of the parabrachial nucleus in rat. *Journal of Cerebral Blood Flow & Metabolism*, *3*(Suppl. 1), S196-S197.

Neiberger, R. E., & Passmore, J. C. (1979). Effects of dopamine on canine intrarenal blood flow distribution during hemorrhage. *Kidney International*, *15*, 219-226.

Ott, C. E., & Vari, R. C. (1979). Renal autoregulation of blood flow and filtration rate in the rabbit. *American Journal of Physiology*, *237*, F479-F482.

Passmore, J. C., Neiberger, R. E., & Eden, S. W. (1977). Measurement of intrarenal anatomic distribution of krypton-85 in endotoxic shock in dogs. *American Journal of Physiology*, *232*, H54-58.

Proctor, K. G. & Busija, D. W. (1985). Relationships among arteriolar, regional, and whole organ blood flow in cremaster muscle. *American Journal of Physiology*, *249*, H34-H41.

Rappaport, A. M., Kawamura, T., Davidson, J. K., Lin, B. J., Ohira, S., Zeigler, M., Coddling, J. A., Henderson, M. J., & Haist, R. E. (1971). Effects of hormones and blood flow on insulin output of isolated pancreas in situ. *American Journal of Physiology*, *221*, 343.

Reddy, V. K., Zamora, C. S., Frandle, K. A., & Samson, M. D., (1981). Regional renal blood flow in ewes. *American Journal of Veterinary Research*, *42*, 1802-1803.

Rundquist, I., Smith, Q. R., Michel, M. E., Ask, P., Öberg, P. A., & Rapoport, S. I. (1985). Sciatic nerve blood flow measured by laser Doppler flowmetry and [^{14}C] iodoantipyrine. *American Journal of Physiology*, *248*, H311-H317.

Schoutens, A., Bergmann, P., & Verhas, M. (1979). Bone blood flow measured by 85 Sr microspheres and bone seeker clearances in the rat. *American Journal of Physiology*, *236*, H1-H6.

Sekins, K. M., Dundore, D., Emery, A. F., Lehmann, J. F., McGrath, P. W., & Nelp, W. B. (1980). Muscle blood flow changes in response to 915 MHz diathermy with surface cooling as measured by Xe^{133} clearance. *Archives of Physical Medicine and Rehabilitation*, *61*, 105-113, 1980.

Seyde, W. C., McGowan, L., Lund, N., Duling, B. & Longnecker, D. E. (1985). Effects of anesthetics on regional hemodynamics in normovolemic and hemorrhaged rats. *American Journal of Physiology*, *249*, H164-H173.

Thurau, K., & Levine, D. Z. (1971). The Renal Circulation. Chapter 1. In C. Rouiller & A. F. Muller (Eds.), *The Kidney Morphology, Biochemistry, Physiology* (pp. 1-70). New York: Academic Press.

Tranquilli, W. J., Parks, C. M., Thurmon, J. C., Benson, G. J., Koritz, G. D., Manohar, M., & Theodorakis, M. C. (1982). Organ blood flow and distribution of cardiac output in nonanesthetized swine. *American Journal of Veterinary Research*, *43*, 895-897.

Tuma, R. F., Irion, G. L., Vasthare, U. S., & Heinel, L. A. (1985). Age-related changes in regional blood flow in the rat. *American Journal of Physiology*, *249*, H485-H491.

Youichi, A., Okahara, T., Kishimoto, T., Yamamoto, K., & Ueda, J. (1973). Relationship between intrarenal distribution of blood flow and renin secretion. *American Journal Physiology*, *225*, 319-323.

239

Radio Frequency Radiation Dosimetry Handbook
(Fifth Edition)

Chapter 8.   Responses to RF Overexposure

Marvin C. Ziskin, M.D.
Director, Center for Biomedical Physics
Professor, Radiology & Medical Physics
Temple University School of Medicine, Philadelphia, PA 19140

ziskin@temple.edu

8.1   Introduction

RF is the abbreviation for radio frequency, and RFR is the abbreviation for radio frequency electromagnetic radiation. RF includes those frequencies between 3 kHz and 300 GHz. The corresponding wavelengths are 100,000 m and 1 mm respectively. People are exposed to RFR from many sources in their daily lives. These sources include radio, television, microwave ovens, radar, and cellular telephones. In medicine, exposures occur in the use of RFR emitting sources such as diathermy machines, patient monitors, MRI machines, electrocautery, and other surgical devices.

This chapter summarizes the biological consequences of exposure to radio frequency electromagnetic energy. It also provides guidance for the proper management of overexposures. An overexposure is defined as an exposure to radio frequency radiation in excess of national safety limit standards. This chapter is written from a physician's point of view.

8.2   Safety Concerns of Electromagnetic Radiation

There are a number of general comments that need to be made concerning the safety of electromagnetic radiation. Highly energetic forms, such as x-rays, are capable of dislodging electrons from atoms. It is this ionizing effect that can alter DNA and produce genetic mutations and other harmful effects. Furthermore, there is no threshold for this type of damage. That is, any amount of ionizing radiation is considered harmful. On the other hand, radio frequency electromagnetic waves do not possess sufficient energy to dislodge electrons and therefore do not pose the ionizing threat of x-rays.

From a medical point of view, the non-ionizing nature of RFR is of utmost importance. RFR exposures do not cause the ionization, free radical production, and subsequent chromosomal damage, which may lead to cancer. Furthermore, there is no convincing evidence suggesting that RFR by any mechanism increases the risk of developing cancer. Whereas the effects of exposure to ionizing radiation are cumulative, this is not true for RFR. That is,

exposures to RFR at levels that individually do not cause any damage will not cause any damage even if repeated multiple times. Furthermore, whereas damage from ionizing radiation has no threshold, all established adverse biological effects from RFR have thresholds below which no harm results regardless of exposure duration.

Radio frequency electromagnetic waves, although non-ionizing, can cause significant biologic damage if the power density is sufficiently high and the exposure duration is sufficiently long. For example, the common microwave oven operating at 2.45 GHz at power densities of 800 W/cm^2 is capable of cooking tissue. Electromagnetic waves at frequencies lower than that of millimeter waves penetrate deeply into the body and cause heating of the entire body. However the penetration of millimeter waves is limited to just the outer layer of the skin, and heating, unless prolonged, remains very superficial.

Nearly all of the known biological effects of radio frequency waves are thermal in nature. That is, the damage results from the magnitude and duration of the temperature elevation induced by absorption of the electromagnetic energy. Absorption of radiated energy depends upon the frequency and tissue properties, and has been studied extensively by many researchers including Dr. William Guy of the University of Washington, Dr. Om Gandhi of the University of Utah, Dr. Kenneth Foster of the University of Pennsylvania, and a number of excellent scientists in military laboratories. The biological effects for both man and animals are well understood, and the scientific literature is extensive. Excellent reviews can be obtained from the web sites of the IEEE Committee on Man and Radiation (IEEE-EMBS COMAR, n.d.), the World Health Organization (WHO, 1993), and the National Council on Radiation Protection and Measurements (NCRP, 1986). A particularly good and comprehensive review is included in the recently published IEEE Standard for Safety Levels with Respect to Human Exposure to Radio Frequency Electromagnetic Fields, 3 kHz to 300 GHz (IEEE Standard C95.1, 2005a). The journal *Bioelectromagnetics* has dedicated a supplement to presenting twelve ―white papers" authoritatively covering many aspects of biological responses to RF radiation (Chou & D'Andrea, 2003; Adair & Black, 2003; D'Andrea, Adair, & de Lorge, 2003; Elwood, 2003; Heynick et al., 2003; Elder, 2003a; D'Andrea, Chou, Johnston, & Adair, 2003; Elder, 2003b; Elder & Chou, 2003; Heynick & Merritt, 2003; Black & Heynick, 2003; Meltz, 2003).

8.3 Radio frequency Radiation Injuries

All established adverse biological effects of RFR are due to heating of the body by the absorption of the incident energy. The resulting temperature elevation depends on how well the body can dissipate the excess heat. In this regard, humans have an excellent capability for maintaining thermal homeostasis. Nevertheless, it is possible in high intensity exposures, for the RFR-induced heating to exceed the body's ability to dissipate the heat, resulting in a temperature elevation capable of destroying tissue. Tissues affected by poor blood perfusion are particularly vulnerable. For example, because of the lack of any blood supply to the lens, cataracts can result from high intensity overexposures.

Temperature elevation, if sufficiently high, causes a number of well-known pathologic consequences. For example, at sustained temperatures above about 43 °C, proteins begin to

241

denature and coagulate. This can lead to cell membrane rupture and cell death. Temperatures above about 60 °C produce clinically recognizable burns. The amount of damage depends on the magnitude and the duration of the temperature elevation. The pathologic processes and histological appearances are similar for all burns. The major difference between ordinary burns and the thermal damage from RFR is in the distribution of the damage. In ordinary burns, heating occurs at the surface of the skin, which is an excellent thermal barrier to deeper penetration. Therefore, the primary site of damage lies within the skin close to the body surface. However, at some frequencies RF energy can penetrate deeper into the body, and heating can occur at places where conventional surface heating cannot reach. In fact, internal heating can be greater than at the skin surface. Medical diathermy is based on the ability of RFR to penetrate deeply and heat internal structures, such as muscles, ligaments, and tendons, without excessive heating of the skin.

8.4   Burns and Pain Thresholds

The temperature at the surface of the skin varies somewhat depending on the ambient temperature. Under typical room temperatures of 22–25 °C, the temperature at the skin surface will be about 34 °C. The ability to sense changes in skin temperature depends on the size and location of the exposed area and on the magnitude and rate of temperature rise. Under ideal conditions one can sense temperature changes as small as 1 °C or less. A change of several degrees is a common experience in our daily lives and creates no problem. However, if the temperature rises 10 °C or more, pain ensues. Numerous studies have shown that the threshold for feeling pain from surface heating is 44-45 °C (Blick et al., 1997; Walters et al., 2000). The higher the temperature elevation the greater is the pain, and if sufficiently high, tissue damage occurs.

The amount of tissue damage depends on the magnitude and duration of the temperature elevation. The threshold for first-degree burns is 55-60 °C. First-degree burns are limited to just the outer layer of the skin, the epidermis, and are accompanied by reddening of the skin and some swelling. The threshold for second-degree burns is 60-65 °C. Second-degree burns affect all layers of the skin and are accompanied with intense pain and blister formation. Temperatures of 70 °C and above lead to third-degree burns which cause extensive damage to the entire skin and underlying muscle, fat, and possibly bone. Affected areas appear charred black, and if greater than 50% of the body surface third-degree burns can be lethal.

First-degree burns heal rapidly without scarring. Second-degree burns heal but may leave some scarring. Third-degree burns are a very serious medical problem. Healing is difficult and often complicated by infection. Third-degree burns usually require skin grafting. There may be extensive scarring with muscle and tendon contractures limiting mobility.

Studies have shown that there are no significant differences in the above thresholds because of gender or race. Furthermore, the above damage thresholds are found to be essentially the same for mice, rats, pigs, as well as man. Studies using rats showed that there were no significant differences between young and old rats in the threshold for tissue damage, but young rats suffered more injury from the most severe exposures.

242

The above analysis shows that there is a significant safety margin between skin temperatures causing pain and those causing burning. Temperatures between 45 and 55 °C will cause significant pain, but unless prolonged should not cause any damage to the skin. Newly developed non-lethal deterrent systems, utilizing high power millimeter waves, are designed to achieve this result. Because of the rapid superficial heating resulting from exposure to the millimeter wave beam, painful skin temperatures will develop within the first few seconds. By limiting the exposure intensity and duration to which any individual would be subjected, it should be possible to avoid injury.

8.5   Ocular Damage

The eye is vulnerable to various forms of radiation. Both ionizing and non-ionizing radiation, if sufficiently intense, can cause intraocular damage. The damage caused by radio frequency radiation results from the elevated temperature when the energy is absorbed by the intraocular tissues. In other parts of the body, there is a substantial blood flow that can effectively remove heat and minimize any increase in temperature. Within the eye, there is no blood flow surrounding the lens, and heat dissipation from this region is greatly diminished. Thermal buildup in the lens can lead to cell damage and cataract formation. Also vulnerable because of its exposed position is the cornea, the outermost covering of the eye consisting of a thin transparent layer of cells. Damage to the cornea, lens, or retina leads to visual impairment. Whereas, damage to the lens and retina tends to be permanent, damage to the cornea usually heals.

Because of the vulnerability of the eye to radiation, the effects of RF radiation on the eye has been studied intensively over many years. Studies of RF induced cataract formation have shown a threshold in rabbits of a specific absorption rate of >150 W/kg in rabbits producing a temperature elevation to 41 °C for a period of 30 minutes (Carpenter, 1979; Foster et al., 1986). Furthermore, near-field exposures producing cataracts were so thermally distressing that whole-body temperature of rabbits rose to lethal levels (Elder, 2003a). The thresholds for humans is believed to be higher, and would be expected to produce unacceptable pain and damage to other parts of the eye and face prior to cataract formation (IEEE COMAR, 2002).

A defect in retinal cone function was reported in a man exposed twice for 15 min to 6000 MHz while inspecting a satellite antenna (Lim et al., 1993). The exposures were sufficiently intense to cause facial erythema, eyelid burns, bilateral foreign body sensation and blurred vision, but no cataracts were reported. These observations support the conclusion that the high exposure levels required to produce cataracts in the human eye would cause undesirable effects on other parts of the eye and face.

Outstanding research on the effect of millimeter waves has been performed by Dr. John D'Andrea and his colleagues at the US Naval Health Research Center. They have clearly established what effects will be seen from high power millimeter exposures to the eye, as well as the thresholds for these effects. Of greatest interest was the effect of 94 GHz as this is the frequency that has been selected for use in a non-lethal deterrent device based on a high power

243

millimeter wave beam. An important reason for choosing 94 GHz is that its penetration into the body is only 0.3 mm (Pakhomov et al., 1998). It doesn't enter into the eye any further than the cornea, and thus the lens, retina, or other intraocular structures are not affected.

Because the amount of heating and potential damage depends on both exposure intensity and duration, the most pertinent physical quantity is energy fluence in units of joules per square centimeter (J/cm^2). The minimal intensity that can be sensed when the eye is exposed to 94 GHz energy is 0.003 J/cm^2 (at 4 mW/cm^2). This is very close to the 4.5 mW/cm^2 threshold for detection of this energy on the skin. The sensation felt at this threshold level is that of warmth, and corresponds to a temperature elevation of 0.1 °C. When the corneal temperature reaches 43 °C, the sensation becomes painful and an involuntary avoidance behavior sets in. This avoidance behavior consists of blinking, turning away from the source, and moving one's hands in front of his eyes. The threshold for the avoidance behavior is 0.4 J/cm^2. Blinking occurs in less than ¼ second. In order to cause corneal damage in an awake human, the corneal temperature would need to rise to 55 °C within this amount of time. The threshold for a minimal lesion is 5 J/cm^2. It consists of a small distinct swelling of the outermost layer of the cornea, and is reversible within 24-48 hours. The rapidity and effectiveness of the avoidance behavior has made it nearly impossible to cause corneal damage to unanesthetized mammals.   In anesthetized animals it was possible to produce irreversible corneal damage when the exposure exceeded 27.7 J/cm^2. This damage would lead to significant corneal scarring and some loss of vision (Chalfin et al., 2002; Foster et al., 2003).

Several studies have recently been performed to investigate whether the wearing of eyeglasses or contact lenses would create any special problem if an individual were exposed to a high power millimeter wave beam.

One investigation was conducted to evaluate what effects eyeglasses, binoculars, or night vision goggles may have on absorption from a 94-GHz beam. Particular attention was paid to the possibility of the production of hotspots by reflections from the eyewear and focusing of the beam on the face. Using human face molds of muscle simulating gel material, it was shown that all face shapes absorb and scatter millimeter waves somewhat differently, due mainly to the shape and size of the nose. However, temperature rise in all cases were very similar and none of the face shapes showed any distinct focusing of the beam or ―hot‖ spots caused by deflection of the beam any more than other shapes that were compared. When wearing no eyewear, it was observed that in all cases the highest temperature increase was located in the area of the cornea closest to the nose. When wearing night vision goggles and binoculars, the hottest spots were located outside the area of the eye, normally on the forehead or nose area. Overall, there was no unusual heating of the surface around the eye or face due to the eyewear and there was no indication of any focusing of the beam towards the area of the eye.

Other studies looked for any effect that the wearing of contact lenses might have on exposure to the eye from a millimeter wave beam. Anesthetized pigs and rhesus monkeys were used. At moderate exposure levels (6 J/cm^2), there were no significant differences or damage observed whether or not contact lenses were worn. At high exposure levels (12 J/cm^2), the heating of the pig eye was slightly greater when contact lenses were present, but the difference was not considered significant. The investigators concluded that, under the conditions of the

244

studies, the wearing of contact lenses during 94-GHz exposure does not pose a greater risk than not wearing contacts. In real life exposures it is expected that alert subjects would blink, close their eyes, and if not constrained would flee from the millimeter wave beam long before tissue damage could occur from heating whether contacts were worn or not.

In summary, 94-GHz exposures produce responses which are time and temperature dependent. Effects on the eye are highly dependent on energy density and, because the effective stimulus is joule heating, exposure duration is very important. The uncomfortable sensations produced by millimeter wave energy are closely tied to cornea and skin temperature. The above studies showed that wearing eyeglasses, contact lens, and other corrective eyewear should not significantly increase the risk of injury. Because of the innate protective spontaneous reactions, 94-GHz millimeter wave beams have a satisfactory margin of safety to prevent serious injury to the eye when utilized as a non-lethal deterrent.

8.6   Internal Organs

Human thermoregulation is well developed and internal temperature is maintained at its "normal" body temperature, which is normally at 37 °C. Body temperature may vary plus or minus 1 °C in a day, or slightly more under vigorous exercise or in febrile conditions. These physiological temperature variations are well handled by the body. Prolonged temperature elevations above 43 °C are dangerous in that they cause protein denaturation, and ultimately cell death. Internal vital organs, such as the brain, heart, liver, and kidneys can be damaged by whole-body heating that occurs from exposure to all RF frequencies except for millimeter waves. The temperature elevation and physiological responses to RF heating has been studied intensively by Dr. Eleanor Adair. She has shown conclusively that exposures to RF levels below national safety limits do not cause sufficient heating of internal organs to cause any damage (Adair & Black, 2003).

RF levels much higher than those permitted by national safety limits are capable of causing significant damage to internal organs. In order for damage to occur, sufficient energy has to reach these structures. The penetration of 94-GHz millimeter waves is so shallow that there is no possibility for the radiation to reach internal organs. The 94-GHz energy never gets beyond the outer layers of the skin. Nevertheless, the temperature of structures close to heated skin can be secondarily elevated by heat conduction through tissue. The amount of secondary heating depends on many factors. The most important are (1) the magnitude and duration of the elevated skin surface temperature, (2) the area of skin that is heated, (3) the distance of the internal structure from the skin surface, (4) blood flow, and (5) the type and amount of intervening tissue, especially fat. Subcutaneous fat is an excellent thermal insulator that serves to help maintain body temperature in both hot and cold climate environmental temperature extremes.

A millimeter wave based non-lethal deterrent system in operation can be expected to raise the skin surface temperature to the point where an individual feels sufficient pain that he will remove himself from the beam. At the millimeter wave intensities being considered, intolerable pain would occur in just a few seconds. Away from the beam the temperature quickly returns to near normal levels. For the brief exposures contemplated, the actual mass of

245

tissue heated is small because of the shallow penetration and this heat is easily dissipated. Most of the absorbed heat is re-radiated to the environment over the next 10-20 seconds. The rest is carried away by the blood that circulates in the skin. The fraction that is conducted to structures deeper than the skin is negligible. Therefore, it is very unlikely for such a deterrent system to cause any detectable temperature rise in any of the internal vital organs.

8.7 Long Term and Delayed Effects

Adverse effects that last longer than 30 days are considered long term effects. Long term effects due to RF overexposures would be those resulting from severe burns. For example, scar formation and contractures following burns are long term effects. These would arise in situations in which the power density was very high and the pain experienced would be excruciating. Severe RF overexposures to the head could result in a post-concussion syndrome (IEEE COMAR, 2002).

Delayed effects are adverse effects that don't show up immediately after sustaining an injury but appear later. For example, cancer may be a delayed effect of exposure to ionizing radiation in that it may not appear for ten years or more. In general, delayed effects would involve changes in gene expression brought about by DNA damage. Therefore there have been many studies investigating the possibility of DNA damage and genotoxicity resulting from RF exposures (Meltz, 2003; Vijayalaxmi et al., 1998; Vijayalaxmi et al., 2001). The weight of the evidence overwhelming indicates that RF does not cause DNA damage of other genotoxicity.

Although the high power millimeter wave based non-lethal deterrent systems are designed to avoid any injury, it is possible that under some circumstances first or second-degree skin burns might occur. First-degree burns cause reddening of the skin and promptly heal with no sequelae. Second-degree burns cause blistering and can lead to scarring. Scarring is a long term effect. In some individuals, scarring leads to keloid formation, a delayed overgrowth of fibrous tissue surrounding the scar. Scars and keloids do not constitute a health issue, just a cosmetic one. Other than these, there are no foreseeable long term or delayed direct effects that could arise from use of the millimeter wave beam. Also, as mentioned previously, thermally induced bioeffects are not cumulative. That is, if a single exposure at a given level doesn't cause an adverse effect; multiple exposures at that level will not cause an adverse effect. Therefore if an individual is subjected to a repeated exposure to RFR on another day, there is no greater risk of injury than on the first day. In fact, experience has shown that individuals once exposed become more knowledgeable and tend to remove themselves from the beam more rapidly. This results in a lesser risk of injury from the second exposure.

8.8 Pregnancy and Reproductive Organs

Rapidly dividing cells are especially sensitive to the destructive action of heating. This is certainly true for sperm cells and for the embryo and developing fetus. Internal temperature elevations of more than 2 °C for an hour or more can suppress spermatogenesis and can cause developmental abnormalities in the fetus (Miller & Ziskin, 1989). The reduction in sperm production is only temporary. However, the fetal effects can be serious and permanent. A particularly vulnerable time is the period of organogenesis which occurs during the first

246

trimester. Possible abnormalities include neurological defects, cleft palate, and orthopedic deformities. Shorter exposure durations require higher temperature elevations to produce the same effects. Temperature elevations smaller than 2 °C do not cause these problems. Exposures to RF at or below national safety limits will not raise body temperature to even a 1 °C elevation, and therefore such exposures will not interfere with pregnancy or other reproductive functions. However, RF overexposures, if sufficiently intense and prolonged do pose a threat (Jensh, 1984a, 1984b).

8.9 Cancer

Because of its seriousness, cancer is always a concern. It is well known that cancer can be caused by ionizing radiation, and many members of the public fear that it may be caused by non-ionizing radiation as well. However, there are many theoretical reasons to refute this belief as well as many experimental results showing that RF radiation is not carcinogenic (Heynick et al., 2003). 24 studies published since 1998 have shown no increase in cancer incidence in animals exposed to RF energy. Therefore, earlier studies reporting effects (5 out of the total of 35) have not been confirmed by more recent and well-designed studies with good exposure assessment.

Because millimeter waves are absorbed entirely within the skin, it is reasonable to assume that should cancer develop from exposure to this energy it would occur in the skin. Therefore, a number of recent studies have carefully examined the possibility that 94-GHz millimeter waves might cause skin cancer or promote the growth of skin cancer. Single and multiple exposures (2 exposures per week for 12 weeks) of 94-GHz radiation to mice do not cause any increase in the initiation or promotion of skin cancer (Mason et al., 2001). These results are credible and consistent with a large body of past experimental results. Although it is scientifically impossible to prove that something can't happen, it would appear there is no statistical evidence to support the likelihood of cancer being caused by RF radiation.

8.10 National Safety Standards

In general, the greater the exposure to RFR the greater will be the likelihood and the severity of an adverse effect. However, if the exposure is below the threshold for all adverse effects, there is no known risk. Thresholds for RFR induced biological effects have been studied for over fifty years. The large literature on this subject has been repeatedly reviewed by professional societies, government agencies, and standard setting organizations. The reproducible adverse biological effect with the lowest threshold is a reduction in the rate of lever-pressing behavior in a number of laboratory animal species, including two types of monkeys. This response was typically observed to occur in association with prolonged (tens of minutes) RFR exposures producing a whole-body rate of energy absorption of 4 W/kg and a modest core temperature elevation of about 1 °C. National standards (IEEE C95.1, 2005a; FCC 96-326, 1996) have set the maximum permissible exposure (MPE) for occupational workers equal to one tenth of this threshold, and equal to one-fiftieth for the general public. Extensive research has shown that the coupling of RF energy into the body depends on the frequency. In

order to compensate for this frequency dependence, the MPE has been designed to vary with frequency in a similar manner. See Tables 8-1 and 8-2.

Table 8-1. Upper Tier (MPE for people in controlled environments).

Frequency range (MHz)	RMS electric field strength (E)[a] (V/m)
0.1–1.0	1842
1.0–30	$1842/f_M$
30–100	61.4
100–300	61.4
300–3000	–
3000–30 000	–
30 000–300 000	–

NOTE—f_M is the frequency in MHz, f_G

[a]For exposures that are uniform over the
field strengths and power densities are co
the exposure fields, as obtained by spatia
an area equivalent to the vertical cross
frequency (see NOTES to Table 8 and Ta

[b]These plane-wave equivalent power den
quencies and are displayed on some instr

248

Table 8-2. Action level (MPE for general public).

Frequency range (MHz)	RMS electric field strength (E)[a] (V/m)	RMS magnetic field strength (H)[a] (A/m)	RMS power density (S) E-field, H-field (W/m^2)	Averaging time[b] $\|E\|^2$, $\|H\|^2$ or S (min)	
0.1–1.34	614	$16.3/f_M$	$(1000, 100\,000/f_M^2)^c$	6	6
1.34–3	$823.8/f_M$	$16.3/f_M$	$(1800/f_M^2, 100\,000/f_M^2)$	$f_M^2/0.3$	6
3–30	$823.8/f_M$	$16.3/f_M$	$(1800/f_M^2, 100\,000/f_M^2)$	30	6
30–100	27.5	$158.3/f_M^{1.668}$	$(2, 9\,400\,000/f_M^{3.336})$	30	$0.0636\,f_M^{1.337}$
100–400	27.5	0.0729	2	30	30
400–2000	–	–	$f_M/200$	30	
2000–5000	–	–	10	30	
5000–30 000	–	–	10	$150/f_G$	
30 000–100 000	–	–	10	$25.24/f_G^{0.476}$	
100 000–300 000	–	–	$(90f_G–7000)/200$	$5048/[(9f_G–700)f_G^{0.476}]$	

NOTE—f_M is the frequency in MHz, f_G is the frequency in GHz.

[a]For exposures that are uniform over the dimensions of the body, such as certain far-field plane-wave exposures, the exposure field strengths and power densities are compared with the MPEs in the Table. For non-uniform exposures, the mean values of the exposure fields, as obtained by spatially averaging the squares of the field strengths or averaging the power densities over an area equivalent to the vertical cross section of the human body (projected area) or a smaller area depending on the frequency (see NOTES to Table 8 and Table 9 below), are compared with the MPEs in the Table.

[b]The left column is the averaging time for $\|E\|^2$, the right column is the averaging time for $\|H\|^2$. For frequencies greater than 400 MHz, the averaging time is for power density S

[c]These plane-wave equivalent power density values are commonly used as a convenient comparison with MPEs at higher frequencies and are displayed on some instruments in use.

Recent research has shown that the MPE safety factor is actually greater than 10 for occupational workers and 50 for the general public for most frequencies and up to 250 for some frequencies. However, for frequencies from 1 to 3 GHz the safety factor may be as small as 25 for a one-year-old child (IEEE C95.1, 2005a).

Injurious exposures generally involve accidental exposure to very high level sources, under conditions in which the exposed individual cannot voluntarily remove himself or herself before excessive heating occurs.

8.11 Likelihood of Overexposure

Because of the promulgation and observance of RFR safety standards and regulations, the incidence of overexposure to the general public is rare. Overexposures, however, do occur when something goes wrong: such as when an engineer is on a roof top adjusting an antenna and someone inadvertently energizes a near-by transmitting antenna. Overexposures also occur sometimes to military personnel who inadvertently find themselves placed within a high power radar beam, or to workers who ignore warning signs and enter into restricted areas. These incidents are most often the result of human error or carelessness. Occupational workers are much more at risk than the general public. Unfortunately, there have also been a few reported incidents of people deliberately exposing others to hazardous levels of RFR; for example, there

249

have been two reported cases of infants being placed in microwave ovens (Alexander et al., 1987).

An overexposure is defined as an exposure exceeding the MPE, as defined in Tables 8-1 and 8-2. However, the greatest exposure to the general public is from medical devices, such as diathermy machines, electrosurgical units, or other catheter-based devices for surgical procedures using microwaves. Typically these machines may emit 100 watts of 2450 MHz RFR, possessing power densities ranging from 100 - 1000 mW/cm^2, or 5 to 50 times higher than the MPE for uncontrolled environments, and capable of producing very high exposures to localized parts of the body. In order to permit physicians to achieve the desired therapeutic benefit, diathermy devices and other devices used in medical treatment are exempted from the national standards. When used according to recommended practice, diathermy is generally considered safe. The clinical experience with diathermy, because of the relatively high RFR exposures, provides a helpful perspective on the possible consequences of overexposures. Non-medical RFR exposure levels are typically 100 or more times lower than those employed in diathermy.

8.12 Signs and Symptoms of RFR Overexposure

The vast majority of RFR overexposures result in no symptoms at all. Because of the large safety margin in existing standards, most people suffer no harm and are not even aware that they were overexposed. Upon learning that they had been exposed, some people develop acute anxiety reactions, and require reassurance if appropriate.

The most common non-psychological symptom of overexposure is an internal warm sensation, located in the region of the body exposed to the RFR beam. The warm sensation turns into pain if the exposure is great enough and the person remains in the beam. Most often, an individual, upon feeling warmth, will move away from the beam and thereby limit the exposure. Because metals are highly conductive and tend to concentrate electromagnetic fields, additional heating could occur in the local vicinity of metallic objects, such as jewelry or metallic implants. Therefore, localized hot sensations and burns are possible even with whole-body exposures. For example, a hot sensation at the site of a metallic watchband (at the time of the overexposure) might be the only complaint from a person who had been overexposed.

The medical consequences of thermal injury depend on what tissues are involved, how well they are perfused, and whether or not they can regenerate. Especially vulnerable to overexposures are the nervous system and the lens of the eye, neither of which regenerate. Heating of the testes can cause a temporary spermatopenia. Many of the acute symptoms, such as nausea, vomiting, headaches, loss of equilibrium, malaise, and fatigue are related to heating of the central nervous system. Some of the latter symptoms may be the result of anxiety rather than overheating per se.

Long term effects can occur with high exposures. In addition to psychological problems, some of the acute symptoms can persist long after the overexposure. Also, organ damage may not be detectable until sometime after an overexposure. For example, cataract formation, dryness in the mouth, and palpitations may not occur immediately following an overexposure.

If an individual received an overexposure to his head, it is also possible for signs and symptoms similar to that of a post-concussion syndrome to develop.

Except for the localized burns when present, there is very little objective medical evidence to substantiate damage from a possible overexposure. Most of the symptoms are non-specific, and it may be impossible to determine if they are in fact due to the overexposure.

8.13 Management of RF Radiation Overexposures

Radiation Incident Evaluation requires the expertise of both health physicists and medical personnel. The health physicist has the responsibility of evaluating the radiation incident. The medical officer or physician is responsible for evaluating the exposed person.

8.14 Role of the Health Physicist

8.14.1 Prevention

The prevention of RFR overexposures is an important duty of a health physicist. The following necessary steps are described in the recently approved IEEE standard, *Recommended Practice for Radio Frequency Safety Programs* (IEEE C95.7, 2005b):

- Be aware of all pertinent safety regulations
- Have a Safety Program for individuals who may be exposed to levels exceeding the MPE lower tier (action level)
- Monitor emissions on a regular basis
- Ensure that appropriate warning signs are posted
- Erect entrance warnings and guards if necessary
- If RFR levels may exceed 10 times the MPE, additional warning is necessary: Use Flashing Lights, Audible Signals, Fences, and/or Interlocks as appropriate.

8.14.2 Assessment

In the event of an overexposure, the health physicist will need to evaluate the nature of the radiation source, the circumstances of the exposure, and the extent of human exposure. Actual measurements are nearly always preferable, but estimates derived from a theoretical analysis are useful if measurements are not possible. In any event, the following information should be obtained.

- Determine the nature of the source:
   - Military or Commercial Designation of Source
   - Operating Frequency
   - Power, Peak and Temporal Average
   - Mode of Operation
   - Pulsing Scheme: Pulse width and Pulse Repetition Frequency
   - Operating Parameters

251

Beam characteristics
Scan or Rotation Rate, if any

- Circumstances of exposure:
  Leaking waveguide?
  Close proximity to antenna?
  Within radar beam?
  Equipment failure?
  Human error on part of operator?
  Human error on part of patient?

- Describe human exposure:
  Geometric relationship between source and human
  Distance to human
  Delineate exposed parts of body
  Estimate power density and duration of exposure
  Obtain any comments or sensations noted by involved personnel at the time of the incident

8.14.3 Follow-Up

- Do what is necessary to correct source of overexposure
- Inspect to see that correction is maintained
- Educate personnel of dangerous situations to avoid reoccurrence

8.15 Role of the Physician

A person brought to a physician because of a suspected RFR overexposure is invariably frightened and agitated. Reassurance to the patient will be helped by knowledge of the extent of the overexposure. The determination of whether or not an overexposure had occurred requires careful analysis by experts trained in RFR measurements and dosimetry. Many times there is actually no overexposure at all. For example, of 330 suspected individual overexposures occurring in US Air Force investigations, only 58 had actually exceeded the MPE (USAF OEHL REPORT, 1984). If no overexposure has occurred, it is only necessary to treat the patient for the anxiety reaction.

Initial Medical Concerns:
  Medical emergency is very unlikely
  Anxiety is likely
  Patient should be calmed and reassured
  Ask Patient to relate facts
  Any acute symptoms will be due to heating: pain, burns, and redness of skin
  In all situations, treat symptomatically

If an overexposure has occurred, an appropriate history and physical examination should be obtained. The patient should be questioned about what was felt during the overexposure. Did

the patient experience a warm sensation in the region of his body exposed to the RFR beam? If this is not the case, the likelihood of an adverse effect is very much lower, unless the individual has a pre-existing neural deficit in the region exposed. The symptoms occurring before and after the overexposure, in addition to those occurring during the overexposure should be recorded, as this information will be required if the incident goes to litigation.

In cases where there is evidence of potential thermal injury, the physical examination should include an ophthalmologic exam, especially for lenticular opacities. If there is any evidence of possible damage, the patient should be referred to an ophthalmologist. The skin should be examined for areas of erythema and for surface burns in the vicinity of metallic objects. A neurologic exam should be performed to evaluate any paresthesias, paralysis, or possible injury to the central nervous system.

Laboratory tests should be performed in accordance with the likelihood and the severity of the overexposure. If there are any cardiac symptoms present, an ECG should be performed. If there is suspicion that internal organ damage has occurred, appropriate serum enzyme levels should be obtained. An x-ray study may be helpful if the patient has any internally implanted metal objects. If there are significant neurologic symptoms, it may be helpful to obtain an EEG and/or an MRI examination of the involved region of the nervous system.

Treatment of the conditions resulting from an RFR overexposure should be the same as that for treating similar injuries from any other cause.

8.16 Special Considerations in the Medical Evaluation of an Overexposed Individual

8.16.1 Ophthalmological Questions

8.16.1.1 In the event of an RF overexposure, when should an ophthalmological examination be performed, and what should the ophthalmologist look for?

The only credible ophthalmologic effects of RF overexposure are those due to thermal mechanisms. Therefore, the pathology to look for would be burns of the eye lids, lenticular cataracts, retinal burns, and other evidences of burns in the surrounding tissues. There are no known pathognomonic RF effects - this means that there are no unique pathologic changes that occur only from RF overexposure and not from other causes.

The medical actions to be taken should be proportional to the likelihood and nature of damage. The hierarchy of indicated medical evaluation should be that by the health physicist, the on-site medical officer, the family practitioner, an ophthalmologist, and ultimately the super specialist for the specific pathology detected. If the health physicist thinks that there has been no overexposure and the exposed individual complains of no ophthalmologic symptoms, no further ophthalmologic examination is called for.

If an overexposure is believed to have occurred and/or the exposed individual has symptoms, then an initial exam by a physician would be appropriate. If the physician is certain

253

that the individual has no eye problem, then it would not be necessary for examination by an ophthalmologist. If, on the other hand, the physician has any doubt about the existence of an eye injury, he would be advised to get an ophthalmology consultation. In most cases of eye damage, adequate care can be provided by the ophthalmologist. Only in very unusual or very severe cases would a super specialist be needed.

The above is based on what the author considers to be good medical practice. Sometimes this has to be modified, especially when there is a high likelihood of litigation. In these cases, it may be advisable for physicians to refer to specialists unless they can be very positive that there is no pathology, and even then it might be prudent to obtain a second opinion. Unfortunately, there is no substantial body of knowledge amongst physicians relative to the specific medical management of RF overexposures and especially RF eye injuries. Therefore, the above comments and recommendations are those of the author.

8.16.1.2 Why does the denaturation of the lens protein following an RFR overexposure continue for a period of 1 hour to 2-3 days?

In general, there are two types of cell death: coagulation necrosis and apoptosis. Coagulation necrosis occurs when the temperature rises so high that there results very rapid protein coagulation and denaturation. The time line for this purely physical reaction starts from the time the temperature exceeds a threshold (time varying) and continually worsens for a matter of an hour or so. Apoptosis, on the other hand, has a lower threshold and involves a biological sequence of steps in a programmed death march, which usually takes 24 to 48 hours or more to become evident. In either case, the dead corneal cells are not removed and the opacity of the lens is affected.

Although generally unaware of non-ionizing radiation effects, physicians are aware of ionizing radiation as a cause of delayed cataract formation, and may mistakenly think that cataracts might be likely following an RF radiation overexposure. Incidentally, in ionizing radiation-induced cataracts, the process is initiated by DNA damage and the resulting cataracts may not become evident for 10 years or more.

8.16.1.3 Does the cataract formation get harder to see as the hours/days tick by?

The cells of the lens that die are not removed as normally occurs in other parts of the body. Therefore, the formation of cataractous changes rarely regresses, and detection of the cataract should not become harder with time. In fact, one would expect cataracts to worsen with time, and their detection to become easier.

8.16.1.4 How reliable is the ophthalmological slit lamp testing to record cataract changes one day after exposure?

The slit lamp is accurate. There will be little variation amongst ophthalmologists unless the cataract is very small. A slit lamp exam one day following an exposure will almost surely detect a cataract that has occurred by that time. Since cataracts formation is naturally so

254

common with advancing age, the real problem with cataracts observed following RF radiation overexposure is proving that an existing cataract was not a result of the exposure.

8.16.1.5 Is there any conceivable circumstance whereby a conscious person would be able to tolerate the sort of extreme and prolonged RF exposure required to induce a cataract?

Under normal circumstances, the possibility of RF radiation overexposure causing cataracts in an exposed individual would be most unlikely. The only exceptions would be if the individual were anesthetized, paralyzed, or confined such that he could not extricate himself from the radiation beam.

8.16.1.6 Is there any evidence of RF induced cataracts at radio broadcast frequencies (say below 700 MHz)?

There are no reports of any individual who has ever developed cataracts because of exposure to radio broadcast frequencies, and I think it would be very unlikely. However, this is no reason to think that it could not happen for any exposure that would raise the in-situ temperature of the lens sufficiently high (above 50 °C) for a sufficiently long time (more than 15 minutes).

8.17 When and Why X-Rays Should Be Obtained

A question may arise concerning the advisability of using x-rays in examining persons who received an RFR overexposure. The concept of using x-rays, an agent known to cause harm, in the evaluation of the effects of RFR, an agent with much less harmful potential, deserves careful consideration.

The decision to perform an x-ray examination is a medical decision based on the anticipated value of the information to be gained compared to the added risk. If a person has been overexposed, but has no symptoms and no internal metallic devices, there is no need for an x-ray.

If a person has been subjected to a severe overexposure and there are signs or symptoms of internal pathology that might be better evaluated by x-rays, then the appropriate radiographic studies should be performed.

A more difficult decision arises when a person who has an internal metallic device such as an internal pacemaker or defibrillator is subject to an RF overexposure.

Some reasons for doing an x-ray examination of implanted metallic objects are as follows:

Detection and Evaluation of:
  1. Deformation, displacement or change in orientation of metal object
  2. Deterioration of metal prosthesis
  3. Breaking of wires in implanted device

255

4. Degenerative changes in bone caused indirectly by a heated metallic implant

Some reasons for not doing an x-ray examination following an RFR overexposure:

1. Radiation hazard:
   There exists a very small but finite risk for producing cancer from an x-ray study. A typical study evaluating metallic implants would subject a patient to a radiation dose of approximately 10 mrem. The average radiation background exposure to a person living in the United States is approximately 300 mrem per year. Therefore, the added risk from such an examination would be considered very small.
2. Cost of study
3. Arousal of patient's concern of damage when in fact there was none.

The decision whether or not to obtain an x-ray study will need to consider the suspected severity of the injuries, the patient's signs and symptoms, the cost, the likelihood of litigation if not performed, and perhaps most importantly the local standard of medical care. All things considered, it is probably advisable to obtain an x-ray examination of any implanted metal object following an RFR overexposure, except in those cases in which the exposure was sufficiently small that any internal damage would be considered highly unlikely.

8.18 Specific Examples of Overexposures

8.18.1 An Antenna Engineer Accidentally Hit with High Level RF and his Body Temperature Rose to 42 °C.

8.18.1.1 If the Body Core Temperature Rose to 42 °C

42 °C is a potentially lethal body core temperature and unless reduced very promptly, the victim will almost certainly die. Immediate actions should include:

1. Removing the victim from further exposure. Turning off the power is best if it can be done promptly. Otherwise shield the victim and/or remove the victim from the radiating beam. The rescuer should minimize exposure to the extent possible and practical.

2. Check for any serious bleeding and/or blockage of breathing. If any, treat this immediately.

3. Cool body temperature as rapidly as possible. Place victim in an ice bath if available. If not available, hose down with cold water. If victim is conscious, have victim drink copious amounts of ice water.

256

4. Shock is likely and potentially lethal, so check blood pressure every 15 minutes for the first hour, and continue until blood pressure becomes stabilized. Treat with drugs (vasopressors), as required.

5. If patient is conscious, the patient will probably be in much pain and will require analgesics, and very possibly narcotics.

6. Transport to hospital. This injury is sufficiently serious that hospitalization will be necessary.

8.18.1.2 If the Temperature Elevation to 42 °C Was Only Superficial

If the temperature of 42 °C was confined to the skin and underlying tissues, but the body core temperature was not significantly elevated, a very different condition would exist. This would in general be much less serious. The severity will depend on the extent and depth of the temperature elevation, as well as the duration. The treatment will depend on the severity. The skin is able to withstand 42 °C without any injury, and if the exposure is limited to a small region of the body, the body's thermoregulatory mechanisms will be capable of preventing injury. Such small overexposures will not lead to the need for any more treatment than just supportive reassurance.

8.19 A Case of Severe Overexposure

A 48-year-old painter was working on an antenna on top of the Sears Building in Chicago when someone, not aware of the painter's presence, accidently turned on a 250,000 watt FM broadcasting transmitter. Within three minutes the painter started to feel a pleasant warm sensation, as it was cold working at such heights. The warm feeling became unpleasantly hot, with pain greater on his legs than his hands, and greater on his right than his left side. Within thirty minutes the leg pain became excruciating and the painter needed help to descend and go to an emergency room at a nearby hospital.

In the emergency room, the patient was anxious and in much pain, especially in his legs. He experienced muscle cramps in his legs and was unable to support his own weight. Laboratory analysis revealed elevated CPK enzyme levels indicating muscle tissue damage. The patient was diagnosed as having deep and superficial burns of the right lower leg and foot. He was treated with narcotics and released the next day.

At one week following the accident, he presented with blistering on his lower right leg and a swollen right foot. His muscles were soft and pliable. He had evidence of neurological damage. He had reduced 2-point discrimination in both feet. He was unable to tolerate the touch of a sock or shoe, a condition called hyperesthesia. He was treated with steroids, leg elevation, and bed rest.

At three months following the accident, the patient showed slow but steady improvement. There was no acute inflammation, but he was weak because of prolonged inactivity. Residual stiffness developed in his right lower leg and ankle. A hyperpigmented scar could be seen on his

257

right lower leg. In addition to the burns, he was diagnosed as having some scarring of tendons in his right leg and foot. He was cleared for light duty, but unable to climb ladders. A course of physical therapy was in progress.

Eight years have passed since the accident. The pain is gone. However, the patient still suffers from a number of symptoms and is psychologically depressed. He experiences a decrease in mental alertness, has difficulty in remembering, and is bothered by occasional headaches. He tires easily. He remains hypersensitive to heat, especially in his legs.

This case is instructive as it shows what may occur in a very severe overexposure and provides a perspective for evaluating the consequences of smaller exposures. It shows that the acute damage that occurs is tissue burning and is accompanied by severe pain.   Late consequences frequently include psychological depression in addition to the functional disabilities resulting from the burns.   Also illustrated by this case is the fact that damage is localized to the regions of the body that are within the radiating beam. Another painter, who at the time of the accident, was working on the other side of the antenna experienced some warmth but no distress or injury.

8.20 Medical Conditions Affecting Severity of Overexposure

8.20.1 Influences of Medications

Drugs can influence the effects of RF exposure in two ways: (1) by directly affecting thermal regulation, and (2) by decreasing awareness of being exposed. Many drugs do both.

Drugs, known as pyretics, actually cause an increase in body temperature, resulting in a feverish condition. Pyrogens include such drugs as interferons, antibacterial agents, amphetamines, and anticholinergic agents. These drugs would of course add to the heat load on a person being over exposed to RF radiation, and if sufficiently intense, would lead to increased tissue damage. The effects would presumably be additive. Other drugs, such as opiates and some hormones are capable of raising the body temperature, albeit to a lesser degree than the pyretics. Alcohol, on the other hand, doesn't cause a temperature elevation directly, but does diminish the body's ability to regulate body temperature.

Many drugs affect alertness and can interfere with one's ability to sense being overexposed to a RF field. These drugs include anesthetics, antihistamines, sedatives, alcohol, tranquilizers, and many psychoactive drugs. Because more damage is expected the longer one is exposed to a high intensity RF field, the presence of these drugs would constitute an elevated risk.

It must be noted that no adverse effect of RF exposure to individuals under the influence of any of the above drugs would be possible unless the exposure was significantly above MPE values. At levels at or below MPE values, RF fields would not adversely affect any individual on or off any of these drugs.

8.20.2 Presence of Medical Devices or Metallic Implants

In general, all metallic objects are conductive and will tend to concentrate electromagnetic fields in their immediate surroundings. Heating effects will be enhanced in the presence of metallic objects, such as jewelry or implanted metallic medical devices. In some industrial accidents where very relatively high RF fields were involved, the only damages noted were skin burns around wrist watches and rings. Thus, the presence of these metallic objects does represent an increased risk. However, it is doubtful that RF fields at or below MPE levels would be concentrated sufficiently to cause any harm to individuals with internal or external metallic objects.

Another concern resulting from RF overexposures is interference with the normal working of cardiac pacemakers, internal defibrillators, and other electronic medical devices. Sufficiently high electric fields can trigger some of these devices, especially if they are not properly designed to suppress electromagnetic interference.

8.20.3 Medical Conditions Associated with Heat Intolerance

There are a number of medical conditions which are marked by a discomfort or worsening of symptoms due to relatively small increases in external temperature. These conditions result from a variety of causes. In general, the distress is temporary and completely relieved once the individual's temperature returns to normal. Some forms of heat intolerance are due to a decreased ability to cool the body by sweating, such as would occur in anhidrosis and some spinal cord injuries. Others are caused by diseases causing an increase in body temperature such as febrile diseases and thyrotoxicosis. Heat intolerance is sometimes associated with some vascular conditions, menopausal heat flashes, and certain drugs. A high incidence (as much as 85%) of heat intolerance occurs in multiple sclerosis, where it is particularly noticeable.

Multiple Sclerosis is a disease of the nervous system characterized by a patchy loss of the myelin surrounding nerve fibers. This loss affects the transmission of nerve impulses and produces the symptoms of multiple sclerosis. The demyelinated nerves are heat sensitive, and small increases in temperature lead to a worsening of clinical symptoms such as muscle weakness and visual blurring. The magnitude of temperature elevation sufficient to induce this unfavorable reaction can be very small, perhaps as small as a few tenths of a degree. The exacerbation of symptoms is temporary, producing no actual tissue damage, and is generally rapidly reversed when the source of the increased temperature is removed. Home air conditioning is frequently prescribed for patients with multiple sclerosis, if they do not have it already.

Very severe RFR overexposures can injure nerves and lead to persistent localized heat intolerances. However, there is no evidence that that would warrant expectation of any neural damage or heat intolerance to RFR exposures that are near or below national safety limits. Furthermore, there is no evidence that chronic exposure to RF fields causes multiple sclerosis or any of the above clinical conditions.

259

8.21 References

Adair, E. R., & Black, D. R. (2003). Thermoregulatory responses to RF energy absorption. *Bioelectromagnetics, 24*(Suppl. 6), S17-S38.

Alexander, R. C., Surrell, J. A., & Cohle, S. D. (1987). Microwave Burns to Children: An Unusual Manifestation of Child Abuse. *Pediatrics*, *79*, 255-60.

Black, D. R. & Heynick, L. N. (2003). Radiofrequency (RF) effects on blood cells, cardiac, endocrine, and immunological functions. *Bioelectromagnetics*, Suppl. 6, S187-S195.

Blick, D. W., Adair, E. A., Hurt, W. D., Sherry, C. J., Walters, T. J., & Merritt, J. H. (1997). Thresholds of Microwave-Evoked Warmth Sensations in Human Skin. *Bioelectromagnetics*, *18*, 403–409.

Carpenter, R. L. (1979). Ocular effects of microwave radiation. *Bulletin of the New York Academy of Medicine*, *55*(11), 1048-1057.

Chalfin, S., D'Andrea, J. A., Comeau, P. D., Belt, M. E., & Hatcher, D. J. (2002). Millimeter wave absorption in the nonhuman primate eye at 35 GHz and 94 GHz. *Health Physics*, *83*(1), 83-90.

Chou, C-K., D'Andrea, J. A. (2003). Reviews of the Effects of RF Fields on Various Aspects of Human Health. *Bioelectromagnetics*, *24*-S6.

D'Andrea, J. A., Adair, E. R., & de Lorge, J. O. (2003). Behavioral and cognitive effects of microwave exposure. *Bioelectromagnetics*, Suppl. 6, S39-S62.

D'Andrea, J. A., Chou, C. K., Johnston, S. A., & Adair, E. A. (2003). Microwave effects on the Nervous System. *Bioelectromagnetics*, Suppl. 6, S107-S147.

Elder J. A. (2003a). Ocular effects of radiofrequency energy. *Bioelectromagnetics,* Suppl. 6, S148-S161.

Elder, J. A. (2003b). Survival and cancer in laboratory mammals exposed to radiofrequency energy. *Bioelectromagnetics,* Suppl. 6, S101-S106.

Elder, J. A., Chou, C. K. (2003). Auditory response to pulsed radiofrequency energy. *Bioelectromagnetics,* Suppl. 6, S162-S173.

Elwood J. M. (2003). Epidemiological studies of radio frequency exposures and human cancer. *Bioelectromagnetics, 24*(Suppl. 6), S63-S73.

Federal Communications Commission. (1996). Guidelines for Evaluating the Environmental Effects of Radiofrequency Radiation. *FCC,* 96-326.

260

Foster, M. R., Ferri, E. S., & Hagan, G. J. (1986). Dosimetric study of microwave cataractogenesis. *Bioelectromagnetics*, *7*, 129 - 140.

Foster, K. R., D'Andrea, J. A., Chalfin, S., & Hatcher, D. J. (2003). Thermal modeling of millimeter wave damage to the primate cornea at 35 GHz and 94 GHz. *Health Physics*, *84*(6), 764-769.

Heynick, L. N., Johnston, S. A., & Mason, P. A. (2003). Radio frequency electromagnetic fields: Cancer, mutagenesis, and genotoxicity. *Bioelectromagnetics*, Suppl. 6, S74-S100.

Heynick, L. N. & Merritt, J. H. (2003). Radiofrequency fields and teratogenesis. *Bioelectromagnetics*, Suppl. 6, S174-S186.

Institute of Electrical and Electronics Engineers, Inc. (IEEE). (2005a). *Standard for Safety Levels with Respect to Human Exposure to Radio Frequency Electromagnetic Fields, 3 kHz to 300 GHz*. (IEEE C95.1). New York: The Institute of Electrical and Electronics Engineers, Inc.

Institute of Electrical and Electronics Engineers, Inc. (IEEE). (2005b). *Recommended Practice for Radio Frequency Safety Programs, 3 kHz to 300 GHz*. (IEEE C95.7). New York: IEEE Institute of Electrical and Electronics Engineers, Inc.

Institute of Electrical and Electronics Engineers, Inc. (IEEE) Committee on Man and Radiation (IEEE COMAR). (2002). Medical Aspects of Radiofrequency Radiation Overexposure. *IEEE Committee on Man and Radiation, Health Physics, 82*, 387-391.

Institute of Electrical and Electronics Engineers, Inc. (IEEE)-Engineering in Medicine and Biology Society (EMBS) Committee on Man and Radiation (IEEE-EMBS COMAR). (n.d.). *COMAR Reports*. Retrieved May 29, 2009, from http://ewh.ieee.org/soc/embs/comar/

Jensh, R. P. (1984a). Studies of the teratogenic potential of exposure of rats tot 600 MHz microwave radiation. I. Morphologic analysis at term. *Radiation Research, 97*, 272-81 1984a.

Jensh, R. P. (1984b). Studies of the teratogenic potential of exposure of rats tot 600 MHz microwave radiation. II. Postnatal psychophysiologic evaluations. *Radiation Research, 97*, 282-301.

Lim, J. I., Fine, S. L., Kues, H. A., & Johnson, M. A. (1993). Visual abnormalities associated with high-energy microwave exposure. *Retina*, *13,* 230-233.

Mason, P. A., Walters, T. J., DiGiovanni, J., Beason, C. W., Jauchem, J. R., Dick, J. E., Mahajan, K., Dusch, S. J., Shields, B., Merritt, J. H., Murphy, M. R., & Ryan, K. L. (2001).

261

Lack of effect of 94-GHz radio frequency radiation exposure in an animal model of skin carcinogenesis. *Carcinogenesis, 22,* 1701-1708.

Meltz, M. L. (2003). Radiofrequency Exposure and Mammalian Cell Toxicity, Genotoxicity, and Transformation. *Bioelectromagnetics,* Suppl. 6, S196-S213.

Miller, M. W. & Ziskin, M. C. (1989). Biological Consequences of Hyperthermia. *Ultrasound in Medicine & Biology*, *15*, 707.

National Council on Radiation Protection and Measurements (NCRP). (1986). *NCRP Report No. 86: Biological Effects and Exposure Criteria for Radiofrequency Electromagnetic Fields*. Bethesda: MD. Retrieved May 29, 2009, from http://www.ncrponline.org/publications/86press.html

Pakhomov, A. G., Akyel, Y., Pakhomova, O. N., Stuck, B. E., & Murphy, M. R. (1998). Current state and implications of research on biological effects of millimeter waves. *Bioelectromagnetics*, *19*, 393-413.

USAF OEHL REPORT. (1984). *The Medical Results of Human Exposures to RadioFrequency Radiation* (Report 85-029CV111ARA). USAF Occupational and Environmental Health Laboratory, Aerospace Medical Division (AFSC), Brooks Air Force Base, TX.

Vijayalaxmi, Frei, M. R., Dusch, S. J., Guel, V., Meltz, M. L., & Jauchem, J. R. (1998). Frequency of micronuclei in the peripheral blood and bone marrow of cancer-prone mice chronically exposed to 2450 MHz radiofrequency radiation. *Radiation Research, 149*, 308-312.

Vijayalaxmi, Pickard, W. F., Bisht, K. S., Leal, B. Z., Meltz, M. R., Roti Roti, J. L., Straube, W. L., & Moros, E. G. (2001). Cytogenetic studies in human blood lymphocytes exposed in vitro to radiofrequency radiation at a cellular telephone frequency. *Radiation Research, 155*, 113-121.

Walters, T. J., Blick, D. W., Johnson, L. R., Adair, E. R., & Foster, K. R (2000). Heating and pain sensations by millimeter waves: Comparison to a simple thermal model. *Health Physics, 78*, 259-267.

World Health Organization (WHO). (1993). *Electromagnetic fields (300 Hz to 300 GHz).* Geneva: World Health Organization*,* Environmental Health Criteria 137. Retrieved May 29, 2009, from http://www.inchem.org/documents/ehc/ehc/ehc137.htm

Radio Frequency Radiation Dosimetry Handbook
(Fifth Edition)

Chapter 9.   Personal Exposure Indicators for Electromagnetic Fields 3 kHz –300 GHz

John A. Leonowich, Ph.D
Staff Scientist
Pacific Northwest National Laboratory
Richland, WA 99352

John.leonowich@pn1.gov

9.1   Introduction – The Need for Incident Field Dosimetry

We are literally surrounded by electromagnetic radiation and fields, from both natural and man-made sources. The identification and control of man-made sources of all forms of non-ionizing radiation has become a high priority of radiation safety professionals in recent years. For the purposes of this chapter, we will consider radio frequency radiation (RFR) to cover the frequencies from 3 kHz to 300 MHz, and microwaves from 300 MHz to 300 GHz, and will use the term RFR interchangeably to describe both. Electromagnetic radiation and fields below 3 kHz are considered Extremely Low Frequency (ELF) and is beyond the scope of this chapter. Unlike x- and gamma radiation, RFR is *non-ionizing*. The energy of any RFR photon is insufficient to produce ionizations in matter. The measurement and control of RFR hazards is therefore fundamentally different from ionizing radiation. The purpose of this chapter is to acquaint the reader with the fundamental issues involved in measuring RFR fields with currently available instrumentation, with particular emphasis on body mounted personal monitoring devices. In a certain sense, personal RFR monitors have existed since the infancy of the science; witnessed by the use of small fluorescent tubes to look for leaks in waveguides. These tubes would illuminate without the presence of an applied current when an intense enough RFR field was present.

Understanding of the physical properties of electromagnetic waves and the components of the electromagnetic spectrum are absolutely essential in order to measure non-ionizing radiation and fields. Electromagnetic energy can have many forms: static electric or magnetic fields; power frequency ELF fields, RFR and microwaves, optical radiations (infrared, light and ultraviolet); and the ionizing radiations. Ionizing radiations, such as x-rays and gamma rays, have extremely high frequencies (i.e., very high energy) and are able to produce ionization (positive and negative electrically charged molecules) by breaking the bonds that hold molecules in cells together. Non-ionizing radiation, on the other hand, has very small amounts of photon energy and is much too weak to be able to break these molecular bonds. Therefore, even high intensity non-ionizing radiation cannot cause ionization or radioactivity in the body. Figure 9-1 below shows the electromagnetic spectrum, along with the frequency and location in the spectrum of each radiation and field.
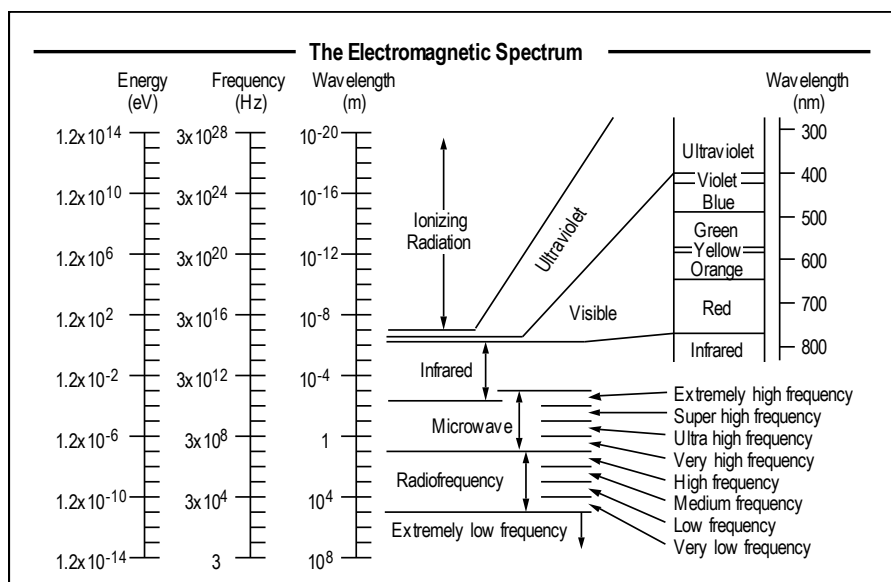
Figure 9-1. The Electromagnetic Spectrum.

There is also a need to measure the fields associated with new modalities such as high-powered microwave (HPM) and ultra-wide band sources (UWB). As these come into more general usage, present day monitors will have to be modified to measure these fields.

9.2   Physics of Electromagnetic Waves

The information in this section is a summation of the basic information required to understand the basic physics of electromagnetic waves. More in-depth treatment of the subject can be found in a number of other references (Leonowich, 1992, 1997).

Electromagnetic energy is propagated through space in the form of a wave as shown in Figure 9-2. For plane waves traveling in free space, the electric field vector **E** and the magnetic field vector **H** are mutually orthogonal and are in phase - i.e. maxima and minima occur at the same point in time and space. The units of **E** are volts/meter (V m^{-1}) and for **H** amperes/meter (A m^{-1}).

DISTRIBUTION A: APPROVED FOR PUBLIC RELEASE; DISTRIBUTION UNLIMITED.
PUBLIC AFFAIRS CASE NO. 11-069
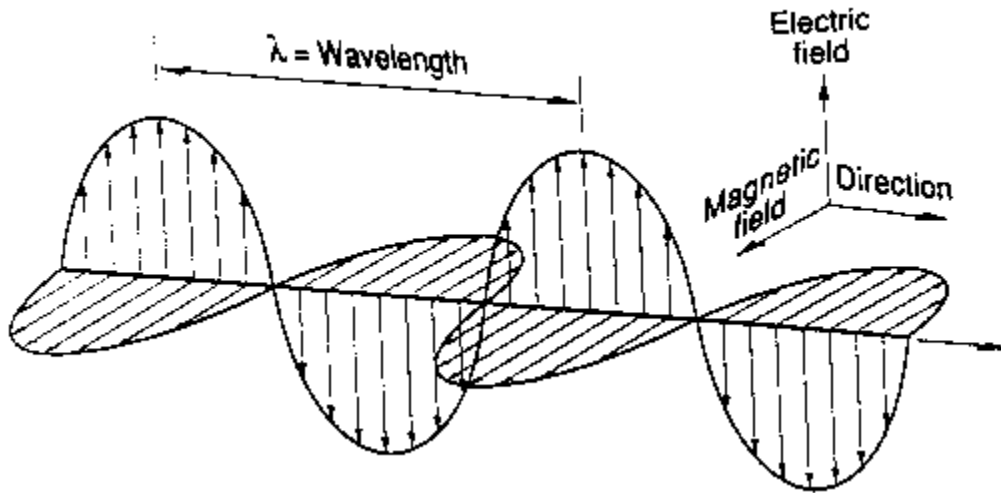
Figure 9-2. Typical electromagnetic wave showing the relationship between the E and H Field vectors.

When RFR is sufficiently far away from a radiation source (the so-called far field), the orthogonal relationship between the **E** and **H** field vectors is taken for granted. The energy carried in an electromagnetic wave is usually expressed in terms of the energy passing through a fixed area per unit time. For an electromagnetic wave this *power density* **S** at any point may be calculated from the vector product of the electric and magnetic field strength vectors, i.e., **E x H** = **P**. **P** is called Poynting's Vector and represents the power density and the direction of energy propagation. The Poynting vector points in the direction in which the electromagnetic wave is traveling, thus transporting energy in that direction. The magnitude of the power density propagated in the wave can be calculated from the vector product:

$$|\mathbf{ExH}| \;=\; |E|\,|H|\;\sin\Theta \;. \tag{1}$$

For $\Theta = 90°$, as is the case for a plane wave in free space:

$$|\mathbf{ExH}| \;=\; |E|\,|H| \;. \tag{2}$$

265

Note that if **E** has dimensions of V m^{-1} and **H** is in units of A m^{-1} the dimensions of **P** and/or **S** are given in W m^{-2}. In the United States, typically in hazard analyses **S** is expressed in milliwatts per square centimeter (mW cm^{-2}). Power density W m^{-2} can be equated to **E** and **H** as follows:

$$\text{Eq. X.3} \quad \mathbf{S} \; = \; \mathbf{E}^2 / 377 \; = \; 377 \, \mathbf{H}^2 . \tag{3}$$

Polarization is another important property of electromagnetic waves and is characterized by the oscillatory behavior and orientation of the electric field vector. A wave referred to as being linearly polarized means that the electric field vector varies in amplitude in only one direction as it travels. It is conventional to describe polarization in terms of the electric field only, not the magnetic field. An electromagnetic wave may exhibit linear, circular, elliptical, or random polarization (such as in a light bulb). A receiver (or absorber) of electromagnetic radiation must have the same sense of polarization as the incident wave for it to be detected or absorb energy from it <u>most efficiently</u>.

Suppose we could "freeze" the motion of an electromagnetic wave traveling in free space that we have previously discussed and take a snapshot of its **E** and **H** fields. The ratio of the electric field strength to the magnetic field strength is known as the characteristic impedance (or wave impedance Z_O) of free space. Therefore:

$$\text{X.4} \quad Z_O \; = \; \left| \mathbf{E/H} \right| . \tag{4}$$

Note that Z_O is the ratio of **E** to **H** and is independent of their absolute magnitudes and has a value of 120π or approximately 377 ohms. Therefore, in the far field, if one can measure either field component (**E** or **H**), it is easy to calculate the other. Unfortunately, in many cases measurements are needed to be made in the so-called "near field", where the orthogonal relationship between **E** and **H** does not hold. In this case, both **E** and **H** fields must be measured. It is usually assumed that near field conditions are present below 300 MHz; certainly this is true for emitters with frequencies below 100 MHz.

Table 9-1 lists both the dose and exposure metrics associated with RFR safety standards. As can be seen, for a very large portion of the RFR spectrum (100 kHz – 10 GHz), Specific Absorption Rate (SAR) in W kg^{-1} is the dose metric of importance. SAR is a measure of the thermal load induced in biological material exposed to RFR. Unfortunately, SAR is a difficult parameter to measure outside of the laboratory. However, it is possible to equate SAR to external **E** and **H** fields, as well as to currents (I) induced in the body. Above 10 GHz, the dose and exposure metric are identical, and can easily be measured by making an **E**-field measurement and using Equation X.3. Therefore, all RFR safety instrumentation measures **E^2**, **H^2** or I^2. **None measure power density directly.**

Table 9-1. Metrics in exposure standards for RFR.

Frequency range	Biomechanism	Dose metric	Exposure metrics*
VLF / LF (3 kHz-10 MHz)	Neuromuscular stimulation	Current density in excitable tissues	E, H, induced currents & contact currents (I)
Intermediate RFR (MF – SHF) (100 kHz–10 GHz)	Tissue heating (whole body and localized); below 10 MHz current density limits are also applied.	Specific Absorption Rate (SAR) in W/kg	E^2, H^2 (<300 MHz), I^2 from induced currents, & contact currents (<100 MHz)
Millimeter Wavelength Microwaves (10 – 300 GHz)	Surface heating	Power Density In W/m^2	E^2, Power Density In W/m^2

*All RFR exposure metric magnitudes are root-mean-squared (RMS) values.

9.3   Development of Broadband Instrumentation for Measuring RFR Fields

Characterization of field strengths for RFR safety applications is a demanding task. High level, or *potentially* high level, fields need to be compared against national and international standards. Standards, while providing excellent information about the field limits and their biological basis, typically provide little information about instrumentation used to demonstrate compliance.

Most measurements are performed with wideband instrumentation consisting of a metering instrument and a broadband field probe. The broadband field probe is comprised of isotropically mounted antennas, which are the detector (in the case of thermocouple arrays) or have a detector at their junction (as a diode based system, see Figure 9-3). The advantages of these types of systems over narrowband (i.e., small frequency range) equipment, is that they are able to measure the total field strength of multiple sources simultaneously. With isotropic sensor designs, wideband sensors can accurately sum these fields, regardless of the polarization employed, or the direction of propagation. This assumes that the detector attached to the antenna is accurately processing the incoming waveform, which is not always the case. Little information is available to the user about how their instrument will fare in other than ideal situations. In most, if not all situations, the detector used will be affected by outside forces. Effects of signal type (frequency, modulation, harmonic content, number of signals) and environment (temperature, humidity, etc.) can seriously degrade measurement accuracy.
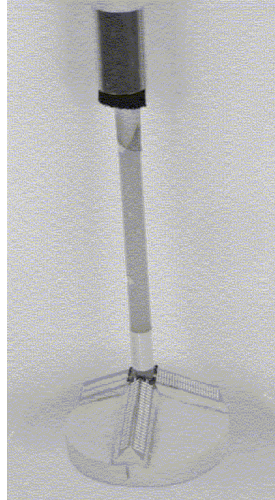
Figure 9-3. Typical isotropic RFR field sensor using three orthogonal elements.

Documents such as IEEE C95.3-2002 (IEEE, 2002), provide detailed information about sensor technology, but very little guidance as to when and where a particular sensor will operate with the highest accuracy. In order to perform proper measurements of radiated fields, an operator needs to be aware of the sensor and its characteristics. This next section introduces the various types of sensors available and their characteristics. The most important are the diode, compensated diode and thermocouple type of sensors.

9.4   Development of RFR Instrumentation

Measurements of RFR fields for safety purposes have been performed over the last 30 years or so with broadband equipment. The average user is usually unaware of design limitations and compromises that different manufacturers have reached for their particular customer base or measurement philosophy. These compromises will dictate how well an instrument will perform in a given RFR environment. Approximately 35 years ago, the commercialization of microwave ovens generated a need for instrumentation operating at 915 and 2450 MHz in order to obtain leakage information for manufacturers and repair organizations. Awareness of RFR energy and its possible effects lead to developments of broader frequency range monitors that at first were circularly polarized in an attempt to respond to all polarizations. These instruments were therefore not isotropic in their detection capability and their effectiveness was markedly affected by geometric considerations. Without prior knowledge of the field to be measured it was therefore quite possible to make a totally erroneous conclusion on the amount of RFR energy present. These initial products were very broadband for their time, covering the spectrum from 1 - 14 GHz by the use of thermistor detectors. While the thermistor was very linear in its response, the receiving antenna design was not, necessitating multiple frequency calibrations to overcome polarization and frequency sensitivity errors of up to 10 decibels (dB). The next generation of these circularly polarized monitors incorporated thermocouple detectors and improved antenna designs that reduced frequency sensitivity errors to about 6 dB. About 25 years ago the first isotropic detection probes came on the market. Electric field probes were made available covering the spectrum from 300 MHz to 18 GHz with

268

a frequency sensitivity of only 3 dB, and a measuring range of 30 dB. During the early 1970's there were also many advances in calibration methods and procedures for quantifying RFR fields from then United States National Bureau of Standards (now NIST). Near field calculations and transverse electromagnetic (TEM cell) developments allowed for even higher calibration accuracies over a broad range of frequencies to uncertainties of ± 0.5 dB. Also in this time period the development of magnetic field probes was accomplished in part to measure the magnetic fields associated with high frequency (HF) communication systems. The impetus for the development of much of this isotropic instrumentation was the United States military, in particular the U.S. Air Force. The development of this broadband instrumentation overcame many of the problems associated with the earlier measurement equipment. Previously tedious measurements with narrowband equipment were replaced with broad sensors covering many decades of frequency. Standards had constant field limits over frequency during this period of time. Approximately 20 years ago, RFR standards became frequency dependent as research determined the need to further limit the fields at the human resonant frequencies, due to increased absorption of RF energy. In addition, fields tested (**E** and/or **H**) changed depending on the particular standard, and frequency of emitters. Sensors have not changed as much as the instrumentation used to display the field detected. The main reason for this is that most limits are still based on the root mean square (RMS), time averaged field level. Since it is the RMS average power level available to do the work, or create the heating of tissue, thermal limits still dominate field limit considerations. New metering instruments simplify the recording of surveys, but the field probe determines the overall accuracy. Some meters can enhance accuracy by compensating for temperature or measurement level errors, particularly when diodes are employed as sensors.

9.5   Detectors for RFR: Diodes Versus Thermocouples

All currently available RFR instrumentation relies on either diodes or thermocouples as detectors. A modern broadband RFR survey meter, incorporating probe, cable and meter is shown in Figure 9-4.

Figure 9-4. Modern Broadband RFR Survey Meter (courtesy of L-3 Communications, NARDA East).

Diode sensors have been used for measurements of RF and microwave power for many years. Semiconductor diodes are used routinely to measure absolute RF power. Diodes exhibit many characteristics that make them desirable for measuring RFR, but also do have disadvantages. They are relatively cheap and rugged. Diodes work well at low RFR field levels when the diode is in its "square law" region. A diode is a non-linear device, which when operated at higher levels will detect peak rather than average levels of RFR, as shown in Figure 9-5. Diodes are therefore not recommended for multiple signals or pulsed environments. They do, however, have intrinsic "zero stability" and seldom drift.
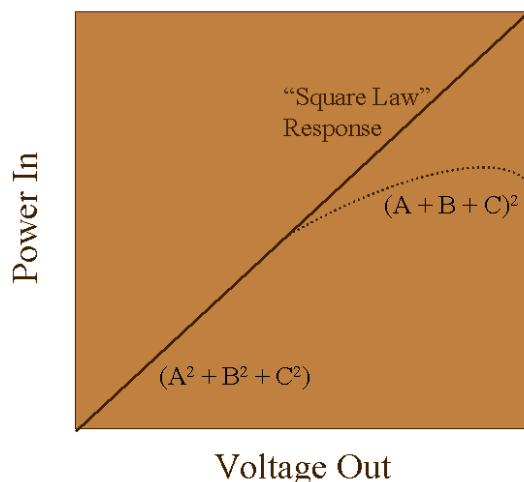
Figure 9-5. Diode linearity versus input level.

The RF induced current in a diode can be represented mathematically as:

$$I = I_s[\exp(V_j/V_t) - 1] . \tag{5}$$

The characteristics of the diode are reflected in the "thermal-voltage", V_t and the reverse saturation current I_s. This current is a function of device area, materials used to form the junction, and temperature. The temperature dependence is very important because most of the change in detector performance can be related to variations in I_s, which changes by approximately a factor of 2 every 20 °C. Therefore, it is imperative that a diode field sensor incorporate at least a basic temperature compensation circuit to correct for I_s variations. There are some improvements to accuracy that metering instruments used with diodes can perform. The most common is to correct for linearity errors in diode detectors. Circuits that compensate diode output will only correct for the diode's response to a particular signal, generally a sinusoid. If the signal is not sinusoidal, the relationship of peak to RMS voltage (power) is different and results in an error for the power measurement. The second accuracy enhancement is to compensate for the diode temperature sensitivity. This sensitivity can be quite large, as much as a 2:1 change for 20 °C. Compensated diode sensors can be utilized for multiple-signal environments, but are not recommended for pulse modulated emitter measurements.

Thermocouple detectors have been the detection technology of choice for sensing microwave frequencies since their introduction in the late 1960's. The main reason for this being that they feature, unlike diodes, inherent square-law detection characteristic (input RF power is proportional to DC voltage out). The energy of the pulse is detected by a series of thermocouples arranged in series to form a resistive dipole antenna. As is well known, energy is deposited at the speed of light. Since thermocouples are heat-based sensors, they are true "averaging detectors." This recommends them for all types of signals formats from CW to complex digital phase modulations.

Thermocouples are based on the fact that dissimilar metals generate a voltage proportional to temperature differences at a hot and cold junction of two metals. Probes that utilize thermocouple detectors function in two different modes. Between 300 MHz and 18 GHz, they operate as a resistive dipole. Above 12 GHz, it utilizes the phase delay of a traveling wave to produce additional output. As a resistive dipole, in the 1500 MHz to 18 GHz region, each probe contains three pair of mutually perpendicular elements, as shown in Figure 9-6. Resistive thermocouples are distributed along the length of the dipole at a spacing that will not permit resonance over the operating range of frequencies. The dipole may be viewed as a group of series-connected small resistive dipoles or as a very low Q resonant circuit.
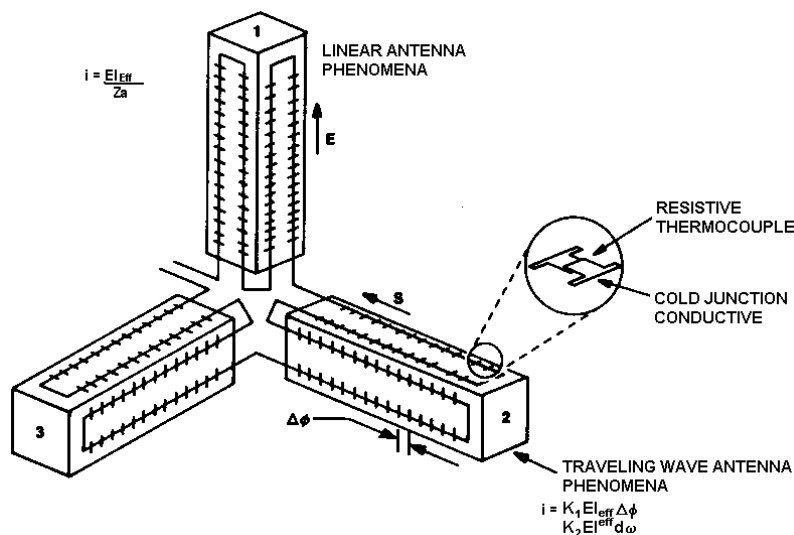
Figure 9-6. Typical thermocouple antenna array (courtesy of L-3 Communications, NARDA East).

Negative points associated with thermocouples are inherently lower output voltage than diodes causing "zero drift" and lower overload level. Early thermocouple based detectors exhibited excellent accuracy in complex, modulated field environments but were limited by overload specifications that a careless operator could exceed, thereby damaging or destroying these probes, although state of the art thermocouples now have overload protection of at least 2000% of full scale reading or 13 dB.

9.6 Measurement Problems and the Selection of Equipment

With any diode-based detector, there will be a point within its dynamic range (or distance from the RFR emitter) where it neither underestimates nor overestimates the average field reading. It may not be accurate except for this one point, or level, in front of the radar. Both diode and thermocouple sensors were recently tested by the author in front of the ROLAND air defense radar system (Figure 9-7). The Roland system features a fast rotating (60-rpm) radar with a minimal pulse width (400 nanoseconds pulse width, 5 kHz pulse repetition frequency). The diode sensor generated a reading that was 6 dB (a factor of four!) lower than the thermocouple probe. This disparity of values was to be expected, since the pulse width is short compared to the period required for a diode to perform accurate detection. In addition, other systems, such as the multi-emitter environment found at many military and telecommunication sites also require the appropriate selection of instrumentation since the RF fields around these systems are quite complex. With appropriate broadband equipment, measuring levels of RF around such systems when the RF levels are within 10 dB of the uncontrolled limits of IEEE or the public limits of the US FCC is entirely feasible. Shaped probe technology, which read out in ―percent of standard,‖ are particularly useful in the multi-emitter environment. It is therefore imperative that the surveyor has comprehensive knowledge of the ambient RF environment before beginning a survey.

Figure 9-7. Roland Air Defense System is an example of a system where diode based detection is inadequate to measure the RFR.

There are presently a number of different companies which market broadband RFR survey equipment. What, then, are some of the attributes of broadband instrumentation that the surveyor should keep in mind when selecting such equipment to perform an RFR field survey? Selection of the appropriate instrument depends on a number of factors that should be clearly understood before the instrument is obtained and include such issues as the ability to do spatial averaging, tolerance to in and out-of-band interference (particularly if magnetic fields are to be measured), and limitations of near field accuracy. Time and spatial averaging, required by the present IEEE RFR standard (IEEE, 1999), is often neglected in practice. Spatial averaging offers a much more useful picture of the actual exposure situation than a single point measurement. Therefore, in performing RFR field measurements where highly localized fields exist, spatial averaging techniques should be applied. In continuous field applications, like those found around RF induction sealers, measurements may be performed at different portions of the body

272

and averaged together manually. In the case of rotating radar where field levels are varying constantly, a time averaging capability is the only way to truly measure, and average, the total exposure. There are currently meters and personal monitors available that can perform this averaging automatically, assisting in determining time averaged exposure. There is at least one meter marketed which can perform spatial averaging over the body or workplace area and show the result automatically. This system has a "pause" feature that allows horizontal and vertical scan averages to be summed so that one can determine averages in multiple planes or for cubic areas. There is no doubt that continued advances in microprocessor technology will produce modules which will be able to perform all these functions, and because of their small size will produce minimal perturbations in the ambient RFR field. Early magnetic field probes of certain designs were not truly isotropic. A phenomena known as "spatial shadowing" existed wherein one or more of the three orthogonally mounted detector loops did not allow the same flux lines to pass through all loops. This was caused by the three loops not having a common vertex. Later designs have corrected this source of error. Nonetheless, these probes were still difficult, if not impossible, to use in multiple emitter applications because of their erroneous response to signals above their operating frequencies. Away from the controlled laboratory environment, where emitters are present throughout the frequency spectrum, large measurement errors are present when an out-of-band transmitter exists nearby a survey area. Newly designed magnetic field probes are now available that greatly enhances the accuracy and operator confidence in magnetic field measurements. Nonetheless, magnetic field measurements of low frequency emitters can be a difficult exercise for the novice surveyor and should not be accomplished without first understanding the limitations of the instrumentation. In addition to the problems associated with magnetic field measurements is the knowledge that in many instances the surveyor will be in the near field region of the emitter, where the RFR environment is very complicated, as shown in Figure 9-8. In order to perform near field surveys accurately the instrument must respond to only one field with no spurious responses; not produce significant scattering; and utilize isotropic, non-directional and non-polarized probes. In conclusion, users must be aware of not only the strong points of a particular system but also its weak points. No single broadband instrument currently available will meet the needs of all users. Even though products might be specified similarly their operation in a given environment may be significantly different. It is therefore important that the radiation protection professional be aware of these differences when choosing one for a particular application. The following guidelines should be useful in selecting a probe and meter for performing a survey: field sensors employing diode detection should only be used for continuous wave (CW) signals; average power measurements on pulsed and complex modulation signals should be measured using thermocouple probes; and finally, compensated diode sensors can be utilized for multiple-signal environments, but are not recommended for pulse modulated emitter measurements.
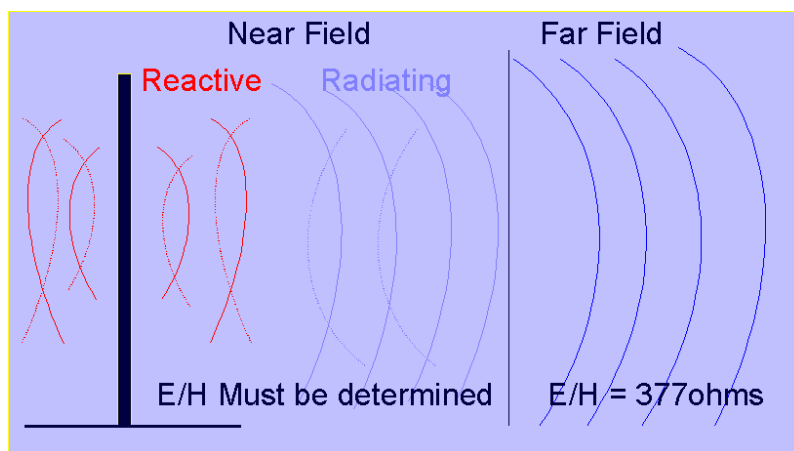
Figure 9-8. The RFR environment in the near field is complicated and requires measurement of both E and H.

9.7 Commercially Available Devices

A subset of broadband instrumentation are the personal monitors. They are not dosimeters in the true sense of the word, rather they are *densitometers*. This section is devoted to a general overview of the commercial personal monitors on the market today. For commercially available monitors, there are various types available to the general public or safety professional use. Designs start from simple detection devices available for $100.00 or less, and more capable units costing over $1,000.00 (in small quantities). The higher end units have performance similar to the broadband instrumentation previously discussed, albeit in a small package. Typical state of the art units are shown in Figure 9-9.

Figure 9-9. Typical RFR personal monitors (Drawings courtesy of Holaday Industries and L-3 Communications, NARDA East).

274

This section is meant to educate the reader about the basic designs, approaches and limitations of commercial instruments. Monitors generally fall into two categories, inexpensive (generally in-accurate) units without any traceability to their function or design, and those sold at higher prices that meet (generally accurate) their published, traceable specifications. The internet is a good source of the first category. Devices such as the ―MicroAlert‖ and others available for relatively little money, are simple diode detection designs that are coupled to an antenna to detect a wide range of frequencies. Because these units are not calibrated over their range of operation their applicability to safety evaluations is negligible. False alarms generated by these units along with their solar and/or temperature inaccuracies make them unsuitable for consideration for use by safety proessionals. The second group of monitors are built by what is now two companies, Hurley-General Microwave (GM, Farmingdale, NY) and L-3 Communications, Narda East (Hauppauge, NY). Previously Wandel and Goltermann (Eningen, Germany) developed the ―RadMan‖ monitor. That business group was purchased by Narda around 2000, and that monitor is now available from Narda as well. The General Microwave monitor is also sold by ETS-Lindgren, who recently purchased Holaday Industries (HI). The models and specifications are listed in Table 9-2 below.

Table 9-2. Commercially available personal monitors (2004).

Model	NARDA B8860 (Nardalert XT)	HI-3510 (GM H600A)	HI-3520 (GM 60A)	NARDA ESM-30 (Rad Man)
Frequency Range	100 kHz to 100 GHz	50 MHz to 2500 MHz	1 to 18 GHz	3 MHz to 40 GHz
Alarm Range	10 to 200% of Std.	0.05 to 20 mW/cm^2	0.05 to 20 mW/cm^2	12.5, 25, 50 and 100% of Std.
Frequency Response	Shaped to Std.	Flat	Flat	Shaped to Std.
Sensor Type	Multiple, Compensated Diode and Thermocouple	Compensated Diode	Thermocouple	Compensated Diode
Field Detected	E-field (see note 1)	H-field	E-field	E and H field
Features	Top mounted, Level Indication LED's, with two programmable alarms (vibration and/or audible). Data logging of exposures. External vibrator, weatherproof pouch	Top mounted LCD display of detected levels, programmable alarm	Top mounted LCD display of detected levels, programmable alarm	Front mounted LED's (4) for display of levels, fixed alarms at 50 and 100%. Removable absorber cap for use off the body.
Calibration Interval	Two years	One year	One year	Three years

Note 1: Manufacturer claims radial field sensor can detect field re-radiated from body, from either an incident E or H field.

275

Shortly before this chapter went to press, information was received of a new personal monitor developed by Antennessa of France (Antennessa, 2003). The DSP090 is a 9 band isotropic personal "dosimeter" (more correctly a densitometer) covering the lower FM band through the upper Universal Mobile Telecommunications – 3rd Generation (UMTS-3G) band. The manufacturer claims a 40 dB dynamic range from 0.05 to 5.0 V m^{-1} (6.63 x 10^{-7} to 6.63 x 10^{-3} mW/cm^2). These are extremely low levels in comparison to the levels measured by the other devices described, which are designed to show compliance with international standards such as IEEE (IEEE, 1999) and the International Commission on Non-Ionizing Radiation (ICNIRP, 1998). Apparently, the device is to be used in on-going epidemiological studies of low-level mobile communications RFR exposures in Europe.

It is important to understand RF personal monitors design, in order to evaluate their performance. One of the main limiting factors in the performance of a personal RF monitor is its ability to function independent of its proximity to the person wearing it, which can give errors greater than 2 dB. This scattering becomes more significant when broadband frequency performance and independence of polarization are required for proper operation. All of the monitors evaluated utilize a design similar to the drawing below (Figure 9-10).
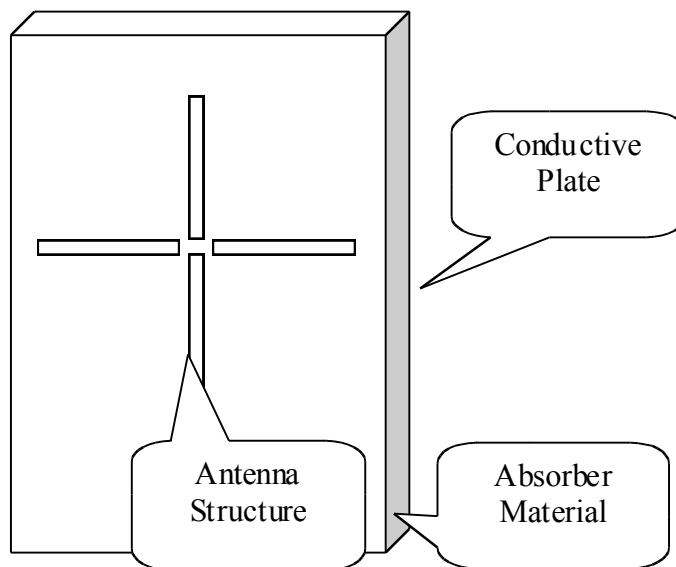
Figure 9-10. Basic RF monitor design to minimize effect of wearer.

All of the monitors tested employ this basic design. For example, the Nardalert XT utilizes the same basic structure, with modifications as is shown in Figure 9-11 below.
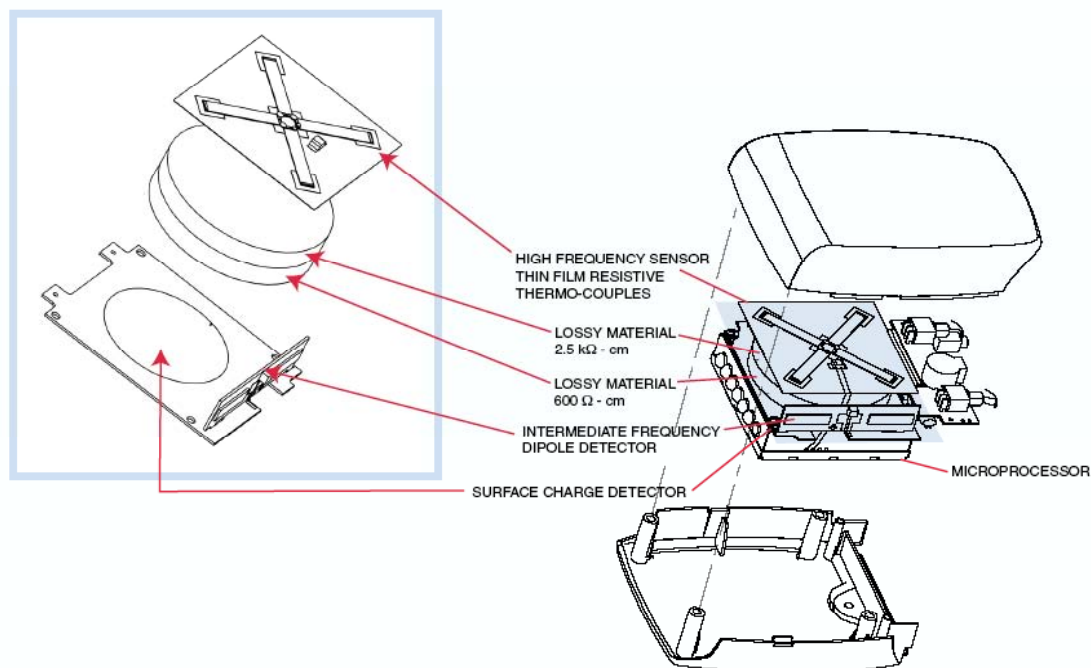
Figure 9-11. Nardalert XT internal view (Drawing courtesy of L-3 Communications, NARDA East).

Some conclusions can be made about the selection of a particular unit based on the following set of criteria:

1. Field sensors employing simple diode detection should only be used for continuous wave (CW) signals. Today, this type of detector is confined to the low-end market not suitable for safety evaluations. Such devices could alert the presence of leakage from a microwave oven, though not necessarily accurately quantify the amount of leakage.

2. Average power measurements on pulsed and complex modulation signals should be measured using thermocouple-based monitors.

3. Compensated diode sensors can be utilized for multiple-signal environments, but are not recommended for pulse modulated emitter measurements. However, due to their relative cost versus a thermocouple based detector, they can be utilized if appropriate correction factors are applied.

4. Although RMS average levels are specified in most exposure situations, if peak pulse power is the desired metric, specialized diode sensors need to be employed. None of the commercial monitors reviewed herein could perform this task at the present time, although the Nardalert XT did respond to a UWB field (see below). Future systems such as HPM and UWB will undoubtedly drive the development of such peak power detectors for general use.

277

5. Meters that operate with diode, or compensated diode, sensors need proper temperature compensation circuitry if systems are going to be operated over wide temperature ranges.

6. Personal RFR monitors are subject to shadowing by the human body. The manufacturer should be consulted to determine the correct placement of the monitor on the body.

9.8 Other Potential Personal RFR Monitors and Future Needs

The instrumentation already discussed allows the surveyor to make measurements of the exposure metrics of E, H which form the basis of all RFR standards. The instrumentation is analogous to ionizing radiation survey meters. These types of units have found wide applicability in the wireless communications industry. Personnel dosimetry similar to thermoluminescent dosimeters (TLDs) for ionizing radiation does not presently exist for RFR. Diazoluminomelanin (DALM) is a unique biopolymer, originally invented by Dr. Johnathan Kiel and co-workers at the U.S. Air Force Research Laboratory, Brooks City-Base, Texas. DALM may have characteristics that can form the basis of a true RFR personal dosimeter. DALM has the properties of luminescence, fluorescence, and slow fluorescence that has a broad optical absorption spectrum. When it is properly activated, it can absorb and store RFR energy, and on subsequent activation, it can release that energy via rapid luminescence followed by slow fluorescence. It has been postulated as a future personnel dosimeter for RFR (Kiel, 2000). It is thought that varying concentrations of DALM on a suitable substrate might form the basis for a personal RFR dosimeter (i.e., whose response at various frequencies is proportional to SAR). Work has also been done on investigating the potential for using a loop antenna with an alarm based on electrochemical changes in DALM to detect magnetic fields passively (Meltz & Smolenski, 2002). As of mid-2004, research on the unique properties of this organic bio-molecule continues.

Another possible personal monitor would be the use of a conducting vest that a person would wear. This concept began as an application of the body mounted antenna being developed by the U.S. Navy for tactical use. In this case the inherent receiving characteristics of the vest (i.e., antenna) would be used to measure the ambient electric field. Work on this device also continues.

Although RMS average field levels are specified in most RFR exposure situations, if peak pulse power is the desired quantity specialized diode sensors need to be employed. None of the commercial sensors reviewed in this chapter could perform this task at the present time. Future military and commercial UWB systems will undoubtedly drive the development of such peak power detectors for *general* use. The Nardalert XT has been tested in a UWB field. The monitor was placed in a GTEM cell, excited by a UWB pulse, perpendicular to the direction of the Electric Field (E-Field). Test conditions were as follows:

Peak E-Field amplitude was adjusted to 100 kV/m (nominal)
Pulse Repetition Frequency: 250 and 500 Hz
Exposure duration: 5 min.

278

Two UWB waveforms per exposure were recorded for a 5-min exposure duration. The Nardalert XT produced results within 3 dB of the expected value, which is within the errors associated with the measurement of a ―traditional" RFR pulse. This encouraging result will no doubt be further investigated as the need for UWB monitors increases.

Another area which will need to be explored in the future is testing of personal RFR monitors to an established standard. For example, ionizing radiation survey instruments are tested to an ANSI standard (ANSI, 2004), and ionizing radiation dosimetry vendors must meet the criteria of the National Voluntary Laboratory Accreditation Program (NVLAP). In addition to testing these devices to established radiation fields, testing is also performed for resistance to environmental conditions (temperature, humidity, mechanical shock) and other factors such as radiated susceptibility and resistance to electostatic discharge.

9.9 Acknowledgments

9.10 References

American National Standards Institute (ANSI). (2004). *American National Standard Performance Criteria for Alarming Personal Radiation Detectors for Homeland Security*. New York, NY: American Standards Instititute, ANSI N42.32, 2004.

Antennessa. (2003). *DSP090 9 Bands Isotropic Selective Personal Dosimeter*. [Product Brochure], Antennessa SA, Plouanze, France.

Institute of Electrical and Electronics Engineers (IEEE). (1999). *IEEE Standard for Safety Levels With Respect to Human Exposure to Radio Frequency Electromagnetic Fields, 3 kHz to 300 GHz (*IEEE C95.1-1998). New York, NY: Institute of Electrical and Electronics Engineers.

Institute of Electrical and Electronics Engineers (IEEE). (2002). *Recommended Practice for Measurements and Computations with Respect to Human Exposure to Radio Frequency Electromagnetic Fields*, 3 kHz to 300 GHz (C95.3-2002). New York, NY: Institute of Electrical and Electronics Engineers.

International Commission on Non-Ionizing Radiation Protection (ICNIRP). (1998). Guidelines for Limiting Exposure to Time-Varying Electric, Magnetic, and Electromagnetic Fields (Up to 300 GHz). *Health Physics*, *74*, 494 – 522.

Kiel, J. L. (2000). Molecular dosimetry. Radio Frequency Radiation Dosimetry and its Relationship to the Biological Effects of Electromagnetic Fields. *Proceedings of the NATO Advanced Research Workshop* (pp. 227-238). Norwell, MA: Kluwer Academic Publishers.

Leonowich, J. A. (1992). Measurement of Radiofrequency Fields. Non-ionizing radiation. *Proceedings of the 2nd International Non-ionizing Radiation Workshop* (pp. 96-124). Vancouver: UBC Press.

Leonowich, J. A. (1997). Introduction and Physics of Non-ionizing radiations (NIR), In: Non-ionizing Radiation: An overview of the Physics and Biology, *Proceedings of the 1997 Health Physics Society Summer School* (pp. 1-16). Madison, WI: Medical Physics Publishing.

Meltz, M. & Smolenski, D. (2002). *Electromagnetic Exposure Indicator* (AFRL-HE-BR-TR-2002-0022). February 2002. (Limited Distribution)

Radio Frequency Radiation Dosimetry Handbook
(Fifth Edition)

Chapter 10. RF Alerting Signs

Richard A. Tell
Richard Tell Associates, Inc.
1872 E. Hawthorne Avenue
Colville, WA 99114

rtell@radhaz.com

10.1 Introduction

Hazard communication is the single most effective factor in maintaining safety in a hazardous environment aside from removing the hazard itself. Such communication can take the form of written or verbal information or some form of safety awareness training. Safety signage represents a common form of communication across a wide range of potential hazards and this applies equally to radio frequency (RF) environments. In fact, RF safety signage constitutes a crucial aspect of most RF safety programs (IEEE, 2005a).

RF safety signage, beyond simply alerting personnel or the public to the fact that a potential hazard may exist, can be used to distinguish between different levels of hazard or the particular nature of the RF hazard. For example, signs are commonly used to indicate areas in which RF field exposures may exceed recommended or regulatory limits of exposure but may also discriminate between different levels of seriousness associated with the potential exposure through the use of certain signal words printed on the sign. Other signs can inform about the potential for excessive contact currents and RF burns. Hence, appropriate RF alerting signs represent an important element of most RF safety programs and their application is likely one of the most cost effective methods for conveying important safety information to persons exposed to potential RF hazards.

Historically, the first RF alerting sign used in the United States (US) was developed for use by the US Navy and, subsequently, the overall Department of Defense, and appears in Figure 10-1. This sign appeared in the first publication of the C95.2 standard developed at the time by the United States of America Standards Institute (USASI, 1966). This particular design remained in use throughout the Department of Defense and was specified in a subsequent standard issued by the US Occupational Safety and Health Administration (OSHA, 1971). While the original sign design specified in 1966 is still used within the US Department of Defense (see Figure 10-2), this sign design was significantly updated and changed with the issuance of a new IEEE standard in 1999 (IEEE, 1999).
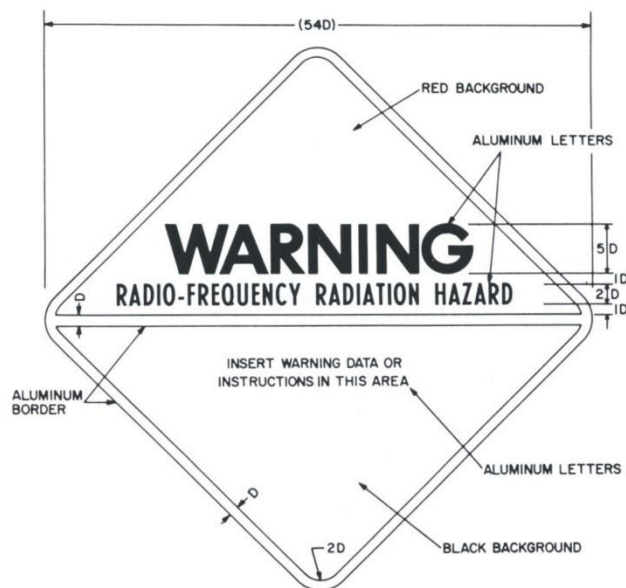
Figure 10-1. Original RF warning sign published in 1966.

Figure 10-2. Current RF alerting sign example used within the US Department of Defense.

282

10.2 Meanings Associated with Different Signs

In the realm of safety signage used in the US, particular signal words have been recommended (ANSI, 2002). A signal word is a word that is displayed prominently, usually at the top of the sign, to convey the degree of safety alerting associated with exposure. For example, the words caution, warning, and danger carry specific meanings in the sense of hazard communication. These words have been adopted for use in recommendations related specifically to RF safety signage in the US (IEEE, 1999).

RF alerting signs can express a wide range of hazard conditions extending from informational signs to danger signs. In each case, signal words are used to express different levels of alerting and, generally, carry the following meanings.

DANGER signs, with a red banner across the top, are to be used to indicate an imminently hazardous situation that, if not avoided, will result in death or serious injury. This signal word is to be limited to the most extreme situations. Figure 10-3 illustrates an example of an RF Danger sign.

Figure 10-3. Example of a DANGER RF alerting sign used to advise of potential RF burn hazards.

WARNING signs, with an orange banner across the top, are to be used to indicate a potentially hazardous situation that, if not avoided, could result in death or serious injury. Figure 10-4 illustrates an example of an RF Warning sign.

283

Figure 10-4. Example of an RF Warning sign following IEEE C95.2-1999.

CAUTION signs, with a yellow banner across the top, are to be used to indicate a potentially hazardous situation that, if not avoided, could result in minor or moderate injury. It may also be used to alert against unsafe practices. Figure 10-5 illustrates an example of an RF Caution sign.
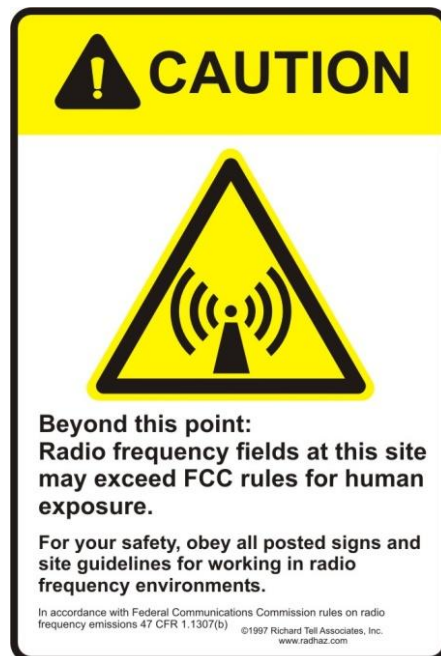
Figure 10-5. Example of an RF Caution sign following IEEE C95.2-1999.

284

NOTICE signs, with a blue banner across the top, are to be used to indicate a statement of organization policy as the message relates directly or indirectly to the safety of personnel or protection of property and this signal word should never be associated with a hazard or hazardous situation in place of *DANGER*, *WARNING*, or *CAUTION*. Figure 10-6 illustrates an example of an RF Notice sign.
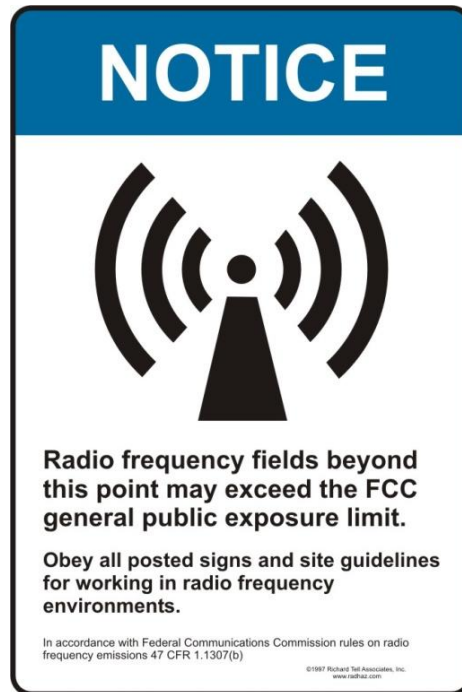
Figure 10-6. Example of an RF Notice sign following IEEE C95.2-1999.

INFORMATION signs, commonly employing a green banner on the sign, are generally used to provide some sort of general instructions relative to safety work practices, reminders of proper safety procedures, or the locations of safety equipment. An example might be a notice to maintain a certain clearance distance from an active antenna or to provide a relevant telephone number to obtain additional information about RF sources at a transmitter site. Figure 10-7 illustrates an example of an RF Information sign.

285
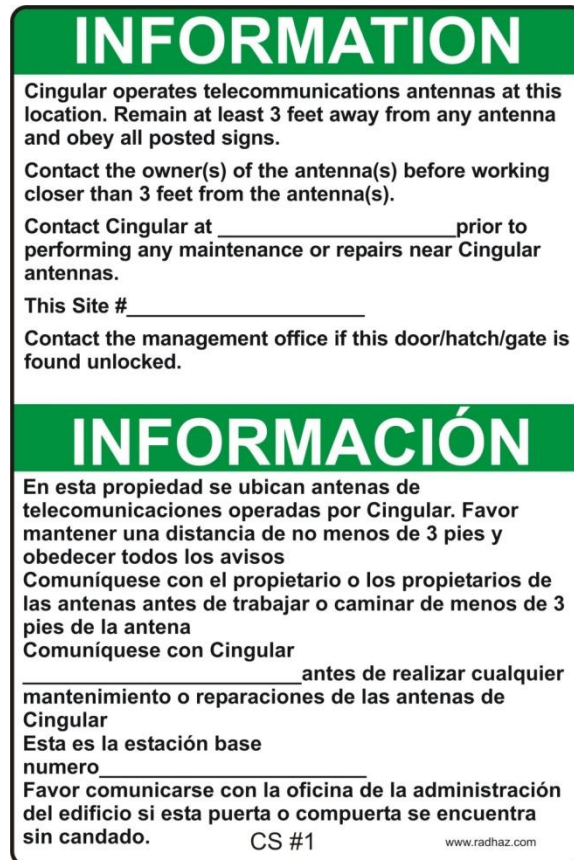
Figure 10-7. Example of an RF Informational sign commonly used at cellular telephone base stations.

10.3 Sign Usage

In the US, these particular signal words have been used to identify areas wherein RF fields may be found that exceed certain field strength levels. The Notice sign is commonly used to alert persons to the possibility that exposure may exceed the exposure limits associated with the general public. This is, for example, considered an Action Level in IEEE C95.1-2005 (IEEE, 2005b) above which an RF safety program is required. The Caution sign is normally used to designate areas in which exposures have the possibility of exceeding the maximum permissible exposure (MPE) specified in IEEE C95.1-2005. The Danger sign, while not normally directly associated with RF field exposure, is used to alert personnel to the potential for RF burns when contacting objects that may represent a direct contact hazard due to tissue damage.

While standard practice in the US is to associate the Caution sign with potential exposure above the MPE, some may argue that such exposures would not be expected to result in a ―minor or moderate injury‖ since the applicable exposure limits are set a safety factor of ten below the exposure that could, if prolonged, result in an adverse health effect. Nonetheless, for practical purposes, the assumption is commonly made that an exposure above the MPE be associated with the use of RF Caution alerting signs. Similar statements could be made about the use of the

286

Danger signal word for exposure to RF fields and this is why, in most situations, the use of the Danger sign is not used.

Detailed specifications as to colors, font sizes, alignment of text, and use of certain symbols are given in IEEE C95.2-1999.

10.4 Application of RF Alerting Signage

RF alerting signs are used to advise persons of the potential for hazards from their exposure to RF fields in a particular area. Installation of signs should follow the guidance discussed above with the sign installed such that it provides the most accurate indication of areas that should be restricted in access. The nature of the site should influence the specific location where signs will be mounted. For example, for a rooftop wireless antenna site, such as used by cellular telephone base stations, ideally the signs, if deemed necessary, should be placed as close to the region of concern as practical since the most intense RF fields will be directly in front of the transmitting antennas. This could be the mounting framework for the antenna(s) or some other location near the point where RF fields exceed the action level or MPE of an RF exposure standard or regulation. In many instances, RF alerting signage may be placed on the roof access door as opposed to the location where excessive exposure could occur. Such mounting points provide little guidance for the person needing access to the roof since it may be assumed that the entire roof is potentially noncompliant with the exposure limits and can, unnecessarily, impact on rooftop operations that might carry no risk of excessive exposure. A similar sign placement strategy should be used in factory environments where occupational exposures may be associated with the use of RF dielectric heat sealers or induction heaters.

Conversely, at high power broadcast sites wherein strong RF fields may encompass a much larger geographic region, the placement of RF alerting signage may not require such specific placement since the spatial distribution of fields can be substantially more widespread. In some cases, however, installation of signs, even at broadcast sites, may be appropriately confined to locations, such as towers, to advise of the potential for excessive exposure when climbing near high power antennas. Such a sign is seen in Figure 10-8. This sign, if the narrative on it is followed by personnel climbing antenna towers supporting active transmitting antennas, has the potential of incorporating the crucial elements of an RF safety program in that it requires that persons accessing the tower be provided with RF safety information and that they make use of RF personal monitors to provide a direct indication of their potential exposure levels.

287

Figure 10-8. Example of an RF Caution sign designed to alert personnel to localized RF exposure on antenna towers following IEEE C95.2-1999.

10.5 References

American National Standards Institute (ANSI). (2002). *American National Standard for Environmental and Facility Safety Signs* (ANSI Standard Z535.2-2002). Rosslyn, VA: National Electrical Manufacturers Association, 1300 N. 17th Street, USA.

Institute of Electrical and Electronics Engineers, Inc. (IEEE). (1999). *IEEE Standard for Radio-frequency Energy and Current Flow Symbols* (IEEE Standard C95.2-1999) (reaffirmed 2005). New York, NY: The Institute of Electrical and Electronics Engineers, 3 Park Avenue, USA.

Institute of Electrical and Electronics Engineers, Inc. (IEEE). (2005a). *IEEE Recommended Practice for Radio Frequency Safety Programs, 3 kHz to 300 GHz* (IEEE Std C95.7-2005). New York, NY: The Institute of Electrical and Electronics Engineers, 3 Park Avenue, USA.

Institute of Electrical and Electronics Engineers, Inc. (IEEE). (2005b). *IEEE Standard for Safety Levels with Respect to Human Exposure to Radio Frequency Electromagnetic Fields, 3 kHz*

to 300 GHz (IEEE Std C95.1-2005). New York, NY: The Institute of Electrical and Electronics Engineers, 3 Park Avenue, USA.

United States of America Standards Institute (USASI). (1966). *USA Standard Radio-Frequency Radiation Hazard Warning Symbol* (USAS Standard C95.2-1966). New York, NY: United States of America Standards Institute.

Occupational Safety and Health Administration (OSHA). (1971). *Occupational Safety and Health Administration.* ―Nonionizing radiation," (29 CFR 1910.97). Washington, DC: Occupational Safety and Health Administration.

Radio Frequency Radiation Dosimetry Handbook
(Fifth Edition)

Chapter 11.   Current Status of EMF Standards and Handbooks - Information for the General Public

Dina Simunic
University of Zagreb
Faculty of Electrical Engineering and Computing
Unska 3
HR-10000 Zagreb, Croatia
Croatia

dina.simunic@fer.hr

11.1   Introduction

The World Health Organization (WHO) International Electromagnetic Fields Project, with 54 participating countries and eight international organizations involved, is a leading institution in the important harmonization process of electromagnetic fields (EMF) legislation, research and information in the world.[1] The process of harmonization is necessary due to increasing public anxiety, which is a consequence of the rapid introduction of new technologies using electromagnetic energy. This legislation harmonization effort consists of three phases:

1. Information gathering of existing regulatory acts in the world;
2. Development of a common framework for harmonization (WHO, 2009);
3. Application of the developed framework, meaning actual harmonization of world EMF legislation.

This paper is a consequence of the first phase, performed during the last two years (2002-2004), where information on EMF standards of 48 countries has been collected. Besides the standards information, information about published handbooks, reports, pamphlets, and fact sheets for general public education have been collected at the same WHO EMF standards database (Simunic & Bullock, 2003). It is important as part of the harmonization process to collect information on both standards and handbooks, because both are integral parts of the overall state of EMF legislation within a country.

EMF legislation is very important at present, but will be even more so in the future, because we already live in an era having extensive applications of electromagnetic fields (e.g., medical therapeutic applications, a variety wireless home appliances and toys, wireless communications). In the future, it is expected that not only communications but also the entire human environment will be connected via wireless devices (e.g., new concepts of ―smart‖ homes and ―smart‖ hospitals).

---

[1] The first WHO Roundtable Meeting with a considerable number of participating countries about harmonization of EMF standards was held November 20, 1998 in Zagreb, Croatia.

Because many of these applications of electromagnetic fields appeared less than 30 years ago (personal communications, electromagnetic therapy), all possible biological effects of EMFs are not yet known. Given the high expectancy for a future ―smart‖ (i.e., ―wireless-human‖) environment, the study of possible biomedical effects of EMFs is a very sensitive field, which will benefit from global harmonization and total knowledge sharing to support progress of the human race.

11.2 WHO International EMF Project Standards Database

The WHO International EMF Project Standards Database (Simunic & Bullock, 2003) relies on results of a questionnaire that was circulated to the member countries in 2002. The WHO standards database is very useful because it enables a thorough and quick overview of existing EMF national legislative instruments from around the world (Simunic & Bullock, 2003).

The questionnaire contains 23 questions pertaining to general details of national legislations:

1. Name of the country
2. Existence of EMF protection at the national level?
3. Description of the legislative instrument type (guidelines, standard, regulation, law,…)?
4. Instrument coverage (national, regional, or local)?
5. Title of the instrument?
6. Who issued the instrument?
7. When it was issued?
8. Are any revisions pending?
9. Are the exposure limits based on International Commission on Non-Ionizing Radiation Protection (ICNIRP) (1998)?
10. Is the instrument voluntary or mandatory?
11. If mandatory, how is compliance verified?
12. Which population group is protected (general public or occupational)?
13. What frequency ranges does the instrument cover?
14. Which quantities are in force for the instrument?
15. What are the basic restriction quantities (ICNIRP or Non-ICNIRP)?
16. If specific absorption rate (SAR) is one of the basic restriction quantities, details about SAR averaging time, averaging mass and measurement method are given
17. Which reference level quantities are applied by the instrument?
18. Which measurement method is applied for determining compliance of the reference level?
19. Are multiple frequency exposures considered in the instrument?
20. Are pulsed field exposures considered in the instrument?
21. Relevant contact persons and agencies to obtain more information about the instrument
22. Who can provide the limit data, as defined in the instrument? (the limit data can be given in separate tables on the national web page, after the general part of the instrument)
23. Is there an EMF handbook for information of general public published at the national level? If yes, the details of the handbook are given (title, editor, publisher,

publication date, number of pages, language, whether it is based on an already published WHO brochure, and contact details to obtain the handbook).[2]

The WHO standards database table is based on the presumption that most countries would implement or have implemented ICNIRP guidelines into their legislative instruments. However, if there are any differences in the exposure limits relative to ICNIRP, these are appended as tables on the same sub-webpage, designed for the whole frequency spectrum (from static electric and magnetic fields to time-varying electric and magnetic fields up to 300 GHz). Also comments are included describing any specificities of the legislative instrument. The first twelve questions require answers that classify the national legislative instruments according to the type (e.g., law, guidelines, standard, regulation, etc.) and give basic information about the instrument, i.e., title, issuing year, issuing institution, nature (mandatory, voluntary), coverage [entire territory of the country (national coverage), or a part of the territory (regional or even local coverage)], definition of protected group of population, frequency range, and about planned revision (in the case of an older legislative act being valid). The second part of the table (questions no. 14-17) deals with the limit values, describing the corresponding applied physical quantities for basic restrictions and reference levels, and describing details about the SAR specifications. Questions 9 and 18 pertain to the details of the required compliance with the instrument. Answers to questions 19 and 20 provide information on existing treatment of multiple frequencies and pulsed field exposures. The next two questions (21 and 22) are related to contact information for the relevant authority or responsible party for the instrument and for the limit data. The last answer in the table (no. 23) gives information about advising the population by means of handbooks (including bibliographic details of any handbooks, brochures, short information papers, such as title, editor, publisher, publication date, number of pages, language, whether it is based on the existing WHO brochure, and contact or ordering details).

11.2.1 International EMF Legislation

Countries throughout the world follow mostly three schemes for EMF exposure standards:

1. Adoption of international ICNIRP guidelines (ICNIRP, 1998) into national legislation as a legally binding instrument;
2. Adoption of international IEEE C95.1 standard (IEEE, 1999) into national legislation as a legally binding instrument;
3. Development of their own separate national standard, based on their own research and experiences (e.g., East European standards).

ICNIRP Guidelines provide two-tier limit values, for occupational and for general public exposures. Restrictions or limits to EMF exposure are called *basic restrictions* and *reference levels*.

Basic restrictions are restrictions on exposure to time-varying electric, magnetic and electromagnetic fields, which are based directly on established health effects and biological considerations. The basic restrictions are based on the following physical quantities: magnetic flux density (B), current density (J), specific energy absorption rate (SAR), specific energy

---

[2] More information about handbooks is given in the next chapter.

absorption (SA) and power density (S). The use of the physical quantity that best describes the basic restrictions depends on the part of the used electromagnetic spectrum. Compliance with the basic restrictions will ensure protection against all known adverse health effects.

Reference levels are derived from the basic restrictions for the condition of maximum coupling of the electromagnetic field to the exposed individual in order to facilitate practical exposure assessment. Since the derivation is based on providing maximum protection, reference levels determine whether the basic restrictions are exceeded, or whether the exposure conditions are well under biological consideration levels. Reference levels consist of the following physical quantities: electric field strength (E), magnetic field strength (H), magnetic flux density (B), power density (S) and limb current (J_L). Besides these, the reference level used to describe perception and other indirect effects is contact current (I_C). Reference levels are calculated from basic restrictions in such a manner as to be ―worst case.‖ This means that compliance of the defined reference level will ensure compliance of the related basic restriction. However, if the measured value exceeds the reference level, this does not necessarily mean that the basic restriction will be exceeded, but rather that it is necessary to perform further evaluations (calculations/measurements of the basic restriction) to determine compliance with the basic restriction.

ICNIRP Guidelines also define a simultaneous exposure to multiple frequency fields for the case of electrical stimulation (from induced current density as well as from electric and magnetic field strength) and for the case of thermal effects (handling of SAR and power density, as well as for electric and magnetic field strength and limb and contact currents).

11.2.2 Regional EMF Legislation

An example of the regional legislation exists in the European Economic Area and it is based on two main documents, European Council (EC) Recommendation 1999/519/EC (EC, 1999) and Directive 2004/40/EC (2004), which follow the ICNIRP Guidelines for general population (1999/519/EC) (EC, 1999) and for occupational (2004/40/EC) (European Parliament and Council of European Union, 2004) exposures. All Member States of the European Union are obliged to adhere to the limit values and EMF physical quantities defined in Directive. As seen from Tables 11-1, 11-2 and 11-3 most of the countries in EEA implemented the Recommendation 1999/519/EC as a mandatory act in the national legislation.

Both documents spell out that the Member States should provide detailed rules in regards to the classification of electromagnetic field sources and measuring practices, by using IEC, CENELEC or a national standard. The Member States may, in accordance with the Treaty Establishing the European Community (1957), provide a higher level of protection than that set out in the mentioned Recommendation or Directive. On the other hand, adoption of EC regulations in the EMF area (in accordance with the Treaty) enforces changes in the existing legislation of some new Member States.

11.2.3 Other National EMF Legislation

In addition to the Member States of the regional EU, most countries in South America, Asia, Australia, New Zealand, and Africa have also adopted ICNIRP Guidelines.

EMF protection on the North American continent (USA and Canada) is based on *maximum permissible exposure* in *controlled* and *uncontrolled environments* from the IEEE C95.-1-1999 Standard (1999). A *controlled environment* corresponds to occupational exposure*,* whereas an *uncontrolled environment* corresponds to the general public (general population) exposure. *Maximum permissible exposure (MPE)* relates to the root mean square (RMS) and peak electric and magnetic field strengths, their squares, or the plane-wave equivalent power densities associated with these fields, and the induced and contact currents to which a person may be exposed without harmful effect and with an acceptable safety factor.

The best example of East European legislation is the Russian Federation's, based on federal law, standards (GOSTs), and sanitary-epidemiological regulations and norms (SanPiNs). Basic restriction physical quantities are based on energy loading, which differs from SAR. The reference level quantities are the same as in ICNIRP.

11.2.4 Overview of Who National EMF Standards Database

Data has been gathered from 48 countries on all continents (31 European countries, 2 Middle East countries, 2 North American countries, 2 South American countries, 8 Asian countries, 2 countries from Australia & Oceania, and 1 country in Africa), which all have EMF legislation. Approximately three fourth of the total countries (36) have adopted ICNIRP guidelines. An approximate one third of the total (i.e., 16) number of countries has stricter legislative acts than ICNIRP. This is mostly valid for specific RF exposure of mobile telephony and thus related more to emission standards. The need for communication about EMF with the general population is particularly high in this segment, because of the specific practices of installing base station transmitters in general public areas. As seen in Tables 11-1, 11-2 and 11-3, almost all countries use a consistent approach across the frequency range (almost the same coverage of static, ELF, and RF legislative acts is present throughout the database).

11.2.4.1 Static Fields

Table 11-1 shows the worldwide policies concerning static fields from WHO EMF Standards Database.

294

Table 11-1. Some worldwide policies concerning static fields.

Legislative Act	Voluntary	Mandatory	Country
ICNIRP 1994 (ICNIRP, 1994)		Australian Radiation Protection and Nuclear Safety Regulations, 1999	Australia
ICNIRP **/No static fields/ (1998)**		480/2000	Czech Republic
	ICNIRP 1998		Malta
	Guidelines for Human Protection from EMF Exposure, 2001		Republic of Korea
	Hazardous Substances Act, 1989, 2001		South Africa
	Limits for Environmental Exposure to Non-ionizing radiation, 2001		Taiwan

Table 11-1. Some worldwide policies concerning static fields (cont.).

Legislative Act	Voluntary	Mandatory	Country
1999/519/EC		Regulation, 2002	Estonia
		Ordinance on non-ionising radiation control, 2002	Finland
		Decret	France
		1105/volII/2000	Greece
		63/2004 (VII.26)ESzCsM, 2004	Hungary
		Planning and Development Act, 2001	Ireland
		151-A/2000	Portugal
	Recommendation		Romania
		Royal Decree 1451/2000	Spain
	SSI FS 2002:3		Sweden
		Ordinance relating to Protection from Non-Ionising Radiation, 814.710, 2000	Switzerland
	NRPB advice vol 15,2, 2004		UK
1999/519/EC with a precaution factor		Ordinance 192/2003, pos.1883[3]	Poland
		Ordinance 204/2003	Croatia[4]
Pre-ENV 50166-1995 **CENELEC, 1995** **Status: withdrawn**	ONORM S1119 /pre-ENV 50166-1995/		Austria
	LVS /pre-ENV 50166-1995/		Latvia
National Act		Sanitary norm 2.2.4.1191-03 "Electromagnetic fields in occupational environments"	Russian Federation[5]
Precautionary/ environmental guidelines		Decree Official Gazette RS, no. 70/96	Slovenia[6]
	1997 Guideline for decision makers on use of the Precautionary Principle		Sweden

---

[3] (http://www.who.int/docstore/peh-emf/EMFStandards/who-0102/Europe/Poland_files/table_pl.htm)

[4] (http://www.who.int/docstore/peh-emf/EMFStandards/who-0102/Europe/Croatia_files/table_hr.htm)

[5] (http://www.who.int/docstore/peh-emf/EMFStandards/who-0102/Europe/Russia_files/table_rs.htm)

[6] The limit values in Slovenia are currently under change (2004, November).

11.2.5 ELF Fields

Table 11-2 shows the worldwide policies concerning ELF fields from WHO EMF Standards Database.

Table 11-2. Some worldwide policies concerning ELF.

Legislative Act	Voluntary	Mandatory	Country
ICNIRP 1998 guidelines for general population		480/2000	Czech Republic
		Decree26BImSchV1996	Germany
	Report on Recommendations for limiting human exposure to time-varying electric, magnetic and electromagnetic fields in the freq. range from 0-300 GHz, 2000 EMF		Malta
	Guidelines for Human Protection from EMF Exposure, 2001		Republic of Korea
	Health Sciences Authority Health and Safety Guideline on EMF Exposure, 2001		Singapore
	Hazardous Substances Act, 1989, 2001		South Africa
	Limits for Environmental Exposure to Non-ionizing radiation, 2001		Taiwan
	1999/519/EC		EC
ICNIRP		2004/40/EC Directive	EC
		UTE C 99-111	France/ 2004/40/EC

297

Table 11-2. Some worldwide policies concerning ELF (cont.).

Legislative Act	Voluntary	Mandatory	Country
1999/519/EC		Regulation, 2002	Estonia
		Ordinance on non-ionising radiation control, 2002	Finland
		Decret 2002-775	France
		63/2004 (VII.26)ESzCsM, 2004	Hungary
		HN 104:2000	Lithuania
		Circular no.1644 (ref. 26/94)	Luxembourg
		Planning and Development Act, 2001	Ireland
		151-A/2000	Portugal
		1999/519/EC	Romania
		1451/2000	Spain
	SSI FS 2002:3		Sweden
	NRPB advice vol 15,2, 2004		United Kingdom
1999/519/EC with a precaution factor		Ordinance 192/2003, pos.1883[7]	Poland
		Ordinance 204/2003	Croatia[8]

Legislative Act	Voluntary	Mandatory	Country
Pre-ENV 50166-1995 **CENELEC, 1995** **Status: withdrawn**	ONORM S1119 /pre-ENV 50166-1995/		Austria
	LVS /pre-ENV 50166-1995/		Latvia
National Act		Ministerial ordinance of Technological Standards for Thermal Facilities based on the Electricity Utilities Industry Law, 1976	Japan
		Sanitary norm 2971-84	Russian Federation[9]

---

[7] (http://www.who.int/docstore/peh-emf/EMFStandards/who-0102/Europe/Poland_files/table_pl.htm)

[8] (http://www.who.int/docstore/peh-emf/EMFStandards/who-0102/Europe/Croatia_files/table_hr.htm)

[9] (http://www.who.int/docstore/peh-emf/EMFStandards/who-0102/Europe/Russia_files/table_rs.htm)

Table 11-2. Some worldwide policies concerning ELF (cont.)

Legislative Act	Voluntary	Mandatory	Country
Precautionary/ environmental guidelines		2001 Environmental guideline of 1μT	Israel
		Italian framework law 36/2001. Decree 2003	Italy
		Decree on Electromagnetic Radiation in the Natural and Living Environment, 1996 Official Gazette RS, no. 70/96	Slovenia
		1999 NIR ordinance plant limits of 1μT at sensitive use locations	Switzerland
	1997 Guideline for decision makers on use of the Precautionary Principle		Sweden
		1999 California EMF program	USA California
Planning guidelines for new facilities	Involve public in decision making process for siting of facilities	Not in close proximity to sensitive areas	Australia, Italy
	Guidelines for the siting of electrical power installations, 1998		Ireland
		―Sensibly dealing with risks" January 2004/State secretary of public housing, spatial Planning and the environment document presented to Parliament.	The Netherlands
		SanPiN 2.1.2.1002-00	Russian Federation
		Connecticut Legislature (US) proposal to restrict power-line installation in sensitive areas.	USA Connecticut
Agreement between industry and government or local municipalities	Prudent Avoidance		Australia

299

11.2.6 RF Fields

Table 11-3 shows the worldwide policies concerning RF fields from WHO EMF Standards Database.

Table 11-3. Some worldwide policies concerning RF.

Legislative Act	Voluntary	Mandatory	Country
ICNIRP		480/2000	Czech Republic
		Degree 26th BlmSchV, 1996	Germany
	Report on Recommendations for limiting human exposure to time-varying electric, magnetic and electromagnetic fields in the freq. range from 0-300 GHz, 2000 EMF		Malta
	Guidelines for Human Protection from EMF Exposure, 2001		Republic of Korea
	Health Sciences Authority Health and Safety Guideline on EMF Exposure, 2001		Singapore
	Hazardous Substances Act, 1989, 2001		South Africa
	Limits for Environmental Exposure to Non-ionizing radiation, 2001		Taiwan
	1999/519/EC		EC
ICNIRP		2004/40/EC Directive	EC
		UTE C 99-111	France/ 2004/40/EC

Table 11-3. Some worldwide policies concerning RF (cont.).

Legislative Act	Voluntary	Mandatory	Country
1999/519/EC		Regulation, 2002	Estonia
		Ordinance on non-ionizing radiation control, 2002	Finland
		Decret 2002-775	France
		63/2004 (VII.26)ESzCsM, 2004	Hungary
		Planning and Development Act, 2001	Ireland
		HN 80:2000	Lithuania
	ITM- CL 179.2		Luxembourg
		151-A/2000	Portugal
	1999/519/EC		Romania
		1451/2000	Spain
	SSI FS 2002:3		Sweden
	NRPB advice vol 15(2), 2004		UK
ICNIRP 1998/ 1999/519/EC with a precaution factor	1105/volII/2000		Greece
		Standard	Luxembourg
		Ordinance 192/2003, pos.1883	Poland
		Ordinance 204/2003	Croatia

301

Legislative Act	Voluntary	Mandatory	Country
Pre-ENV 50166-1995 **CENELEC, 1995** **Status: withdrawn**	ONORM S1120 /pre-ENV 50166-1995/		Austria
	LVS /pre-ENV 50166-1995/		Latvia
National Act		Radio-Radiation Protection Guidelines for Human Exposure to EMF, 1997	Japan
		Sanitary norm 2.2.4.1191-03	Russian Federation[10]
Precautionary/ environmental guidelines		Italian framework law 36/2001. Decree 2003.GU n.199	Italy
		Decree on Electromagnetic Radiation in the Natural and Living Environment, 1996	Slovenia
		NIR ordinance relating to Protection from Non-Ionizing Radiation	Switzerland
	1997 Guideline for decision makers on use of the Precautionary Principle		Sweden

---

[10] (http://www.who.int/docstore/peh-emf/EMFStandards/who-0102/Europe/Russia_files/table_rs.htm)

302

11.3 EMF Handbooks Information for General Public

Handbooks are valuable tools for education of the general public. Regarding the field of biological effects of electromagnetic fields, the first handbook was the *Radiofrequency Radiation Dosimetry Handbook* (Durney, Massoudi & Iskander, 1986). This handbook was published in 1978, 1980 and 1986 and it has been internationally recognized. Since many generations of experts and scientists have learned the basics of electromagnetic dosimetry from it, it represents one of the cornerstone publications in the field of bioelectromagnetics. The *RFR Dosimetry Handbook* was written for readers having some engineering and scientific knowledge and background, to promote deepening knowledge about electromagnetic fields dosimetry.

Meanwhile, the world has perceived an introduction of a lot of new kinds of wireless communications, as well as the other applications of EMF technology. Thus, the task of the *International EMF Dosimetry Handbook* is to update the existing *RFR Dosimetry Handbook* and to include data and knowledge, gathered since 1986. The readers still remained professionals interested in EMF dosimetry, i.e., electrical engineering professionals, epidemiologists, medical professionals, biologists conducting experiments ―in vivo" and ―in vitro" and governmental professionals establishing exposure standards.

On the other hand, this paper gives insights and information from national governmental bodies on the topic of biomedical effects of electromagnetic fields to the general public in the WHO. The overview at the database shows that the available materials from different countries are written using different approaches, being the consequence of different cultures around the globe. The general public in some countries has very brief material at its disposal (fact sheets and press releases); in other countries there are elaborate and extensive state-of-the-science reviews (reports).

Literature about EMF available to the general public around the world has in this paper been classified as statements, reports, handbooks, pamphlets, fact sheets and videos.

Statements are usually given by internationally recognized bodies or organizations like WHO and ICNIRP. When the general public has a high concern in a specific topic, a statement is given on the specific topic by a political organization (e.g., EU Statement).

Reports are very detailed and elaborate materials (up to 250 pages), intended for educated readers to deepen knowledge in the field, and giving state-of-the-science review.

Handbooks educate readers on specific topics in an accessible and easily understandable way, usually in the form of a book. The average size is up to 40 pages.

Pamphlets are materials of a shorter length (up to 4 pages), with the main purpose being to provide some basic information about the topic to readers.

Fact sheets are even shorter than pamphlets (usually 1 page only), but still provide basic information about a topic.

Video is a modern and very practical means to inform general public, by giving the basic information of the topic in audio-visual way.

303

11.3.1 Concept of "Ideal Information for the General Public"

The ideal statement is brief information given by an internationally recognized body or organization, or in some cases, a political organization about the specific topic.

The ideal report gives a state-of-the-science review for educated readers (scientists in the field) to deepen knowledge in the field and in general; it is not intended as information for the general public. However, sometimes it is used as information for the general public, as well.

Based on the information from the WHO database, the "ideal handbook" for the general public has the following characteristics:

- relatively brief (20-30 pages)

- topic specific (radiation and health)

- source/technology specific (e.g., today actual topic of mobile telephony system)

- contents explains:

    - basics of radiation concepts (ionizing, non-ionizing)

    - basics of electromagnetics

    - basics of specific technology (e.g., mobile telephony system)

    - basics of known biomedical effects

    - existing EMF research from the scientific literature

    - coupling biomedical effects with the existing national standard

    - national standard

    - international EMF standard-setting and research organizations, standards and guidelines

    - siting the electromagnetic source

    - compliance of the source with the existing national standard

    and giving

    - contact details (address[11] where to ask for more details).

The ideal pamphlet has the same characteristics (topic and source/technology specific) as "the ideal handbook," except that it is very brief (up to 4 pages).

The ideal fact sheet is even shorter than "the ideal pamphlet" with only one page of information about specific technologies and compliance with limits on the national standards.

The ideal video is published by a national government and explains the basics of technology with audiovisual examples.

---

[11] Usually this is only the mailing address of the national authority. In a number of cases Internet addresses for the relevant institutions are given.

Table 11-4 contains a classification based on length and content of handbooks from different countries.

Table 11-4. Classification of Information for the General Public in the WHO Database.

Country	Handbook	Pamphlet	Fact Sheet	Video	Report
Austria					x
Australia	x	x	x		x
Belgium			x		
Canada			x		x
Croatia	in preparation				
France	x		x		x
Germany	x	x	x		x
Hungary	x		x		x
Ireland	x				
Israel	x		x		
Italy			x		
Japan	x		x		
Malaysia	x				
New Zealand	x		x		
Peru	x				
Poland	in preparation				
Russia	x				
Slovenia	x		x		x
Sweden	x				
Switzerland	in preparation				
Taiwan	x				
Turkey			x		
United Kingdom	x	x	x	x	x
United States of America	x	x	x		x

305

As an example of report, the Austrian Ministry of Health has published two extensive 1996 reports (in German) for low-frequency and high-frequency electromagnetic fields: *Studie Dokumentierter Forschungsresultate über die Wirkung Elektromagnetischer Felder, Teil 1: Niederfrequente Elektrische und Magnetische Felder* (*Study of the Documented Research Results on the Effects of Low Frequency Electric and Magnetic Fields*) and *Teil 2: Hochfrequente Elektromagnetische Felder* (*Study of the Documented Research Results on the Effects of High Frequency Electromagnetic Fields*).

The general public in Australia (and the worldwide general public via the Internet) has at its disposal a series of eleven fact sheets about EMF and health, in English. The information is published by Committee on Electromagnetic Energy Public Health Issues, which includes representatives from the Australian Department of Communications, Information Technology and the Arts, the Australian Radiation Protection and Nuclear Safety Agency (ARPANSA), the Australian Communications Authority (ACA), and the National Health and Medical Research Council (NHMRC). The Fact Sheets explain the very basics of electromagnetic energy and its effects (No. 1), touch upon the topic of mobile phones (No. 5), gives levels of RF EM power density in the form of a pie chart (No. 6), discusses the interference of mobile phones with pacemakers, hearing aids and other devices (No. 8), a very simplified approach to the operation of a mobile telephony system (No. 9), the basics of broadcast towers (No. 10), and addresses the question of use of mobile phones by children (No. 11) (Committee on Electromagnetic Energy Public Health Issues, 2008). A handbook, *Radiofrequency Electromagnetic Energy, Mandatory Human Exposure Standards and Compliance Framework*, has been published by Australian Communications Authority in 1999.

The Belgian public is informed via the Internet sites of the Ministry of Health and the Belgian Health Council.

In Canada there are no published handbooks for the general public, but *Health Canada* has three reports, one about ELF and two about RF, at the website (http://www.hc-sc.gc.ca/hecs-sesc/ccrpb/electro.htm): ―Health Effects and Exposure Guidelines Related to Extremely Low Frequency (ELF) 50/60 Hz Electric" and ―Magnetic Fields - an Overview, Potential Health Risks of Radiofrequency Fields from Wireless Telecommunications Devices," both released in 1998, and ―Measurement of Cellular Base-Station Emissions Using a Newly Developed RF Field Mapping System," from 2003. Besides these reports, the website has information about microwave ovens in the paper ―Radiation Leakage of Before-Sale and Used Microwave Ovens*"* (published in 2000), a frequently-asked-questions document ―Safety of Exposure to Radiofrequency Fields - Frequently Asked Questions (Fact Sheet)*"* (1997), and short information pages about electric and magnetic fields at ELF – ―It's Your Health: Electric and Magnetic Fields at Extremely Low Frequencies," about microwave ovens ―It's Your Health: Radiation Safety of Microwave Ovens," about cellular phones ―It's Your Health: Safety and Safe Use of Cellular Phones," and about computer monitors and other video display terminals ―It's Your Health: Safety of Exposure to Electric and Magnetic Fields from Computer Monitors and Other Video Display Terminals."

The general public in some countries uses e-mail (e.g., Czech Republic, also via website[12]) or telephone (e.g., Croatia) to get answers on the most frequently asked questions.

---

[12] Internet site: (http://web.telecom.cz/hygpraha/ohzpp9.htm)

Some countries (e.g., Croatia) have a system where the relevant ministry, e.g., Ministry of Health, upon requests and concerns from the citizens, will organize measurements at a site. Regarding EMF publications, there is on-going effort to produce a pamphlet for the general public in Croatia.

The general public in France has at its disposal information from three sources – the French Health Ministry, the French Environmental Health and Safety Agency, and the Ecology Ministry, represented by INERIS.[13] This information is in the form of a report (i.e, the *Zmirou Report*, 2001), a leaflet (*Mobile Phones: Health & Security*, 2002), a statement (*AFSSE Statement on Mobile Phone and Health*, 2003, in English and French), and a press release (*Communiqué de Presse Concernant l'avis de l'AFSSE*, 2003). A handbook is also available, by Flammarion Médecine-Sciences, Paris, entitled *Les Effets Biologiques des Rayonnements Non Ionisants*, 2001.

Several brochures have been published in Germany by different government agencies: the Federal Office for Radiation Protection (*Deutsches Mobilfunk-Forschungsprogramm*), the Radiation Protection Commission (*Grenzwerte und Vorsorgemaßnahmen zum Schutz der Bevölkerung vor Elektromagnetischen Feldern*), and the Ministry for Environment, Nature Conservation and Reactor Security.

Hungary has three publications on mobile phones (―Base Stations,‖ 2004; ―Mobile Phone and Our Life,‖ 2001 and ―Facts on Mobile and Antennas,‖ 1999) and two publications on EMF-ELF (―EMF in Our Environment,‖ 2004 and ―Electromagnetic Fields and Our Environment,‖ 2002). Colorful poster has been distributed in schools in 2002 on mobile phones. It can be also found on the Internet address at: http://www.szezam.hu/htemobil/indexlogok.html.

Ireland has a 22-page booklet published by the Electricity Supply Board (ESB) in 1994 entitled *Electric and Magnetic Fields in the Environment*.

In Israel most of the information is on the Internet pages of the Ministry of Environment. The Radiation Safety Division (SOREQ) published a pamphlet *Radiation From Mobile Phones*.

Italy has some information in the form of the fact sheets on the Elettra web site.

The Japan Electrical Safety and Environment Technology Laboratories in 2001 published a brochure on ELFs *Electromagnetic Fields and Health*, while the Japan Ministry of Public Management, Home Affairs, Posts and Telecommunications (MPHPT) recently (in 2004) published a colorful brochure on RF *Radio Waves and a Safe Life*.

The Malaysia Comunications and Multimedia Commission in 2003 published a brochure on mobile phones entitled *Radiation, Mobile Phones, Base Stations and Your Health*.

New Zealand's government (New Zealand National Radiation Laboratory, NZ Ministry of Health and Ministry for the Environment/Ministry of Health) published one

---

[13] INERIS Internet site: (http://toxi.ineris.fr/activites/neurotoxicologie/neurotoxicologie.php)

handbook describing the basics of electromagnetic fields and the known health effects, *Your Health and Fields from Electric Lines*, and three publications on RF fields and health, which are all found on the Internet. These booklets, pertaining to the bioeffects of RF exposure, describe operation of cellular phone networks, and present results of national base stations site measurements by the National Radiation Laboratory (booklet *Cellsites*), give basic data about *Safety of Cellphones*, and give descriptions about radio frequency fields and technology, an overview of health effects and exposure standards by presenting the basics of laboratory and epidemiological studies, present the policy on exposures to radio frequency fields, guidance on environmental effects, and the standardization organizations (booklet *National Guidelines for Managing the Effects of Radiofrequency Transmitters*).

Peru has a handbook on mobile telephony, published by Instituto Nacional de Investigacion y Capacitacion de Telecomunicaciones, Institute of Telecommunications, INICTEL.

In Poland there is an on-going effort to produce a handbook entitled *Electroenergetic Lines and Stations in the Environment*.

Russia informs the public about non-ionizing radiation with a publication entitled *Human Being in the Electromagnetic Field* from 1998.

Slovenia has an elaborate handbook (*Vpliv Neionizirnih Elektromagnetnih Sevanj na Biološke Sisteme*, translation *Effects of Non-ionizing Electromagnetic Fields on Biological Systems*, published in 1999), explaining bioeffects for the entire spectrum (from 0 to 300 GHz). The Forum EMS published brochure *Mobile Telephony and Health* in 2004.

In Switzerland there is an ongoing effort to produce a handbook to contain general information for the public.

Sweden informs the public about non-ionizing radiation mostly via the websites of the Swedish Radiation Protection Authority, Statens strålskyddsinstitut (http://www.ssi.se). These websites are very useful and information-filled. The handbook published by six authorities (Swedish Radiation Protection Authority, Social Welfare Agency, Swedish Work Environment Authority, National Post and Telecom Authority, Electrical Safety Administration, National Board of Housing, Building and Planning) gives a very short description of electromagnetic fields (differences between ionizing and non-ionizing radiation), a mobile telephony system, and proven thermal effects of non-ionizing radiation.

Taiwan uses a translation of the USA handbook *EMF Questions and Answers*, released in 2003.

Turkey has no published handbook, but information about EMF can be found at Internet sites published in Turkish.

The National Radiological Protection Board of United Kingdom has published different information sheets about EMFs at the website (www.nrpb.org/press/information_sheets), and also released several studies and recently an educational video. Department of Health has published a pamphlet (*Mobile Phone Base Stations and Health)*.

308

The United States of America has two brochures published by the National Institute of Environmental Health Sciences' National Institute of Health (NIEHS/NIH) – *EMF. Questions and Answers* in 2002, and the earlier *Questions and Answers - EMF in the Workplace*, from 1996. The public can obtain information about the topic of wireless phones on the cooperative FDA/FCC Internet site (http://www.fda.gov/cellphones/).

Insight into WHO database information to the general public shows that there is a balanced approach according to frequency ranges in the world. Most countries inform their citizens about both ELF and RF specific topics.

Table 11-5 gives an overview of coverage of information accessible to the general public according to frequency ranges.

309

Table 11-5. Classification of information for the general public in the WHO Database according to considered frequency spectrum.

Country	ELF	RF
Austria	x	x
Australia	x	x
Belgium		x
Canada	x	x
Croatia	in preparation	
France	x	x
Germany	x	x
Hungary	x	x
Ireland	x	
Israel	x	x
Italy	x	x
Japan	x	x
Malaysia		x
New Zealand	x	x
Peru		x
Poland	in preparation	
Russia	x	x
Slovenia	x	x
Sweden	x	
Switzerland	in preparation	
Taiwan	x	
Turkey		x
United Kingdom	x	x
United States of America	x	x

All data about EMF handbooks and pamphlets from the WHO standards database is included in Appendix.

11.4   Conclusion

This paper has described the WHO database of compiled national legislative acts and of known published information (in the form of printed publications or at the specific websites) concerning EMF exposures for the general public. The EMF standards harmonization effort requires as the first phase having a thorough overview of the world's EMF legislative instruments, in order to proceed to the second phase of defining the harmonized instrument and to finally achieve the third phase of the real harmonization.

The information in the database has been gathered from 48 countries from all over the world, which all have EMF legislation (31 European countries, two Middle East countries, two North American countries, two South American countries, eight Asian countries, two countries from Australia and Oceania and one country in Africa). Approximately three-fourths of the total countries (36) have adopted ICNIRP guidelines. Approximately one-third of the total (i.e., 16) number of countries have limits that are stricter than ICNIRP in their legislative instruments. The stricter limits are mostly specific for RF exposure of mobile telephony, as a consequence of the risk perceived by the general population. Concerning the considered frequency range, the data from the WHO database show that almost all the countries have a balanced approach, i.e., almost the same coverage of ELF and RF EMFs in their legislative instruments.

Approximately half of the countries in the WHO database currently have or are preparing information on EMF and health for the general public. The information can take the form of a report, handbook, pamphlet, a fact sheet or a video. In the text, the information has been classified according to contents and length, as well as frequency range. Most of the considered countries have published handbooks (14). After that, the preferences are reports (12 countries), fact sheets (10) and finally pamphlets (9). Two countries are in the process of preparing the handbook. The second classification has been made according to the used frequency spectrum. It is evident that the countries have a balanced frequency approach in presenting biomedical effects of electromagnetic fields to the public.

In this paper, the concept of the ―ideal EMF information/report/handbook/ pamphlet/ factsheet/video for general public" has been introduced. The ideal handbook/pamphlet should be of a shorter length (20-30 pages/2-3 pages) and should be topic specific (radiation and health) with explanation of radiation concept (ionizing vs. non-ionizing). It is advisable that it is source/technology specific (power lines/microwave ovens/mobile telephony system) with explanation of basics of electromagnetics and of specific technology. The handbook should further explain biomedical effects and on-going EMF research from the existing body of scientific literature and couple them to explain foundations of existing national and international standards. In the final part, it should give details on siting electromagnetic sources in an urban/rural environment and explain the conduction of compliance of the source with the existing national standard. At the end, the contact data of the relevant institution should be given, where members of the general population can request more details on the topic. The ideal fact sheet should be much shorter with a brief paragraph on specific technology and compliance with limits in the national standards.

The EMF legislation and information for the general public about EMFs are very important in the on-going harmonization process, which is led by the WHO International EMF Project. The topic of EMFs is important because of the rapid development of new

wireless technologies, which will be very soon applied in the whole new wireless world of the 21st century.

11.5 Acknowledgment

The author would like to thank T. Harrington for editorial comments and review.

11.6 References

Committee on Electromagnetic Energy Public Health Issues. (2008). *EME Series Fact Sheets*. Retrieved on July 6, 2009, from http://www.arpansa.gov.au/eme/index.cfm.

Durney, C. H., Massoudi, H., & Iskander, M. F. (1986). *Radiofrequency Radiation Dosimetry Handbook*. USAF School of Aerospace Medicine.

European Council (EC). (1999). *Council Recommendation on the limitation of exposure of the general public to electromagnetic fields (0 Hz to 300 GHz).* 1999/519/EC.

European Parliament and Council of European Union. (2004). *Directive 2004/40/EC of the European Parliament and of the Council of 29 April 2004 on the minimum health and safety requirements regarding the exposure of workers to the risks arising from physical agents (electromagnetic fields)* (18th individual Directive within the meaning of Article 16(1) of Directive 89/391/EC), European Parliament.

Institute of Electrical and Electronics Engineers, Inc. (IEEE). (1999*). IEEE Standard for Safety Levels with Respect to Human Exposure to Radio Frequency Electromagnetic Fields, 3 kHz to 300 GHz* (Std C95.1-1999). New York, NY: Institute of Electrical and Electronics Engineers.

International Commission on Non-Ionizing Radiation Protection (ICNIRP). (1994). Guidelines on limits of exposure to static magnetic fields. *Health Physic Society*, *66*(1), 100-106.

International Commission of Non-Ionizing Radiation Protection (ICNIRP). (1998). ICNIRP Guidelines for limiting exposure to time-varying electric, magnetic and electromagnetic fields (up to 300 GHz), *Health Physics*, *74*(4), 494-522.

Simunic, D. & Bullock, S. (2003). *WHO International EMF Project Standards Database. EMF World Wide Standards*. Retrieved May 4, 2009, from http://www.who.int/docstore/peh-emf/EMFStandards/who-0102/Worldmap5.htm.

Treaty Establishing the European Community. (1957, March 25). Rome. Retrieved June 23, 2009, from http://www.hri.org/docs/Rome57/.

World Health Organization. (2009). Framework for developing health-based EMF standards. Retrieved July 21, 2009, from http://www.who.int/peh-emf/standards/framework/en/index.html.

11.7 APPENDIX - EMF Handbooks from the WHO Standards Database

The following list is based on information known and available at the time of writing (Nov. 2004), and may not be an exhaustive compilation of all relevant documents. Please contact the author (dina.simunic@fer.hr) with information and suggestions about other documents for future inclusion.

	Country	Title	Author	Year	Remarks	Source
	Reports					
[1]	Austria	Studie Dokumentierter Forschungsresultate über die Wirkung elektromagnetischer Felder, Teil 1: Niederfrequente elektrische und magnetische Felder	B. Kunsch, G. Neubauer, H. Garn, E. Bonek. N. Leitgeib, G. Magerl, and O. Jahn, Forshungsbericht herausgeben vom Bundesministerium für Gesundheit und Konsumenschutz – Sektion III # OEZFS-A-3909 (Ministry of Health)	1996	German, ELF, 270 pp.	Hrn. MinRat DI Hohenberg Bundesministerium für Land-, Forst-, Umwelt und Wasserwirtschaft Sektion I, Abteilung 8 Radetzkystraße 2 A-1030 Wien
[2]	Austria	Studie Dokumentierter Forschungsresultate über die Wirkung elektromagnetischer Felder, Teil 2: Hochfrequente elektromagnetische Felder	B. Kunsch, G. Neubauer, H. Garn, E. Bonek. N. Leitgeib, G. Magerl, and O. Jahn, Forshungsbericht herausgeben vom Bundesministerium für Gesundheit und Konsumenschutz – Sektion III # OEZFS-A-3910 (Ministry of Health)	1996	German, RF, 380 pp.	Hrn. MinRat DI Hohenberg Bundesministerium für Land-, Forst-, Umwelt und Wasserwirtschaft Sektion I, Abteilung 8 Radetzkystraße 2 A-1030 Wien
[3]	Belgium	GSM, Mobile Telephony, is it safe?	Health Council	2002	French, 54 pp.	(http://www.health.fgov.be/CSH_HGR/Francais/Brochures/DeGSMeindversiefr1.html)
[4]	Canada	A review of the Potential Health Risks of Radiofrequency Fields from Wireless Telecommunications Devices	Expert Panel of Royal Society of Canada	1999	RF, 155 pp.	(http://www.rsc.ca//files/publications/expert_panels/RF//RFreport-en.pdf)
[5]	Canada	Recent Advances in Research on Radiofrequency Fields and Health:2001-2003	Expert Panel of Royal Society of Canada	2003	RF, 52 pp	(http://www.rsc.ca//files/publications/expert_panels/RF//expert_panel_radiofrequency_update2.pdf)
[6]	Canada	Environmental Health Criteria 137 - Electromagnetic Fields (300 Hz to 300 GHz)	International Programme on Chemical Safety (IPCS) INCHEM	1993		(http://www.inchem.org/documents/ehc/ehc/ehc137.htm)
[7]	Canada	Environmental Health Criteria 16 - Radiofrequency and Microwaves	International Programme on Chemical Safety (IPCS) INCHEM	1981		(http://www.inchem.org/documents/ehc/ehc/ehc016.htm)
[8]	Canada	Update Recent Advances in		2001	RF, 15 pp, published	(http://taylorandfrancis.metapress.com/app/home/contribution.asp?wa

	Country	Title	Author	Year	Remarks	Source
		Research on Radiofrequency Fields and Health			in Journal of Toxicology and Environmental Health Part B: Critical Reviews, vol. 4, no. 1 pp. 145-159	sp=3d325dwvrq5knj8h9j5m&referrer=parent&backto=searcharticlesresults,29,32;homemain,1,1;)
[9]	Canada	A review of the Potential Health Risks of Radiofrequency Fields from Wireless Telecommunications Devices – update report	D. Krewski, C. V. Byus, B. W. Glickman, W. G. Lotz, R. Mandeville, M. L. McBride, F. S. Prato, D. F. Weaver	2001	Published in Journal of Toxicology and Environmental Health Part B: Critical Reviews, vol. 4, no. 1 pp. 1-143.	(http://taylorandfrancis.metapress.com/app/home/contribution.asp?wasp=3d325dwvrq5knj8h9j5m&referrer=parent&backto=searcharticlesresults,28,32;homemain,1,1;)
[10]	Finland	STUK-A161, Radiation safety of handheld mobile phones and base stations	Jokela, K., Leszczynski, D., Paile, W., Salomaa, S., Puranen, L., Hyysalo, P.	1999	English, 76 pp.	(http://www.stuk.fi/julkaisut/stuk-a/stuk-a161.html)
[11]	France	Report of Parliament's Evaluation "Mobile Telephony and Health"	Ministry of Health	2002	French, RF	(http://www.sante.gouv.fr/htm/dossiers/telephon_mobil/1tele.htm), (http://www.senat.fr/rap/r02-052/r02-052.html), (http://www.senat.fr/rap/r02-052/r02-0521.pdf)
[12]	France	"Zmirou Report" - Les Telephones Mobiles, Leurs Stations de Base et la Sante - Etat des connaissances et recommandations	Ministry of Health	2001	French, English, RF, 270 pp.	(http://www.sante.gouv.fr/htm/dossiers/telephon_mobil/2tele.htm), (http://www.sante.gouv.fr/htm/dossiers/telephon_mobil/pdf/teleph_01_01.pdf), (http://www.sante.gouv.fr/htm/dossiers/telephon_mobil/teleph_uk.htm), (http://www.sante.gouv.fr/htm/dossiers/telephon_mobil/pdf/teleph_uk.doc)
[13]	France	Mobile Telephones, Health and Security	Commission of Consumers Security	2002	French, RF	(http://www.cscnet.org/Commun/AVIS/telecell.htm)
[14]	France	Report of Experts Mandated by French Environmental Health and Safety Agency	French Environmental Health and Safety Agency	2003	French	(http://www.afsse.fr/)
[15]	Germany	Human Health RF EMF Effects	Author: J. Silny, Regional Environmental Office of Baden-Wuerttemberg	2003	German, 89 pp.	(http://www2.lfu.baden-wuerttemberg.de/lfu/abt3/e-smog/literaturstudie_silny.pdf)
[16]	The Netherlands	Mobile Telephones: An Evaluation of Health Effects	Health Council of the Netherlands	2002	English, 96 pp.	(http://www.gezondheidsraad.nl/pdf.php?ID=858)
[17]	The Netherlands	Health effects of exposure to radiofrequency electromagnetic fields: Recommendations for research	Health Council of the Netherlands	2003	Dutch (1-68)+ English (69-122) 122 pp.	(http://www.gr.nl/pdf.php?ID=886%20)
[18]	Slovenia	Effects of non-ionizing electromagnetic fields on biological systems	D. Miklavcic, P. Gajsek, Faculty of Electrical Engineering, University of Ljubljana	1999	Slovenian, 210 pp.	damijan.miklavcic@fe.uni-lj.si
[19]	Sweden	Recent Research on Mobile Telephony and Cancer and Other Selected Biological Effects: First annual report from SSI's Independent Expert Group on	International Independent Expert Group of the Swedish Radiation Protection Authority, SSI	2003	28 pp.	(http://www.ssi.se/english/EMF_)

	Country	Title	Author	Year	Remarks	Source
		Electromagnetic Fields				
[20]	Sweden	Epidemiologic Studies of Cellular Telephones and Cancer Risk, A Review	J.D. Boice, J.K. McLaughlin, SSI Report	2002	38 pp.	(http://www.ssi.se/ssi_rapporter/pdf/ssi_rapp_2002_16.pdf)
[21]	Sweden	SAR and radiation effect for 21 mobile phones	G. Anger SSI Report	2002	Swedish, 93 pp.	(http://www.ssi.se/ssi_rapporter/pdf/ssi_rapp_2002_01.pdf)
[22]	Switzerland	Nichtionisierende Strahlung: Vergleichsmessungen an Mobilfunk-Basisstationen	H. Ryser, METAS-Berichte	2002	German, 35 pp.	(http://www.metas.ch/de/publication/docu/mobilfunk_basisstationen.pdf)
[23]	United Kingdom	Mobile Phones and Health	Independent Expert Group on Mobile Phones, Stewart Report	2000	160 pp.	(http://www.iegmp.org.uk/report/text.htm)
[24]	United Kingdom	Review of the Scientific Evidence for Limiting Exposure to Electromagnetic Fields (0-300 GHz)	Documents of the NRPB, Vol. 15, No. 3	2004	215 pp.	(http://www.nrpb.org/publications/documents_of_nrpb/pdfs/doc_15_3.pdf)
[25]	United Kingdom	Particle Deposition in the Vicinity of Power Lines and Possible Effects on Health: Report of an independent Advisory Group on Non-ionising Radiation and its Ad Hoc Group on Corona Ions	Documents of the NRPB, Vol. 15, No. 1	2004	55 pp.	(http://www.nrpb.org/publications/documents_of_nrpb/pdfs/doc_15_1.pdf)
[26]	United Kingdom	Health Effects from Radiofrequency Electromagnetic Fields: Report of an independent Advisory Group on Non-ionising Radiation	Documents of the NRPB, Vol. 14, No. 2	2003	177 pp.	(http://www.nrpb.org/publications/documents_of_nrpb/pdfs/doc_14_2.pdf)
[27]	United Kingdom	ELF Electromagnetic Fields and Neurodegenerative Disease: Report of an Advisory Group on Non-Ionising Radiation	Documents of the NRPB, Vol. 12, No. 4	2001	24 pp.	(http://www.nrpb.org/publications/documents_of_nrpb/pdfs/doc_12_4.pdf)
[28]	United Kingdom	Possible Health Effects from Terrestrial Trunked Radio (TETRA): Report of an Advisory Group on Non-Ionising Radiation	Documents of the NRPB, Vol. 12, No. 2	2001	86 pp.	(http://www.nrpb.org/publications/documents_of_nrpb/abstracts/absd12-2.htm)
[29]	United Kingdom	Exposure to Radio Waves Near Mobile Phone Base Stations	NRPB	2000	55 pp.	(http://www.nrpb.org/publications/archive/reports/2000/nrpb_r321.pdf)
[30]	United Kingdom	Mobile Phones and Health	British Medical Association, Board for Science and Education	2001	19 pp.	(http://www.bma.org.uk/ap.nsf/650f3eec0dfb990fca25692100069854/80256b140033ce0780256b1a004dd03c/$FILE/Mobile phones.pdf)
[31]	United Kingdom	Mobile phones & health - an update	BMA	2004		(http://www.bma.org.uk/ap.nsf/content/mobphonupd?opendocument&highlight=2,mobile)
[32]	United States of America	NIEHS Report on Health Effects from Exposure to Power-Line Frequency Electric and Magnetic Fields	NIEHS	1999	67 pp.	(http://www.niehs.nih.gov/emfrapid/html/EMF_)
[33]	European	Opinion on possible health effects	Scientific Steering	1998	11 pp.	(http://europa.eu.int/comm/food/fs/sc/ssc/out19_en.html)

	Country	Title	Author	Year	Remarks	Source
	Commission	from exposure to electromagnetic fields (0 Hz- 300 GHz)	Committee of the EC			
[34]	Canada/WHO	Health risks of electromagnetic fields. Part I: Evaluation and assessment of electric and magnetic fields.	Habash RW, Brodsky LM, Leiss W, Krewski D, Repacholi M.	2003	Published in Critical Reviews in Biomedical Engineering, vol. 31, no. 3, pp. 141-195.	(http://www.begellhouse.com/journals/4b27cbfc562e21b8,1279f8172a 33ead5,71202be37bebbc37.html)
[35]	Canada/WHO	Health risks of electromagnetic fields. Part II: Evaluation and assessment of radio frequency radiation.	Habash RW, Brodsky LM, Leiss W, Krewski D, Repacholi M.	2003	Published in Critical Reviews in Biomedical Engineering, vol. 31, no. 3, pp. 197-254.	(http://www.begellhouse.com/journals/4b27cbfc562e21b8,1279f8172a 33ead5,48fda0935b1b7699.html)
[36]	Canada/WHO	Health risks of electromagnetic fields. Part III: Risk analysis.	Brodsky LM, Habash RW, Leiss W, Krewski D, Repacholi M.	2003	Published in Critical Reviews in Biomedical Engineering, vol. 31, no. 4, pp. 333-354.	(http://www.begellhouse.com/journals/4b27cbfc562e21b8,48a5227c1 17355d2,45e02ad644f07b0e.html)
	Handbooks					
[37]	Australia	Radiofrequency Electromagnetic Energy, Mandatory human exposure standards and compliance framework	Australian Communications Authority	1999	Handbook, RF 29 pp.	(http://www.narda-sts.com/pdf/normen/emrhandbook_australia.pdf)
[38]	Canada	Health Effects And Exposure Guidelines Related To Extremely Low Frequency (ELF) 50/60 Hz Electric And Magnetic Fields - An Overview	Working Group of the Federal-Provincial Territorial Radiation Protection Committee	1998	Handbook, ELF, 15 pp	(http://www.hc-sc.gc.ca/hecs-sesc/ccrpb/publication/elf_guidelines/toc.htm)
[39]	Canada	Measurement Of Cellular Base-Station Emissions Using A Newly Developed RF Field Mapping System	Health Canada	2003	RF, 10 pp	(http://www.hc-sc.gc.ca/hecs-sesc/ccrpb/publication/report_globe_system_03march03/toc.htm)
[40]	Canada	Radiation Leakage of Before-Sale and Used Microwave Ovens	Authors: A. Thansadote, D.W. Lecuyer, G.B. Gajda	2000	Microwave World, 21(1), p. 4-8, article, 5 pp	(http://www.hc-sc.gc.ca/hecs-sesc/ccrpb/pdf/microwave-)
[41]	France	Biological Effects of Non-ionizing Radiation	Author: A. Duchene, J. Joussot-Dubien	2001	French, Flammarion Médecine-Sciences, Paris, 95 pp	(http://medecine.flammarion.com/)
[42]	Germany	German Mobile Telephony Research Program	Federal Office for Radiation Protection	2003	German, RF, 26 pp	(http://www.bfs.de)
[43]	Germany	Mobile Telephony: How does it operate?	Federal Office for Radiation Protection	2003	German, RF, 20 pp	(http://www.bfs.de/elektro/papiere)
[44]	Germany	Limit Values and Measures for Protection of General Public from Electromagnetic Fields	Commission for Radiation Protection	2001	German, 66 pp	(http://www.bmu.de/files/elektroma_felder.pdf)
[45]	Germany	General Public Protection of Exposure to Electromagnetic Fields	Commission for Radiation Protection	1999	German, 116 pp	(http://www.ssk.de/)
[46]	Ireland	Electric and Magnetic Fields in the Environment	Electricity Supply Board	1994	22 pp	Electricity Supply Board Lower Fitzwilliam Street, Dublin 2.
[47]	Israel	Radiation from Mobile Phones	SOREQ NRC 3	2002	Hebrew, 16 pp.	(http://www.radiation-safety-)
[48]	Japan	Electromagnetic Fields and Health	Japan Electrical Safety, Environment Technology Laboratories	2001	Japanese, 14 pp.	(http://www.jet.or.jp/e_health/)

	Country	Title	Author	Year	Remarks	Source
[49]	Japan	Radio Waves and a Safe Life	Ministry of Public Management, Home Affairs, Posts and Telecommunications, MPHPT	2004	Japanese, 12 pp.	(http://www.tele.soumu.go.jp/j/ele/body/emf_pamphlet.pdf)
[50]	Malaysia	Radiation, Mobile Phones, Base Stations and Your Health	Malaysian Communications and Multimedia Commission	2003	32 pp.	(http://www.who.int/peh-emf/publications/en/mcmcradiationmobilephonebk.pdf)
[51]	New Zealand	Your Health and Fields from Electric Lines	New Zealand National Radiation Laboratory, NZ Ministry of Health	2001	ELF, 21 pp.	(http://www.nrl.moh.govt.nz/EMF.)
[52]	New Zealand	Cellsites	NZ National Radiation Laboratory, NZ Ministry of Health	2001	RF, 12 pp.	(http://www.nrl.moh.govt.nz/Cellsites_booklet.pdf)
[53]	New Zealand	National Guidelines for Managing the Effects of Radiofrequency Transmitters	Ministry of Environment, Ministry of Health	2000	RF, 94 pp.	(http://www.mfe.govt.nz/publications/rma/radio-freq-guidelines-dec00.html)
[54]	Peru	Mobile Telephony and Health	V.Cruz Ornetta, INICTEL	2003	Spanish, 24 pp.	(http://www.who.int/peh-emf/publications/en/esp_mobphonehealthbk.pdf)
[55]	Russia	Human Being in Electromagnetic Field	Centre for Electromagnetic Safety, RF SRC–Institute of Biophysics	1998	Russian, 12 pp.	CEMS@tesla.ru
[56]	Taiwan	EMF. Questions and Answers	Author: NIEHS, NIH, Research Triangle Park, NC, USA Publisher: National Association for Radiation Protection (NARP, Taiwan)	2003	Classic Chinese, 64 pp.	
[57]	UK	Mobile phone network development: code of best practice	Office of the Deputy Prime Minister 26 Whitehall London SW1A 2WH Tel: 020 7944 4400	2002		(http://www.odpm.gov.uk/stellent/groups/odpm_control/documents/contentservertemplate/odpm_index.hcst?n=2348&l=2)
[58]	USA	EMF. Questions and Answers	National Institute of Environmental Health Sciences, National Institute of Health, Research Triangle Park, NC, USA	2002	64 pp.	(http://www.niehs.nih.gov/emfrapid/booklet/home.htm)
[59]	USA	Questions and Answers - EMF in the Workplace	NIEHS	1996		(http://www.niehs.nih.gov/emfrapid/html/Q&A-Workplace.html)
[60]	WHO	Establishing a Dialogue on Risks from EMFs	WHO	2002		(http://www.who.int/peh-emf/publications/en/EMF_)
	Pamphlets					
[61]	Australia	Mobile Phones… your health and regulation of radiofrequency	Australian communications Authority	2001	4pp.	(http://www.aca.gov.au/consumer_info/issues_alerts/emr_pamphlet.pdf)

	Country	Title	Author	Year	Remarks	Source
		electromagnetic radiation				
[62]	Canada	Safety and Safe Use of Cellular Phones	Health Canada		English, Leaflet, 2 pp.	(http://www.hc-sc.gc.ca/english/pdf/iyh/cellphone_e.pdf)
[63]	France	AFSSE statement on mobile phones and health				(http://www.afsse.fr/documents/Afsse.statement.on.mobile.phones.and.health.)
[64]	Germany	Radiation topics: Mobile Telephony and Transmitters	Federal Office for Radiation Protection	2001	German, Leaflet, 4 pp.	(http://www.bfs.de/)
[65]	Germany	Radiation Topics: Radio and Microwave Radiation Protection	Federal Office for Radiation Protection	2002	German, leaflet, 4 pp.	(http://www.bfs.de/)
[66]	New Zealand	Safety of Cellphones	NZ National Radiation Laboratory, NZ Ministry of Health	2000	RF, 4 pp.	(http://www.nrl.moh.govt.nz/Cellphones_IS21.pdf)
[67]	Slovenia	Electromagnetic radiation: Mobile Telephony and Health	Forum EMS	2004	Slovenian, 16 pp.	(http://www.forum-ems.si/s_files/pdf/zlozenka.pdf)
[68]	Sweden	Radiation from mobile telecommmunication system. An information of six authorities	Swedish Radiation Protection Authority, Social Welfare Agency, Swedish Work Environment Authority, National Post and Telecom Authority, Electrical Safety Administration, National Board of Housing, Building and Planning	2002	Swedish, 12 pp.	(http://www.ssi.se/ickejoniserande_stralning/mobiltele/stralning_mobil.pdf)
[69]	Sweden	Reduction of electric and magnetic fields in buildings	Y.Hamnerius, M.Persson, S.Wijk SSI, NCC and Chalmers	2004	Swedish, 18 pp.	(http://www.ssi.se/forskning/Rapporter/P1361 Slutrapport EoM fält populärversion.pdf)
[70]	United Kingdom	Mobile Phone Base Stations and Health	Department of Health	2000	leaflet; 2 pp., folded sheet	(http://www.dh.gov.uk/assetRoot/04/05/77/42/04057742.pdf)
[71]	United Kingdom	Mobile Phones and Health	Department of Health	2000	leaflet; 2 pp., folded sheet	(http://www.dh.gov.uk/assetRoot/04/05/77/43/04057743.pdf)
[72]	United Kingdom	Understanding Radiation: Radio Waves	NRPB			(http://www.nrpb.org/understand/radiowaves/radiowaves.htm)
[73]	United Kingdom	Mobile Phones and Health: Guidance from the Dept. Of Health	Department of Health	2001	guidance	(http://www.hse.gov.uk/lau/lacs/60-7.htm)
	Fact sheets					
[74]	Australia	Electromagnetic energy and its effects	ARPANSA		Fact sheet no.1	(http://www.arpansa.gov.au/pubs/eme_comitee/fact1.pdf)
[75]	Australia	About mobile phones	ARPANSA		Fact sheet no.5	(http://www.arpansa.gov.au/pubs/eme_comitee/fact5.pdf)
[76]	Australia	About mobile phone networks	ARPANSA		Fact sheet no.6	(http://www.arpansa.gov.au/pubs/eme_comitee/fact6.pdf)
[77]	Australia	Potential interference of mobile phones with pacemakers, hearing aids and other devices	ARPANSA		Fact sheet no.8	(http://www.arpansa.gov.au/pubs/eme_comitee/fact8.pdf)
[78]	Australia	What about base stations and telecommunications towers – are there any health effects?	ARPANSA		Fact sheet no.9	(http://www.arpansa.gov.au/pubs/eme_comitee/fact9.pdf)

	Country	Title	Author	Year	Remarks	Source
[79]	Australia	What about broadcast towers – are there any health effects?	ARPANSA		Fact sheet no.10	(http://www.arpansa.gov.au/pubs/eme_comitee/fact10.pdf)
[80]	Australia	Mobile phones and children	ARPANSA		Fact sheet no.11	(http://www.arpansa.gov.au/pubs/eme_comitee/fact11.pdf)
[81]	Australia	Electromagnetic energy (EME) emissions information FAQ	Department of Communications, Information Technology and the Arts			(http://www.dcita.gov.au/tel/faqs/telecommunications_)
[82]	Belgium		Belgian Health Council			(http://www.health.)
[83]	Belgium		Ministry of Health			(http://www.infogsm.be/)
[84]	Canada	Safety of exposure to RF - FAQ		1997	5 pp.	
[85]	Canada	It's Your Health: Electric and Magnetic Fields at Extremely Low Frequencies				(http://www.hc-sc.gc.ca/english/iyh/environment/)
[86]	Canada	It's Your Health: Radiation Safety of Microwave Ovens				(http://www.hc-sc.gc.ca/english/iyh/products/micro_ovens.html)
[87]	Canada	It's Your Health: Safety and Safe Use of Cellular Phones				(http://www.hc-sc.gc.ca/english/iyh/products/cellphones.htm)
[88]	Canada	It's Your Health: Safety of Exposure to Electric and Magnetic Fields from Computer Monitors and Other Video Display Terminals				(http://www.hc-sc.gc.ca/english/iyh/products/vdt.html)
[89]	Czech Republic					(http://web.telecom.cz/hygpraha/ohzpp.htm)
[90]	Italy	Electromagnetic Fields	Foundation Elettra 2000		Basic terms of EMF, GSM, health risk	(http://www.elettra2000.it/corso/campi.htm)
[91]	Nordic Authorities	Mobile Telephony and Health	Danish National Board of Health, Radiation and Nuclear Safety Authority of Finland, Icelandic Radiation protection Institute, Norwegian Radiation Protection Authority, Swedish Radiation Protection Authority	2004	English, leaflet, 2 pp.	(http://www.ssi.se/ickejoniserande_stralning/mobiltele/NordicMobilPress2004.pdf)
[92]	Turkey	Gazi University, Faculty of Medicine			Turkish	(http://www.med.gazi.edu.tr/departments/biophysisc/biophysics.htm)
[93]	United Kingdom	IEGMP, Base Stations, Ofcom's Role, Exposure Guidelines	Office of Communications			(http://www.ofcom.org.uk/consumer_guides/mob_phone_base_stat/faqs/faq_general/?a=87101)
[94]	United Kingdom	Mobile Phones & Health – an Update	The British Medical Association	2004		(http://www.bma.org.uk/ap.nsf/content/mobphonupd?opendocument&highlight=2,mobile)
[95]	United Kingdom	Mobile Phones and Health: Guidance from the Dept. Of Health	Department of Health	2001	guidance	(http://www.hse.gov.uk/lau/lacs/60-7.htm)
[96]	United States of America	Cell Phone Facts	Food and Drug Administration, Federal Communications Commission	2003		(http://www.fda.gov/cellphones/)
[97]	United States of	Cellular and PCS Base Stations	Federal Communications			(http://www.fcc.gov/oet/rfsafety/cellpcs.html)

	Country	Title	Author	Year	Remarks	Source
	America		Commission			
[98]	United States of America	Cellular Telephone Use and Cancer	National Cancer Institute	2002		(http://cis.nci.nih.gov/fact/3_72.htm)
[99]	United States of America	Mobile Phone (Cell Phone) Base Stations and Human Health	Medical College of Wisconsin, JE Moulder	2004	FAQ	(http://www.mcw.edu/gcrc/cop/cell-phone-health-)
[100]	EC, EMF-Net	Effects of the Exposure to EMFs: From Science to Public Health and Safer Workplace	European Commission, 6th Framework (2004-2008)	2004	Press releases	(http://www.jrc.cec.eu.int/emf-net/press.cfm)
	Statements					
[101]	ICNIRP	Use of the ICNIRP EMF Guidelines, ICNIRP Homepage, 1999.				(http://www.icnirp.de/documents/use.htm)
[102]	ICNIRP	Statement related to the Use of Security and Similar Devices utilizing Electromagnetic Fields. Health Physics, Vol. 87, No 2, 2004.				(http://www.icnirp.de/documents/EASD.pdf)
[103]	ICNIRP	Statement on Medical Magnetic Resonance (MR) Procedures: Protection Of Patients. Health Physics, Vol. 87, No 2, 2004.				(http://www.icnirp.de/documents/MR2004.pdf)
[104]	European Commission	Electromagnetic fields				(http://www.europa.eu.int/comm/health/)
	Videos					
[105]	United Kingdom	Mobile Telephony and Health	NRPB	2003		(http://www.nrpb.org/publications/educational/video/mobilephone.pdf)

Radio Frequency Radiation Dosimetry Handbook
(Fifth Edition)

Chapter 12. Radio Frequency/Microwave Safety Standards

R. C. Petersen
P.O. Box 386
Bedminister, NJ 07921-0386

r.c.petersen@ieee.org

12.1 Introduction

Radio frequency (RF)/microwave safety standards generally refer to standards, regulations, recommendations and guidelines that specify basic restrictions and exposure limits for the purpose of protecting human health. Contemporary standards are based on the results of critical evaluation and interpretation of the relevant scientific research – ideally, all laboratory and epidemiology research that relates any biological response, from short-term and long-term exposure, would be included. From this evaluation, a threshold is established for the most sensitive confirmed response that could be considered harmful to humans. To account for uncertainties in the data and to increase confidence that the limits are well below the levels at which an adverse effect could occur, the resulting threshold is lowered by a somewhat arbitrary safety factor. RF safety standards have evolved over several decades from a simple single value that is applicable over a broad band of frequencies e.g., 10 MHz to 100 GHz, to sophisticated frequency and time dependent limits that cover a much greater frequency range, e.g., 3 kHz to 300 GHz. The early single-value limits were usually expressed in terms of incident power density and were based on simple models predicting whole-body heating; contemporary standards address effects associated with electrostimulation at low frequencies, effects associated with whole-body heating, effects associated with surface heating and usually include limits on induced and contact, exposure to pulses of high peak but low average power, and localized exposure. The evolution of the development of the standards and guidelines developed by committees of the American National Standards Institute (ANSI), the International Commission on Non-Ionizing Radiation Protection (ICNIRP), the Institute of Electrical and Electronics Engineers (IEEE) and the National Council on Radiation Protection and Measurements (NCRP) is described below.

12.2 The Early Years

Although the interest in the potential effect on humans exposed to RF energy goes back almost a century, it was only toward the end of World War II that a concerted effort was made to try to understand the interaction of RF energy with biological systems and, from this understanding, establish criteria to protect against effects that could be considered harmful. The effort in the United States mainly stemmed from anecdotal reports of various effects by radar technicians and others who came in contact with various military radars, e.g., temporary male sterility from exposure to radar beams, the induction of opacities in the lens of the eye. Although by this time the heating effects of RF energy were well-understood and the technology had been applied in medicine for decades, e.g., RF diathermy, the anecdotal

reports in conjunction with studies reporting lens opacities in the eyes of subject animals exposed to microwave energy (e.g., Richardson, et al., 1948; Clark et al., 1949; Daily, et al., 1952) and a report of cataracts in a radar technician (Hirsch & Parker, 1952), resulted in a coordinated effort to understand the interaction of RF/microwave energy with biological systems and to establish safety limits. As clearly evidenced by the several orders of magnitude differences between the protection guides initially adopted by different organizations worldwide during the mid to late 1950's, there was little agreement as to suitable protection criteria or an appropriate rationale for establishing these criteria.

Organized efforts to seek an understanding of the possible interaction mechanisms and the effects on human beings of exposure to electromagnetic energy at RF/microwave frequencies began in the United States with a number of meetings and symposia. Such meeting included the ―Symposium on Physiologic and Pathologic Effects of Microwaves" held at the Mayo Clinic in 1955, the ―First Annual Tri-Service Conference on Biological Hazards of Microwave Radiation" and the ―Second Annual Tri-Service Conference on Biological Hazards of Microwave Radiation," in 1957 and 1958, respectively (Mumford, 1960). The purpose of these meetings was to bring together key researchers in the radiation hazards area in order to discuss ongoing research and identify needed research and, ultimately, establish science-based safety limits. As pointed out by Mumford (1960), during the time period of these symposia, and even before, a number of widely different exposure limits were recommended and used by different organizations in the US. These recommendations, expressed in terms of incident power density, ranged from 100 μW/cm^2 to 100 mW/cm^2. The upper level was based on an apparent threshold for opacities in the lens of the eye (cataracts), which was estimated by Hirsch and Parker (1952) to be of the order of 100 mW/cm^2. Others, e.g., Williams et al. (1956) and Ely et al. (1957) found higher thresholds but there was general agreement that 100 mW/cm^2 should be considered an approximate threshold for biological damage, i.e., levels above this value were considered hazardous and should be avoided. In 1953, one Department at Bell Telephone Laboratories added a 30 dB safety factor to the level considered hazardous and adopted 100 μW/cm^2 as a safe level. In 1954 General Electric adopted 1 mW/cm^2 as a safe level, some organizations informally adopted 10 mW/cm^2 as a potentially hazardous level, and still others merely adopted 100 mW/cm^2 as a hazardous level without specifying a safe limit. Based on a number of animal studies and discussions at the symposia noted above, it became apparent by the late 1950's that 100 μW/cm^2 was too conservative, 100 mW/cm^2 was probably not conservative enough and most organizations adopted an exposure limit of 10 mW/cm^2 as recommended by Schwan and Li (1956). This value was based on a simple thermal model that limited the rise in core temperature of an exposed individual to less than 1 $^\circ$C, assuming that about half of the incident energy was absorbed. The frequency range was 10 MHz to 100 GHz.

12.3 ASA C95.1-1966 and ANSI C95.1-1974

In 1960, the first formal RF safety standards project was approved in the US when the American Standards Association (ASA)[16] approved the initiation of Radiation Hazards Standards Project C95 and the establishment of a committee (C95), which was charged with developing standards through an open consensus process. The scope of the committee was ―*Hazards to mankind, volatile materials, and explosive devices which are created by man-*

---

[16] The American Standards Association later became the American National Standards Institute (ANSI) that now serves as a clearing house for standards developed through an open consensus process.

made sources of electromagnetic radiation. The frequency range of interest extends presently from 10 kHz to 100 GHz. It is not intended to include infrared, X-rays or other ionizing radiation" (ASA, 1966). The C95 Committee, co-sponsored by the Department of the Navy (Bureau of Ships), and the American Institute of Electrical Engineers,[17] was chaired by Schwan; there were six members on the committee, including the chairman. The committee deliberated for approximately six years and in 1966 the first C95.1 standard, ASA C95.1-1966, was published (1966). The exposure limit was presented as a ―Radiation Protection Guide" (RPG), defined as the radiation level which should not be exceeded without careful consideration of the reasons for doing so. The RPG for whole-body exposure was 10 mW/cm^2 across the frequency spectrum from 10 MHz to 100 GHz. Included were an averaging time of 6 minutes and a corresponding energy density limit of 1 mWh/cm^2. The 6 min averaging time appears to have come from the diathermy literature, although this is not stated in the standard. It is noted that the RPG is applicable in moderate thermal environments and that under conditions of moderate to severe heat stress the RPG should be reduced accordingly. The entire standard is less than one and one-half pages in length. Although some at the time considered the RPGs only applicable in the occupational environment, nowhere in the standard is this stated or implied.

A revision of ASA C95.1-1966 was published in 1974 by the American National Standards Institute (ANSI) as ANSI C95.1-1974 (1974). The normative part of the standard was still less than two pages in length; the RPGs for continuous whole-body exposure, expressed in terms of incident power density and energy density, remained at 10 mW/cm^2 and 1 mWh/cm^2, respectively. Because it was then recognized that important exposures could occur in the near field, particularly in the workplace, limits were also given separately in terms of mean squared electric and magnetic field strengths. Although the mean-squared electric and magnetic field strengths were each based on an equivalent power density of 10 mW/cm^2, it was considered important to assess each independently, at least at frequencies below 300 MHz. It is noted in the standard that the RPGs were based on the currently available literature; it was the consensus of the committee that effects associated with tissue heating remain dominant, and the RPGs should protect against such effects. It is also noted that at the time, sufficient information concerning modulation effects, peak power effects and frequency dependent effects was not adequate to substantiate adjustments to the RPGs to account for these effects (ANSI, 1974). The frequency range over which the RPGs applied remained 10 MHz to 100 GHz. During the eight-year development of the 1974 revision, the working group (Subcommittee 4)[18] had grown considerably in size, totaling almost 70 members.

12.4 ANSI C95.1-1982 Standard and the National Council on Radiation Protection and Measurements (NCRP) Recommendations (1986)

Each revision of the C95.1 standard was more scientifically sound, albeit more complex than its predecessor, with major changes appearing in ANSI C95.1-1982 (the revision of ANSI C95.1-1974). These changes were related to the significant advances that

---

[17] In 1963 the American Institute of Electrical Engineers merged with the Institute of Radio Engineers to form a new professional society, the Institute of Electrical and Electronics Engineers (IEEE).

[18] At the time (1974), the C95 Committee consisted of the following seven subcommittees: SC1 (Techniques, Procedures and Instrumentation); SC2/3 Terminology and Units of Measurements); SC4 (Safety Levels and/or Tolerances with Respect to Personnel); SC5 (Safety Levels and/or Tolerances with Respect to Electro-Explosive Devices); SC6 (Safety Levels and/or Tolerances with Respect to Flammable Materials); SC7 (Medical Surveillance).

occurred in the 1970s in instrumentation and the techniques for measuring complex electromagnetic fields and, most important, in the field of RF dosimetry. Advances in dosimetry included the use of numerical techniques to study energy absorption patterns in simple spheroidal and block models of humans and animals and the use of thermography to study the absorption characteristics of complex realistic models of animals and anthropomorphic models of humans. These studies led to a clearer understanding of the frequency-dependent absorption by objects in an RF field, in particular the pronounced resonance over a narrow range of frequencies, the extent of which depended on the geometry and orientation of the object in the field. Under optimal exposure conditions, i.e., conditions yielding maximal absorption, it was found that the absorption cross section at resonance could be 2-3 times greater than the geometrical cross section (Durney et al., 1978) (see Figure 12-1). From this understanding, it became apparent that realistic future protection guides should be frequency-dependent, something that was studied by Soviet scientists in the early 1960s, cf. Pressman (1970). Thus, while the RPGs in the 1966 and 1974 C95.1 standards were independent of frequency, by the mid 1970's it was recognized that the amount of RF energy absorbed by an object in the field would be frequency dependent—as should the RPGs.

RF dosimetry studies, i.e., the study of RF absorption in models of humans and animals, were carried out by Guy (1975, 1974), Guy et al. (1976), Gandhi et al. (1977, 1976), Durney (1980), Durney et al. (1978), Hagmann and Gandhi (1979), and others, using thermographic techniques and numerical modeling. These studies led to an understanding of how the incident and internal electromagnetic fields are related as a function of frequency, field polarization, and size, geometry, orientation and composition of the object in the field. They also led to the recognition of the need for a dosimetric quantity to relate the incident fields to the internal fields, a quantity that would be more directly related to a biological effect than the incident fields alone. This need became very apparent during the literature evaluation that led to the 1982 standard where the general criticism of the growing body of literature was a complete lack of consistency in reported results, particularly with respect to the field parameters necessary for determining the internal field distributions or energy absorbed from the field. In many cases only the incident power density was reported without mention of other parameters necessary for estimating these quantities and, hence, made the comparison of studies difficult at best. This lack of consistency and completeness also helped explain large differences in the incident power density reported for the same biological effect in different animal species, and in the same animal species under different exposure conditions. It was agreed that an appropriate quantity for establishing meaningful thresholds and allowing comparison across frequency and animal species should be analogous to ―dose,‖ and ―dose rate‖ used by the ionizing radiation community. This then would be the basic parameter that should be reported so that the results of studies at different frequencies, using different animal species and widely different exposure conditions e.g., plane wave, TEM cell, cylindrical cavity, could be compared. Once a threshold for an adverse effect is determined in terms of the ―dose rate,‖ i.e., the rate at which energy is absorbed from the field, the growing understanding of RF dosimetry would provide the means for relating this threshold to the incident fields and, with a suitable safety factor, to realistic frequency-dependent RPGs.

324
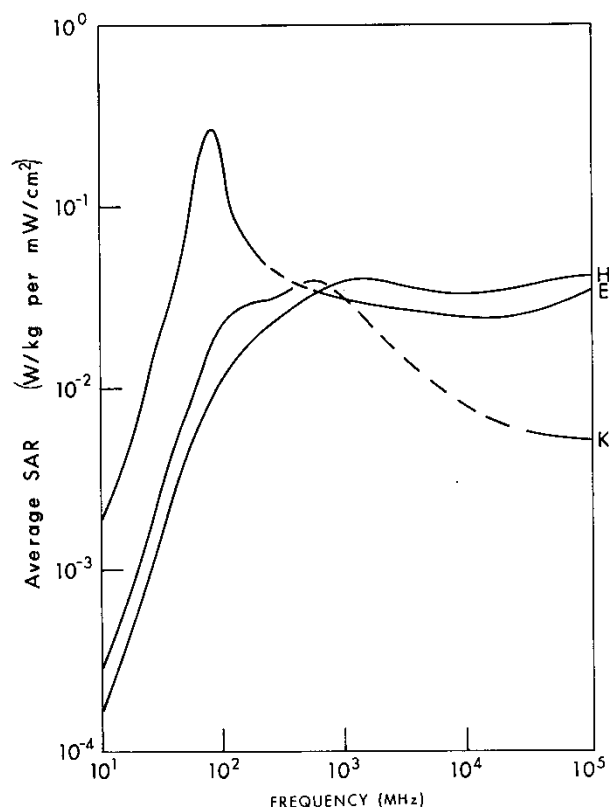
Figure 12-1. Calculated whole-body average SAR versus frequency for simple models of the average man for three standard polarizations. The incident power density is 1 mW/cm2. Curves E and H refer to exposure geometries where the major axis of the body is aligned with the electric field (E) and the magnetic field (H), respectively; K refers to the geometry where the direction of propagation is in the direction of the major axis of the body (From Durney et al., (1978)).

Various quantities and terms were proposed for an appropriate dosimetric quantity including ―absorbed power density" expressed in units of W/cm^3 or W/kg, and ―dose," and ―dose rate," i.e., the energy imparted to a unit mass of biological material (dose) and the rate at which energy is imparted to unit mass (dose rate). After considerable discussion and debate within C95 Subcommittee 4 (SC4) during the 1970's, there was consensus that dose and dose-rate were appropriate. To avoid confusion and the connotation associated with terms traditionally used in ionizing radiation protection, ―dose" and ―dose rate" were named ―specific absorption" (SA), defined as the incremental energy absorbed by (dissipated in) an incremental mass, and ―specific absorption rate" (SAR), defined as the time rate of incremental energy absorbed in (dissipated in) an incremental mass—specific meaning that it is unique to RF/microwave frequencies. The units of SA and SAR are J/kg and W/kg respectively. Although SA and SAR first appear as the defining RF dosimetric quantities in the 1981 NCRP Scientific Committee 39 Report (No. 67) (NCRP, 1981), it had already been accepted by C95 SC4 in the late 1970s during the development of C95.1-1982 and was used effectively to compare the results of studies in the database in order to determine a SAR threshold for effects considered adverse. From this threshold and the results of the increasing number of dosimetry studies, frequency-dependent limits expressed in terms of the incident fields were derived. These limits were called Radio frequency Protection Guides (RFPGs) in

325

order to mitigate confusion with the term RPG used by the ionizing radiation community. Compliance with the RFPGs, ensures that the SAR remains below the threshold (with an adequate margin of safety) under various exposure conditions and for various size humans from infants to adults.

As indicated above, the 1966 and 1974 C95.1 standards were based on the assumption that effects to protect against are related to gross thermal effects associated with elevations in core temperature. By 1980, however, a number of studies reporting effects that occurred at levels where significant temperature increases were not observed or expected (i.e., ―athermal effects‖) began to appear in the scientific literature. These studies warranted careful examination and were included in the list of citations considered by SC4 during the development of the 1982 C95.1 standard. (It is pointed out in the 1982 standard that ―classification and judgment of findings were made without prejudgment of mechanisms of effects. The subcommittee‗s intent was that of protecting exposed human beings from harm by any mechanism, including those arising from excessive elevations of body temperature‖ (ANSI, 1982, p. 13). During the literature selection process that led to ANSI C95.1-1982, several hundred experimental studies reporting effects associated with RF energy were reviewed and a select list of 32 studies was compiled in accordance with the following criteria: demonstrability (positive effects), relevance, reproducibility and dosimetric quantifiability (i.e., was the SAR reported or was there enough information in the report regarding the exposure setup to allow determination of the SAR).

Studies that demonstrated general evidence of morbidity or debilitation, chronic or acute, were emphasized (ANSI, 1982). The bias toward positive findings added a degree of worst-case conservatism to the resulting exposure limits. When positive results were demonstrated for a specific biological endpoint by several laboratories, those studies that demonstrated the effect at the lowest SAR and longest exposure duration were selected. Biological endpoints were grouped in the 15 categories shown in Table 12-1 along with the number of studies that met the selection criteria in each category. Reports of specific effects induced by low frequency amplitude-modulated RF carriers, e.g., calcium efflux from chick brain tissue, were included but were not considered adverse for the following reasons: inability of the SC4 members to relate the effect to human health; the narrow range of effective modulation frequencies; the study author‗s finding that the effect is reversible. The studies were reviewed by the biologists on SC4 and also by the physically trained scientists and engineers with emphasis on reliability, evidence of adverse effects, and whether the study had been independently replicated in another laboratory. The engineers also determined the SAR for each of the studies.

Following the critical evaluation of the selected studies, the subcommittee agreed that the most sensitive, reliable confirmed biological response that could be considered potentially harmful to humans is disruption of food-motivated learned behavior. Even though this effect is, modest, transient and represents an adaptive response, it serves to identify a threshold for potentially harmful effects (ANSI, 1982). It was also assumed that while behavioral disruption was demonstrated to be transient and reversible after acute exposure, chronic exposure could lead to irreversible injury. The threshold for behavioral disruption was found to reliably occur within a narrow range of whole-body average SARs between approximately 4 to 8 W/kg, across animal species from rodents to primates, frequencies from 600 MHz to 2450 MHz, and incident power densities that ranged from 10 to 50 mW/cm^2. Thus it was agreed by SC4 that the appropriate biological endpoint for acute exposures should be

disruption of behavior, and the corresponding threshold, in terms of whole-body average SAR, should be set at 4 W/kg. That is, SAR values above 4 W/kg could produce adverse effects while SARs below 4 W/kg were not shown to result in effects that could be considered hazardous.

Table 12-1. Category of exemplary reports selected from the experimental literature by SC4 for the development of ANSI C95.1-1982.

Environmental factors (effects of temperature on the specific endpoint – 3 studies

Behavior and physiology – 6 studies

Immunology – 4 studies

Teratology – 1 study

Central nervous system/blood-brain barrier – 4 studies

Cataracts – no reliable studies were found reporting cataracts at levels $\leq$ 10 mW/cm^2

Genetics (no reliable studies were found reporting genetic effects at levels $\leq$ 10 mW/cm^2

Human studies – no reliable human studies were found

Thermoregulation and metabolism – 5 studies

Biorhythms – 1 study

Endocrinology – 3 studies

Development – 3 studies

Evoked auditory response (RF hearing) – no studies

Hematology – 2 studies

Cardiovascular – 1 study

There was considerable deliberation during the development of ANSI C95.2-1982 as to an appropriate margin of safety and whether a single frequency-dependent RFPG should apply to exposures of the public and the worker. In order to ensure an adequate margin of safety, a safety factor of 10 was incorporated, which was considered adequate to protect members of the public and the worker because of the conservatism already built into the 4 W/kg threshold. Thus, a whole-body average SAR value of 0.4 W/kg was adopted as the basis of the standard (basic restriction) from which the frequency-dependent RFPGs (also called derived limits, investigation levels, reference levels) would be derived.

By 1980, the field of RF dosimetry had advanced to the point where reliable techniques were available to determine the incident power density that would limit the whole-body average SAR to a specific value. Theoretical analyses were carried out to determine the magnitude of the incident fields that would limit the whole-body average SAR to 0.4 W/kg under worst-case exposure conditions, i.e., conditions that would maximize energy absorption. The results of these analyses demonstrated that under plane wave exposure conditions, energy absorption in models of humans, ellipsoids, animals, etc., is generally maximal when the major axis of the exposed object is aligned with E-field vector of the incident field and, under these exposure conditions, absorption increases with the square of frequency, reaches a maximum (resonance), then decreases linearly with increasing frequency over a limited range of frequencies, and then remains relatively constant. Work by Gandhi (1980) and others showed that under these conditions, maximum absorption (resonance) occurs when the length of the long axis of the exposed object is approximately 0.36 to 0.4 wavelengths. For example,

327

the resonant frequency varies from about 79 MHz to 54 MHz, respectively, when the height of the body ranges from 1.52 m to 1.98 m. Moreover, it was found that when the object is in contact with a ground plane, the resonant frequency is about one-half the value found when it was not in contact. Data were compiled from a number of dosimetry studies and a family of resonance curves and plotted as a function of whole-body average SAR versus frequency for humans ranging in size from infants to tall adults, both in and not in conductive contact with a ground plane and with the long axis of the body parallel to the E-field vector of the incident field. The result of this exercise, normalized to an incident power density of 1 mW/cm^2 (which limits the maximum SAR at resonance to 0.4 W/kg) is shown in the Appendix of C95.1-1982, (ANSI, 1982). The RFPGs were obtained by rearranging these data to determine the maximum incident power density that would limit the whole-body average SAR to 0.4 /kg across the frequency range of interest. The results showed that the incident power density required to maintain an essentially constant SAR in humans of all sizes could be approximated by a broad resonance curve that decreased as 900/f^2 up to 30 MHz, above which it remained constant up to 300 MHz, then rose as f/300 to 1500 MHz, above which it remained relatively constant at 5 mW/cm^2. Although the limiting incident power density continues to increase with decreasing frequency for frequencies below 30 MHz, the RFPG was limited to 100 mW/cm^2 for frequencies below 3 MHz to prevent reactions at the body surface caused by the relatively high E-fields (> 600 V/m), e.g., perception and electric shock. The averaging time remained 6 min over the entire frequency range. There was some concern by members of the subcommittee about the 6 min averaging time as it applies to pulses of high peak power but low average power because time averaging single pulses of extremely short duration, e.g., a few microseconds, leads to unrealistically high exposure limits. No agreement was reached on how to treat this situation and, therefore, there are no explicit peak power limitations in the 1982 standard.

In addition to RFPGs for whole-body exposures, the 1982 standard contained the following exclusions: 1) The RFPG for whole-body exposure at frequencies between 300 kHz and 100 GHz could be exceeded if it could be shown using laboratory techniques that the resulting SAR averaged over the whole body would not exceed 0.4 W/kg and the peak spatial average SAR could not exceed 8 W/kg as averaged over any one gram of tissue. The 8 W/kg was based on the peak to average SAR values reported in a number of animal studies where it was found that typically the peak to average SAR ratio was 20 to 1; 2) At frequencies between 300 kHz and 1 GHz, the RFPGs could be exceeded if the RF input power to the devices is 7 W or less, which is based on limiting the peak spatial-average SAR to 8 W/kg.

Finally, the standard contained the following caveat: ―Because of the limitations of the biological effects database, these guides are offered as upper limits of exposure, particularly for the population at large. Where exposure conditions are not precisely known or controlled, exposure reduction should be accomplished by reliable means to values as low as reasonably achievable" (ANSI, 1982, p. 11). This last sentence often has been quoted out of context by applying it to RF exposure in general.

12.5 NCRP Report No. 86

A number of important events occurred during the interval between approval of ANSI C95.1-1982 and IEEE C95.1-1991, including comprehensive reviews of the extant RF bioeffects literature by a scientific committee of the National Council on Radiation Protection

and Measurements (NCRP).[19] Although NCRP is concerned mostly with ionizing radiation, in 1973 Scientific Committee 53 (SC53 – now SC89-5) was convened to carry out a comprehensive review the scientific literature and make recommendations for limiting exposures to RF energy. SC53 consisted of 6 members, 5 advisory members and 5 consultants (NCRP, 1986) – 8 of whom were at the time also members of SC4 of the ANSI C95 committee. Whereas SC4 adopted criteria for selecting studies specifically relevant to standard setting (e.g., demonstration of positive effects, relevance, reproducibility, dosimetric quantifiability), and consequently reviewed in detail a relatively small number of reports, SC53 carried out complete review of the literature and close to 1000 studies were included in the NCRP literature evaluation (the literature cutoff date was 1982 but a few 1983 references are included). With the quality of the selected reports ranging from excellent to poor, including some which appear to be nothing more than anecdotal reports, value judgments had to be made in interpreting and assessing the quality of each of the studies. Reports were divided roughly by biological endpoint into the categories shown in Table 12-2.

Table 12-2. Category of reports reviewed NCRP SC53 SC4 during the development of NCRP Report 86 (NCRP, 1986).

Macromolecular and cellular effects

Chromosomal and mutagenic effects

Carcinogenesis

Effects on growth, reproduction and development

Effects on the hematopoietic and immune systems

Effects on the endocrine system

Effects on cardiovascular function

Interaction with the blood-brain-barrier

Interactions with the central nervous system

Behavioral effects

Cataractogenesis

Human studies

Thermoregulatory response in human beings

Mechanisms of interactions

As did SC4 of the C95 committee, the members of SC53 also concluded that the most sensitive and statistically significant biological endpoint was behavioral disruption. Although the carrier frequencies for behavioral disruption ranged from 225 to 5800 MHz, across animal species from laboratory rats to rhesus monkeys (see Table 12-3), the incident power densities ranged from 8 to 140 mW/cm^2 and the exposure conditions included near field, far field, planewave, multipath, CW and modulated RF, the SAR threshold for behavioral disruption narrowly ranged from 3 to 9 W/g, which is in fair agreement with the threshold reported in ANSI C95.1-1982.

---

[19] NCRP is a non-profit corporation chartered by the U.S. Congress. The Charter of the NCRP includes as one of its objectives ―To collect, analyze, develop and disseminate in the public interest information and recommendations about (a) protection against radiation (referred to herein as radiation protection) and (b) radiation measurements, quantities and units, particularly those concerned with radiation protection.‖ Although more focused on ―ionizing radiation,‖ e.g., X-rays, gamma-rays, nuclear radiation, NCRP has developed several reports that address radiofrequency issues.

Table 12-3. Comparison of power density and SAR thresholds for behavioral disruption in trained laboratory animals (from Osepchuk & Petersen, 2001).

Species and Conditions	225 MHz (CW)	1.3 GHz (Pulsed)	2.45 GHz (CW)	5.8 GHz (Pulsed)
Norwegian Rat				
Power Density	—	10 mW/cm^2	28 mW/cm^2	20 mW/cm^2
SAR	—	2.5 W/kg	5.0 W/kg	4.9 W/kg
Squirrel Monkey				
Power Density	—	—	45 mW/cm^2	40 mW/cm^2
SAR	—	—	4.5 W/kg	7.2 W/kg
Rhesus Monkey				
Power Density	8 mW/cm^2	57 mW/cm^2	67 mW/cm^2	140 mW/cm^2
SAR	3.2 W/kg	4.5 W/kg	4.7 W/kg	8.4 W/kg

For the frequency range where surface effects predominate, SC53 went further than the C95 committee and recommended lowering the RFPG if there is a likelihood of coming into contact with grounded metallic objects. To prevent RF burns at the point of contact, the recommendation was to lower the RFPG such that the induced RF current does not exceed 200 mA. This is to be done on a case by case basis.

Recommendations, based on the low-frequency modulation-specific effects literature, e.g., calcium efflux studies, were also included. It was pointed out that it is not known whether these affects lead to a risk to human health, but the reliability of the studies and their independent confirmation in avian and mammalian species dictates the need for caution (NCRP, 1986). The recommendation is as follows: ―If the carrier frequency is modulated at a depth of 50 percent or greater at frequencies between 3 and 100 Hz, the exposure criteria for the general population shall also apply to occupational exposures" (NCRP, 1986, p. 286). The incorporation of this caveat, which was based on reported frequency and intensity ―windows," was extremely controversial and has not been accepted by other standard-setting bodies or incorporated into contemporary science-based standards and guidelines.

Although the RFPGs in the 1982 C95.1 standard and the NCRP Report are far more realistic and sophisticated than those used before 1982, both suffer serious shortcomings, including the following: 1) There are no limitations on peak power for pulses of high intensity but low average power—the 6 min averaging time allows exposure to short pulses in excess of those known to cause burns at frequencies where the energy is deposited superficially, i.e., frequencies above a few GHz; 2) There is no explicit guidance to limit induced current at the lower frequencies, i.e., frequencies below a few MHz, to prevent electric shock and RF burns; 3) The magnetic field strength limits, which correspond to the equivalent plane wave power density of the RFPG, is unrealistic at the low frequencies where the magnetic field is inefficiently coupled to the body; 4) No clear distinction is made between whole-body and partial-body exposure (Petersen, 1991). Many of these issues were addressed in the next

330

revision of the 1982 C95.1 standard, i.e., IEEE C95.1-1991.[20] Table 12-4 is a comparison of the rationale between NCRP Report 86 and ANSI C95.1-1982.

Table 12-4. Comparison of rationale: ANSI/NCRP (from Petersen, 1991).

Parameter	ANSI C95.1-1982	NCRP Report No. 86
Recognition of whole-body resonance	Yes	Yes
Incorporation of dosimetry(SAR)	Yes	Yes
Database of experimental literature	Relatively small (32 citations)	Large
Most significant biological endpoint	Behavioral disruption	Behavioral disruption
Whole-body average SAR associated with behavioral disruption	4-8 W/kg	3-9 W/kg
Limiting whole-body average SAR	0.4 W/kg	0.4 W/kg 0.08 W/kg*
Averaging time	6 min	6 min 30 min*
Criterion for limits below 3 MHz	Surface effects, e.g., perception, electric shock (E-field))	Surface effects, e.g., perception, electric shock (E-field).
Criterion for localized exposure	Whole-body average SAR < 0.4 W/kg Peak spatial average SAR < 8 W/kg	Peak spatial average SAR < 8 W/kg Peak spatial average SAR < 2 W/kg*
Special criterion for modulated fields	No	Yes (for occupational exposure)
Specific limits for high peak, low average power pulses	No	No

*General population

12.6 Institute of Electrical and Electronics Engineers (IEEE) C95.1-1991[21]

Almost immediately after ANSI C95.1-1982 was published, Subcommittee IV of the ANSI C95 Committee began work on the next revision with emphasis on addressing some of the recognized shortcomings mentioned above. As with the earlier revisions, the literature was culled for relevant studies and a total of 321 papers were identified by the Literature Surveillance Working Group. (See Figure 12-2 for a graphical depiction of the literature evaluation process.) Although most of the selected reports were published before 1985,

---

[20] During the period the revision of ANSI C95.1-1982 was developed (1982-1990), ANSI ceased sponsoring standards committees and instead became a clearing house for standards developed by committees accredited by ANSI. Although the C95 committee became an ANSI Accredited Standards Committee (ANSI ASC C95), there was consensus of the membership that it would be beneficial to explore the possibility of operating under the sponsorship of the Institute of Electrical and Electrical Engineers (IEEE), which is also an ANSI accredited standards developer. After several meetings with IEEE staff, in 1989 the C95 committee began operating as a Standards Coordinating Committee (SCC28 – now the International Committee on Electromagnetic Safety – ICES) under the sponsorship and subject to the rigid rules, procedures, and oversight of the IEEE Standards Board (now the IEEE Standards Association Standards Board – SASB).

[21] IEEE is a non-profit technical professional society with more than 365,000 members in 150 countries. Within IEEE are 39 societies, including the Consumer Electronics Society, Education Society, Electromagnetic Compatibility Society, Engineering in Medicine and Biology Society, Information Theory Society, Neural Networks Society, Society on Social Implications of Technology. While many IEEE societies sponsor standards committees, when the scope of a proposed standard overlaps the scope of several societies, ―Standards Coordinating Committees" (SCC) are established to develop such standards. IEEE membership is not a requirement for participation on an IEEE SCC or on any of its subcommittees.

several reports, particularly those relating to shock, burns and peak-power effects, were published after 1985. Those peer-reviewed studies that reported effects at whole-body average SARs less than 10 W/kg, and which also met the criteria of the Engineering, Biological and Statistical Evaluation Working Groups, were sent to the Risk Assessment Working Group, whose charge was to determine the threshold SAR above which potentially deleterious effects are likely to occur in humans, even if the effects are reversible (IEEE C95.1, 1991). As in the case of ANSI C95.1-1982 and the NCRP Report, the working group concluded that a threshold SAR of 4 W/kg is appropriate to protect against behavioral disruption, which was once again found to be the most sensitive and reliable biological endpoint. Without saying that behavioral disruption is a ―thermal‖ effect, it was noted that behavioral disruption in laboratory animals was accompanied by a core temperature increase of approximately 1 °C and the effect, regardless of the interaction mechanism, was reversible. Effects reported to be non-thermal, e.g., modulation specific effects such as changes in calcium efflux from chick brain tissue, were again considered but it was the consensus of the Risk Assessment Working Group that such effects were inconsistent, could not be related to human health, and, therefore, not useful for standard setting. It was also the consensus of the Risk Assessment Working Group that a safety factor of 10 to account for dosimetric, biological and other uncertainties would provide an adequate margin of safety, thereby yielding a basic restriction of 0.4 W/kg in terms of whole-body average SAR.
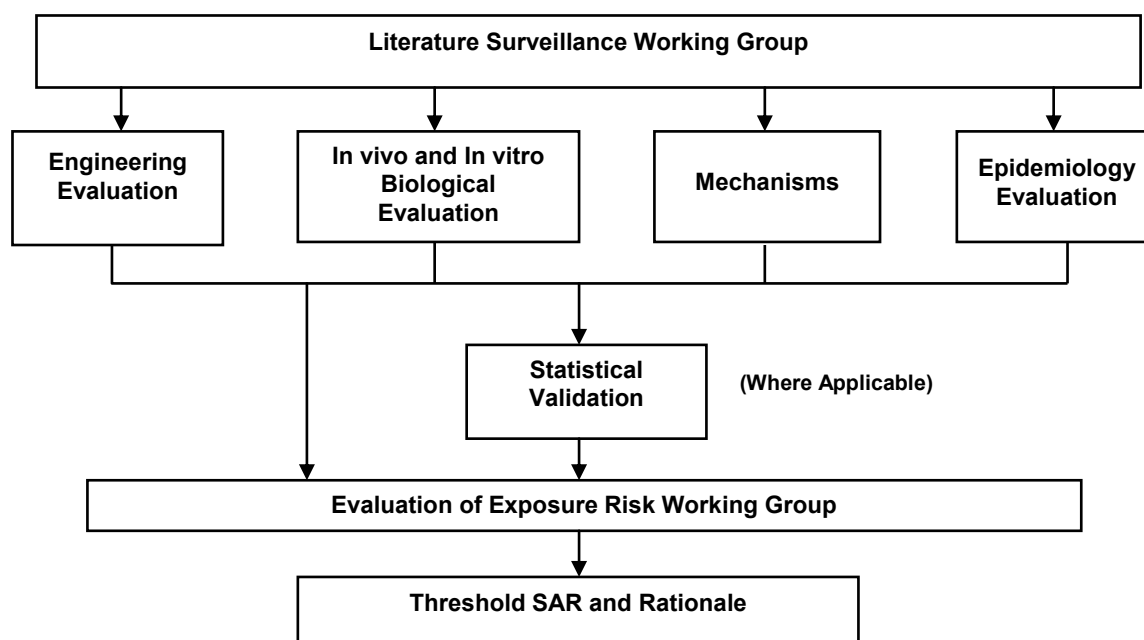
Figure 12-2. Graphical depiction of the ANSI/IEEE literature evaluation process.

Unlike C95.1-1982, however, which consisted of a single tier that was considered protective of all, the SC4 Societal Implications Working Group recommended following NCRP and including a separate lower tier for exposures that take place in *uncontrolled environments.* Their recommendation was based on the following argument (IEEE C95.1, 1991): ―To some, it would appear attractive and logical to apply a larger, or different, safety factor to arrive at the guide for the general public. Supportive arguments claim subgroups of greater sensitivity (infants, the aged, the ill, and the disabled), potentially greater exposure durations (24-hr/day vs. 8-hr/day), adverse environmental conditions (excessive heat and/or

humidity), voluntary vs. involuntary exposure, and psychological/emotional factors that can range from anxiety to ignorance. Non-thermal effects, such as efflux of calcium ions from brain tissues, are also mentioned as potential health hazards" (IEEE C95.1, 1991, p. 23). However, this is followed by ―The members of Subcommittee IV believe the recommended exposure levels should be safe for all, and submit as support for this conclusion the observation that no reliable scientific data exist indicating that:

(1) Certain subgroups of the population are more at risk than others

(2) Exposure duration at ANSI C95.1-1982 levels is a significant risk,

(3) Damage from exposure to electromagnetic fields is cumulative, or

(4) Nonthermal (other than shock) or modulation-specific sequelae of exposure may be meaningfully related to human health" (IEEE C95.1, 1991, p. 23)

and ―no verified reports exist of injury to human beings or of adverse effects on the health of human beings who have been exposed to electromagnetic fields within the limits of frequency and SAR specified by previous ANSI standards, including ANSI C95.1-1982" (IEEE C95.1, 1991, p. 23). Thus, any scientific justification for the lower tier is tenuous at best. However, the C95 standards are developed through an open consensus process and the majority of the voting members agreed that a lower tier is appropriate.

The lower tier was derived by reducing the upper tier value by a factor of 5, at least in the resonance region where SAR is important resulting in a whole-body average SAR of 0.08 W/kg. However, unlike other standards and guidelines that set limits based on population groups, i.e., an upper tier for occupational exposure and a lower tier for exposure of the general population, the committee concluded that it would be more meaningful to address the exposure environment rather than the exposed population to help clarify the assignment of an appropriate set of limits to personnel, particularly in the workplace. Thus, the derived limits of the upper tier, now referred to as maximum permissible exposure values (MPE) to be consistent with the use of the term in other standards relating to non-ionizing radiation protection, e.g., the laser safety standards ANSI Z136.1 and IEC 60825, apply to exposures in *controlled environments*; the MPEs of the lower tier apply to exposures in *uncontrolled environments*. Controlled environments are considered locations where exposures may be incurred by individuals who are aware of and have control of their potential for exposure, e.g., as a concomitant of their employment, or by other cognizant persons; uncontrolled environments are locations where there is exposure of individuals who have no knowledge or control of their exposure (in living quarters, offices or in workplaces where there are no expectations that exposure levels may exceed the MPE recommended for lower tier). See Figure 12-3 for graphical representation of the IEEE C95.1-1991 MPEs.
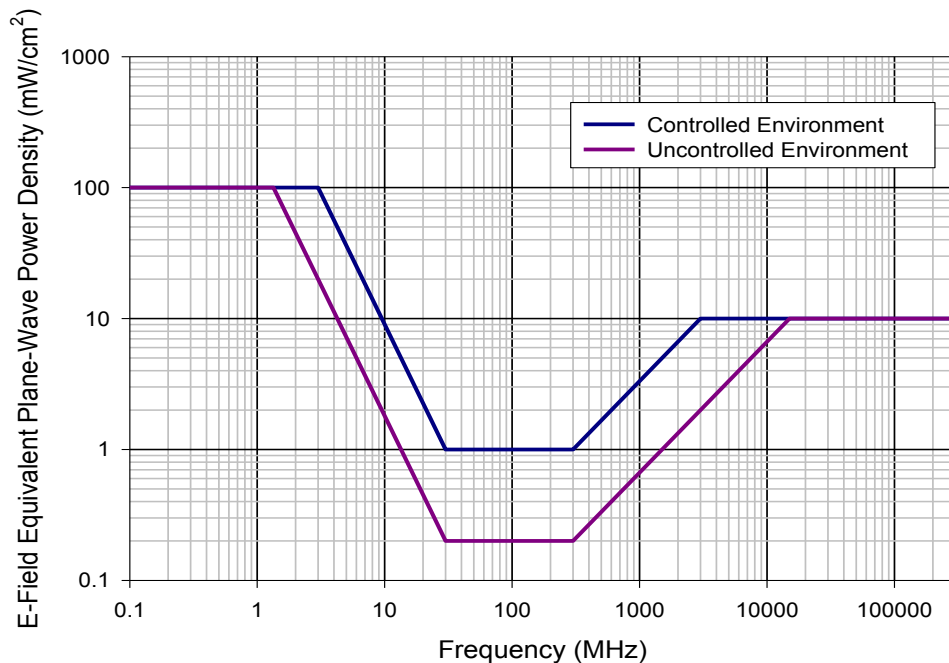
Figure 12-3. Graphical representation of the C95.1-1991 MPEs expressed in terms of the E-field equivalent plane wave power density.

In addition to a lower tier and the use of exposure environments rather than exposed populations, a number of other significant changes appear in the 1991 revision of ANSI C95.1-1982. These include the following:

1. *Increased frequency range*: The frequency range of the 1982 C95.1 standard is 300 kHz to 300 GHz; the frequency range of the 1991 standard is 3 kHz to 300 GHz.

2. *Magnetic field limits*: The magnetic field limits, which correspond to the equivalent free-space power density of the RFPGs in the 1982 standard, were relaxed in the 1991 standard at frequencies below 3 MHz in order to more realistically reflect the contribution of the magnetic field to the SAR.

3. *Power density limits at quasi-optical frequencies*: The MPEs in terms of incident power density were relaxed from 5 mW/cm^2, the value in the 1982 standard for frequencies above 1.5 GHz, to 10 mW/cm^2 for frequencies above 3 GHz (exposures in controlled environments) and for frequencies above 15 GHz (exposures in uncontrolled environments). This more realistically reflects biological effects associated with surface heating where the penetration depth is comparable to that of infrared radiation (IR). This is consistent with the corresponding MPEs at IR wavelengths found in the laser safety standards, e.g., ANSI Z136.1 and IEC 60825, for exposure to large area beams (greater than 1,000 cm^2) (ANSI, 2007; IEC, 2001).

4. *Averaging time*: More realistic averaging times are incorporated in the 1991 standard in order to address a number of issues including exposure to short high peak power pulses. The averaging time is as follows: In the frequency region where surface heating predominates, the averaging times decrease with increasing frequency. For exposures in controlled environments, the averaging time now decreases from a value of 0.1 h at 15 GHz to 10 s at 300 GHz and decreases from 0.5 h at 15 GHz to 10 s at 300 GHz for exposures in uncontrolled environments. The shorter averaging time mitigates against

334

conditions where skin burns could occur from short but intense exposures to small areas of the skin, which would be permitted with the longer averaging times found in the NCRP recommendations and the 1982 ANSI C95.1 standard. For example, an averaging time of 0.1 h at wavelengths where the penetration depth is comparable to that of the far-IR would allow a 0.5-s exposure to small areas of the skin that exceeds the $1.2 - 2.4 \times 10^4$ mW/cm^2 skin burn threshold reported by Evans et al. (1955). At 300 GHz, the 10-s averaging time is consistent with the corresponding averaging time at 300 GHz found in the laser safety standards and guidelines.

5. *Peak power limits*: Peak power limitations have been incorporated to preclude high specific absorption (SA) that could result from exposure to increasingly short, high-amplitude pulses. Specifically, for exposures to pulsed RF fields of pulse durations less than 100 ms and frequencies in the range of 100 kHz to 300 GHz, the MPE in terms of peak power density for a single pulse is limited to the MPE (under normal averaging time conditions) multiplied by the averaging time in seconds, divided by five times the pulse width in seconds, i.e.,

$$Peak\ MPE = \frac{MPE \times Time\ (\sec onds)}{5 \times Pulsewidth\ (\sec onds)}.$$

If more than five pulses occur during the averaging time, normal time averaging will further reduce the permissible peak power. In addition, a peak E-field limit of 100 kV/m is included and takes precedence over the SA limits above. The peak power limits are based on the literature on the evoked auditory response in humans (microwave hearing) and RF energy induced unconsciousness (stun effect) in rodents. The SA limits are conservative with respect to the stun effect but the peak power density limits are above the threshold for microwave hearing, which while annoying, is not considered harmful.

6. *Partial-body exposure*: Most situations, particularly in the workplace, exposures are to non-uniform fields over portions of the body and not to uniform plane-wave fields. It was therefore decided that it is appropriate to address such situations with criteria that would allow relaxation of the MPEs under partial-body exposure conditions. Specifically, the spatial peak mean squared field strengths and the equivalent power density permitted under partial-body exposure conditions are allowed to exceed the spatial average (as averaged over the projected area of the body), as a function of frequency, up to a factor of 20 times. This relaxation is based on animal studies and dosimetric studies which show that under uniform plane-wave exposure conditions, the spatial peak SAR exceeds the whole-body average SAR by a factor of about 20 times. The use of the partial-body relaxation provision is limited because of the accompanying caveat ―The following relaxation of power density limits is allowed for exposure of all parts of the body except the eyes and the testes" (IEEE C95.1, 1991, p. 20). This precludes practical implementation in many exposure scenarios. The reasoning behind inclusion of the caveat was concern that at frequencies where the penetration depth was comparable to that in the IR portion of the spectrum, the relaxation would allow exposures to the eye that would exceed the IR MPEs for the eye and skin in the laser safety standards―even with the reduced averaging time.

7. *Induced and contact current limits*: Induced and contact current limits are incorporated to protect against surface effects (e.g., shocks and burns) associated with electric-field induced currents which predominate at frequencies below a few MHz. For the controlled environment, the maximum contact current and the induced RF current through each foot is limited to $1000\,f$ mA ($0.003 < f \leq 0.1$ MHz) and 100 mA (0.1 MHz $< f < 100$ MHz) and

335

to 450 f mA (0.003 < f ≤ 0.1 MHz) and 45 mA (0.1 MHz < f < 100 MHz) for the uncontrolled environment. The averaging time is 1 s. Guidance is also included on how measurements of foot and contact current should be performed.

8. *Minimum measurement distance*: In order to minimize the problem of proximity effects, i.e., erroneous measurement results associated with coupling between the sensor (antenna) elements in the instrument and the reactive fields from re-radiating structures, a minimum separation distance of 20 cm from any object is recommended.

9. *Low power device exclusion*: This exclusion pertains to devices that emit RF energy without control or knowledge of the user. It is generally applied to hand-held devices such as two-way radios. Specifically, at frequencies between 100 kHz and 450 MHz, the MPE may be exceeded if the radiated power is 7 W or less for the controlled environment and less than 1.4 W for the uncontrolled environment. At frequencies between 450 and 1500 MHz, the MPE may be exceeded if the radiated power is 7(450/f) W or less for the controlled environment and less than 1.4(450/f) W for the uncontrolled environment. This exclusion does not apply to devices with the radiating structure maintained within 2.5 cm of the body, e.g., personal wireless communication devices such as mobile telephones.

10. *SAR Exclusions*: As in the 1982 standard, the SAR exclusion allows exposures in excess of the MPEs if it can be shown by reliable means (e.g., laboratory studies) that the whole-body average and peak spatial-average SAR (basic restrictions) are not exceeded. Unlike the SAR exclusions in the 1982 C95.1 standard, which were applicable over the entire frequency range of 300 kHz to 300 GHz, and did not specify a geometric shape for the 1-g averaging volume for localized exposure, the 1991 standard specifies a realistic frequency range of 100 kHz to 6 GHz and an averaging volume in the shape of a cube to eliminate the problem of grossly overestimating the peak spatial-average SAR at frequencies where the depth of penetration is superficial, i.e., at millimeter-wave frequencies. Limiting the frequency range to that where SAR is meaningful and assigning a cubic geometry to the averaging volume more accurately represents the potential for hazard. The recommended whole-body average SAR exclusion for exposures in controlled environments remains the same as that for the single-tier exclusion in the 1982 C95.1 standard, i.e., 0.4 W/kg (but applicable over the narrower frequency range indicated above). The corresponding value for exposures in uncontrolled environments is 0.08 W/kg. The peak spatial-average SAR is 8 W/kg and 1.6 W/kg for the uncontrolled and uncontrolled environments, respectively (but applicable over a narrower frequency range and averaged over any 1-g of tissue in the shape of a cube). The following additional SAR exclusion is included: for exposure of the extremities, i.e., the hands, wrists, feet and ankles, the MPEs can be exceeded provided the peak spatial-average SAR of 20 W/kg (controlled environment) and 4 W/kg (uncontrolled environment) in any 10-g of tissues in the shape of a cube is not exceeded (and the induced current and contact current limits are not exceeded).

Compared with the RFPGs found in the 1982 C95.1 standard and the NCRP recommendations, the 1991 MPEs are far more complex and sophisticated. The complexity in application and measurement is more than offset by having scientifically defensible limits that realistically address known RF hazards by ensuring that the thresholds for adverse effects are not exceeded.

The 1991 standard was approved by the IEEE Standards Board in 1991 and published in 1992. It was also approved for use as an American National Standard by ANSI in 1992. At the time IEEE C95.1-1991 was approved, SC4 had 125 members; approximately 72% from

336

the research community (including university, military and public health service laboratories), the rest from industry (~10%), industry (consulting ~3%), government (administration ~4%), and general public and independent consultants (~11%). At the same time C95.1-1991 was approved, IEEE C95.3-1991 was also approved (IEEE C95.3, 1991). C95.3-1991 was developed by SC1 (Techniques, Procedures, and Instrumentation) and replaces ANSI C95.3-1973 (ANSI, 1973) and ANSI C95.5-1981 (ANSI, 1981). This recommended practice describes instrumentation, measurement techniques and computational techniques that can be employed to assess compliance with the basic restrictions and MPEs of the C95.1 standards.

In 1997, C95.1-1991 was reaffirmed (without change); in 1999, Supplement 1 was approved to address certain ambiguities in the 1991 standard. A definition of *spatial average* and recommendations on how spatial average should be measured, i.e., by scanning (with a suitable measurement probe) a planar area equivalent to the area occupied by a standing adult human (projected area), is included in Supplement 1. Also, the averaging time for induced and contact current was increased from 1 s to 6 min for frequencies where heating predominates, i.e., above 100 kHz, and rms ceiling values of 500 and 220 mA for the controlled and uncontrolled environments, respectively, were added as were E-field limits (expressed as a percentage of the MPEs) below which induced current measurements are not required. A detailed description of how induced and contact current should be measured was also added. There were also a number of other changes including the clarification of *averaging volume* as it applies to average spatial-peak SAR, clarification of the term *radiated power* as it applies to low-power hand-held devices, and clarification of the measurement distance requirements for certain direct radiators (the separation distance for measurements made in proximity to any *directly radiating* structure or any of its attachments was reduced to 5 cm but remained at 20 cm for indirect radiators and reflectors).

In 2004, a request from IEEE SCC34[22] led to the development of an amendment (C95.1b-2004) that helped clarify issues relating to the determination of the peak spatial-average SAR associated with the use of hand-held mobile transceivers intended to be operated placed against the side of the head. This amendment, which was approved in 2004, assigns the same basic restrictions to the pinna as those applicable to the extremities, i.e., peak spatial-average SAR values of 20 and 4 W/kg, for the controlled and uncontrolled environments, respectively, averaged over any 10 g of tissue in the shape of a cubical volume surrounding an *evaluation point*. For this purpose, the *evaluation point* is defined as ―either the geometric center of the electric field probe sensors at a site used for experimental SAR measurement, or the location of the incremental volume (voxel) in a numerical computation.‖

12.7 International Commission on Non-Ionizing Radiation Protection (ICNIRP) Guidelines

The most commonly used standards throughout the world are based on the IEEE C95 standards, the recommendations of the National Council on Radiation Protection and Measurements (NCRP), and the guidelines of the International Radiation Protection Association's (IRPA) International Commission on Non-Ionizing Radiation Protection

---

[22] IEEE SCC34 was a standards coordinating committee established in 1995 to develop product standards relative to the safe use of electromagnetic energy. At the time, SCC34 SC2 was developing a standard (IEEE 1528) for measuring the peak spatial-average SAR from RF-emitting devices intended to be operated while placed next to the head (mobile telephones).

(ICNIRP).[23]   Like IEEE and NCRP, ICNIRP is an organization with established scientific committees that review the literature and make recommendations regarding exposure to RF/microwave energy. The most recent ICNIRP guidelines were approved in November 1997 and published in 1998 (ICNIRP, 1998). At the time the guidelines were developed, the Commission included the participation of 17 scientists and 11 external experts from 12 different countries, including Sweden, Australia, Great Britain, Germany, Poland, and the US. Like IEEE and NCRP, ICNIRP carried out an extensive review and interpretation of the literature, from which exposure guidelines were developed. As in the case of the ANSI, IEEE and NCRP committees, the ICNIRP guidelines are based on studies reporting established effects.   In agreement with the rationale of C95.1-1991, ICNIRP also found that the established effects that should be used for developing exposure criteria were surface effects at the lower frequencies, e.g., electrostimulation, shocks and burns, and effects associated with tissue heating at the higher frequencies. Although a number of in vitro studies were reviewed, the focus was on in vivo studies. A number of epidemiological studies of reproductive outcome and cancer were reviewed, but because of the lack of adequate exposure assessment and inconsistency of results these studies were found to be of little use for establishing science-based exposure criteria.   Studies reporting athermal effects, including ―window effects,‖ e.g., effects associated with ELF amplitude modulated (AM) RF fields, were also considered, but ICNIRP concluded ―Overall, the literature on athermal effects of AM electromagnetic fields is so complex, the validity of reported effects so poorly established, and the relevance of the effects to human health is so uncertain, that it is impossible to use this body of information as a basis for setting limits on human exposure to these fields" (ICNIRP, 1998, p. 507).

Like the ANSI/IEEE and NCRP committees, ICNIRP determined that SAR is the valid dosimetric parameter over the broad whole-body resonance region and also found that the most reliable and sensitive indicator of potential harm was behavioral disruption, with a threshold SAR of 4 W/kg. A safety factor of 10 was incorporated for exposure in the workplace, and an additional factor of 5 for exposure of the general public yielding maximum whole-body average SAR values of 0.4 and 0.08 W/kg, respectively (called basic restrictions). In addition, basic restrictions in terms of peak spatial-average SAR of 10 and 2 W/kg averaged over any 10 g contiguous tissue are recommended for localized exposure. The somewhat less arbitrary ICNIRP peak spatial-average SAR limits are thought to be based on effects to the eye. Specifically, the threshold associated with the induction of lens opacities in the eyes of rabbits has been shown to be greater than 100 W/kg. The mass of the eye is about 10 g – by incorporating safety factors of 10 and 50 times, the resulting peak spatial-average values are 10 and 2 W/kg averaged over any 10 g of contiguous tissue for occupational exposure and exposure of the public, respectively.

There are also a number of differences between the ICNIRP derived limits (called reference levels) and the MPEs found in the 1991 IEEE standard but these differences are

---

[23] As indicated on their website ―ICNIRP's beginnings go back to 1973 when, during the 3rd International Congress of the International Radiation Protection Association (IRPA), for the first time, a session on non-ionizing radiation protection was organized" (ICNIRP, 2007, p. 1). This was followed in 1974 by the formation of a working group on non-ionizing radiation, in 1975 by a study group to review the field of non-ionizing radiation, in 1977 by the creation of the International Non-Ionizing Radiation Committee (INIRC), and in 1992 ICNIRP was chartered as an independent non-profit scientific body. ICNIRP is also a formally recognized non-governmental organization in non-ionizing radiation for the World Health Organization and the International Labour Office. The work of ICNIRP is carried out by the main Commission, with support of consulting members and four Standing Committees; Epidemiology, Biology, Physics and Engineering and Optical Radiation.

mostly related to engineering issues, e.g., models used to relate the incident fields to the basic restrictions, and differences in philosophy of determining safety factors, and not with any specific biological response or its threshold. Differences between the ICNIRP guidelines and the C95.1-1991 standard include a broader frequency range for the ICNIRP guidelines (0 to 300 kHz[24] compared with 3 kHz to 300 GHz for C95.1-1991), different values for the induced and contact current limits, a slightly higher basic restriction for localized exposure, (10 and 2 W/kg for the upper and lower tiers, respectively, compared with 1.6 and 8 W/kg in C95.1-1991), a different averaging volume for the localized exposure basic restriction ("over any 10 g of contiguous tissue" compared with "over any 1 g of tissue in the shape of a cube" in C95.1-1991, a broader resonance region (10 to 400 MHz compared with 30 to 300 MHz in C95.1-1991), a broader frequency range over which SAR applies (100 kHz to 10 GHz compared with 100 kHz to 6 GHz in C95.1-1991), and lower peak-power limits. The ICNIRP peak power limits are based on the evoked auditory response (microwave hearing) whereas the C95.1-1991 limits are based on the stun-effect in small animals (with a suitable margin of safety). That is, while ICNIRP considers "microwave hearing" a harmful effect, it is considered a possible annoyance in the C95.1-1991 standard—but not a hazard. There are a number of other minor differences.

12.8 IEEE Process

Compared with other committees that develop recommendations and guidelines for exposure to RF/microwave energy, e.g., ICNIRP and NCRP, C95 committees are by far the largest, most innovative, and had the greatest influence on RF/microwave safety standards worldwide (Petersen, 1999). The subcommittees are open to anyone with a direct material interest and the standards development process has always been open, formal and transparent at every level, i.e., the process is different from that of other committees, such as ICNIRP and NCRP, which tend to be closed, informal and somewhat non-transparent. While the committee operated as an ANSI committee during the development of the 1991 C95.1 standard, then as an ANSI Accredited Standards Committee, then, during the last two years a committee sponsored by the IEEE SASB, in each instance it was subject to the formal rules of the sponsoring organization to ensure due process at every level. In order to understand how the IEEE committees function, the process will be described briefly before discussing the latest revision of the C95.1 standard (IEEE C95.1-2005).

The standards coordinating committees that operate under the sponsorship of the IEEE SASB must rigidly adhere to the policies and procedures of the IEEE, IEEE SASB and the approved polices of the committees. In general, the process begins with the submittal of a Project Authorization Request (PAR) to the New Standards Committee (NesCom), a standing committee of the IEEE SASB. (See Figure 12-4 for a flowchart that depicts the process.) The PAR outlines the scope and purpose of the proposed standard, the reasons for developing the standard, the number of members of the working group, when the draft will be ready for sponsor ballot, potential conflicts with the scope of other standards or standards projects, plus a number of other questions that must be answered by the submitter. Once deemed complete and accurate by NesCom, a recommendation can be made to the SASB for approval. Following SASB approval, the working group (in this case SC4) can move forward with the development of drafts. In accordance with IEEE SASB and ICES procedures, the membership of SC4 consists of volunteers representing all stakeholders (membership is open to all parties with a direct material interest – IEEE membership is not required). The

---

[24] Basic restrictions are provided over the frequency range extending from "up to 1 Hz" to 300 GHz.

membership of SC4 consists of volunteers in engineering, physics, statistics, epidemiology, life sciences, medicine, and the public with a balance of representatives from government, industry, academia, and the general public. This wide-ranging participation, including thorough discussions and open decision making, is the hallmark of the process that led to C95.1-2005 (IEEE C95.1, 2006).
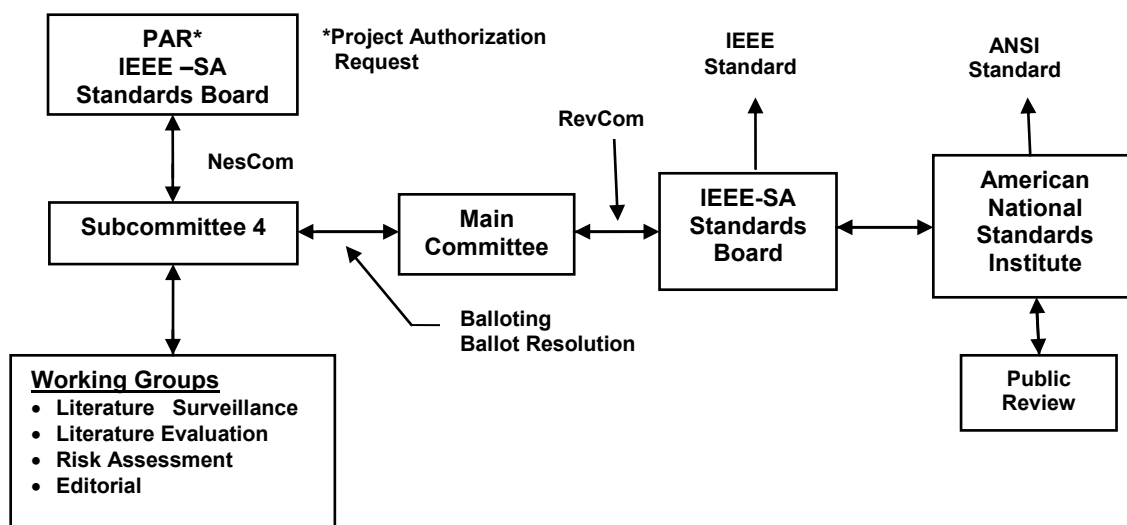
Figure 12-4. Flowchart of IEEE process for development of C95.1 standards.

When a draft is finally approved by the working group, following the same process mandated for sponsor balloting described below, (except that balloting is carried out by SC4—not the IEEE SA Balloting Center), the draft is submitted to the IEEE SA Balloting Center for sponsor ballot (i.e., by the parent committee – SCC28). Sponsor balloting begins when the IEEE Balloting Center notifies members of the balloting pool that a standard is ready for sponsor ballot and invites members to join the Ballot Group for that standard. The balloting pool consists of the parent committee members (SCC28 – now Technical Committee 95 of the IEEE International Committee on Electromagnetic Safety—ICES)[25] plus all interested parties that may have joined the balloting pool. The balloting pool is open to any IEEE Standards Association (IEEE SA) member, or any non-member who elects to pay a nominal fee to vote and receive drafts. Members of the parent committee who wish to vote, but are not members of the IEEE SA, first have to be approved by the SASB. Requests from the sponsor chair to the SASB secretary outlining why these individuals should be permitted

---

[25] In order to provide a better description of the international aspects of its activities, the name ―IEEE International Committee on Electromagnetic Safety‖ (ICES) was approved for use by the IEEE SASB in 2000. Then, in March 2005, the IEEE SASB approved a new committee, still called ICES, which includes two technical committees: TC34 (formerly SCC34) and TC95 (formerly SCC28). This new committee operates as a standards coordinating committee (SCC39) under the sponsorship of the IEEE SASB. Currently the membership of the two technical committees (not including subcommittee members) stands at approximately 150 professionals, with a balance of disciplines and a balanced representation from the medical, scientific, engineering, industrial, government, and military communities, representing 26 countries. ICES is now international and influence of the C95 standards is now global in scope. Through the World Health Organization‗s standards harmonization effort, ICES is working closely with other expert groups toward the development a single science-based global standard.

to vote, what they bring to the committee, etc., are usually placed on the consent agenda of the next quarterly SASB meeting and, unless pulled off for discussion, are approved with the agenda. During this time the standard usually undergoes a mandatory editorial review by IEEE Standards Department project editors, a review by SCC10 (Terms and Definitions – to ensure that all terms and definitions are in accord with IEEE definitions where such definitions exist), SCC14 (Quantities, Units, and Letter Symbols – to ensure consistent use of units and letter symbols), and, in some cases, a legal review.

Approval at the sponsor level requires a 75% response from the members of the Ballot Group (including abstentions) and 75% affirmative votes (the ratio of positive to positive plus negative votes) after ballot resolution. Attempts must be made to resolve every negative ballot and every substantive comment that accompanied a ballot, and their resolution (by an ad hoc ballot resolution working group) must be circulated to the Ballot Group to allow each member to confirm, change his or her vote or comment (only on issues raised during the initial ballot or previous recirculation ballot). Once a consensus is achieved the standard, ballot results, copies of the PAR, copies of the recirculation ballots, ballot resolution, and other relevant material are submitted to the SASB Review Committee (RevCom), also a standing committee of the IEEE SASB. RevCom reviews the scope of the standard to ensure that it is in accord with the scope of the PAR, that the draft has gone though legal review (when necessary), editorial review, review by SCC10, and SCC14 and that the Policies and Procedures of the sponsor and those of the IEEE SASB have been meticulously followed to ensure that the process was open, transparent, and due process was afforded at every level. When these conditions are met, RevCom can deem the ballot valid and recommend approval by the IEEE SASB. (RevCom deals only with procedural issues—not technical issues.) Once approved, the draft standard becomes an IEEE standard and is forwarded to ANSI for public comment and recognition as an American National Standard. Because of the potential sensitivity of the C95 standards, ICES Policies and Procedures require formal balloting at the working group level adhering strictly to IEEE SASB procedures, i.e., all members of SC4 are invited to join the ballot group, all comments submitted with each ballot are addressed, each revised draft resulting from ballot resolution and all comments and their disposition are circulated to all members of the ballot group to allow them to reaffirm or change their original vote.

12.9 IEEE C95.1-2005

C95.1-2005 is far more detailed and inclusive than its predecessor C95.1-1991. The 2005 standard is divided into two major parts—normative and informative. The normative part contains the scope and purpose, the normative references, definitions, recommendations (basic restrictions and MPEs), rules for assessing compliance and the role of an RF safety program. The informative part contains seven Annexes. The first three explain the revision process, summaries of the literature by biological endpoint, and the rationale for the revision. Examples of practical applications of the standard to typical exposure situations are also included as is a glossary of commonly used terms, the bibliography of seminal papers from the International EMF Project (IEEE/WHO) database that are cited in establishing the basic restrictions and thresholds, and a bibliography of other cited publications.

At the time C95.1-2005 was approved, SC4 had 132 members, 42% from outside the US representing 23 countries. Of the 132 members, 36 were from academia, 56 from laboratories and administrative branches of federal agencies and the Department of Defense,

22 were from industry, 26 were independent consultants, and 2 represented the general public. Of these, 73 participated in the balloting, 57 approved, 5 disapproved with comments and 11 abstained, resulting in 92% approval. During sponsor balloting, the Ballot Group had 59 members, 58 returned ballots, 51 approved, 2 disapproved with comments, 1 disapproved without comments and 4 abstained, resulting in 96% approval. The standard has grown in length from less than one and one-half pages (C95.1-1966) to more than 250 pages—the majority of which addresses the literature reviews and evaluations and the rationale, particularly as it applies to changes.

As with the earlier C95.1 standards, the revision of the 1991 standard began with the identification of relevant papers by the SC4 Literature Surveillance Working Group. The focus was on the identification of reliable studies reporting biological responses – from reversible effects and responses of adaptation to irreversible and biologically harmful effects. At the literature evaluation cutoff date, 31 December 2003, the Literature Surveillance Working Group identified over 2200 papers from a number of databases and inputs from federal agencies and other organizations that were regularly polled. Findings of studies published between 1950 and December 2003 were considered, including a number of studies reviewed for C95.1-1991. Although the literature cutoff date was December 2003, a few papers published in 2004 and 2005 were included. New insights gained from improved experimental and numerical methods and a better understanding of the effects of acute and chronic RF electromagnetic field exposures of animals and humans were considered during the evaluation process. Every attempt was made to include and to evaluate all of the relevant literature in the database, with emphasis on studies carried out under low level exposure conditions where increases in temperature could not be measured or were not expected. SC4 agreed that only peer-reviewed papers and technical reports of original research would constitute the primary database on which any risk analysis would be based. Abstracts and presentations at scientific meetings or technical conferences were expressly excluded. A list of all 1143 papers that were evaluated during the development of C95.1-2005 can be found in Annex E of the standard.[26]

The literature evaluation was carried out by the Engineering, Epidemiology, In vivo, and In vitro Working Groups (WGs). In addition, a Mechanisms Working Group was established to evaluate the technical significance of particular interaction mechanisms with regard to standard-setting. The Engineering WG was tasked with assessing of the exposure systems, field characteristics and measurements, dosimetry, specific absorption rates, induced currents and fields, and temperature/humidity measurements and whether or not the information provided was sufficient to allow a full understanding of how the experiment was performed.

The Epidemiology WG was originally tasked with the evaluation of each paper for study design and population segments, quality of the methods and implementation, merit of data acquisition and analysis for specific endpoints, and presence or absence of positive statistical associations. Similarly, the In Vivo and In Vitro WGs examined the technological methodologies employed in each published paper, including the exposure conditions, specific organ systems and/or biological endpoints, the engineering and statistical methodologies employed, and the relevance of each study for standard-setting. The in vitro papers typically emphasized possible effects at the cellular level, including those on cell viability and

---

[26] The complete list of papers in the IEEE/WHO database is available online at Internet site http://www10.who.int/peh-emf/emfstudies/IEEEdatabase.cfm

proliferation, genotoxicity, cell transformation, molecular synthesis, and cell function; the in vivo papers typically examined possible effects of exposure on the whole organism or on specific organ systems, including effects on the embryo/fetus, reproductive ability, immunological system, functional alterations of the metabolic or thermoregulatory system, various histological endpoints, and behavioral changes.

Many of the evaluations went through a formal process beginning with the chair of each WG providing copies of each paper to two independent reviewers, together with specially designed and approved review forms. These forms were in a computer format that required numerical scoring by individual reviewers for entry into a computerized database. When a review was completed, the reviewer gave the paper an overall technical merit rating on a 5-point scale. The rating scale was: Very High = 5; Moderately High = 4; Acceptable = 3; Low = 2; and Very Low = 1. For ratings of 1 or 2, a request was made for justification for the low score in writing by the reviewer. Strong discordance between the two reviews of a given paper required a third independent review. Periodically, the chair of each WG would submit a summary of the completed evaluations to the Chair of the Risk Assessment WG (RAWG) whose charge was to evaluate the implied risk for human beings of exposure to RF electromagnetic fields.

After several years it became clear that the literature evaluation process would not be completed on time following the formal protocol described above. While the engineering WG evaluated nearly all of the papers in the database and the In Vivo WG evaluated more than 90% of their assigned papers, few epidemiology and in vitro papers were evaluated by members of their respective WGs because of a lack of qualified reviewers. Rather than try to evaluate every paper in the database following the protocol described above, certain individuals with considerable expertise in specific areas volunteered or were asked to prepare review papers and summarize their findings in specific topic areas. These included, for example, cancer induction or promotion, teratologic effects, ocular effects, epidemiology, thermoregulation, and animal behavior. In each topic area, one of the goals was to search for definable hazards. The texts and conclusions of the various review papers were made available to the RAWG; the summaries and conclusions from each review paper, which appear in Annex B of C95.1-2005, were further enhanced by 12 review papers published in Supplement 6, 2003 of *Bioelectromagnetics* (Greenebaum, 2003). These included reviews of the epidemiology and in vitro literature. The evaluation process took advantage of all completed evaluations in the computerized database plus the review papers.

The overall results of the literature evaluation and review process were used to determine the thresholds of individual responses and dose response functions, i.e., the lowest level at which a potential harmful effect occurs and the function that relates dose rate, e.g., SAR, to response magnitude. The weight of evidence approach was used throughout to develop the thresholds and dose response functions, i.e., the same approach used to develop guidance for assessment of risk from chemical and other physical agents known to be hazardous.[27] SC4 agreed that the recommendations (basic restrictions and MPEs) should protect against ―*established adverse health effects in human beings associated with exposure to electric, magnetic and electromagnetic fields in the frequency range of 3 kHz to 300 GHz*‖

---

[27] For purposes of this standard, the weight of scientific evidence is defined as ―the outcome of assessing the published information about the biological and health effects from exposure to RF energy. This process includes evaluation of the quality of test methods, the size and power of the study designs, the consistency of results across studies, and the biological plausibility of dose-response relationships and statistical associations.‖

343

(IEEE C95.1, 2006, p. 1). The term adverse health effect is defined as ―A biological effect characterized by a harmful change in health" (IEEE C95.1, 2006, p. 4). Notes to the definition point out that 1) ―adverse effects do not include biological effects without a harmful health effect, changes in subjective feelings of well-being that are a result of anxiety about RF effects or impacts of RF infrastructure that are not physically related to RF emissions, or indirect effects caused by electromagnetic interference with electronic devices" (IEEE C95.1, 2006, p. 4), and 2) ―sensations (perceptions by human sense organs) per se are not considered adverse effects. Thus a sensation of warmth at millimeter and other wavelengths and the microwave auditory effect under the underlying special conditions are not recognized as effects to be protected against by this standard. Painful or aversive electrostimulation resulting from exposure at frequencies below 0.1 MHz is treated as an adverse effect" (IEEE C95.1, 2006, p. 4). This definition, though somewhat narrower than the WHO definition of adverse effect, i.e., ―A biological effect that has a detrimental effect on mental, physical and/or general well being of exposed people, either in the short-term or long term" (cf. WHO, 2006, p. 7), was chosen to eliminate some of the ambiguity and subjectivity associated with the broader definition.

Once the hazard threshold was identified and enough supporting information was available, a safety factor was applied to the threshold to derive the basic restrictions and MPEs based on the best available scientific information using the conservative approach common in standard setting. The safety factor, which is influenced by the uncertainty in the knowledge of the degree of hazard associated with the hazard threshold, is selected to prevent exceeding the hazard threshold value with a sufficiently wide margin. The magnitude of a safety factor in the 2005 standard ranges from unity at low frequencies, where effects associated with electrostimulation occur, e.g., sensation, to significantly greater values at frequencies where heating effects occur, i.e., above 100 kHz. In all cases, however, the selection of the appropriate safety factor was based on informed expert opinion after considering the underlying biological and engineering uncertainties applicable to the exposed population for a broad range of exposure conditions.

The results of the literature evaluation and review process by the SC4 working groups did not provide evidence that would warrant a change in the scientific basis for the adverse effect level for frequencies between 100 kHz and 3 GHz. The threshold value for whole-body average SAR was again found to be 4 W/kg, and again the most reliable reproducible biological endpoint was found to be behavioral disruption of food-motivated behavior in laboratory animals, including non-human primates. Although this conclusion was based on the results of animal studies, it was agreed that whole-body average SARs above 4 W/kg could be potentially harmful in humans. This is the same threshold SAR and endpoint found during the development of C95.1-1982, C95.1-1991, the 1986 NCRP report and the 1998 ICNIRP guidelines. The upper boundary of the frequency range over which whole-body average SAR is considered the appropriate basic restriction metric was reduced from 6 GHz in the 1991 standard to 3 GHz based on RF penetration depth calculations. Also, peak spatial-average SAR values were changed from 1.6 W/kg and 8 W/kg for the lower and upper tiers to 2 W/kg and 10 W/kg, respectively, and the corresponding tissue averaging mass was changed from 1g to 10 g. This change is based partially on the biologically based rationale of ICNIRP related to exposure of the eyes, the extensive theoretical biophysical research quantifying RF energy penetration in biological tissue, and the desire to harmonize with the ICNIRP guidelines where scientifically justified.

344

The rationale to set exposure limits for effects associated with electrostimulation at the lower frequencies and temperature-related effects at higher frequencies is explained thoroughly in the standard. Improved numerical and measurement methods in RF dosimetry have increased knowledge about the SAR-temperature relationship following RF energy deposition in human tissue, which is essential when assessing potential biological and health effects of RF exposures. A number of special considerations have been reviewed and are explained in detail in the annexes of the standard.

The 2005 standard incorporates a reasonably large margin of safety and, unlike the earlier standards, an RF safety program is required to provide part of the margin of safety for those exposed above the lower tier, now called an "action level," rather than exposures in uncontrolled environments. The choice of the term "action level" for the lower tier, rather than limits for the "general public" or "uncontrolled environment," stems from the fact that the committee concluded that the weight of scientific evidence supports the conclusion that there is no measurable risk associated with RF exposures below the basic restrictions of the *upper tier* of this standard. The lower tier, with an additional safety factor, recognizes public concerns and also supports the process of harmonization with other recommendations and guidelines, e.g., the NCRP recommendations and the ICNIRP guidelines, and defines the level above which implementation of an RF safety program is recommended. The purpose of the action level is to initiate measures, i.e., implementation of an RF safety program as defined in IEEE C95.7-2005 (2006), to prevent exposures above the upper tier. (The basic restrictions and MPEs of the lower tier can be used for the general population.) The standard is especially conservative, since the safety factors are applied against perception phenomena (electrostimulation and behavioral disruption), which are far less serious effects than any permanent pathology or even reversible tissue damage that could occur at much higher exposure levels than those for perception phenomena (IEEE C95.1-2005, 2006).

This revision of IEEE Std C95.1 maintains many of the characteristics of the previous standard but also contains a number of differences from earlier editions that address new dosimetry findings and that simplify the use and application of the standard. These similarities and differences are described in Annex C of C95.1-2005 and are summarized below.

12.10 Similarities

- All relevant reported biological effects at either low ("non-thermal") or high ("thermal") levels were evaluated. Research on the effects of chronic exposure and speculations on the biological significance of low-level interactions have not changed the scientific basis of the adverse effect level.
- Whole-body average and peak spatial-average SAR remain the basic restrictions over much of the RF spectrum and remain the same as in the earlier standards and guidelines, i.e., 0.4 and 0.08 W/kg.
- The MPE for exposures in controlled environments remain the same as in C95.1-1991.
- The averaging time remains 6 min for frequencies below 3 GHz for effects associated with tissue heating; but the averaging time for effects associated with electrostimulation is now 0.2 s for an rms measurement (not 1 s as in the 1999 Supplement to C95.1-1991 (IEEE C95.1b, 2004).

12.11 Differences

- Both C95.1-1991 and C95.1-2005 contain two tiers. While the weight of scientific evidence supports the conclusion that no measurable risk is associated with RF exposures below the limits of the upper tier, it is impossible to scientifically prove absolute safety and, hence, a lower tier has been set with an extra margin of safety. The lower tier recognizes public concerns, takes into account uncertainties in laboratory data and in exposure assessment, and supports the process of harmonization with other standards, e.g., the NCRP recommendations and the ICNIRP guidelines. While the basic restrictions and MPEs of the upper tier in both standards apply to exposures in controlled environments; the lower tier of the 2005 standard is now an *action level*, rather than specific limits for exposures in uncontrolled environments. This action level, above which an RF safety program shall be implemented to protect against exposures that exceed the upper tier, is tied to C95.7-2005 (RF safety programs) (IEEE C95.7, 2006). For practical purposes, however, the lower tier may also be used for the general public.

- The upper frequency boundary over which the whole-body average SAR is deemed to be the basic restriction (i.e., the ―resonance‖ region) has been reduced from 6 GHz to 3 GHz.

- The lower tier MPEs for long-term exposure are different from those in C95.1-1991 and are in general more restrictive between 300 MHz and 300 GHz.

- The peak spatial-average SAR values have been changed from 1.6 W/kg and 8 W/kg for lower and upper tiers to 2 W/kg and 10 W/kg, respectively.

- The averaging mass for determining the peak spatial-average SAR has been changed from 1 g of tissue in the shape of a cube to 10 g of tissue in the shape of a cube.

- Although implicit in previous versions of the C95.1 standard, e.g., as a SAR exclusion, the present standard explicitly relies on ―basic restrictions.‖

- The C95.1-2005 requires the development and implementation of an RF safety program in controlled environments.

- A more realistic averaging time (based on thermal modeling by Riu and Foster (1999) for both the upper and lower tiers has been incorporated for frequencies above 3 GHz to take into account penetration depth, which decays rapidly above 5 GHz. (This resolves the need for the caveat ―except for the eyes and testes‖ (IEEE C95.1, 1991, p. 20) associated with the partial-body relaxation criteria found in the 1991 standard.)

- The upper frequency at which maximum induced and contact currents are specified is now 110 MHz compared with 100 MHz in the previous standard.

- The frequency at which the upward ramp begins for the relaxation of the power density limits for localized exposure has been changed from 6 GHz to 3 GHz.

In recognition of the differing impact of exposure to particular frequencies, the standard provides sections devoted to three frequency bands: 3 kHz to 5 MHz, 100 kHz to 3 GHz, and 3 GHz to 300 GHz. The limits in the first band, which protects against adverse effects associated with electrostimulation, overlaps the second band where the limits also protect against effects associated with heating. The limits in the third band protect against

346

effects associated with heating, particularly superficial heating. Differences between C95.1-1991 and C95.1-2005 within each of these bands are as follows:

- **3 kHz to 5 MHz:** The basic restrictions, based on effects associated with electrostimulation, are now provided in terms of the *in situ* electric fields for different regions of the body. Magnetic field MPEs are specified for the arms and legs and for the head and torso. The electric field MPE for exposure of the whole body has been increased for exposures in controlled environments; the corresponding magnetic field MPE, with separate requirements for different regions of the body, has been increased for exposures in controlled environments and for the lower tier (action level), and have been made frequency dependent. Formulas for determining maximum permitted peak electric fields for both *in situ* and environmental conditions are included.

- **100 kHz to 3 GHz:** The peak spatial-average SAR criteria for localized exposure of any tissue excluding the hands, wrists, forearms, feet, ankles, lower legs and pinnae, have been relaxed from 8 W/kg and 1.6 W/kg to 10 W/kg and 2 W/kg for the upper and lower tiers, respectively. The corresponding averaging mass has been increased from 1 g to 10 g of tissue in the shape of a cube.[28] The peak spatial-average SAR for the hands, wrists, forearms, feet, ankles, lower legs and pinnae, remains 20 W/kg for the upper tier and 4 W/kg for the lower tier. The contact current limits for the frequency range of 100 kHz to 110 MHz have been subdivided into touch and grasping conditions, with the grasping condition confined to the controlled environment. The permissible touch contact current has been reduced for both the controlled environment and the lower tier (action level). In the transition region where effects associated with electrostimulation and tissue-heating occur (100 kHz to 5 MHz), the basic restrictions and MPEs for both must be met. In order to harmonize with ICNIRP, the frequency dependence of the MPEs for frequencies between 300 MHz and 300 GHz has changed and the values made more stringent, but only for the lower tier.

- **3 GHz to 300 GHz:** The upper frequency of the SAR region has been reduced from 6 GHz to 3 GHz to better reflect the quasi-optical nature of tissue interactions. As indicated above, the principal change has been in the values and frequency dependence of the MPEs above 300 MHz for the lower tier, but the MPE at 300 GHz and the corresponding averaging time remains the same as in C95.1-1991.

As in the earlier standards, the recommendations are expressed in terms of basic restrictions MPEs, i.e., reference levels, investigation levels. The basic restrictions are limits on the *in situ* electric field strength for the brain, heart, extremities and other tissues (different limits for each) for frequencies between 3 kHz and 100 kHz, whole-body average SAR and peak spatial-average SAR (with relaxed limits for the extremities and the pinna) for frequencies between 100 kHz and 3 GHz, and incident power density for frequencies between 3 GHz and 300 GHz. The MPEs, which are derived from the basic restrictions, are limits on external fields and induced and contact current. In the region where effects associated with electrostimulation predominate, i.e., between 3 kHz and 100 kHz (up to 5 MHz for certain pulsed fields), the MPEs are expressed in terms of the external electric and magnetic field strengths for the head and torso with separate values for the limbs. MPEs for the undisturbed

---

[28] The rationale for changing the peak spatial-average SAR and averaging volume was in part the desire to harmonize with the ICNIRP guidelines where scientifically justified and in part based on recent theoretical biophysical research and thermophysiological data showing the inability of RF energy to cause significant local temperature increases in small tissue volumes for inducing adverse health effects 0.

electric field strength (absent a person) are also provided for frequencies between 3 kHz and 100 kHz. In the region where whole-body heating predominates (100 kHz to 3 GHz), the MPEs are expressed in terms of the incident electric and magnetic field strengths for frequencies up to 300 MHz for the upper tier (exposures in controlled environments) and up to 400 MHz for the lower tier (action level – general public) above which the MPEs for both tiers are expressed in terms of the plane-wave equivalent power density. In the transition region of 0.1 to 5 MHz, each of the two sets of MPEs and basic restrictions apply. In this transition region, the MPEs and basic restrictions based on heating will be more restrictive for long-term exposures to CW fields, while the MPEs and basic restrictions based on the effects of electrostimulation will be more restrictive for short-term exposure, e.g., short isolated pulses of low duty factor. For frequencies greater than 3 GHz, the MPEs and basic restrictions are expressed in terms of incident power density and are equivalent. Figure 12-5 and Figure 12-6 are graphical representations of the C95.1-2005 MPEs for the upper tier (exposures in controlled environments) and the lower tier (action levels), respectively. Figure 12-7 shows a comparison of the C95.1-2005 MPEs (in terms of the E-field equivalent power density) with the corresponding MPE of the 1998 ICNIRP guidelines. Table 12-5 is a comparison of features of the ICNIRP guidelines with the corresponding features of IEEE C95.1-2005.
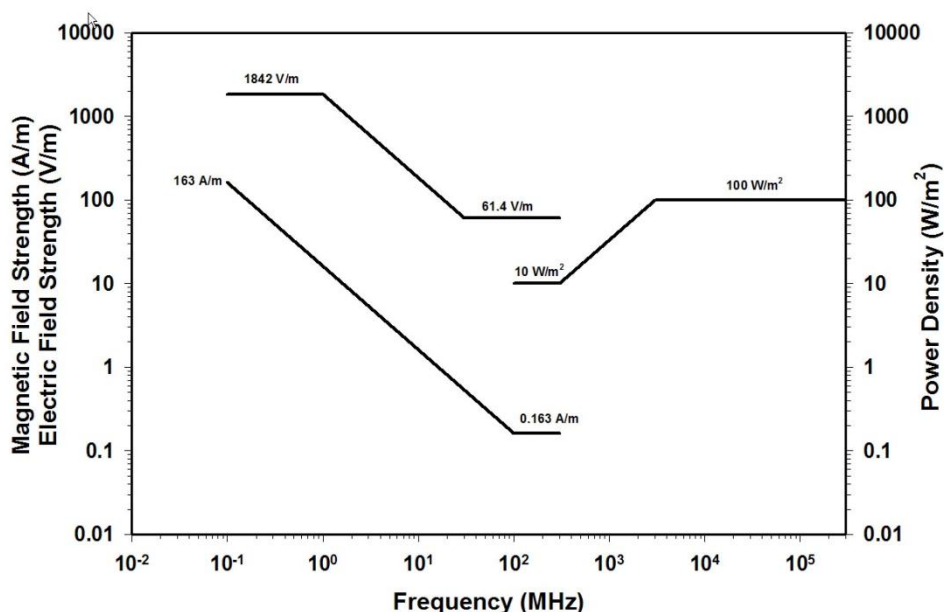
Figure 12-5. Graphical representation of the C95.1-2005 MPEs for the upper tier in the frequency region where effects associated with heating predominate (from IEEE C95.1-2005, 2006).

348
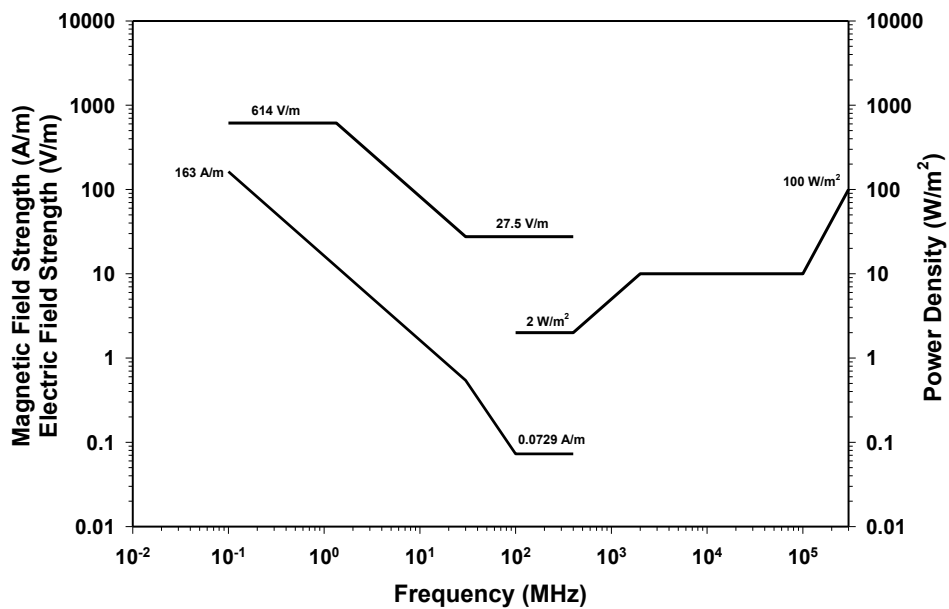
Figure 12-6. Graphical representation of the C95.1-2005 MPEs for the lower tier in the frequency region where effects associated with heating predominate (IEEE C95.1-2005, 2006).
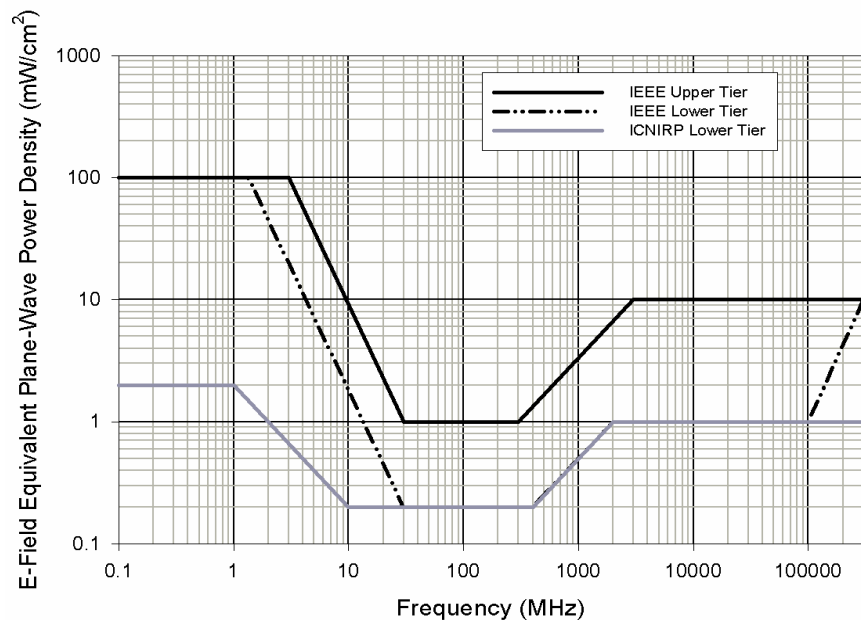
Figure 12-7. Comparison of the C95.1-2005 MPEs (lower tier - expressed in terms of E-field equivalent power density) with the ICNIRP MPEs for the general public. The upper tier MPEs of C95.1-2005 are the same as the C95.1-1991 MPEs.

349

Table 12-5. Comparison of 1998 ICNIRP guidelines and C95.1-2005: Region where the predominant interaction mechanism is tissue heating.

Parameter	ICNIRP	IEEE C95.1-2005
Frequency range	~ 100 kHz to 300 GHz	~ 100 kHz to 300 GHz
Recognition of whole-body resonance	Yes	Yes
Incorporation of dosimetry(SAR)	Yes	Yes
Database of experimental literature	Large	Large (~1100 citations)
Most significant biological endpoint	Behavioral disruption (associated with ~ 1°C temperature rise)	Behavioral disruption (associated with ~ 1°C temperature rise)
Whole-body average SAR associated with behavioral disruption	1-4 W/kg	~ 4W/kg
Limiting whole-body average SAR	0.4 W/kg (Occupational)	0.4 W/kg (Controlled Environment)
– Applicable frequency range	0.08 W/kg (General Public)	0.08 W/kg (Action Level)
	100 kHz to 10 GHz	100 kHz to 3 GHz
Peak spatial-average SAR (localized exposure)	10 W/kg (Occupational)	10 W/kg (Controlled Environment)
	2 W/kg (General Public)	2 W/kg (Action Level)
–Averaging volume	10 g of contiguous tissue	10 g of tissue in the shape of a cube
–Averaging time	6 min (Occupational)	6 min (Controlled Environments)
	6 min (General Public)	30 min (Action Level)
Limits for extremities		
–Upper tier	20 W/kg (limbs)	20 W/kg (extremities including pinnae)
–Lower tier	4 W/kg (limbs)	4 W/kg (extremities including pinnae)
–Applicable frequency range	$100 \text{ kHz} < f \leq 10 \text{ GHz}$	$100 \text{ kHz} < f \leq 3 \text{ GHz}$
Averaging time ($f > 100$ kHz)		
–Upper tier	6 min ($f \leq 10$ GHz) decreasing to 10 s at 300 GHz	6 min ($f \leq 3$ GHz) then decreasing to 10 s at 300 GHz)
–Lower tier	6 min ($f \leq 10$ GHz) decreasing to 10 s at 300 GHz	6 min (3 kHz $\leq f \leq$ 1.34 MHz). E^2 and H^2 have different averaging times for 1.34 MHz $< f \leq$ 100 MHz but both are equal to 30 min at 100 MHz. For 100 MHz $< f \leq$ 5 GHz the averaging time is 30 min and then decreases to 10 s at 300 GHz.
Induced and contact current limits		
–Upper tier	40 mA (limb currents)	90 mA (each foot)
–Lower tier	20 mA (limb current)	45 mA (each foot)
–Applicable frequency range	$100 \text{ kHz} \leq f \leq 110 \text{ MHz}$	$100 \text{ kHz} \leq f \leq 110 \text{ MHz}$
Special criterion for modulated fields	No	No
Specific limits for high peak, low average power pulses	Yes—Based on evoked auditory response (—microwave hearing")	Yes—Based on the stun-effect
RF safety program	Not specifically	Yes – IEEE C95.7-2005. The BRs and MPEs of the lower tier (action level) are linked to an RF safety program to mitigate against exposures that could exceed the BRs and MPEs of the upper tier.

350

12.12 Other RF Standards

There are a number of other standards available for assessing compliance with the C95.1 standards and the ICNIRP guidelines. These include measurement standards, such as IEEE C95.3-2002 (2002), which describes measurement and computational techniques for assessing human exposure to electric, magnetic and electromagnetic fields, instrument types and limitations, measurement uncertainties, plus a number of other instrument and measurement issues. Although the scope of the standard covers the frequency range of 100 kHz to 300 GHz, its practical range of applicability is closer to 100 kHz to few GHz. There are also a number of product standards available for assessing compliance of specific products, such as hand-held mobile telephones intended to be operated while placed next to the head, with the basic restrictions (peak spatial-average SAR) found in C95.1-2005 and the ICNIRP guidelines. These include IEEE 1528-2003 (2003), IEEE 1528a-2005 (2006) and IEC 62209 (2005). These standards describe in detail the procedures for determining the peak spatial-average SAR in an anthropomorphic model of the human head (filled with liquid head-tissue simulant) by means of a robotically-controlled miniature electric field probe. Calibration techniques, measurement uncertainties, recipes for the tissue-equivalent liquids and techniques for measuring their electric properties are just a few of the issues addressed in these standards. These IEEE and IEC standards are in complete harmony. Neither of these standards specifies a specific basic restriction—they can be used for conformity assessment against any commonly used value and averaging mass. Similar standards are now under development to carry out the same assessments using numerical simulations, e.g., FDTD techniques. An IEC project team is now in the process of developing a standard specific to assessing human exposure to mobile telephone base stations.

IEEE C95.7-2005 (RF safety programs) presents guidelines and procedures that can form the basis of a RF safety program for controlling hazards associated with RF sources that operate in the frequency range of 3 kHz to 300 GHz (IEEE C95.7-2005, 2006). C95.7 is a general-purpose standard with the goal of preventing potentially hazardous exposures to electromagnetic fields, currents, and/or contact voltages. The standard is modeled somewhat after the laser safety standards, e.g., ANSI Z136.1 (ANSI, 2007) and IEC 60825-1 (2001), where areas in which exposure may be possible are characterized into one of four exposure categories according to the potential risk for exposure in excess of prescribed limits and then specifying the appropriate controls to reduce the likelihood of over-exposure. This standard is designed to complement the IEEE C95 family of standards but may find use in the development of effective programs to ensure conformance with other guidelines, standards, or regulations. Warning signs and labels, which generally are part of any safety program, can be found in IEEE C95.2-1999 (1999).

12.13 Summary

Contemporary science-based RF/microwave safety standards and guidelines are based on in-depth evaluations and interpretations of the extant scientific literature. This is an on-going process and, as such, the recommendations in terms of safe limits of exposure evolve as the research becomes more focused and the quality of the research improves. The simple single value frequency-independent limit proposed more than five decades ago has evolved into the sophisticated rather complex standards and guidelines now used throughout the world. The biggest influence on the direction of the standards was the better understanding of dosimetry issues gained through the thermographic studies and numerical modeling that began

in the 1970's. This provided the means for establishing meaningful parameters for relating the external fields to the internal fields and provided the means for readily comparing study results. The concept of SAR, first proposed in 1981 for use as a basic restriction over a limited frequency range, led to the current whole-body average SAR 4 W/kg threshold for adverse effects (behavioral disruption), which has not changed even though the literature database has grown tremendously during that time. Although the MPEs of IEEE C95.1-2005 may differ slightly from those of the 1997 ICNIRP guidelines, the differences are minor and have to do with the engineering aspects of relating the incident fields to the internal fields and the assigned margins of safety—not with philosophical differences in the interpretation of the biology. With each revision, the basic restrictions and derived limits (reference levels, MPEs) of the two most often cited standards and guidelines, i.e., the C95.1 standards and the ICNIRP guidelines, converge.

Both the ICNIRP guidelines and C95.1 standards are living documents. If any new adverse effect is established which would require a change in the standard, for example, the standard can be promptly revised by amendments. The IEEE committee continues the literature surveillance and evaluation of the bioeffects research for the next revision. The future replacement of peak SAR by temperature or temperature increase was discussed as a possibility during development of the 2005 standard; dosimetry studies are now in progress to identify the relationship between temperature rise and peak spatial average SAR for future consideration.

12.14 References

American National Standards Institute (ANSI). (1974). *Safety Level of Electromagnetic Radiation With Respect to Personnel* (C95.1-1974). New York, NY: American National Standards Institute.

American Standards Association (ASA). (1966). *Safety Level of Electromagnetic Radiation with Respect to Personnel* (C95.1-1966). New York, NY: United States of America Standards Institute.

American National Standards Institute (ANSI). (1982). *American National Standard Safety Levels with respect to Human Exposure to Radio Frequency Electromagnetic Fields, 300 kHz to 100 GHz* (C95.1-1982). New York, NY: American National Standards Institute.

American National Standards Institute (ANSI). (1973). *American National Standard Techniques and Instrumentation for the Measurement of Potentially Hazardous Electromagnetic Radiation at Microwave Frequencies* (C95.3-1973). New York, NY: American National Standards Institute.

American National Standards Institute (ANSI). (1981). *American National Standard Recommended Practice for the Measurement of Hazardous Electromagnetic Fields - RF and Microwave* (C95.5-1981). New York, NY: American National Standards Institute.

American National Standards Institute (ANSI). (2007). *American National Standard for the Safe Use of Lasers* (Z136.1). New York, NY: American National Standards Institute.

Clark, J. W., Hines, H. M. & Salisbury, W. W. (1949). Exposure to microwaves. *Electronics*, *22*, 66-67.

Daily, L. Jr., Wakim, K. G., Herrick, J. F., Parkhill, E. M. & Benedict, W. L. (1952). The effects of microwave diathermy on the eye of the rabbit. *American Journal of Ophthalmol*ogy, *35*, 1001-1017.

Durney, C. H. (1980). Electromagnetic dosimetry for models of humans and animals: A review of theoretical and numerical techniques. *Proceedings of the IEEE*, *68*.

Durney, C. H., Johnson, C. C., Barber, P. W., Masoudi, H., Iskander, M. F., Lords, J., Ryser, D. K., Allen, S. L. & Mitchell,. J. C. (1978). *Radiofrequency Dosimetry Handbook*, Second Edition (Report SAM-TR-78-22). Brooks Air Force Base, Texas: USAF School of Aerospace Medicine.

Ely, T. S., Goldman, D. E., Hearon, J. Z., Williams, R. B., & Carpenter, H. M. (1957). *Heating Characteristics of Laboratory Animals Exposed to Ten-Centimeter Microwaves*. Naval Med. Res. Report. Project NM001 056.13.02.

Evans, E., Brooks, J., Schmidt, F, Williams, R., & Ham, W. T., Jr. (1955). Flash burn studies on human volunteers. *Surgery*, *37*, 280-297.

Gandhi, O. P. (1980). State of knowledge for electromagnetic absorbed dose in man and animals. *Proceedings of the IEEE*, *68*, 24-32.

Gandhi, O. P., Hunt, D. L. & D'Andrea, J. A. (1977). Deposition of electromagnetic energy in animals and in models of man with and without grounding and reflector effects. *Radio Science*, *12*(6S), 39-48.

Gandhi, O. P., Sedigh, K., Beck, G. S. & Hunt, E. L. (1976). Distribution of electromagnetic energy deposition in models of man with frequencies near resonance. In C. C. Johnson & M. L. Shore (Eds.), *Biological Effects of Electromagnetic Waves* (Vol. 2, pp. 44-67). DHEW Publications (FDA), 77-8011.

Greenebaum, B. (Ed.). (2003). Editor's note: Reviews of the effects of RF fields on various aspects of human health. *Bioelectromagnetics*, Suppl. 6, Wiley-Liss.

Guy, A. W. (1974). Quantitation of induced electromagnetic field patterns in tissue, and associated biological effects. In P. Czerski (Ed.), *Biological Effects and Health Hazards of Microwave Radiation* (pp. 203-216). Warsaw: Polish Medical Publishers.

Guy, A. W. (1975). Analyses of electromagnetic fields induced in biological tissues by thermographic studies on equivalent phantom models. *IEEE Transactions on Microwave Theory and Techniques*, MTT-*19*, 205-214.

Guy, A. W., Weber, M. D. & Sorensen, C. C. (1976). Determination of power absorption in man exposed to high-frequency electromagnetic fields by thermographic measurements on scale models. *IEEE Transactions on Medical Electronics*, *23*, 361-371.

Hagmann, M. J. & Gandhi, O. P. (1979). Numerical calculations of electromagnetic energy deposition in models of man with grounding and reflector effects. *Radio Science*, *14*(6S), 23-29.

Hirsch, F. T. & Parker, J. T. (1952). Bilateral lenticular opacities occurring in a technician operating a microwave generator. *American Medical Association Archives of Industrial Health*, *6*, 512-517.

Institute of Electrical and Electronics Engineers, Inc. (IEEE). (1991). *IEEE Standard for Safety Levels with Respect to Human Exposure to Radio Frequency Electromagnetic Fields, 3 kHz to 300 GHz* (C95.1-1991). New York, NY: IEEE. Retrieved May 5, 2009, from
http://ieeexplore.ieee.org/stamp/stamp.jsp?tp=&arnumber=159488&isnumber=4177

Institute of Electrical and Electronics Engineers, Inc. (IEEE). (2004). *IEEE Standard for Safety Levels with Respect to Human Exposure to Radio Frequency Electromagnetic Fields, 3 kHz to 300 GHz - Amendment 2: Specific Absorption Rate (SAR) Limits for the Pinna* (C95.1b-2004). New York, NY: IEEE.

Institute of Electrical and Electronics Engineers, Inc. (IEEE). (2006). *IEEE Standard for Safety Levels with Respect to Human Exposure to Radio Frequency Electromagnetic Fields, 3 kHz to 300 GHz* (C95.1-2005). New York, NY: IEEE.

Institute of Electrical and Electronics Engineers, Inc. (IEEE). (1999). *IEEE Standard for Radio-Frequency Energy and Current-Flow Symbols* (C95.2-1999*)*. New York, NY: IEEE.

Institute of Electrical and Electronics Engineers, Inc. (IEEE). (1991). *IEEE Recommended Practice for the Measurement of Potentially Hazardous Electromagnetic Fields - RF and Microwave* (C95.3-1991). (Replaces ANSI C95.3-1973 and ANSI C95.5-1981)

Institute of Electrical and Electronics Engineers, Inc. (IEEE). (2002). *Recommended Practice for Measurements and Computations of Radio Frequency Electromagnetic Fields With Respect to Human Exposure to Such Fields, 100 kHz–300 GHz* (C95.3-2002). New York, NY: IEEE.

Institute of Electrical and Electronics Engineers, Inc. (IEEE). (2006). *IEEE Recommended Practice for Radiofrequency Safety Programs* (C95.7-2005). New York, NY: IEEE.

Riu, P. J. & Foster, K. R. (1999). Heating of tissue by near-field exposure to a dipole: a model analysis. *IEEE Transactions on Biomedical Engineering*, *46*, 911 – 917.

Institute of Electrical and Electronics Engineers, Inc. (IEEE). (2003). *IEEE Recommended Practice for Determining the Peak Spatial-Average Specific Absorption Rate (SAR) in the Human Head from Wireless Communications Devices: Experimental Techniques* (1528-2003). New York, NY: IEEE.

Institute of Electrical and Electronics Engineers, Inc. (IEEE). (2006). *IEEE Recommended Practice for Determining the Peak Spatial-Average Specific Absorption Rate (SAR) in the Human Head from Wireless Communications Devices: Measurement Techniques*

Amendment 1: CAD File for Human Head Model (SAM Phantom) (1528a-2005). New York, NY: IEEE.

International Commission on Non-Ionizing Radiation Protection (ICNIRP). (1998). Guidelines for limiting exposure to time-varying electric, magnetic, and electromagnetic fields (up to 300 GHz). *Health Physics*, *74*, 494 - 522.

International Commission on Non-Ionizing Radiation Protection (ICNIRP). (2007). *Aim & Roots*. Retrieved May 2, 2009, from http://www.icnirp.org/aim.htm

International Electrotechnical Commission (IEC). (2001). *IEC Standard Safety of Laser Products - Part 1: Equipment Classification, Requirements and User's Guide* (60825-1). International Electrotechnical Commission, Geneva.

International Electrotechnical Commission (IEC). (2005). *Human Exposure to Radio Frequency Fields from Hand-held and Body-mounted Wireless Communication Devices – Human Models, Instrumentation, and Procedures – Part 1: Procedure to Determine the Specific Absorption Rate (SAR) for Hand-held Devices used in Close Proximity to the Ear (Frequency Range of 300 MHz to 3 GHz)*(62209-1). Geneva: International Electrotechnical Commission.

Mumford, W. W. (1960). Some technical aspects of microwave radiation hazards. *Proceedings of the IRE*, 427–447.

National Council on Radiation Protection & Measurements (NCRP). (1981). *Radiofrequency Electromagnetic Fields – Properties, Quantities and Units, Biophysical Interaction, and Measurements* (NCRP Report No. 67). Bethesda, MD: National Council on Radiation Protection and Measurements.

National Council on Radiation Protection & Measurements (NCRP). (1986). *Biological Effects and Exposure Criteria for Radiofrequency Electromagnetic Fields* (NCRP Report No. 86). Bethesda, MD: National Council on Radiation Protection and Measurements.

Osepchuk, J. M. & Petersen, R. C. (2001). Safety Standards for Exposure to Electromagnetic Fields. *IEEE Microwave Magazine*, *2*(2), 57-69.

Petersen, R. C. (1991). Radiofrequency/Microwave Protection Guides. *Health Physics*, *61*(1).

Petersen, R.C. (1999). Radiofrequency safety standards-setting in the United States. In Bersani (Ed.), *Electricity and Magnetism in Biology and Medicin*e (pp. 761-764). New York: Plenum Press.

Pressman. S. (1970). *Electromagnetic Fields and Life* (Translation by Sinclair, F. L.,). New York: Plenum Press.

Richardson, A. M., Duane, T. D. & Hines, H. M. (1948). Experimental lenticular opacities produced by microwave irradiation. *Archives of Physical Medicine*, *29*, 765-769.

Riu P. J. & Foster, K. R. (1999). Heating of tissue by near-field exposure to a dipole: a model analysis. *IEEE Transactions on Biomedical Engineering*, *46*, 911-917.

Schwan, H. P. & Li, K. (1956). The mechanism of absorption of ultrahigh frequency electromagnetic energy in tissues as related to the problem of tolerance dosage. *IRE Transactions on Medical Electronics*, *ME-4*.

Williams, D. B., Mohahan, J. P., Nicholson W. J., & Aldrich, J. J. (1956). Biologic effects studies on microwave radiation, time and power thresholds for the production of 12.3 cm microwaves. *IRE Transactions on Medical Electronics*, *ME-4*, 17-22.

World Health Organization (WHO). (2006). *Model legislation for electromagnetic fields protection.* Retrieved May 1, 2009, from http://www.who.int/peh-emf/standards/EMF.

Radio Frequency Radiation Dosimetry Handbook
(Fifth Edition)

Chapter 13.   Terahertz-Frequency Bioeffects: Models and Standards

Robert J. Thomas[a], Jason A. Payne[a], C. D. Clark III[b], Douglas N. Goddard[b], Jill S. McQuade[a], Gavin D. Buffington[c], Paul D. S. Maseberg[c], Sirley Marques-Bonham[a], Kalyn M. Haeuser[a], Matthew A. Haeuser[a], and William P. Roach[a]

[a]Air Force Research Laboratory, 8262 Hawks Road, Brooks City-Base, TX 78235-5147
[b]Northrop Grumman, 4241 Woodcock Dr. Ste. B100, San Antonio, TX 78228-1330
[c]Fort Hays State University, Department of Physics, Hays, KS 67601-4099

Robert.Thomas@brooks.af.mil

13.1 Introduction

Electromagnetic radiation sources of terahertz frequencies are currently of interest for numerous applications in material science, security, and medical fields (Dobroiu et al., 2006; Dragoman & Dragoman, 2004; Fitzgerald et al., 2002). Recent technology advances have led to high-brightness sources (Williams, 2006b; Williams, 2006a; Carr et al., 2002). Systems currently under construction and identified as terahertz sources range in output from approximately 100-GHz to 10-THz frequencies or wavelengths of 30 μm to 3 mm. Among application-specific spectroscopic investigations, optical properties of tissues have now been examined in this frequency range (Pickwell et al., 2004; Pickwell et al., 2005).

In the employment of these new systems, safety is of interest to application developers, as output limitations will affect performance. Exposure limits for the 100-GHz to 10-THz frequency band fall within the overlapping ranges of laser safety limits and radio frequency limits. Commonly accepted exposure limit standards for lasers include the ANSI Z136.1 American National Standard for Safe Use of Lasers (American National Standards Institute, 2000), and the International Electrotechnical Commission (IEC) 80625-1 Standard (International Electrotechnical Commission IEC, 2001). These standards extend to a maximal wavelength of 1 mm (300 GHz). Radio frequency exposure limits are commonly determined from the IEEE C95.1 Standard (IEEE 2005), which begin with 300 GHz and extend to lower frequencies.

Laser and radio frequency exposure limits are defined very differently. Laser exposure limits are typically defined by a maximum permissible exposure (MPE) which is expressed as irradiance $[W\ cm^{-2}]$ for continuous-wave exposure, or radiant exposure $[J\ cm^{-2}]$ for pulsed exposures. The exposure limits are influenced by the exposure duration and wavelength of the optical radiation. Radio frequency exposure limits, or permissible exposure limits (PELs) may be expressed in the same units, or as maximal specific absorption rate (SAR), expressed in units of watts per kilogram $[W\ kg^{-1}]$. In

357

order to make a meaningful comparison of exposures, it may be necessary to translate between values (SAR and PEL), through more detailed knowledge of the interaction of the radio frequency radiation and the body or tissues of interest. This is due to the fact that the PEL computation often requires a detailed measurement or computation of the beam propagation and interaction.

Historically, safety analyses for optical laser exposures have been designed to define the threshold level for tissue damage, while radio frequency exposure limits have been based upon a psychophysical assessment of perception thresholds. To date, no systematic experimental studies have documented damage thresholds to living tissues in the terahertz range of electromagnetic frequencies (0.1 - 20 THz). Exposure limits exist as extrapolated estimates at the extreme bounds of current occupational safety standards for lasers and radio frequency sources. Additionally, there are disagreements between the two extrapolated values, in some temporal regions from the radio frequency side and the optical side, which may not be resolved until experiments are performed at the terahertz frequencies of concern.

Recently, there has been renewed interest in the absorption and dispersion spectra of liquids (Kindt & Schmuttenmaer, 1996) at the low-frequency end ($1 - 30 \ cm^{-1}$) of the far-infrared spectrum. This part of the spectrum is quite important as it falls between the microwave region and far-infrared optical region. The responses that are probed at those frequencies bridge the infrared-radio frequency gap between bulk dielectric relaxation, oscillatory, and intermolecular motions and electronic transitions. Technical limitations have, in the past, prevented extensive study in this region, but the advent of new femtosecond-pulse-initiated terahertz sources has enabled new study and analyses (Carr et al., 2002).

Most relevant to the question of exposure limits to terahertz sources is the measurement of fundamental parameters required for the assessment of tissue heating and subsequent injuries. Recent works by Pickwell et al. (Pickwell et al., 2004; Pickwell et al., 2005) have applied a terahertz-frequency source to the detection of basal cell carcinoma. The data available span the frequency range of approximately 0.1 - 2.0 THz and represent an excellent basis for initial assessments. Here these measurements are applied through a more complete derivation of dielectric parameters using the Debye models (Yu et al., 2005), assessing propagation and absorption strengths, heat transfer, and subsequent damage.

13.2 Methods

13.2.1 Electro-Optical Properties

Permittivity measurements at microwave to far-infrared frequencies have been reported for a number of electrolyte and non-electrolyte systems (Barthel & Buchner, 1991). They expand the knowledge of processes which produce an understanding of the electromagnetic properties that provide insight on the interplay of orientational, intramolecular, kinetic, bonding, diffusional or migrational modes. To deal with

358

complicated relaxation behavior, detected through a broad-frequency coverage of responses, the analysis of experimental data is based upon a suite of distinct relaxation processes. These may be Debye processes [Equation (1)] with discrete relaxation times or more or less broad relaxation time distributions around the relaxation time (τ_j), characterized by the parameters $\alpha_j > 0$ for symmetric and $\beta_j < 1$ for asymmetric distributions, with

$$\hat{\epsilon}(\omega) = \epsilon_\infty + (\epsilon - \epsilon_\infty) \sum_{j=1}^{n} \frac{g_j}{[1+(i\omega\tau_j)^{1-\alpha_j}]_j^\beta} \ . \tag{1}$$

Equation (1) contains Debye processes $(\alpha_j = 0, \beta_j = 1)$, Cole-Cole processes $(0 < \alpha_j < 1, \beta = 1)$ and Cole-Davidson processes $(\alpha_j = 0, 0 < \beta < 1)$ where n is the number of separable dispersion steps j of relaxation time τ_j, and dispersion amplitude $(\epsilon - \epsilon_\infty)$, and weight g_j (Barthel & Buchner, 1991).

Studies to date for terahertz imaging (Pickwell et al., 2004; Pickwell et al., 2005) have successfully characterized skin (epidermis and dermis) through the double-Debye formulation of Equation (1) over the 0.1 to 2.0 THz frequency range. This formulation of the dielectric properties for a given tissue are calculated by Equation (2), where $\epsilon_s, \epsilon_2, \epsilon_\infty, \tau_1$ and τ_2 are the double-Debye parameters, representing a simple expansion of two terms in Equation (1).

$$\hat{\epsilon}(\omega) = \epsilon_\infty + \frac{\epsilon_s - \epsilon_2}{1 + i\omega\tau_1} + \frac{\epsilon_2 - \epsilon_\infty}{1 + i\omega\tau_2} \ . \tag{2}$$

The values of the parameters found in Table 3.5 were taken from Pickwell et al. (2005) for both *ex-vivo* epidermis and water. Expanding on the analysis of Pickwell et al. (2005), values for refractive index, $n(\omega)$; linear absorption coefficient, $\alpha(\omega)$; and conductivity, $\sigma(\omega)$, for water, dermis, and epidermis were derived through Equations (3 - 8).

$$\hat{\epsilon}(\omega) = \epsilon'^{(\omega)} - i\epsilon''(\omega) \ . \tag{3}$$

$$\hat{n}(\omega) = n(\omega) - ik(\omega) \ . \tag{4}$$

$$n(w) = \left[\frac{\sqrt{\epsilon'^2 + \epsilon''^2} - \epsilon'^2}{2}\right]^{\frac{1}{2}} \ . \tag{5}$$

$$k(w) = \left[\frac{\sqrt{\epsilon'^2 + \epsilon''^2} - \epsilon'^2}{2}\right]^{\frac{1}{2}} \ . \tag{6}$$

$$\alpha(\omega) = \frac{2\omega}{c} k(\omega) \,. \tag{7}$$

$$\sigma(\omega) = \epsilon_0 \omega [\epsilon''(\omega)] \,. \tag{8}$$

These values, along with relative permittivity values for 0.2 to 2.0 THz, appear in Figure 13-1. Specific values at 1 THz appear in Table 13-1. With all the values obtained, formulations are applied to address propagation and the subsequent derivation of source terms for heat transfer.
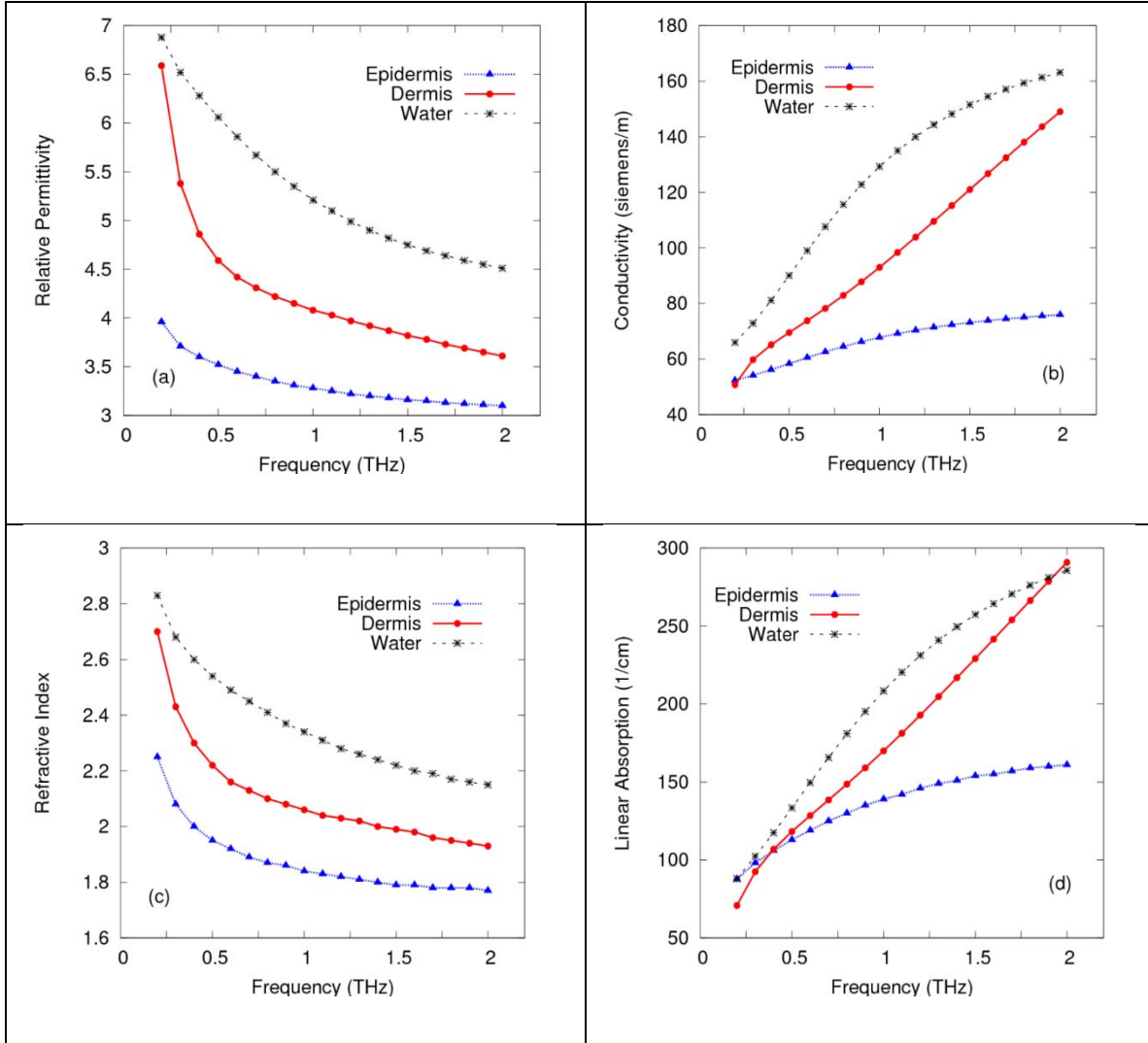
Figure 13-1. (a) Frequency-dependent permittivity, (b) conductivity, (c) refractive index, and (d) linear absorption values for skin tissues and water.

Table 13-1. Electromagnetic and optical parameters of tissue layers employed in heat transfer modeling at 1-THz frequency.

Layer Name	Relative Permittivity ϵ/ϵ_0	Conductivity σ [$Siemens\ m^{-1}$]	Absorption μ_a [cm^{-1}]
Water	5.21	129	208
Epidermis	3.28	67.8	139
Dermis	4.08	93.0	170

13.2.2 Heat Transfer Models

A two-dimensional representation of tissue constructs was selected with the assumption of cylindrical symmetry. The model, implemented numerically, computes an approximate solution to the bio-heat equation, expressed in cylindrical coordinates by Equation (9) (Takata et al., 1977; Mainster et al., 1970). The tissue (skin) is modeled as a two-layer structure of large radial extent. Layer axial dimensions representative of the measured values for tissues are listed in Table 13-2. Each layer is assumed to be homogeneous in optical and physical properties, each of which is listed in Table 13-2. In the limit of very large area exposures, a solution was developed for the one-dimensional form of Equation (9), which solves only the axial dependence of temperature with time.

$$\rho c_p \frac{\partial v}{\partial t} = \frac{k}{r}\frac{\partial v}{\partial r} + \frac{\partial}{\partial r}\left(k\frac{\partial v}{\partial r}\right) + \frac{\partial}{\partial z}\left(k\frac{\partial v}{\partial z}\right) + A + \bar{q} \ . \tag{9}$$

Table 13-2. Thermal parameters and densities of tissue layers employed in heat transfer modeling and water.

Layer Name	Layer Thickness [μm]	Density [$g\ cm^{-3}$]	Specific Heat [$J\ g^{-1}K^{-1}$]	Thermal Conductivity [$W\ cm^{-1}K^{-1}$]
Water	-	1.000	4.1868	6.28 x 10^{-3}
Epidermis	68	1.210	2.2440	2.00 x 10^{-3}
Dermis	-	1.060	3.6630	4.90 x 10^{-3}

The solution of Equation (9) represents the temperature rise [°C] in the tissue as a function of time and position. The source term $A = A(z, r, t)$, represents energy from the laser absorbed per unit time and volume [$J\ cm^{-3}\ sec^{-1}$]. The term $\bar{q} = \bar{q}(z, r, t)$ represents energy transfer per unit time and volume from blood flow (perfusion) within the tissue [$J\ cm^{-3}\ sec^{-1}$]. The value $k = k(z)$ is the thermal conductivity [$J\ cm^{-1}\ sec^{-1}\ K^{-1}$], $c_p = c_p(z)$ is the specific heat [$J^{-1}g\ K^{-1}$] of the layer at constant pressure, $\rho(z)$ is the layer density [$g\ cm^{-3}$], with z specifying the axial coordinate in the tissue.

The bio-heat equation is solved numerically, employing an alternating-direction implicit (ADI) finite-difference method (Peaceman & Rachford, 1955) for a two-dimensional (2-D) solution and the Crank-Nicholson method for a one-dimensional (1-D) solution where the radial coordinate is ignored (Ozisik, 1994). The numerical solution is

361

performed on a grid which is uniformly spaced within the region of the beam interaction. A stretched-grid scheme (Takata et al., 1977) extends the computational region to limit boundary effects other than at the tissue-air interface.

13.2.3 Source Term Representation

The heat source term for the formulation of the thermal model was examined through two differing approaches. These approaches are labeled as an ―optical model‖ and a ―radio frequency model.‖ In the optical model formulation, the time-dependent solution to Equation (9) is determined for a source term, $A(z, r, t)$, defined by Equation (10). A localized heat source term was estimated from a simple linear absorption commonly used for optical frequencies. The time dependent amplitude is assumed to be a square pulse temporal profile with an optional Gaussian or top-hat spatial distribution in the radial coordinate. Because optical scattering within the tissue is insignificant at terahertz frequencies, the model ignores scattering and approximates the light propagation using a Beer's law approximation (Welch & van Gemert, 1995).

$$A(z,r,t) = h(z,r)H_0(\lambda,t)\mu_a(z,\lambda).$$ (10)

This source term provides a time-dependent description of the linear absorption of optical energy as a function of depth in the tissue, complete with spectral and radial dependence of energy being absorbed. The variable λ refers to the wavelength of the terahertz source. The function $h(z,r)$ specifies the relative irradiance for a given position in the cylindrical coordinate system and includes losses due to linear absorption. This term also addresses the focusing of the beam through the tissues using a specified beam-waist location and a hyperbolic function to assign beam radius as a function of position. The function $H_0(\lambda, t)$ provides the maximum irradiance per wavelength division at a given time [$W\ cm^{-2}\ nm^{-1}$]. The value $\mu_a(z,\lambda)$ represents the absorption coefficient [cm^{-1}] at a given wavelength within the tissue, which is determined by the tissue type at the given axial depth, z.

In the radio frequency formulation of the source term, a one-dimensional finite-difference time-domain (FDTD) method was used to predict the SAR within single and multi-layer skin slab models. The FDTD method is an explicit time-domain numerical approach for solving Maxwell's equations in a discretized space (Yee, 1966; Taflove & Hagness, 2000). This method has become widely used for predicting the electromagnetic fields and energy absorption rates within digital voxelized models. Equations (11-12) below give the FDTD update equations for the electric field (E_x) in the x direction and the magnetic field (H_y) in the y direction, respectively.

$$E_x\Big|_k^{n+\frac{1}{2}} = \left[\frac{1-\frac{\sigma_k \Delta t}{2\epsilon_k}}{1+\frac{\sigma_k \Delta t}{2\epsilon_k}}\right] E_x\Big|_k^{n-\frac{1}{2}} + \left[\frac{\frac{\Delta t}{\epsilon_k}}{1+\frac{\sigma_k \Delta t}{2\epsilon_k}}\right]\left[\frac{H_y\big|_{k-\frac{1}{2}}^n - H_y\big|_{k+\frac{1}{2}}^n}{\Delta z}\right].$$ (11)

362

$$H_y\big|_k^{n+1} = \left[\frac{1-\frac{\sigma_k^*\Delta t}{2\mu_k}}{1+\frac{\sigma_k^*\Delta t}{2\mu_k}}\right] H_x\big|_k^n + \left[\frac{\frac{\Delta t}{\mu_k}}{1+\frac{\sigma_k^*\Delta t}{2\mu_k}}\right]\left[\frac{E_x\big|_{k-\frac{1}{2}}^{n+\frac{1}{2}}-E_x\big|_{k+\frac{1}{2}}^{n+\frac{1}{2}}}{\Delta z}\right]. \tag{12}$$

In Equations (11-12), σ is the conductivity in Siemens per meter, μ is the permeability in henrys per meter, and σ^* is the magnetic loss term in ohms per meter. Assuming zero magnetic loss, the localized SAR values within the tissue were calculated by Equation (13). The index k represents the discretized axial coordinate, $z = k\Delta z$, and n indicates the time step, $t = n\Delta t$. The SAR value is subsequently defined from the electric field strength and the density of the tissue, as given by Equation (13).

$$SAR = \frac{\sigma|E|^2}{\rho}. \tag{13}$$

In Equation (13), ρ is the density, and $|E|^2$ is the root-mean-square of the electric field. The 1-D SAR was mapped to a 2-D spatial function (Gaussian or top-hat) proportional to the incident irradiance distribution for cases when the 2-D heat transfer model was employed.

13.2.4 Boundary Conditions

Surface boundary conditions were addressed by Equation (14). A negative z-axis outward surface normal is assumed. The rate at which energy is lost through the surface composed of three effects. The first term on the right hand side of Equation (14) represents the convective loss rate from a dry skin surface due to convective heat transfer. The convective loss is proportional to the difference in ambient temperature and the tissue's surface temperature. The value h_e represents the convective heat transfer coefficient [$W\ cm^{-2}$], and v_e represents the ambient temperature relative to the tissue baseline or core body temperature. The second term represents the radiative loss from the surface, proportional to the difference in temperatures to the fourth power. Here, σ_s is the Stefan-Boltzmann constant, ϵ_σ is the emissivity of the tissue, and θ and θ_e are the absolute surface temperature and ambient temperature [Kelvin], respectively. The third term provides an energy loss rate from evaporation, and is defined in Equation (15).

$$k\frac{\partial v}{\partial z}\big|_{z_{min}} = h_e(v-v_e) + \sigma_s\epsilon_\sigma(\theta^4-\theta_e^4) + Q_{vap}. \tag{14}$$

Equation (14) is important to the correct prediction of surface temperatures within the skin for strongly absorbed wavelengths. Equation (15) follows the approach of Torres et al. (1993) providing a mathematical approximation to the surface energy loss rate due to evaporative effects. The approach is based upon the heat and mass transfer boundary layer analogy for evaporative cooling. This provides a method by which the surface temperature behavior can be mapped to ambient temperature, and ambient relative

humidity. In the numerical simulation, the second term in the right-hand side of Equation (14) is made linear in temperature through a simple Taylor series approximation (Ozisik, 1994).

$$Q_{vap} = h_{fg}h_m[\rho_{sat}(T_s) - \rho_\infty] \ .$$

(15)

In Equation (15), Q_{vap} is the vaporization loss term $[W\ cm^{-2}]$, $\rho_{sat}(T_s)$ is the mass density of saturated water vapor $[g\ cm^{-3}]$ at the temperature of the tissue surface, ρ is the density of water vapor in the the air $[g\ cm^{-3}]$ at the ambient temperature T_e, h_{fg} is the phase-change enthalpy $[J\ g^{-1}]$ of water at the temperature of the tissue surface, and h_m is the convection mass transfer coefficient $[cm\ s^{-1}]$. These coefficients are given by Torres et al. (1993), and derived from citations therein, expressed by Equations (16) and (17) with the air temperature, T_e, expressed in degrees Celsius (Chen et al., 2006). In the equations below, the various numerical coefficients have units which produce terms of $[cm\ s^{-1}]$.

$$h_m = \frac{h_e}{\rho_a c_a L_e^{2/3}} \approx h_e\ (T_e \cdot 1 \times 10^{-4} + 9 \times 10^{-3}) \ .$$

(16)

$$\rho_{sat}(T) \approx T^4 \cdot 4 \times 10^{-11} - T^3 \cdot 6 \times 10^{-10}$$
$$+ T^2 \cdot 1.96 \times 10^{-9} + T \cdot 1.534 \times 10^{-8} + 6.1098 \times 10^{-7} \ .$$

(17)

Other boundary conditions include an insulating boundary at the maximum radial coordinate, established within the computational space at a distance at which no significant terahertz-source energy is transferred. In addition, the assumption that the first derivative of the temperature, with respect to the radial coordinate, approaches zero at $r = 0$, is employed. The maximum axial coordinate (z_{max}) is held to a constant initial baseline temperature of the tissue (i.e., body temperature), selected at a depth where no significant source energy is transferred during the simulation.

One important aspect of this surface boundary condition is that without a source term, $A(z,\ r,\ t) = 0$, a tissue construct initialized to a uniform temperature will develop a thermal gradient for most common ambient conditions. For example, a tissue construct with a core temperature of 37 ºC placed in contact with room temperature (20 ºC) air, will cool at the surface. This implies that one must first run the numerical model to thermal equilibrium to accurately represent the skin surface, or provide a steady-state, time independent solution. These conditions were examined for the effects on tissue response and predicted damage thresholds (Clark et al., 2007). As a consequence, the heat transfer model was employed with an equilibrium state prior to simulating an exposure to the terahertz beam.

13.2.5 Damage Models

The potential for the thermal response of skin tissue was evaluated under the assumption of a single rate process model for damage. A common model in thermal damage studies, the activation energy and rate for tissue damage through protein denaturation, is measured experimentally. Measured or predicted thermal response, or time-temperature history of the tissue, is linked to the thermal damage rate-process and assigned a probability of causing tissue damage. Damage to the tissue is evaluated through an Arrhenius damage integral given by Equation (18).

$$\Omega(z, r) = C \int_{1_1}^{t_2} exp(\frac{-E_a}{RT(t)}) \, dt \, . \tag{18}$$

In Equation (18), R is the universal gas constant, T represents the absolute temperature of a given coordinate at a given time, $T(z, r, t)$, and t_1 and t_2 represent the initial and final simulation times used in the solution of Equation (9). The variable C is a normalizing constant (sec^{-1}) and E_a the activation energy for a reactive process ($J \, Mole^{-1}$). Values for C and E_a exist in the literature and are based upon differing assumptions about tissue types and geometry. Because of this, damage threshold parameters ($C = 3.1 \times 10^{98} s^{-1}, E_a = 6.28 \times 10^5 J \, Mole^{-1}$) consistent with the models documented in the literature (Welch & van Gemert, 1995) were selected. This provides a self-consistent result which can be compared to previous modeling studies which have been experimentally validated (Chen et al., 2005). Values of this damage integral approaching $\Omega = 1$, indicate irreversible thermal damage to the tissue at a given location for our study, and are commonly referenced as second-degree burns (Takata et al., 1977).

13.3 Results and Discussion

In order to estimate a threshold for injury for exposures of the skin to terahertz exposures, a number of parameters were examined to determine their effect on predictions of thermal response. The time-temperature response dictates the predicted injury threshold, and is a parameter which can be measured experimentally at the tissue surface or within the tissue. In addition, a comparison was made of both optical and radio frequency representations of source terms for the models.

13.3.1 Energy Deposition Rates

A central axial distribution of the SAR values used in the radio frequency implementation for a two-layer skin model and a uniform water slab is shown in Figure 13-2. The increased absorption rate of energy near the interface of the epidermis and dermis is clearly marked. A larger absorption rate is seen near the surface, assuming an extrapolated water value, but with a lower absorption rate deeper in the tissues. As the terahertz frequencies are strongly absorbed by the surface, it is anticipated that the water approximation would produce larger surface temperature increases for comparable

irradiance levels and, as a result, lower damage thresholds. Also shown in the figure is the linear absorption model source term, expressed in $W\ cm^{-3}$. The trends are quite similar, although the common units of each representation (i.e., SAR incorporates density) cause a slight variation in the trends.
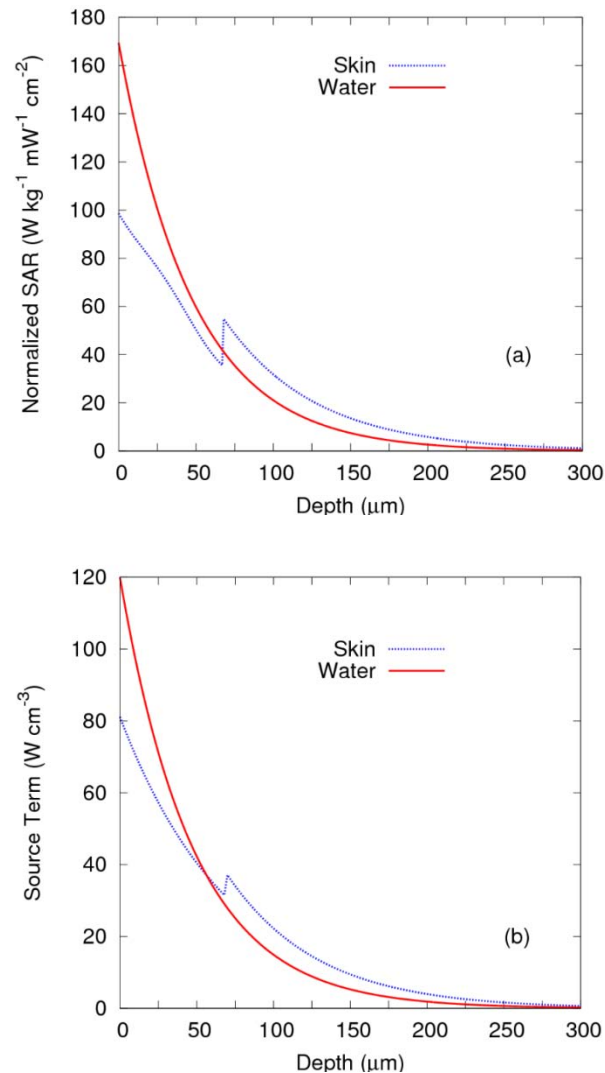
Figure 13-2. Axial distribution of the source term (a) Normalized SAR (b) Linear Absorption, for two-layer skin model and water for a 1-Wcm^{-2}, 1-THz exposure along $r = 0$.

Figure 13-3 provides a direct comparison of the 2-D distributions of source terms for the two representations. The top panel shows a 1-THz frequency SAR model energy deposition rate for the baseline two-layer skin model. Here the beam is a Gaussian distribution, 1-cm (at e^{-1}) diameter, 1-W beam. The panel at the bottom shows the same rate for the linear absorption case. The radio frequency and optical representations agree fairly well, with a slightly larger source term in the epidermis layer. The radio frequency

representation includes the contributions of reflections at the epidermis-dermis interface. This is due to the fact that the FDTD method is bi-directional, while internal surface reflections were ignored for the optical model.
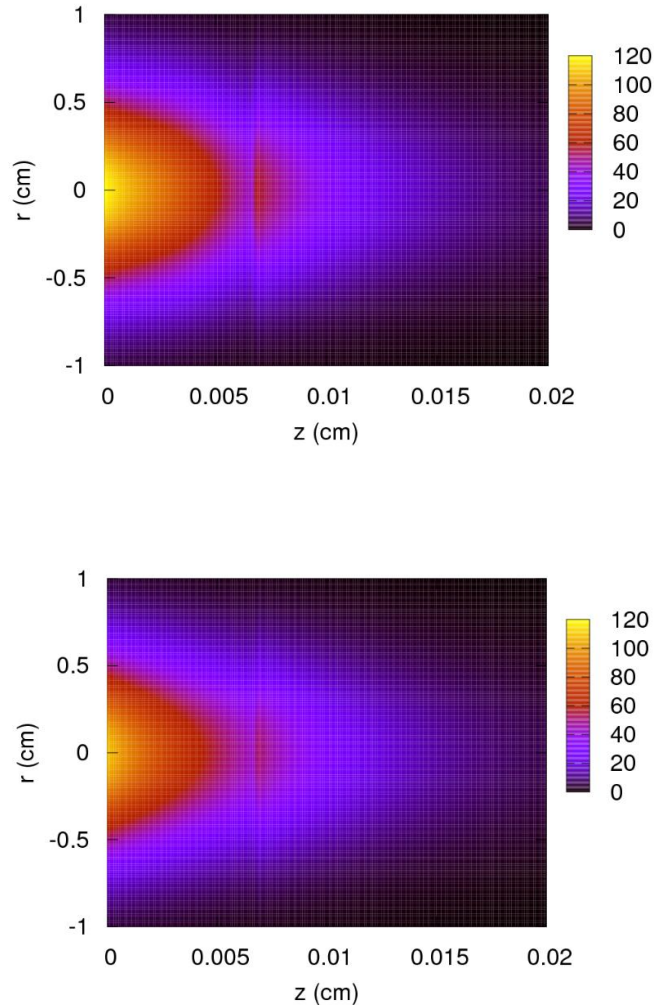
Figure 13-3. (top) Two layer source term from radio frequency FDTD-SAR [Wcm⁻³]. (bottom) Two-layer source term from linear absorption model.

13.3.2 Thermal Response

The thermal response of tissues was determined for a number of exposure time, beam diameter, irradiance magnitude, and surface boundary conditions. The parameter space represents a large number of permutations. Therefore, it was decided to closely examine a nominal exposure condition of a 1-THz frequency, Gaussian spatial distribution (measured at e^{-1} irradiance) with varying diameter and ten-second exposure duration. A baseline configuration with a core tissue temperature of 37 ºC and an ambient

367

air temperature of 20 ºC at fifty percent relative humidity was selected. From this nominal condition, variations of single parameters were examined.

Figure 13-4 demonstrates a typical surface temperature within a two-layer skin simulation as a function of time during a 10-second, 1-THz exposure, with the peak Gaussian beam irradiance set to a constant $2\,W\,cm^{-2}$ for each curve. The temperature rise at the tissue surface reaches its maximum value much more quickly for the smaller beam diameters, as the effects of radial thermal diffusion contribute more significantly. Beyond diameters of about one centimeter, little difference is seen in the thermal behavior. The limiting one-dimensional, or infinite extent, model result is also shown to illustrate that the thermal response asymptotically approaches a maximal temperature rise. This also illustrates the good agreement between separate model implementations (1-D vs. 2-D) for validation purposes. As the bio-heat equation is a linear differential equation to a first approximation (boundary losses are non-linear), it can be inferred that the same plateau, as a function of beam size, will occur for other irradiance values greater than the surface energy loss rate.
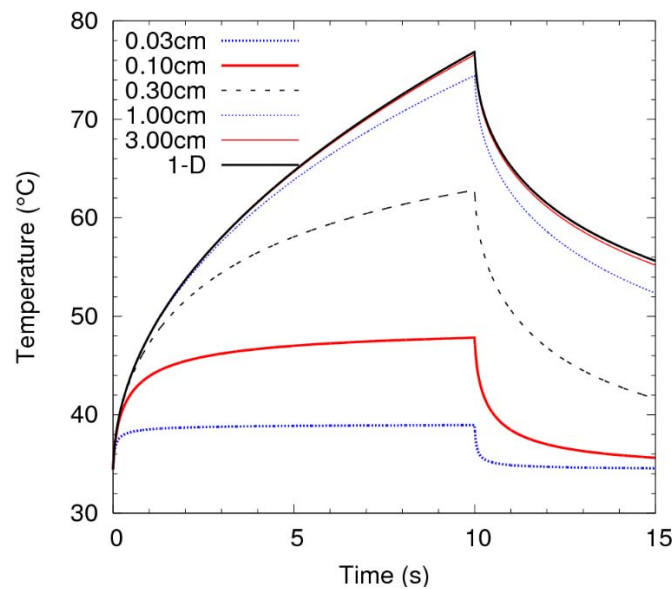
Figure 13-4. Thermal response of the skin surface as a function of time for a 2-W *cm*⁻², 1-THz, 10-sec exposure for the two-dimensional linear absorption model.

The cooling time is also relatively short as the terahertz pulse is turned off, with the tissue surface returning to within approximately one-half the initial surface temperature rise after about 500 *ms* for small beams, and more slowly (over about 5 *s*) for the large-beam (1-D) limit. For these simulations, both the optical and radio frequency approach were compared. Results were in agreement to within about five percent in total temperature shift, with maximum temperature values agreeing to within about 1.0 ºC.

Initial and boundary condition effects are demonstrated by Figures 13-5 and 13-6. Figure 13-5 illustrates a typical equilibrium condition, demonstrating the axial

temperature distribution at equilibrium for the case of $h_e = 1.5 \times 10^{-3} W\ cm^{-2}$ (Takata et al., 1977) and a perfusion rate (Welch & van Gemert, 1995) of $3.0 \times 10^{-3} g\ cm^{-3} s^{-1}$ within the dermis layer, and no radiative or evaporative effects. The resultant temperature difference at the surface is approximately 2.4 ºC. This gradient is consistent with measured values and numerical estimates found elsewhere in a more detailed examination (Clark et al., 2007).

The boundary condition effect on thermal response of the tissue surface is demonstrated in Figure 13-6. Calculations in the variation of thermal response for conditions of $1 W\ cm^{-2}$ and $2 W\ cm^{-2}$ show that ambient temperature effect on response over the first ten seconds of exposure is minimal. The ambient temperature shift of more than twenty degrees results in less than one degree difference in the tissue maximum temperature response.
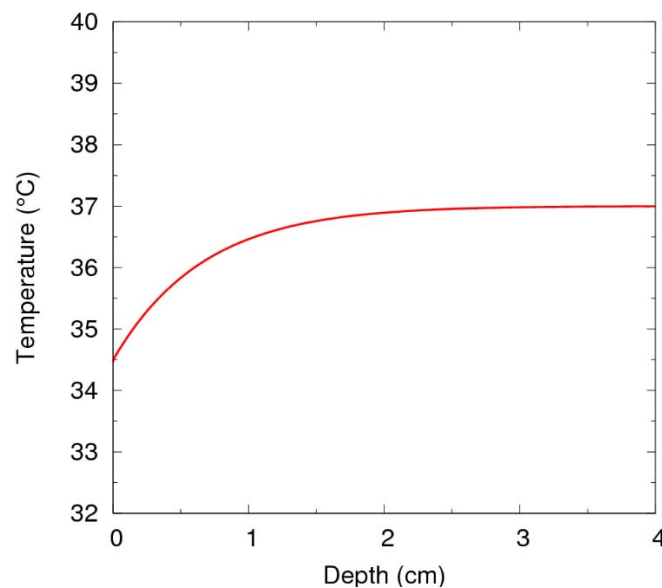
Figure 13-5. Initial axial temperature distribution within a tissue simulation.

369
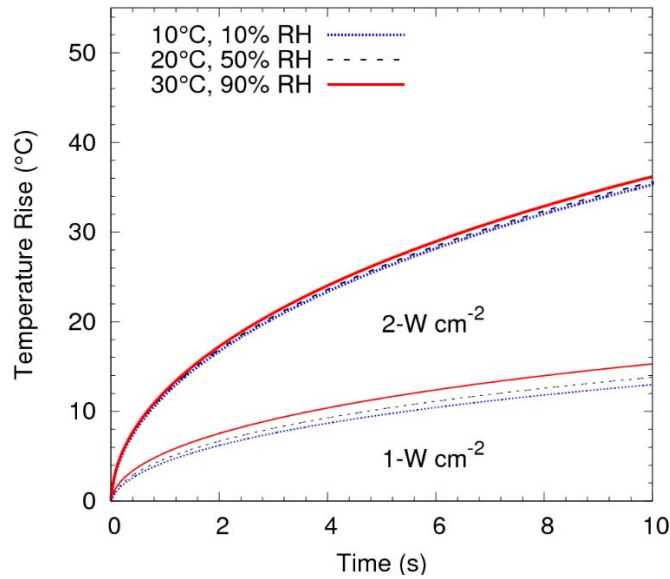
Figure 13-6. Effect of ambient temperature on maximum surface temperature.

13.3.3 Injury Thresholds

The finite-difference, heat transfer model, coupled to a linear absorption or FDTD-SAR source term, includes an option to search through source power and estimate a threshold for damage. As an initial estimate of damage thresholds for a terahertz-frequency source, a convergence criterion of about five percent in damage integral value was the exit criteria for the search. As the threshold was estimated, approximate damage depth was recorded along with the peak temperature rise achieved during the simulation of temperature response to a given frequency and exposure time.

Figure 13-7 summarizes the estimated damage thresholds for both a 1-D model as well as a 2-D model for a $2 - cm$ Gaussian beam diameter (e^{-1}), 1-THz frequency exposure. Estimates were made for a threshold criterion of $\Omega = 1$ at any point within the tissue. The figure demonstrates the effect of increasing exposure duration over the range of one microsecond to ten seconds. The damage trends roughly reflect the exposure limit trends of the ANSI Z136.1-2000 Standard (American National Standards Institute, 2000) for a 1-mm wavelength (0.3-THz frequency) condition, the upper wavelength limit of this standard. The exposure limit is shown as the dashed line in the figure. Panel (a) of the figure shows damage thresholds and exposure limits as a function of irradiance. Panel (b) of the figure illustrates damage thresholds relative to the exposure limit in terms of radiant exposure [$J\ cm^{-2}$]. The figure illustrates the constant-fluence thermal damage threshold plateau from one microsecond to approximately one millisecond. In Figure 13-7, the damage thresholds remain above the exposure limit across all exposure times. At the shortest exposure durations, the thermal damage threshold is separated from the exposure limit by a factor of more than fifty. At longer durations, beyond about 100 *ms*, the 1-D prediction diverges from the 2-D model, depending upon the beam diameter. Larger exposures are required in this region to compensate for the radial loss and to

370

achieve sufficient temperature to induce damage. Calculations performed also demonstrated the effect of including a range of evaporative and radiative boundary conditions in the estimation of the damage threshold. The calculation shows that the evaporative boundary effect plays a significant role only above about one second. At ten seconds exposure, for example, the predicted damage threshold is increased by a factor of only about ten to twenty percent, due to the additional energy loss with evaporative cooling. Here, additional energy is required to produce the same temperature rise, and therefore an injury.
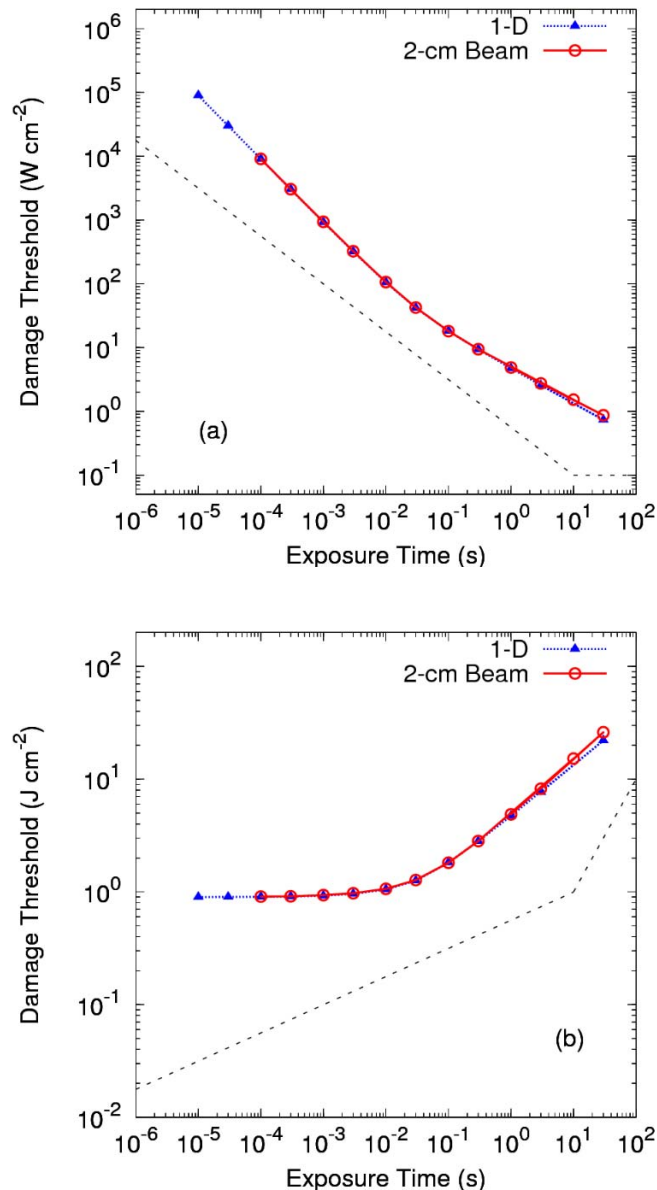
Figure 13-7. Summary of computed damage thresholds as a function of exposure time for one-dimensional simulations and a 2-D simulation of 2-cm beam diameter (Gaussian distribution), 1-THz exposures. Panel (a) shows the threshold as irradiance (W *cm*^-2) and (b) shows the same results as radiant exposure (J *cm*^-2).

371
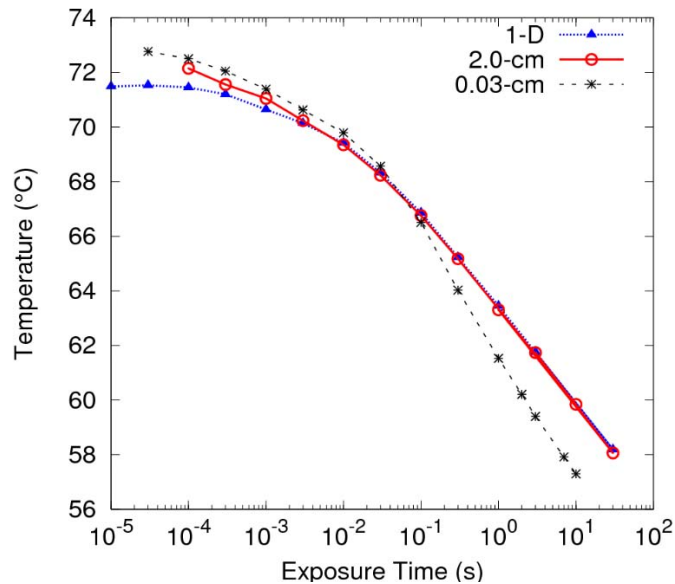
Figure 13-8. Summary of computed temperature rise at the damage threshold for a number of beam diameter values (Gaussian distribution), 1-THz exposures.

Temperature response of tissue at the damage threshold was recorded for all calculations. The results are shown in Figure 13-8. The figure depicts the maximum temperature achieved during exposure for each time shown in Figure 13-7. At short pulse durations, the temperature increase required to injure the tissue is estimated to be near 35 ºC or approximately 72 ºC in absolute temperature. The temperature required for damage decreases as exposure duration increases to approximately one second of exposure, where the temperature increase needed for damage is approximately 21 ºC or a net tissue temperature of 58 ºC. As the damage threshold irradiance is larger for the small beam, it was anticipated that the temperature increase would occur earlier in the pulse, as shown in Figure 13-9, providing a balancing area for the damage integral, and counteracting radial diffusion losses.

The damage threshold as a function of beam diameter is illustrated in Figure 13-10. For strongly absorbed wavelengths (frequencies), a weak dependence on beam diameter is expected for short exposure durations. For long exposures, where heat transport is significant, an increase in threshold is anticipated. The figure illustrates that below about 10-ms exposure, a differing threshold can be seen in the calculation. Beyond this exposure time the threshold increases for smaller beam diameters, and for the range considered (0.03 cm to 3.00 cm), varies by a factor of one order of magnitude at the longest exposure time. The 1-D limit is approached for exposures of up to 10-s duration for beam diameters as small as 0.3 cm.

372
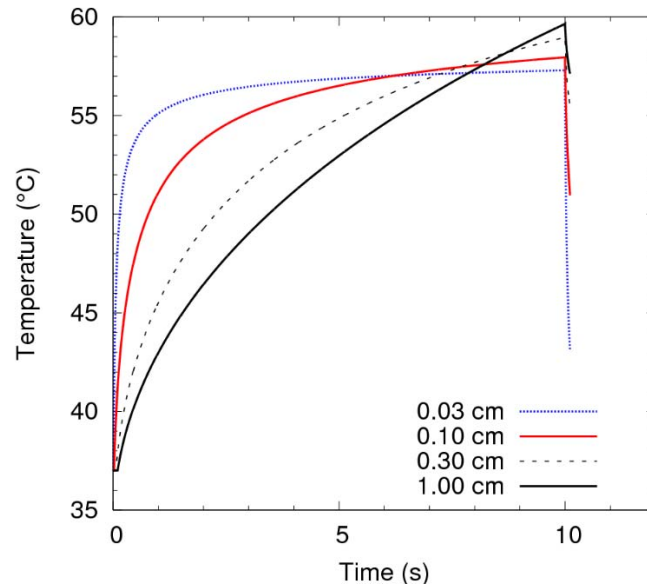
Figure 13-9. Thermal response of the skin surface as a function of time at the computed damage threshold for 1-THz, 10-sec exposures for the two-dimensional linear absorption model.
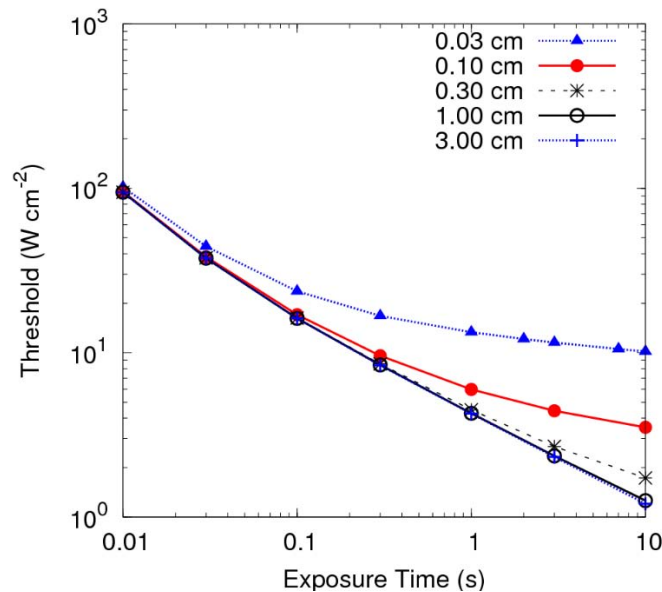
Figure 13-10. Beam diameter (Gaussian e⁻¹ irradiance point) dependence of damage threshold for differing exposure durations at 1 THz.

Figure 13-11 demonstrates the effect of various frequencies in the range of 0.2 to 2.0 THz, for a 0.1, 1.0 and 10-s exposure for large beams. The simulations were run using the two-layer skin model, extrapolating linear absorption properties of the tissue using the Pickwell et al. (2005; 2004) data found in Table 13-1. Although there is a significant

373

change in absorption properties over this range, there is only a very weak dependence of damage threshold on frequency. This is due to the fact that axial thermal diffusion takes place quickly over the scale of the absorption, making the thermal penetration depth large compared with the absorption coefficient. The thermal penetration depth, $z_{therm}[cm]$, can be estimated (Niemz, 2004) for any exposure duration from Equation 19, and is compared with the absorption coefficient over the frequency range of 0.1 to 2.0 THz. See also Figure 13-12.

$$z_{therm}(t) = \sqrt{4t \frac{k}{\rho c_p}} \ . \tag{19}$$

$$\tau_r = \frac{\rho c_p}{4k\mu_a^2} . \tag{20}$$

A thermal relaxation time, $\tau_r[sec]$, can then be computed (Niemz, 2004) according to Equation (20). For example, for a 200-cm^{-1} absorption coefficient and using the thermodynamic properties of water, thermal relaxation will take place over a time scale of about 250 μs (see also Figure 13-12). Therefore, the damage threshold remains nearly a constant function of frequency in the terahertz frequency range for exposure durations of greater than this thermal diffusion time. Furthermore, the damage threshold should become nearly a constant in terms of the fluence [$J\ cm^{-2}$] delivered to the surface for times much shorter than this thermal diffusion time. This is indeed reflected in Figure 13-7, where the log-log plot presented in panel (b) shows a nearly constant value below 1-ms exposure duration.
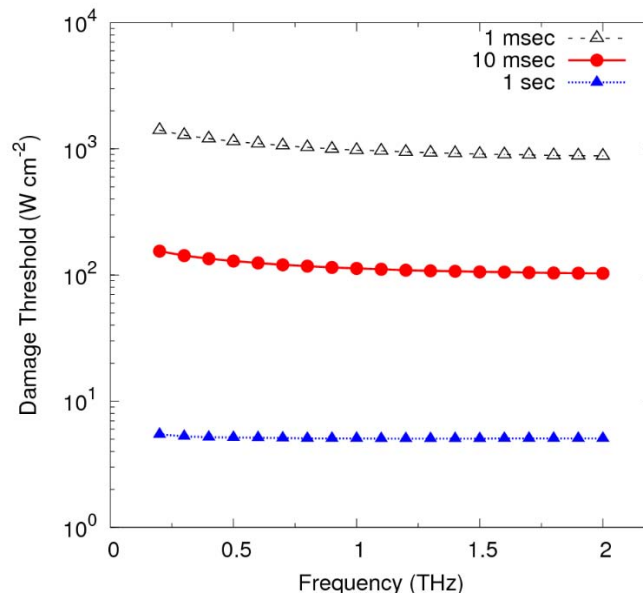
Figure 13-11. Frequency dependence of damage thresholds for three differing exposure times for the 1-D linear absorption model.
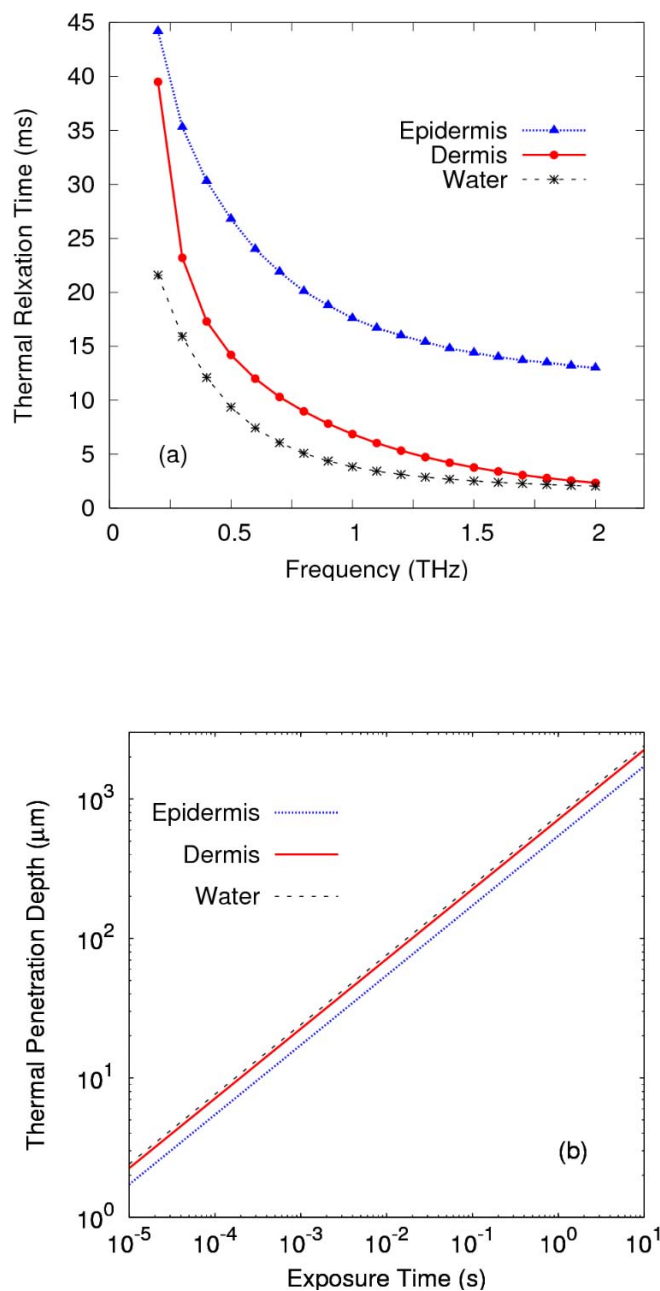
Figure 13-12. (a) Thermal relaxation times and (b) thermal penetration depth of skin tissues and water.

13.3.4 Experimental Comparison

Although no experimental data currently establish terahertz-frequency damage thresholds for the skin, a number of studies exist using strongly absorbed optical frequencies (Chen et al., 2005; Brownell et al., 1968; Brownell et al., 1969; Brownell et al., 1971; Brownell & Stuck, 1972; Rockwell & Goldman, 1974; Bostick et al., 2005).

375

These studies span the range of absorption coefficients of interest and should compare for exposure times greater than the corresponding thermal confinement time. The literature available for comparison includes a number of carbon dioxide laser exposure conditions conducted by Brownell and Rockwell, a few holmium laser exposure conditions recently characterized by Chen, and a single, pulsed-laser data point at deuterium-fluoride (multiple) wavelengths.

The experimental data largely consist of points which can be characterized as large-beam exposures, near the 1-D limit presented here. Figure 13-13 shows the experimental data superimposed with model calculations for a 1-THz frequency beam. Table 13-3 provides additional experimental details regarding beam diameter, profile, exposure time, and lesion characterization. The experimental data compare favorably, and agree to within about fifty percent of the predicted threshold fluence, despite the widely varying wavelength and skin types. From the Brownell data, it is seen that the prediction is bracketed by the measured erythemia threshold and the threshold for immediate whitening of the skin, characteristic of a third-degree burn. The largest discrepancy occurs for the deuterium-fluoride short-pulse system, which disagrees by a factor of about three. A careful examination of the literature shows that this beam was highly non-uniform and perhaps subject to an overprediction of the irradiance present.
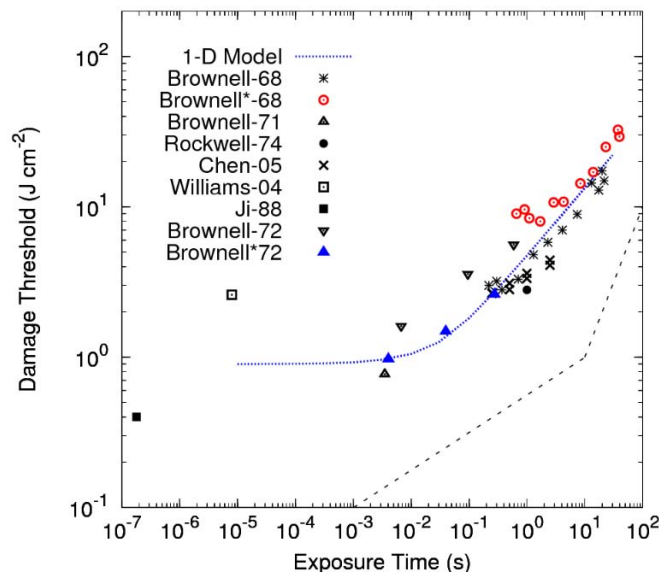
Figure 13-13. A comparison of 1-THz damage threshold estimates to experimental data from other strongly absorbed wavelengths. Citations marked with an asterisk indicate blistering threshold endpoints. The dashed line in the lower right is the applicable ANSI Z136.1-2000 exposure limit.

376

Table 13-3. A summary of historical experimental data for comparison to THz damage models.

Reference	Wave-length [μm]	μ_a [cm^{-1}]	Beam Dia. [cm]	Exp Time [s]	Damage Threshold [$J\ cm^{-2}$]	End-Point
(Brownell et al., 1969)	10.6	260	1.9	0.22	3.0	Erythema
(Brownell et al., 1969)	10.6	260	1.9	0.30	3.2	Erythema
(Brownell et al., 1969)	10.6	260	1.9	0.37	2.8	Erythema
(Brownell et al., 1969)	10.6	260	1.9	0.71	3.3	Erythema
(Brownell et al., 1969)	10.6	260	1.9	1.3	4.8	Erythema
(Brownell et al., 1969)	10.6	260	1.9	2.3	5.8	Erythema
(Brownell et al., 1969)	10.6	260	1.9	4.1	7.0	Erythema
(Brownell et al., 1969)	10.6	260	1.9	7.4	8.9	Erythema
(Brownell et al., 1969)	10.6	260	1.4	13.1	14.4	Erythema
(Brownell et al., 1969)	10.6	260	1.4	17.4	12.9	Erythema
(Brownell et al., 1969)	10.6	260	1.4	19.9	17.3	Erythema
(Brownell et al., 1969)	10.6	260	1.4	21.6	14.9	Erythema
(Brownell et al., 1969)	10.6	260	1.9	0.66	9.0	White Burn
(Brownell et al., 1969)	10.6	260	1.9	0.91	9.6	White Burn
(Brownell et al., 1969)	10.6	260	1.9	1.1	8.4	White Burn
(Brownell et al., 1969)	10.6	260	1.9	1.7	8.0	White Burn
(Brownell et al., 1969)	10.6	260	1.9	2.9	10.7	White Burn
(Brownell et al., 1969)	10.6	260	1.9	4.3	10.8	White Burn
(Brownell et al., 1969)	10.6	260	1.4	8.4	14.3	White Burn
(Brownell et al., 1969)	10.6	260	1.4	14.0	17.0	White Burn
(Brownell et al., 1969)	10.6	260	1.4	23.0	25.0	White Burn
(Brownell et al., 1969)	10.6	260	1.4	37.4	32.5	White Burn
(Brownell et al., 1969)	10.6	260	1.4	39.6	29.3	White Burn
(Brownell et al., 1971	10.6	260	2.0	3.5×10^{-3}	0.77	Erythema
(Brownell & Stuck, 1972)	10.6	260	1.26	590×10^{-3}	5.60	Blister
(Brownell & Stuck, 1972)	10.6	260	1.33	95.4×10^{-3}	3.57	Blister
(Brownell & Stuck, 1972)	10.6	260	0.80	6.71×10^{-3}	1.61	Blister
(Brownell & Stuck, 1972)	10.6	260	1.26	275×10^{-3}	5.60	Erythema
(Brownell & Stuck, 1972)	10.6	260	1.33	39.6×10^{-3}	3.57	Erythema
(Brownell & Stuck, 1972)	10.6	260	0.80	4.05×10^{-3}	1.61	Erythema
(Rockwell & Goldman, 1974)	10.6	260	1.0	1.0	2.8	Erythema
(Chen et al., 2005)	2.0	20-60	1.1	0.25	2.65	Erythema
(Chen et al., 2005)	2.0	20-60	1.1	0.5	3.10	Erythema
(Chen et al., 2005)	2.0	20-60	1.1	1.0	3.61	Erythema
(Chen et al., 2005)	2.0	20-60	1.1	2.5	4.42	Erythema
(Chen et al., 2005)	2.0	20-60	1.4	0.25	2.67	Erythema
(Chen et al., 2005)	2.0	20-60	1.4	0.5	2.81	Erythema
(Chen et al., 2005)	2.0	20-60	1.4	1.0	3.34	Erythema
(Chen et al., 2005)	2.0	20-60	1.4	2.5	4.09	Erythema
(Ji & Liangshun, 1988)	10.6	260	1.0	180×10^{-9}	0.40	Erythema
(Bostick et al., 2005)	3.8	37	2.0	8.0×10^{-6}	2.6	Erythema

13.3.5 Exposure Limits

The results here can be considered with regard to currently accepted exposure limits for both radio frequency and optical radiation. Figure 13-14 provides a comparison of radio frequency (IEEE, 2005) and laser (American National Standards Institute, 2000) exposure limits near the bounding 1-mm (300 GHz) wavelength (frequency).

For the optical wavelength region of 2.6 μm to 1.0 mm, the ANSI Z136.1-2000 Standard dictates a time-varying exposure limit of 0.56 $t^{-3/4} W\ cm^{-2}$ for exposure times of 1.0 $\times$ 10^{-7} seconds to 10 seconds, and a constant irradiance of 0.1$W\ cm^{-2}$ for exposure times greater than 10 seconds. These exposure limits are for peak exposures integrated and averaged over an 11-mm diameter limiting aperture. For large beam exposures exceeding 10 seconds in duration, where the cross-sectional area of the exposed region is 100 cm^2 to 1000 cm^2, the exposure limit scales downward with area, to account for thermo-regulatory stress, and is given as 10$A_s W\ cm^{-2}$, where A_s is the area in cm^2. For large-beam exposures exceeding 10 seconds, where the cross-sectional area exceeds 1000 cm^2, the exposure limit is 0.01 $W\ cm^{-2}$. The impact of this scaling is illustrated as a rectangular box in the lower right of Figure 13-14, showing the region of lowered exposure limits for large beam, long-term exposures. Although the long-term, 1-D damage threshold approaches the ANSI Z136.1 long exposure-duration limit shown in Figure 13-7, this 1-D assumption also implies a large beam exposure area, for which the lower region of exposure limit provides compensation. As was shown in Figure 13-10, the damage threshold is larger as beam diameter decreases for longer exposure times.

Radio frequency exposure limits can be determined from the IEEE C95.1-1995 Standard (IEEE, 2005). This standard begins with 300 GHz at its upper bound and addresses lower frequencies. For frequency bands up to 300 GHz, the exposure limit values for the general public are given as $[(90f_G-7000)/200]W\ m^{-2}$, where f_G is a frequency in GHz. The averaging time is $(5048/[(9f_G - 700)f_G^{(-0.476)}])$ minutes for this exposure limit. In controlled environments, as defined by the standard, the exposure limit in the range of 30-300 GHz is 100 $W\ m^{-2}$, with an averaging time of $2.524/f_G^{0.476}$ minutes. These restrictions have been adopted in order to protect against tissue heating effects in these frequency ranges.

For the purpose of comparing to laser standards at frequencies above 300 GHz, the extrapolated values for the THz region are provided in Figure 13-14, assuming that the same trends hold, including expressions for averaging times. As an example, the exposure limit values for 300-GHz to 2-THz exposure are illustrated as the three dashed lines in Figure 13-14. The lines are in increasing frequency order for the figure, with 2-THz having the lowest extrapolated exposure limit. Although the C95.1-1995 Standard does not specifically extend to this optical region of the spectrum, it is of interest to see how similar exposure limits might be extended. The figure does not illustrate the ―Controlled Environment,‖ where personnel are trained in the establishment of a safety program and are aware of the risks. Shown is the ―General Public‖ condition where persons exposed have no knowledge or control of their exposure. The General Public

378

values are the least restrictive, and were therefore selected for discussion here. We note that a discrepancy is introduced, resulting in an increased exposure limit, due to the fact that we are extrapolating beyond 300 GHz. The C95.1-1995 expressions for averaging time are being defined by frequency, and perhaps would require revision above 300 GHz such that the General Public margin of safety would be maintained.

At short exposure times, it is also seen that the ANSI Z136.1-2000 exposure limit trend diverges from the predicted damage threshold curve, but the C95.1-1995 trends mimic the slope of these estimated damage thresholds. The damage threshold behavior is more accurately represented by the constant radiant exposure value of approximately 0.1 $J\ cm^{-2}$ below about 1 ms, and therefore mimics the C95.1-1995 Standard. The predicted temperature rise at threshold does not exceed the boiling point of water at room temperature and pressure, and therefore should not require an additional examination of ablative or other mechanisms to explain damage threshold trends. Therefore, it may be safe to assume that short-pulse ($<1\ ms$) THz exposure limits, as derived from the Z136.1-2000 Standard, might be relaxed to follow those of the C95.1-1995 Standard. This relaxation would provide the commonly accepted factor of ten between damage threshold and exposure limit.

It is of interest to note comparisons in the case of the General Public exposure definition, where the radio frequency standard is applied to those with no knowledge of the exposure such as in the work environment. Here, an assumed extrapolation increases the permitted exposures for durations greater than a few hundred milliseconds, with a 2-THz exposure of about 0.1 $W\ cm^{-2}$ permitted. This extrapolation and relaxation would therefore contradict the laser exposure limit, which is more restrictive for long-term, large-beam exposures, prescribing only 0.01 $W\ cm^{-2}$ as an exposure limit for these cases.

Also of interest is the fact that radio frequency exposure limits have historically been based upon a psychophysical assessment of perception thresholds. With respect to this philosophy, warmth detection thresholds and discomfort elicitation thresholds may be estimated in the THz region. These can then be compared to exposure limits from both the C95.1-1995 and Z136.1-2000 Standards. Warmth detection thresholds in the radio frequency range have been shown to vary with respect to frequency (Blick et al., 1997). However, thermal modeling analysis of these empirical data has shown that warmth detection occurs at a temperature rise of 0.07 ºC at or near the skin's surface, irrespective of incident frequency (Riu et al., 1996). This has been validated for exposures of a few seconds. Additionally, heating of the skin to 43-46 ºC has been shown to evoke discomfort for rapid heating and slow heating, respectively (IEEE, 2005). More specifically, a threshold of 45 ºC has been observed for evoking ―pin-prick" sensation during a brief ($3-10\ sec$) thermal stimulus (Hardy et al., 1952).

These warmth detection and discomfort threshold temperatures have been used in order to predict the power densities required to elicit these responses in the terahertz region. The damage, discomfort (at 44 ºC) and warmth detection thresholds at 1 THz are also illustrated in Figure 13-14 for comparison to exposure limits. Again, the values for the General Public, as given at 300 GHz, are extrapolated to 1 THz. For all exposure

379

durations up to 10 s, the C95.1-1995 Standard is adequate to prevent uncomfortable stimulations, but may not guard against the thermal detection of energy in the terahertz region.
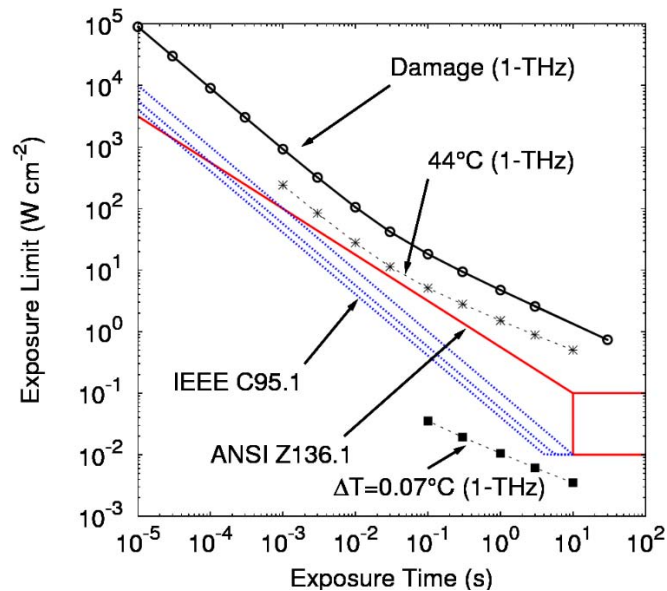
Figure 13-14. A comparison of various thresholds and exposure limits for frequencies near 1 THz (see text).

13.4 Conclusions

The modeling presented here provides an initial insight into injury thresholds from terahertz-frequency electromagnetic radiation. The computation has taken the approach of establishing a nominal exposure condition, based upon initial applications in this frequency range. From this, one can see the sensitivity of the results to various parameters such as exposure duration, exposure area, electromagnetic frequency, and ambient conditions.

For a nominal one-second, continuous-wave exposure with a 2-cm beam diameter, the damage threshold for a second-degree burn to the skin is approximately $5\,W\,cm^{-2}$ for a 1-THz frequency. It is found that injury thresholds will vary only weakly as a function of frequency in the 0.1 to 10-THz range, due to the strong surface absorption effects on a scale less than the thermal diffusion length for exposures greater than a few hundred microseconds. This generalization argues for simple exposure limit definitions in the terahertz frequency range which are nearly constant for the region spanned by both laser and radio frequency exposure limits.

Damage threshold estimates for terahertz frequencies for large beams can be effectively determined by a 1-D heat transfer model with appropriate source term definition. Damage thresholds as a function of beam size are determined to be independent of beam diameter above about 2-3 cm. Below this diameter, damage

380

thresholds will vary abruptly with regard to beam irradiance. Threshold estimates (experimental or theoretical) based upon beams of less than about 1 cm will underpredict damage thresholds in terms of irradiance, as they will experience significant thermal diffusion effects sufficient to increase the damage threshold.

Other factors examined only weakly influenced the thermal response and damage threshold predictions. Ambient temperature makes only a small contribution to the thermal response, less than 0.2 ºC for each 10 ºC temperature shift within the range of 0-100 ºC. The thermal gradient at the surface of the tissue also contributes only a small influence to the threshold for injury. At 1.0-s exposure, the thermal gradient at the tissue surface is overcome in less than 0.1 seconds. Small corrections to damage thresholds at short exposure durations are therefore anticipated, as energy delivered within this time will be required to raise the temperature of the tissue by about 2-3 ºC, resulting in an increased damage threshold of at most about ten to fifteen percent (Clark et al., 2007) within the regime of thermal effects. This work has found that perfusion rates have a notable effect only at longer exposure durations beyond about ten seconds. At longer time scales it will be necessary to examine in more detail the thermo-regulatory response of the body as a whole.

Finally, it is concluded that extending the accepted exposure limit from the laser standards at 1-mm wavelength would result in sufficient safety factors to 0.2 THz. For short exposure times ($< 1 \times 10^{-3}$s), it may be possible to relax laser exposure limits to conform to radio frequency limit trends. For longer exposure times, it may also be possible to relax radio frequency exposure limits to follow the laser standard guidance. However, it is recommended that the community await confirming experimental evidence from the laboratories. These experiments can be guided by this theoretical work in terms of selection of relevant exposure conditions and examination of sensitivity to ambient or other conditions.

13.5 Acknowledgments

13.6 References

American National Standards Institute. (2000). Z136.1 American National Standard for Safe Use of Lasers. Laser Institute of America. Orlando, FL; ISBN 0-912035-65-X.

Barthel, J. & Buchner, R. (1991). High-frequency permittivity and its use in the investigation of solution properties. *Pure and Applied Chemistry*, *63*, 1473–1482.

Blick, D. W., Adair, E. R., Hurt, W. D., Sherry, C. J., Walter, T. J., & Merritt, J. H. (1997). Thresholds of microwave-evoked warmth sensations in human skin. *Bioelectromagnetics*, *18*, 403–409.

Bostick, A. C., Johnson, T. E., Randolph, D. Q., & Winston, G. C. (2005). Response of pigmented porcine skin (*Sus scrofa domestica)* to single 3.8 micron laser radiation pulses, *Photonic Therapeutics and Diagnostics*, *5686*, 668–673.

Brownell, A. & Stuck, B. (1972). Ocular and skin hazards from *CO*2 laser radiation. *Proceedings of the 1972 Army Science Conference*, 123–128, US Army.

Brownell, A. S., Hysell, D. K., & Parr, W. H. (1971). *Millisecond Exposure of Porcine Skin to Simulated CO2 Laser Radiation* (US Army Technical Report USAMRL 953). Fort Knox, KY: US Army Medical Research Laboratory.

Brownell, A. S., Parr, W. H., Hysell, D. K., & Dedrick, R. S. (1968). *CO2 Laser Induced Skin Lesions* (Final Report) (US Army Technical Report USAMRL RN 769). Fort Knox, KY: US Army Medical Research Laboratory.

Brownell, A. S., Parr, W.H., Hysell, D. K., & Dedrick, R. S. (1969). Skin and carbon dioxide laser radiation. *Archives of Environmental Health*, *18*, 437–442.

Carr, G. L., Martin, M. C., McKinney, W. R., Jordan, K., Neil, G. R., & Williams, G. P. (2002). Very high power THz radiation at Jefferson Lab. *Journal of Physics in Medicine and Biology*, *47*, 3761–3764.

Chen, B., O'Dell, D. C., Thomsen, S., Rockwell, B. A., & Welch, A. J. (2005). Porcine skin *ED*50 damage thresholds for 2,000 nm laser irradiation. *Lasers in Surgery and Medicine*, *37*, 373–381.

Chen, B., Thomsen, S., Thomas, R. J., & Welch, A. J. (2006). Modeling thermal damage in skin from 2000-nm laser irradiation. *Journal of Biomedical Optics, 11*(6), 064028.

Clark, C. D., Thomas, R. J., Maseberg, P. D. S., Buffington, G. D., Irvin, L. J., Stolarski, J., & Rockwell. B. A. (2007). Modeling of surface thermodynamics and damage thresholds in the IR and THz regime. *Optical Interactions with Tissues and Cells XVIII*, *643505*, 1–12, SPIE.

Dobroiu, A., Otani, C., & Kawase, K. (2006). Terahertz-wave sources and imaging applications. *Measurement Science and Technology, 17*, R161–R174.

Dragoman, D., & Dragoman, M. (2004). Terahertz fields and applications. *Progress in Quantum Electronics*, *28*, 1–66.

382

Fitzgerald, A. J., Berry, E., Zinovev, N. N., Walker, G. C., Smith, M. A., & Chamberlain, J. M. (2002). An introduction to medical imaging with coherent terahertz frequency radiation. *Physics in Medicine and Biology*, *47*, R67–R84.

Hardy, J., Wolff, H. G., & Goodel, H. (1952). *Pain Sensations and Reactions*. Baltimore, MD: Williams and Wilkins.

Institute of Electrical and Electronics Engineers, Inc. (IEEE). (2005). *Standard for Safety Levels with Respect to Human Exposure to Radio Frequency Electromagnetic Fields, 3-KHz to 300 GHz* (C95.1-2005). IEEE, New York.

International Electrotechnical Commisssion IEC. (2001). *60825-1 2001 Safety of Laser Products - Part 1: Equipment Classification, Requirements and User's Guide*. IEC, Geneva, Switzerland.

Ji, C., & Liangshun, S. (1988). Research on human skin injury thresholds for pulsed carbon dioxide lasers. *Jiguang Jishu* (Laser Technology), 12, 39–42.

Kindt, J. T., & Schmuttenmaer, C. A. (1996). Far-infrared dielectric properties of polar liquids probed by femtosecond terahertz pulse spectroscopy. *Journal of Physical Chemistry*, *100*(24), 10373–10379.

Mainster, M. A., White, T. J., Tips, J. H., & Wilson, P. W. (1970). Transient thermal behavior in biological systems. *Bulletin of Math Biophysics, 32*, 303–314.

Niemz, M. H. (2004). *Laser-Tissue Interactions, Fundamentals and Applications, Biological and Medical Physics, Biomedical Engineering* (3rd revised ed.). New York: Springer-Verlag.

Ozisik, M. (1994). *Finite Difference Methods in Heat Transfer* (1st ed.). Boca Raton, FL: CRC Press.

Peaceman, D. W. & Rachford, H. H. (1955). The numerical solution of parabolic and elliptic differential equations. *Journal of the Society for Industrial and Applied Mathematics*, *3*, 28–41.

Pickwell, E., Cole, B., Fitzgerald, A. J., Wallace, V., & Pepper, M. (2004). Simulation of terahertz pulse propagation in biological systems. *Applied Physics Letters*, *84*, 2190-2192.

Pickwell, E., Fitzgerald, A., Cole, B., Taday, P., Pye, R., Ha, T., Pepper, M., & Wallace, V. (2005). Simulating the response of terahertz radiation to basal cell carcinoma using ex vivo spectroscopy measurements. *Journal of Biomedical Optics, 10*, 064021.

Riu, P. J., Foster, K. R., Blick, D. W., & Adair, E. R. (1996). A thermal model for human thresholds of microwave-evoked warmth sensations. *Bioelectromagnetics, 18*, 578–583.

Rockwell, R. J. & Goldman, L. (1974). *Research on Human Skin Laser Damage Thresholds* (USAF Technical Report DERM-LL-74-1003). Brooks AFB, TX: USAF School of Aerospace Medicine.

Taflove, A. & Hagness, S. C. (2000). *Computational Electrodynamics - The Finite-Difference Time-Domain Method* (2nd ed.). Norwood, MA: Artech House.

Takata, A. N., Zaneveld. D., & Richter, M. S. (1977). *SAM-TR-77-38 Laser Induced Thermal Damage of Skin* (USAF Technical Report SAM-TR-77-38). Brooks AFB, TX: USAF School of Aerospace Medicine.

Torres, J. H., Motamedi, M., Pearce, J. A., & Welch, A. J. (1993). Experimental evaluation of mathematical models for predicting the thermal response of tissue to laser irradiation. *Applied Optics, 32*, 597–606.

Welch, A. J. & van Gemert, M. J. C. (1995). *Optical-Thermal Response of Laser-Irradiated Tissue, Lasers, Photonics, and Electro-Optics* (1st ed.). New York: Plenum Press.

Williams, G. (2006a). Filling the THz gap. *Reports on Progress in Physics*, *69*.

Williams, G. (2006b). Next generation accelerator-based light sources for IR microscopy and spectroscopy. *Journal of Infrared Physics and Technology, 49*.

Yee, K. S. (1966). Numerical solution of initial boundary value problems involving Maxwell's equations in isotropic media. *IEEE Transactions Antennas and Propagation, 14*, 302–307.

Yu, B. L., Yang, Y., Zeng, F., Xin, X., & Alfano, R. R. (2005). Reorientation of the H_2O cage studied by terahertz time-domain spectroscopy. *Applied Physics Letters*, *86*, 061912.

IEC, See International Electrotechnical Commission, 40, 293, 333, 334, 351, 355, 357, 383

IEEE, See Institute of Electrical and Electronics Engineers, 1, 2, 3, 4, 31, 34, 40, 41, 42, 43, 44, 45, 46, 67, 68, 97, 98, 100, 111, 113, 114, 117, 121, 122, 124, 125, 147, 168, 170, 171, 201, 209, 218, 219, 241, 243, 247, 249, 251, 261, 268, 272, 276, 279, 281, 283, 284, 285, 286, 287, 288, 292, 294, 312, 321, 323, 328, 331, 332, 333, 336, 337, 338, 339, 340, 341, 342, 344, 345, 346, 348, 349, 350, 351, 352, 353, 354, 355, 356, 357, 378, 379, 383, 384

Impedance method, 10, 11, 38, 41, 45

In vivo, vii, 102, 178, 182, 303, 342, 343

Induced current density, 1, 293

Induced currents, 14, 25, 27, 28, 32, 40, 66, 73, 90, 267, 335, 342

Injuries, 148, 253, 254, 256, 259, 358

Institute of Electrical and Electronics Engineers, 44, 261, 279, 288, 312, 321, 323, 331, 354

Instrumentation, 49, 267, 268, 323, 337, 352, 355

Internal E-field, 18

International Commission on Non-Ionizing Radiation Protection, 44, 279, 312, 321, 337, 355

International Electrotechnical Commission, 355, 357

International EMF Project, 291, 312, 341

Laboratory animal, 66, 121, 131, 140, 141, 183, 247, 330, 332, 344

Learning, 106, 108, 116, 118, 123, 250

Legislative act, 292, 294, 311

Long-term exposure, 321, 346, 348, 378

Low frequency, 13, 41, 273, 306, 326

Magnetic field, 2, 10, 11, 12, 13, 27, 29, 32, 34, 37, 38, 39, 41, 42, 43, 44, 45, 49, 118, 154, 172, 173, 263, 264, 265, 266, 269, 272, 278, 292, 293, 294, 306, 307, 312, 316, 318, 323, 325, 330, 334, 347, 362

Magnetic flux density, 292, 293

Man, 7, 8, 15, 45, 47, 48, 50, 51, 66, 126, 127, 129, 133, 134, 136, 137, 138, 143, 159, 162, 163, 168, 169, 171, 173, 194, 195, 201, 204, 241, 242, 243, 263, 322, 325, 353, 354

Maximum permissible exposure, 2, 3, 247, 286, 294, 333, 357

Measurement, vii, 18, 47, 53, 54, 55, 57, 60, 63, 65, 70, 72, 75, 76, 82, 85, 91, 92, 95, 97, 134, 178, 182, 201, 223, 224, 263, 266, 267, 268, 270, 272, 274, 279, 291, 336, 337, 345, 351, 358

Memory, 6, 26, 27, 35, 106, 116, 148

Metabolic heat production, 126, 127, 129, 130, 131, 136, 137, 140, 147, 159, 161, 163, 164

Metabolism, 123, 175, 176, 177, 178, 179, 181, 182, 236, 238, 327

Microdosimetry, 75, 76, 84, 85, 96

Microwave, ix, 1, 2, 40, 42, 67, 69, 70, 74, 75, 76, 77, 78, 79, 80, 81, 82, 83, 86, 87, 91, 92, 97, 98, 99, 100, 101, 102, 103, 104, 105, 106, 107, 109, 113, 114, 115, 116, 117, 118, 119, 120, 121, 122, 123, 125, 151, 152, 164, 166, 167, 168, 169, 170, 172, 173, 174, 218, 240, 241, 250, 260, 261, 264, 268, 270, 271, 277, 306, 311, 316, 321, 322, 325, 335, 338, 339, 344, 350, 351, 353, 354, 355, 356, 358, 382, 384

Microwave exposure, 76, 78, 105, 106, 107, 115, 118, 119, 123, 164, 260, 261

Microwave heating, 77, 79, 81, 82, 120, 218

Military, 101, 153, 241, 249, 269, 272, 278, 321, 337, 340

Millimeter wave, 209, 210, 211, 213, 219, 241, 243, 244, 245, 246, 247, 261, 262

Mobile phones, 113, 211, 306, 307, 314, 315, 318

Modeling, 4, 5, 67, 102, 127, 133, 155, 156, 158, 168, 175, 181, 184, 192, 202, 203, 204, 214, 217, 261, 324, 351, 361, 365, 380

Models, viii, 1, 6, 10, 12, 15, 22, 26, 29, 31, 32, 33, 34, 35, 36, 38, 39, 40, 42, 43, 45, 46, 66, 67, 72, 155, 156, 158, 168, 173, 175, 177, 199, 202, 203, 212, 213, 214, 215, 216, 217, 218, 275, 321, 324, 325, 327, 339, 353, 354, 358, 362, 365, 377, 384

Modulation, 150, 267, 273, 277, 323, 326, 330, 332, 333

Mouse, 50, 51, 54, 65, 112, 116, 120, 121, 172

MPE, See Maximum permissible exposure, 2, 247, 248, 249, 250, 251, 252, 258, 259, 286, 287, 294, 333, 335, 336, 345, 347, 348, 357

MRI, See Magnetic Resonance Imaging, 6, 13, 14, 15, 27, 31, 41, 42, 147, 153, 154, 155, 156, 157, 165, 218, 220, 240, 253

Nanopulse, 111, 112

National Council on Radiation Protection and Measurements, 241, 262, 321, 323, 329, 337, 355

National Radiological Protection Board, 28, 45, 308

NCRP, See also National Council on Radiation Protection and Measurements, 241, 262, 321, 323, 325, 328, 329, 330, 331, 332, 335, 336, 337, 338, 339, 344, 345, 346, 355

Near-field, vii, 2, 4, 5, 18, 40, 64, 66, 243, 354, 356

Near-field exposure, vii, 2, 243, 354, 356

Non-ionizing, viii, 240, 241, 243, 247, 254, 263, 301, 304, 308, 311, 314, 333, 338

Non-thermal effects, 69